TESIS DE LA UNIVERSIDAD DE ZARAGOZA

2025

89

Jorge Perpiñán Hinarejos

# Innovative proposals for the integration of Power to Gas systems in the Iron and Steel Industry

Director/es
Bailera Martín, Manuel
Peña Pellicer, María Begoña

http://zaguan.unizar.es/collection/Tesis

ISSN 2254-7606

Prensas de la Universidad
Universidad Zaragoza

Universidad de Zaragoza
Servicio de Publicaciones

ISSN 2254-7606

Universidad Zaragoza
1542

Tesis Doctoral

# INNOVATIVE PROPOSALS FOR THE INTEGRATION OF POWER TO GAS SYSTEMS IN THE IRON AND STEEL INDUSTRY


Autor

Jorge Perpiñán Hinarejos

Director/es

Bailera Martín, Manuel
Peña Pellicer, María Begoña

**UNIVERSIDAD DE ZARAGOZA**
**Escuela de Doctorado**


2024


**Repositorio de la Universidad de Zaragoza – Zaguan http://zaguan.unizar.es**

Universidad Zaragoza
1542

Tesis Doctoral

# Innovative proposals for the integration of Power to Gas systems in the Iron and Steel Industry.


Autor

Jorge Perpiñán Hinarejos

Directores

Begoña Peña Pellicer

Manuel Bailera Martín

Tutora

Begoña Peña Pellicer

**UNIVERSIDAD DE ZARAGOZA**

Escuela de ingeniería y arquitectura


**2024**

Dedico este trabajo a mi familia y mis amigos, quienes han estado a mi lado apoyándome en todo momento y brindándome su amor, comprensión y motivación. Sin ellos, este logro no habría sido posible.

# Innovative proposals for the integration of Power to Gas systems in the Iron and Steel Industry.

Jorge Perpiñán Hinarejos

Memoria presentada por Jorge Perpiñán a la Universidad de Zaragoza para la obtención del título de Doctor con Mención de Doctorado Internacional

**Tutores**
Begoña Peña Pellicer *Universidad de Zaragoza (Spain*)

**Director**
Begoña Peña Pellicer *Universidad de Zaragoza (Spain*)
Manuel Bailera Martín *Universidad de Zaragoza (Spain)*

# Index

INDEX ..... 4
LIST OF TABLES ..... 6
LIST OF FIGURES ..... 7
NOMENCLATURE ..... 9
LIST OF PUBLICATIONS ..... 10
AGRADECIMIENTOS ..... 13
PROLOGUE ..... 14
PRÓLOGO ..... 15
ABSTRACT ..... 16
RESUMEN ..... 19
1. GENERAL INTRODUCTION ..... 22
1.1. FRAMEWORK AND MOTIVATION ..... 22
1.2. PROPOSED LOW-CARBON TECHNOLOGY FOR HIGH-TEMPERATURE INDUSTRIAL PROCESSES ..... 24
1.3. OBJECTIVES, TASKS, AND STRUCTURE OF THE THESIS ..... 28
2. METHODOLOGY ..... 32
2.1. METHODOLOGY OF SYSTEMATIC REVIEWS ..... 32
2.2. MODELLING AND SIMULATION ..... 33
2.3. TECHNICAL INDICATORS AND ECONOMIC ANALYSIS ..... 38
2.4. EXPERIMENTAL PROCEDURE AND FACILITIES ..... 41
2.5. DATA PROCESSING AND ARTWORK ..... 44
3. POTENTIAL OF PTG INTEGRATION IN INDUSTRY ..... 45
3.1. POWER TO GAS IN THE GLASS INDUSTRY ..... 45
3.2. POWER TO GAS IN THE STEEL INDUSTRY ..... 51
3.3. DISCUSSION AND CONCLUSIONS OF PRELIMINARY STUDIES ..... 55
4. POWER TO GAS INTEGRATION IN THE IRON AND STEEL INDUSTRY ..... 57
4.1. CARBON CAPTURE TECHNOLOGIES IN BLAST FURNACE ROUTE ..... 57
4.2. PROPOSAL AND ASSESSMENT OF PTG INTEGRATION ..... 61
4.3. REVIEW ON PTG IN BF-BOF ROUTE ..... 75
5. MODELLING PTG SYSTEMS FROM EXPERIMENTAL TESTS ..... 80
5.1. MODELLING METHANATION FROM EXPERIMENTS (TRL 4) ..... 80
5.2. AMINE SCRUBBING MODELLING FROM EXPERIMENTS (TRL 6) ..... 84
6. CONCLUDING REMARKS ..... 89
6.1. CONCLUSIONS ..... 89
6.2. CONCLUSIONES ..... 91

**6.3. CONTRIBUTIONS ..... 95**

**6.4. ON-GOING AND FUTURE WORK ..... 96**

**BIBLIOGRAPHY ..... 98**

**ANNEXES ..... 109**

**A I&S INDUSTRY: $CO_2$ EMISSIONS AND STATE OF THE ART ..... 109**

**A.1. ENERGY CONSUMPTION AND $CO_2$ EMISSIONS ..... 109**

**A.2. MAIN PATHWAYS FOR STEELMAKING PRODUCTION ..... 110**

**A.2.1. LOW-CARBON APPROACHES FOR STEELMAKING INDUSTRY ..... 113**

**B FUNDING AND COLLABORATIONS ..... 119**

**C IMPACT FACTOR AND CATEGORY ..... 121**

**D AUTHOR CONTRIBUTION ..... 122**

**E PUBLISHED PAPERS ..... 126**

# List of tables

Table 1. General comparison of CCS processes and technologies [11], [12]. ..... 26
Table 2. Features of cell electrolysis technologies [13]. ..... 26
Table 3. Technical data of reactors for catalytic methanation [9], [14], [19]–[30]. ..... 27
Table 4. Technical data of reactors for biological methanation [9], [14], [19]–[30]. ..... 28
Table 5. Structure of the thesis: Objectives, tasks, outcomes, and thesis chapter. The numbering of the papers and conferences correspond to the ones indicated in the Section List of publications. ..... 28
Table 6. Aspen property methods for each process of sections 3 and 4. The selection of each property method was done according to the Methods Assistant of Aspen Plus [37]. ..... 34
Table 7. Input data of CaL system [41], [42]. ..... 36
Table 8. Description of variables in equations (3)-(6). ..... 39
Table 9. Data for the economic analysis of the PtG integration ..... 40
Table 10. Input data of the conventional container glass production plant [65]. ..... 47
Table 11. Comparison of KPIs for the low-carbon concepts (P: purchased; S-C: self-consumption) ..... 50
Table 12. Main steelmaking production routes: BF-BOF, Scrap-EAF and DR-EAF [76], [77]. ..... 52
Table 13. Status of main near-zero emission technologies in the iron and steel sector [76]. ..... 52
Table 14. BF technology and PtG component breakdown for Cases 1-6. ..... 62
Table 15. Summary of BF results from this study and literature. ..... 67
Table 16. Breakdown of $CO_2$ recycling. ..... 71
Table 17. Economic KPIs [46], [73]–[75]. ..... 72
Table 18. Classification of approaches to integrate PtG in blast furnace ironmaking. ..... 75
Table 19. Summary of all potential PtG integrations in BF ironmaking, according to the renewable fuel produced: A (SNG from pure $CO_2$), B (SNG from sweet gas), C (SNG from BFG), D ($H_2$), and E (Syngas from $CO_2$ electrolysis). (*) Poor performance expected a priori. ..... 77
Table 20. Main inputs and outputs for the Aspen Plus model. ..... 86
Table 21. Pilot Plant vs. Aspen Plus Model Outputs. ..... 87
Table 22. Main steelmaking production routes: BF-BOF, Scrap-EAF and DR-EAF [76], [77]. ..... 113
Table 23. Status of main near-zero emission technologies in the iron and steel sector [76]. ..... 115
Table 24. Journals where the manuscripts in the Doctoral Thesis were published. Journals where the manuscripts of the Doctoral Thesis were published. ..... 121

# List of figures

Figure 1. (Left) Total $CO_2$ emissions ($Gt_{CO2}$/year) from energy combustion and industrial processes, 1900-2021 [3]. (Right) Global energy-related $CO_2$ emissions by sector [4]. ..... 23
Figure 2. Direct $CO_2$ emissions from industry in the Net Zero Scenario, 2000-2030 [5]..... 23
Figure 3. Simplified process flow diagram of a Power to Gas system with a closed carbon loop. ..... 25
Figure 4. Thesis structure. Roman numbers indicate the related paper included in this thesis. 29
Figure 5. Flow diagram for systematic reviews. ..... 33
Figure 6. $CO_2$ capture with chemical absorption. ..... 36
Figure 7. Process flow diagram of the Calcium Looping system ..... 37
Figure 8. Methanation system scheme ..... 38
Figure 9. Methanation test facility. ..... 41
Figure 10. Methanation reactor (without external insulation). ..... 42
Figure 11. Flow scheme of the carbon capture pilot plant (adapted from [63]). ..... 44
Figure 12. Conventional glass plant, base case. ..... 46
Figure 13. Process flow diagram of the low-carbon concepts. Case 1: basic PtG integration (solid lines). Case 2: PtG with CaO recycling (solid and pink dashed lines). Case 3: PtG with oxy-melting furnace (solid and green dashed lines). Case 4: PtG with Power Plant (solid and red dotted lines). ..... 48
Figure 14. Main steel production pathways and material flows in 2019 [76]. ..... 51
Figure 15. Process flow diagram of the reference ironmaking plant (Case 0). ..... 53
Figure 16. Process flow diagram of the power to methane integration in ironmaking with oxy-fuel combustion and top gas recycling (Case 1) ..... 54
Figure 17. Process flow diagram of the COG methanation integration in ironmaking with oxy-fuel combustion and top gas recycling (Case 2) ..... 55
*Figure 18. Carbon capture routes in the BF-BOF route.* ..... 58
*Figure 19. Number of scientific papers organised by year and technology.* ..... 58
Figure 20. Comparison of KPIs obtained from the literature for different CC technologies. ..... 59
Figure 21. Process flow diagram of a) Base case, b) BF+Amine+Meth., c) OBF+Amine+Meth., d) OBF+Amine+Meth.+TGR, e) OBF+Meth., f) OBF+Meth.+CO2, g) OBF+H2. ..... 63
Figure 22. Process flow diagrams of the hierarchy blocks. Blue lines: steam streams. ..... 64
Figure 23. Reducing agents and preheated gas injected in the blast furnace. The gaseous reducing agents include SNG, TGR and $H_2$. Cases in Figure 21. ..... 66
Figure 24. Total coal consumption broken down according to its final used form, see Figure 21. ..... 67
Figure 25. Blast furnace gas composition (vol%) for the cases of Figure 21. ..... 68
Figure 26. PEM size and sold gases for the cases of Figure 21. ..... 69
Figure 27. Total $CO_2$ emissions and $CO_2$ recycled in PtG, pre-heating gas, and TGR. ..... 70
Figure 28. Energy penalty in the cases of Figure 21. ..... 71
Figure 29. Specific $CO_2$ avoidance cost and implementation cost. Cases in Figure 21. ..... 73
Figure 30. Specific CC cost in €/$t_{CO2}$ as a function of the $CO_2$ taxes and the electricity price for an OBF with two auxiliary fuel injections (113 $kg_{SNG}/t_{HM}$ and 270 $kg_{TGR}/t_{HM}$), an electrolyser of 741 MW, and an amine scrubbing of 305 $kg_{CO2}/t_{HM}$ (Case 3). ..... 74
Figure 31. Summary of the different options for PtG-BF integrations, in terms of A) gas recycling, and B) renewable fuel injection. C) Nomenclature. ..... 76
Figure 32. Experimental design to evaluate catalyst performance. Sensitivity analysis on temperature (yellow), GHSV (red) and $H_2$:$CO_2$ ratio (blue). ..... 81

Figure 33. $CO_2$ conversion at the outlet vs. isothermal temperature of reactor. Each point corresponds to one steady state operation. GHSV = 10000$h^{-1}$; $H_2$:$CO_2$ ratio = 4; P = 1 atm. ..... 82
Figure 34. $CO_2$ conversion at the outlet vs. GHSV. Each point corresponds to one steady state operation. T = 350 °C; $H_2$:$CO_2$ ratio = 4; P = 1 atm. ..... 82
Figure 35. $CO_2$ conversion at the outlet vs. $H_2$:$CO_2$ ratio at the inlet. Each point corresponds to one steady state operation. GHSV = 10000 $h^{-1}$; T = 350 °C; P = 1 atm. ..... 83
Figure 36. Process flow diagram for the methanation plant in Aspen Plus (4-reactor configuration). ..... 84
Figure 37. Process flow diagram for the carbon capture plant in Aspen Plus. ..... 85
Figure 38. Inner absorber Temperature: Pilot Plant (•) vs. Model (–). Stage 1 and stage 30 are the top and the bottom of the absorber, respectively. ..... 88
Figure 39. Specific Carbon Capture Duty: Pilot Plant (·) vs. Model (-) at Stripper Pressures of 1.8 (orange) or 2.0 bar (blue). ..... 88
Figure 40.Cumulative direct emission reductions by mitigation strategy in the sustainable development scenario between 2020 and 2050 [76]. ..... 110
Figure 41. Main steel production pathways and material flows in 2019 [76]. ..... 113
Figure 42. TRL scale applied by the IEA [76]. ..... 114

# Nomenclature

| Abbreviation | Meaning |
|---|---|
| AFT | Adiabatic Flame Temperature |
| AHF | Air Heating Furnace |
| ASU | Air Separation Unit |
| BF-BOF | Blast Furnace-Basic Oxygen Furnace |
| BFG | Blast Furnace Gas |
| BOFG | Basic Oxygen Furnace Gas |
| CaL | Calcium Looping |
| CC | Carbon Capture |
| CCUS | Carbon Capture Utilization and Storage |
| ChL | Chemical Looping |
| COG | Coke Oven Gas |
| DRI | Direct Reduced Iron |
| EAF | Electric Arc Furnace |
| FSCM | Fixed Site Carrier Membrane |
| GHG | Green House Gas |
| GWP | Global Warming Potential |
| HM | Hot Metal |
| HRC | Hot Rolled Coil |
| I&S | Iron and Steel |
| IEA | International Energy Agency |
| IRR | Internal Rate of Return |
| LHV | Lower Heating Value |
| MDEA | Methyldiethanolamine |
| NGCC | Natural Gas Combined Cycle |
| OBF | Oxygen Blast Furnace |
| OtherL | Other Looping Processes |
| Oxy-TGR | Oxy-Top Gas Recycling |
| PCI | Pulverised Coal Injection |
| PEM | Proton Exchange Membrane |
| Post-chem | Post-combustion CC with chemical absorption |
| Post-memb | Post-combustion CC with membranes |
| PP | Power Plant |
| PPAs | Power purchase agreements |
| Pre-adsor | Pre-combustion CC with physical adsorption |
| Pre-chem | Pre-combustion CC with chemical absorption |
| Pre-memb | Pre-combustion CC with membranes |
| PtG | Power to Gas |
| SEWGS | Sorption Enhanced Water Gas Shift |
| SNG | Synthetic Natural Gas |
| SPECCA | Specific Primary Energy Consumption for $CO_2$ Avoided |
| tCS | Ton of Crude Steel |
| TGR | Top Gas Recycling |
| tHM | Ton of Hot Metal |
| TRL | Technology Readiness Level |
| TSA | Temperature Swing Adsorption |
| VPSA | Vacuum Pressure Swing Adsorption |
| WGS | Water Gas Shift |
| α, β, γ | Parameters for Economic Analysis |

# List of publications

This thesis is presented as a compendium of publications. The thesis is supported by several original publications developed by the author and his co-authors during the thesis period. The author has explicit authorization by all his co-authors to use their content as part of this thesis. A complete copy of the publications is presented in Section E

i. Cristian Barón, Jorge Perpiñán, Manuel Bailera, Begoña Peña. 2023. "*Techno-economic assessment of glassmaking decarbonization through integration of calcium looping carbon capture and power-to-gas technologies*". Sustainable Production and Consumption 41 (2023) 121–133. doi: 10.1016/j.spc.2023.07.029

ii. Jorge Perpiñán, Manuel Bailera, Luis M. Romeo, Begoña Peña, and Valerie Eveloy. 2021. "*$CO_2$ Recycling in the Iron and Steel Industry via Power-to-Gas and Oxy-Fuel Combustion*." Energies 14(21):7090. doi: 10.3390/en14217090.

iii. Jorge Perpiñán, Begoña Peña, Manuel Bailera, Valerie Eveloy, Pravin Kannan, Abhijeet Raj, Pilar Lisbona, and Luis Miguel Romeo. 2022. "*Integration of Carbon Capture Technologies in Blast Furnace Based Steel Making: A Comprehensive and Systematic Review*." Fuel 336 (2023) 127074. doi: 10.1016/j.fuel.2022.127074.

iv. Jorge Perpiñán, Manuel Bailera, Begoña Peña, Luis Miguel Romeo, and Valerie Eveloy. 2022. "*Technical and Economic Assessment of Iron and Steelmaking Decarbonization via Power to Gas and Amine Scrubbing*." Energy 276 (2023) 127616. doi: 10.1016/j.energy.2023.127616

v. Jorge Perpiñán, Manuel Bailera, Begoña Peña, Luis M. Romeo, and Valerie Eveloy. 2023. "*High Oxygen and SNG Injection in Blast Furnace Steelmaking with Power to Gas Integration and $CO_2$ Recycling*." Journal of Cleaner Production 405 (2023) 137001. doi: 10.1016/j.jclepro.2023.137001.

vi. Jorge Perpiñán, Manuel Bailera, Begoña Peña, Pravin Kannan, Valerie Eveloy, and Luis M. Romeo. 2023. "*Power to Gas and Top Gas Recycling Integration in an Oxygen Blast Furnace Steelmaking Industry*." Journal of CO2 Utilization 78 (2023) 102634. doi: 10.1016/j.jcou.2023.102634.

vii. Jorge Perpiñán, Manuel Bailera, and Begoña Peña. 2023. "*Full oxygen blast furnace steelmaking: from direct hydrogen injection to methanized BFG injection*." Energy conversion and management 295 (2023) 117611. doi: 10.1016/j.enconman.2023.117611

viii. Jorge Perpiñán, Manuel Bailera, and Begoña Peña. 2024. "*Outline of all potential Power to Gas integrations in blast furnace ironmaking: A systematic review*". Renewable and Sustainable Energy Reviews 201 (2024) 114605. Doi: 10.1016/j.rser.2024.114605.

ix. Manuel Bailera, Pilar Lisbona, Begoña Peña, Andreina Alarcón, Jordi Guilera, Jorge Perpiñán, and Luis Miguel Romeo. 2022. "*Synthetic Natural Gas Production in a 1 KW Reactor Using Ni-Ce/$Al_2O_3$ and Ru-Ce/$Al_2O_3$: Kinetics,*

*Catalyst Degradation and Process Design*." Energy 256 (2022) 124720. doi: 10.1016/j.energy.2022.124720.

In addition, the author has collaborated in other papers not directly related to the subject of the thesis but developed within the research group framework. For this reason, these publications are included in Section Annex B.

Furthermore, during the course of this research, the author has actively participated in various conferences and scientific gatherings related to the field of study. These conferences have provided valuable opportunities for the exchange of ideas, networking, and staying updated with the latest developments in the research domain. The underlined name indicates the presenter.

i. Jorge Perpiñán. "*Innovative proposals for the integration of Power to Gas systems in the Iron and Steel Industry*". IX Jornada de Doctorandos del Programa de Doctorado en Ingeniería Mecánica. 9th May 2023, Zaragoza, Spain.
ii. Jorge Perpiñán, Manuel Bailera, Begoña Peña, Luis M. Romeo. "*Evaluación de la integración de la tecnología 'Power to Gas' en la industria siderúrgica*". 4th Conference on 'Aportando Valor al $CO_2$'. 10-11th May 2023, Bilbao, Spain.
iii. Jorge Perpiñán, Manuel Bailera, Begoña Peña, Luis M. Romeo. "*Metano sintético para reducir las emisiones de $CO_2$ en la industria siderúrgica*". 1st Iberus Connect Doctoral Students Congress. 28th April 2023, Zaragoza, Spain.
iv. Jorge Perpiñán, Manuel Bailera, Begoña Peña, Luis M. Romeo, Valerie Eveloy and Mohamed Ali. "*Technical viability of different Power to Gas integration configurations in a BF-BOF iron and steel plant*". 16th International Conference on Greenhouse Gas Control Technologies (GHGT-16). 23-27th October 2022, Lyon, France.
v. Jorge Perpiñán, Manuel Bailera, Begoña Peña and Luis M. Romeo. "*Technical viability of different Power to Gas integration configurations in a BF-BOF iron and steel plant*". XII National and III International Conference on Engineering Thermodynamics (12CNIT-2022), 29th June – 1st July 2022, Madrid, Spain.
vi. Begoña Peña, Manuel Bailera, Belén Zalba, Pilar Lisbona, Jorge Perpiñán. "*Improving the long-term learning in Engineering Thermodynamics through spaced review to overcome Ebbinghaus' forgetting curve*". XII National and III International Conference on Engineering Thermodynamics (12CNIT-2022), 29th June – 1st July 2022, Madrid, Spain.
vii. Jorge Perpiñán, Manuel Bailera, Begoña Peña and Luis M. Romeo. "*Techno-economic viability of different Power to Gas integration configurations in a BF-BOF iron and steel plant*". EGATEC 2022 conference. Hamburg, the 14th of June 2022.
viii. Jorge Perpiñán, Manuel Bailera, Luis Miguel Romeo, Pilar Lisbona, Begoña Peña. "*Decarbonization of blast furnace steelmaking through Power to Gas: from direct $H_2$ injection to full blast furnace gas methanation*" XIII National and III International Conference on Engineering Thermodynamics (13CNIT-2023), 29th November – 1st December 2023, Castellón, Spain.

ix. Manuel Bailera, Jorge Perpiñán, Pilar Lisbona, Luis Miguel Romeo, Begoña Peña. "*Techno-economic assessment and comparison of different power to gas integrations for the reduction of $CO_2$ emissions in the Iron and Steel industry*". 37th International Conference on Efficiency, Cost, Optimization, Simulation and Environmental Impact of Energy Systems (ECOS 2024), 30th June – 5th July.

Lastly, the author has also contributed to one book chapter.

i. Sara Pascual, Manuel Bailera, Jorge Perpiñán and Pilar Lisbona. Chapter eight - CO2 conversion to methane. Advances and Technology Development in Greenhouse Gases: Emission, Capture and Conversion. Carbon Dioxide Conversion to Chemicals and Energy. 2024, Pages 165-193. Doi: 10.1016/B978-0-443-19235-7.00019-1

# Agradecimientos

Quiero expresar mi profunda gratitud a mis directores de tesis, Begoña y Manuel, así como a Luis Miguel y Pilar, por darme la oportunidad de embarcarme en una carrera investigadora y por su apoyo incondicional desde el principio. Agradezco enormemente todo lo que me han enseñado, tanto en los momentos gratificantes como en los desafiantes, y por su constante motivación y compartir su invaluable experiencia.

También quiero agradecer a mis compañeros Javi, Alex y Cristian, por hacer que el día a día sea más llevadero y ameno. Mi agradecimiento también a Daria y Silvia por el tiempo agradable durante sus estancias, y a Irmela, Michael y el resto del equipo de K1-MET por hacer de mi estancia en Linz una experiencia maravillosa.

De manera personal, quiero expresar mi agradecimiento a mi familia y a Alicia, por su amor incondicional, confianza y apoyo inquebrantable durante todo este tiempo.

Sin todos ellos, esta tesis no habría sido posible.

# Prologue

After graduating in Mechanical Engineering in 2018, I entered the Official Master in Renewable Energies and Energy Efficiency of the University of Zaragoza. The first time I heard about Power to Gas was thanks to Professor Luis M. Romeo, who proposed me to study this new technology in my Final Master's Work, co-directed also by Manuel Bailera. This work analysed the integration of Power to Gas in the steel industry, with the objective of reducing coal consumption and $CO_2$ emissions, and increasing the consumption of renewable energy. The trajectory followed during this master would later be awarded, in 2021 with the Extraordinary Prize of End of Master Degree, by the University of Zaragoza.

Power to Gas technology is the cornerstone of one of the research lines of the Energy and CO2 research group. I had the opportunity to be part of this team and work on three publicly funded projects on Power to Gas in the steel industry, during the period 2021-2023, among which is the CIRA-080-2020 project funded by Khalifa University.

Currently, the line of research is continued at the University of Zaragoza, through the projects DIS-HYCOME (PID2021-126164OB-I00) and DEC-I&S (TED2021-130000B-I00). These projects aim to deepen the integration of Power to Gas technology in the steel industry, through different configurations, technologies and concepts.

# Prólogo

Tras graduarme en Ingeniería Mecánica en 2018, ingresé en el Máster Oficial en Energías Renovables y Eficiencia energética de la Universidad de Zaragoza. La primera vez que oí hablar del Power to Gas fue gracias al profesor Luis M. Romeo, quien me propuso estudiar esta novedosa tecnología en mi Trabajo Fin de Máster, co-dirigido también por Manuel Bailera. Este trabajo analizaba la integración del Power to Gas en la industria siderúrgica, con el objetivo de reducir el consumo de carbón y las emisiones de $CO_2$, y aumentar el consumo de energía renovable. La trayectoria seguida durante este máster sería más tarde premiada, en 2021 con el Premio Extraordinario Fin de Máster Universitario, por la Universidad de Zaragoza.

La tecnología Power to Gas es el pilar fundamental de una de las líneas de investigación del grupo de investigación Energía y $CO_2$. Tuve la oportunidad de formar parte de este equipo y trabajar en tres proyectos de financiación pública sobre Power to Gas en la industria siderúrgica, durante el periodo 2021-2023, entre los que se encuentra el proyecto CIRA-080-2020.

Actualmente, la línea de investigación es continuada en la Universidad de Zaragoza, a través de los proyectos DIS-HYCOME (PID2021-126164OB-I00) y DEC-I&S (TED2021-130000B-I00). Estos proyectos pretenden profundizar en la integración de la tecnología Power to Gas en la industria siderúrgica, mediante diferentes configuraciones, tecnologías y conceptos.

# Abstract

Global $CO_2$ emissions from energy combustion and industrial processes reached their highest annual level ever in 2021, experiencing a 6% increase compared to 2020. This pushed emissions to a total of 36.3 gigatonnes (Gt) in 2021. Coal contributed significantly to the emissions increase, responsible for over 40% of them, reaching a record of 15.3 Gt. Natural gas emissions also exceeded 2019 levels at 7.5 Gt.

The industrial sector emitted 9.4 Gt of $CO_2$ in 2021, comprising a quarter of global emissions. The iron and steel (I&S) industry is a major emitter, responsible for 11% of industry-related $CO_2$ emissions. The Net Zero Emissions scenario envisions reducing industrial emissions to about 7 Gt of $CO_2$ by 2030 through improved energy efficiency, increased renewable energy adoption, and low-carbon production processes. In the Net Zero Scenario, around 60% of emission reductions in heavy industries by 2050 will rely on proven technologies that are not yet ready for the market.

Hence, the primary objective of this thesis is to deepen into innovative technologies that can contribute to the achievement of the Net Zero Scenario for the industry in general, with a special focus on the iron and steel industry. One promising approach is Power to Gas (PtG). PtG involves using renewable electricity to power electrolysers that decompose water, generating green hydrogen. This hydrogen can then be combined with $CO_2$ to produce synthetic natural gas, which can be utilized as a fuel within the industry. This process effectively recycles $CO_2$ and prevents its release into the atmosphere.

To achieve this primary objective, two preliminary studies were done in two different industries: glass and steel. The results were published in two papers:

i. Cristian Barón, Jorge Perpiñán, Manuel Bailera, Begoña Peña. 2023. "*Techno-economic assessment of glassmaking decarbonization through integration of calcium looping carbon capture and power-to-gas technologies*". Sustainable Production and Consumption 41 (2023) 121–133. doi: 10.1016/j.spc.2023.07.029

ii. Jorge Perpiñán, Manuel Bailera, Luis M. Romeo, Begoña Peña, and Valerie Eveloy. 2021. "*$CO_2$ Recycling in the Iron and Steel Industry via Power-to-Gas and Oxy-Fuel Combustion*." Energies 14(21):7090. doi: 10.3390/en14217090.

PtG technology offers significant potential for decarbonizing the glassmaking and steel industries. The glass sector can achieve more significant reductions in carbon intensity compared to the steel industry, for which, due to its complexity, lower reductions are achievable. This highlights the substantial emission-reduction potential of PtG technology, emphasizing the need for additional research within the steel industry to attain higher emission reductions. Despite the promising aspects, it is crucial to acknowledge that the associated costs are currently high. However, there is potential for significant cost reduction through adjustments in electricity pricing and $CO_2$ tax. Consequently, carbon capture in the steel industry and PtG integration in this sector are further investigated, with the outcomes detailed in the following publications:

iii. Jorge Perpiñán, Begoña Peña, Manuel Bailera, Valerie Eveloy, Pravin Kannan, Abhijeet Raj, Pilar Lisbona, and Luis Miguel Romeo. 2022. "*Integration of*

*Carbon Capture Technologies in Blast Furnace Based Steel Making: A Comprehensive and Systematic Review*." Fuel 336 (2023) 127074. doi: 10.1016/j.fuel.2022.127074.

iv. Jorge Perpiñán, Manuel Bailera, Begoña Peña, Luis Miguel Romeo, and Valerie Eveloy. 2022. "*Technical and Economic Assessment of Iron and Steelmaking Decarbonization via Power to Gas and Amine Scrubbing*." Energy 276 (2023) 127616. doi: 10.1016/j.energy.2023.127616

v. Jorge Perpiñán, Manuel Bailera, Begoña Peña, Luis M. Romeo, and Valerie Eveloy. 2023. "*High Oxygen and SNG Injection in Blast Furnace Steelmaking with Power to Gas Integration and $CO_2$ Recycling*." Journal of Cleaner Production 405 (2023) 137001. doi: 10.1016/j.jclepro.2023.137001.

vi. Jorge Perpiñán, Manuel Bailera, Begoña Peña, Pravin Kannan, Valerie Eveloy, and Luis M. Romeo. 2023. "*Power to Gas and Top Gas Recycling Integration in an Oxygen Blast Furnace Steelmaking Industry*." Journal of CO2 Utilization 78 (2023) 102634. doi: 10.1016/j.jcou.2023.102634.

vii. Jorge Perpiñán, Manuel Bailera, Begoña Peña, Valerie Eveloy, and Luis M. Romeo. 2023. "*Full oxygen blast furnace steelmaking: from direct hydrogen injection to methanized BFG injection*." Energy conversion and management 295 (2023) 117611. doi: 10.1016/j.enconman.2023.117611

viii. Jorge Perpiñán, Manuel Bailera, Begoña Peña and Luis M. Romeo. 2024. "*Outline of all potential Power to Gas integrations in blast furnace ironmaking*". Renewable and Sustainable Energy Reviews. doi: 10.1016/j.rser.2024.114605.

The successful integration of PtG faces two main challenges: the need for higher TRLs for components like oxygen blast furnaces, methanation or carbon capture; and addressing the associated high costs, in terms of CAPEX and OPEX.

The second part of this thesis focuses on experimenting with different Power to Gas system components. It specifically involves investigating the methanation reaction at TRL 4 and examining the carbon capture stage at TRL 6. The methanation reaction was conducted at UNIZAR's facilities, where various catalysts were compared, and the conversion of $CO_2$ to methane was studied. The carbon capture research took place at voestalpine and K1-MET's facilities, focusing on amine scrubbing for capturing $CO_2$ from actual flue gases generated at the steel site (voestalpine, Linz, Austria). The results of both experiments have been gathered in the following papers:

ix. Manuel Bailera, Pilar Lisbona, Begoña Peña, Andreina Alarcón, Jordi Guilera, Jorge Perpiñán, and Luis Miguel Romeo. 2022. "*Synthetic Natural Gas Production in a 1 KW Reactor Using Ni-Ce/$Al_2O_3$ and Ru-Ce/$Al_2O_3$: Kinetics, Catalyst Degradation and Process Design*." Energy 256 (2022) 124720. doi: 10.1016/j.energy.2022.124720.

Among the key findings an innovative approach in the glass industry combining Calcium-Looping and $CO_2$ methanation is proposed and analysed, achieving up to 80% emission reduction with specific energy penalties of 35.8 MJ/$kg_{CO2}$. In the iron and steel sector, various PtG integration scenarios were examined, with an oxygen blast furnace with $CO_2$ methanation and top gas recycling emerging as the most effective, offering

substantial $CO_2$ reductions (30 %), lower energy penalty (12 MJ/$kg_{CO2}$) and cost-efficiency (216 €/$t_{CO2}$ and 130 €/$t_{HM}$) without the need for geological storage. Experimental tests validated the efficacy of nickel-based catalysts in a 1 kW reactor for methanation, and an Aspen Plus model based on this data identified the 3-reactor configuration as the most suitable for methanation plant design, reducing catalyst mass while achieving 95% methane content in synthetic gas. Experimental tests on an amine carbon capture plant identified optimal operating conditions for minimizing energy requirements at a liquid-to-gas ratio of 4.5 and an Aspen Plus model for carbon capture was validated with data from these tests.

# Resumen

Las emisiones globales de $CO_2$ provenientes de la combustión de energía y de procesos industriales alcanzaron su nivel anual más alto en 2021, experimentando un aumento del 6% en comparación con 2020. Esto llevó las emisiones a un total de 36,3 gigatoneladas (Gt) en 2021. El carbón contribuyó significativamente al aumento de las emisiones, siendo responsable de más del 40% de ellas, alcanzando un récord de 15,3 Gt. Las emisiones de gas natural también superaron los niveles de 2019 con 7,5 Gt.

El sector industrial emitió 9,4 Gt de $CO_2$ en 2021, comprendiendo una cuarta parte de las emisiones globales. La industria del hierro y el acero es una de las mayores emisoras, responsable del 11% de las emisiones de $CO_2$ relacionadas con la industria. El escenario de Emisiones Netas Cero prevé reducir las emisiones industriales a aproximadamente 7 Gt de $CO_2$ para 2030 mediante una mejor eficiencia energética, una mayor adopción de energías renovables y procesos de producción de bajo carbono. En el Escenario de Cero Neto, alrededor del 60% de las reducciones de emisiones en las industrias pesadas para 2050 dependerán de tecnologías que aún no están listas para el mercado.

Por lo tanto, el objetivo principal de esta tesis es profundizar en las tecnologías innovadoras que pueden contribuir a lograr el Escenario de Cero Neto para la industria en general, con un enfoque especial en la industria del hierro y el acero. Un enfoque prometedor es la tecnología Power to Gas (PtG). PtG implica el uso de electricidad renovable para alimentar electrolizadores que descomponen el agua, generando hidrógeno verde. Este hidrógeno puede luego combinarse con $CO_2$ para producir gas natural sintético, que puede ser utilizado como combustible dentro de la industria. Este proceso recicla efectivamente el $CO_2$ y previene su liberación a la atmósfera.

Para lograr este objetivo principal, se realizaron dos estudios preliminares en dos industrias diferentes: vidrio y acero. Los resultados se publicaron en dos artículos:

i. Cristian Barón, Jorge Perpiñán, Manuel Bailera, Begoña Peña. 2023. "*Techno-economic assessment of glassmaking decarbonization through integration of calcium looping carbon capture and power-to-gas technologies*". Sustainable Production and Consumption 41 (2023) 121–133. doi: 10.1016/j.spc.2023.07.029

ii. Jorge Perpiñán, Manuel Bailera, Luis M. Romeo, Begoña Peña, and Valerie Eveloy. 2021. "*$CO_2$ Recycling in the Iron and Steel Industry via Power-to-Gas and Oxy-Fuel Combustion*." Energies 14(21):7090. doi: 10.3390/en14217090.

La tecnología PtG ofrece un potencial significativo para la descarbonización de las industrias del vidrio y del acero. El sector del vidrio puede lograr reducciones más significativas en la intensidad de carbono en comparación con la industria del acero, para la cual, debido a su complejidad, se logran reducciones menores. Esto resalta el considerable potencial de reducción de emisiones de la tecnología PtG, enfatizando la necesidad de investigación adicional en la industria del acero para lograr mayores reducciones de emisiones. A pesar de los aspectos prometedores, es crucial reconocer que los costes asociados son actualmente altos. Sin embargo, existe potencial para una reducción significativa de costes mediante ajustes en los precios de la electricidad y el

impuesto al $CO_2$. En consecuencia, se investigan más a fondo la captura de carbono en la industria del acero y la integración de PtG en este sector, con los resultados detallados en las siguientes publicaciones:

iii. Jorge Perpiñán, Begoña Peña, Manuel Bailera, Valerie Eveloy, Pravin Kannan, Abhijeet Raj, Pilar Lisbona, and Luis Miguel Romeo. 2022. "*Integration of Carbon Capture Technologies in Blast Furnace Based Steel Making: A Comprehensive and Systematic Review*." Fuel 336 (2023) 127074. doi: 10.1016/j.fuel.2022.127074.

iv. Jorge Perpiñán, Manuel Bailera, Begoña Peña, Luis Miguel Romeo, and Valerie Eveloy. 2022. "*Technical and Economic Assessment of Iron and Steelmaking Decarbonization via Power to Gas and Amine Scrubbing*." Energy 276 (2023) 127616. doi: 10.1016/j.energy.2023.127616

v. Jorge Perpiñán, Manuel Bailera, Begoña Peña, Luis M. Romeo, and Valerie Eveloy. 2023. "*High Oxygen and SNG Injection in Blast Furnace Steelmaking with Power to Gas Integration and $CO_2$ Recycling*." Journal of Cleaner Production 405 (2023) 137001. doi: 10.1016/j.jclepro.2023.137001.

vi. Jorge Perpiñán, Manuel Bailera, Begoña Peña, Pravin Kannan, Valerie Eveloy, and Luis M. Romeo. 2023. "*Power to Gas and Top Gas Recycling Integration in an Oxygen Blast Furnace Steelmaking Industry*." Journal of CO2 Utilization 78 (2023) 102634. doi: 10.1016/j.jcou.2023.102634.

vii. Jorge Perpiñán, Manuel Bailera, Begoña Peña, Valerie Eveloy, and Luis M. Romeo. 2023. "*Full oxygen blast furnace steelmaking: from direct hydrogen injection to methanized BFG injection*." Energy conversion and management 295 (2023) 117611. doi: 10.1016/j.enconman.2023.117611

viii. Jorge Perpiñán, Manuel Bailera, Begoña Peña and Luis M. Romeo. 2024. "*Outline of all potential Power to Gas integrations in blast furnace ironmaking*". Renewable and Sustainable Energy Reviews. doi: 10.1016/j.rser.2024.114605.

La integración exitosa de PtG enfrenta dos desafíos principales: la necesidad de mayores TRL para componentes como los altos hornos de oxígeno, la metanización o la captura de carbono; y abordar los altos costes asociados, en términos de CAPEX y OPEX.

La segunda parte de esta tesis se centra en experimentar con diferentes componentes del sistema Power to Gas. Específicamente, implica investigar la reacción de metanización en TRL 4 y examinar la etapa de captura de carbono en TRL 6. La reacción de metanización se llevó a cabo en las instalaciones de UNIZAR, donde se compararon varios catalizadores y se estudió la conversión de $CO_2$ a metano. La investigación sobre captura de carbono tuvo lugar en las instalaciones de voestalpine y K1-MET, enfocándose en la absorción con aminas para capturar $CO_2$ de gases de combustión reales generados en la planta siderúrgica (voestalpine, Linz, Austria). Los resultados de ambos experimentos se han recopilado en los siguientes artículos:

ix. Manuel Bailera, Pilar Lisbona, Begoña Peña, Andreina Alarcón, Jordi Guilera, Jorge Perpiñán, and Luis Miguel Romeo. 2022. "*Synthetic Natural Gas Production in a 1 KW Reactor Using Ni-Ce/$Al_2O_3$ and Ru-Ce/$Al_2O_3$: Kinetics,*

*Catalyst Degradation and Process Design*." Energy 256 (2022) 124720. doi: 10.1016/j.energy.2022.124720.

Entre los hallazgos clave, se propone y analiza un enfoque innovador en la industria del vidrio que combina Calcium-Looping y metanización de $CO_2$, logrando hasta un 80% de reducción de emisiones con penalizaciones energéticas específicas de 35,8 $MJ/kg_{CO2}$. En el sector del hierro y el acero, se examinaron varios escenarios de integración de PtG, emergiendo un alto horno de oxígeno con metanización de $CO_2$ y reciclaje de gas superior de horno como el más efectivo, ofreciendo reducciones sustanciales de $CO_2$ (30 %), menor penalización energética (12 $MJ/kg_{CO2}$) y eficiencia en costes (216 €/$t_{CO2}$ y 130 €/$t_{HM}$) sin necesidad de almacenamiento geológico. Las pruebas experimentales validaron la eficacia de los catalizadores a base de níquel en un reactor de 1 kW para la metanización, y un modelo de Aspen Plus basado en estos datos identificó la configuración de 3 reactores como la más adecuada para el diseño de la planta de metanización, reduciendo la masa del catalizador mientras se lograba un contenido de metano del 95% en el gas sintético. Los experimentos en la planta de captura de carbono con aminas identificaron condiciones óptimas de operación para minimizar el consumo energético en una relación líquido-gas (L/G) de 4,5, y un modelo de Aspen Plus para captura de carbono fue validado con datos de estos experimentos.

# 1. General introduction

The present thesis is part of the doctoral program in Mechanical Engineering at the University of Zaragoza, with a research stay conducted at K1-MET in Linz, Austria. It aligns with various policies such as carbon emission reduction and circular economy initiatives. This thesis aims to contribute to the current European plan to reduce "hard-to-abate" industrial emissions, enhance Europe's energy independence while maintaining competitiveness, and address existing gaps (Section 1.1). The proposed solution is based on the Power to Gas concept, which closes the carbon loop using renewable sources (Section 1.2). The objectives, activities, and structure of the thesis are outlined at the end of this chapter (Section 1.3).

## 1.1. Framework and motivation

In recent years, Europe has spearheaded ambitious initiatives aimed at tackling pressing environmental challenges and fostering sustainable development. Central to these efforts are flagship programs such as the Green Deal [1] and the Net Zero Industry Act [2], which seeks to transform the continent into a climate-neutral economy by 2050. The European Green Deal provides an action plan, to boost the efficient use of resources by moving to a clean, circular economy and to restore biodiversity and cut pollution. It embraces several policy areas: economy decarbonization, increase of energy efficiency, deployment of renewable energies, electrification of the economy, energy storage technologies, solutions based on nature, circular economy, ecology restauration and enhanced resilience of economic sectors. The Net Zero Industry Act is a legislative framework aimed at achieving net-zero carbon emissions in the industrial sector. It outlines measures and targets to reduce greenhouse gas emissions from industrial processes and operations, with the ultimate goal of aligning industrial activities with climate neutrality objectives.

$CO_2$ emissions from industrial processes and power generation is rising significantly, experiencing in 2021 a 6% increase compared to 2020. This pushed emissions to a total of 36.3 gigatonnes (Gt) as shown in Figure 1 (left). Coal usage was responsible for more than 40% of the global $CO_2$ emissions growth in 2021, reaching a record of 15.3 Gt. $CO_2$ emissions from natural gas accounted for 7.5 Gt, due to increased demand in all sectors [3].

Due to the heavy reliance on fossil fuels, the power sector (including electricity and heat) is the largest contributor to carbon emissions, accounting for almost 40% of global energy-related emissions [4], as depicted in Figure 1 (right). Coal-fired power generation stands as the primary source of energy-related emissions, contributing to 10 $Gt_{CO2}$ or 29% of total energy-related $CO_2$ emissions in 2018.

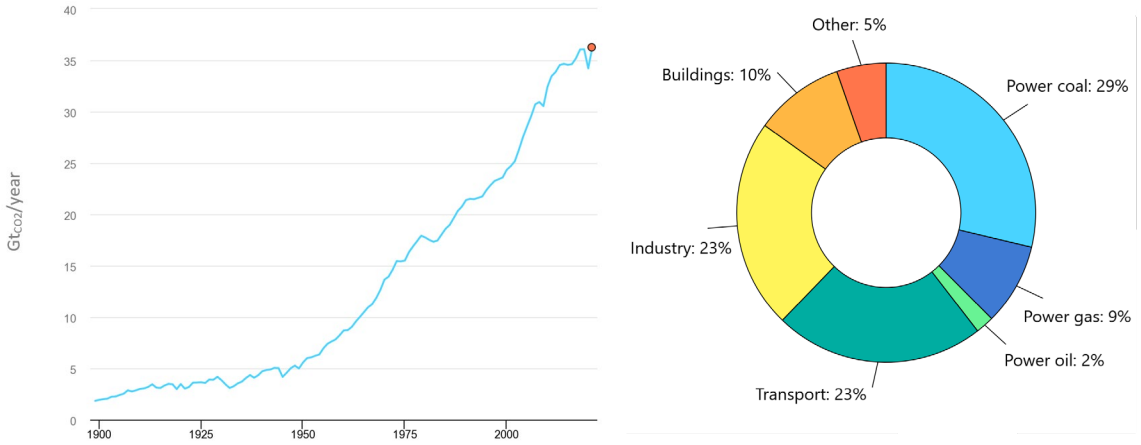


*Figure 1. (Left) Total $CO_2$ emissions ($Gt_{CO2}$/year) from energy combustion and industrial processes, 1900-2021* [3]*. (Right) Global energy-related $CO_2$ emissions by sector* [4].

In 2021, industrial activity directly emitted 9.4 Gt of $CO_2$, constituting a quarter of global emissions (excluding indirect emissions from electricity used in industrial processes) [5]. In the Net Zero Emissions by 2050 Scenario, it is projected that industrial emissions will decrease to approximately 7 $Gt_{CO2}$ by 2030, despite the expected growth in industrial production [5]. Some progress has been made in enhancing energy efficiency and increasing the adoption of renewable energy, along with positive policy measures and innovation. However, the pace of progress is insufficient. It is crucial to achieve greater material and energy efficiency, accelerate the adoption of renewable fuels, and expedite the development and deployment of low-carbon production processes, including carbon capture and storage and hydrogen technologies [6], see Figure 2.

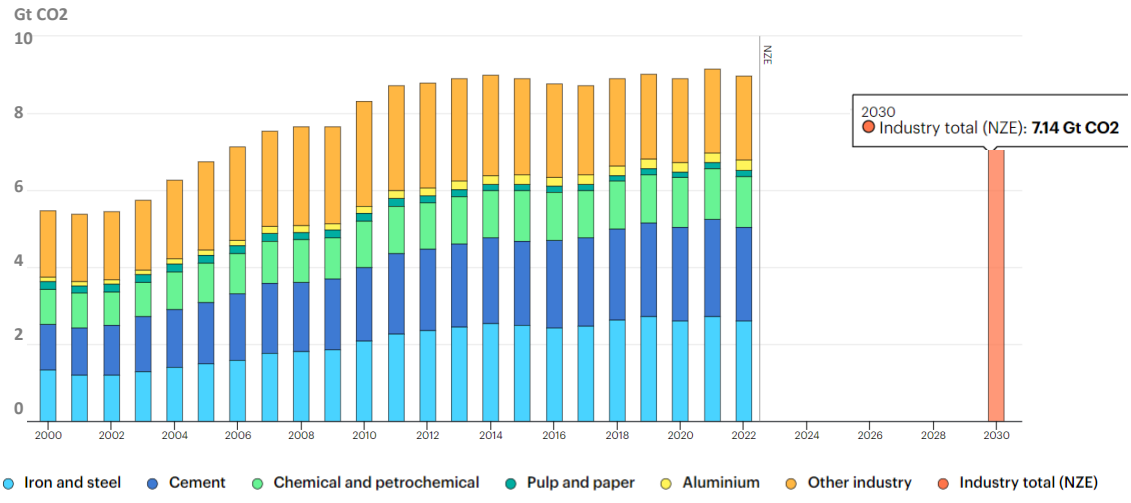


*Figure 2. Direct $CO_2$ emissions from industry in the Net Zero Scenario, 2000-2030* [5].

In the Net Zero Scenario, various technological pathways are envisioned, including the adoption of production methods incorporating hydrogen, carbon capture, use and storage (CCUS), direct electrification, energy storage and other innovative approaches specific to certain products [7]. As a result, these technologies could experience increased deployment by 2030, including commercialization and early

implementation. The share of electricity in the sector's final consumption could rise from 21% to nearly 30% by 2030, with a larger proportion of that electricity generated from near-zero emission sources. The demand for hydrogen could also increase significantly from 55 Mt in 2021 to approximately 85 Mt in 2030. Additionally, $CO_2$ captured through CCUS could undergo a substantial increase from 4 Mt in 2021 to around 300 Mt by 2030 [5]. The adoption of other innovative production methods will vary across different industries.

Many industrial processes involve chemical reactions and high-temperature heat that cannot currently be decarbonized with commercially available technologies, such as in the iron and steel industry, the cement industry or the glass industry [8]. In the Net Zero Scenario, around 60% of emission reductions in heavy industries by 2050 will rely on proven technologies that are not yet ready for the market. Numerous global efforts in industrial innovation are currently underway. It is crucial to accelerate the development and deployment of key low-emission technologies by ensuring sufficient funding for research and development, as well as demonstration projects.

Major industrial $CO_2$ emitters include the iron and steel industry, contributing 2.6 $Gt_{CO2}$ annually, and the cement industry, emitting approximately 2.4 $Gt_{CO2}$. The chemical and petrochemical sector adds around 1.3 $Gt_{CO2}$, while the glass industry contributes 0.1 $Gt_{CO2}$ annually, see Figure 2 [5]. These industries are key sources of global industrial emissions, necessitating focused efforts on adopting low-emission technologies to align with the objectives of the Net Zero Scenario.

## 1.2. Proposed low-carbon technology for high-temperature industrial processes

Power to gas (PtG) includes technologies that converts electricity generated from renewable sources into hydrogen or methane gas [9]. This process involves electrolysis to split water molecules into hydrogen and oxygen. The produced hydrogen can then be further utilized in various applications such as energy carrier, transportation fuel, or as a feedstock for industrial processes.

One notable advantage of power to gas systems is their capability to recycle $CO_2$ continuously, thereby preventing its release into the atmosphere [10], see Figure 3. This concept involves capturing $CO_2$ emissions from industrial processes and utilizing it alongside hydrogen in the methanation process to produce synthetic methane. This process not only helps to reduce greenhouse gas emissions but also enables the utilization of $CO_2$ as a valuable resource. Additionally, it enables indirect electrification of high-temperature heat and the production of renewable fuels.

The state of the art of the main components involved in PtG systems, the electrolyser, the carbon capture and the methanation plant, is briefly outlined in the following paragraphs.

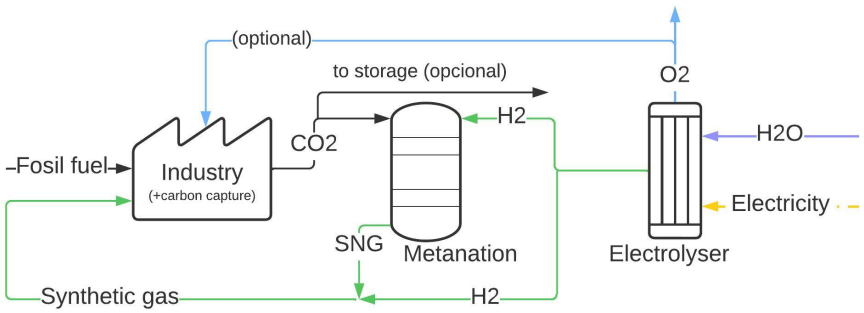


*Figure 3. Simplified process flow diagram of a Power to Gas system with a closed carbon loop.*

**Carbon capture**

Various configurations of carbon capture exist, including post-combustion capture, which involves capturing $CO_2$ from exhaust gases after combustion; pre-combustion capture, which entails capturing $CO_2$ before combustion, such as in solid fuel gasification processes, and extracting it from the produced syngas; oxy-fuel combustion, which involves combustion with pure oxygen and recycled flue gas, generating a $CO_2$-rich flue gas suitable for capture; chemical looping, which uses solid materials to transfer oxygen and facilitate combustion or gasification, producing a purer $CO_2$ stream; and direct air capture, which involves capturing $CO_2$ directly from ambient air [11]. Table 1 shows the advantages, disadvantages and TRL level of each carbon capture configuration. These configurations employ different technologies, including chemical absorption, physical adsorption, calcium looping, and others.

**Electrolyser**

The electrolysis of water is a thermo-chemical process that involves the decomposition of water molecules ($H_2O$) into hydrogen gas ($H_2$) and oxygen gas ($O_2$) using an electrical current. There are three main types of electrolysers: alkaline electrolysis (AE), proton exchange membrane electrolysis (PEM), and solid oxide electrolysis (SOEC). Each type has distinct characteristics in terms of efficiency, operating temperature, and pressure requirements, see Table 2.

The AE and the PEM are considered mature technologies, while the SOEC is still in the development phase. Technology maturity is typically associated with costs and durability. Currently, AE is the most cost-effective and reliable option, although it has limitations such as corrosion and restricted operating pressure and load ranges. However, PEM is regarded as the preferred choice for Power to Gas plants [9] due to its ability to handle intermittent energy inputs and its operational flexibility, including operating at pressures of up to 100 bar. On the other hand, the SOEC technology needs further demonstration. Operating at high temperatures, the SOEC exhibits accelerated electrolysis kinetics, making it a promising option. However, the durability of ceramic materials at high temperatures and during long-term operation remains a challenge that needs to be addressed [9].

*Table 1. General comparison of CCS processes and technologies* [11], [12].

| Capture type | Advantages | Disadvantages | TRL |
|---|---|---|---|
| Post-combustion | Ease of retrofitting | Poor process efficiency<br>High operational costs | 7-9 |
| Pre-combustion | High process efficiency and $CO_2$ concentration<br>Retrofit possible | Heat transfer efficiency issues<br>High Capex costs | 6-8 |
| Oxy-fuel combustion | High $CO_2$ concentration in reduced gas volumes<br>Potential for easier CO2 purification | Energy intensive and costly<br>Difficult to retrofit<br>High oxygen production costs | 5-7 |
| Chemical looping | Purer $CO_2$ content<br>Lower energy penalty | Scale-up challenges, process still in low TRL<br>Complex system integration<br>No retrofit possible | 5-7 |
| Direct air capture | Can capture $CO_2$ from the ambient air<br>Address historical emissions<br>Flexible siting | High energy requirements<br>Currently expensive<br>Low $CO_2$ concentration in air leading to large volumes processed | 3-5 |
| **Technology** | **Advantages** | **Disadvantages** | **TRL** |
| Chemical absorption | Well-established and scalable<br>Can be tailored to target specific gases or contaminants | Energy Intensive<br>Can cause corrosion<br>Solvent degradation | 8-9 |
| Physical adsorption | Lower energy requirements<br>Adsorbents can often be regenerated | Limited for low $CO_2$ concentrations<br>Lower $CO_2$ purity than Chemical absorption | 6-7 |
| Calcium looping | High $CO_2$ capture efficiency<br>Cost-Effective (cheap limestone)<br>Potential for heat integration | High energy demand<br>Material degradation<br>Complexity of operation with hight temperature reactions | 5-7 |
| Chemical looping | High $CO_2$ capture efficiency<br>Fuel flexibility (including coal or biomass) | Complex process<br>Material costs (oxygen carriers) | 5-7 |

*Table 2. Features of cell electrolysis technologies* [13].

| Feature | AE | PEM | SOEC |
|---|---|---|---|
| Maturity | Mature | Mature | Development |
| Temperature (°C) | 40-90 | 20-100 | 600-1000 |
| Pressure (bar) | <30 | <100 | - |
| Efficiency (%) | 62-82 | 67-82 | - |
| Cold start up time (min) | 15-20 | 5 | >60 |

**Methanation**

Methanation is the process of converting hydrogen gas and carbon dioxide into methane through biological or catalytic reactions. Biological methanation, also known as biological methanogenesis, utilizes microorganisms (archaea) activity to convert $H_2$ and $CO_2$ into methane under anaerobic conditions. Catalytic methanation employs heterogeneous catalysts to facilitate the chemical reaction between $H_2$ and $CO_2$, producing methane as the desired product [9], [14].

Catalytic methanation is an efficient process (≈75%) that operates at high pressure and low temperature. The process is suitable for integration with existing industrial infrastructure, and its high reaction rate allows for scalability (GHSV > 2000 $h^{-1}$). However, catalytic methanation is sensitive to contaminants in the $CO_2$ stream and has limited operational flexibility under load variations, see Table 3. Some of the most relevant catalytic methanation projects are the Audi e-gas plant by ETOGAS in 2013 (6000 kW of electrolyser) [15], the Store&GO – Falkenhagen project in 2013 (2000 kW of electrolyser) [16], the JUPITER 1000 project in 2018 (1000 kW of electrolyser) [17], and the MethFuel project in 2020 (1000 kW of electrolyser) [18].

*Table 3. Technical data of reactors for catalytic methanation* [9], [14], [19]–[30].

| | **Adiabatic fixed bed** | **Cooled fixed bed** | **Structured reactor** | **Fluidized bed reactor** | **3-phase reactor** |
|---|---|---|---|---|---|
| Temperature (°C) | 250 - 700 | 250 - 500 | 250 - 300 | 300 - 400 | 300 - 350 |
| Pressure (bar) | 1 - 100 | 1 - 100 | 1 - 20 | 1 - 12 | 20 |
| Load range (%) | 40 - 100 | 30 - 100 | 30 - 100 | 50 - 100 | 20 - 100 |
| GHSV ($h^{-1}$) | < 5000 | < 6000 | < 3000 | <60000 | < 1000 |
| $CH_4$ content (%) | > 90 | > 90 | > 90 | > 90 | > 90 |
| N° of stages | 2 - 7 | 1 - 2 | 1 - 2 | 1 - 2 | 1 - 2 |
| Heat use | High | High | Regular | Regular | Regular |
| Tolerance to impurities | Low | Low | Low | Low | Regular |

Biological methanation utilizes methanogenic archaea to convert $CO_2$ and $H_2$ into methane. These archaea can tolerate impurities such as $H_2S$, NOX, and $NH_3$, allowing for the use of biogas and syngas as $CO_2$ sources, see Table 4. Some of the most relevant biological methanation projects are the P2G-BioCat by Electrochaea in 2014 (1000 kW of electrolyser) [31], Pirmasens-Winzeln Energy Park by Technische Universität Clausthalin 2016 (2500 kW of electrolyser) [32], and HyCAUNAIS by Storengy in 2018 (1000 kW of electrolyser) [33].

When integrating Power to Gas in the industry, the selection of an appropriate methanation process is crucial. Biological methanation is not chosen due to its low GHSV, limiting methane production rates. Among catalytic methanation options, structured, fluidized, and three-phase reactors are excluded due to their lower TRL. However, when comparing adiabatic and cooled fixed bed reactors, both exhibit high GHSV and TRL. The cooled fixed bed reactor stands out as the preferred choice with the ability to operate at lower temperatures and requiring fewer stages [9], [34].

*Table 4. Technical data of reactors for biological methanation* [9], [14], [19]–[30].

| | **Continuous stirred tank reactors** | **Fixed bed reactors** | **Trickled bed reactors** |
|---|---|---|---|
| Temperature (°C) | 20 - 70 | 20 - 65 | 37 - 55 |
| Pressure (bar) | 1 - 3 | 1 | 1 |
| Load range (%) | 10 - 100 | 0 - 100 | 0 - 100 |
| GHSV ($h^{-1}$) | 10 - 300 | 1-30 | < 1 |
| $CH_4$ content (%) | 5 - 85 | 15 - 90 | 94 - 98 |
| N° of stages | 1 | 1 | 1 |
| Heat use | Low | Low | Low |
| Tolerance to impurities | High | High | High |

## 1.3. Objectives, tasks, and structure of the thesis

To support the attainment of the above-mentioned targets, this thesis has a primary goal: to propose and assess innovative Power to Gas configurations within the industrial sector. The aim is to indirectly electrify high-temperature processes and decarbonize the chosen industry through renewable energies and circular economy principles. Table 5 outlines the tasks, papers, conferences, and corresponding thesis sections undertaken to realize this primary goal.

*Table 5. Structure of the thesis: Objectives, tasks, outcomes, and thesis chapter. The numbering of the papers and conferences correspond to the ones indicated in the Section List of publications.*

| **Primary goal:** To propose and assess innovative Power to Gas configurations within the industrial sector | |
|---|---|
| **Objectives / Tasks** | **Chapter / Outcomes** |
| SO1. To select the target industry | 3. Potential of PtG integration in industry |
| *T 1.1: Preliminary study on PtG integration in the glass industry.* | *Paper i* |
| *T 1.2: Preliminary study on PtG integration in the I&S industry* | *Paper ii* |
| SO2. To propose and assess PtG integration concepts in the I&S industry | 4. Power to gas integration in the iron and steel industry |
| *T 2.1: State of the art of the carbon capture technologies in the I&S industry* | *Paper iii* |
| *T 2.2: Modelling of conventional I&S plant* | *Paper iv, Conferences i* |
| *T 2.3: Modelling of amines-methanation concept* | *Paper iv, Conferences i, ii, iii, iv, v* |
| *T 2.4: Modelling of $O_2$ enrichment of air* | *Paper v, Conferences ii, iv, v* |
| *T 2.5: Modelling of top gas recycling concept* | *Paper vi, Conferences iv, v* |
| *T 2.6: Modelling of direct BFG methanation* | *Paper vii, Conferences iv, v, viii* |
| *T 2.7: Modelling of direct hydrogen injection* | *Paper vii, Conferences iv, v, viii* |
| *T 2.8: Techno-economic comparison* | *Paper viii, Conferences vi, vii, ix* |
| SO3. To model PtG technologies from experimental data | 5. Modelling PtG systems from experimental tests |
| *T 3.1: Modelling methanation from experiments at TRL 4.* | *Paper ix* |
| *T 3.2: Modelling of amine scrubbing capture system and experimental validation in the I&S industry at TRL 6.* | |

The thesis has three specific objectives. Firstly, to select the target industry, from the preliminary analysis of different energy-intensive industries. Secondly, to introduce novel PtG concepts within the target industry with the aim of reducing $CO_2$ emissions. In particular, carbon capture, oxygen enrichment, top gas recycling, or BFG methanation, among others, are integrated in the I&S industry. Thirdly, to develop realistic models for the main PtG components, such as methanation or amine scrubbing, adjusted and validated with experimental data.

The novel configurations proposed in this thesis seek to reduce $CO_2$ emissions by a minimum of 30%, aligning with the 2030 objectives, and to lay the groundwork for future PtG systems capable of achieving even greater reductions, potentially reaching net-zero emissions.

In addition to the chapters outlined in Table 5, Chapter 2 details the methodology, while Chapter 6 presents the conclusions.

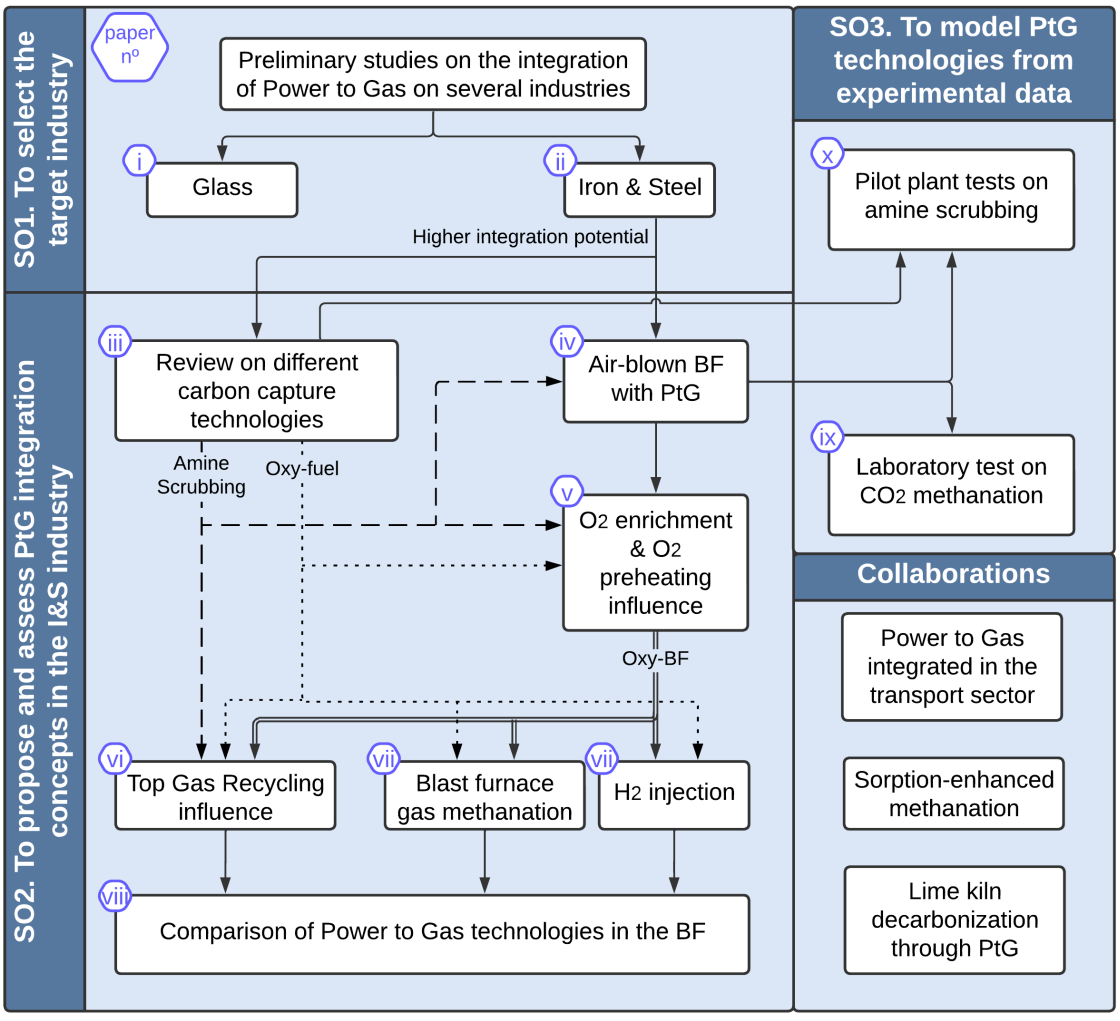


*Figure 4. Thesis structure. Roman numbers indicate the related paper included in this thesis.*

**SO1. To select the target industry.**

Power to Gas technology has been studied in the literature as a technology for energy storage [35]. It has a great potential to solve some energy-related issues such as intermittent power generation, electrical grid stability or large-distance electricity

transport [35]. However, a knowledge gap is found when applying this technology in the 'hard to abate' industrial sector as a way of recycling carbon and reducing emissions.

So, the first objective of this thesis is to highlight the importance of this issue, assess the potential of the Power to Gas technology in different industries, and select the most appropriate industry with the greatest potential for emissions reduction (Chapter 3). To reach this goal, two different industries are addressed: glass (Task 1.1) and steel (Task 1.2) industries. The industry showing higher potential for implementation, I&S industry, is further studied in the following tasks.

**SO2. To propose and assess PtG integration concepts in the I&S industry.**

The objective is to propose and evaluate Power to Gas integration concepts in the I&S industry. Once the I&S industry is chosen for further study with PtG technology, various PtG integrations are compared with a reference BF-BOF plant using techno-economic indicators to assess viability (Chapter 4).

To achieve this, a literature review is conducted on carbon capture systems within the I&S industry (Task 2.1). Then, a reference plant is modelled and validated using bibliographic data (Task 2.2). This reference plant should represent the state-of-the-art blast furnace route and encompass a holistic view of the iron and steel industry, including the blast furnace, sinter, coke oven, and power plant, among others.

Six different configurations for PtG integration are proposed. The first configuration (Task 2.3) employs amine scrubbing for $CO_2$ capture from blast furnace gas, followed by methanation. The synthetic natural gas (SNG) produced is then recycled to the blast furnace, reducing reliance on fossil fuels and emissions. In the second configuration (Task 2.4), oxygen from the electrolyser is used to enrich the air injected into the blast furnace. The third option (Task 2.5) involves using $CO_2$-lean gases (mainly CO and $H_2$) after amine scrubbing as a reducing agent in the oxygen blast furnace, known as top gas recycling (TGR). The fourth option (Task 2.6) modifies the second by directing blast furnace gas to the methanation reaction to convert CO2 and CO into $CH_4$, without amine scrubbing. The last option (Task 2.7) involves directly injecting hydrogen into the oxygen blast furnace, simplifying the configuration, and eliminating the need for carbon capture or a methanation stage.

**SO3. To model PtG technologies from experimental data.**

Currently, power to gas systems are not yet deployed at full scale, and most technologies remain commercially unavailable. Particularly within the iron and steel industry, the adoption of low-carbon technologies is minimal. To contribute to the development and deployment of these technologies in the industrial sector, the third task of this thesis focuses on experimental investigation of power to gas components, specifically methanation (Task 3.1) and $CO_2$ capture (Task 3.2), along with the development and validation of simulation models (Chapter 5).

The $CO_2$ capture component is examined to assess its effectiveness in capturing and purifying $CO_2$ emissions from the iron and steel industry. A detailed model, validated with experimental data, will analyse key performance indicators such as reboiler duty, liquid-to-gas ratio, and $CO_2$ concentration.

The methanation component is studied to evaluate its capacity to convert captured $CO_2$ into methane gas, which can serve as a renewable energy source. Methanation tests will assess the $CO_2$ conversion rate and selectivity of the system.

# 2. Methodology

To effectively accomplish the objective of proposing and assessing the integration of Power to Gas technologies in industry requires to carry out a variety of tasks for which the application different methodologies is needed. The revision of the state of the art, mandatory as starting point to select possible technologies and to propose innovative low carbon solutions, has followed the systematic methodology presented in Section 2.1. The modelling of the different industrial plants has been performed with help of two simulation softwares, EES and Aspen Plus®. The main assumptions and hypothesis, the general procedure and the description of the models are summarized in Section 2.2. The proposed integrations in industry are assessed from the technical and economic point of view. To this end, meaningful parameters are defined in Section 2.3 for insight and comparison purposes. The procedure for adjustment and validation of simulation models of carbon capture and methanation from experimental data is accounted for in Section 2.4. Finally, the artwork is presented in Section 2.5.

## 2.1. Methodology of systematic reviews

A comprehensive understanding of the current state of the art is indispensable in academic pursuits, serving as the foundational background for informed research. Equally crucial is a meticulous examination of the methodology employed in reviewing this state of the art.

The present thesis employed a systematic review approach to identify pertinent literature on the respective topics. Utilizing the PRISMA 2020 systematic approach [36], the Web of Science search engine was selected for its advanced search capabilities and comprehensive database coverage. The search focused on scientific journals and conferences within the chosen search engine. Employing a set of keywords relevant to the topic field, the search generated a specific number of entries. Subsequently, a screening process based on article abstracts was conducted, leading to the selection of final articles for inclusion in the review. The chosen articles were then categorized and addressed in the review paper, see Figure 5.

The PRISMA 2020 guidelines offer a structured framework for conducting systematic reviews and meta-analyses, ensuring transparency and rigor in the research process. The guidelines encompass various aspects of the review process, from the initial search strategy to the interpretation and discussion of results.

It starts with a clear title and abstract summarizing the rationale, objectives, methods, results, and conclusions. The introduction provides context for the research topic and states the review's objectives or questions. Detailed methods include eligibility criteria, information sources, search strategy, selection process, data collection, and risk of bias assessment. The results section describes the study selection process, characteristics of included studies, risk of bias assessment, and results of individual studies and syntheses. Discussion section interpret the findings in the context of existing evidence, acknowledge limitations, and discuss implications for practice, policy, and

future research. Additionally, information on registration, support, competing interests, and data/materials availability should be included.

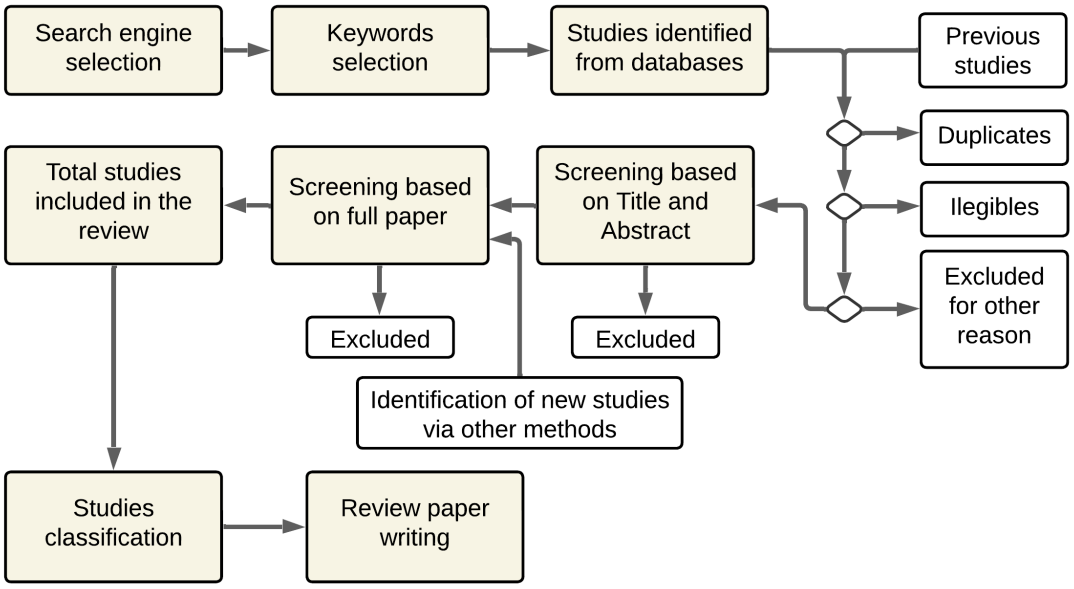


*Figure 5. Flow diagram for systematic reviews.*

## 2.2. Modelling and simulation

In order to accomplish the technical and economic assessment of the proposed low carbon technologies, the design and modelling were performed with aid of two specialized software tools Engineering Equation Solver (EES) and Aspen Plus®.

The general assumptions include steady-state condition and chemical equilibrium, ideal gases for gaseous species, and thermal losses disregarded. The modelling methodology is based on overall mass and energy balances in steady state, applied to each equipment of the plant layouts. When necessary, data from literature are used.

The first approach to the problem was performed by using the EES software for the simplicity of programming and the previous experience. It served to carry out the preliminary viability study of PtG integration in the iron and steel industry. EES is a commercial software package designed for solving systems of coupled non-linear equations. With a repertoire of specialized functions and equations, it proves particularly valuable for addressing thermodynamics and heat transfer problems. However, it faces limitations when analysing complex process flow diagrams due to its design, hindering its effectiveness for a comprehensive modelling. Additionally, EES lacks accurate calculation capabilities for chemical reactions and equilibrium, limiting its suitability for tasks requiring detailed modelling of chemical processes.

The Aspen Plus® excels in simulating large processes with high accuracy. The model library encompasses various components such as mixers, phase separators, heat exchangers, distillation columns, reactor pressure changers manipulators, etc. Through the interconnection of these unit operations, users can formulate a process flow diagram (PFD) for an entire plant. It offers comprehensive process modelling

capabilities, including reaction kinetics, phase equilibrium, and heat/mass transfer. It provides extensive thermodynamic libraries and a user-friendly interface, facilitating easy model building and modification. Aspen Plus also features powerful optimization tools. For these reasons, the remaining studies were based in Aspen Plus models. Table 6 details the property method employed in each Aspen-simulated process, accompanied by a brief description.

*Table 6. Aspen property methods for each process of sections 3 and 4. The selection of each property method was done according to the Methods Assistant of Aspen Plus* [37].

| Process | Property method | Description |
|---|---|---|
| Glassmaking plant<br>I&S plant<br>ASU | PENG-ROB | The PENG-ROB property method uses the Standard Peng-Robinson cubic equation of state for all thermodynamic properties except liquid molar volume. API method for liquid molar volume of pseudo components and the Rackett model for real components. |
| Rankine Power Plant | PR-BM | Recommended option for Power industries. The PR-BM property method uses the Peng Robinson cubic equation of state with the Boston-Mathias alpha function for all thermodynamic properties. |
| Electrolyser | ELECNRTL | This property method is appropriate for aqueous and mixed solvent applications. The ELECNRTL property method is the most versatile electrolyte property method. It can handle very low and very high concentrations. |
| Calcium Looping | SOLIDS | The SOLIDS property method is designed for many kinds of solids processing. The properties of solids and fluid phases cannot be calculated with the same type of models. Therefore the components are distributed over the substreams of types MIXED (liquid and gas), CISOLID (conventional solids) and NCSOLID (non-conventional solids) and their properties are calculated with appropriate models |
| Methanation | RKSMHV2 | The RKSMHV2 property method is based on the Redlich-Kwong-Soave MHV2 equation-of-state model for gases, which is an extension of the Redlich-Kwong-Soave equation of state. |
| Amine scrubbing | ENRTL-RK | The ENRTL-RK property method is based on the Unsymmetric Electrolyte NRTL property model. It uses: The Redlich-Kwong equation of state for vapor phase properties. The unsymmetric reference state (infinite dilution in aqueous solution) for ionic species. Henry's law for solubility of supercritical gases. Unsymmetric Electrolyte NRTL method of handling zwitterions |

In the Aspen Plus simulations, a convergence tolerance of 0.0001 is applied to key parameters such as concentrations, temperatures, and flow rates to ensure precise results. The simulation allows up to 50 errors before interruption, with corrective

actions taken by the user based on error information to aid convergence. A maximum of 1,000 flowsheet evaluations is set to achieve steady-state conditions. For looping configurations, the initial calculation uses default values, while subsequent iterations leverage results from previous calculations to improve convergence efficiency. These measures ensure that the simulations reach a consistent and reliable steady state before finalizing the results.

In addition to EES and Aspen, Excel is used for organizing and analysing the data generated during the Power to Gas integration analysis. Excel provides a versatile platform for data management, manipulation, and statistical analysis, facilitating a comprehensive evaluation of the results obtained from the simulations. It is primarily used for data treatment and analysis of the EES and Aspen results, as well as for calculating key performance indicators used in each study.

The following subsections detail the hypothesis and initial data used in the different power to gas models: carbon capture, methanation and electrolyser.

**PEM electrolyser**

The PEM electrolyser operates at 1.5 bar and 80 °C, producing hydrogen and oxygen with an energy consumption of 3.8 $kWh_e/Nm^3$ [38]. The water used enters the system at ambient conditions of 25 °C and 1 atm.

In EES, the electrolyser is assumed to generate separate streams of pure $O_2$ and $H_2$, while the methanation process produces pure methane. In Aspen, to be more realistic, the outlet hydrogen stream drags 2 mol of $H_2O$ per mole of $H_2$ (which are condensed and recirculated), and 0.1% of $O_2$ (which is purified). The outlet oxygen flow has only traces of hydrogen (0.01%) [38], [39].

**Amine scrubbing carbon capture**

The amine scrubbing models used in Section 4 are developed from a predefined Example File of Aspen (reactor and process design in [40]), see Figure 6. The model fixes a 90% $CO_2$ capture from the incoming stream using a 50wt% methyldiethanolamine (MDEA) and water solvent. Prior to entering the capture unit, the water content of the BFG is condensed, and then the gas is diverted to the absorption column.

This absorption column, consisting of 15 stages, has gas entry at the bottom (stage 15) and lean solvent entry at the top (stage 1). Clean gas exits from the top at atmospheric pressure and 42 °C. Rich solvent, loaded with $CO_2$, exits from the bottom at 43 °C and 1.1 bar (loading of 0.2 $kmol_{CO2}/kmol_{MDEA}$). The rich solvent is then heated to 100 °C in a heat recovery exchanger that cools the lean solvent from the stripper (from 112 °C to 56 °C) before re-entering the absorber [40].

The stripper column, comprising 19 stages with condenser and reboiler stages, further processes the rich solvent. The condenser's reflux ratio is 0.01, and the reboiler's boil-up ratio is 0.1 [40]. In the stripper, the rich solvent enters at the second stage and descends as $CO_2$ is released. The lean solvent exits from the last stage, and $CO_2$ exits from the first stage. A condenser then cools the $CO_2$-rich stream from 85 °C to 35 °C, achieving 95vol% $CO_2$ purity. The condensed solvent is recirculated to the absorber along with the lean solvent [40].

Ultimately, a makeup stream, mixed with the lean solvent prior to entering the absorber, is introduced to compensate for water and MDEA losses in both the clean gas and $CO_2$ streams.

Additionally, a new monoethanolamine (MEA) model is developed based on experimental data. The experimental test methodology is detailed in Section 2.4.2, and the developed model is presented in Section 5.2

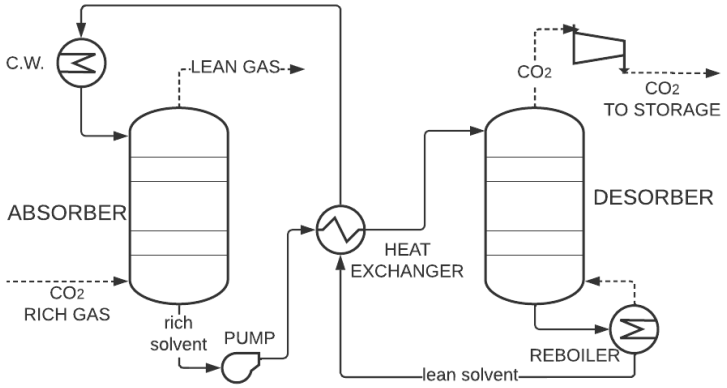


*Figure 6. $CO_2$ capture with chemical absorption.*

**Calcium looping carbon capture**

The Calcium Looping technology is applied in the glass industry study (chapter 3) to leverage synergies between the two processes, as they both utilize the same raw material, limestone. The carbon capture model follows the scheme shown in Figure 7, where the main components are the calciner and the carbonator. In Aspen Plus, these components are modelled as stoichiometric reactors with 90% (to $CO_2$) and 100% conversion, respectively [41], calculating the chemical composition of the $CO_2$ gas and the clean gas.

Table 7 provides the operational parameters, regarding mass ratios and temperatures, used for the modelling.

*Table 7. Input data of CaL system* [41], [42].

| **Variable** | **Units** | |
|---|---|---|
| *Ratios* | | |
| Inlet Limestone / Inlet $CO_2$ | $mol_{CaCO3}$ / $mol_{CO2}$ | 0.05 |
| Recirculated CaO / Introduced $CO_2$ | $mol_{CaO}$ / $mol_{CO2}$ | 10 |
| Purged CaO [18] | % | 4 |
| *Streams* | | |
| Calciner Exit (a) | °C | 950 |
| $CO_2$ (b) | °C | 50 |
| Carbonator Exit (c) | °C | 650 |
| Clean Gas (d) | °C | 90 |
| Carbonator Entry (e) | °C | 700 |

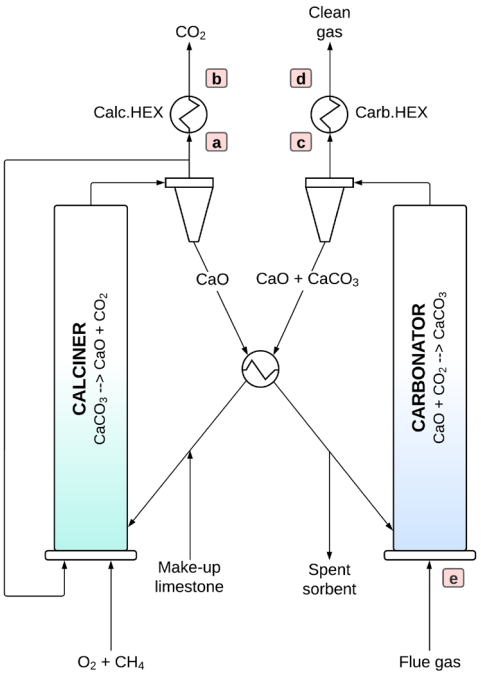


*Figure 7. Process flow diagram of the Calcium Looping system*

In the carbonator, the exothermic carbonation reaction takes place, where the $CO_2$ in the flue gas reacts with CaO to form $CaCO_3$. The resulting limestone ($CaCO_3$) is then transported to the calciner, where it undergoes an endothermic decomposition process, regenerating the CaO and releasing $CO_2$ ($\Delta H$ = 177.9 kJ/mol). The thermal energy required for this process is provided by the oxy-combustion of the SNG produced in the PtG system. To maintain proper conditions, a $CO_2$ recirculation loop is implemented at the exit of the calciner to prevent hot spots. The recirculated $CO_2$ is adjusted to achieve 21% $O_2$ at the calciner's entrance, simulating air conditions. Stoichiometric oxygen quantity is introduced, and complete combustion is assumed.

A sorbent purge is included before the carbonator's entrance. Additionally, recuperative heat exchangers are incorporated at the exit of each reactor to improve the process's thermal efficiency. These heat exchangers offer the opportunity to recover residual heat, which can be used for steam production in a Rankine cycle. Furthermore, a solid-particle heat exchanger is employed to preheat the limestone while cooling the CaO, optimizing the overall heat transfer.

**Methanation plant**

Two different models of methanation plants have been developed. First, the EES approach (Section 3.2) uses a black box with fixed values (300 °C, 30 bar, and 100% CH4). Second, a more detailed approach is conducted in Aspen Plus® (Sections 3.1 and 4.2).

Due to the high TRL, high carbon conversion rate and commercial maturity, the methanation system developed in Aspen, as shown in Figure 8, consists of two isothermal fixed-bed reactors [43], [44], following the Sabatier reaction described in Eq. (1) [45]. The first methanation reactor operates at a temperature of 350 °C, while the second reactor operates at 300 °C, both at a pressure of 5 bar and with a Gas Hourly

Space Velocity (GHSV, Eq. (2)) of 5000 $h^{-1}$ [46]. The $H_2$ produced in the electrolyser is compressed and combined with $CO_2$ from the carbon capture system in a stoichiometric ratio of 4:1. The gas mixture is preheated to 250 °C before entering the first methanation stage, which is modelled as a Gibbs reactor to simulate equilibrium conditions. The outlet flow is then cooled to 100 °C in a flash separator to condense the water, and subsequently reheated to 250 °C before entering the second reactor. The resulting stream of Synthetic Natural Gas is separated from water at 25 °C in a second flash separator, reaching a purity of 94.77% $CH_4$ (3.96 % $H_2$, 0.77% $CO_2$ and 0.50% $H_2O$).

$$\mathrm{CO_2 + 4H_2 \Leftrightarrow CH_4 + 2H_2O} \qquad \Delta H_{298} = -164.9\ \mathrm{kJ/mol} \tag{1}$$

$$\mathrm{GHSV} = \frac{volume\ flow\ of\ reactants}{catalyst\ mass\ /\ bulk\ density\ of\ the\ catalyst} \quad [h^{-1}] \tag{2}$$

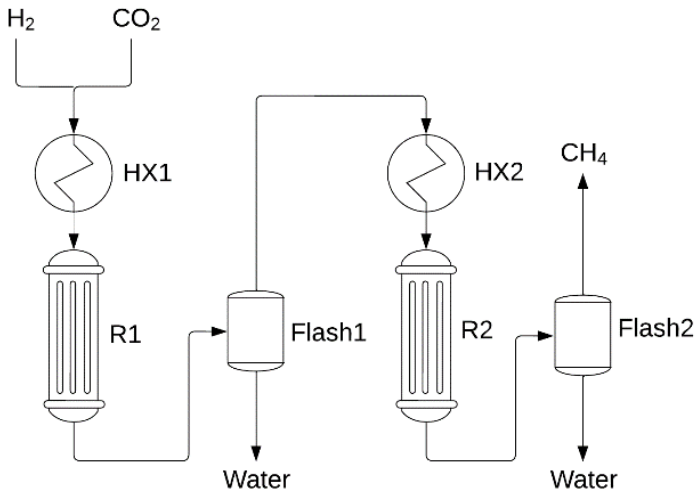


*Figure 8. Methanation system scheme*

Additionally, a third model in Aspen Plus® varies the number of reactors (Section 5.1) to assess the impact of this variation.

## 2.3. Technical indicators and economic analysis

Certain technical indicators are defined for comparison purposes. The most important are the coal-equivalent replacement ratio (coal-e RR) and the energy penalty. The former was defined as the sum of the pulverized coal and coking coal replaced by the reducing agent (SNG, $H_2$ or other) (Eq. (45)). The latter was defined as the net energy consumed in the industry per kg of $CO_2$ avoided with the PtG-steelmaking integration (Eq. (4)). Units and description of equation variables are in Table 8.

$$Coal - e\ RR\ = \frac{\Delta \dot{m}_{PCI} + \Delta \dot{m}_{CokingCoal}}{\Delta \dot{m}_{SNG} + \Delta \dot{m}_{TGR}}\ \left[kg_{Coal}/kg_{ReducingGas}\right] \tag{3}$$

$$E_{penalty} = \frac{\Delta E_{cons} - \Delta E_{coal} \cdot \eta_{elec} - \Delta E_{gases} \cdot \eta_{elec}}{\Delta \dot{m}_{CO2}}\ [MJ/kg_{CO_2}] \tag{4}$$

*Table 8. Description of variables in equations (3)-(6).*

| Variable | Units | Description |
|---|---|---|
| $\Delta\dot{m}_{PCI}$ | $kg_{PCI}/t_{HM}$ | Savings in PCI consumption |
| $\Delta\dot{m}_{CokingCoal}$ | $kg_{CokingCoal}/t_{HM}$ | Savings in coking coal consumption |
| $\Delta\dot{m}_{SNG}$ | $kg_{SNG}/t_{HM}$ | Increase in SNG injection |
| $\Delta\dot{m}_{TGR}$ | $kg_{TGR}/t_{HM}$ | Increase in TGR injection |
| $\Delta E_{cons}$ | $MJ/t_{HM}$ | Increase in electricity consumption in the industry |
| $\Delta E_{coal}$ | $MJ/t_{HM}$ | Savings in coal energy |
| $\Delta E_{gases}$ | $MJ/t_{HM}$ | Increase in excess sold gases |
| $\eta_{elec}$ | - | Energy conversion factor coal to electricity (0.33) |
| CAPEX | M€ | Capital Expenditure |
| OPEX | M€/year | Operational Expenditure |
| Incomes | M€/year | Operational Incomes |
| Loan amortizat. | Years | Process of paying off a loan over time |
| CO2 avoided | $t_{CO_2}/h$ | CO2 avoided per hour |
| Operating hours | $h/year$ | Operating hours per year |

In order to assess the economic viability of the proposed technologies, a comprehensive economic analysis is conducted with literature data and performed in Microsoft Excel spreadsheets. The developed cost model provides estimates for CAPEX (M€), OPEX (M€/year), Incomes (M€/year), and specific costs for the implementation of the low carbon technologies (€/$t_{CO2}$ and €/$t_{HRC}$ or €/$t_{glass}$), taking as reference a configuration of the conventional industry. Detailed components can be found in

Table 9, while specific costs are calculated using Eq. (5) and Eq. (6).

$$\mathrm{CO_2\ Avoidance\ Cost} = \frac{\left(\frac{\mathrm{Capex}}{\mathrm{Loan\ amortization}} + \mathrm{Opex} - \mathrm{Incomes}\right)}{\mathrm{CO_2\ avoided} \cdot \mathrm{Operating\ hours}} \quad \left[\frac{€}{t_{CO_2}}\right] \tag{5}$$

$$\mathrm{Specific\ Implementation\ Cost} = \frac{\left(\frac{\mathrm{Capex}}{\mathrm{Loan\ amortization}} + \mathrm{Opex} - \mathrm{Incomes}\right)}{\mathrm{Steel\ Production} \cdot \mathrm{Operating\ hours}} \quad \left[\frac{€}{t_{HRC}}\right] \tag{6}$$

The economic analysis focuses on the investment required for PtG-industry integration, which includes the implementation of the PEM, methanation stage, and carbon capture. A discount factor of 4% with a loan amortization period of 20 years is assumed. The carbon capture and PtG systems are assumed to operate for 8000 hours per year based on previous studies [47]. A carbon tax value of 84.28 €/$t_{CO2}$ [48] and a renewable electricity consumption cost of 77 €/MWh are also considered.

The initial capital expenditure (CAPEX) for the PtG integration encompasses the carbon capture, electrolysis, and methanation plant, the heat exchanger network, the blast furnace retrofitting, as well as other direct and indirect costs. The annual operational expenditure (OPEX) includes expenses related to catalyst renovation, water consumption by the electrolyser, amine or limestone renovation, purchased electricity, and operation and maintenance (O&M) costs. The annual incomes are derived from savings on $CO_2$ taxes and coal, as well as revenue generated from the sale of unused oxygen and steel gases (BFG, BOFG, and COG) in the case of steelmaking.

*Table 9. Data for the economic analysis of the PtG integration*

| | Cost equation (M€) or (M€/y) | Parameters α, β, γ | Eq. | Ref. |
|---|---|---|---|---|
| **CAPEX** | | | | |
| Amine Plant | | | | |
| Overall Cost | $26.094\cdot(\alpha/408)^{0.65}$ | α= $CO_2$ captured [t/h] | (7) | [49] |
| Calcium Looping | | | | |
| Calciner | $0.193\cdot\alpha^{0.65}$ | Thermal power [$MW_t$] | (8) | [50] |
| Carbonator | $0.217\cdot\alpha + 3.83$ | Low heating value [$MW_t$] | (9) | [50] |
| Electrolysis | | | | |
| Overall Cost | $400\cdot10^{-6}\cdot\alpha$ | α= Power [kW] | (10) | [51] |
| Methanation | | | | |
| $H_2$ compressor | $0.267\cdot(\alpha/445)^{0.67}$ | α= Power [kW] | (11) | [52] |
| $CO_2$ compressor | $0.267\cdot(\alpha/445)^{0.67}$ | α= Power [kW] | (12) | [52] |
| Reactors | $300\cdot10^{-6}\cdot\alpha$ | α= SNG power [$kW_{SNG}$] | (13) | [53] |
| Catalyst | $0.1875\cdot\alpha$ | α= Volume of catalyst [$m^3$] | (14) | [52] |
| Heat exchangers | $(9016.3+721.3\cdot(\alpha^{0.8}))\cdot10^{-6}$ | α= Area [$m^2$] | (15) | [54] |
| BF retrofitting | $0.5\cdot\alpha$ | α= BF construction cost | (16) | [55] |
| Other direct costs | | | | |
| Installation | $10\%\cdot\alpha$ | α= Total equipment costs [M€] | (17) | [49] |
| Instr. & control | $4\%\cdot\alpha$ | α= Total equipment costs [M€] | (18) | [49] |
| Piping | $16\%\cdot\alpha$ | α= Total equipment costs [M€] | (19) | [49] |
| Electrical | $5\%\cdot\alpha$ | α= Total equipment costs [M€] | (20) | [49] |
| Building | $5\%\cdot\alpha$ | α= Total equipment costs [M€] | (21) | [49] |
| Land | $1\%\cdot\alpha$ | α= Total equipment costs [M€] | (22) | [49] |
| Indirect costs | | | | |
| Engineering | $7\%\cdot\alpha$ | α= Total direct costs [M€] | (23) | [49] |
| Legal expenses | $2\%\cdot\alpha$ | α= Total CAPEX [M€] | (24) | [49] |
| Construction expenses | $4\%\cdot\alpha$ | α= Total CAPEX [M€] | (25) | [49] |
| Contingency | $7\%\cdot\alpha$ | α= Total CAPEX [M€] | (26) | [49] |
| **OPEX** | | | | |
| Amine renovation | $3204\cdot10^{-6}\cdot\alpha$ | α= MDEA renovation [$t_{CO2}$/y] | (27) | [56] |
| Catalyst renovation | $15\%\cdot\alpha$ | α= Initial catalyst cost [M€] | (28) | [47] |
| Limestone | $10^{-5}\cdot\alpha$ | α= Limestone consumed [t/y] | (29) | [57] |
| Electricity | $\alpha\cdot\beta\cdot\gamma\cdot10^{-6}$ | α= Electricity purchased [$MWh/t_{HM}\cdot h^{-1}$], β= Operating hours [h/y], γ= Electricity cost [€/MWh] | (30) | - |
| Water | $1.47\cdot10^{-6}\cdot\alpha$ | α= Water consumption [$m^3$/y] | (31) | [58] |
| O&M | $3\%\cdot\alpha$ | α= Total CAPEX [M€] | (32) | [49] |
| **INCOMES** | | | (33) | |
| Coal | $130.43\cdot10^{-6}\cdot\alpha$ | α= Coal saved [$t_{Coal}$/y] | (34) | [59] |
| Natural Gas | $7.87\cdot10^{-4}\cdot\alpha$ | α= NG saved [$t_{NG}$/y] | (35) | [60] |
| Oxygen | $80\cdot10^{-6}\cdot\alpha$ | α= $O_2$ generated [$t_{O2}$/y] | (36) | [61] |
| $CO_2$ taxes | $84.28\cdot10^{-6}\cdot\alpha$ | α= $CO_2$ saved [$t_{CO2}$/y] | (37) | [48] |
| Steel gases | $(15+\alpha\cdot\beta/13)\cdot10^{-6}\cdot\gamma$ | α= Natural gas price [€/MWh] β= Steel gases LHV [kWh/kg] γ= Steel gases generated [MWh/y] | (38) | - |

## 2.4. Experimental procedure and facilities

To tackle the objective SO3, different PtG subsystems have been further studied, in order to obtain reliable models validated with experimental data. The Power to Gas systems consider key components, including carbon capture, a PEM electrolyser, and a methanation plant. Due to the commercial maturity of PEM electrolysers, our study focused on a TRL 4 methanation plant to investigate catalyst kinetics and process design (Task 3.1); and on a TRL 6 carbon capture pilot plant to explore the potential of carbon capture technology from real flue gases in the I&S industry (Task 3.2).

### 2.4.1. Methanation tests (TRL 4)

The experimental study performed in a 1 kW fixed bed reactor have three main goals: firstly, to test and compare the performance of pellet catalysts of nickel and ruthenium at pilot plant scale; secondly, to develop and validate kinetic models from the experimental data; and thirdly, to identify a configuration that minimizes catalyst usage while maintaining high methane content in the outlet gas. To this end, Aspen Plus is employed to model and optimize a methanation plant with multiple reactors in series. The model operates with the data obtained from the experimental tests, under the property method RKSMHV2.

The methanation plant is located in UNIZAR, Spain, and depicted in Figure 9. The facility consists of a $CO_2$ cylinder (≥99.5% purity, Air products x50S) linked to a mass flow controller (EL-Flow Bronkhorst® model Fe201CV-RAD-22-K, range 0.16-0.80 kg/h), a $H_2$ cylinder (≥99.5% purity, Air products x50S) connected to a mass flow controller (EL-Flow Bronkhorst® model F-201AV-RAD-22-V, range 0.003-0.15 kg/h), a ceramic heater (custom-made by Tellsa SL) for pre-heating the reagent mixture in stainless steel 310 and stainless steel 304 flanges (≤400 °C), a fixed bed reactor (tube design), three electrical resistances wound around the reactor (3 x 500 W, annealed copper, model Electricfor FFC4 T-175-E), a custom-made water condenser (Tellsa SL), and a burner (custom-made by Tellsa SL) for co-firing synthetic methane with butane [62]. Additionally, for cleaning and safety purposes, the facility included an entry for $N_2$ ($N_2$ bottle, ≥99.998% purity, Air products x50S).

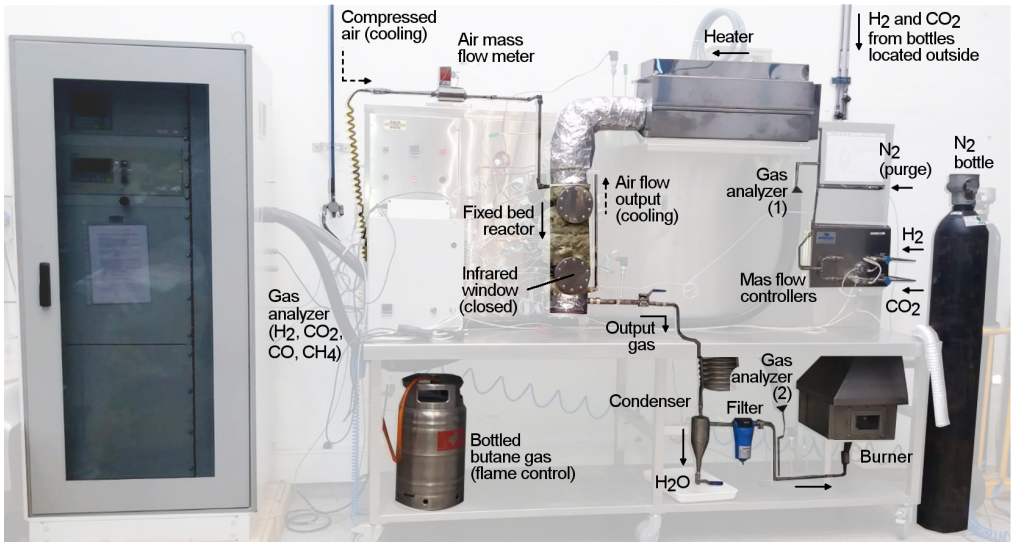


*Figure 9. Methanation test facility.*

The gas composition was assessed both before and after the methanation step using a gas analyser, which included a thermal conductivity detector (Calomat 6, Siemens) for quantifying $H_2$ and an infrared detector (Ultramat 23, Siemens) for quantifying $CO_2$, $CH_4$, and CO. Pressure and temperature at various locations in the setup were measured using standard instrumentation and monitored through a Labview system.

The reactive channel utilized a tubular fixed bed measuring 30 mm in diameter and 490 mm in length. Catalyst spheres, when prepared, were combined and loaded with alumina spheres (3.56 mm in diameter, true density of 3.81 g/cm3, Goodfellow AL60-SP-000122) to ensure a uniform temperature distribution along the axis. To position the catalytic bed correctly, two layers of inert alumina spheres, each 35 mm thick, were employed, and a 60 mm layer of quartz wool was placed at the bottom.

The thermal design of the reactor was structured as a co-current "double pipe" system (see Figure 10). In this setup, air circulated through the outer tube (100 mm outer diameter) to cool it, while the reactants flowed through the inner tube (30 mm inner diameter and 620 mm length). Nine thermocouples were evenly positioned along the reactor's length, each separated by 50 mm, and they were in contact with the inner tube's wall.

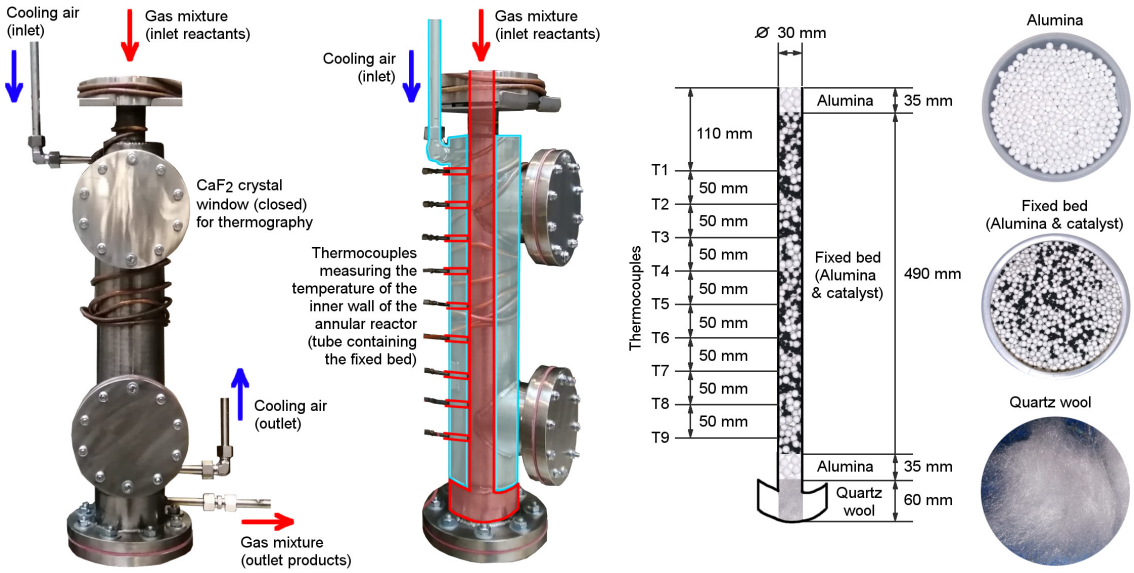


*Figure 10. Methanation reactor (without external insulation).*

The activation of the catalyst was carried out by passing a pure hydrogen flowrate of 0.015 kg/h during 3 h at 200-400 °C. After activation, the mass flows of $H_2$ and $CO_2$ corresponding to the operating point under study were set in the mass flow controllers. When the conversion and temperature of the reactor was stable, the measurement in the gas analyser was recorded. The experimental plan was designed to evaluate the performance of both catalysts at different steady conditions of (GHSV = 8000-16000 $h^{-1}$), molar ratio (3.5-5.5) and activation operating temperature (T = 250-450 °C), gas hourly space velocity temperature (T = 200-400 °C). The operating pressure

was 1 bar. Experimental tests, results, and the Aspen Plus model are detailed in Section 5.1 and paper ix.

### 2.4.2. Carbon capture tests (TRL 6)

The pilot plant, jointly operated since Q4 2022 by voestalpine and K1-MET in Linz, Austria, features a carbon capture system comprising two reactors (absorber and stripper) and auxiliary equipment like heat exchangers, blowers, and pumps. This facility captures $CO_2$ from flue gases originating from a power plant within the voestalpine iron and steel industry, which is fuelled by a combination of steel gases and natural gas. It is worth noting that this pilot plant design draws inspiration from its predecessor [63], which was previously utilized in a coal power plant setting. The pilot plant works through a scada system that controls the pumps, blower and the desorption´s unit resistance. Modelling and results are shown in Section 5.2.

In reference to Figure 11, there are several components situated before the absorber. These include a quench, a flue gas blower, a cooler, and a pre-scrubber. Condensate generated within the heat exchanger is effectively separated in a phase separator located adjacent to the flue gas cooler. The pre-scrubber operates using an aqueous NaOH solution in a closed circuit, reducing the $SO_x$ content in the flue gas to levels below 10 ppm.

A water washing section, equipped with a demister unit, is situated at the top of the absorption unit. This section prevents solvent loss by cooling the treated gas.

The $CO_2$-enriched solvent is gathered in the absorber sump and then pumped to the desorber column. In the main heat exchanger, the temperature of the $CO_2$-enriched solvent is raised.

The regeneration of the solvent takes place in the desorption unit, requiring heat to be supplied to the desorption unit sump via an electric heating rod. The resulting $CO_2$:$H_2O$ gas mixture moves through the desorption unit in a counter-current manner relative to the enriched solvent, from bottom to top. Structured packings inside the desorber column promote intense interaction between the gas and liquid phases. Similar to the absorption unit, the top of the desorber column features a washing section and a demister.

After passing through the demister, the $CO_2$:$H_2O$ gas mixture is cooled again in the overhead condenser, producing condensate collected in the phase separator. A pressure retention valve is used to maintain a constant pressure within the desorption unit.

One typical performance parameter in this kind of installation is the liquid-to-gas (L/G) ratio. The L/G ratio of an amine carbon capture plant represents the ratio between the liquid (comprising MEA and water, in l/h) and the volume of gas treated (flue gas flow rate, in Nm3/h or m3/h), is expressed in units of l/$Nm^3$ or l/$m^3$, where $Nm^3$ represents cubic meters at normal pressure, and $m^3$ refers to cubic meters at operating pressure. Typical values range from 2 to 7 l/$Nm^3$.

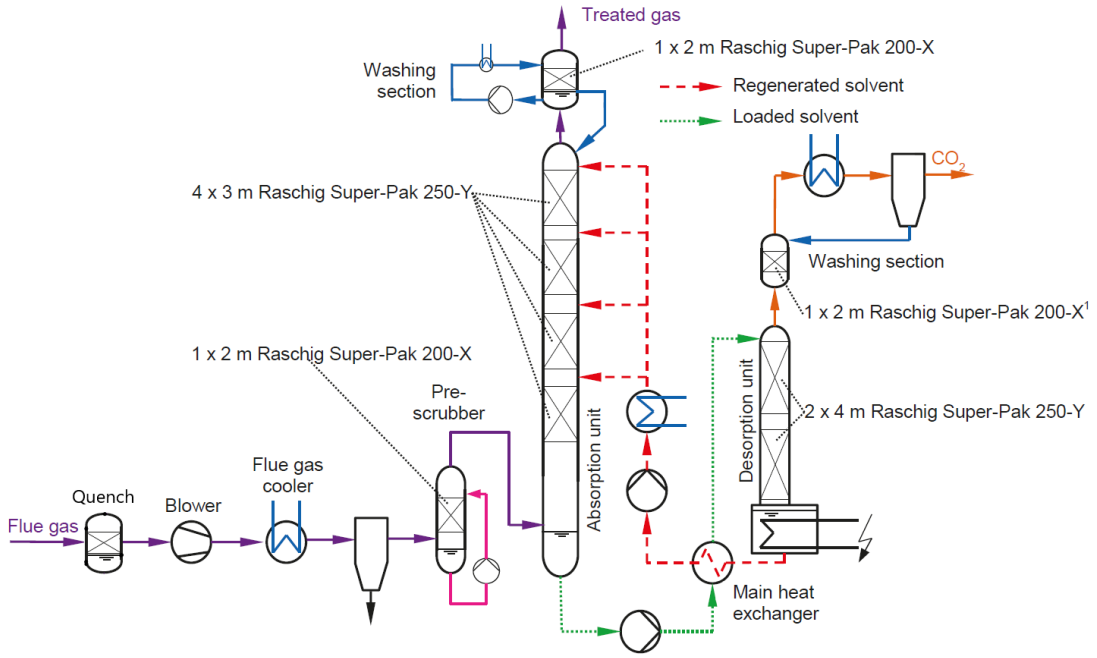


*Figure 11. Flow scheme of the carbon capture pilot plant (adapted from* [63]*).*

## 2.5. Data processing and artwork

A systematic methodology was consistently applied to graphics and tables throughout the document to improve comparison and understanding. This ensured uniformity and clarity in data presentation. By maintaining consistency in formatting and layout across graphics, tables, and artwork, readability was enhanced, allowing for easier comparisons across sections. This systematic approach was diligently followed to ensure a uniform style throughout both the thesis and associated publications. Adhering to a standardized framework for graphical visualization enhanced coherence and clarity, improving the comprehensibility of the conveyed information.

The software tools utilized for generating graphs, process flow diagrams, and Sankey diagrams are Origin Pro, Lucidchart and Illustrator, and Sankey Flow Show, respectively.

Origin Pro is utilized as the primary software for creating graphs in this study. This is a comprehensive software package selected for its diverse graphing capabilities, customizable features, and statistical analysis functions.

Process flow diagrams developed for illustrating the sequential steps and interactions within a system is performed through Lucidchart and Illustrator. Lucidchart is a versatile online tool that enables the creation of professional-looking diagrams with a user-friendly interface and a wide range of predefined shapes and symbols. Illustrator, on the other hand, provides advanced design capabilities, allowing for further customization and refinement of the process flow diagrams.

Sankey diagrams is used for visualizing complex flow and energy distribution within a system. Sankey Flow Show was employed to generate Sankey diagrams in this study. It offers intuitive drag-and-drop functionality and various layout options to effectively represent the flow of material, energy, or any other relevant variables.

# 3. Potential of PtG integration in industry

In order to propose PtG concepts that actually have a relevant impact on the reduction of carbon emissions of industrial sector, an initial assessment across different case studies is here performed to select the most suitable for the detailed analysis. On the one hand, various strategies are investigated in section 3.1 for the glass industry, preselected for its significance in Aragón (Spain). On the other hand, two configurations of PtG integration are presented in section 3.2 for the iron and steel industry, chosen due to its high $CO_2$ emissions and urgent need for decarbonization. Section 3.3 provides a comprehensive discussion of the outcomes obtained for the different industries.

## 3.1. Power to gas in the glass industry

### 3.1.1. General overview and state of the art

The glass industry, heavily reliant on fossil fuels like natural gas (4-17 GJ/$t_{glass}$) [64]), emits substantial $CO_2$, with container and flat glass subsectors contributing significantly to global and European production emissions. Melting, forming, and other processes comprise glassmaking, with melting being the most energy- and carbon-intensive. Container glass melting consumes 75-85% of total energy and accounts for 75% of $CO_2$ emissions [65]. Energy-efficient measures like cullet recycling may reduce emissions and enhance energy efficiency by up to 3% per 10% cullet increment [64]. External cullet usage varies by industry, with container and glass wool sectors utilizing up to 95% cullet [66]. Specific energy consumption and emissions depend on factors such as glass type, melting technology, and cullet fraction, as well as primary fuels. Chinese glass plants, relying heavily on coal, exhibit higher combustion-related emissions compared to those in the US and Europe, which mainly use natural gas. European plants achieve higher recycling rates and lower emissions compared to their Chinese counterparts [67], [68].

Possible decarbonization options include waste heat recovery, process intensification, and fuel substitution [64]. Waste heat recovery encompasses preheating combustion gases, cullet, or batch, thermo-chemical heat recovery, and heat-to-power conversion using technologies like Organic Rankine Cycles, steam turbines, or thermoelectric generators. Process intensification aims to enhance energy efficiency through improved burner or furnace design and advanced process control, commonly implemented in European and US industries, limiting their $CO_2$ reduction potential [66]. Fuel substitution involves using gaseous energy carriers like biogas, hydrogen, or synthetic methane, or employing electric furnaces. All-electric melting technology, while established at small scales (up to 250 t/h)., faces challenges in design, control, flexibility, and lifespan, particularly unsuitable for high-quality glass production requiring stable batch layers and limited cullet usage [66]. Direct hydrogen combustion presents different behavior, necessitating further research into its effects on glass quality and

process adaptation. Few PtG-related modeling papers exist in literature, notably exploring power-to-hydrogen processes for oxyfuel glass melting [69] and $CO_2$ separation for low-emission glass melting [70].

The present work represents the first comprehensive study about the integration of Power to Gas technology in a glassmaking plant: $CO_2$ captured from the glass melting furnace reacts with green hydrogen to produce synthetic methane, which in turn is used in the melting process. The primary objectives of this research are to propose, model in Aspen Plus and assess from technical, economic, and environmental point of view novel low-carbon concepts based in Power to Gas technology to significantly reduce the net emissions. Regarding the analysis of the economic viability, two scenarios are considered: purchasing renewable electricity and using a photovoltaic power plant for self-consumption.

### 3.1.2. Reference case

The base case study (Case 0) replicates the typical scheme of a conventional glass plant, incorporating the essential processes of real container glassmaking, such as batch preparation, melting and fining, forming, annealing, surface treatment, and inspection. Every subsystem has been modelled as a hierarchy in Aspen Plus, following the methodology explained in Section 2.2 and taken the design data from the literature [64], [65]. Figure 12 visually represents the direct $CO_2$ emissions stemming from NG combustion, with the assumption that the electricity consumed is generated from renewable resources.

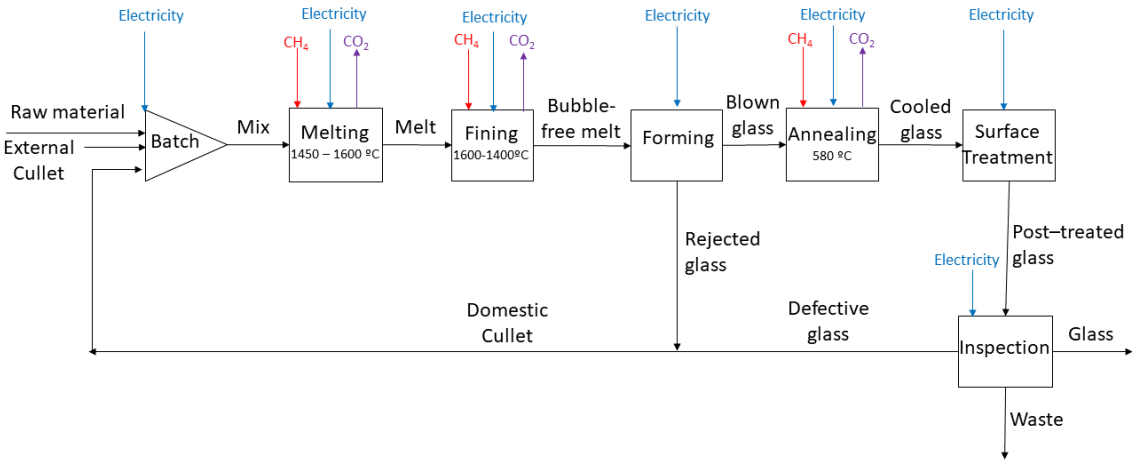


*Figure 12. Conventional glass plant, base case.*

Batch preparation involves the thorough mixing of raw materials and recycled cullet in order to achieve the desired composition. The raw material comprises various compounds, including network formers, fluxing agents, stabilizers, colorants, and fining agents, but only the main materials have been considered (Table 10). Typically, the mixture is moistened with 2-4 wt% water to ensure uniformity [64].

*Table 10. Input data of the conventional container glass production plant* [65].

| Variable | Units | Case 0 | Variable | Units | Case 0 |
|---|---|---|---|---|---|
| *Raw material* | | | *Cullet ratios* | | |
| Silica Sand | $kg/t_{glass}$ | 191 | Rejected glass | $kg/t_{glass}$ | 22 |
| Dolomite | $kg/t_{glass}$ | 34 | Defective glass | $kg/t_{glass}$ | 89 |
| Limestone | $kg/t_{glass}$ | 24 | *Glass composition* | | |
| Sodium Carbonate | $kg/t_{glass}$ | 57 | $SiO_2$ | wt% | 73.26 |
| Sodium Sulphate | $kg/t_{glass}$ | 2 | $Na_2O$ | wt% | 12.61 |
| External Cullet | $kg/t_{glass}$ | 744 | CaO | wt% | 9.92 |
| Domestic Cullet | $kg/t_{glass}$ | 111 | MgO | wt% | 2.55 |

The mixture is then directed to the melting furnace, which operates continuously at high temperatures (1500 °C). In this furnace, the solid material undergoes various phases, including heating and melting of solid particles, evaporation of water, and occurrence of chemical reactions. Heat transfer occurs through thermal radiation from the natural gas flame of the burners installed above and through convection from the molten material below. The melting furnace also facilitates the necessary reactions to achieve the desired glass composition. The decomposition of raw materials (silica, soda ash, limestone, and dolomite) releases $CO_2$, resulting in the formation of $SiO_2$, $Na_2O$, CaO, and MgO, see Eq. (39) to Eq. (42). The fining process purifies and homogenizes the molten glass at 1500 °C.

$$Na_2CO_3(s) \rightarrow Na_2O(s) + CO_2(g) \qquad \Delta H_{298} = 273.3\ kJ/mol \qquad (39)$$

$$CaMg(CO_3)_2\ (s) \rightarrow CaCO_3(s) + CO_2(g) + MgO(s) \qquad \Delta H_{298} = 68.9\ kJ/mol \qquad (40)$$

$$CaCO_3(s) \rightarrow CaO(s) + CO_2(g \qquad \Delta H_{298} = 177.9\ kJ/mol \qquad (41)$$

$$Na_2SO_4(s) \rightarrow Na_2O(s) + SO_3(g) \qquad \Delta H_{298} = 522.4\ kJ/mol \qquad (42)$$

The conditioned glass is then processed in forming machines to obtain the desired container shape. Any rejected glass is recycled back to the melting stage. The glass that meets the quality requirements, blown at 500 °C, proceeds to the annealing stage, where internal stresses are relieved to enhance crack resistance, at 580 °C. Subsequently, the glass undergoes surface treatment, which involves coating with organic compounds to enhance physical and optical properties, such as lubricity and increased strength. Defects are identified during the final inspection stage, contributing to the domestic cullet pool.

The Aspen model of the conventional glass plant has been validated with bibliographic data [65], [71]. Deviation values of the main mass flows are below 3.5 % except for MgO, which is a minority compound that weighs <3 wt% of the final glass composition. The specific glass composition is variable depending on the manufacturer, the colour and quality of the produced glass. Nevertheless, these deviations have little effect in the global mass and energy balances. According to that, the presented Aspen model can be considered representative of container glassmaking process.

### 3.1.3. Proposed integration concepts

Four different concepts are designed and analysed (Figure 13), incorporating Power to Gas and carbon capture technologies (paper i, Annex E). These concepts include a PEM electrolyser powered by renewable energy, a Calcium Looping carbon capture system, and a catalytic methanation reactor. Waste heats from the glassmaking process are utilized for pre-heating batch, air, or natural gas [64].

In Case 1, a PtG system is integrated into a conventional glassmaking plant to produce synthetic natural gas (SNG), according to the configuration depicted in solid lines in Figure 13. This process involves reducing captured $CO_2$ from the glassmaking process's flue gas with hydrogen generated in the PEM electrolyser. The methanation system generates SNG and is sized to meet the thermal requirements of both the melting furnace and the calciner in the CaL system. The carbon capture system is sized to capture the necessary amount of $CO_2$ from the flue gas, with the remaining flue gas emitted into the atmosphere. Additionally, the PEM electrolyser is sized to meet the hydrogen demand, while the produced oxygen is utilized for oxy-combustion in the calciner. This case serves as the starting point for the subsequent cases.

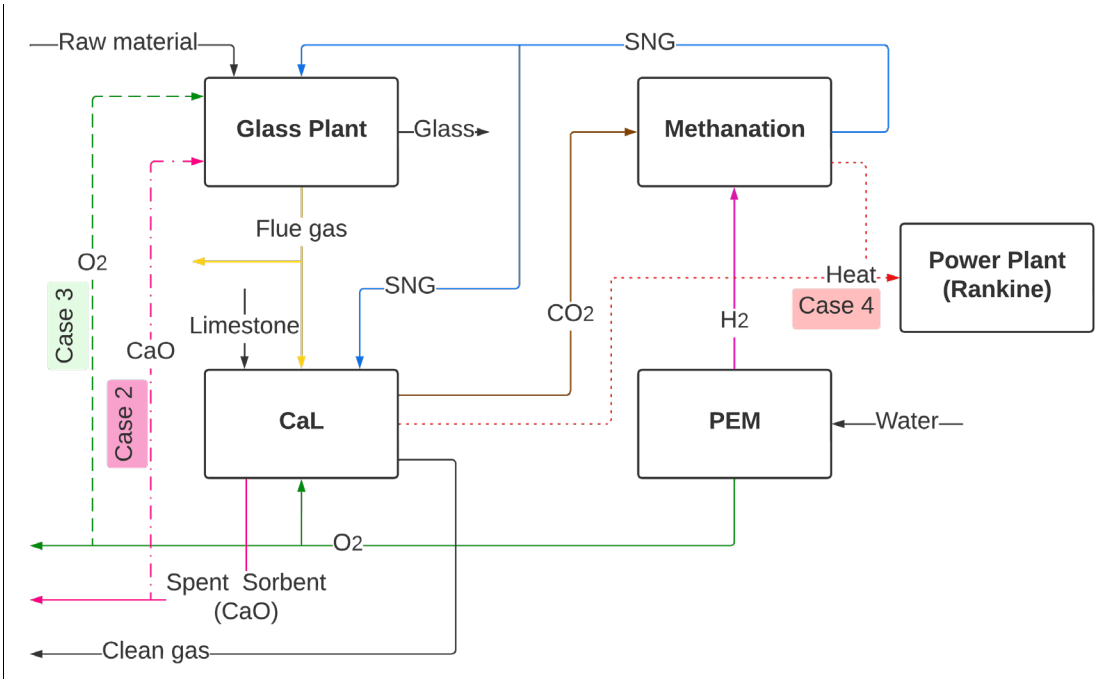


*Figure 13. Process flow diagram of the low-carbon concepts.*
*Case 1: basic PtG integration (solid lines). Case 2: PtG with CaO recycling (solid and pink dashed lines). Case 3: PtG with oxy-melting furnace (solid and green dashed lines). Case 4: PtG with Power Plant (solid and red dotted lines).*

In Case 2, in addition to the integration of PtG, certain fraction of the purged CaO from the CaL capture system is used to replace the equivalent raw material in the glassmaking process (pink dash-dotted line). The quantities of recycled CaO and limestone are calculated to maintain the same composition in the final glass product. This modification is expected to reduce $CO_2$ emissions through three mechanisms: (i) the batch material is pre-heated with the high-temperature purged CaO (at 700 °C); (ii) the reduction of the overall input raw material flow, as 1 kg of CaO is equivalent to 1.79

kg of $CaCO_3$; (iii) the avoidance of the indirect emissions associated with the fuel combustion required for $CaCO_3$ decomposition.

In Case 3, the excess oxygen produced by the PEM electrolyser is utilized for oxy-combustion in the fining and annealing furnaces (green dashed line), resulting in a reduction in both natural gas consumption and $CO_2$ emissions. Since the amount of oxygen required is lower than the amount produced by the electrolyser, there is no need for an air separation unit and the surplus is sold for external uses. The oxy-combustion in the melting furnace is not considered in this work, since not enough oxygen is produced in the electrolyser and the use of an air-separation unit would result in additional economic and energetic penalties.

Finally, in Case 4, waste heat from the methanation and capture systems is recovered for power generation in a Rankine power plant with three evaporators, three turbines, and four pressure levels (red dotted lines) [71]. The heat streams analysis was done through a Pinch analysis.

The economic analysis for the PV farm considered an initial investment of 620 €/kW and a typical utilization factor in Spain of 25% (1990 h/year) [72].

### 3.1.4. Results and conclusions

After the reference case validation, and simulating the four different concepts proposed, 17 techno-economic KPIs are defined and calculated (Table 11). KPIs 1–6 are identical in Cases 1, 3 and 4, while little differences are obtained in Case 2. This is because the CaL and methanation systems remain unchanged through these cases. Specifically for Case 2, carbonator volume is slightly higher (KPI 2), while the thermal demand in the melting stage and, therefore, the SNG required decrease (KPI 5). Accordingly, such reduction results in smaller amounts of thermal energy consumption in CaL per ton of glass produced (KPI 4), and smaller volume of the methanation reactor (KPI 6).

The NG consumption per glass mass produced (KPI 8) and the $CO_2$ emissions (KPI 9) are significantly reduced for the proposed PtG concepts with respect to the reference plant for which these figures are 111 $kg_{NG}/t_{glass}$ and 355 $kg_{CO2}/t_{glass}$, respectively. The remaining quantities are due to some NG consumption in other processes, like the annealing. In Case 3, the values of KPIs 8 and 9 are even lower due to the oxy-combustion technology employed in these processes, that directly reduce the NG consumed in such secondary processes. On the contrary, the electricity consumption (KPI 10) increases more than ten times in all cases with respect to Case 0 (216 $kWh_e/t_{glass}$). In the least favourable case (Case 1), the electricity consumption increases up to 3026.38 $kWh_e/t_{glass}$, which implies an energy penalty for the carbon capture of 35.83 $MJ_e/kg_{CO2}$ (KPI 11). It is a quite high value with regards to conventional CCS energy penalties ranging between 1 and 6 $MJ/kg_{CO2}$, depending on the technology used.

The recirculation of CaO in Case 2, which lowers the thermal demand in the melting furnace, provides further reductions in $CO_2$ emissions (−2.27 percentage points, pp, with respect to Case 1), specific electricity consumption (−2.12 pp) and energy penalty of carbon capture (−5.53 pp). Regarding NG savings, no additional benefits are

obtained, since the melting furnace in Case 1 uses 100 % SNG, as also occurs in Case 2 and 4.

*Table 11. Comparison of KPIs for the low-carbon concepts (P: purchased; S-C: self-consumption)*

| KPI | Related to | Description | Units | Case 1 | Case 2 | Case 3 | Case 4 |
|---|---|---|---|---|---|---|---|
| **1** | CaL | *Calciner volume* | $m^3_{cal}/kg_{CO2}$ | 4.26 | 4.25 | 4.26 | 4.26 |
| **2** | CaL | *Carbonator volume* | $m^3_{car}/kg_{CO2}$ | 16.36 | 16.71 | 16.35 | 16.35 |
| **3** | CaL | *$CO_2$ energy requirements* | $kWh_t/kg_{CO2}$ | 1.21 | 1.22 | 1.21 | 1.21 |
| **4** | CaL | *Thermal energy demand* | $kWh_t/t_{glass}$ | 456.77 | 450.33 | 456.77 | 456.77 |
| **5** | Methanation | *SNG production* | $kg_{SNG}/t_{glass}$ | 133.29 | 130.48 | 133.29 | 133.29 |
| **6** | Methanation | *Reactor volume* | $m^3_{reactor}/t_{glass}$ | 468.3 | 458.31 | 468.25 | 468.25 |
| **7** | Rankine | *Electricity generation* | $kWh_e/t_{glass}$ | - | - | - | 346.89 |
| **8** | Operation | *NG consumption* | $kg_{NG}/t_{glass}$ | 13.5 | 13.5 | 5.8 | 13.5 |
| **9** | Operation | *$CO_2$ emissions* | $kg_{CO2}/t_{glass}$ | 72 | 62 | 51 | 72 |
| **10** | Operation | *Electricity consumption* | $kWh_e/t_{glass}$ | 3026 | 2967 | 3026 | 2681 |
| **11** | Operation | *Energy penalty* | $MJ/kg_{CO2}$ | 35.8 | 33.9 | 33.3 | 31.4 |
| **12** | Economics | *20-year balance* | M€ | *P:* -151.3 | *P:* -136.0 | *P:* -133.5 | *P:* -123.1 |
| | | | | *S-C:* -139.2 | *S-C:* -123.0 | *S-C:* -121.4 | *S-C:* -105.5 |
| **13** | Economics | *CAPEX* | M€ | *P:* -36.8 | *P:* -32.9 | *P:* -33.4 | *P:* -41.0 |
| | | | | *S-C:* -68.3 | *S-C :* -63.7 | *S-C:* -64.9 | *S-C:* -68.6 |
| **14** | Economics | Opex | | P: -151.3 | P: -136.0 | P: -133.5 | P: -123.1 |
| | | | | S-C: -139.2 | S-C: -123.0 | S-C: -121.4 | S-C: -105.0 |
| **15** | Economics | *Annual benefits* | M€/y | *P:* -8.4 | *P:* -7.6 | *P:* -0.4 | *P:* -6.0 |
| | | | | *S-C:* -5.2 | *S-C:* -4.4 | *S-C:* -4.2 | *S-C:* -2.7 |
| **16** | Economics | *Carbon Abatement Cost* | $€/t_{CO2}$ | *P:* 436.5 | *P:* 378.9 | *P:* 357.4 | *P:* 343.9 |
| | | | | *S-C:* 367.0 | *S-C:* 344.8 | *S-C:* 292.7 | *S-C:* 261.2 |
| **17** | Economics | *Glass Production Cost* | $€/t_{glass}$ | *P:* 164.8 | *P:* 140.1 | *P:* 134.9 | *P:* 129.9 |
| | | | | *S-C:* 138.6 | *S-C:* 127.5 | *S-C:* 110.5 | *S-C:* 98.6 |

The implementation of oxy-combustion in fining and annealing stages (Case 3) reduces specific $CO_2$ emissions and NG consumption in 6 and 7 pp, respectively, with regards to Case 1, reaching NG consumption as low as 5.79 $kg_{NG}/t_{glass}$. Electricity consumption does not vary with respect to Case 1 (Fig. 8), while energy penalty is reduced by 6.9 pp. This decrease is directly related to the increase in energy efficiency through oxy-combustion.

Finally, the only effect of the inclusion of a power plant in Case 4 is the reduction in electricity consumption and energy penalty by 11.4 pp and 12.3 pp regarding Case 1. Considering a net glass production of 250 $t_{glass}$/day, the size of the Rankine cycle is 3.6 $MW_e$.

As for the economic analysis, the nominal power of the solar system is determined based on the maximum electricity consumption without energy storage. Consequently, electricity is purchased during hours without sunlight. In both scenarios, the capital expenditure (CAPEX) and operational expenditure (OPEX) are significantly high, resulting in a high carbon abatement cost ranging 261 $€/t_{CO2}$ and 499 $€/t_{CO2}$. The implementation costs are also substantial between 99 $€/t_{glass}$ and 165 $€/t_{glass}$, respectively (see Table 11).

One of the main advantages of the proposed concept is its versatility, as it does not change the current glassmaking process. It should also be noted that the improvements analysed here separately can be combined to optimize the system. The

carbon abatement costs are in the line of other industrial integrations of Power to Gas, ranging from 261 to 367 €/$t_{CO2}$ [73]–[75]. In spite of these high figures, the proposed concepts may be profitable under future scenarios with high carbon taxes, high prices of fossil fuels and low prices of renewable electricity, as it has been demonstrated in later studies [72].

## 3.2. Power to gas in the steel industry

### 3.2.1. General overview and state of the art

The iron and steel sector holds the top position in terms of $CO_2$ emissions among heavy industries and ranks second in terms of energy consumption. This sector is directly responsible for emitting 2.6 gigatonnes of carbon dioxide (Gt of $CO_2$) annually, accounting for 7% of the global emissions from the energy system [76].

The primary production of crude steel involves three main phases: raw material preparation, ironmaking, and steelmaking (Figure 14). Two main pathways exist: the blast furnace-basic oxygen furnace (BF-BOF) and the direct reduced iron-electric arc furnace (DR-EAF). The BF-BOF route dominates the market, constituting around 70% of global steel production and approximately 90% of primary steel production [76].

Regardless the ironmaking route selected in primary production (BF or DR), the supply of carbon monoxide and hydrogen are essential for reducing the iron ore (Eq (43) – Eq (44)). The generation of these gases relies almost entirely on fossil fuels. Coal and its derivative coke, along with natural gas to a lesser extent, are the main primary energy sources of these inputs.

$$Fe_2O_3 + 3CO \rightarrow 2Fe + 3CO_2 \qquad \Delta H = -27.52\ kJ/mol \qquad (43)$$

$$Fe_2O_3 + 3H_2 \rightarrow 2Fe + 3H_2O \qquad \Delta H = +88.44\ kJ/mol \qquad (44)$$

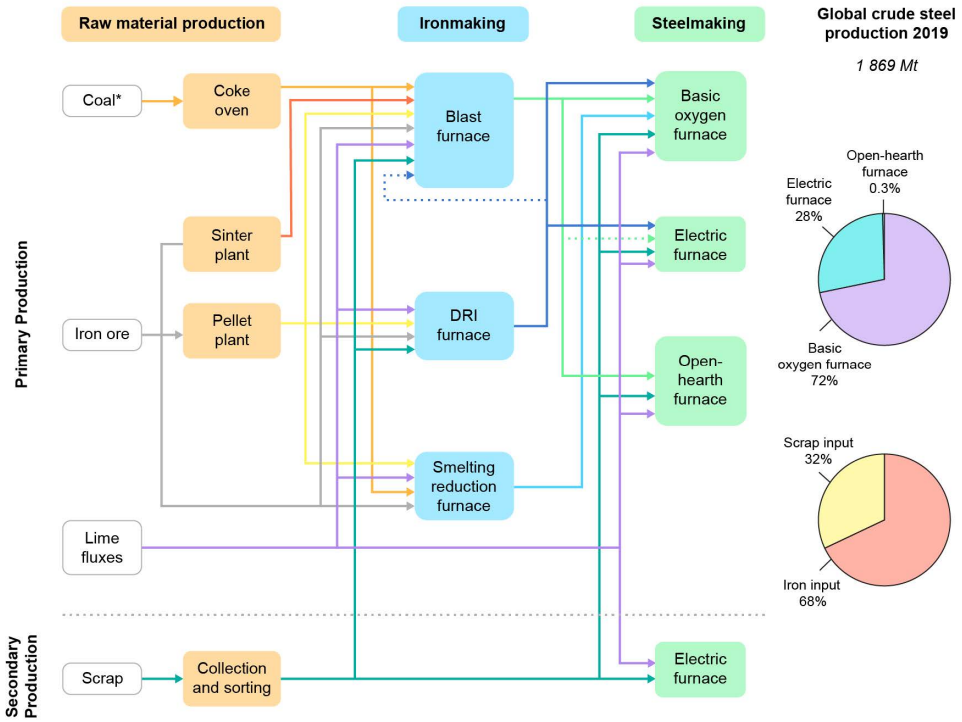


*Figure 14. Main steel production pathways and material flows in 2019* [76].

The production cost of steel heavily relies on the cost of key inputs, namely iron ore, scrap, and energy (Table 12). These raw materials and energy inputs typically constitute 60-80% of the total production cost [76].

*Table 12. Main steelmaking production routes: BF-BOF, Scrap-EAF and DR-EAF* [76], [77]

| **Steelmaking production route** | **BF-BOF** | **Scrap-EAF** | **DR-EAF** |
|---|---|---|---|
| Steel world production (%) | 72% | 21% | 7% |
| Main inputs | Iron ore, coal and coke | Scrap and electricity | Iron ore, NG, scrap and electricity. |
| Energy consumption (GJ/$t_{Steel}$) | 21.4-22.7 | 2.1-5.2 | 17.1-21.8 |
| $CO_2$ emissions ($t_{CO2}$/$t_{Steel}$) | 2.2 | 0.3 | 1.4 |
| Costs (USD/$t_{Steel}$) | 330-460 | 330-510 | 400-600 |

A number of innovation efforts are aiming to lower emissions. These technologies can be classified as: CCUS (Carbon capture, utilization and storage), Hydrogen, Direct electrification and Bioenergy. In Table 13, the current TRL (technology readiness level), the expected horizon of availability and the anticipated weight in the Net Zero Emissions (NZE) scenario are summarized [76].

*Table 13. Status of main near-zero emission technologies in the iron and steel sector* [76].

| **Technology** | **TRL** | **Year Available** | **Importance for NZE** |
|---|---|---|---|
| **CCUS (Carbon capture, utilization and storage)** | | | |
| Blast furnace: off-gas hydrogen enrichment and/or $CO_2$ removal for use or storage | 5 | 2030 | Very High |
| Blast furnace: Converting off-gases to fuels | 8 | Today | Medium |
| Blast furnace: Converting off-gases to chemicals | 7 | 2025 | Medium |
| DR: Natural gas-based with $CO_2$ capture | 9 | Today | Very high |
| Smelting reduction: with CCUS | 7 | 2028 | Very high |
| **Hydrogen** | | | |
| Blast furnace: electrolytic $H_2$ blending | 7 | 2025 | Medium |
| DR: Natural gas-based with high levels of electrolytic $H_2$ blending | 7 | 2030 | High |
| DR: Based solely on electrolytic $H_2$ | 5 | 2030 | Very high |
| Smelting reduction: $H_2$ plasma reduction | 4 | - | Medium |
| Ancillary processes: $H_2$ for high temperature heat | 5 | 2025 | High |
| **Direct electrification** | | | |
| Electrolysis: Low-temperature | 4 | - | Medium |
| Electrolysis: High-temperature molten oxide | 4 | - | Medium |
| **Bioenergy** | | | |
| Blast furnace: Torrefied biomass | 7 | 2025 | Medium |
| Blast furnace: Charcoal | 10 | Today | Medium |

An extended state of the art for low-carbon approaches in the iron and steel industry can be found in Annex A.

The study presented in the following sections aims to integrate the methanation of green hydrogen and carbon from flue gases of the steel industry in order to produce synthetic methane for use in the blast furnace process to produce elemental iron. The

proposed concept, modelled in EES, combines various technologies including oxy-combustion in the blast furnace, catalytic methanation, and top gas recycling.

### 3.2.2. Reference plant

The integrated route for iron and steelmaking consists of several components including a sintering process, coke oven, hot stoves, blast furnace, air separation unit, basic oxygen furnace, and casting. The block diagram of the reference plant model is shown in Figure 15. The main input mass flows include iron ore, coal (converted to coke in the coke oven or pulverized, PCI), and air (used for combustion in the BF and for oxygen production in the ASU). Processes requiring high-temperature heat are supplied by utilizing part of the internal fuel gases produced in the coke oven, BF, and BOF. Additionally, a power plant, sized to make the industry self-sufficient, utilizes the remaining coke oven gas (COG), blast furnace gas (BFG), and basic oxygen furnace gas (BOFG), as well as high-temperature gas streams from cooling processes (sinter, slag, and coke cooling). An overall efficiency of 17.9% is assumed [78], due to the low temperatures of the heat recovery flows and the limited calorific value of the fuel gases (high $CO_2$ and $N_2$ content).

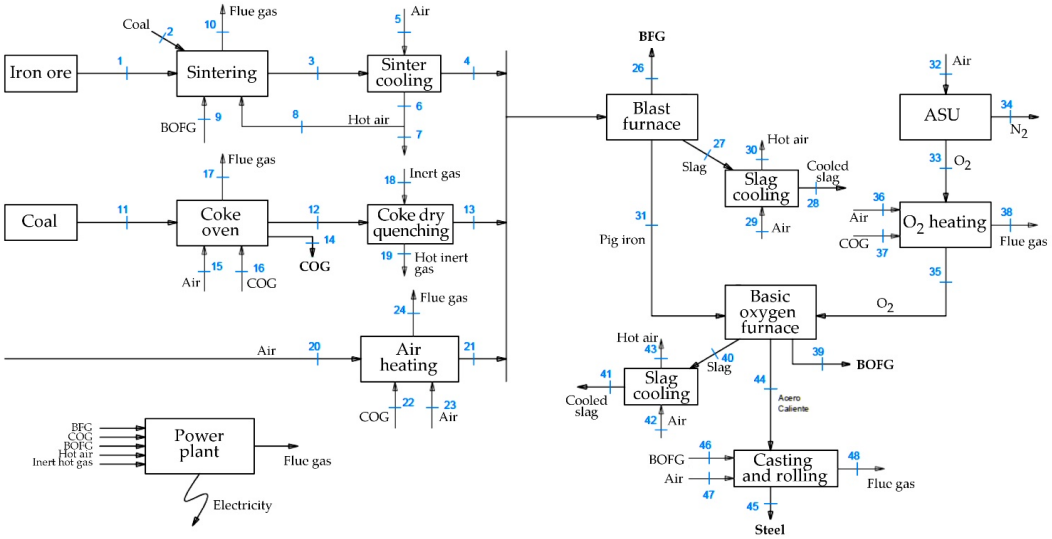


*Figure 15. Process flow diagram of the reference ironmaking plant (Case 0).*

The ironmaking process has a total electricity consumption of 874 MJ/$t_{Steel}$, while the power plant generates 1260 MJ/$t_{Steel}$, making the overall process self-sufficient (typical power productions in on-site plants are around 1300 MJ/$t_{Steel}$ [79]). The total $CO_2$ emissions of the plant amount to 1718 kg/$t_{Steel}$, with BFG being the primary source (1368 kg/$t_{Steel}$). Literature suggests that BF $CO_2$ emissions can range between 1270 and 1550 kg/$t_{Steel}$, with total emissions going up to 2200 kg/$t_{Steel}$ [76], [78]. The analysis is performed in specific units referred to a ton of crude steel, but later a typical production of 320 $t_{steel}$/h is considered. All results lay within reasonable limits when compared with bibliography, thus validating the results of the reference case [80].

### 3.2.3. Power to Gas integration

The proposed PtG concepts (paper ii, Annex E) combine oxy-blast furnace (OBF), PEM electrolyser for green $H_2$ production and top gas recycling (TGR) in Case 1, while COG is used as hydrogen source in Case 2, eliminating the need of electrolyser.

In the former case, both oxy-combustion and top gas recycling (TGR) technologies are applied simultaneously (Figure 16). The blast furnace uses the $O_2$ by-produced in the electrolyser, with synthetic methane partially replacing coke. The pure oxygen is introduced through the tuyeres instead of hot air to achieve nitrogen-free BFG (composed solely of $CO_2$ and CO). The oxy-BF gas (OBFG) is divided into three streams: for top gas recycling (stream 175), for the power to gas plant (176) and for synthetic methane production (174). The direct methanation of oxy-BF gas reduces the size of the methanation reactor due to the absence of nitrogen and also reduces the hydrogen consumption due to the presence of CO in the gas. TGR is implemented to dilute the pure oxygen stream, resulting in a 40% $O_2$–60% $CO_2$ ratio in the OBF. Preheating blocks for $O_2$ + BFG and $CH_4$ are also modelled.

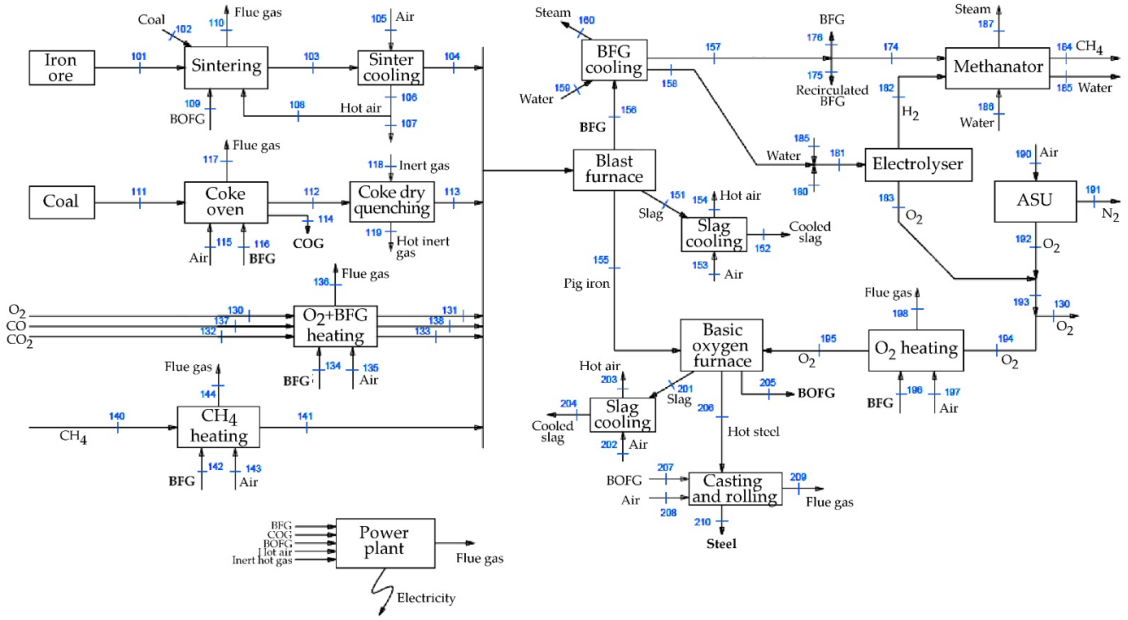


*Figure 16. Process flow diagram of the power to methane integration in ironmaking with oxy-fuel combustion and top gas recycling (Case 1)*

This first integration results in a reduction of 50 $kg_{Coke}/t_{Steel}$, with a replacement ratio of 1.3 $kg_{SNG}/kg_{Coke}$. This substitution necessitates a total of 27 $kg_{H2}$ per ton of steel (corresponding to a 432 $MW_e$ electrolyser). Consequently, the electricity consumption increases up to 6136 $MJ/t_{Steel}$, with the electrolyser accounting for 81% of the total consumption. The $CO_2$ emissions decrease to 1582 $kg_{CO2}/t_{Steel}$, representing an 8% reduction compared to the reference case. This reduction in $CO_2$ emissions results in an energy penalty of 34 $MJ/kg_{CO2}$.

In the second PtG integration, COG (56% $H_2$, 30% $CH_4$, 10% CO, 5% $CO_2$, 1% $O_2$ and 5% $N_2$ [81]) is used as hydrogen source for the methanation (Figure 17). The same amount of SNG is produced, resulting in equivalent coke replacement and $CO_2$ emission

reduction. However, Case 2 achieves significantly lower electricity consumption and energy penalty, with values of 1382 MJ/$t_{Steel}$ (58% higher compared to the reference case) and 4.9 MJ/$kg_{CO2}$, respectively.

Savings in $CO_2$ emissions with either of the two PtG implementations were 8%, with a reduction in coal fuel of 12.8%. The second case also uses the $H_2$ from the COG, avoiding the need for an electrolyser. Under this framework, the only competitive option is Case 2, whose energy penalization is in the range of conventional amine carbon capture [82]. Moreover, it has the advantage of reducing the fuel consumption and reducing geological storage, which are additional benefits regarding economic costs compared to conventional carbon capture and storage.

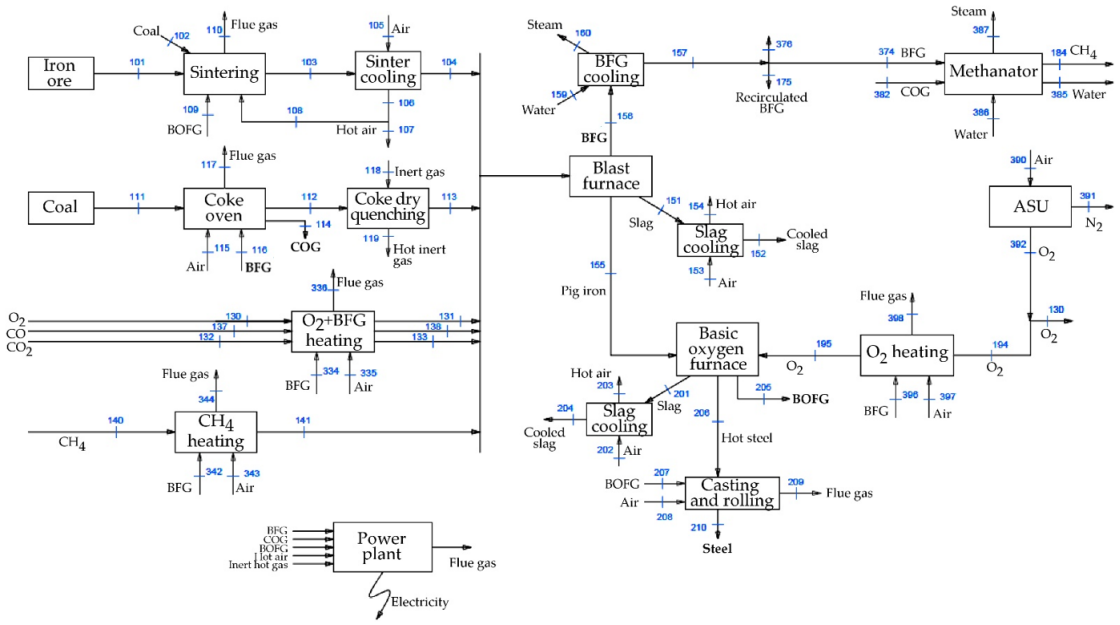


*Figure 17. Process flow diagram of the COG methanation integration in ironmaking with oxy-fuel combustion and top gas recycling (Case 2)*

## 3.3. Discussion and conclusions of preliminary studies

The glassmaking and steel industries can benefit from implementing Power to Gas technology for decarbonisation. However, several factors need to be considered when evaluating which industry is better suited for PtG integration.

In terms of carbon intensity, the glass industry can reduce $CO_2$ emissions by up to 80%, and the steel industry by 8%. This emphasizes the significant emissions reduction potential in the glassmaking industry, while further research is needed in the steel industry. Energy consumption and associated penalties should also be considered when implementing PtG technology. The energy penalty for decreasing $CO_2$ emissions in a PtG system ranges from 31 MJ/$kg_{CO2}$ to 36 MJ/$kg_{CO2}$. The iron and steel industry demonstrates additional benefits concerning the energy penalty, which can be reduced to 5 MJ/$kg_{CO2}$ if coke oven gas is used as a hydrogen source.

The steel industry offers more integration possibilities due to the availability of different off-gases with diverse compositions, beyond just flue gases with $CO_2$ and $N_2$.

For example, methanation of blast furnace gas or coke oven gas ($CH_4$, $CO_2$, CO, $H_2$) can be explored.

Regarding technological maturity, the oxygen blast furnace in the steel industry is still under development (TRL 6-7) [83], as well as the oxy-combustion glass furnaces [84] and the calcium looping technology [85]. On the other hand, other PtG components such as methanation, electrolyser, and amine carbon capture are commercially available (TRL 9).

Despite achieving higher $CO_2$ emission reductions in the glassmaking industry, further research in the steelmaking industry is crucial due to its inherent challenges in decarbonisation and the potential for more synergistic opportunities.

# 4. Power to gas integration in the iron and steel industry

Various tasks are necessary to conduct the techno-economic evaluation of the proposed PtG concepts aimed at reducing $CO_2$ emissions in the I&S industry. The state of the art regarding carbon capture in the I&S industry, serving as a starting point, is revised in Section 4.1. The modelling of different industrial configurations has been performed using Aspen Plus. The description of the models, techno-economic indicators, and results are summarized in Section 4.2. Additionally, to contextualize the results and compare them with other literature, a second review was conducted. This review compares the configurations analysed in this thesis with others found in existing literature, as detailed in Section 4.3.

## 4.1. Carbon capture technologies in blast furnace route

### 4.1.1. General approach

Following the methodology presented in Section 2.1 [36], a systematic review is carried on the application of carbon capture (CC) in the BF-BOF route of steelmaking. The search strategy involves conducting a set of seven searches combining terms related to the industrial process and CC. A total of 1569 entries are obtained from these searches. Screening of the retrieved articles is performed based on their abstracts, with a focus on experimental or theoretical studies actually applying any form of carbon capture on the BF-BOF route. This screening process results in the selection of 120 articles, which are further classified into the four categories of CC: post-combustion, looping cycles, oxy-combustion, and pre-combustion. Within each category, specific CC technologies are identified, such as chemical absorption, physical adsorption, membranes, calcium looping, chemical looping, and sorption enhanced water gas shift (SEWGS), see Figure 18. Articles unrelated to CC, as well as those addressing other steelmaking routes or not relevant to the research focus, are excluded.

Figure 19 displays the number of scientific papers organized by year and technology to highlight the most studied or novel technologies. For oxy blast furnaces with top gas recycling (oxy-TGR), only the decrease of $CO_2$ due to injecting TGR is considered, excluding the decrease that would be achieved by storing the pure $CO_2$ from the CC stage underground. However, pre-combustion with adsorption (pre-adsor) technology is typically coupled with oxy-BF and TGR, and the combined benefit is taken into account for this technology. Oxy-TGR is the most studied technology with 30 published papers starting in 2004, followed by post-chem, pre-chem, and pre-adsor with 22, 13, and 17 papers, respectively, starting between 2007 and 2010. Among the novel technologies, such as pre- and post-memb, SEWGS, CaL, ChL, and OtherL, investigation in the iron and steel industry began between 2014 and 2016, having fewer than 6 published papers for each.

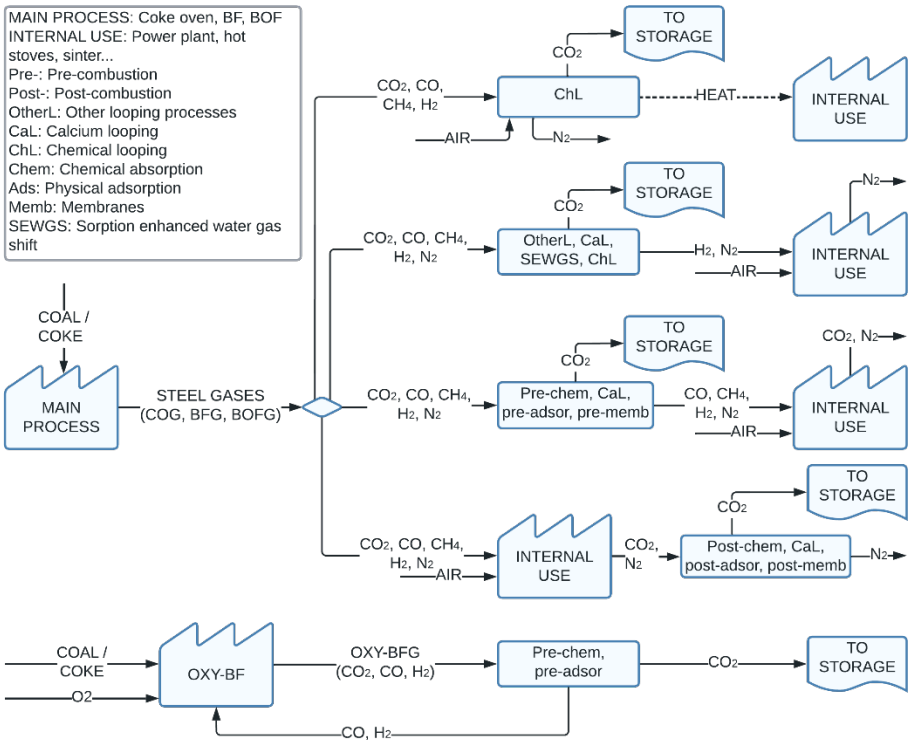


*Figure 18. Carbon capture routes in the BF-BOF route.*

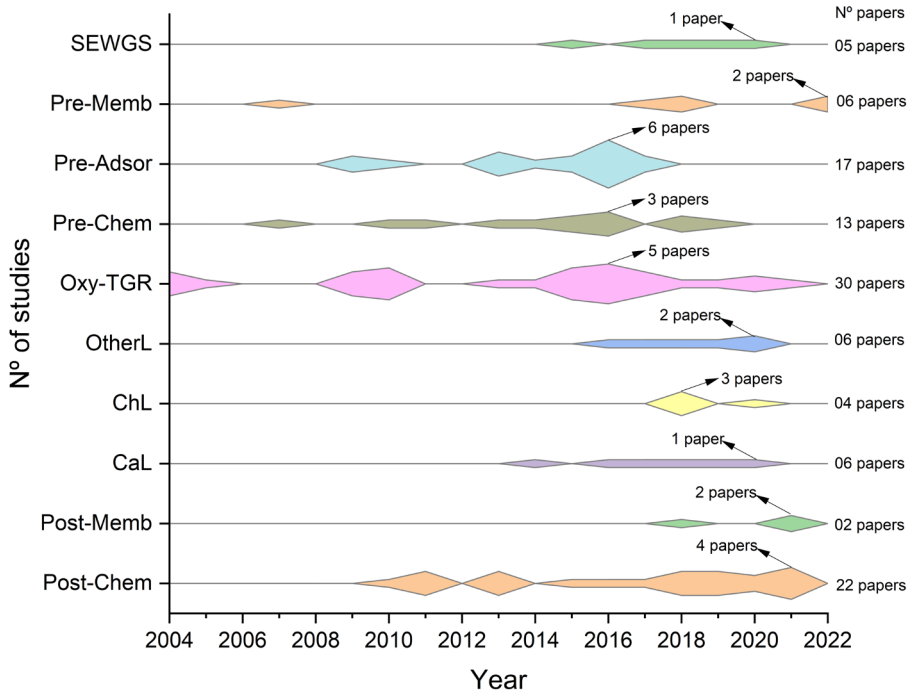


*Figure 19. Number of scientific papers organised by year and technology.*

### 4.1.2. Key findings

The review (paper iii, Annex E) describes and compares the integration of CC technologies in the BF-BOF steel industry in terms various KPIs: thermal penalty (MJ/$kg_{CO2}$), electrical penalty (MJ/$kg_{CO2}$), economic cost ($/$t_{CO2}$), $CO_2$ emission reduction

($kg_{CO2}/t_{HM}$), $CO_2$ purity (%), and TRL. Figure 20 gathers for each KPI the minimum, the maximum, the average, and all sampled values collected from the literature, given direct insight of the differences among technologies.

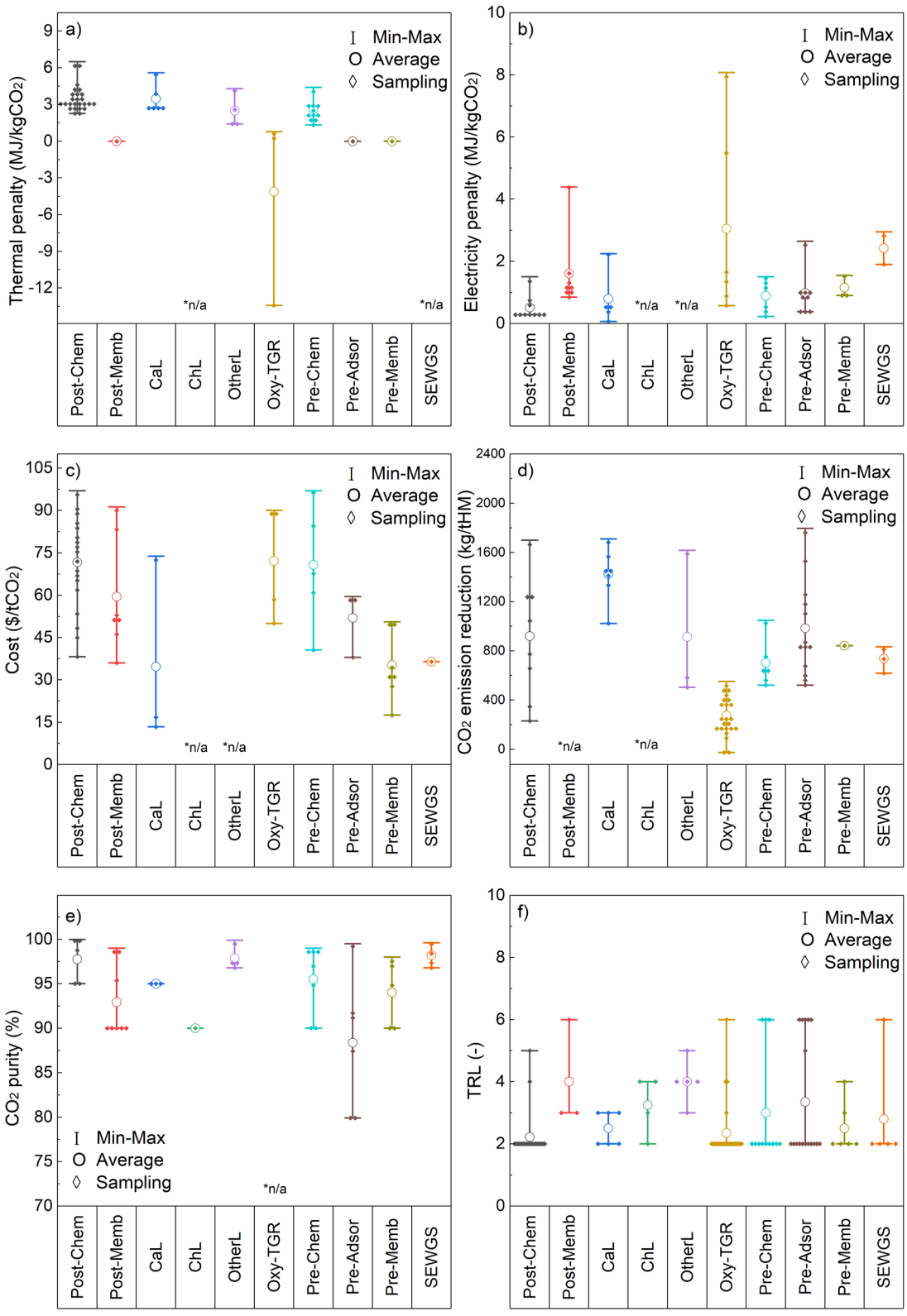


*Figure 20. Comparison of KPIs obtained from the literature for different CC technologies.*

The thermal penalty (subfigure a) ranges from 1.3 to 6.2 MJ/$kg_{CO2}$ for post-combustion chemical absorption (post-chem), calcium looping (CaL), other looping processes (OtherL), and pre-combustion chemical absorption (pre-chem). Oxy-TGR stands out with a thermal energy consumption range of 0.3–0.8 MJ/$kg_{CO2}$, and one study even calculates a negative penalty (-13.4 MJ/$kg_{CO2}$) [86]. Post- and pre-combustion with membranes (post-memb and pre-memb), chemical looping (ChL), pre-adsor, and sorption-enhanced water gas shift (SEWGS) either have negligible consumption or lack available data (n/a).

As for electricity penalty (subfigure b), post-chem, CaL, and pre-chem have the lowest consumption, averaging less than 1 MJ/$kg_{CO2}$. This is due to their primarily thermal process energy consumption, with minimal electricity usage related to $CO_2$ compression (up to 100–150 bar). Post-memb, pre-memb, SEWGS, and pre-adsor technologies involve gas compression for $CO_2$ capture, resulting in higher average electricity penalties ranging from 1 to 3 MJ/$kg_{CO2}$. Post-memb, in particular, has one outlier data point much higher than the rest (4.4 MJ/$kg_{CO2}$) due to capturing $CO_2$ from sinter flue gas with very low $CO_2$ content, requiring greater compression. Oxy-TGR exhibits the widest range of electricity penalties due to very different implementation configurations, ranging from under 1 MJ/$kg_{CO2}$ to over 8 MJ/$kg_{CO2}$.

Most published economic analyses have focused on post-chem technology, with more than 19 samples compared to less than 7 for the other technologies. Post-chem, oxy-TGR, and pre-chem have higher average economic costs, around 70 \$/$t_{CO2}$, while the other technologies range between 30 \$/$t_{CO2}$ and 60 \$/$t_{CO2}$ (subfigure c). Regarding the potential $CO_2$ mitigation (subfigure d), some configurations like Post-Chem, CaL and Pre-adsor can achieve reduction of almost 80%, considering that typical emissions from the BF-BOF route range between 2000 and 2200 $kg_{CO2}/t_{HM}$ [87]. However, most published works are simulations with low TRL (TRL 2-4, subfigure f), not accounting for physical or economic constraints of actual facilities. The maximum amount of $CO_2$ captured to date is 1270 $kg_{CO2}/t_{HM}$, achieved at TRL 6 in a pilot plant within the ULCOS project [88], with VPSA technology.

Among the technologies analyzed, only pre-adsor achieves a $CO_2$ purity lower than 90%, with an average of 88% and a minimum of 80% (subfigure e). Membranes are the only technology with an average purity below 95% due to economic considerations.

### 4.1.3. Conclusions

The main bottlenecks for the rapid development of all CC technologies are the high costs and the unavailability of underground storage. For promising technologies like membranes, CaL, and OtherL, low TRL and the absence of pilot plants are additional obstacles that slow down their development. Furthermore, pre-combustion CC technologies face technical limitations due to the CO and $CH_4$ present in energetic streams like BFG, COG, and BOFG, which are latter combusted, converted into $CO_2$, and emitted to the atmosphere. Partial solutions include injecting CO as a reducing agent in the BF or implementing a water gas shift prior to pre-combustion CC, but these approaches have their own economic and technical limitations.

In the BF-BOF route, the main $CO_2$ streams have a similar $CO_2$ content (i.e., 15–28 %vol) and similar pressures (from atmospheric to 2 bar). Therefore, where the CC stage is implemented is not a relevant criterion to select the CC system, as it will behave similarly. Taking into account the KPIs analysed, pre-adsor is found to be the most promising technology for capturing $CO_2$ in the I&S industry, according to its high TRL and $CO_2$ emission reduction at reasonable cost and penalty. In addition, it exhibits synergies with oxy-blast furnaces and top gas recycling, enhancing the benefits. The main drawback of this technology is the level of $CO_2$ purity (88 % on an average), that is lower than for other technologies.

The chosen technologies for further study in subsequent sections, in conjunction with power to gas, are amine scrubbing carbon capture, oxy-blast furnace, and top gas recycling. These technologies offer promising prospects for reducing $CO_2$ emissions in the iron and steel industry while addressing specific challenges such as cost-effectiveness, technical feasibility, and synergy potential with other decarbonization measures.

## 4.2. Proposal and assessment of PtG integration

### 4.2.1. Process description and case studies

The selection of six distinct cases for study within the I&S industry is motivated by the pursuit of synergistic combinations of various technologies aimed at reducing $CO_2$ emissions. By integrating technologies such as amines, top gas recycling, and oxy-blast furnace with the Power to Gas approach, the aim is to explore the viability of diverse pathways. Each case represents a unique configuration of these technologies, offering different advantages and challenges.

In Figure 21a, the base case represents a conventional plant. In the proposed low-carbon concepts, the systems outside the dashed frame remain essentially unchanged. So, subfigures b-e include the new configuration inside such box, whose components are summarized in Table 14. The simulated cases are the following:

- **BASE CASE:** Conventional BF-BOF plant (paper iv, Annex E).
  A reference plant is designed for comparison purposes, including sinter strand, coke oven, blast furnace (BF, including hot stoves), air separation unit, basic oxygen furnace, casting-rolling stages and a combined cycle power plant. The mass flow inputs to the system are iron ore, coal, air, scrap, and flux.
- **CASE 1 (BF+Amine+Meth.):** $CO_2$ methanation with air-blow blast furnace (paper iv, Annex E).
  Amine scrubbing is used to capture $CO_2$ from a part of the BFG, while a PEM electrolyser produces green $H_2$. A methanation plant produces SNG which is injected into the BF to continuously recycle the $CO_2$ and to reduce coal consumption. The $O_2$ from the electrolyser is used in part to cover the demand in the BOF, avoiding the expensive ASU, while the surplus is sold to interested industries. The resulting clean gas from the amine scrubbing (stream clean-BFG) is mixed with the rest of the BFG.

- **CASE 2 (OBF+Amine+Meth.):** $CO_2$ methanation with oxygen blast furnace (paper v, Annex E).
  This case study differs from the prior one in employing pure oxygen for an OBF configuration. Pure oxygen allows for additional reducing agents (SNG or other) in the furnace, reducing the required coal and therefore increasing the avoided $CO_2$ emissions.
- **CASE 3 (OBF+Amine+Meth.+TGR):** $CO_2$ methanation and top gas recycling integrated in an oxygen blast furnace (paper vi, Annex E).
  Unlike case 2, this study employs the preheated clean-BFG stream into the OBF's tuyeres, constituting a TGR concept. The Power to Gas and TGR are coupled with the aim of reducing the methanation plant size and, therefore, the electrolyser power and costs.
- **CASE 4 (OBF+Meth.):** BFG methanation with an oxygen blast furnace (paper vii, Annex E).
  Starting from case 2, the amine scrubbing is eliminated and the OBFG is directly fed into the methanation plant, enabling the reaction between green $H_2$ and $CO/CO_2$, present in the OBFG. The objective is to reduce PEM size and costs.
- **CASE 5 (OBF+Meth.+$CO_2$):** $CO_2$ recycling via lean-$H_2$ BFG methanation integrated in an oxygen blast furnace (paper vii, Annex E).
  Similar to case 4, this study employs lean-$H_2$ methanation, resulting in unreacted $CO_2$. The resulting syngas (primarily $CO_2$ and $CH_4$) is injected into the OBF's tuyeres. The objectives are to increase $CO_2$ recycling and decrease the PEM size.
- **CASE 6 (OBF+$H_2$):** Hydrogen injection in an oxygen blast furnace (paper vii, Annex E).
  Direct $H_2$ injection into the OBF's tuyeres is performed without any carbon recycling technology. The objective of this case is to design a more simplistic configuration without carbon recycling, while maintaining high carbon avoidance rates and relatively low costs.

*Table 14. BF technology and PtG component breakdown for Cases 1-6.*

| Case Study | Case 1 | Case 2 | Case 3 | Case 4 | Case 5 | Case 6 |
|---|---|---|---|---|---|---|
| OBF | | x | x | x | x | x |
| Amine | x | x | x | | | |
| Methanation | x | x | x | x | x | |
| TGR | | | x | | | |
| Electrolyser | x | x | x | x | x | x |

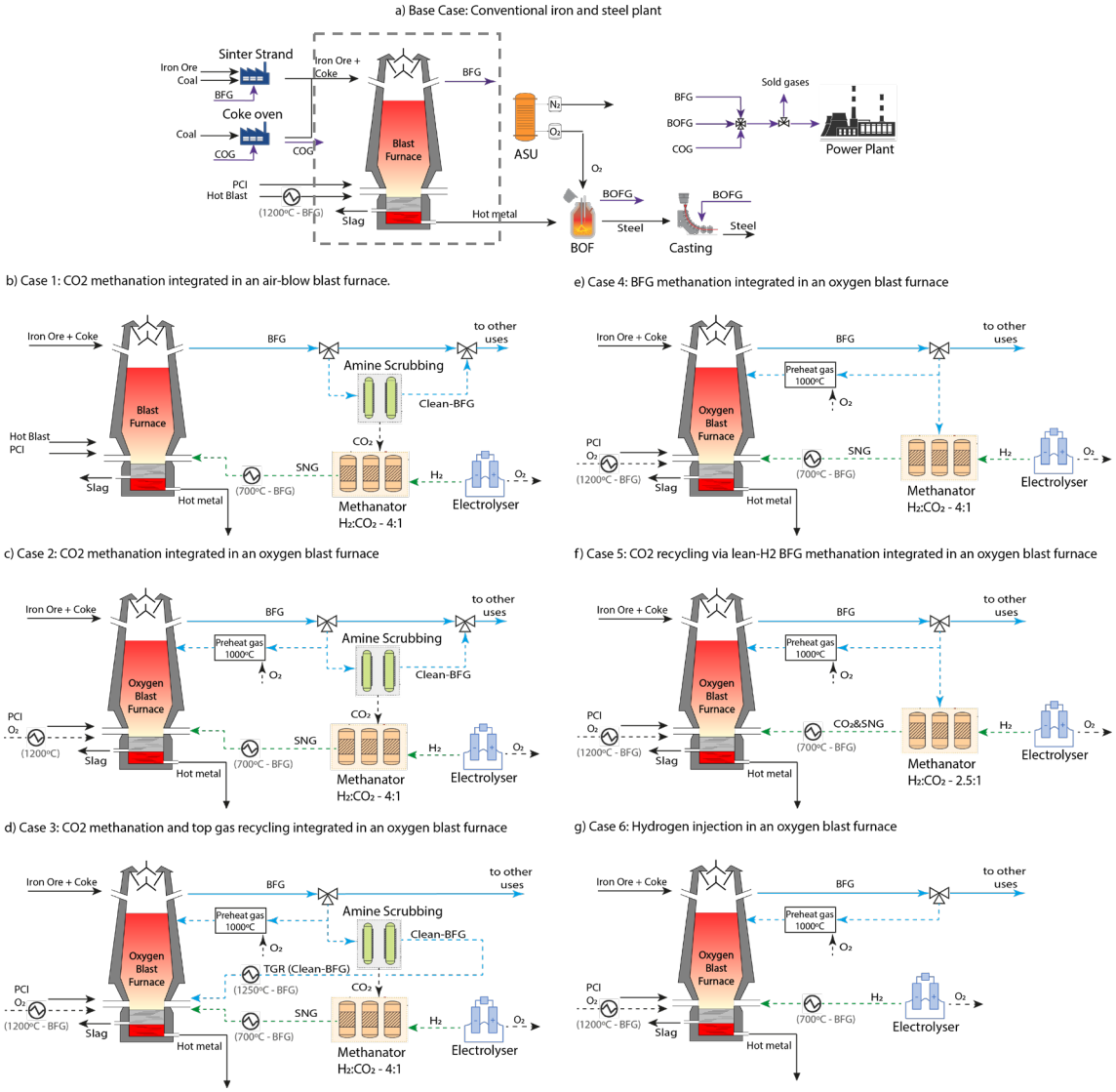


*Figure 21. Process flow diagram of a) Base case, b) BF+Amine+Meth., c) OBF+Amine+Meth., d) OBF+Amine+Meth.+TGR, e) OBF+Meth., f) OBF+Meth.+CO2, g) OBF+H2.*

## 4.2.2. Modelling and simulation

### Reference plant of conventional BF-BOF steelmaking

The conventional iron and steel plant producing 320 $t_{HM}$/h [89] is assumed as base case according to the process flow diagram (PFD) of Figure 21a. Each hierarchy, modelled and simulated in Aspen Plus®, consolidates essential sub-models of the associated processes (Figure 22). The sinter process represents fine ore particle agglomeration, achieved through initial fusion driven by coal combustion [90]. The initial step involves heating a blend of iron ore, coal (5wt%), and limestone to 800 °C utilizing BFG as fuel, followed by coal combustion at 1262 °C to create sinter [78], [90]. The coke oven emulates coal-to-coke transformation in anaerobic conditions. COG combustion (indirect heat exchange) elevates temperature to 1100 °C, yielding coke and coke oven gas. Subsequently, the coke is cooled to 150 °C through coke dry quenching (CDQ).

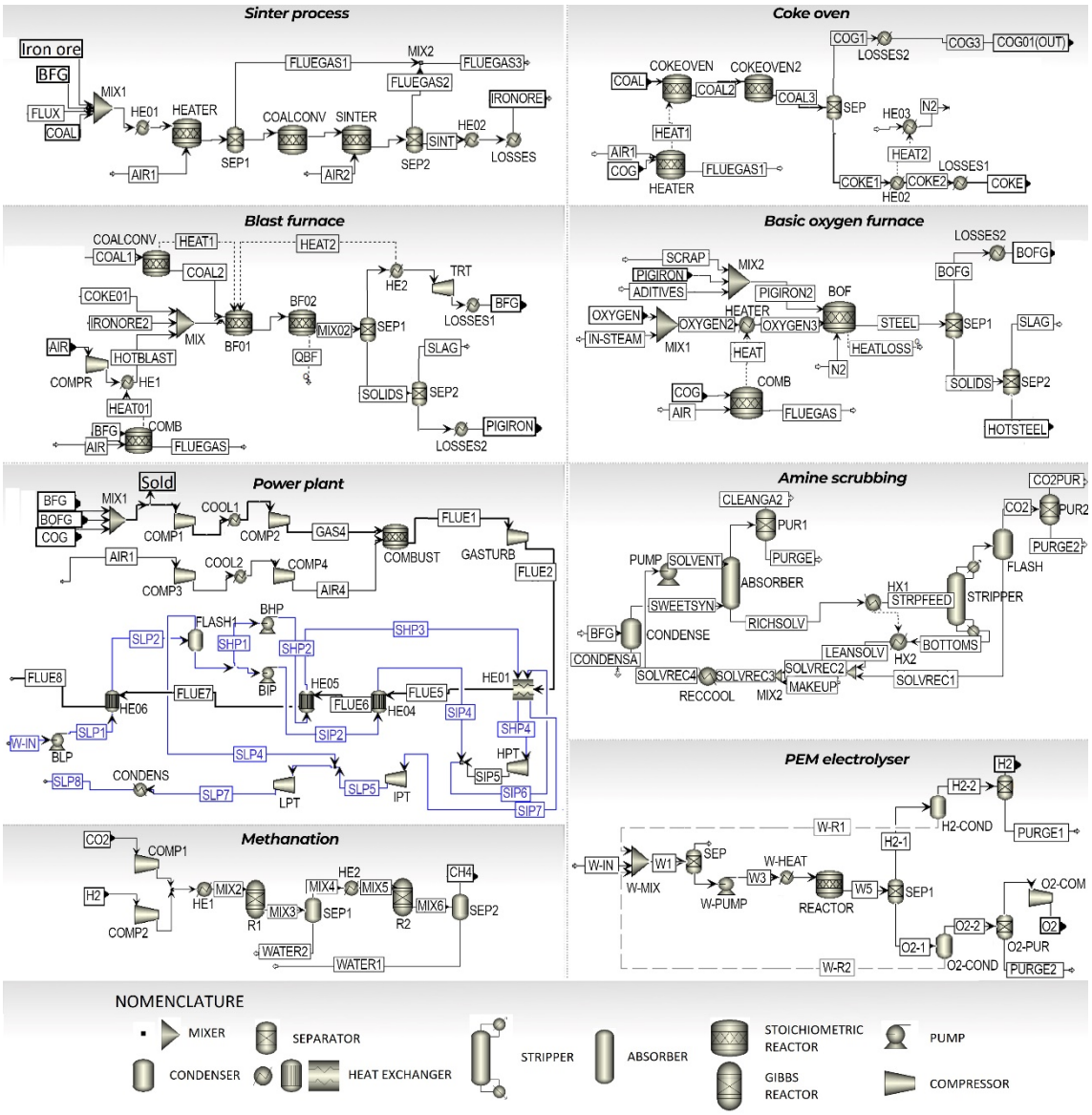


*Figure 22. Process flow diagrams of the hierarchy blocks. Blue lines: steam streams.*

The Blast Furnace hierarchy includes hot stoves and a detailed blast furnace. In the hot stoves, air is pressurized to 5 bar and indirectly heated to 1200 °C. Within the blast furnace, the initial reactor reduces iron oxides to metallic iron, and a subsequent reactor adjusts BFG composition based on CO and $H_2$ utilization (Eq.(45) and Eq.(46),respectively). Initial parameters include a pulverized coal rate of 150 kg/$t_{HM}$, $H_2$ utilization of 0.47, and 4.5wt% carbon content in hot metal [90], [91]. Additional parameters (BFG temperature and composition, air and coke flow rates, flame temperature) are derived via a revised Rist diagram [92]–[94], and subsequently integrated into the Aspen Plus model as inputs. When introducing SNG to the BF, the coal rate decreases while keeping the total coke input constant. Once all coal is substituted, coke usage begins to decrease.

$$\mu_{CO} = CO_2/(CO_2 + CO) \quad (45)$$

$$\mu_{H2} = H_2O/(H_2O + H_2) \quad (46)$$

The BOF transforms hot metal (4.5wt% C) into steel (0.267wt% C) through $O_2$ blowing, reacting with carbon to generate CO and $CO_2$. As this reaction is highly exothermic, 150 kg/$t_{HM}$ of scrap (0.267wt% C) is introduced to capitalize on this energy [79], [95]. The melted scrap blends with the hot metal, increasing steel production and regulating process temperature (1650 °C [89], [96]). Nitrogen injection from the BOF base promotes mixture stirring [89]. A portion of BOFG preheats the oxygen inlet stream to 1650 °C. $O_2$ is produced in the ASU via the Hampson-Linde cycle, following an example block in the Aspen Plus repository (Power, Coal gasification, IGCC [97]), so it is not included in Figure 22. The ASU separates oxygen at -189 °C through 94% purity liquefaction [98]–[100].

According to the actual BF-BOF facilities [71], [79], the Power Plant is simulated as a combined cycle, utilizing unused BFG, COG, and BOFG and 100 $MW_e$ net power, [78]. The gas turbine cycle comprises two-stage air compression with intercooling preceding the combustion chamber, along with a single expansion turbine for flue gas. The turbine experiences inlet conditions of 27 bar pressure and 1389 °C temperature [101]. The HRSG (heat recovery steam generator) block includes four counter-current heat exchangers that transfer energy from flue gases to steam (HE01, HE04-HE06), reaching a maximum steam temperature of 560 °C [101]. The steam power cycle encompasses three expansion stages, aligned with high, intermediate, and low-pressure turbines (HPT, IPT, and LPT blocks).

**Oxygen blast furnace**

In Cases 2-6, oxygen blast furnace is considered [102], [103]. The decreased bosh gas volume in the OBF, due to the lack of nitrogen, causes that preheating of the burden in the upper part tends to be insufficient in comparison with the conventional BF, which leads to low BFG temperature. Temperature drop below 100 °C can generate significant water condensation problems. In order to compensate for the insufficient heat supply in the shaft, it is necessary to inject preheating gas into the upper shaft. A fuel (usually BFG) is burned with pure oxygen and the flue gas is injected at 1000 °C in the upper part of the BF. In this study, the required amount of preheating gas is calculated to achieve a temperature of 150 °C in the BFG.

**Power to gas components**

Amine scrubbing, PEM electrolyser and methanation process are modelling with respective hierarchies, following the general procedure explained in Section 2.2. For each case, the maximum amount of reducing gas (SNG, TGR or $H_2$) is injected, firstly to reduce the pulverised coal injection (PCI) and, once it is over, to substitute the coke rate. The amount of reducing gas is limited by the adiabatic flame temperature (AFT), which should not be dropped below 2000 °C for technical reasons [104]. Consequently, the oxygen enrichment increases the AFT and the reducing gas injection lowers it, reaching equilibrium at 2000 °C in the AFT. Knowing the amount of reducing gas, the methanation plant, the amine scrubbing system and the PEM electrolyser are sized. The oxygen by-produced in the electrolyser is used to eliminate the ASU and to feed the BOF and hot blast enrichment necessities.

### 4.2.3. Blast furnace indicators

Various parameters are compared to assess the BF performance: amount of reducing agents and pre-heating gas, coal consumption and BFG composition (detailed results in papers iv-vii, Annex E). In Figure 23, the specific mass flow of pre-heating gas and reducing agents in the BF, namely coke, PCI, SNG, TGR and $H_2$, are compared for the different configurations. The pre-heating gas injection, required under OBF conditions to maintain the BFG temperature at 150 °C, ranges from 205 to 260 $kg_{BFG}/t_{HM}$ in all cases. Notably, the OBF considered in Cases 2-6 involves a greater reduction in coke consumption compared to the air blast furnace except in Case 5, for which the $CO_2$ injection entails poor performance. Injection of SNG, TGR, and $H_2$ produces similar reductions in coke and PCI, with slightly better outcomes for SNG injection (Cases 2 and 4).

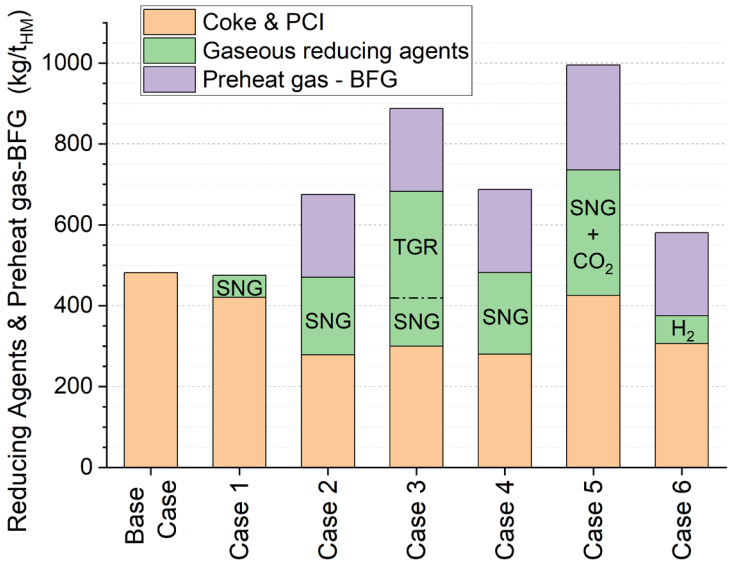


*Figure 23. Reducing agents and preheated gas injected in the blast furnace. The gaseous reducing agents include SNG, TGR and $H_2$. Cases in Figure 21.*

Specifically, in the reference case, consumption stands at 332 $kg_{coke}/t_{HM}$ and 150 $kg_{PCI}/t_{HM}$. In Case 1 (BF+Amine+Meth.), PCI injection is reduced to 88.8 $kg/t_{HM}$ by injecting 53.6 $kg_{SNG}/t_{HM}$ into an air-blow blast furnace. In Cases 2-4 and 6, the operation under oxy-combustion conditions enables complete substitution of PCI, alongside partial substitution of coke. Coke consumption ranges from 279 to 307 $kg_{coke}/t_{HM.}$ The $CO_2$ injection into the BF's tuyeres in Case 5 (OBF+Meth.+$CO_2$) assists in AFT control but does not yield significant reductions in fossil fuel consumption. In particular, the injection of 310 $kg_{SNG}/t_{HM}$ with 35.8% $CO_2$ in the BF results in a coke rate of 426 $kg_{coke}/t_{HM}$. In Table 15, these results are compared with similar studies reported in the bibliography [105]–[107]. Sahu et al. [105] investigated the impact of the nature of the fuel and burden of the OBF process with top gas recycling, Zhang et al. [106] and Li et al. [107] studied the medium (50% $O_2$) and full (98% $O_2$) oxygen enriched blast furnace with top gas recycling. The obtained results align with the ones obtained in the present work.

*Table 15. Summary of BF results from this study and literature.*

| | **BF/OBF** | **Coke** | **PCI** | **Reducing Gas** | **Ref.** |
|---|---|---|---|---|---|
| | - | $kg_{coke}/t_{HM}$ | $kg_{PCI}/t_{HM}$ | $kg_{Red.Gas}/t_{HM}$ | - |
| Base Case | BF | 332 | 150 | 0 | This work |
| Case 1 | BF | 332 | 88.8 | 54 (SNG) | This work |
| Case 2 | OBF | 279 | 0 | 192 (SNG) | This work |
| Case 3 | OBF | 300 | 0 | 113+270 (SNG+TGR) | This work |
| Case 4 | OBF | 280 | 0 | 202 (SNG) | This work |
| Case 5 | OBF | 426 | 0 | 310 (SNG) | This work |
| Case 6 | OBF | 307 | 0 | 69 ($H_2$) | This work |
| Sahu et al. | Full OBF | 323-342 | 200 | 615 (TGR) | [105] |
| Zhang et al. | Medium OBF | 300 | 126 | 781 (TGR) | [106] |
| Zhang et al. | Full OBF | 200 | 205 | 525 (TGR) | [106] |
| Li et al. | Medium OBF | 337 | 150 | 619 (TGR) | [107] |
| Li et al. | Full OBF | 200 | 205 | 875 (TGR) | [107] |

Regarding the total coal consumption, Figure 24 breaks down the use in the form of sintering coal, PCI, and coking coal. Sintering coal remains constant at 75 $kg_{coal}/t_{HM}$, as the PtG integration has no influence on the sintering process. PCI is partially substituted in the air blast furnace (Case 1) and fully substituted under oxy-fuel operation. As already seen in Figure 23, $CO_2$ injection in the BF (Case 5) implies minimal reduction of total coal consumption (4%). In summary, the PtG integration in an air blast furnace reduces coal consumption by 9%, while OBF technology (Cases 2-4 and 6) allows reductions of 28-33%.

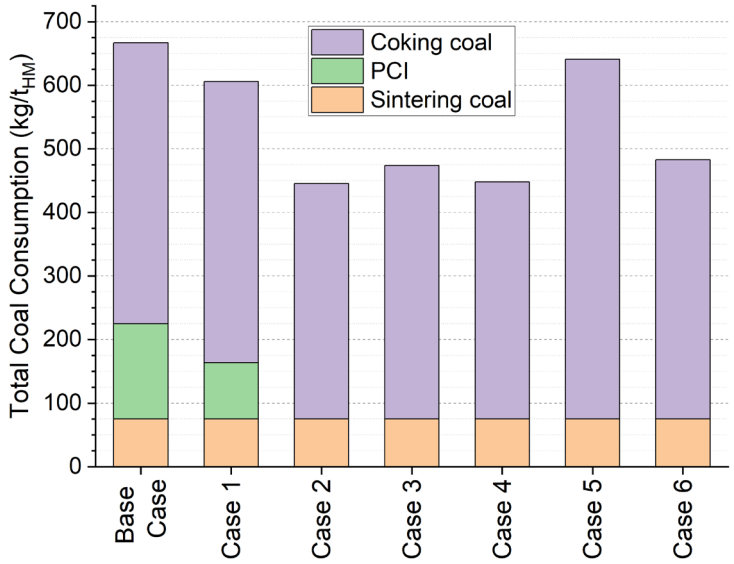


*Figure 24. Total coal consumption broken down according to its final used form, see Figure 21.*

The effects of PtG integration into the composition of BFG are shown in Figure 25. The composition relies heavily on two factors: (i) the injection of air/oxygen and (ii) the injection of $H_2$-rich/CO-rich reducing gas. In the base case and Case 1 (BF+Amine+Meth.), over half of the composition is $N_2$. Conversely, Cases 2-6 show minimal $N_2$ content. Case 6 (OBF+H2) contains the highest $H_2$ content, achieved by

injecting pure $H_2$ into the BF, followed by Cases 2 (OBF+Amine+Meth.) and 4 (OBF+Meth.), which use SNG injection. The combination of low SNG injection and increased TGR in Case 3 and the $CO_2$ injection in Case 5 results in the lower $H_2$ content.

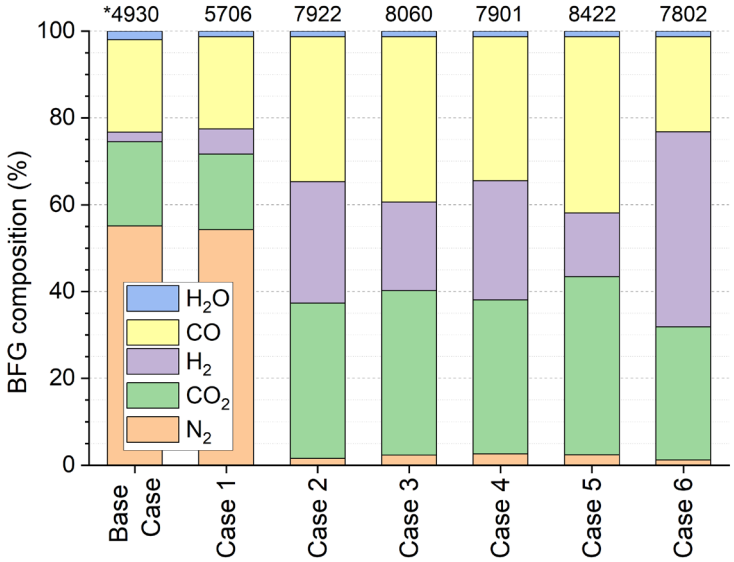


*Figure 25. Blast furnace gas composition (vol%) for the cases of Figure 21.*
**Figures on top of the composition bars represent the BFG energy content in MJ/$t_{HM}$.*

The energy content of the BFG, indicated at the top of Figure 25, takes into account both the lower heating value (LHV) of the gas (MJ/$kg_{BFG}$) and the mass flow rate ($kg_{BFG}/t_{HM}$), providing the energy content in MJ/$t_{HM}$. Higher energy content is achieved for OBF due to the almost absence of $N_2$ and the increased injection of gaseous reducing agents, nearly doubling the values from the base case. These values are in accordance with the literature, specifically Pistorius et al. [108] reported similar amounts of NG resulting in 7000–8000 MJ/$t_{HM}$.

### 4.2.4. Technical and environmental indicators

Specific indicators related to energy penalty, PEM capacity, sold gases and $CO_2$ emissions are here presented and compared to assess the viability of the proposed low-carbon concepts. General definitions were explained in Section 2.3, while details for each simulated case are further discussed in papers iv-vii (Annex E).

Regarding PEM electrolyser, specific installed capacity in MW/($t_{HM}$/h) is represented in Figure 26 for the simulated cases. The corresponding net PEM sizes are easily obtained by multiplying those specific values by the hot metal production, for example 320 $t_{HM}$/h in the present work. It is noticed that higher reducing gas injection leads to larger installed capacity. Specifically, PEM size decreases when (i) co-injecting TGR with SNG, (ii) methanizing BFG, and (iii) using a low $H_2$:$CO_2$ ratio in the methanation stage. In agreement with the data of Figure 23, Case 1 (BF+Amine+Meth.) requires the smallest PEM size because lower SNG mass flow is needed with respect to the other cases. Conversely, the largest PEM size is obtained in Case 2 (OBF+Amine+Meth.) due to the substantial $CO_2$ quantities to be methanized. On the contrary, Case 3 (OBF+Amine+Meth.+TGR) requires barely half the electrolyser power of Case 2 despite

methanizing $CO_2$, due to the co-injection of large amounts of TGR, reducing SNG requirements. In Case 4 (OBF+Meth.) and Case 5 (OBF+Meth.+$CO_2$), methanization of BFG, containing CO and $H_2$, significantly reduces the demand for $H_2$. Specifically, Case 4 uses an $H_2$:$CO_2$ ratio of 4, while Case 5 uses a ratio of 2.5, explaining the lower PEM size in the latter. Finally, the direct injection of the $H_2$ produced by the PEM in Case 6 (OBF+$H_2$) results in a relatively high electrolyser size, similar to that in Case 4.

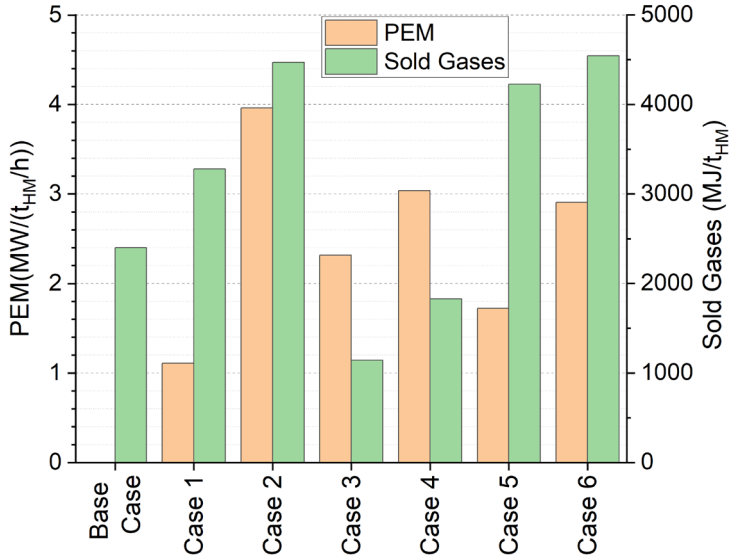


*Figure 26. PEM size and sold gases for the cases of Figure 21.*

Regarding oxygen flows, in Case 1, $O_2$ produced by the PEM is entirely sold to nearby industries, while in Cases 2-6, is used in the oxygen blast furnace which requires large quantities. In Cases 2, 4, and 6, where the electrolyser is large enough, the air separation unit is not required. However, in Cases 3 and 5, a small ASU, producing 63 and 179 $kg_{O2}/t_{HM}$, respectively, is necessary. These oxygen flows are relatively small when compared to the oxygen consumed by the OBF, ranging from 268 to 437 $kg_{O2}/t_{HM}$.

The PEM electricity consumption accounts for 78-92% of the total electricity consumption depending on the case, creating an almost linear dependency between the size of the electrolyser and the total electricity consumption. If an ASU is required it will increase the total electricity consumption, but its consumption is almost negligible with regards to the PEM consumption, barely affecting the results. The electricity consumption is 4965 $MJ/t_{HM}$ for the air blast furnace (Case 1), and between 7925 and 15597 $MJ/t_{HM}$ for the oxygen blast furnaces (Cases 2-6). These figures are higher than the 950 $MJ/t_{HM}$ in the base case and will be determinant in the economic analysis.

Regarding the gases sold to nearby industries, including BFG, BOFG, and COG, the specific energy content is calculated according to the LHV in order to be quoted later as fuel. It is 2400 $MJ/t_{HM}$ in the base case (Figure 26) and decreases to 1143 $MJ/t_{HM}$ and 1828 $MJ/t_{HM}$ in Cases 3 and 4, where BFG is either used as TGR or directly in the methanation stage. Despite the use of BFG in the methanation stage in Case 5, the energy of the sold gases increases up to 4227 $MJ/t_{HM}$ due to the higher LHV of BFG, a result of increased coke consumption in the BF. In Cases 1 and 2, where only $CO_2$ is used in the methanation stage or in Case 6 with no methanation, the energy of sold gases increase to values ranging from 3278 $MJ/t_{HM}$ to 4542 $MJ/t_{HM}$. Ideally, lower levels of sold

gases are desirable, as this indicates higher plant efficiency. Selling a significant amount of gases means the sale of expensive $H_2$ produced by the electrolysis at a lower price. According to Figure 26, the best option to have low levels of sold gases is to combine Power to Gas with Top Gas Recycling (Case 3).

The $CO_2$ emissions and the $CO_2$ recycled in internal loops are compared in Figure 27. The integration of PtG into an air blast furnace (Case 1) results in a 9% reduction of $CO_2$ emissions compared to the base case (1943 $kg_{CO2}/t_{HM}$). For PtG integration with OBF via SNG injection (Cases 2 – OBF+Amine+Meth. and 4 – OBF+Meth.), the $CO_2$ emission reduction is approximately 34%, the highest among the cases. Slightly lower reductions, around 29%, are observed when using TGR (Case 3) or direct $H_2$ injection (Case 6). If $CO_2$ is injected into the blast furnace, as in Case 5 (OBF+Meth.+$CO_2$), the emission reduction is minimal, only 5%. This can be attributed to the coke rate, where higher carbon input as coke leads to increased carbon output in the form of $CO_2$ emissions. Table 16 breaks down the recycling of $CO_2$ emissions through PtG, TGR, or preheat gas. Only cases with OBF have pre-heating gas, and only Case 3 incorporates TGR. From the comparison with the final $CO_2$ emissions to the atmosphere, the importance of maintaining a closed carbon loop is emphasised.

Previous studies have reported $CO_2$ emissions ranging from 868 to 1180 $kg_{CO2}/t_{HM}$ in BF-TGR concepts [109], [110]. In comparison, the $CO_2$ emissions from the OBF-PtG concepts of the present study are lower, ranging from 738 to 833 $kg_{CO2}/t_{HM}$ (not to be confused with the total emissions of the entire I&S industry, 1279 – 1387 $kg_{CO2}/t_{HM}$ in Figure 27). Concerning BF emissions alone, the TGR setup shows higher $CO_2$ flow rates, but a significant portion should be geologically stored (300-700 $kg_{CO2}/t_{HM}$). Therefore, the environmental impact of the TGR configuration depends on the availability of storage sites.

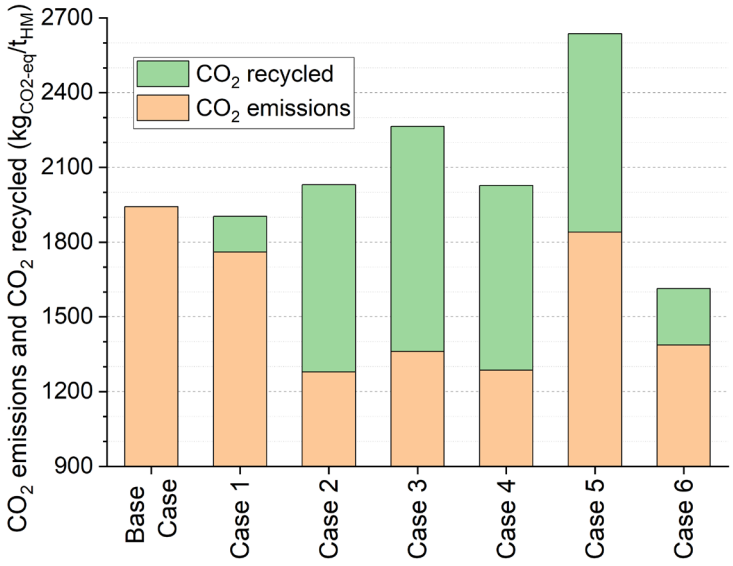


*Figure 27. Total $CO_2$ emissions and $CO_2$ recycled in PtG, pre-heating gas, and TGR.*

*Table 16. Breakdown of $CO_2$ recycling.*

| Case | $CO_2$ recycled | $CO_2$ recycled - PtG | | $CO_2$ recycled - TGR | | $CO_2$ recycled – Preheat | |
|---|---|---|---|---|---|---|---|
| | $kg_{CO2}/t_{HM}$ | $kg_{CO2}/t_{HM}$ | % | $kg_{CO2}/t_{HM}$ | % | $kg_{CO2}/t_{HM}$ | % |
| Base | 0.0 | 0.0 | - | 0.0 | - | 0.0 | - |
| Case 1 | 143.6 | 143.6 | 100 | 0.0 | 0 | 0.0 | 0 |
| Case 2 | 751.4 | 513.2 | 68 | 0.0 | 0 | 238.2 | 32 |
| Case 3 | 902.8 | 298.8 | 33 | 364.6 | 40 | 239.3 | 27 |
| Case 4 | 740.8 | 506.3 | 68 | 0.0 | 0 | 234.5 | 32 |
| Case 5 | 796.0 | 491.0 | 62 | 0.0 | 0 | 305.0 | 38 |
| Case 6 | 227.0 | 0.0 | 0 | 0.0 | 0 | 227.0 | 100 |

The specific energy penalty (Figure 28) is calculated as the net energy consumed per kilogram of $CO_2$ avoided in order to later quantify the related costs. There are mainly two influential magnitudes: electricity consumption and avoided $CO_2$ emissions. As a result, the energy penalty is relatively high if electrolysis is involved, particularly when compared to amine carbon capture technology (3 – 6 $MJ/t_{CO2}$ [111]). Case 1 (BF+Amine+Meth.) and Case 2 (OBF+Amine+Meth.) involve similar energy penalty (16 and 17 $MJ/t_{CO2}$, respectively), as they both perform $CO_2$ methanation. The lowest energy penalty among the PtG concepts (12 $MJ/t_{CO2}$) is presented by Case 3 (OBF+Amine+Meth.+TGR) because it requires least amount of SNG due to TGR injection, resulting in the smallest PEM capacity. In Case 4 (OBF+Meth.) and Case 5 (OBF+Meth.+$CO_2$), the BFG to be methanized already contains CO and $H_2$, reducing the PEM size, especially in Case 5. However, while Case 4 achieves significant $CO_2$ avoidance (14 $MJ/t_{CO2}$), Case 5 barely reduces $CO_2$ emissions, resulting in the highest specific energy penalty (60 $MJ/t_{CO2}$). In Finally, in absence of methanation (Case 6), the energy penalty is 14 $MJ/t_{CO2}$. In summary, decreasing the PEM size through BFG methanation or TGR gas injection leads to lower penalties, while injecting $CO_2$ into the BF performs poorly significantly increasing the energy penalty.

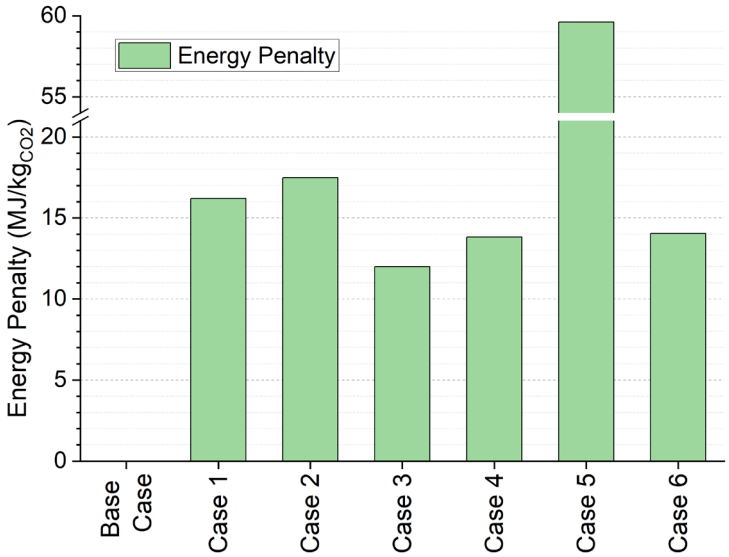


*Figure 28. Energy penalty in the cases of Figure 21.*

### 4.2.5. Economic analysis

The economic analysis is focused in KPIs as CAPEX, OPEX, Incomes and specific carbon avoidance costs, as it was explained in Section 2.3. The final objective is to assess the economic viability of the proposed low-carbon concepts according to the specific implementation cost (€/$t_{HRC}$). The analysis assumed a loan amortization period of 20 years, PtG system operating for 8000 hours per year [47], carbon tax value of 84.28 €/$t_{CO2}$ [48], and renewable electricity price of 77 €/MWh. The initial capital expenditure (CAPEX) for the PtG integration includes amine, electrolysis and methanation plants, the heat exchangers network, the BF retrofitting, and other direct and indirect costs. The annual operational expenditure (OPEX) is composed of the catalyst renovation, the water consumed by the electrolyser, the amine renovation, the purchased electricity and the operation and maintenance (O&M). The annual incomes are the saved $CO_2$ taxes and coal, and the sold oxygen and steel gases (BFG, BOFG and COG). The specific costs, in €/$t_{CO2}$ and €/$t_{HRC}$, are calculated using Eq. (5) and Eq. (6) defined in Section 2.3.

The PEM constitutes the largest item of the CAPEX, accounting for 35% to 43% of the total cost. Purchased electricity is the predominant contributor to the OPEX, making up 94% to 95% of the expenses. The primary source of revenue comes from $CO_2$ taxes, which range from 33% to 67%. Main economic parameters for Cases 1-6 are gathered in Table 17, while specific $CO_2$ avoidance cost and implementation cost are compared in Figure 29.

*Table 17. Economic KPIs* [46], [73]–[75].

| **Case Study** | **CAPEX** | **OPEX** | **INCOMES** | **$CO_2$ Avoid. Cost** | **Specific Impl. Cost** |
|---|---|---|---|---|---|
| | M€ | M€/y | M€/y | €/$t_{CO2}$ | €/$t_{HRC}$ |
| **Case 1** BF+Amine+Meth. | 268 | 221 | 102 | 283 | 52 |
| **Case 2** OBF+Amine+Meth. | 1167 | 835 | 294 | 352 | 233 |
| **Case 3** OBF+Amine+Meth.+TGR | 784 | 490 | 195 | 216 | 130 |
| **Case 4** OBF+Meth. | 931 | 640 | 248 | 260 | 171 |
| **Case 5** OBF+Meth.+CO2 | 635 | 397 | 30 | 1518 | 155 |
| **Case 6** OBF+H2 | 870 | 594 | 288 | 245 | 136 |

The lowest specific implementation cost is obtained for Case 1 (BF+Amine+Meth.), in agreement with the lowest requirement of SNG (Figure 23) and, consequently, the smallest PEM power (Figure 26). Among the remaining cases with OBFs, Case 3 (OBF+Amine+Meth.+TGR) boasts the lowest specific implementation cost and $CO_2$ avoidance cost (€/$t_{CO2}$) due to its smaller electrolyser and high $CO_2$ avoidance rate. Conversely, Case 5 (OBF+Meth.+$CO_2$), characterized by a very low $CO_2$ avoidance rate, experiences a significant increase in the $CO_2$ avoidance cost, exceeding 1500 €/$t_{CO2}$. In summary, combining PtG technology with top gas recycling yields the most favourable cost outcomes, making it a recommended choice. However, the direct $H_2$ injection case is also recommended due to its implementation simplicity (no loopings or recycling).

It is worth noting that the steel price in 2022 was around 660–1400 €/$t_{HRC}$ [112], so the specific implementation cost of the proposed concepts represents a 4–35% increase in the actual steel price, depending on the case (9-20% increase for Case 3). A recent study conducted by Subraveti et al. [113] analysed CCS costs in a steel plant (47% capture with a 13% increase in cost), concluding that, for instance, the cost of a bridge increases only 1%. This implies that the costs incurred for implementing the PtG system in steelmaking, despite being significant, would have a limited impact on the final product competitiveness.

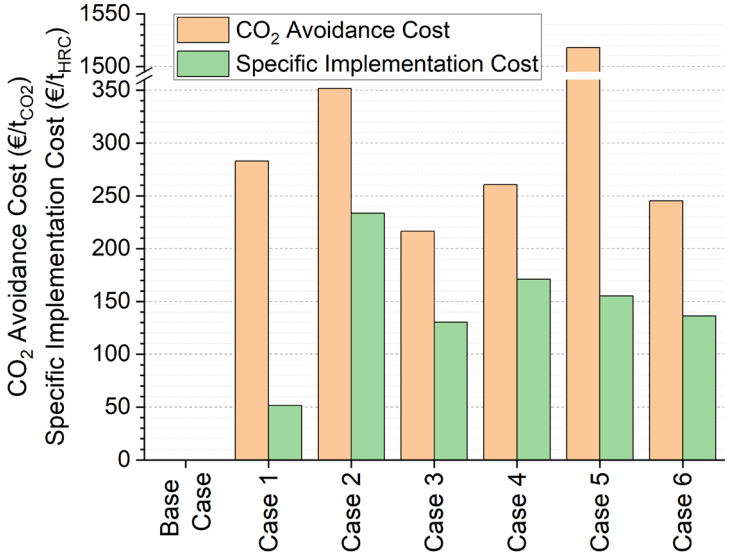


*Figure 29. Specific $CO_2$ avoidance cost and implementation cost. Cases in Figure 21.*

For the Case 3 with lower $CO_2$ avoidance cost, a sensitivity analysis was performed. The $CO_2$ taxes and the electricity price were varied, looking for those combinations that make the PtG-steelmaking integration economically viable (Figure 30). Today, with an electricity price of 77 €/MWh and a $CO_2$ tax of 84 €/$t_{CO2}$, the specific CC cost is 216 €/$t_{CO2}$. Negative costs (i.e., actual benefits) could be achieved under certain scenarios. For the limit of specific CC cost of 0 €/$t_{CO2}$, a maximum electricity price of 21 €/MWh should be paid, or a minimum $CO_2$ tax of 300 €/$t_{CO2}$ should apply. However, these prices or taxes do not guarantee a profitable investment, since the CAPEX should also be amortized. To amortize CAPEX in 20 years (i.e., total investment pay-back of 20 years), the electricity price should be 18 €/MWh, or the $CO_2$ tax 313 €/$t_{CO2}$, or an intermediate combination of both parameters, resulting in a specific CC cost of -13 €/$t_{CO2}$ or -8 €/$t_{HM}$. With an electricity price of 35 €/MWh (cost of production for wind power [114]), and a $CO_2$ tax of 150 €/$t_{CO2}$, the pay-back is 20 years and the investment would be profitable.

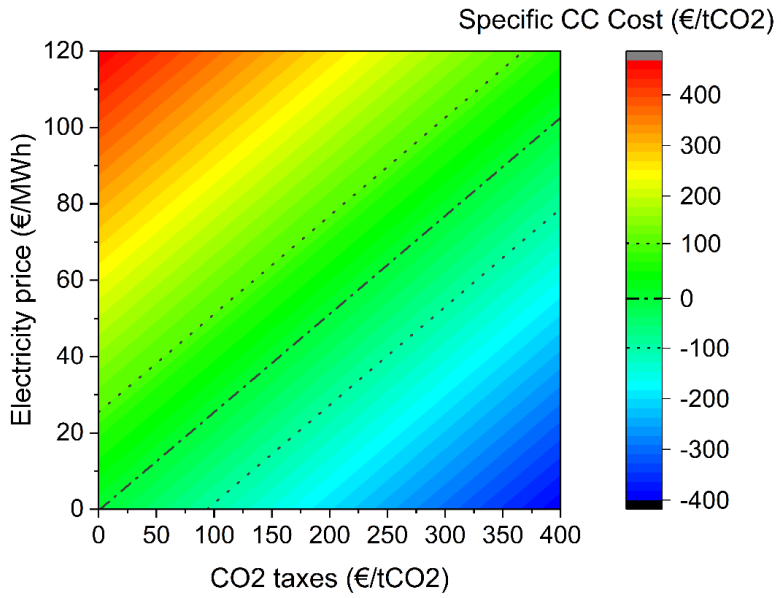


*Figure 30. Specific CC cost in €/$t_{CO2}$ as a function of the $CO_2$ taxes and the electricity price for an OBF with two auxiliary fuel injections (113 $kg_{SNG}/t_{HM}$ and 270 $kg_{TGR}/t_{HM}$), an electrolyser of 741 MW, and an amine scrubbing of 305 $kg_{CO2}/t_{HM}$ (Case 3).*

### 4.2.6. Discussion and conclusions

In this study, various configurations were analysed to assess the feasibility and effectiveness of integrating power to gas and other decarbonization measures into blast furnace operations. Initially, amine carbon capture and $CO_2$ methanation were applied in a conventional blast furnace. Additional technologies, such as top gas recycling, BFG methanation, $CO_2$ recycling, or direct $H_2$ injection, were then layered onto this configuration.

The effectiveness of $CO_2$ reduction in conventional blast furnaces is somewhat limited, primarily due to the constraint of the adiabatic flame temperature. Substituting pure oxygen for air (oxygen blast furnace) alleviates this limitation, enabling larger PtG facilities and thus higher carbon savings. However, this improvement leads to a significant increase in PEM size, energy consumption, and costs. Given that the PEM and its associated electricity usage are primary cost drivers, alternative configurations are explored.

One such configuration is TGR, where clean BFG from the amine scrubbing process is injected into the blast furnace tuyeres. This reduces $H_2$ requirements at the methanation plant, resulting in a decrease in PEM size and sold gases, and achieving lower carbon avoidance costs. Another option is direct BFG methanation, which also reduces $H_2$ requirements, although not to the same extent as TGR. $CO_2$ recycling by adjusting the $H_2$:$CO_2$ ratio in methanation yields poor outcomes due to the significant cooling effect of $CO_2$ on the adiabatic flame temperature.

Simplified configurations, such as direct hydrogen injection into the blast furnace, offer a straightforward solution without looping, yielding favourable results in terms of $CO_2$ savings and costs, but are not optimal compared to other options.

In conclusion, our analysis suggests that the recommended approach is Case 3, which performs at the same time $CO_2$ methanation and top gas recycling in an oxygen blast furnace. In spite of slightly higher emissions compared to some other cases, this configuration, stands out as the most favourable, as it features the lowest sold gases, energy penalty and cost.

## 4.3. Review on PtG in BF-BOF route

The PtG-steelmaking configurations analysed in the previous section apply in situations where $CO_2$ storage is not available and shaft injection in the blast furnace is not considered. If these options are taking into account, other possible configurations can be analysed.

A systematic comparison was conducted with literature data in paper viii (Annex E), encompassing all conceivable PtG configurations. The review was carried out following the methodology presented in Section 2.1 [36]. Two sets of search terms were established: the first set related to blast furnaces and the second set about Power to Gas technologies. A total of 78 entries were obtained in the Web of Knowledge website. Afterwards, only articles presenting applications of any form of Power to Gas on the blast furnace route are finally selected. Articles focusing solely on $CO_2$ emission reduction, fuel consumption reduction, methane production for sale, hydrogen production, or not addressing the blast furnace or carbon recycling through Power to Gas were excluded from the review. This screening process yielded a total of 20 articles.

*Table 18. Classification of approaches to integrate PtG in blast furnace ironmaking.*

| **Criterion** | **Approach** | **Options** |
|---|---|---|
| Combustion regime (2 options) | Air-blown | |
| | Oxy-fuel | |
| Type of top gas recirculation (8 options, Figure 31A) | No recirculation | |
| | Single, located at | Tuyeres |
| | | Shaft |
| | | Upper zone |
| | Double, located at | Tuyeres and shaft |
| | | Tuyeres and upper zone |
| | | Shaft and upper zone |
| | Triple, located at | Tuyeres, shaft and upper zone |
| Type of renewable gas produced (5 options, Figure 31B) | Synthetic natural gas from the methanation of | Pure $CO_2$ from amine scrubbing |
| | | Sweet gas from amine scrubbing |
| | | Blast furnace gas |
| | Hydrogen from electrolysis | |
| | Syngas from $CO_2$ electrolysis | |
| Injection location of the renewable gas (3 options, Figure 31B) | Tuyeres | |
| | Shaft | |
| | Tuyeres and shaft | |

To obtain all the potential integrations, the different approaches that can be followed when integrating PtG are combined. In Table 18 and Figure 31, the different strategies are classified in terms of: (i) combustion regime, (ii) top gas recirculation, (iii) produced renewable gas, and (iv) location of the injection of the renewable gas. TGR may be performed at three different levels: tuyere, shaft or upper zone. Similarly, the renewable gas can be injected in the tuyeres or in the shaft. The possible location of these gases can be seen at the left of Figure 31 (tuyeres, shaft or upper zone). Regarding methanation, the carbon source may be the $CO_2$ diverted from the carbon capture, the $CO_2$-lean gas (sweet gas), or simply the BFG.

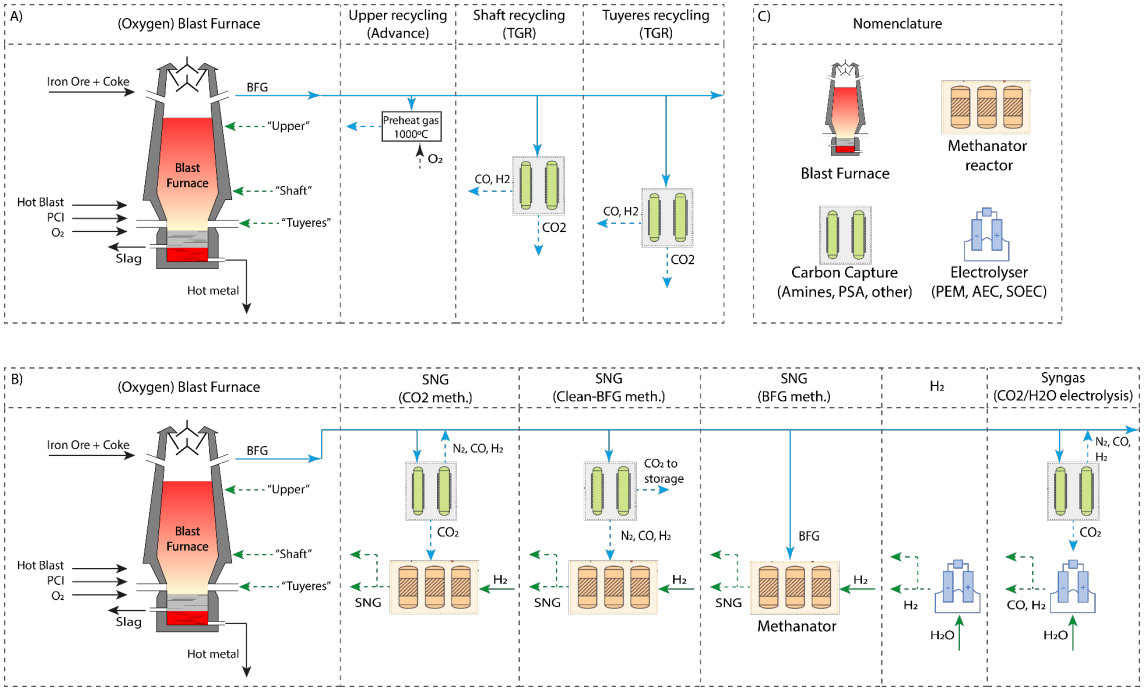


*Figure 31. Summary of the different options for PtG-BF integrations, in terms of A) gas recycling, and B) renewable fuel injection. C) Nomenclature.*

The entire review encompasses a total of 240 integration configurations, resulting from the combination of 2 regimes, 8 top gas recycling methods, 5 renewable gases, and 3 injection locations. Table 19 provides a summary of all these potential integrations in two main blocks, distinguishing between air blown and OBF regimes. Those previously examined in the literature includes the reference, while those not deemed worthwhile due to anticipated poor performance are indicated with *. The type of renewable fuel produced is denoted by A (SNG from pure $CO_2$), B (SNG from sweet gas), C (SNG from BFG), D ($H_2$), and E (Syngas from $CO_2$ electrolysis).

Configurations with anticipated poor performance often involve injecting significant amounts of $N_2$ into the blast furnace, leading to notable reductions in the adiabatic flame temperature and low fossil fuel replacement ratios. These issues primarily occur in air-blown regimes when top gas is recycled or when methanation consumes BFG without prior separation. To mitigate these problems, oxy-fuel regimes

are recommended, as they result in lower $N_2$ concentrations in the BFG, typically around 1% - 2%. As for the $N_2$, the recirculation of $CO_2$ is also discouraged for the same reasons, when methanation operates under sub-stoichiometric ratios ($H_2$:$CO_2$ < 4) [73], $CO_2$ electrolysis has low conversion rates [115], or top gas recycling occurs without prior carbon capture to remove $CO_2$ from the BFG [80]. Please note that none of these three possibilities are considered in the review.

*Table 19. Summary of all potential PtG integrations in BF ironmaking, according to the renewable fuel produced: A (SNG from pure $CO_2$), B (SNG from sweet gas), C (SNG from BFG), D ($H_2$), and E (Syngas from $CO_2$ electrolysis). (*) Poor performance expected a priori.*

| **Combustion regime: Air-blown** | | | |
|---|---|---|---|
| **Type of top gas recirculation** | **Injection location of the renewable gas:** | | |
| | **Tuyeres** | **Shaft** | **Tuyeres & Shaft** |
| No recirculation | A [109][46], B* [109], C* [109], D [109][116][117], E [115][118] | A, B*, C*, D, E | A, B*, C*, D, E |
| Single | | | |
| Tuyeres | A*, B*, C*, D*, E* | A*, B*, C*, D*, E* | A*, B*, C*, D*, E* |
| Shaft | A*, B*, C*, D*, E* | A*, B*, C*, D*, E* | A*, B*, C*, D*, E* [119] |
| Upper | A*, B*, C*, D*, E* | A*, B*, C*, D*, E* | A*, B*, C*, D*, E* |
| Double | | | |
| Tuyeres & shaft | A*, B*, C*, D*, E* | A*, B*, C*, D*, E* | A*, B*, C*, D*, E* |
| Tuyeres & upper | A*, B*, C*, D*, E* | A*, B*, C*, D*, E* | A*, B*, C*, D*, E* |
| Shaft & upper | A*, B*, C*, D*, E* | A*, B*, C*, D*, E* | A*, B*, C*, D*, E* |
| Triple | | | |
| Tuyeres & shaft & upper | A*, B*, C*, D*, E* | A*, B*, C*, D*, E* | A*, B*, C*, D*, E* |
| **Combustion regime: Oxy-fuel** | | | |
| **Type of top gas recirculation** | **Injection location of the renewable gas:** | | |
| | **Tuyeres** | **Shaft** | **Tuyeres & Shaft** |
| No recirculation | A, B, C, D, E | A, B, C, D, E | A, B, C, D, E |
| Single | | | |
| Tuyeres | A [109][92], B [109], C [109][80], D [109], E | A, B, C, D, E | A, B, C, D, E |
| Shaft | A, B, C, D, E | A, B, C, D, E | A, B, C, D, E |
| Upper | A [75], B, C [73], D [73], E | A, B, C, D, E | A, B, C, D, E |
| Double | | | |
| Tuyeres & shaft | A, B, C, D, E | A, B, C, D, E | A, B, C, D, E |
| Tuyeres & upper | A [74], B, C, D, E | A, B, C, D, E | A, B, C, D, E |
| Shaft & upper | A, B, C, D, E | A, B, C, D, E | A, B, C, D, E |
| Triple | | | |
| Tuyeres & shaft & upper | A, B, C, D, E | A, B, C, D, E | A, B, C, D, E |

### 4.3.1. Discussion and conclusions

Several KPIs were compared for the different PtG configurations, among of which the most relevant are fuel consumption, $CO_2$ emissions, surplus steel gases, energy penalty, electrolyser size and cost, as defined in Section 2.3.

In terms of fuel consumption, oxygen blast furnaces exhibit 18% reduction in total coal consumption compared to air-blown furnaces. Moreover, upper recycling configurations further enhance this reduction by injecting higher volumes of synthetic gas. Among these configurations, the use of SNG from either $CO_2$ or BFG methanation achieves the lowest total coal consumption at 370 kg/$t_{HM}$. Concerning $CO_2$ emissions, PtG systems offer limited benefits in reducing $CO_2$ emissions for air-blown blast furnaces, resulting in specific $CO_2$ emissions consistently above 1000 $kg_{CO2}/t_{HM}$ in the BF. However, further emissions reductions can be realized by implementing this technology in OBFs, with emissions dropping below 800 $kg_{CO2}/t_{HM}$, especially when underground storage is available, resulting in net emissions of 435 $kg_{CO2}/t_{HM}$ in the BF.

In air-blown blast furnaces utilizing PtG, the surplus steel gases contain 27% more energy compared to conventional blast furnaces. Oxygen blast furnace configurations that combine tuyere gas recycling with PtG minimize energy wastage while remaining self-sufficient. Excess energy in these OBFs varies from 267 MJ/$t_{HM}$ to 4542 MJ/$t_{HM}$. The energy penalty typically falls within the range of 10 to 20 MJ/$t_{HM}$, with oxygen blast furnaces generally demonstrating better performance on average. The most efficient configuration involves the simultaneous use of both tuyere and upper recycling injections.

The sizes of electrolysis units, measured in specific power capacity, are primarily influenced by the $H_2$ content in the BFG. This, in turn, is somewhat affected by the chosen configuration. In air-blown BF, electrolyser sizes typically range from 0.2 to 2.2 MW/($t_{HM}$/h), while for OBFs range from 1.0 to 4.0 MW/($t_{HM}$/h). A significant advantage of integrating electrolysis is the availability of $O_2$ to replace the ASU, which becomes unnecessary in many integration scenarios. Only OBFs with TGR in the tuyere still require an ASU, although the size decreases to an average of 145 $kg_{O2}/t_{HM}$, compared to the 250-350 $kg_{O2}/t_{HM}$ of an OBF without PtG.

Regarding economic costs, the analysis presented in this thesis (Chapters 3-4) is pioneer, as no other studies have explored this aspect. Depending on the approach (air-blown BF, oxygen BF, or oxygen BF with $CO_2$ storage), the most feasible configurations among the studied in literature and this thesis are:

- Air-blown blast furnace: Utilizing $H_2$ as a reducing agent injected through the tuyeres, produced with a PEM electrolyser, and without TGR. This configuration results in $CO_2$ emissions of 1060 $kg_{CO2}/t_{HM}$.
- Oxygen blast furnace: Employing SNG from BFG methanation as a reducing agent injected through the tuyeres, $H_2$ produced with a PEM electrolyser, and featuring TGR in the upper part (advanced OBF). $CO_2$ emissions to the atmosphere amount to 747 $kg_{CO2}/t_{HM}$. This configuration corresponds to Case 4 in the present thesis (Section 4.2).
- Oxygen blast furnace combined with geological storage: Using SNG from sweet-BFG methanation as a reducing agent injected through the tuyeres, $H_2$ produced by electrolysis, and implementing TGR in the tuyeres. $CO_2$ emissions to the atmosphere and to storage amount to 435 $kg_{CO2}/t_{HM}$ and 490 $kg_{CO2}/t_{HM}$, respectively.

There remains considerable potential for further investigation to assess the full capabilities of these technologies in reducing carbon emissions in the iron and steel industry. Future studies should validate technologies that have demonstrated promising outcomes, notably advanced oxygen blast furnaces with upper recycling. Additionally, addressing the current high costs of these systems and prioritizing efforts to reduce the energy penalty associated with green hydrogen production are essential steps forward.

# 5. Modelling PtG systems from experimental tests

In order to achieve a better approach to real systems, models adjusted with experimental data have been developed for the most critical components of the PtG systems, methanation and carbon capture. The modelling of a methanation plant (TRL 4), where the process is analysed based on empirical data, is discussed in Section 5.1. The modelling of an amine scrubbing pilot plant (TRL 6), where the efficiency and the energy consumption of the system are validated using experimental data, is discussed in Section 5.2.

## 5.1. Modelling methanation from experiments (TRL 4)

The primary novelty in this study lies in the comparison between nickel and ruthenium as catalysts on a larger scale, along with the comprehensive performance assessment in the 1 kW fixed bed reactor described in Section 2.4.1. This entails the development of kinetic models tailored for this scale (paper ix, Annex E). This section is structured into distinct segments, covering experimental tests, catalyst performance evaluation, and the design and modelling in Aspen Plus of a methanation plant to provide SNG with 95% methane purity.

This study employs two spherical catalysts, with a diameter of 2.0-2.2 mm, distinguished by their active phase: Ni and Ru. Both catalysts are $CeO_2$-promoted and supported on γ-alumina spheres. The selection of catalyst composition has been guided by prior research on $CeO_2$-promoted Ni and Ru catalysts [120]. The samples of Ru and Ni catalysts were developed and characterized by the "Instituto de Investigación de la Energía de Cataluña" (IREC), involving Scanning Electron Microscopy (SEM) for morphology, Energy Dispersive X-ray (EDX) for elemental composition, Helium Pycnometry for true densities, Hydrogen Temperature Programmed Reduction ($H_2$-TPR) to assess reducibility, Nitrogen Physisorption for textural analysis, X-ray Diffraction (XRD) for crystalline structure, and CO-Chemisorption to determine metal dispersion [121]. These analyses provide critical insights into the catalysts' physical and chemical properties, enhancing our comprehension of their behaviour and performance. IREC's findings favoured the Ni-based catalyst, which exhibits superior physicochemical properties in the studied reactor, with a lower decrease in surface area and metal dispersion compared to the Ru-based catalyst.

### 5.1.1. Experimental tests

The experimental plan (see Figure 32) is designed to assess the performance of these catalysts under wide range of steady-state conditions, including operating temperatures (250-450 °C), gas hourly space velocities (GHSV, Eq. (2)) ranging from 8000 to 16000 $h^{-1}$, molar $H_2$:$CO_2$ ratios from 3.5 to 5.5, and activation temperatures (200-400 °C). The experiments are conducted at a pressure of 1 bar, with the base case set at 350

°C, a GHSV of 10000 $h^{-1}$, and an $H_2$:$CO_2$ ratio of 4. The experimental design comprises 13 independent points for each catalyst, and each experiment is repeated twice (at different activation temperatures), resulting in a total of 52 measured data points. The activation of the catalyst is carried out by passing a pure hydrogen flowrate of 0.015 kg/h during 3 h at 200-400 °C. The experimental values obtained from the tests have been utilized to formulate a new kinetic model in Aspen Plus [121].

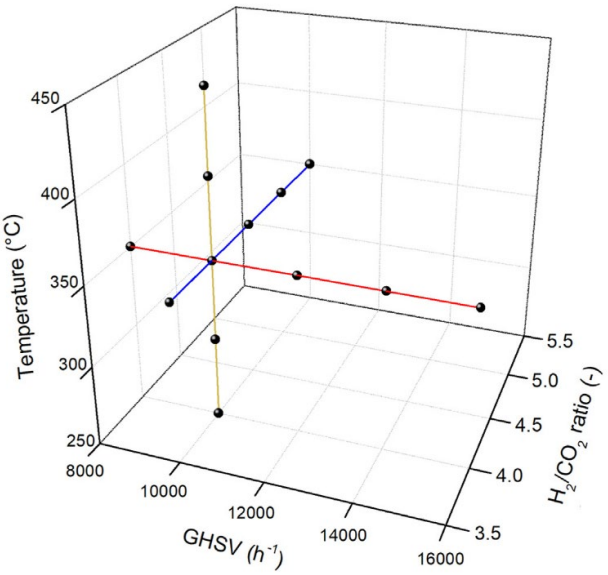


*Figure 32. Experimental design to evaluate catalyst performance. Sensitivity analysis on temperature (yellow), GHSV (red) and $H_2$:$CO_2$ ratio (blue).*

### 5.1.2. Performance of the catalysts

The impact of activation temperature is examined for both catalysts. Across most points studied, similar $CO_2$ conversion rates are observed regardless of the temperature. Consequently, it can be concluded that within the 200-300 °C range, there is no notable influence of reduction temperature on the Ru-based catalyst. In the case of the Ni-based catalyst (activated at 300 °C and 400 °C), improved activity is observed for two operating points corresponding to conditions far from equilibrium, while at high $CO_2$ conversions, activation temperature has no discernible effect. Given the negligible variation in $CO_2$ conversion with the activation procedure in most cases, an intermediate value of 300 °C is chosen for the reduction protocol during the catalyst performance comparison.

The influence of methanation temperature on $CO_2$ conversion is assessed using experimental tests with both catalysts activated at 300 °C, conducted under atmospheric pressure, a gas hourly space velocity of 10000 $h^{-1}$, and an $H_2$:$CO_2$ ratio of 4. The results depicted in Figure 33 follow the typical curve of $CO_2$ methanation conversion versus temperature, consistent with predictions from the kinetic model (paper ix, Annex E). Ni-based catalyst exhibits higher conversion rates for every tested temperature, with similar conversions achieved at temperatures above 350 °C. According to the kinetic model, the activity of the Ni-based catalyst is approximately three times higher than that

of the Ru-based catalyst at 275 °C, while their activities are nearly identical at temperatures exceeding 375 °C due to reaching equilibrium.

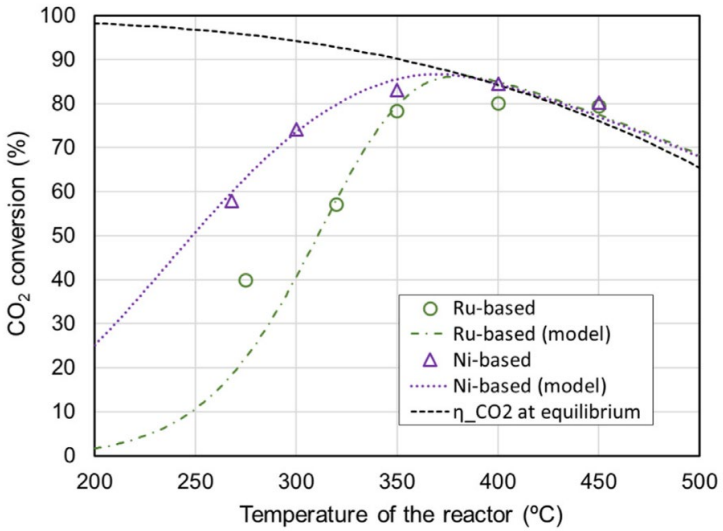


*Figure 33. $CO_2$ conversion at the outlet vs. isothermal temperature of reactor. Each point corresponds to one steady state operation. GHSV = 10000$h^{-1}$; $H_2$:$CO_2$ ratio = 4; P = 1 atm.*

The impact of gas flowrate is also assessed through experimental tests conducted with both catalysts activated at 300 °C, under atmospheric pressure, a constant temperature of 350 °C, and an $H_2$:$CO_2$ ratio of 4. Ni-based catalyst consistently outperformed the Ru-based catalyst across all tested GHSV ranging from 8000 to 16000 $h^{-1}$. Both catalysts exhibit a coherent and analogous trend, with conversion decreasing as gas flowrate through the reactor increases (Figure 34). Notably, the carbon conversion achieved with the Ni-based catalyst at double the flowrate (16000 $h^{-1}$) is similar to that attained with the Ru-based catalyst at 8000 $h^{-1}$. Consequently, the Ni-based catalyst demonstrated the capability to handle twice gas flowrate without affecting carbon conversion, with a wider disparity between conversions observed at higher GHSV.

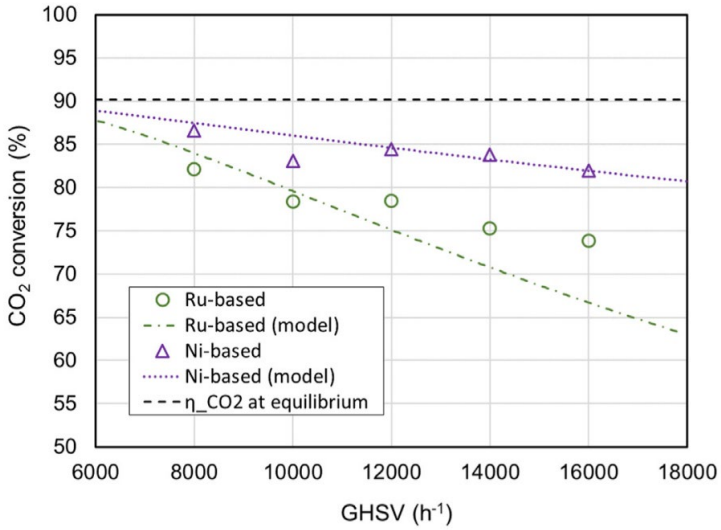


*Figure 34. $CO_2$ conversion at the outlet vs. GHSV. Each point corresponds to one steady state operation. T = 350 °C; $H_2$:$CO_2$ ratio = 4; P = 1 atm.*

Lastly, the impact of increasing the $H_2$:$CO_2$ ratio is analysed through experimental tests conducted under atmospheric pressure, a constant temperature of 350 °C, and a gas hourly space velocity of 10000 $h^{-1}$. Once again, the Ni-based catalyst outperformed the Ru-based catalyst, exhibiting a linear increase in carbon conversion with the $H_2$:$CO_2$ ratio until reaching equilibrium conditions. The Ni-based catalyst has approximately 6%-8% higher activity than the Ru-based catalyst within $H_2$:$CO_2$ ratios ranging from 3.5 to 5 (see Figure 35).

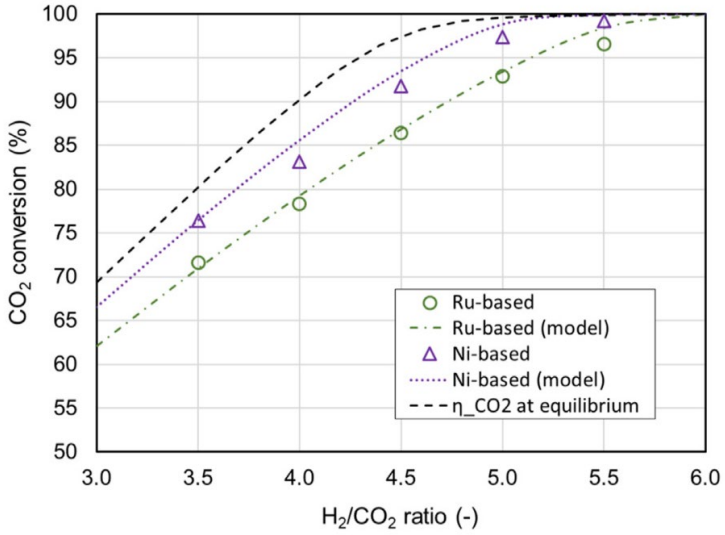


*Figure 35. $CO_2$ conversion at the outlet vs. $H_2$:$CO_2$ ratio at the inlet. Each point corresponds to one steady state operation. GHSV = 10000 $h^{-1}$; T = 350 °C; P = 1 atm.*

### 5.1.3. Aspen Plus model

A kinetic model is developed for each catalyst using the experimental data from this study [121]. The model is based in the equation proposed by Falbo et al. [122], which is a modification of the model reported by Lunde et al. [123]. The mean squared error (MSE) is minimized by using the Powell Method [60], resulting in MSE of 7.4% for the Ru-based catalyst and 1.4% for the Ni-based catalyst. This adjusted kinetic model is implemented in Aspen Plus® to evaluate a methanation plant targeting a 95 vol% methane content in the synthetic natural gas [82]. A standard reactor configuration in series with intermediate condensers is adopted (Figure 36).

The simulation employs the RKSMHV2 property method provided by Aspen Plus. An optimization procedure utilizing the Sequential Quadratic Programming (SQP) method is followed to minimize the required catalyst quantity while ensuring a 95 vol% $CH_4$ concentration in the final gas. This optimization involves varying reactor temperatures, catalyst masses, and the number of reactors (2, 3, or 4 reactors in series). Technical constrains of typical methanation plants (GHSV ≤ 5000 $h^{-1}$ and T ≥ 300 °C [9]) are also considered. For the process design, we assume the use of Ni-based catalysts, recognized in the experimental tests as the optimal choice.

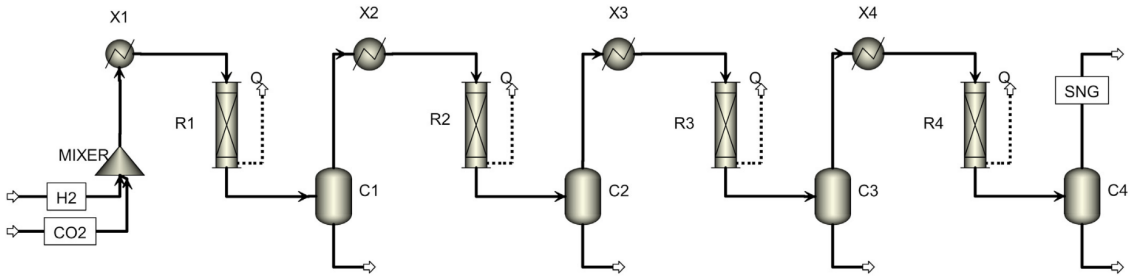


*Figure 36. Process flow diagram for the methanation plant in Aspen Plus (4-reactor configuration).*

When considering 2 reactors in series, this configuration is feasible only if we disregard technical constraints (GHSV and T). With 3 reactors in series, a substantial reduction in catalyst mass is observed, requiring nearly a quarter of the catalysts needed for 2 reactors. However, when using 4 reactors in series, only an additional 10% reduction in catalyst mass is achieved. This marginal reduction may not justify the added cost of a fourth reactor and increased energy consumption for preheating. In terms of plant design, the 3-reactor configuration emerges as the most suitable choice.

### 5.1.4. Conclusions

The Ni-based catalyst exhibited higher $CO_2$ conversion rates under all tested conditions in agreement with the literature. Specifically, the activity of the Ni-based catalyst was three times greater than that of the Ru-based catalyst at 275 °C, while at temperatures exceeding 375 °C, the activities were nearly equivalent due to reaching equilibrium.

Regarding plant design, various potential configurations of a methanation plant were assessed in Aspen Plus for the Ni-based catalyst. It was determined that the three-reactor configuration was the most suitable design, due its lower catalyst requirement and fewer reactors.

## 5.2. Amine scrubbing modelling from experiments (TRL 6)

This section delves into the critical aspect of carbon capture (CC) with amine scrubbing. In particular, the experiments performed in the pilot facility installed in voestalpine I&S plant (Section 2.4.2) serve for the development and validation of an Aspen Plus model.

### 5.2.1. Experimental tests

The pilot plant (Figure 11) captures $CO_2$ from the flue gas stream originated in the power plant of the I&S plant. The CC facility employs as solvent a solution of monoethanolamine (MEA) consisting of 30 wt% MEA and 70 wt% water. The solvent circulates continuously in a closed loop between the absorber and the desorber (stripper).

The primary objective of the experimental plan is to determine the specific energy required by the carbon capture system (MJ/$kg_{CO2}$). To achieve this, the carbon capture rate is fixed at 90%, and the flue gas flow rate and composition remain constant

at 70 $m^3$/h and 25% $CO_2$, respectively. To identify the optimal operating conditions that minimize the specific energy requirement, the L/G ratio and the stripper pressure are varied.

The experimental data registered from the pilot plant are used to adjust and validate the Aspen model presented in the following section. The registered data comprised mass flow rates, temperatures, pressures and reboiler duty.

### 5.2.2. Aspen Plus model

The carbon capture system is modelled and simulated using Aspen Plus® software, employing the ENRTL-RK property method for calculations. The main equipment of the pilot plant is simulated with respective Aspen model blocks. To streamline the model and maintain simplicity, certain auxiliary components, including the quench, blower, and pre-scrubber, were omitted from the simulation. The input parameters for this model encompass the mass flow rate, composition, and temperature of the flue gas as it enters the absorber. The Aspen flowsheet is shown in Figure 37.

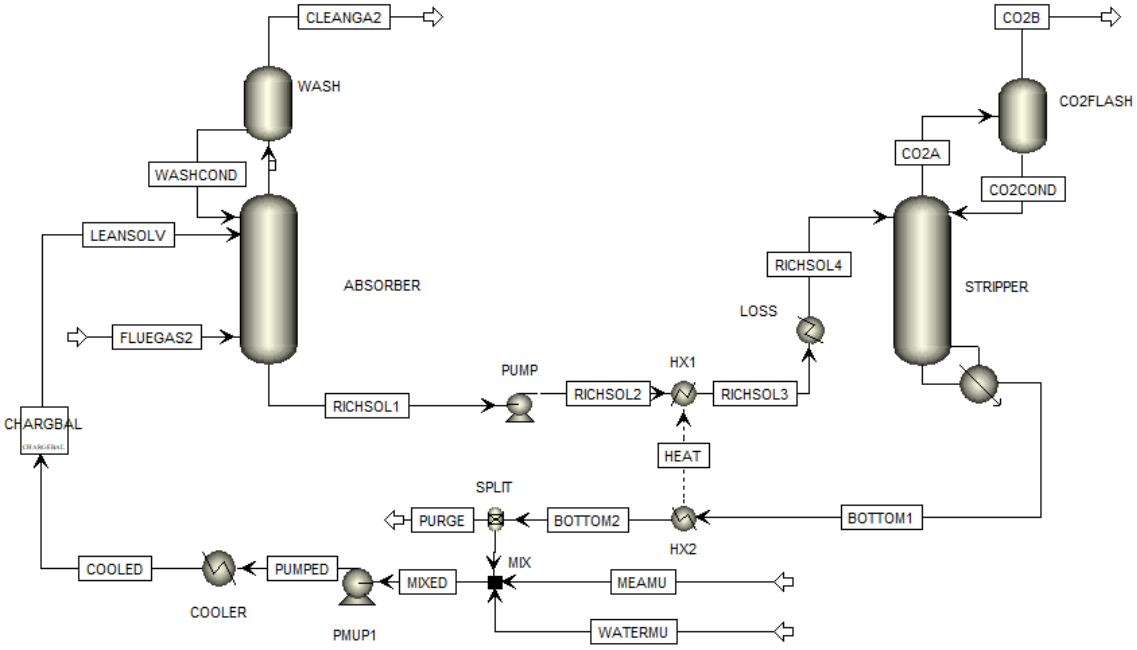


*Figure 37. Process flow diagram for the carbon capture plant in Aspen Plus.*

The absorber is represented using a RadFrac model employing the Rate-Based calculation method. It comprises 30 stages without condenser or reboiler components. The Vapor-Liquid phase option is chosen as applicable. Inlet streams consist of lean solvent and condensed water from the washing section entering at stage 1 (the top of the absorber), while the flue gas enters at stage 30 (the bottom of the absorber). A pressure loss of 0.025 bar is specified. For the column internals, a rating model has been developed, utilizing Rasching Super-Pak 200X metal packing. The absorber tower stands at a height of 12 m with a diameter of 0.15 m. Regarding the internal modelling of the absorber, a reaction condition factor of 0.9 and a film discretization ratio of 10 are considered. To predict mass transfer coefficients and interfacial areas, the correlations

of Bravo et al. are applied, and for heat transfer coefficients, the Chilton and Colburn correlation is used [124].

The washing section for the retention of MEA residuals, positioned above the absorber, cools the gas to 42 °C. It is represented using a Flash2 model, and no pressure loss is accounted for in this stage.

The modelling of the stripper, or desorber, is similar to that of the absorber regarding internal correlations and packing type. It employs a RadFrac model utilizing the Rate-Based calculation method. This configuration comprises 24 stages, with a Kettle-type reboiler [125]. The condenser, however, is modelled separately outside the RadFrac model to faithfully replicate the pilot plant diagram. The reboiler has a maximum electric power of 30 kW. Inlet streams at stage 1 (the top of the stripper) integrate the condensate from the condenser and the rich solvent. The stripper operates at a pressure of 1.8 bar, with a specified pressure loss of 0.05 bar. The stripper tower has dimensions of 8 meters in height and 0.1 meters in diameter. It is important to note that, for both the absorber and the stripper, heat loss from the column is not considered [124].

The $CO_2$ cooler (or condenser), situated atop the stripper, is responsible for cooling the gas to 6 °C. This component is represented using a Flash2 model, and no pressure loss is taken into account in this stage.

The heat exchanger connecting the rich and lean solvents employs two independent Heater models, linked by a heat flow. To maintain a specific temperature difference, the hot outlet (lean stream out) is fixed to be +5 °C relative to the cold inlet (rich stream in). The outlet temperature of the lean stream is determined through an energy balance calculation. Another heat exchanger, also utilizing a Heater model, is configured to cool the lean stream to 40 °C before it enters the absorber.

*Table 20. Main inputs and outputs for the Aspen Plus model.*

| **Variable** | **Composition** | **Mass flow rate** | **Temperature** | **Other** |
|---|---|---|---|---|
| Lean stream | Input | Input | Input | - |
| Flue gas | Input | Input | Input | - |
| Clean gas | Output | Output | Input | - |
| $CO_2$ | Output | Output | Input | - |
| Makeup water | Input | Output | Input | - |
| Makeup MEA | Input | Output | Input | - |
| Absorber (temperature profile) | - | - | Output | - |
| Reboiler | - | - | Output | - |
| Capture ratio | - | - | - | Input |
| Specific duty | - | - | - | Output |
| L/G ratio | - | - | - | Input |
| Absorber pressure | - | - | - | Input |
| Stripper duty | - | - | - | Output |
| Stripper pressure | - | - | - | Input |

Both pumps, operating within the rich and lean streams, are simulated using the Pump model with 0.75 efficiency and driver efficiency of 0.9. A purge is incorporated into the system for addressing potential calculation loop issues and facilitating the

measurement of necessary renovation and makeup. This component is represented using a Split model and is configured to purge 1% of the lean stream.

Two calculators are required: one for MEA makeup and the other for water makeup. The MEA makeup calculator determines the total amount of MEA lost in the clean and $CO_2$ streams, including the purge stream. Similarly, the water makeup calculator performs a similar calculation, considering water loss and accounting for the water content in the flue gas entering the absorber. A single design spec is required to establish the desired carbon capture ratio, typically set at 90%. This is achieved by adjusting the reboiler power. Main inputs and outputs to the model are gathered in Table 20.

### 5.2.3. Results and model validation

For the purpose of model validation, a rigorous comparison is conducted between the data obtained from the pilot plant and the predictions made by the model. This comparison specifically focuses on a critical operating point where the L/G ratio is set at 4.5. The selection of this point is based on the fact that it represents the point with lower consumption according to the pilot plant data. At this particular point, a consistent flue gas flow rate of 70 $m^3/h$, with a $CO_2$ content of 25% (dry basis), is utilized. Significant variables, including temperatures, power requirements, and specific carbon capture duties, are analysed and compared.

Table 21 displays the key outputs for both the pilot plant and Aspen Plus model, demonstrating consistent results with errors below 8% for all magnitudes. Figure 38 illustrates absorber profile temperature for both the pilot plant and the Aspen model, indicating a strong agreement between the two datasets, with errors below 4%.

*Table 21. Pilot Plant vs. Aspen Plus Model Outputs.*

| Variable | Pilot Plant | Aspen Model | Units | Error (%) |
|---|---|---|---|---|
| $CO_2$ concentration in $CO_2$ stream | - | 99.3 | % (wet) | - |
| $CO_2$ concentration in clean gas | 3 | 3 | % | 0 |
| Clean gas flow rate (dry) | 51.3 | 55.1 | $Bm^3/h$ | 7.4 |
| Temperature rich solvent | 48.7 | 45.9 | °C | -5.7 |
| Temperature rich solvent after HX | 101.4 | 103.3 | °C | 1.9 |
| Temperature reboiler | 121.1 | 121.2 | °C | 0.1 |
| Reboiler duty | 24.6 | 26.5 | kW | 7.7 |
| Lean mass flow rate | 315 | 315 | l/h | n/a |
| Specific CC Duty | 3.36 | 3.51 | $MJ/kg_{CO2}$ | 4.5 |

Additionally, the validation process extends beyond this point to provide a thorough evaluation of the model's performance across different L/G ratios and their corresponding specific carbon capture duties. Figure 39 presents these findings for stripper pressures of 1.8 and 2.0 bars. The Aspen Plus model shows a comparable trend to the pilot plant, although with slightly higher duties in the 4 to 5 $l/m^3$ ratio range. Notably, as the stripper pressure increases, the duty decreases. The error is in all cases below 6%.

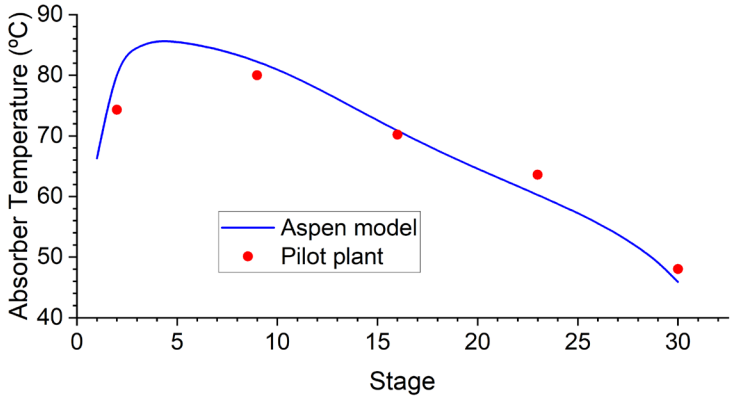


*Figure 38. Inner absorber Temperature: Pilot Plant (•) vs. Model (–). Stage 1 and stage 30 are the top and the bottom of the absorber, respectively.*

In summary, the study presented successfully validates the Aspen Plus model. We compared pilot plant data and model predictions, emphasizing an L/G ratio of 4.5 for its lower consumption. Results show strong consistency, with errors below 8%. The novelty of this work lies in its rigorous validation approach with experimental data registered in large-scale (TRL 6), which ensures the reliability of the model for industrial applications. Moreover, the demonstrated accuracy and efficiency of the model underscore its potential to enhance process optimization and resource utilization in relevant industries, thus garnering considerable interest in both academic and industrial circles.

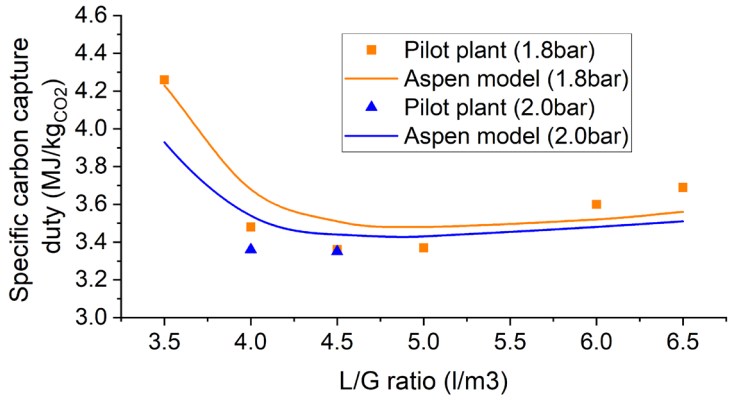


*Figure 39. Specific Carbon Capture Duty: Pilot Plant (·) vs. Model (-) at Stripper Pressures of 1.8 (orange) or 2.0 bar (blue).*

# 6. Concluding remarks

## 6.1. Conclusions

The industrial sector is a formidable contributor to CO2 emissions, making it imperative to intensify efforts aimed at emissions reduction. Achieving net-zero emissions in this sector is an ambitious but essential goal. Notably, the iron and steel industry, responsible for approximately 11% of global industry-related emissions, represents a significant challenge in this regard. To address these challenges, this thesis has focused on the potential of Power to Gas technology as a transformative solution for decarbonizing this industry and, by extension, heavy industries at large.

The core objective of this research was to propose innovative Power to Gas configurations within industry settings that enable closed-loop $CO_2$ recycling while enhancing efficiency, resource utilization, and profitability. This goal was pursued through three specific objectives:

**(i) Preliminary study on power to gas integration in the industry sector.**

With the aim of selecting a target industry, the glass and steel industries were examined. In the iron and steel industry, a novel concept of an oxygen blast furnace with blast furnace gas methanation was analysed. When hydrogen consumed in methanation is produced by a green PEM electrolyser, an 8% reduction in $CO_2$ emissions can be achieved with an energy penalty of 34 MJ/$kg_{CO2}$. Using COG as the hydrogen source achieves the same carbon abatement with an energy penalty of 4.9 MJ/$kg_{CO2}$. The primary difference in energy penalty arises from the electricity consumption by the electrolyser in the first scenario, highlighting the need to reduce hydrogen consumption or find cheaper hydrogen sources. The energy penalty with COG is similar to that of an amine scrubbing plant (3-4 MJ/$kg_{CO2}$).

Regarding the glass industry, combining CaL and methanation achieved an 80% reduction in $CO_2$ emissions with an energy penalty of 35.8 MJ/$kg_{CO2}$. Implementing the recycling of spent sorbent (CaO) from CaL improved the emissions reduction by 2.3 percentage points (pp) and decreased the energy penalty to 33.9 MJ/$kg_{CO2}$. Using the oxygen from the electrolyser in the glass furnaces provided an additional 6.0 pp reduction in emissions and reached 33.3 MJ/$kg_{CO2}$ in the energy penalty. Adding a Rankine power plant achieved a further reduction in the energy penalty, with 31.4 MJ/$kg_{CO2}$. The economic analysis reveals high costs of 344-437 €/$t_{CO2}$ and 130-165 €/$t_{glass}$ if all electricity is purchased, and of 261-367 €/$t_{CO2}$ and 99-139 €/$t_{glass}$ if part of it is self-consumed, especially if compared with the current CCS cost of 67-116 €/$t_{CO2}$ (amines 46-74 €/$t_{CO2}$, transport 19 €/$t_{CO2}$/1,500kg, and storage 3,6-23 €/$t_{CO2}$ [11]) with storage and glass price of 400-500 €/$t_{glass}$.

Compared to conventional $CO_2$ reduction technologies like amine scrubbing with carbon storage, PtG offers several advantages. These include CaO recycling, heat recovery, reduced fossil fuel use, and continuous $CO_2$ recycling, eliminating the need for storage. However, PtG has higher energy penalties and costs. Nonetheless, significant investments in projects such as ULCOS-BF [126], IGAR [127], COURSE50 [128] and

STEPWISE [129] support BF decarbonization, and initiatives like HyGlass [130], HyNet [131] and Kopernikus P2X [132] support glassmaking decarbonization.

While the glass industry achieves significant $CO_2$ emissions reductions, it faces substantial carbon abatement costs and implementation expenses, potentially affecting its competitiveness, especially in comparison to current glass prices. Likewise, the implementation of PtG in the iron and steel industry brings challenges and opportunities. Further research is vital for the steelmaking sector due to its unique decarbonization challenges and the potential for synergistic opportunities.

**(ii) Reduction of $CO_2$ emissions and coal consumption in the iron and steel industry by power to gas technology.**

With the objective of reducing $CO_2$ emissions and coal consumption in the iron and steel industry, a comprehensive techno-economic analysis was undertaken employing Power to Gas technology. Various integration scenarios involving $CO_2$ methanation within the blast furnace were explored, leading to valuable insights.

The integration of Power to Gas into an air-blown blast furnace (Case 1) demonstrated technical feasibility but revealed limitations in $CO_2$ reduction due to constraints related to the adiabatic flame temperature. Using pure oxygen instead of air (Case 2) led to significant improvements in $CO_2$ avoidance but incurred higher costs and energy consumption, primarily driven by the PEM. Incorporating TGR (Case 3) reduced $H_2$ requirements, resulting in the lowest carbon avoidance costs. Blast furnace gas methanation (Case 4) achieved $CO_2$ emission reductions comparable to Case 2 but with lower costs. Adjusting the $H_2$:$CO_2$ ratio (Case 5) for $CO_2$ reduction faced challenges related to $CO_2$ injection into the blast furnace. Considering a loop-free configuration with direct $H_2$ injection (Case 6) offered easier implementation but lower $CO_2$ avoidance rates. Each case presents unique trade-offs, emphasizing the importance of carefully selecting the integration approach based on specific objectives and constraints.

In summary, simultaneous $CO_2$ methanation and top gas recycling in an oxygen blast furnace emerges as the most profitable option. While it achieves slightly lower $CO_2$ avoidance rate (30 %) compared to some other scenarios (up to 34 %), it stands out for reduced sold gas volume (1143 $MJ/t_{HM}$), lower energy penalty (12 $MJ/kg_{CO2}$), and costs (216 $€/t_{CO2}$ and 130 $€/t_{HM}$). This configuration can cut $CO_2$ emissions from 1943 $kg_{CO2}/t_{HM}$ to 1362 $kg_{CO2}/t_{HM}$, all without the need for geological storage. In the case of a 320 $t_{HM}$/h blast furnace, this translates to reducing 186 $t_{CO2}$/h, or 1500 $kt_{CO2}$ annually (assuming 8000 operating hours per year). On a global scale, considering steel production in 2020 (1.9 Gt/year) and the BF-BOF route's share (70%) [76], this setup could potentially save as much as 773 million tons of $CO_2$ per year, compared with the 6341 $Mt_{CO2}$ emitted globally by the industry.

To ensure economic viability, electricity prices and $CO_2$ taxes are critical. To amortize CAPEX in 20 years, electricity prices should be around 18 €/MWh or $CO_2$ taxes around 313 $€/t_{CO2}$. For instance, with an electricity price of 35 €/MWh (wind power production cost) and a $CO_2$ tax of 150 $€/t_{CO2}$, the investment becomes profitable after 20 years. Although initial costs may be high, decarbonization technologies offer long-term economic benefits. However, careful consideration of market conditions and policy support is essential for their viability.

This study is aligned with the R&D projects on technologies to decarbonize blast furnace operations performed by the I&S industries. Initiatives like ULCOS-BF [126], IGAR [127], COURSE50 [128] and STEPWISE [129] focus on blast furnace decarbonization through similar technologies, such as carbon capture and TGR. Current industry practices include implementing technologies like CCS, as well as injecting $H_2$ and COG into the blast furnace. These efforts highlight the industry's commitment to transitioning towards more sustainable and environmentally friendly production methods.

**(iii) Experimental tests at TRL 4-6 of various components of the power to gas technology.**

With the purpose of developing reliable models on the most critical PtG components, various experimental tests were conducted focused on Methanation at TRL 4 and Amine Scrubbing at TRL 6.

Methanation experiments, conducted in UNIZAR's laboratory, compared nickel and ruthenium catalysts in a 1 kW fixed bed reactor. The catalysts' activation temperature was found to have limited influence on $CO_2$ conversion within the 200-400 °C temperature range. Gas flow rate experiments revealed that Ni-based catalysts could handle twice the gas flow rate compared to Ru-based catalysts. Increasing the $H_2$:$CO_2$ ratio improved carbon conversion, with the nickel-based catalyst consistently outperforming the ruthenium-based catalyst by 6-8%. A kinetic model was also developed in Aspen Plus with the experimental data, to assess a methanation plant aiming for 95% methane content in the final synthetic gas. Among the different configurations, the 3-reactor configuration emerged as the most suitable choice for plant design, offering a substantial reduction in catalyst mass while meeting technical constraints.

Carbon capture experiments were conducted in voestalpine and K1-MET installations. During these tests, $CO_2$ was captured from real flue gases of the steel industry using an amine scrubbing cycle (30wt% MEA). The study varied the liquid-to-gas (L/G) ratio and desorber pressure to identify optimal operating conditions for minimizing specific energy requirements, finding an optimal point at a ratio of 4.5. Aspen Plus software was used to simulate the carbon capture process. The model results were compared to those from the pilot plant, demonstrating strong consistency with errors below 8%. In summary, the study successfully validated the Aspen Plus model, affirming its accuracy in predicting carbon capture performance under various operating conditions.

## 6.2. Conclusiones

El sector industrial es un contribuyente formidable a las emisiones de $CO_2$, lo que hace imperativo intensificar los esfuerzos dirigidos a la reducción de emisiones. Lograr emisiones netas cero en este sector es un objetivo ambicioso pero esencial. En particular, la industria del hierro y el acero, responsable de aproximadamente el 11% de las emisiones globales relacionadas con la industria, representa un desafío significativo en este sentido. Para abordar estos desafíos, esta tesis se ha centrado en el potencial de la tecnología Power to Gas como una solución transformadora para descarbonizar esta industria y, por extensión, las industrias pesadas en general.

El objetivo principal de esta investigación fue proponer configuraciones innovadoras de Power to Gas en entornos industriales que permitan el reciclaje en un bucle cerrado de $CO_2$ al tiempo que mejoran la eficiencia, la utilización de recursos y la rentabilidad. Esta meta se consiguió a través de tres objetivos específicos:

**(i) Estudio preliminar sobre la integración de Power to Gas en el sector industrial.**

Con el objetivo de seleccionar una industria objetivo, se examinaron las industrias del vidrio y del acero. En la industria del hierro y el acero, se analizó un concepto novedoso de un alto horno de oxígeno con metanización de gas de horno alto. Cuando el hidrógeno consumido en la metanización es producido por un electrolizador PEM verde, se puede lograr una reducción del 8% en las emisiones de $CO_2$ con una penalización energética de 34 MJ/$kg_{CO2}$. Usando COG como fuente de hidrógeno se logra la misma reducción de carbono con una penalización energética de 4.9 MJ/$kg_{CO2}$. La principal diferencia en la penalización energética surge del consumo de electricidad por parte del electrolizador en el primer escenario, lo que destaca la necesidad de reducir el consumo de hidrógeno o encontrar fuentes de hidrógeno más baratas. La penalización energética con COG es similar a la de una planta de absorción de aminas (3-4 MJ/$kg_{CO2}$).

En cuanto a la industria del vidrio, la combinación de CaL y metanización logró una reducción del 80% en las emisiones de $CO_2$ con una penalización energética de 35.8 MJ/$kg_{CO2}$. La recirculación del sorbente gastado (CaO) de CaL mejoró la reducción de emisiones en 2.3 puntos porcentuales (pp) y disminuyó la penalización energética a 33.9 MJ/$kg_{CO2}$. El uso del oxígeno del electrolizador en los hornos de vidrio proporcionó una reducción adicional de 6.0 pp en las emisiones y alcanzó 33.3 MJ/$kg_{CO2}$ en la penalización energética. La introducción de una planta de potencia tipo Rankine logró una mayor reducción en la penalización energética, con 31.4 MJ/$kg_{CO2}$. El análisis económico revela altos costes de 344-437 €/$t_{CO2}$ y 130-165 €/$t_{vidrio}$ si se compra toda la electricidad, y de 261-367 €/$t_{CO2}$ y 99-139 €/$t_{vidrio}$ si parte de ella es de autoconsumo, especialmente si se compara con el costo actual de CCS de 67-116 €/$t_{CO2}$ (aminas 46-74 €/$t_{CO2}$, transporte 19 €/$t_{CO2}$/1,500kg, y almacenamiento 3,6-23 €/$t_{CO2}$ [11]) con almacenamiento y precio del vidrio de 400-500 €/$t_{vidrio}$.

Comparado con tecnologías convencionales de reducción de $CO_2$ como la absorción de aminas con almacenamiento de carbono, PtG ofrece varias ventajas. Estas incluyen el reciclaje de CaO, la recuperación de calor, la reducción del uso de combustibles fósiles y el reciclaje continuo de $CO_2$, eliminando la necesidad de almacenamiento. Sin embargo, PtG tiene mayores penalizaciones energéticas y costes. No obstante, inversiones significativas en proyectos como ULCOS-BF [126], IGAR [127], COURSE50 [128] y STEPWISE [129] apoyan la descarbonización del alto horno, e iniciativas como HyGlass [130], HyNet [131] y Kopernikus P2X [132] apoyan la descarbonización de la fabricación de vidrio.

Mientras que la industria del vidrio logra reducciones significativas en las emisiones de $CO_2$, muestra costes sustanciales de abatimiento de carbono y gastos de implementación, lo que puede afectar su competitividad, especialmente en comparación con los precios actuales del vidrio. Del mismo modo, la implementación de PtG en la industria del hierro y el acero trae desafíos y oportunidades. Es vital realizar

más investigaciones en el sector de la fabricación de acero debido a sus desafíos únicos de descarbonización y al potencial de oportunidades sinérgicas.

**(ii) Reducción de emisiones de $CO_2$ y consumo de carbón en la industria del hierro y el acero mediante tecnología Power to Gas.**

Con el objetivo de reducir las emisiones de $CO_2$ y el consumo de carbón en la industria del hierro y el acero, se llevó a cabo un análisis tecno-económico integral empleando la tecnología Power to Gas. Se exploraron varios escenarios de integración que involucraban la metanización de $CO_2$ junto con el alto horno, lo que llevó a obtener valiosos descubrimientos.

La integración de Power to Gas en un alto horno con aire (Caso 1) demostró la viabilidad técnica pero reveló limitaciones en la reducción de $CO_2$ debido a las restricciones relacionadas con la temperatura adiabática de llama. El uso de oxígeno puro en lugar de aire (Caso 2) llevó a mejoras significativas en la reducción de $CO_2$ pero incurrió en mayores costes y consumo de energía, impulsados principalmente por el electrolizador PEM. La incorporación de TGR (Caso 3) redujo los requisitos de $H_2$, resultando en los costes de emisión de carbono más bajos. La metanización de gas de alto horno (Caso 4) logró reducciones de emisiones de $CO_2$ comparables al Caso 2 pero con costes más bajos. Ajustar el ratio $H_2$:$CO_2$ (Caso 5) para la reducción de $CO_2$ enfrentó desafíos relacionados con la inyección de $CO_2$ en el alto horno. La consideración de una configuración sin bucle en base a inyección directa de $H_2$ (Caso 6) ofreció una implementación más fácil pero menores tasas de reducción de $CO_2$. Cada caso presenta compensaciones únicas, destacando la importancia de seleccionar cuidadosamente el enfoque de integración basado en objetivos y restricciones específicos.

En resumen, la metanización simultánea de $CO_2$ y el reciclaje de gas superior (TGR) en un alto horno de oxígeno emergen como la opción más rentable. Aunque logra una tasa de reducción de $CO_2$ ligeramente menor (30 %) en comparación con algunos otros escenarios (hasta 34 %), se destaca por el menor volumen de gas vendido (1143 $MJ/t_{HM}$), menor penalización energética (12 $MJ/kg_{CO2}$) y costes (216 €/$t_{CO2}$ y 130 €/$t_{HM}$). Esta configuración puede reducir las emisiones de $CO_2$ de 1943 $kg_{CO2}/t_{HM}$ a 1362 $kg_{CO2}/t_{HM}$, todo sin la necesidad de almacenamiento geológico. En el caso de un alto horno de 320 $t_{HM}$/h, esto se traduce en una reducción de 186 $t_{CO2}$/h, o 1500 $kt_{CO2}$ anualmente (asumiendo 8000 horas de operación por año). A escala global, considerando la producción de acero en 2020 (1.9 Gt/año) y la participación de la ruta BF-BOF (70%) [76], esta configuración podría ahorrar hasta 773 millones de toneladas de $CO_2$ por año, en comparación con las 6341 $Mt_{CO2}$ emitidas globalmente por la industria.

Para asegurar la viabilidad económica, los precios de la electricidad y los impuestos al $CO_2$ son críticos. Para amortizar el CAPEX en 20 años, los precios de la electricidad deben estar alrededor de 18 €/MWh o los impuestos al $CO_2$ alrededor de 313 €/$t_{CO2}$. Por ejemplo, con un precio de la electricidad de 35 €/MWh (coste de producción de energía eólica) y un impuesto al $CO_2$ de 150 €/$t_{CO2}$, la inversión se vuelve rentable a los 20 años. Aunque los costes iniciales pueden ser altos, las tecnologías de descarbonización ofrecen beneficios económicos a largo plazo. Sin embargo, es esencial

considerar cuidadosamente las condiciones del mercado y el apoyo de políticas para su viabilidad.

Este estudio está alineado con los proyectos de I+D sobre tecnologías para descarbonizar las operaciones de altos hornos realizados por las industrias de I&S. Iniciativas como ULCOS-BF [126], IGAR [127], COURSE50 [128] y STEPWISE [129] se centran en la descarbonización de altos hornos a través de tecnologías similares, como la captura de carbono y el TGR. Las prácticas actuales de la industria incluyen la implementación de tecnologías como CCS, así como la inyección de $H_2$ y COG en el alto horno. Estos esfuerzos destacan el compromiso de la industria con la transición hacia métodos de producción más sostenibles y respetuosos con el medio ambiente.

**(iii) Pruebas experimentales en TRL 4-6 de varios componentes de la tecnología Power to Gas.**

Con el propósito de desarrollar modelos fiables de los componentes más críticos de la tecnología PtG, se realizaron varias pruebas experimentales centradas en la metanización en TRL 4 y la absorción con aminas en TRL 6.

Los experimentos de metanización, realizados en los laboratorios de UNIZAR, compararon catalizadores de níquel y rutenio en un reactor de lecho fijo de 1 kW. Se encontró que la temperatura de activación de los catalizadores tenía una influencia limitada en la conversión de $CO_2$ dentro del rango de temperatura de 200-400 °C. Los experimentos de caudal de gas revelaron que los catalizadores a base de níquel podían manejar el doble del flujo de gas en comparación con los catalizadores a base de rutenio. El aumento de la relación $H_2$:$CO_2$ mejoró la conversión de carbono, con el catalizador a base de níquel superando consistentemente al catalizador a base de rutenio en un 6-8%. También se desarrolló un modelo cinético en Aspen Plus con los datos experimentales, para evaluar una planta de metanización que obtiene un contenido de metano del 95% en el gas sintético final. Entre las diferentes configuraciones, la configuración de 3 reactores surgió como la opción más adecuada para el diseño de la planta, ofreciendo una reducción sustancial en la masa del catalizador mientras se cumplen las restricciones técnicas.

Los experimentos de captura de carbono se realizaron en las instalaciones de voestalpine y K1-MET. Durante estas pruebas, se capturó $CO_2$ de gases de combustión reales de la industria del acero utilizando un ciclo de absorción con aminas (MEA al 30%). El estudio varió la relación líquido-gas (L/G) y la presión del desorbedor para identificar las condiciones óptimas de operación para minimizar el consumo energético, encontrando un punto óptimo en un ratio de 4.5. Se utilizó el software Aspen Plus para simular el proceso de captura de carbono. Los resultados del modelo se compararon con los de la planta piloto, demostrando una fuerte consistencia con errores por debajo del 8%. En resumen, el estudio validó con éxito el modelo de Aspen Plus, afirmando su precisión en la predicción del rendimiento de captura de carbono bajo diversas condiciones de operación.

## 6.3. Contributions

This thesis falls within the domain of engineering and presents innovative solutions to address technical challenges hindering the progress of emerging technologies. The primary focus of this work is to mitigate the substantial carbon dioxide emissions associated with industrial processes, with a particular emphasis on the iron and steel industry. It contributes to the existing knowledge gap in BF decarbonization through PtG and carbon recycling. The contributions made in this research can be summarized as follows:

1) **Broadened Scope of Power to Gas Applications:** This thesis extends the application of Power to Gas technology to diverse industries, including glass and steel. Notably, the research demonstrates that the glass industry can achieve high levels of emissions reductions, showcasing the adaptability and effectiveness of Power to Gas in diverse industrial settings. Regarding the steel industry, due to its intricate structure, further research was needed. This thesis deepened in this aspect for the first time, contributing novel insights to the existing literature (see contribution 3).
2) **Comprehensive Review of Carbon Capture Technologies:** A systematic review and classification of carbon capture technologies applied to the BF-BOF steelmaking route was performed, providing detailed comparisons of thermal and electrical penalties, economic costs, $CO_2$ emission reductions, and TRL.
3) **Innovative Power to Gas Configurations for Steel Industry:** This work introduces novel Power to Gas configurations tailored specifically for the steel industry. These configurations integrate various technologies such as oxygen blast furnaces, Top Gas Recycling, and BFG methanation. While the thermochemical models of individual sub-systems have been previously documented in the literature, their combined application with Power to Gas in the iron and steel industry is a unique contribution of this thesis. This integration allows for a quantitative assessment of synergies and carbon abatement potential within the proposed configurations. Additionally, this thesis is the only study to have conducted an economic analysis in these specific configurations.
4) **Comprehensive Review of PtG Technologies in I&S:** A systematic review and classification of different power to gas technologies applied to the BF-BOF steelmaking route was performed, providing for the first time detailed comparisons of fossil fuel consumption, carbon conversion technology, injection point, electrolyser size, energy penalty, $CO_2$ emissions and costs.
5) **Comparative Analysis of Ni and Ru-Based Catalysts:** The primary novel contribution of this study is the detailed comparison between Ni and Ru-based catalysts is conducted in a 1 kW methanation fixed-bed reactor. Key performance indicators such as GHSV, $H_2$:$CO_2$ ratio, temperature, and $CO_2$ conversion are examined. This analysis provides valuable insights into catalyst selection for methanation processes, offering guidance for future implementations. Additionally, the developed methanation model

minimizes the required catalyst quantity while ensuring a high methane concentration (95 vol%) in the synthetic natural gas. It can serve as a reference for designing full-scale installations and optimizing operational parameters.

6) **Development of a Comprehensive Carbon Capture Model:** An entirely new model is developed to simulate the carbon capture process using amines, specifically tailored and validated for real gases produced in the iron and steel industry. This model can be used at industrial level to determine the minimum thermal consumption by adjusting the Liquid-to-Gas (L/G) ratio.

## 6.4. On-going and future work

To capitalize on the work developed in this thesis, it is crucial to outline future research directions. While significant progress has been made, much work remains in the field, and the results have generated new questions and areas for exploration. To address the challenges encountered in this work, the following options for future research stages should be considered:

i. **Further synergy assessment:** Further exploration of synergistic configurations, like within the glass industry, is worth considering. While individual options have undergone assessment, the cumulative impact of integrating them remains undiscovered.

ii. **PtG Implementation in Other Industries:** Expanding PtG implementation beyond steelmaking to industries like cement or chemicals holds promise for reducing CO2 emissions. Investigating PtG's feasibility and benefits in these sectors could open up new avenues for carbon mitigation efforts.

iii. **Sulphur Influence:** The presence of sulphur gases in BFG poses a potential threat to various components of the PtG system, including the carbon capture and methanation plants. To assess and mitigate this issue, two independent projects are currently underway: DIS-HYCOME (PID2021-126164OB-I00) and DEC-I&S (TED2021-130000BI00).

iv. **Exploration of Alternative Configurations:** To enhance energy efficiency and further reduce $CO_2$ emissions, it is advisable to investigate alternative configurations. These configurations may incorporate technologies such as Solid Oxide Electrolyzer Cells (SOEC), Power to Syngas, Water Gas Shift or Shaft Injection.

v. **Biomass and Charcoal Integration:** Future research should also explore the integration of biomass and charcoal within PtG systems, with a particular focus on determining the most effective utilization method. This investigation should consider their potential roles in replacing coke, substituting pulverized coal injection (PCI), or serving as gaseous bio-reducing agents.

vi. **Alternative Sources of $H_2$**: Since hydrogen is the main cost factor in the current scenarios, identifying more economical sources of $H_2$ is essential. Future research should explore alternatives to electrolytic $H_2$, such as biomass-to-hydrogen conversion, natural gas reforming with carbon

capture, or photoelectrochemical water splitting, to reduce overall costs and enhance the feasibility of PtG systems.

vii. **Behaviour of Blast Furnace under Low Coke Rate:** Another important path for future research is to study the behaviour of blast furnaces when subjected to high quantities of reducing gas injection and reduced coke rates. Understanding the operational dynamics and potential challenges in such scenarios will provide valuable insights for optimizing PtG-integrated processes in the iron and steel industry.

viii. **Low-Carbon Approaches in the I&S Industry:** While technologies like DR, Hisarna, Corex, or Finex represent low-carbon alternatives in the iron and steel industry, they still generate $CO_2$ emissions. Power to Gas technology has the potential to contribute to further emissions reduction in conjunction with these approaches.

ix. **Life Cycle Assessment (LCA) Integration:** Incorporating LCA methodologies is crucial to accurately evaluate the overall environmental impact of PtG implementation in various industries. Assessing PtG's sustainability across its entire life cycle, from raw material extraction to end-of-life disposal, will provide valuable insights into its true environmental footprint and help guide decision-making towards more sustainable practices.

# BIBLIOGRAPHY


[1] E. Commission, “Delivering the European Green Deal,” 2021. https://commission.europa.eu/strategy-and-policy/priorities-2019-2024/european-green-deal/delivering-european-green-deal_en (accessed Jun. 15, 2023).

[2] E. Union, “Net Zero Industry Act,” 2023. https://single-market-economy.ec.europa.eu/publications/net-zero-industry-act_en

[3] I. E. Agency, “Global Energy Review: CO2 Emissions in 2021, IEA, Paris,” 2022. [Online]. Available: https://www.iea.org/reports/global-energy-review-co2-emissions-in-2021-2

[4] International Energy Agency, “The role of CCUS in low-carbon power systems, IEA, Paris,” 2020. doi: 10.1787/7be68d30-en.

[5] International Energy Agency, “Industry, IEA, Paris. Sectoral overview.,” 2020. [Online]. Available: https://www.iea.org/reports/industry

[6] E. Commision, “REPowerEU: A plan to rapidly reduce dependence on Russian fossil fuels and fast forward the green transition,” 2022. https://ec.europa.eu/commission/presscorner/detail/en/IP_22_3131 (accessed Jun. 12, 2023).

[7] M. Sustainability, “The net-zero challenge: Accelerating decarbonization worldwide,” 2022. [Online]. Available: https://www.mckinsey.com/capabilities/sustainability/our-insights/the-net-zero-challenge-accelerating-decarbonization-worldwide

[8] Z. Fan and S. J. Friedmann, “Low-carbon production of iron and steel: Technology options, economic assessment, and policy,” *Joule*, pp. 1–34, 2021, doi: 10.1016/j.joule.2021.02.018.

[9] M. Götz *et al.*, “Renewable Power-to-Gas: A technological and economic review,” *Renew. Energy*, vol. 85, pp. 1371–1390, 2016, doi: 10.1016/j.renene.2015.07.066.

[10] L. M. Romeo and M. Bailera, “Design configurations to achieve an effective CO2 use and mitigation through power to gas,” *J. CO2 Util.*, vol. 39, no. December 2019, pp. 1–10, 2020, doi: 10.1016/j.jcou.2020.101174.

[11] W. Y. Hong, “A techno-economic review on carbon capture, utilisation and storage systems for achieving a net-zero CO2 emissions future,” *Carbon Capture Sci. Technol.*, vol. 3, no. December 2021, p. 100044, 2022, doi: 10.1016/j.ccst.2022.100044.

[12] M. R. Rahimpour, M. Farsi, and M. A. Makarem, *Advances in carbon capture. ISBN: 978-0-12-819657-1*.

[13] K. Ghaib and F. Z. Ben-Fares, “Power-to-Methane: A state-of-the-art review,” *Renew. Sustain. Energy Rev.*, vol. 81, no. June 2017, pp. 433–446, 2018, doi: 10.1016/j.rser.2017.08.004.

[14] B. Lecker, L. Illi, A. Lemmer, and H. Oechsner, “Biological hydrogen methanation – A review,” *Bioresour. Technol.*, vol. 245, no. September, pp. 1220–1228, 2017, doi: 10.1016/j.biortech.2017.08.176.

[15] O. Strohbach, “Audi e-gas plant stabilizes electrical grid,” *Press Release - Audi MediaInfo - Technology and Innovation Communications*, 2015.

[16] “Store&GO project.” https://www.storeandgo.info/index.html (accessed Sep. 11, 2024).
[17] GRTgaz, “Jupiter 1000 project - Web Page.” https://www.jupiter1000.eu/english (accessed Sep. 11, 2024).
[18] “MethFuel Project Website.” https://www.ise.fraunhofer.de/en/research-projects/methquest-methfuel.html (accessed Sep. 11, 2024).
[19] E. K. Vakkilainen, “Fluidized Bed Boilers for Biomass,” *Steam Gener. from Biomass*, pp. 211–236, 2017, doi: 10.1016/b978-0-12-804389-9.00010-1.
[20] J. Y. Ahn *et al.*, “Developing Ni-based honeycomb-type catalysts using different binary oxide-supported species for synergistically enhanced CO2 methanation activity,” *Fuel*, vol. 250, no. April, pp. 277–284, 2019, doi: 10.1016/j.fuel.2019.03.123.
[21] C. Bassano, P. Deiana, L. Lietti, and C. G. Visconti, “P2G movable modular plant operation on synthetic methane production from CO2 and hydrogen from renewables sources,” *Fuel*, vol. 253, no. May, pp. 1071–1079, 2019, doi: 10.1016/j.fuel.2019.05.074.
[22] H. S. Jee, N. Nishio, and S. Nagai, “Continuous CH4 Production from H2 and CO2 by Methanobacterium thermoautotrophicum in a fixed-bed reactor,” *J. Ferment. Technol.*, vol. 66, no. 2, pp. 235–238, Jan. 1988, doi: 10.1016/0385-6380(88)90054-4.
[23] E. C. Bugante, Y. Shimomura, T. Tanaka, M. Taniguchi, and S. Oi, “Methane production from hydrogen and carbon dioxide and monoxide in a column bioreactor of thermophilic methanogens by gas recirculation,” *J. Ferment. Bioeng.*, vol. 67, no. 6, pp. 419–421, 1989.
[24] H. Porté, P. G. Kougias, N. Alfaro, L. Treu, S. Campanaro, and I. Angelidaki, “Process performance and microbial community structure in thermophilic trickling biofilter reactors for biogas upgrading,” *Sci. Total Environ.*, vol. 655, pp. 529–538, 2019, doi: 10.1016/j.scitotenv.2018.11.289.
[25] M. Burkhardt and G. Busch, “Methanation of hydrogen and carbon dioxide,” *Appl. Energy*, vol. 111, pp. 74–79, 2013.
[26] T. Schaaf, J. Grünig, M. R. Schuster, T. Rothenfluh, and A. Orth, “Methanation of CO2 - storage of renewable energy in a gas distribution system,” *Energy. Sustain. Soc.*, vol. 4, no. 1, pp. 1–14, 2014, doi: 10.1186/s13705-014-0029-1.
[27] “Liten Annual Report 2014,” CEA Tech, 2014.
[28] G. Benjaminsson, J. Benjaminsson, and R. Boogh Rudberg, “Power-to-Gas – A technical review. Report.,” 2013.
[29] J. Lefebvre, M. Götz, S. Bajohr, R. Reimert, and T. Kolb, “Improvement of three-phase methanation reactor performance for steady-state and transient operation,” *Fuel Process Technol*, vol. 132, pp. 83–90, 2015.
[30] J. Li *et al.*, “Enhanced fluidized bed methanation over a Ni/Al2O3 catalyst for production of synthetic natural gas,” *Chem. Eng. J.*, vol. 219, pp. 183–189, 2013, doi: 10.1016/j.cej.2013.01.005.
[31] D. Hofstetter, “Biocatalytic Methanation with Methanogenic Archaea for Power-to-Gas Energy Storage. Conference proceeding.,” 2014.
[32] PFI Germany, “Biomethane for the Gas Grid of Municipal Utility Companies,” 2016. http://newsletter.pfi-biotechnology.de/nl_dez_2016/img/Biomethane.pdf
[33] “HyCAUNAIS project website.” https://www.europe-

bfc.eu/beneficiaire/hycaunais/ (accessed Sep. 11, 2024).
[34] X. Su, J. Xu, B. Liang, H. Duan, B. Hou, and Y. Huang, “Catalytic carbon dioxide hydrogenation to methane: A review of recent studies,” *J. Energy Chem.*, vol. 25, no. 4, pp. 553–565, 2016, doi: 10.1016/j.jechem.2016.03.009.
[35] M. Bailera, P. Lisbona, L. M. Romeo, and S. Espatolero, “Power to Gas projects review: Lab, pilot and demo plants for storing renewable energy and CO2,” *Renew. Sustain. Energy Rev.*, vol. 69, no. November 2016, pp. 292–312, 2017, doi: 10.1016/j.rser.2016.11.130.
[36] M. J. Page *et al.*, “The PRISMA 2020 statement: An updated guideline for reporting systematic reviews,” *BMJ*, vol. 372, 2021, doi: 10.1136/bmj.n71.
[37] Aspen Technology Inc., “Physical Property Models - Reference Manual.” AspenTech, 2019.
[38] “NEL Hydrogen,” 2019. https://nelhydrogen.com/ (accessed Mar. 02, 2022).
[39] A. Zaccara *et al.*, “Renewable hydrogen production processes for the off-gas valorization in integrated steelworks through hydrogen intensified methane and methanol syntheses,” *Metals (Basel).*, vol. 10, no. 11, pp. 1–24, 2020, doi: 10.3390/met10111535.
[40] F. Shi, *Reactor and Process Design in Sustainable Energy Technology*. Elsevier, 2014.
[41] C. O. Domínguez, R. C. Ramírez, and J. M. V. Millán, “The Calcium-Looping process for advancing in the development of both CO2 capture and thermochemical energy storage systems,” *PhD Thesis, Univ. Sevilla*, no. July, 2018.
[42] C. Ortiz, J. M. Valverde, and R. Chacartegui, “Energy Consumption for CO2 Capture by means of the Calcium Looping Process: A Comparative Analysis using Limestone, Dolomite, and Steel Slag,” *Energy Technol.*, vol. 4, no. 10, pp. 1317–1327, 2016, doi: 10.1002/ente.201600390.
[43] S. Rönsch *et al.*, “Review on methanation - From fundamentals to current projects,” *Fuel*, vol. 166, pp. 276–296, 2016, doi: 10.1016/j.fuel.2015.10.111.
[44] K. Izumiya and I. Shimada, “Methane producing technology from CO2 for carbon recycling,” in *The First Symposium on Carbon Ultimate Utilization Technologies for the Global Environment, CUUTE-1*, 2021, pp. 34–35.
[45] K. Müller, F. Rachow, J. Israel, and D. Schmeiber, “Sabatier based CO2-Methanation under oxyfuel conditions. Conference proceedings.,” May 2014.
[46] J. Perpiñán, M. Bailera, B. Peña, L. M. Romeo, and V. Eveloy, “Technical and economic assessment of iron and steelmaking decarbonization via power to gas and amine scrubbing,” *Energy*, vol. 276, p. 127616, 2023, doi: 10.1016/j.energy.2023.127616.
[47] M. Bailera, S. Espatolero, P. Lisbona, and L. M. Romeo, “Power to gas-electrochemical industry hybrid systems: A case study,” *Appl. Energy*, vol. 202, no. 2017, pp. 435–446, 2017, doi: 10.1016/j.apenergy.2017.05.177.
[48] Sendeco2, “sendeco2,” 2022. https://www.sendeco2.com/es/precios-co2%0A (accessed Mar. 02, 2022).
[49] M. R. M. Abu-Zahra, J. P. M. Niederer, P. H. M. Feron, and G. F. Versteeg, “CO2 capture from power plants. Part II. A parametric study of the economical performance based on mono-ethanolamine,” *Int. J. Greenh. Gas Control*, vol. 1, no. 2, pp. 135–142, 2007, doi: 10.1016/S1750-5836(07)00032-1.

[50] E. De Lena *et al.*, “Techno-economic analysis of calcium looping processes for low CO2 emission cement plants,” *Int. J. Greenh. Gas Control*, vol. 82, pp. 244–260, Mar. 2019, doi: 10.1016/J.IJGGC.2019.01.005.

[51] L. A. TURNER, “OpenForum2022 (bloomberg (BNEF) report: 1H 2022 Hydrogen Market Outlook),” 2022. [Online]. Available: https://www.rechargenews.com/energy-transition/will-us-and-european-green-hydrogen-markets-soon-be-flooded-by-cheap-chinese-electrolysers-/2-1-1165966

[52] M. De Saint Jean, P. Baurens, C. Bouallou, and K. Couturier, “Economic assessment of a power-to-substitute-natural-gas process including high-temperature steam electrolysis,” *Int. J. Hydrogen Energy*, vol. 40, no. 20, pp. 6487–6500, 2015, doi: 10.1016/j.ijhydene.2015.03.066.

[53] M. Lehner, R. Tichler, H. Steinmüller, and M. Koppe, *Power-to-Gas: Technology and Business Models*. 2014. [Online]. Available: https://link.springer.com/book/10.1007/978-3-319-03995-4?noAccess=true

[54] Aspen Technology Inc., “Aspen Energy Analyzer.” AspenTech, 2019.

[55] “IEA - Iron & Steel Roadmap,” 2020. https://www.iea.org/reports/iron-and-steel-technology-roadmap. (accessed Apr. 26, 2022).

[56] A. L. Kohl and R. B. Nielsen, *Gas Purification*. 1997. doi: https://doi.org/10.1016/B978-0-88415-220-0.X5000-9.

[57] C. Ortiz, J. M. Valverde, R. Chacartegui, L. A. Perez-Maqueda, and P. Giménez, “The Calcium-Looping (CaCO3/CaO) process for thermochemical energy storage in Concentrating Solar Power plants,” *Renew. Sustain. Energy Rev.*, vol. 113, p. 109252, Oct. 2019, doi: 10.1016/J.RSER.2019.109252.

[58] G. Benjaminsson, J. Benjaminsson, and R. B. Rudberg, “Power-to-Gas - A technical review. Report.,” 2013. [Online]. Available: http://sgc.camero.se/ckfinder/userfiles/files/SGC284_eng.pdf

[59] “Quarterly Coal Report July–September 2021. U.S. Department of Energy,” 2021. [Online]. Available: https://www.eia.gov/coal/production/quarterly/pdf/qcr-all.pdf

[60] T. Economics, “Trading Economics. Natural gas.” https://tradingeconomics.com/commodity/natural-gas (accessed Jul. 01, 2022).

[61] M. Hurskainen, “Industrial oxygen demand in Finland.” 2017. [Online]. Available: https://www.vttresearch.com/sites/default/files/julkaisut/muut/2017/VTT-R-06563-17.pdf

[62] M. Bailera, B. Peña, P. Lisbona, J. Marín, and L. M. Romeo, “Lab-scale experimental tests of power to gas-oxycombustion hybridization: System design and preliminary results,” *Energy*, vol. 226, 2021, doi: 10.1016/j.energy.2021.120375.

[63] D. Markus Rabensteiner, “Evaluation of CO2 absorption solvents for post-combustion capture on the basis of pilot plant studies on hard coal-fired power plants. Doctoral thesis.,” 2016.

[64] M. Zier, P. Stenzel, L. Kotzur, and D. Stolten, “A review of decarbonization options for the glass industry,” *Energy Convers. Manag. X*, vol. 10, no. February, p. 100083, 2021, doi: 10.1016/j.ecmx.2021.100083.

[65] I. Papadogeorgos and K. M. Schure, “Decarbonisation Options for the Dutch Container and Tableware Glass Industry,” 2019. [Online]. Available:

https://www.pbl.nl/sites/default/files/downloads/pbl-2019-decarbonisation-options-for-the-dutch-container_and_tableware_glass_industry_3720.pdf
[66] U. S. D. of Energy, “Energy and environmental profile of the U.S. glass industry,” 2002, [Online]. Available: https://www.nrel.gov/docs/fy02osti/32135.pdf
[67] B. Maria, A. Soria, A. Schmitz, and J. Kamin, “Energy consumption and CO2 emissions of the European glass industry,” vol. 39, pp. 142–155, 2011, doi: 10.1016/j.enpol.2010.09.022.
[68] P. Hu, Y. Li, X. Zhang, Z. Guo, and P. Zhang, “CO2 emission from container glass in China, and emission reduction strategy analysis,” vol. 3004, no. May, 2018, doi: 10.1080/17583004.2018.1457929.
[69] S. Gärtner *et al.*, “Simulation and techno-economic analysis of a power-to-hydrogen process for oxyfuel glass melting,” *Energies*, vol. 14, no. 24, pp. 1–24, 2021, doi: 10.3390/en14248603.
[70] S. Gärtner, T. Marx-Schubach, M. Gaderer, G. Schmitz, and M. Sterner, “Techno-Economic Analysis of Carbon Dioxide Separation for an Innovative Energy Concept towards Low-Emission Glass Melting,” *Energies*, vol. 16, no. 5, 2023, doi: 10.3390/en16052140.
[71] G. Manzolini, A. Giuffrida, P. D. Cobden, H. A. J. van Dijk, F. Ruggeri, and F. Consonni, “Techno-economic assessment of SEWGS technology when applied to integrated steel-plant for CO2 emission mitigation,” *Int. J. Greenh. Gas Control*, vol. 94, no. February 2019, p. 102935, 2020, doi: 10.1016/j.ijggc.2019.102935.
[72] C. Barón, J. Perpiñán, M. Bailera, and B. Peña, “Techno-economic assessment of glassmaking decarbonization through integration of calcium looping carbon capture and power-to-gas technologies,” *Sustain. Prod. Consum.*, vol. 41, pp. 121–133, 2023, doi: 10.1016/j.spc.2023.07.029.
[73] J. Perpiñán, M. Bailera, and B. Peña, “Full oxygen blast furnace steelmaking: from direct hydrogen injection to methanized BFG injection,” *Energy Convers. Manag.*, vol. 295, p. 117611, 2023, doi: 10.1016/j.enconman.2023.117611.
[74] J. Perpiñán, M. Bailera, B. Peña, P. Kannan, V. Eveloy, and L. M. Romeo, “Power to Gas and Top Gas Recycling integration in an oxygen blast furnace steelmaking industry,” *J. CO2 Util.*, vol. 78, p. 102634, 2023, doi: 10.1016/j.jcou.2023.102634.
[75] J. Perpiñán, M. Bailera, B. Peña, L. M. Romeo, and V. Eveloy, “High oxygen and SNG injection in blast furnace steelmaking with Power to Gas integration and CO2 recycling,” *J. Clean. Prod.*, vol. 405, p. 137001, 2023, doi: 10.1016/j.jclepro.2023.137001.
[76] International Energy Agency, “Iron and Steel Technology Roadmap, IEA, Paris,” 2020. https://www.iea.org/reports/iron-and-steel-technology-roadmap (accessed Apr. 26, 2022).
[77] World Steel Association, “WorldSteel.” https://worldsteel.org/steel-topics/statistics/world-steel-in-figures-2022/
[78] J. Wu, R. Wang, G. Pu, and H. Qi, “Integrated assessment of exergy, energy and carbon dioxide emissions in an iron and steel industrial network,” *Appl. Energy*, vol. 183, pp. 430–444, 2016, doi: 10.1016/j.apenergy.2016.08.192.
[79] H. He, H. Guan, X. Zhu, and H. Lee, “Assessment on the energy flow and carbon emissions of integrated steelmaking plants,” *Energy Reports*, vol. 3, pp. 29–36, 2017, doi: 10.1016/j.egyr.2017.01.001.

[80] J. Perpiñán, M. Bailera, L. M. Romeo, B. Peña, and V. Eveloy, “CO2 Recycling in the Iron and Steel Industry via Power-to-Gas and Oxy-Fuel Combustion,” *Energies*, vol. 14, p. 7090, 2021, doi: 10.3390/en14217090.

[81] K. He and L. Wang, “A review of energy use and energy-efficient technologies for the iron and steel industry,” *Renew. Sustain. Energy Rev.*, vol. 70, no. September 2016, pp. 1022–1039, 2017, doi: 10.1016/j.rser.2016.12.007.

[82] M. Bailera, P. Lisbona, B. Peña, and L. M. Romeo, *Energy Storage*. Cham: Springer International Publishing, 2020. doi: 10.1007/978-3-030-46527-8.

[83] W. Zhang, J. Dai, C. Li, X. Yu, Z. Xue, and H. Saxén, “A Review on Explorations of the Oxygen Blast Furnace Process,” *Steel Res. Int.*, vol. 92, no. 1, 2021, doi: 10.1002/srin.202000326.

[84] J. Raič *et al.*, “CFD simulation aided glass quality and energy efficiency analysis of an oxy-fuel glass melting furnace with electric boosting,” *Energy Convers. Manag. X*, vol. 15, no. June, 2022, doi: 10.1016/j.ecmx.2022.100252.

[85] B. Arias *et al.*, “Operating Experience in la Pereda 1.7 MWth Calcium Looping Pilot,” *Energy Procedia*, vol. 114, pp. 149–157, 2017, doi: 10.1016/j.egypro.2017.03.1157.

[86] P. Jin, Z. Jiang, C. Bao, S. Hao, and X. Zhang, “The energy consumption and carbon emission of the integrated steel mill with oxygen blast furnace,” *Resour. Conserv. Recycl.*, vol. 117, pp. 58–65, 2017, doi: 10.1016/j.resconrec.2015.07.008.

[87] “International Energy Agency, Iron and Steel Technology Roadmap.,” 2020. https://www.iea.org/reports/iron-and-steel-technology-roadmap (accessed Apr. 26, 2022).

[88] G. Danloy *et al.*, “ULCOS - Pilot testing of the low-CO2 Blast Furnace process at the experimental BF in Lulea,” *Rev. Metall. Cah. D’Informations Tech.*, vol. 106, no. 1, pp. 1–8, 2009, doi: 10.1051/metal/2009008.

[89] “Steelmaking technologies. CISDI ingeniering CO. LTD,” 2022. http://www.cisdigroup.com/4-steelmaking.html (accessed Apr. 26, 2022).

[90] K. T. M. A. Babich, D. Senk, H. W. Gudenau, *IRONMAKING. ISBN: 3861309971.* 2008.

[91] A. K. Biswas, *Principles of blast furnace ironmaking. Theory and practice*. Cootha Publishing house, 1981.

[92] M. Bailera, T. Nakagaki, and R. Kataoka, “Revisiting the Rist diagram for predicting operating conditions in blast furnaces with multiple injections,” 2021, doi: 10.12688/openreseurope.14275.1.

[93] M. Bailera, “DISIPO project. Personal communication (mbailera@unizar.es),” 2022. Accessed: Jul. 12, 2022. [Online]. Available: https://cordis.europa.eu/project/id/887077/es

[94] M. Bailera, T. Nakagaki, and R. Kataoka, “Extending the operating line methodology to consider shaft and preheating injections in blast furnaces,” *ISIJ Int.*, vol. 62, no. 12, pp. 1–12, 2022, doi: 10.2355/isijinternational.ISIJINT-2022-111.

[95] L. V. Fisher and A. R. Barron, “The recycling and reuse of steelmaking slags — A review,” *Resour. Conserv. Recycl.*, vol. 146, no. January, pp. 244–255, 2019, doi: 10.1016/j.resconrec.2019.03.010.

[96] Pasquale Cavaliere, “Clean Ironmaking and Steelmaking Processes. Efficient

Technologies for Greenhouse Emissions Abatement", doi: https://doi.org/10.1007/978-3-030-21209-4.

[97] Aspen Technology Inc., "Aspen Examples - Reference Manual." AspenTech, 2019.

[98] Y. A. Alsultanny and N. N. Al-Shammari, "Oxygen specific power consumption comparison for air separation units," *Eng. J.*, vol. 18, no. 2, pp. 67–80, 2014, doi: 10.4186/ej.2014.18.2.67.

[99] A. Darde, R. Prabhakar, J. P. Tranier, and N. Perrin, "Air separation and flue gas compression and purification units for oxy-coal combustion systems," *Energy Procedia*, vol. 1, no. 1, pp. 527–534, 2009, doi: 10.1016/j.egypro.2009.01.070.

[100] M. Aneke and M. Wang, *Improving the Energy Efficiency of Cryogenic Air Separation Units (ASU) through Compressor Waste Heat Recovery using Direct Binary Heat Engine Cycle*, vol. 37, no. June. Elsevier, 2015. doi: 10.1016/B978-0-444-63576-1.50090-X.

[101] R. Kehlhofer, R. Bachmann, H. Nielsen, and J. Warner, "Combined-cycle gas & steam turbine power plants-PennWell." 1999.

[102] T. Ariyama, M. Sato, T. Nouchi, and K. Takahashi, "Evolution of blast furnace process toward reductant flexibility and carbon dioxide mitigation in steel works," *ISIJ Int.*, vol. 56, no. 10, pp. 1681–1696, 2016, doi: 10.2355/isijinternational.ISIJINT-2016-210.

[103] M. Sato, K. Takahashi, T. Nouchi, and T. Ariyama, "Prediction of next-generation ironmaking process based on oxygen blast furnace suitable for CO2 mitigation and energy flexibility," *ISIJ Int.*, vol. 55, no. 10, pp. 2105–2114, 2015, doi: 10.2355/isijinternational.ISIJINT-2015-264.

[104] J. G. Peacey and W. G. Davbenport, *The Iron Blast Furnace. Theory and Practice (1979)*. 1979. doi: ISBN 0-08-023258-2.

[105] R. K. Sahu, S. K. Roy, and P. K. Sen, "Applicability of Top Gas Recycle Blast Furnace with Downstream Integration and Sequestration in an Integrated Steel Plant," *Steel Res. Int.*, vol. 1, no. 5, pp. 502–516, 2015, doi: 10.1002/srin.201400196.

[106] W. Zhang, J. Zhang, and Z. Xue, "Exergy analyses of the oxygen blast furnace with top gas recycling process," *Energy*, vol. 121, pp. 135–146, 2017, doi: 10.1016/j.energy.2016.12.125.

[107] C. L. Li, Q. G. Xue, Y. L. Liu, Z. S. Dong, G. Wang, and J. S. Wang, "Comprehensive analysis on material and exergy balances of oxygen blast furnace," *Ironmak. Steelmak.*, vol. 46, no. 8, pp. 761–770, 2019, doi: 10.1080/03019233.2017.1410947.

[108] P. C. Pistorius, J. Gibson, and M. Jampani, "Natural gas utilization in blast furnace ironmaking: Tuyere injection, shaft injection and prereduction," *Miner. Met. Mater. Ser.*, no. 9783319510903, pp. 283–292, 2017, doi: 10.1007/978-3-319-51091-0_26.

[109] M. Bailera, T. Nakagaki, and R. Kataoka, "Limits on the integration of power to gas with blast furnace ironmaking," Elsevier, Sep. 2022. doi: 10.1016/J.JCLEPRO.2022.134038.

[110] R. Kumar Sahu, C. Halder, and P. K. Sen, "Optimization of Top Gas Recycle Blast Furnace Emissions with Implications of Downstream Energy," *steel Res. Int.*, vol. 87, no. 9, pp. 1190–1202, Sep. 2016, doi: 10.1002/srin.201500312.

[111] J. Perpiñán *et al.*, “Integration of carbon capture technologies in blast furnace based steel making: a comprehensive and systematic review,” *Fuel*, 2023, doi: 10.1016/j.fuel.2022.127074.
[112] “Marketwatch web page (HRC steel),” 2022. https://www.marketwatch.com/investing/index/steel?countryCode=XX (accessed Jul. 25, 2022).
[113] S. G. Subraveti, E. Rodriguez, A. Ramirez Ramirez, and S. Roussanaly, “Is CCS Really so Expensive? An Analysis of Cascading Costs and CO2 Emissions Reduction of Industrial CCS Implementation Applied to a Bridge,” *Environ. Sci. Technol.*, 2022, doi: 10.2139/ssrn.4278030.
[114] “IRENA,” 2022. https://www.irena.org/costs/Power-Generation-Costs (accessed May 10, 2022).
[115] K. Suzuki, K. Hayashi, K. Kuribara, T. Nakagaki, and S. Kasahara, “Quantitative evaluation of CO2 emission reduction of active carbon recycling energy system for ironmaking by modeling with aspen plus,” *ISIJ Int.*, vol. 55, no. 2, pp. 340–347, 2015, doi: 10.2355/isijinternational.55.340.
[116] C. Yilmaz, J. Wendelstorf, and T. Turek, “Modeling and simulation of hydrogen injection into a blast furnace to reduce carbon dioxide emissions,” *J. Clean. Prod.*, vol. 154, pp. 488–501, 2017, doi: 10.1016/j.jclepro.2017.03.162.
[117] J. Kim *et al.*, “An integrative process of blast furnace and SOEC for hydrogen utilization: Techno-economic and environmental impact assessment,” *Energy Convers. Manag.*, vol. 250, no. August, p. 114922, 2021, doi: 10.1016/j.enconman.2021.114922.
[118] K. Hayashi *et al.*, “Process evaluation of use of high temperature gas-cooled reactors to an ironmaking system based on active carbon recycling energy system,” *ISIJ Int.*, vol. 55, no. 2, pp. 348–358, 2015, doi: 10.2355/isijinternational.55.348.
[119] Y. Hu *et al.*, “Opportunities to reduce energy consumption and $CO_2$ emissions from ironmaking blast furnace using $CO_2$ electrolysis to CO for carbon recycling,” *J. Clean. Prod.*, vol. 389, no. January, p. 135997, 2023, doi: 10.1016/j.jclepro.2023.135997.
[120] A. Alarcón, J. Guilera, J. A. Díaz, and T. Andreu, “Optimization of nickel and ceria catalyst content for synthetic natural gas production through CO2 methanation,” *Fuel Process. Technol.*, vol. 193, no. May, pp. 114–122, 2019, doi: 10.1016/j.fuproc.2019.05.008.
[121] M. Bailera *et al.*, “Synthetic natural gas production in a 1 kW reactor using Ni-Ce/Al2O3 and Ru-Ce/Al2O3: Kinetics, catalyst degradation and process design,” *Energy*, vol. 256, p. 124720, 2022, doi: 10.1016/j.energy.2022.124720.
[122] L. Falbo, M. Martinelli, C. G. Visconti, L. Lietti, C. Bassano, and P. Deiana, “Kinetics of CO2 methanation on a Ru-based catalyst at process conditions relevant for Power-to-Gas applications,” *Appl. Catal. B Environ.*, vol. 225, no. August 2017, pp. 354–363, 2018, doi: 10.1016/j.apcatb.2017.11.066.
[123] P. J. Lunde and F. L. Kester, “Rates of methane formation from carbon dioxide and hydrogen over a ruthenium catalyst,” *J. Catal.*, vol. 30, no. 3, pp. 423–429, 1973, doi: 10.1016/0021-9517(73)90159-0.
[124] Y. Zhang and C. C. Chen, “Modeling CO2 absorption and desorption by aqueous monoethanolamine solution with Aspen rate-based model,” *Energy Procedia*,

vol. 37, pp. 1584–1596, 2013, doi: 10.1016/j.egypro.2013.06.034.
[125] D. C. Thomas, *Carbon Dioxide Capture for Storage in Deep Geologic Formations – Results from the CO2 Capture Project*, vol. 1. 2005. doi: 10.1016/B978-008044570-0/50099-4.
[126] M. Abdul Quader, S. Ahmed, S. Z. Dawal, and Y. Nukman, "Present needs, recent progress and future trends of energy-efficient Ultra-Low Carbon Dioxide (CO2) Steelmaking (ULCOS) program," *Renew. Sustain. Energy Rev.*, vol. 55, pp. 537–549, Mar. 2016, doi: 10.1016/J.RSER.2015.10.101.
[127] ArcelorMittal, "ArcelorMittal Climate Action Report 2," 2021, [Online]. Available: https://corporate.arcelormittal.com/sustainability/climate-action-reports
[128] S. Tonomura, "Outline of course 50," *Energy Procedia*, vol. 37, pp. 7160–7167, 2013, doi: 10.1016/j.egypro.2013.06.653.
[129] H. A. J. Van Dijk *et al.*, "Stepwise project: Sorption-enhanced water-gas shift technology to reduce carbon footprint in the iron and steel industry," *Johnson Matthey Technol. Rev.*, vol. 62, no. 4, 2018, doi: 10.1595/205651318X15268923666410.
[130] "HyGlass, 2020. IN4climate. NRW.," 2020. https://www.in4climate.nrw/best-practice/2020 /hyglass/. (accessed Jun. 03, 2024).
[131] G. Morris, "NSG to Test Hydrogen Fuel for Glassmaking at St Helens Site. Glass International.," 2020. https://www.glass-international.com/news/ (accessed May 08, 2023).
[132] Kopernikus, "Kopernikus Project: P2X.," 2022.
[133] K. E. Daehn, A. C. Serrenho, and J. M. Allwood, "How Will Copper Contamination Constrain Future Global Steel Recycling?," *Environ. Sci. Technol.*, 2017, doi: 10.1021/acs.est.7b00997.
[134] Y. Ujisawa, S. Tonomura, N. Ishiwata, Y. Nabeshima, and K. Saito, "Topic: CO2 Breakthrough Program by COURSE50 in Japanese Steel Industry Sector," *Energy Technol. Roadmaps Japan Futur. Energy Syst. Based Feasible Technol. Beyond 2030*, pp. 1–573, 2016, doi: 10.1007/978-4-431-55951-1_29.
[135] ArcelorMittal, "ArcelorMittal (2017), Integrated Annual Review," 2017. https://www.arcelormittal-reports.com/reports/integrated-2017/index.php
[136] ArcelorMittal, "ArcelorMittal (2019), Launch of the '3D' Project for the Capture and Storage of CO2," 2019. https://automotive.arcelormittal.com/news_and_stories/news/2019DMXproject
[137] ArcelorMittal, "ArcelorMittal Climate Action Report 1," no. May, 2019, [Online]. Available: https://corporate.arcelormittal.com/sustainability/arcelormittal-climate-action-report
[138] Saarstahl, "Sustainable Steel Production at the Saar: Dillinger and Saarstahl Are for the First Time Using Hydrogen in Blast Furnaces to Reduce Carbon Emissions," 2019. https://www.saarstahl.com/sag/en/group/media/press/sustainable-steel-production-at-the-saar-dillinger-and-saarstahl-are-for-the-first-time-using-hydrogen-in-blast-furnaces-to-reduce-carbon-emissions-88595.shtml
[139] STEPWISE, "STEPWISE: A H2020 Project," 2020. https://www.stepwise.eu/project/
[140] LanzaTech, "World First Products made from Recycled Pollution Reduce

Emissions and Keep Carbon in the Ground!," 2019. https://renewable-carbon.eu/news/world-first-products-made-from-recycled-pollution-reduce-emissions-and-keep-carbon-in-the-ground/
[141] LanzaTech, "World's First Commercial Waste Gas to Ethanol Plant Now in Operation," 2018. https://aclima.eus/worlds-first-commercial-waste-gas-to-ethanol-plant-now-in-operation/
[142] ArcelorMittal, "Steelanol Open Door," 2022. http://www.steelanol.eu/en/news/steelanol-opendoor
[143] FReSMe, "FReSMe," 2020. http://www.fresme.eu/about.php
[144] E. Commission, "European Commission (2019), From Residual Steel Gasses to Methanol, CORDIS EU research results," 2019. https://cordis.europa.eu/project/id/727504
[145] Thyssenkrupp, "Thyssenkrupp (2020), The Carbon2Chem Project," 2020. https://www.thyssenkrupp.com/en/newsroom/content-page-162.html
[146] Thyssenkrupp, "Thyssenkrupp (2020), Targeting a Future Without CO2 : Our Climate Strategy for Sustainable Steel Production," 2020. https://www.thyssenkrupp-steel.com/en/company/sustainability/climate-strategy/?gclid=EAIaIQobChMIgL2O88zv6AIV1O5RCh2W2wacEAAYASAAEgI08PD_BwE
[147] Carbon4PUR, "Carbon4PUR (2020), At a Glance," 2020. https://www.carbon4pur.eu/about/at-a-glance/
[148] ADNOC, "ADNOC (Abu Dhabi National Oil Company) (2017), ADNOC and Masdar's Carbon Capture Facility Holds Key to Limiting Industrial CO2 Emissions," *2017*. https://www.adnoc.ae/en/news-%0Aand-media/press-releases/2017/adnoc-and-masdars-carbon-capture-facility-holds-key- to-limiting-industrial-co2-emissions
[149] Ternium, "Ternium (2018), Low Carbon Energy Cases at Ternium, presentation at American steel expert's dialogue in the framework of the IEA Global Sustainable Technology Roadmap for Iron and Steel," 2018. https://iea.blob.core.windows.net/assets/imports/events/64/LowcarbonenergycasesatTernium.pdf
[150] Primetals, "Primetals," 2023. https://www.primetals.com/
[151] Tata Steel, "HISARNA Building a sustainable steel industry," 2022, [Online]. Available: www.tatasteeleurope.com/en/innovation/hisarna
[152] Thyssenkrupp, "World first in Duisburg as NRW economics minister Pinkwart launches tests at thyssenkrupp into blast furnace use of hydrogen," 2019. https://www.thyssenkrupp.com/en/newsroom/press-releases/world-first-in-duisburg-as-nrw-economics-minister-pinkwart-launches-tests-at-thyssenkrupp-into-blast-furnace-use-of-hydrogen-17280.html
[153] Tenova, "Tenova (2018), HYL News," 2018. https://www.tenova.com/fileadmin/user_upload/HYL_News_-_December_2018.pdf
[154] SALCOS, "SALCOS (2019), Salzgitter Low CO2 Steelmaking," 2019. https://salcos.salzgitter-ag.com/en/index.html (accessed Sep. 11, 2024).
[155] M. Pei, M. Petäjäniemi, A. Regnell, and O. Wijk, "Toward a fossil free future with hybrit: Development of iron and steelmaking technology in Sweden and Finland," *Metals (Basel).*, vol. 10, no. 7, pp. 1–11, 2020, doi:

10.3390/met10070972.
[156] ArcelorMittal, “ArcelorMittal (2019), Hydrogen-Based Steelmaking to Begin in Hamburg,” 2019. https://corporate.arcelormittal.com/media/case-studies/hydrogen-based-steelmaking-to-begin-in-hamburg
[157] Iberdrola and H. G. Steel, “Iberdrola y H2 Green Steel firman acuerdo de hidrógeno verde de 2.300 millones de euros,” *2021*. https://www.iberdrola.com/sala-comunicacion/noticias/detalle/acuerdo-hidrogeno-verde-iberdrola-h2-green-steel
[158] K1-MET, “K1-MET.” https://www.k1-met.com/
[159] H. Y. Sohn, Y. Mohassab, M. Elzohiery, D. Fan, and A. Abdelghany, “Status of the Development of Flash Ironmaking Technology,” in *Applications of Process Engineering Principles in Materials Processing, Energy and Environmental Technologies. The Minerals, Metals & Materials Series. Springer, Cham.*, 2017. doi: 10.1007/978-3-319-51091-0_2.
[160] J. Wiencke, H. Lavelaine, P. J. Panteix, C. Petitjean, and C. Rapin, “Electrolysis of iron in a molten oxide electrolyte,” *J. Appl. Electrochem.*, vol. 48, no. 1, pp. 115–126, 2018, doi: 10.1007/s10800-017-1143-5.
[161] B. Metal, “Molten Oxide Electrolysis for steel decarbonization,” 2019. https://www.bostonmetal.com/green-steel-solution/
[162] R. Nascimento, A. Almeida, E. Oliveira, A. De Jesus, and R. L. De Moraes, “18 months of charcoal fines’ injection into Gusa Nordeste’s blast furnaces,” *3rd Int. Meet. Ironmak.*, no. 1, pp. 845–856, 2012, [Online]. Available: https://foundrygate.com/upload/artigos/18%2520Months%2520of%2520Charcoal%2520Fines%25 27Injection%2520into%2520Gusa%2520Nordeste%2527s%2520Blast%2520Furnaces.pdf

# Annexes

## A I&S industry: $CO_2$ emissions and state of the art

### A.1. Energy consumption and $CO_2$ emissions

The iron and steel sector holds the top position in terms of $CO_2$ emissions among heavy industries and ranks second in terms of energy consumption. This sector is directly responsible for emitting 2.6 gigatonnes of carbon dioxide (Gt of $CO_2$) annually, accounting for 7% of the global emissions from the energy system. When considering indirect emissions from the power sector and the combustion of steel off-gases, the iron and steel sector's contribution to energy system $CO_2$ emissions increases to 10% [76]. Currently, the steel industry is the largest consumer of coal among industrial sectors, with coal meeting approximately 75% of its energy demand. Coal is utilized for generating heat and producing coke, a crucial component in the chemical reactions necessary for steel production from iron ore.

To achieve energy and climate goals, it is essential to address existing infrastructure. Global crude steel production capacity has more than doubled in the past two decades, with the majority of the growth occurring in China. Currently, around 85% of the total steel production capacity is situated in emerging economies. This rapid expansion has resulted in a relatively young global blast furnace fleet, averaging around 13 years of age, which is less than one-third of their typical lifespan. If these plants and other assets in the steel industry continue to operate until the end of their typical lifespans under current conditions, they could contribute to cumulative emissions of approximately 65 $Gt_{CO2}$. This would consume a significant portion of the $CO_2$ budget compatible with a sustainable transition for the sector, leaving little room for capacity additions that will be necessary in the coming decades [76].

The adoption of new technologies and infrastructure must occur at a rapid pace. In the Net Zero Emissions pathway, global deployment of one hydrogen-based direct reduced iron (DRI) plant per month is required after the technology's market introduction, see Figure 40. This would increase electricity demand by 720 terawatt hours by 2050, equivalent to 60% of the sector's current total electricity consumption. Simultaneously, the deployment of carbon capture, utilization, and storage (CCUS) equipped plants would necessitate approximately 400 Mt of $CO_2$ capture globally in 2050, equivalent to installing a large-scale CCUS facility (capturing 1 million tonnes of CO2 per year) every 2-3 weeks starting from 2030 [76].

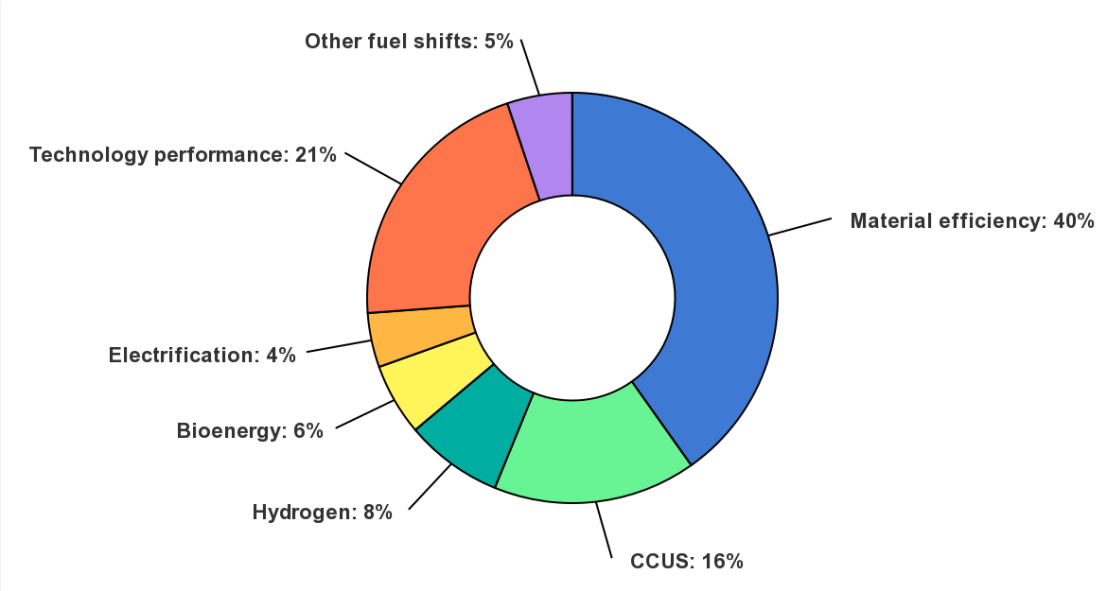


*Figure 40.Cumulative direct emission reductions by mitigation strategy in the sustainable development scenario between 2020 and 2050 [76].*

## A.2. Main pathways for steelmaking production

In the steelmaking process today, the primary inputs include iron ore, energy (mainly coal, natural gas, and electricity), limestone, and steel scrap. Iron ore and scrap are utilized as the metallic charge for the process. Energy inputs are required to generate heat for melting the metallic input and, in the case of iron ore, to chemically reduce it by removing oxygen. The reducing agents responsible for removing oxygen from iron ore molecules are carbon monoxide and hydrogen. This reduction process results in the formation of $CO_2$ and $H_2O$ as final products, which is an exothermic reaction. On the other hand, reduction by carbon leads to the formation of CO as the final product, which is an endothermic reaction [90], see Eq (47) – Eq (58).

The production of carbon monoxide and hydrogen, which are essential for reducing iron ore, relies almost entirely on fossil fuels. Coal and its derivative coke, along with natural gas to a lesser extent, are the main primary energy sources of these inputs.

The primary production of crude steel involves three main phases: raw material preparation, ironmaking, and steelmaking (Figure 14). In the raw material preparation phase, after mining and beneficiation, the iron ore undergoes processing before it can be used in the ironmaking stage. This processing involves the production of sinter or pellets, depending on the iron content of the ore and the desired quality of the pellets or sinter. These processes typically consume 1-3 gigajoules (GJ) per tonne of pellets or sinter [76]. Another input, coke, requires an intermediate step of transformation. Coking coal, a specific type of hard coal with a high carbon content, is heated to approximately 1100 °C in a coke oven in the absence of air. This process eliminates volatile components and results in the production of coke, a predominantly carbon-based substance with excellent compressive strength. Scrap metal also undergoes some preparation, often separated from other materials using magnets, before it is utilized in steelmaking [133].

Indirect Reduction:

$$3Fe_2O_3 + CO \rightarrow 2Fe_3O_4 + CO_2 \qquad \Delta H = -52.85\ kJ/mol \tag{47}$$

$$3Fe_2O_3 + H_2 \rightarrow 2Fe_3O_4 + H_2O \qquad \Delta H = -4.86\ kJ/mol \tag{48}$$

$$Fe_3O_4 + CO \rightarrow 3FeO + CO_2 \qquad \Delta H = +36.46\ kJ/mol \tag{49}$$

$$Fe_3O_4 + H_2 \rightarrow 3FeO + H_2O \qquad \Delta H = +84.45\ kJ/mol \tag{50}$$

$$FeO + CO \rightarrow Fe + CO_2 \qquad \Delta H = -17.13 kJ/mol \tag{51}$$

$$FeO + H_2 \rightarrow Fe + H_2O \qquad \Delta H = +30.86\ kJ/mol \tag{52}$$

Overall global reactions of Indirect Reduction:

$$Fe_2O_3 + 3CO \rightarrow 2Fe + 3CO_2 \qquad \Delta H = -27.52\ kJ/mol \tag{53}$$

$$Fe_2O_3 + 3H_2 \rightarrow 2Fe + 3H_2O \qquad \Delta H = +88.44\ kJ/mol \tag{54}$$

Direct Reduction:

$$3Fe_2O_3 + C \rightarrow 2Fe_3O_4 + CO \qquad \Delta H = +119.62\ kJ/mol \tag{55}$$

$$Fe_3O_4 + C \rightarrow 3FeO + CO \qquad \Delta H = +208.93\ kJ/mol \tag{56}$$

$$FeO + C \rightarrow Fe + CO \qquad \Delta H = +155.34\ kJ/mol \tag{57}$$

Overall global reaction of Direct Reduction:

$$Fe_2O_3 + 3C \rightarrow 2Fe + 3CO \qquad \Delta H = +483.89\ kJ/mol \tag{58}$$

During the ironmaking phase, various methods, as depicted in Figure 14, are employed to reduce iron ore into elemental iron. These methods include the blast furnace, DR furnace, and smelting reduction furnace. Subsequently, in the steelmaking phase of primary production, final steel is manufactured through processes like the basic oxygen furnace, electric arc furnace, and open hearth furnace. The secondary production route also employs the electric arc furnace.

In the industry, within the primary production route, two main production pathways exist: the blast furnace-basic oxygen furnace (BF-BOF) and the direct reduced iron-electric arc furnace (DR-EAF). The BF-BOF route predominates, constituting around 70% of global steel production and approximately 90% of primary production [76]. Within this route, coke and iron ore are introduced into the blast furnace from the top. Simultaneously, hot air, pulverized coal, or natural gas is injected through tuyeres at the lower furnace section, creating a counter-current process where iron ore descends while reducing gases rise. The blast furnace yields molten iron, commonly referred to as "hot metal" or "pig iron," with temperatures ranging from 1400 to 1500 °C. This hot metal, often combined with scrap, is transferred to the BOF. Oxygen injection in the BOF reduces the carbon content from around 4-5% to the specified level for the particular steel grade, typically approximately 0.25%.

The other primary route of production, DR-EAF, differs from the BF-BOF route in several key aspects [76]:

- Iron ore type: In the DR-EAF route, high-quality DR pellets are typically used, whereas the BF-BOF route offers more flexibility to utilize iron ore with higher impurities, including a combination of pellets, fines, sinter, and lump ore.
- State of material reduction: The DR furnace reduces the iron ore in a solid state, contrasting with the blast furnace where reduction occurs in the liquid phase. After reduction, the DR is melted in the EAF, often alongside some scrap metal.
- Main reducing agents: Carbon and carbon monoxide are the primary reduction agents in the BF-BOF route, while the DR-EAF pathway involves a more balanced utilization of hydrogen and carbon monoxide.
- Energy input balance: Presently, DR-EAF facilities primarily employ natural gas to produce the reducing syngas (carbon monoxide and hydrogen). In contrast, BF-BOF producers primarily rely on coke and coal, with less frequent use of natural gas injection.

Smelting reduction is an ironmaking process that enables the direct use of iron ore fines, eliminating the need for agglomerated pellets or sinter, as well as the requirement for a coke oven or coking coal. Despite the availability of several designs for smelting reduction, its widespread adoption in the industry remains limited. The open-hearth furnace is an outdated alternative to the BOF, has become obsolete due to its lower energy efficiency and has been mostly phased out.

The secondary production route (Figure 14) primarily relies on electricity to melt recycled steel in an electric furnace. In some cases, a small amount of natural gas or coal is used to create a protective slag foam. The process of heating the scrap metal to temperatures as high as 1800 °C also requires the consumption of highly conductive graphite electrodes.

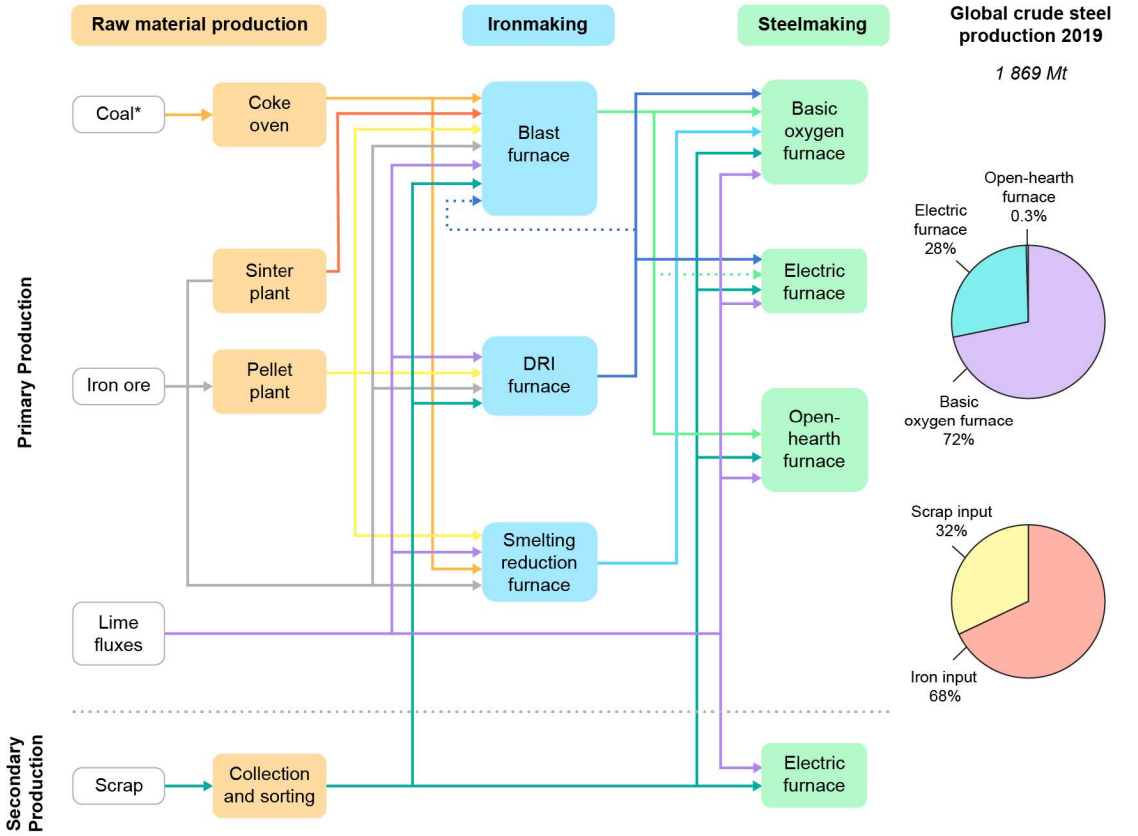


*Figure 41. Main steel production pathways and material flows in 2019 [76].*

The production cost of steel heavily relies on the cost of key inputs, namely iron ore, scrap, and energy (Table 12). These raw materials and energy inputs typically constitute 60-80% of the total production cost [76].

*Table 22. Main steelmaking production routes: BF-BOF, Scrap-EAF and DR-EAF [76], [77]*

| **Steelmaking production route** | **BF-BOF** | **Scrap-EAF** | **DR-EAF** |
|---|---|---|---|
| Steel world production (%) | 72% | 21% | 7% |
| Main inputs | Iron ore, coal and coke | Scrap and electricity | Iron ore, NG, scrap and electricity. |
| Energy consumption ($GJ/t_{Steel}$) | 21.4-22.7 | 2.1-5.2 | 17.1-21.8 |
| $CO_2$ emissions ($t_{CO2}/t_{Steel}$) | 2.2 | 0.3 | 1.4 |
| Costs ($USD/t_{Steel}$) | 330-460 | 330-510 | 400-600 |

### A.2.1. Low-carbon approaches for steelmaking industry

In a low-carbon future, new technologies that are not yet commercially available are becoming increasingly important. A range of technologies is currently being developed, and their timing of introduction and deployment rate in the Sustainable Development Scenario depend on their Technology Readiness Level (TRL). The TRL scale used in this section follows the framework provided by the IEA [76], which ranges from TRL 1 to 11. This scale represents the progression from the initial concept (TRL 1) to commercial operation (TRL 9) in relevant environments, and ultimately to predictable growth (TRL 11), as shown in Figure 42. Technologies beyond TRL 9 require further development for integration into existing systems or scalability. To address this, the IEA

expanded the TRL scale by adding two additional levels: TRL 10, where the technology is commercially viable and competitive but requires further innovation for integration into energy systems and value chains at scale, and TRL 11, where the technology has achieved predictable growth.

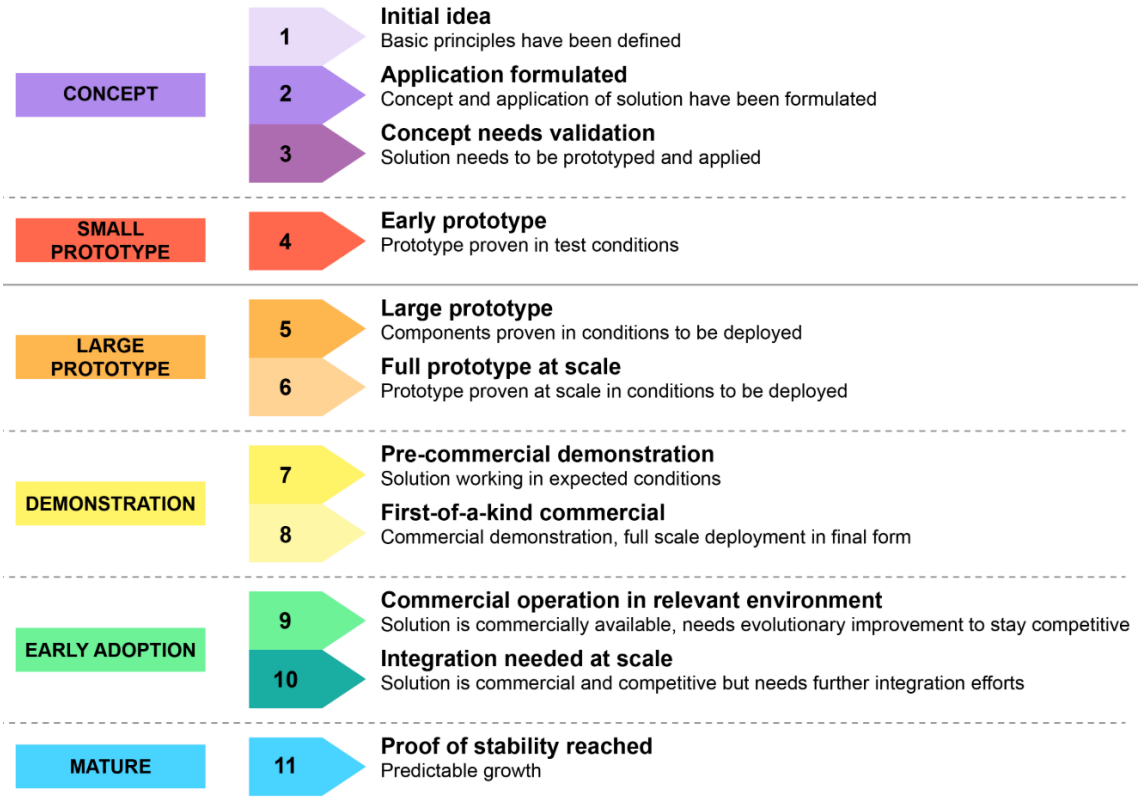


*Figure 42. TRL scale applied by the IEA [76].*

A number of innovation efforts are aiming to lower emissions from conventional blast furnace production. These technologies can be classified as: CCUS (Carbon capture, utilization and storage), Hydrogen, Direct electrification and Bioenergy, see Table 13.

**CCUS.** Blast furnace technology of off-gas hydrogen enrichment and/or $CO_2$ removal for use or storage. Currently at TRL 5, it is expected to be available by 2030. Its importance in addressing emissions is considered very high. Here is the deployment status:

- Japan's COURSE 50 project has completed its initial experimental testing phase and aims to achieve full commercial scale by 2030. It can be deployed in conjunction with CCUS [134].
- The utilization of top-gas recycling through vacuum pressure swing adsorption has been proven in an experimental blast furnace under the ULCOS project. ArcelorMittal has developed various concepts such as the IGAR project and the "3D" project, with the goal of achieving industrial-scale implementation by 2025-2027 [135]–[137].
- The ROGESA project in Germany is piloting the use of $H_2$-rich coke oven gas in a blast furnace, with plans to implement it in two blast furnaces during the 2020s [138].

- The STEPWISE project in Sweden is piloting a technology to decarbonize blast furnace gas for power production, with a capacity to remove 14 tons of $CO_2$ per day [139].

*Table 23. Status of main near-zero emission technologies in the iron and steel sector [76]. Where NZE is Net Zero Emissions.*

| Technology | TRL | Year Available | Importance for NZE |
|---|---|---|---|
| **CCUS (Carbon capture, utilization and storage)** | | | |
| Blast furnace: off-gas hydrogen enrichment and/or $CO_2$ removal for use or storage | 5 | 2030 | Very High |
| Blast furnace: Converting off-gases to fuels | 8 | Today | Medium |
| Blast furnace: Converting off-gases to chemicals | 7 | 2025 | Medium |
| DR: Natural gas-based with $CO_2$ capture | 9 | Today | Very high |
| Smelting reduction: with CCUS | 7 | 2028 | Very high |
| **Hydrogen** | | | |
| Blast furnace: electrolytic $H_2$ blending | 7 | 2025 | Medium |
| DR: Natural gas-based with high levels of electrolytic $H_2$ blending | 7 | 2030 | High |
| DR: Based solely on electrolytic $H_2$ | 5 | 2030 | Very high |
| Smelting reduction: $H_2$ plasma reduction | 4 | - | Medium |
| Ancillary processes: $H_2$ for high temperature heat | 5 | 2025 | High |
| **Direct electrification** | | | |
| Electrolysis: Low-temperature | 4 | - | Medium |
| Electrolysis: High-temperature molten oxide | 4 | - | Medium |
| **Bioenergy** | | | |
| Blast furnace: Torrefied biomass | 7 | 2025 | Medium |
| Blast furnace: Charcoal | 10 | Today | Medium |

**CCUS.** Blast furnace technology of converting off-gases to fuels. Currently at TRL 8, it is already available today. Its importance in addressing emissions is considered medium. Here is the deployment status:

- The first commercial plant, operated by LanzaTech, Shougang Group, and TangMing, started operation in China in 2018. In its first year, it produced 30 million litters of ethanol for sale [140], [141].
- In 2022, a second large-scale plant has been constructed in Ghent, Belgium, as part of the Steelanol/Carbalyst project by ArcelorMittal and LanzaTech. This plant has a capacity of 80 million liters of ethanol [127], [142].
- The FReSMe project, led by a consortium of European partners, is piloting the conversion of steel off-gas to methanol at a rate of 1 ton per day. This project builds upon the research from the STEPWISE project on $CO_2$ capture and the MefCO2 project on methanol production from $CO_2$ [143], [144].

**CCUS.** Blast furnace technology of converting off-gases to chemicals. Currently at TRL 7, it is expected to be available by 2025. Its importance in addressing emissions is considered medium. Here is the deployment status:

- The Carbon2Chem pilot plant in Germany, initiated by thyssenkrupp in 2018, has successfully produced ammonia and methanol from steel off-gases. The project aims to establish an industrial-scale plant by 2025 [145], [146]
- The Carbon4PUR project, led by a consortium of 11 partners across Europe, focuses on converting steel off-gases to polyurethane foams and coatings. The project is currently in the pilot phase, producing 20 tons per year [147]

**CCUS.** DR technology, based on natural gas and equipped with $CO_2$ capture. Currently at TRL 9, it is already available today. Its importance in addressing emissions is considered very high. Here is the deployment status:

- In Abu Dhabi, a plant has been operating since 2016 with a $CO_2$ capture capacity of 0.8 million tonnes per year. The captured $CO_2$ is utilized for Enhanced Oil Recovery (EOR) at a nearby oilfield [148].
- Ternium operates two plants in Mexico since 2008, capturing 5% of emissions (combined 0.15-0.20 million tonnes per year). The captured $CO_2$ is used in the beverage industry. Plans are underway to increase the capture capacity [149]
- Orinoco Iron in Venezuela has a commercial Finmet plant that has been operating since 1998. The plant uses amine-based $CO_2$ separation, achieving close to 100% $CO_2$ concentrations. However, the captured $CO_2$ is currently not utilized or stored [150]

**CCUS.** Smelting reduction with CCUS. Currently at TRL 7, it is expected to be available by 2028. Its importance in addressing emissions is considered very high. Here is the deployment status:

- The HIsarna pilot plant, developed by the ULCOS consortium, is currently operational at a Tata Steel plant in Ijmuiden, Netherlands. It produces 60 kt of steel, but CCS implementation has not yet been applied [151]. A demonstration-scale plant (0.5 Mt/yr) at TRL 8 is expected in India between 2023-27, and an industrial-scale plant (1.5 Mt/yr) with CCS at TRL 9 is planned in the Netherlands between 2027-33.
- Initial testing of amine-based $CO_2$ scrubbing in FINEX plant [150]

**Hydrogen.** Blast furnace technology with electrolytic $H_2$ blending. Currently at TRL 7, it is expected to be available by 2025. Its importance in addressing emissions is considered medium. Here is the deployment status:

- Since 2019 thyssenkrupp has been testing the use of hydrogen in a blast furnace in Germany, replacing a proportion of injected coal [152]

**Hydrogen.** DR technology, based on natural gas, with high levels of electrolytic $H_2$ blending. Currently at TRL 7, it is expected to be available by 2030. Its importance in addressing emissions is considered high. Here is the deployment status:

- In the 1990s, Tenova conducted tests in Mexico, achieving 90% hydrogen utilization in a DR production of 9 kt/yr [153]
- Salzgitter steelworks is carrying out a MW-scale electrolyser demonstration in Germany and conducting a feasibility study to integrate a hydrogen DR plant into the existing site as part of the SALCOS project [154].
- Thyssenkrupp is planning to build commercial DR plants incorporating hydrogen by the mid-2020s [146].

**Hydrogen.** DR technology based solely on electrolytic hydrogen. Currently at TRL 5, it is expected to be available by 2030. Its importance in addressing emissions is considered very high. Here is the deployment status:

- The HYBRIT project in Sweden started operating a pilot plant in August 2020, with plans for a 1 Mt/yr demonstration plant by 2025 [155].
- ArcelorMittal is leading the design of a pilot plant in Hamburg, scheduled for construction by 2030 [156].
- Thyssenkrupp aims to transition to full hydrogen reduction in the future [146].
- A full-scale zero carbon-emissions steel plant is set to be operational in Sestao by 2025, producing 1 Mton per year [127].
- Iberdrola and H2 Green Steel plan to build a commercial DR plant with a 1 GW electrolyser for the production of 2.5-5 Mt/year by 2025 [157].

**Hydrogen.** Smelting reduction technology based on $H_2$ plasma reduction. Currently at TRL 4, with an expected availability date yet to be determined. Its importance in addressing emissions is considered medium. Here is the deployment status:

- The SuSteel research project at the voestalpine plant in Austria is currently in the process of upscaling a 100 g reactor to a 50 kg batch operation [150], [158].
- Flash ironmaking technology is under development at the University of Utah, and a mini pilot reactor has been commissioned [159].

**Direct electrification.** Electrolysis with low-temperature electrolyser. Currently at TRL 4, with an expected availability date yet to be determined. Its importance in addressing emissions is considered medium. Here is the deployment status:

- The Siderwin project is building upon the ULCOWIN process (electrowinning) developed by the ULCOS programme. They are working towards the establishment of a pilot-scale plant by the end of 2020 (Siderwin, 2019)

**Direct electrification.** Electrolysis with high-temperature molten oxide electrolyser. Currently at TRL 4, with an expected availability date yet to be determined. Its importance in addressing emissions is considered medium. Here is the deployment status:

- The ULCOS proposed concept called MIDEIO during its 2004-12 work programme [160], and further research at MIT led to the founding of

Boston Metal. Boston Metal commissioned its first prototype cell in 2014, producing more than 1 ton of metal. They are currently aiming to establish a pilot-scale plant [161].

**Bioenergy.** Blast furnace technology with torrefied biomass. Currently at TRL 7, it is expected to be available by 2025. Its importance in addressing emissions is considered medium. Here is the deployment status:

- The Torero partnership project is conducting tests on the use of bio-coal, specifically torrefied waste wood, as a partial substitute for coal in ArcelorMittal's plant in Ghent, Belgium. The large-scale demonstration of this technology is expected to be operational by the end of 2024 [127].

**Bioenergy.** Blast furnace technology with charcoal. Currently at TRL 10, it is already available today. Its importance in addressing emissions is considered medium. Here is the deployment status:

- Charcoal is currently being commercially used as a substitute for a portion of the coal used in blast furnaces, primarily in Brazil. Ongoing development efforts aim to optimize charcoal production and improve its product specifications for steel production [162].

The extent to which emissions are reduced by these methods depends on various factors. Using $CO_2$ twice through CCU reduces emissions compared to unabated steel production with fossil fuel-based fuel or chemical production outside the steel sector. However, it may result in higher emissions compared to using zero-emission energy or CCS for both steel production and external fuel or chemical production. Exceptions for a circular and emission-free $CO_2$ loop exist, such as using steel off-gases for fuel production and utilizing this product as furnace fuel.

# B Funding and collaborations

Throughout the development of this thesis, various tasks were undertaken in collaboration with different projects and organizations:

- "Decarbonization of Iron&Steel industry through green hydrogen and CO2 recirculation (**DEC-I&S**)" Spanish Ministry of Science and Innovation (TED2021-130000B-I00).
- "Decarbonization of Iron&Steel industry through green HYdrogen, CO2 capture and MEthanation (**DIS-HYCOME**)" Spanish Ministry of Science and Innovation (PID2021-126164OB-I00).
- "Development, evaluation and optimization of sustainable power-to-gas schemes for energy-intensive industrial metal manufacturing processes" Competitive Internal Research Award (**CIRA-080-2020**).
- "Decarbonisation of carbon-intensive industries (Iron and Steel Industries) through Power to gas and Oxy-fuel combustion (**DISIPO**)" European Union's Horizon 2020 (No 887077).
- "Ramon y Cajal programme (**RYC2022-038283-I**)" MCIN/ AEI/ 10.13039/ 501100011033 and the European Social Fund Plus (FSE+)
- **K1-MET GmbH**, Linz, is also acknowledged for hosting the research stay of the researcher.

In addition to the main focus of this thesis, a collaboration is extended to several related works in the field. While these works are not the primary focus of my research, they are nonetheless valuable contributions that have helped to advance the understanding and application of power to gas technology. The following list provides an overview of these collaborative works, including papers and conferences. By examining these works in conjunction with my main research, readers can gain a more comprehensive understanding of the current state-of-the-art in this field and the potential for future advancements and fields of research.

The collaboration between myself and other researchers has resulted in the following additional papers and conferences:

a) Alexander García-Mariaca, and Jorge Perpiñán. 2023. "*Techno-economic analysis of the integration of PtG and carbon capture and storage in the transport sector*". In preparation.
b) Laura Gómez, Jorge Perpiñán, Isabel Martinez, Manuel Bailera, and Begoña Peña. "C*omparative analysis of sorption enhanced methanation and conventional methanation for methane production*." In preparation.
c) Manuel Bailera, Irmela Kofler, Jorge Perpiñán, Andreas Spanglang. 2023. "*Decarbonisation pathways based on Power to Gas for lime kilns in ironmaking plants*" In preparation.
d) Jorge Perpiñán, Michael Derntl, Irmela Kofler, Begoña Peña, and Manuel Bailera. "*Aspen Plus and GProms simulation models for $CO_2$ removal with MEA: Validation of models with experimental data*." In preparation.
e) Begoña Peña, Manuel Bailera, Belén Zalba, Pilar Lisbona, Jorge Perpiñán. "*Improving the long-term learning in Engineering Thermodynamics through*

*spaced review to overcome Ebbinghaus' forgetting curve*". XII National and III International Conference on Engineering Thermodynamics (12CNIT-2022), 29th June – 1st July 2022, Madrid, Spain.

f) Jorge Perpiñán, Manuel Bailera, Luis Miguel Romeo, Pilar Lisbona, Begoña Peña. 2024. "*Decarbonization of blast furnace steelmaking through Power to Gas: from direct H2 injection to full blast furnace gas methanation*" 13CNIT 2024.

g) Manuel Bailera, Jorge Perpiñán, Pilar Lisbona, Luis Miguel Romeo, Begoña Peña. "*Techno-economic assessment and comparison of different power to gas integrations for the reduction of CO2 emissions in the Iron and Steel industry*" ECOS 2024.

h) Cristian Barón, Manuel Bailera, Jorge Perpiñán, Pilar Lisbona, Begoña Peña "*Modelling of carbon capture through Calcium Looping technology for the integration in a blast furnace-based iron and steel industry*" Sdewes 2024

i) Begoña Peña, Manuel Bailera, Jorge Legaz, Cristian Barón, Silvia Garlatti, M. Zampilli, K. L. Slopiecka, Jordi Guilera, Elena Martín, Francesco Fantozzi, Luis M. Romeo, Pilar Lisbona. "*Development, testing, performance analysis and modelling of a biochar based catalyst for methanation reaction*" Sdewes 2024.

# C Impact factor and category

Below is the impact factor, category and quartile of the journals in which the manuscripts comprising this Doctoral Thesis have been published. The information has been obtained from the Journal Citations Reports®, with the most recent data belonging to the year 2022.

*Table 24. Journals where the manuscripts in the Doctoral Thesis were published. Journals where the manuscripts of the Doctoral Thesis were published.*

| Paper | Journal | Impact Factor | Thematic Area 1 | Thematic Area 2 | Cites Scopus |
|---|---|---|---|---|---|
| i. | Sustainable Production and Consumption | 12.1 | Environmental studies Q1, 7th/128 | Green & sustainable science & technology Q1, 6th/46 | 4 |
| ii. | Energies | 3.2 | Energy & fuels Q3, 80th/119 | - | 19 |
| iii. | Fuel | 7.4 | Energy & Fuels Q2, 32nd/119 | Chemical engineering Q1, 19th/142 | 42 |
| iv. | Energy | 8.9 | Energy & Fuels Q1, 23rd/119 | Thermodinamics Q1, 3rd/663 | 13 |
| v. | Journal of Cleaner Production | 11.1 | Environmental Engineering Q1, 8th/55 | Environmental Sciences Q1, 22nd/275 | 13 |
| vi. | Journal of CO2 Utilization | 7.7 | Multiidisciplinary Chemistry Q1, 37th/178 | Chemical Engineering Q1, 16th/142 | 2 |
| vii. | Energy Conversion and Management | 10.4 | Energy & Fuels Q1, 17th/119 | Mechanics Q1, 3rd/137 | 3 |
| viii. | Renewable and Sustainable Energy Reviews | 15.9 | Energy & Fuels Q1, 8th/119 | Green & sustainable science & technology Q1, 2nd/46 | 0 |
| ix. | Energy | 8.9 | Energy & Fuels Q1, 23rd/119 | Thermodinamics Q1, 3rd/663 | 7 |

Scopus cites date: 09-Sept-2024

# D Author contribution

In compliance with the regulations regarding the submission of theses by compendium of publications (Agreement of June 25, 2020, of the University Governing Council, which approves the Regulations on Doctoral Theses of the University of Zaragoza, BOUZ 7-20), the contribution of the author of this thesis, Jorge Perpiñán, is detailed below, along with the contribution of the other co-authors, as it appears in each publication.

i. Cristian Barón, Jorge Perpiñán, Manuel Bailera, Begoña Peña. 2023. "*Techno-economic assessment of glassmaking decarbonization through integration of calcium looping carbon capture and power-to-gas technologies*". Sustainable Production and Consumption 41 (2023) 121–133. doi: 10.1016/j.spc.2023.07.029.

Contributions: Conceptualization, J.P., M.B., C.B. and B.P.; methodology, C.B., J.P. and M.B.; model, C.B. and J.P.; validation, C.B.; formal analysis, C.B.; writing—original draft preparation, C.B.; writing—review and editing, J.P. and B.P.; visualization, C.B., J.P. and B.P.; supervision, M.B., B.P. and J.P.; project administration, M.B. and B.P.; funding acquisition, M.B., B.P.

In this paper, the thesis author supervised the model and methodology development, collaborated with and guided the first author in analyzing and discussing the results, and oversaw the final version of the manuscript.

ii. Jorge Perpiñán, Manuel Bailera, Luis M. Romeo, Begoña Peña, and Valerie Eveloy. 2021. "*$CO_2$ Recycling in the Iron and Steel Industry via Power-to-Gas and Oxy-Fuel Combustion*." Energies 14(21):7090. doi: 10.3390/en14217090.

Author Contributions: Conceptualization, J.P., M.B., L.M.R. and B.P.; methodology, J.P. and M.B.; model, J.P. and M.B.; validation, J.P. and M.B.; formal analysis, J.P.; writing—original draft preparation, J.P. and M.B.; writing—review and editing, V.E.; visualization, J.P. and M.B.; supervision, M.B., L.M.R., B.P. and V.E.; project administration, M.B., L.M.R., B.P. and V.E.; funding acquisition, M.B., L.M.R. and V.E.

In this paper, the thesis author was responsible for developing the model, detailing each process, and balancing the mass and energy streams. He contributed to the analysis, discussion, and graphical representation of the results. Additionally, he prepared the initial manuscript draft and coordinated the contributions of the other authors to ensure coherence and served as the corresponding author, managing communication with the journal and reviewers. He also ensured that the reviewers' comments were implemented according to the journal's quality standards.

iii. Jorge Perpiñán, Begoña Peña, Manuel Bailera, Valerie Eveloy, Pravin Kannan, Abhijeet Raj, Pilar Lisbona, and Luis Miguel Romeo. 2022. "*Integration of Carbon Capture Technologies in Blast Furnace Based Steel Making: A Comprehensive and Systematic Review*." Fuel 336 (2023) 127074. doi: 10.1016/j.fuel.2022.127074.

Author Contributions: Conceptualization, J.P., M.B., and B.P.; methodology, J.P., and M.B.; formal analysis, J.P.; writing—original draft preparation, J.P., P.K., A.R., P.L., M.B., B.P., L.M.R., and V.E.; writing—review and editing, M.B., and B.P; visualization, J.P. and M.B.; supervision, M.B. and B.P.; project administration, M.B. and L.M.R.; funding acquisition, M. B. L.M.R. and V.E.

In this review paper, the thesis author conducted the literature search, distributed tasks among the co-authors, and was in charge of writing key sections, including the introduction, systematic review approach, post-combustion technology, comparison of carbon capture technologies, and conclusions. He gathered the contributions from the other authors, ensuring cohesiveness and coherence throughout the document. Additionally, he refined the paper to maintain consistency and clarity, served as the corresponding author, managed communication with the journal and reviewers, and ensured that the reviewers' comments were implemented according to the journal's quality standards.

iv. Jorge Perpiñán, Manuel Bailera, Begoña Peña, Luis Miguel Romeo, and Valerie Eveloy. 2022. "*Technical and Economic Assessment of Iron and Steelmaking Decarbonization via Power to Gas and Amine Scrubbing*." Energy 276 (2023) 127616. doi: 10.1016/j.energy.2023.127616.

Author Contributions: Conceptualization, J.P., M.B., and B.P.; methodology, J.P., M.B. and B.P.; model, J.P. and M.B.; formal analysis, J.P.; writing—original draft preparation, J.P. and M.B.; writing—review and editing, M.B., B. P., L.M.R., and V.E.; visualization, J.P. and M.B.; supervision, M.B. and B.P.; project administration, M.B. and L.M.R.; funding acquisition, M. B. L.M.R. and V.E.

In this paper, the thesis author developed the model, described each process, and balanced the mass and energy streams. He handled the analysis, discussion, and visual representation of the results. Furthermore, he wrote the initial draft of the manuscript and coordinated the input from the other authors to maintain consistency throughout the work. Acting as the corresponding author, he managed communication with the journal and reviewers, ensuring that all feedback was addressed in line with the journal's quality requirements.

v. Jorge Perpiñán, Manuel Bailera, Begoña Peña, Luis M. Romeo, and Valerie Eveloy. 2023. "*High Oxygen and SNG Injection in Blast Furnace Steelmaking with Power to Gas Integration and $CO_2$ Recycling*." Journal of Cleaner Production 405 (2023) 137001. doi: 10.1016/j.jclepro.2023.137001.

Author Contributions: Conceptualization, J.P., M.B. and B.P.; methodology, J.P., M.B. and B.P.; model, J.P. and M.B.; formal analysis, J.P.; writing—original draft, J.P.; writing—review and editing, M.B., B.P., L.M.R. and V.E.; visualization, J.P. and M.B.; supervision, M.B., B.P. and L.M.R.; project administration, M.B., B.P., L.M.R. and V.E.; funding acquisition, M.B., B.P., L.M.R. and V.E.

For this paper, the thesis author was responsible for developing the model, detailing each process, and balancing the mass and energy streams. He managed the

analysis, discussion, and graphical representation of the results. Additionally, he prepared the initial manuscript draft, coordinated the contributions of the other authors to ensure coherence, and served as the corresponding author, overseeing communication with the journal and reviewers. He also ensured that the reviewers' comments were addressed in accordance with the journal's quality standards.

vi. Jorge Perpiñán, Manuel Bailera, Begoña Peña, Pravin Kannan, Valerie Eveloy, and Luis M. Romeo. 2023. "*Power to Gas and Top Gas Recycling Integration in an Oxygen Blast Furnace Steelmaking Industry*." Journal of CO2 Utilization 78 (2023) 102634. doi: 10.1016/j.jcou.2023.102634.

Author Contributions: Conceptualization, J.P., M.B. and B.P.; methodology, J.P., M.B. and B.P.; formal analysis, J.P.; visualization, J.P., M.B.; software, J.P., M.B.; writing - original draft, J.P.; writing - review & editing, M.B., B.P., P.K. V.E., L.M.R.; supervision, M.B., B.P.; project administration, M.B., B.P, L.M.R., V.E. ; funding acquisition, M.B., B.P, L.M.R., V.E.

In this paper, the thesis author developed the model, described each process, and balanced the mass and energy streams. He handled the analysis, discussion, and visual representation of the results. Furthermore, he wrote the initial draft of the manuscript and coordinated the input from the other authors to maintain consistency throughout the work. Acting as the corresponding author, he managed communication with the journal and reviewers, ensuring that all feedback was addressed in line with the journal's quality requirements.

vii. Jorge Perpiñán, Manuel Bailera, and Begoña Peña. 2023. "*Full oxygen blast furnace steelmaking: from direct hydrogen injection to methanized BFG injection*." Energy conversion and management 295 (2023) 117611. doi: 10.1016/j.enconman.2023.117611.

Author Contributions: Conceptualization, J.P., M.B. and B.P.; methodology, J.P., M.B. and B.P.; formal analysis, J.P.; visualization, J.P., M.B.; software, J.P., M.B.; writing - original draft, J.P.; writing - review & editing, M.B., B.P.; supervision, M.B., B.P.; project administration, M.B., B.P.; funding acquisition, M.B., B.P.

For this paper, the thesis author was responsible for developing the model, detailing each process, and balancing the mass and energy streams. He managed the analysis, discussion, and graphical representation of the results. Additionally, he prepared the initial manuscript draft, coordinated the contributions of the other authors to ensure coherence, and served as the corresponding author, overseeing communication with the journal and reviewers. He also ensured that the reviewers' comments were addressed in accordance with the journal's quality standards.

viii. Jorge Perpiñán, Manuel Bailera, and Begoña Peña. 2024. "*Outline of all potential Power to Gas integrations in blast furnace ironmaking: A systematic review*". Renewable and Sustainable Energy Reviews 201 (2024) 114605. Doi: 10.1016/j.rser.2024.114605.

Author Contributions: Conceptualization, J.P., M.B. and B.P.; methodology, J.P., M.B. and B.P.; formal analysis, J.P.; writing—original draft preparation, J.P. and M.B.; writing—review and editing, M.B. and B.P.; visualization, J.P. and M.B.; supervision, M.B., and B.P.; project administration and funding acquisition, M.B., and B.P.

In this review paper, the thesis author conducted the literature search, assigned tasks to the co-authors, and wrote key sections, including the introduction, an overview of potential power-to-gas integrations in blast furnace ironmaking, a review of these integrations, a discussion and comparison of various approaches, future trends for integrating power-to-gas with blast furnace ironmaking, and the conclusions. He gathered contributions from the other authors to ensure cohesiveness and coherence throughout the document. Additionally, he polished the paper for consistency and clarity, served as the corresponding author, managed communication with the journal and reviewers, and ensured that reviewers' feedback was incorporated according to the journal's quality standards.

ix. Manuel Bailera, Pilar Lisbona, Begoña Peña, Andreina Alarcón, Jordi Guilera, Jorge Perpiñán, and Luis Miguel Romeo. 2022. "*Synthetic Natural Gas Production in a 1 KW Reactor Using Ni-Ce/$Al_2O_3$ and Ru-Ce/$Al_2O_3$: Kinetics, Catalyst Degradation and Process Design*." Energy 256 (2022) 124720. doi: 10.1016/j.energy.2022.124720.

Author Contributions: Conceptualization, M.B., P.L., B.P., A.A., J.G., LM.R.; Methodology, M.B., B.P., A.A., J.G.; Software, M.B.; Validation, M.B., B.P., A.A., J.G.; Formal analysis, M.B., B.P., A.A., J.G.; Investigation, M.B., P.L., B.P., A.A., J.G., LM.R., J.P.; Writing e original draft, M.B., P.L., A.A., J.G.; Visualization, M.B., A.A., J.G.; Funding acquisition, M.B., P.L., B.P., LM.R.

For this paper, the thesis author was involved in the investigation and contributed to the overall conceptualization of the results. He assisted with laboratory tests and focused on visualizing the results.

# E Published papers

Sustainable Production and Consumption 41 (2023) 121–133

Contents lists available at ScienceDirect

Sustainable Production and Consumption

journal homepage: www.elsevier.com/locate/spc

# Techno-economic assessment of glassmaking decarbonization through integration of calcium looping carbon capture and power-to-gas technologies

Cristian Barón, Jorge Perpiñán, Manuel Bailera, Begoña Peña *

*Escuela de Ingeniería y Arquitectura, Universidad de Zaragoza, María de Luna 3, 50018 Zaragoza, Spain*

ARTICLE INFO

Editor: Dr. José María Ponce-Ortega

*Keywords:*
Power-to-gas
Glass industry
Methanation
Carbon capture
Calcium looping
Decarbonization
Electrification

ABSTRACT

Glass industry involves high temperature melting processes mainly based on fossil fuel combustion so far. This paper proposes the integration of Power to Gas and carbon capture to reduce the $CO_2$ emissions, as well as the dependency on fossil fuels. Four novel concepts, modelled in Aspen Plus, are analyzed separately and compared with a conventional glass plant in terms of $CO_2$ reduction potential and energy and economic penalties. The economic scenarios of full electricity purchase and full self-production with a photovoltaic plant are compared. The reference case, also modelled in Aspen Plus, has been validated with bibliographic data, being deviations of the main parameters <6 %. The low-carbon alternatives take advantage of the synergies between the different technologies: Calcium Looping, methanation and glassmaking processes. The main results show great reductions in fossil natural gas consumption as well as in $CO_2$ emissions, specifically up to 95 % and 87 %, respectively. Furthermore, the different assessed low-carbon strategies may be combined to reach higher savings of $CO_2$ emisions, reducing economic penalties.

## 1. Introduction

Decarbonization of energy-intensive industries involving high-temperature processes is an overriding target to ensure an increase of the global average temperature below 1.5 °C compared to pre-industrial levels (The Paris Agreement, 2015). Among these industries, glass-making presents specific energy consumption (SEC) of 4–17 GJ/$t_{glass}$ (Zier et al., 2021) with a global production of close to 130 million tons in 2020 (Furszyfer Del Rio et al., 2022), which represents one of the highest production volumes per capita worldwide. Glass industry is extremely diverse, being container and flat glass the most important sectors. Specifically, these end products account for 80 % of the global and European glass production, emitting around 81 $Mt_{CO2}$ (Westbroek et al., 2021) and 18 $Mt_{CO2}$ (Zier et al., 2021) per year, respectively.

Glassmaking involves five main processes: batch preparation, melting, forming, annealing and finishing. Melting stage is the most energy- and carbon-intense, as the (minimum) theoretical energy requirement is established between 2.8 and 3.0 GJ/$t_{glass}$ (Conradt, 2019) (for instance, SEC for melting soda-lime is 2.68 GJ/$t_{glass}$ (Zier et al., 2021)). Melting process for container glass represents 75–85 % of total energy consumption and around 75 % of $CO_2$ emissions (Papadogeorgos and Schure, 2019). The average energy consumption of container glass furnaces was estimated in 5150 MJ/$t_{glass}$ (normalized to 50 % cullet and to the primary energy equivalent to oxygen production for oxy-fuel furnaces). The best furnace reached 3700–3800 MJ/$t_{glass}$, but batch pre-heating decreases energy consumption up to 3670 MJ/$t_{glass}$ and all-electric furnaces up to 3100–3200 MJ/$t_{glass}$ (Conradt, 2019).

Glass recycling (cullet) saves energy and emissions, as the chemical decomposition of carbonates is already complete. This results in direct savings (no-process related emissions and increase of 2.5–3.0 % energy efficiency for each 10%wt cullet) and indirect savings derived from the reduction of primary raw material which avoids the corresponding preparation processes, such as soda production (Zier et al., 2021). External cullet is mainly used in container and glass wool industries, with maximum cullet percentages between 70 % (white/flint) and 95 % (green) depending on the glass color, while typical levels for flat glass are around 25 % (Conradt, 2019).

According to these data, SEC and $CO_2$ emissions strongly depend on different factors, such as the kind and color of glass, melting technology and cullet fraction, but also on primary fuels. Chinese container glass industry strongly relies on coal (44.3 %), in contrast to U.S. and Europe which primarily base their production on natural gas (80 % and 90 %, respectively). In addition, EU-28 glass industry operates with higher

* Corresponding author.
*E-mail addresses:* cbaron@unizar.es (C. Barón), jorge.perpinan@unizar.es (J. Perpiñán), mbailera@unizar.es (M. Bailera), bpp@unizar.es (B. Peña).

https://doi.org/10.1016/j.spc.2023.07.029
Received 12 April 2023; Received in revised form 27 July 2023; Accepted 29 July 2023
Available online 5 August 2023
2352-5509/© 2023 The Authors. Published by Elsevier Ltd on behalf of Institution of Chemical Engineers. This is an open access article under the CC BY-NC-ND license (http://creativecommons.org/licenses/by-nc-nd/4.0/).

**Nomenclature**

| | |
|---|---|
| AEL | alkaline water electrolysis |
| CAPEX | CAPital EXpenditures |
| CaL | calcium looping |
| EU ETS | European Emissions Trading System |
| GHSV | gas hourly space velocity |
| HP/IP/LP | high/medium/low pressure |
| KPI | key parameter indicator |
| NG | fossil natural gas |
| PtG | power to gas |
| PEM | polymer electrolyte membrane |
| PV | photovoltaic |
| SEC | specific energy consumption |
| OPEX | OPerational EXpenditures |
| RH | reheater |
| SH | superheater |
| SNG | synthetic natural gas |
| SOEC | solid oxide electrolysis cell |
| TCR | thermo-chemical heat recovery |
| cal | calciner of CaL |
| car | carbonator of CaL |

cullet rates (65 %) than Chinese plants where the recycling is as low as 28 % (Zier et al., 2021). These differences are reflected in higher combustion-related emissions for China (0.69 $t_{CO2}/t_{glass}$) with respect to U.S. and Europe (0.50 $t_{CO2}/t_{glass}$ and 0.47 $t_{CO2}/t_{glass}$, respectively) (Schmitz et al., 2011; Hu et al., 2018). An additional 0.15 $t_{CO2}/t_{glass}$ from the dissociation of carbonates in raw materials should be added (Furszyfer Del Rio et al., 2022).

Waste heat recovery, process intensification and fuel substitution are other decarbonization options which have been investigated to a greater or lesser extent (Zier et al., 2021). The first block includes preheating of inlet gases, cullet or batch; heat to power and building heating. The second kind of measures aims to increase energy efficiency of the melting process, for instance, through enhanced burners or furnace designs, improvement of batch or advanced process control. These strategies are usually implemented in the European and U.S. industry, and therefore, the potential for global $CO_2$ reduction is limited (Conradt, 2019). Regarding fuel substitution, gaseous energy carriers, such as biogas, hydrogen or synthetic methane, or electric furnaces may be considered. All-electric melting technology is well established only at small scale (up to 250 t/h). Although some projects expect to reach higher capacities, the complex design and control of such furnaces, the low flexibility and short lifetimes are challenging and will require future research efforts to solve these drawbacks. Furthermore, the all-electric furnaces are not appropriate for high-quality glass where especially stable batch layer is needed, and the use of cullet is limited, reducing the possibility of recycling (Conradt, 2019). As for the direct use of hydrogen, the different combustion behavior results in higher adiabatic temperatures and changes in thermal radiation properties, being necessary further research about the effects on glass quality and the investment in process adaptation.

Carbon capture, utilization and storage technologies have not been explored from glass furnace gases. However, the current carbon uses involves a very small fraction of the $CO_2$ emitted (<1 %) and geological $CO_2$ storage exhibits important concerns related to available locations, security, economic viability and social acceptance (Dowell et al., 2017).

According to those arguments, the present work represents the first comprehensive study about the integration of Power to Gas technology in a glassmaking plant: $CO_2$ captured from the glass melting furnace reacts with green hydrogen to produce synthetic methane, which in turn is used in the melting process. Given the greater relevance of the container industry (>50 % of world production), the case study has focused on the container manufacturing process. The primary objectives of this research are to propose, model and assess from technical, economic and environmental point of view novel low-carbon concepts based in Power to Gas technology to significantly reduce the net emissions. After the State of the Art summarized in Section 2, the case studies and the methodology are presented in Section 3. Results and discussion is found in Section 4, while conclusions are gathered in Section 5.

## 2. Literature review

### 2.1. Decarbonization options

Research has addressed decarbonization of glassmaking industry from three different perspectives: energy efficiency, material recycling and fuel substitution (Table 1). The former includes waste heat recovery and process intensification. According to the literature (Rozendaal et al., 2017) only heat recovery is performed in practice from exhaust gases, because of operational problems related to fouling, unprofitability and lack of proximity between source of heat and possible uses. The heat recovery has been only implemented for batch and cullet preheating (see a full revision in (Zier et al., 2021)), reaching energy savings in the range of 10–20 %. Waste heat recovery has been also proposed for oxygen and natural gas preheating, but only theoretical studies are found (Kim et al., 2016). Power generation from waste heat would be also carried out through thermal cycles (Pili et al., 2020; Danieli et al., 2019), and thermoelectric generators, but this research lines are scarcely explored so far. Pili et al. (Pili et al., 2020) investigated from a general perspective the potential of Heat to Power by means of an Organic Rankine Cycle (ORC) in the glass industry, among others. The work considered mean values of temperature and three scenarios of recoverable heat obtaining promising results, but the detailed integration in a specific glass plant was not performed. Danieli et al. (2019) compared different heat recovery configurations based in Joule-Brayton cycles and ORC to exploit the energy content of flue gas of regenerative hollow glass furnaces. For a medium-size furnace (345 t/day) net power of 0.7–1.2 MW were obtained with payback about five years. In spite of the interest of these works to increase energy efficiency, the potential for $CO_2$ emissions reduction is very limited. Regarding process intensification, the optimization of furnace or burner design (Zier et al., 2021; Yu et al., 2014), and operation conditions (Tiozzo et al., 2017; Council GMI et al., 2004) efficiency, but economic costs may do such measures unprofitable and the potential as mitigation measure of carbon emissions is low.

In addition to the reuse of glass products and the eco-design, which

**Table 1**
Input data of the conventional container glass production plant (Papadogeorgos and Schure, 2019).

| Variable | Units | Case 0 |
|---|---|---|
| Raw material | | |
| Silica Sand | $kg/t_{glass}$ | 191 |
| Dolomite | $kg/t_{glass}$ | 34 |
| Limestone | $kg/t_{glass}$ | 24 |
| Sodium carbonate | $kg/t_{glass}$ | 57 |
| Sodium sulphate | $kg/t_{glass}$ | 2 |
| External cullet | $kg/t_{glass}$ | 744 |
| Domestic cullet | $kg/t_{glass}$ | 111 |
| Cullet ratios | | |
| Rejected glass | $kg/t_{glass}$ | 22 |
| Defective glass | $kg/t_{glass}$ | 89 |
| Glass composition | | |
| SiO2 | %wt | 73.26 |
| Na2O | %wt | 12.61 |
| CaO | %wt | 9.92 |
| MgO | %wt | 2.55 |

are beyond the scope of this revision, the increase of material efficiency is mainly focused on glass recycling, mixing cullet with raw material in the melting furnace. The beneficits are the saving of 1.2 t of virging material per tonne of cullet and 60 % of $CO_2$ emissions in the glass-making process, as melting of cullet requires 70–75 % less energy (Furszyfer Del Rio et al., 2022) Despite glass may be 100 % recycled in theory, the mixing of different colours, contamination with non-glassy materials, restrictions imposed for quality reasons and limitations in the recycling infrastructure reduce the actual potential of glass recycling (see (Furszyfer Del Rio et al., 2022) for further discussion). Alternative materials based in biomass ash have been investigated by Deng and co-workers (Deng et al., 2023), but the fractions allowed are below 5 wt% and only for green container glass.

Regarding fuel substitution, it exhibits a very significant mitigation potential of $CO_2$ emissions. Fiehl et al. (Fiehl et al., 2017) presented the sole study about co-firing of biogas coming from agricultural residues in a full-size industrial glass melting furnace. No negative effects were observed in glass quality or refractory with 30 % energy share of biogas. Nevertheless, the limited availability and the variability in gas composition are important concerns that must be solved. The combustion of pulverized biomass is feasible from a theoretical point of view (Jonson et al., 2008), but the effects of calcium and other pollutant compounds must be clarified. On the contrary, hydrogen is a promising energy carrier which has been considered in different recent projects: HyGlass (HyGlass, 2020), HyNet (Morris, 2020) and Kopernikus P2X (Kopernikus, 2022). Gärtner et al. (Gärtner et al., 2021) simulated the integration of Power-to-$H_2$ in an oxyfuel melting furnace, obtaining reductions up to 60 % in specific carbon dioxide emissions with increase of 25 % in specific energy demand. Some attempts have been also done to develop an experimental facility operated with hydrogen (Flammatec, 2020) but there are many barriers for the deployment of hydrogen as direct fuel in melting furnaces, such as lower radiation heat transfer and lower volumetric energy content (Furszyfer Del Rio et al., 2022) which imply development of new hydrogen burners, retrofitting of existing facilities and further research to optimize the operation conditions.

### 2.2. Research gaps and novel contributions

Decarbonization of glass industry is a complex problem without unique solution. Carbon capture technologies and Power to Methane must be added to the picture shown in the literature review, as an alternative for $CO_2$ mitigation in current facilities without important changes in process and equipment. Only one study has been published to this respect (Gärtner et al., 2023), but the scope of the model is limited to the amine-based carbon capture.

To date, there is no comprehensive study about the integration of Power to Methane in the glass industry. In the present work, a holistic perspective is adopted to take advantage from the existing synergies between the involved technologies. The Aspen model integrates: glass industry, methanation system, Calcium-Looping (CaL) capture system, PEM electrolyzer and power plant. Four novel integrated concepts are analyzed from the technical and economic point of view to show separately the effect of each improvement measure on $CO_2$ reduction and economic penalty. These concepts have not been explored for the glass industry so far in literature. Furthermore, the assessment of synergies presented in this work between the glass melting process, methanation, carbon capture and oxy-combustion to effectively reduce $CO_2$ emissions is completely novel in literature.

## 3. Methods

The present work is focused on the container industry which represents 47 % of the total glass industry accounted for in the European Emissions Trading System (EU ETS) (Zier et al., 2021). Specifically, the most common melting technology based in fossil natural gas has been considered as base case. A novel Power-to-Gas (PtG) integration concept is proposed to reduce gas natural consumption and $CO_2$ emissions, while the potential benefit of three variants is assessed to reduce energy penalty or raw material. For comparison purposes, the analysis has been performed in specific units (per ton of glass product, $t_{glass}$) and afterwards sized to net amounts for a glass plant of medium size (250 $t_{glass}$/day).

### 3.1. Case studies

#### 3.1.1. Conventional Glass production process: base case

The base case study (Case 0) is represented in Fig. 1, considering the typical scheme of a conventional glass plant. The main processes of real container glassmaking are contemplated (Zier et al., 2021; Papadogeorgos and Schure, 2019): batch preparation, melting and fining, forming, annealing, surface treatment and inspection. The main energy consumption (fossil natural gas, NG) takes place in the high temperature processes that occur in the melting, fining and annealing stages. Additionally, electricity is consumed to a lesser extent in every analyzed process. Only direct $CO_2$ emissions, related to NG combustion, are represented in Fig. 1, since the electricity is considered generated from renewable resources. If this were not the case, the indirect emissions associated to electricity production should be accounted for in the global balance.

Batch preparation serves to properly mix the raw materials and the cullet (recycled glass). Raw material is a mixture of different compounds (glass formers, fluxing agents, stabilizers, colorant and fining agents), among which silica sand is the main component. The cullet glass comes both from glass that does not meet the quality requirements in fining or inspection stages (domestic cullet) and from specific recovery plants (external cullet). Usually, the resulting mixture is moistened with 2–4 wt % water to ensure homogeneity (Zier et al., 2021). Energy consumption of batch plants (electricity) represents about 4 % of total energy demand (Pellegrino, 2002).

The mixture is driven to the melting furnace which is continuously operated at high temperatures (between 1450 °C and 1600 °C) and is responsible for the main energy expenditure of the whole plant (75–85 %). The income solid material passes different phases, through which the solid particles are heated and melted, water is evaporated and different chemical reactions take place. Heat is transferred by thermal radiation from the NG flame to the above-installed burners and by convection from the molten material below. Besides natural convection, electrodes (electric boosting) and bubblers located at the bottom of the furnace generates forced recirculation movement. The essential reactions required to obtain the desired glass composition also occur in the melting furnace. The decomposition of the raw material (silica, soda ash, limestone and dolomite) to give rise to $SiO_2$, $Na_2O$, CaO and MgO liberates $CO_2$ and $SO_2$. The dissolved gases form bubbles that are removed at high temperature in the fining processes with help of fining agents, such as $Na_2SO_4$ (Hujová and Vernerová, 2017). In addition, the molten glass is purified and homogenized before leaving the forehearth (Pellegrino, 2002; Beerkens, 2008). In order to increase the thermal efficiency of the melting furnace, it is also equipped with a regenerative heat exchanger. Its purpose is to pre-heat the gases that enter the furnace using the enthalpy of the hot gases that leave the furnace. In this way, less energy is needed and $CO_2$ emissions and NG consumption are reduced.

The conditioned glass enters the forming machines to receive the proper container shape. The electricity consumption for glass blowing and air compression represents 5–6 % of the total energy. Some rejected glass is recycled to the melting stage. The post-formed glass that meets quality requirements is driven to the annealing stage, where internal stresses are removed, providing strength to cracks. Energy demand (NG and electricity) of this third furnace accounts for 4–5 % of the total energy consumption (Pellegrino, 2002). Afterwards, surface treatment, consisting in glass coating with organic compounds, gives proper physical (lubricity, further strength) and optical properties. Defects are

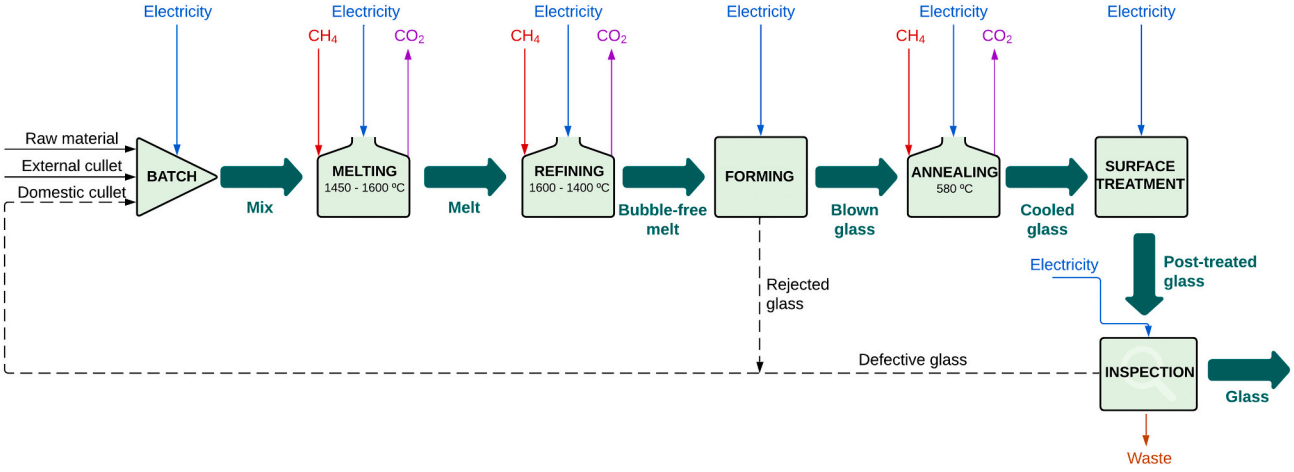


**Fig. 1.** Base case corresponding to a conventional glass plant (own elaboration).

detected in the final inspection stage, contributing to the domestic cullet.

### 3.1.2. *Low-carbon concepts*

The conventional glassmaking plant has been integrated with a PtG system in different configurations as it is shown in Fig. 2. Case 1 in solid line serves as the starting point for Cases 2–4. Each modification with respect to Case 1 is indicated in dashed lines: pink for Case 2, green for Case 3 and orange for Case 4. The main additional equipment consists of a PEM electrolyzer powered by renewable energy, a CaL carbon capture system and a catalytic methanation reactor. PEM technology has been selected instead of SOEC (solid oxide electrolysis cell) because of its current higher commercial development (TRL-7 vs. TR-5) and instead of AEL (alkaline) which exhibits less flexibility in load-following operation with renewable generation systems (Subramani et al., 2015). Despite amine scrubbing is well-established as capture technology in power plants (90–95 % capture ratio, and specific penalties of 2.9–6.5 MJ/$kg_{CO2}$ for MEA and 2.9–3.1 MJ/$kg_{CO2}$ for MDEA (Perpiñán et al., 2023)), Calcium Looping has been considered in the present work. The latter offers additional integration advantages with the glassmaking process, because spent lime can be reutilized (see Fig. 2).

In Case 1, synthetic natural gas (SNG) is produced in the methanation system by combining the captured $CO_2$ from the glassmaking process with the hydrogen from the electrolyzer. The methanation system is sized to produce enough SNG to cover the thermal necessities of both the melting furnace and the calciner of the CaL system, in such a way that carbon follows a closed loop. Likewise, the capture system receives the necessary flow of flue gas to capture the $CO_2$ required in methanation. The rest of the flue gas is cleaned before being emitted into the atmosphere, as in the conventional glass plant. Meanwhile, PEM electrolyzer is sized to cover the demanded hydrogen. The by-produced $O_2$ is used internally for oxy-combustion in the calciner. In the economic assessment, the excess $O_2$ is supposed to be sold to other industries. It is noteworthy that the consumed electricity is considered carbon-neutral.

In Case 2, some of the CaO purged in the CaL capture system replaces part of the raw material of the glassmaking process. The new amount of limestone is calculated in the model to obtain the same glass composition in the output of the melting furnace. This strategy involves some benefits, since the equivalent quantities of limestone ($CaCO_3$) do not have to be introduced and decomposed (strongly endothermic reaction). Specifically, the corresponding raw material, the related reaction energy and the direct process emissions are saved, reducing economic costs and

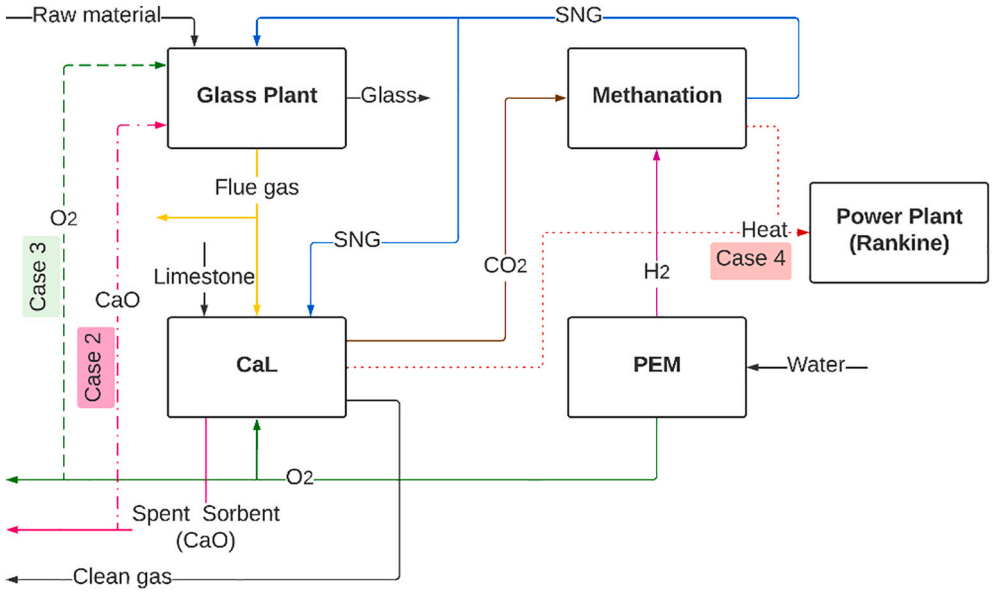


**Fig. 2.** The different analyzed low-carbon concepts: Case 1 includes the mass flows indicated in solid line, while the Cases 2–3 are represented in dashed lines (own elaboration).

environmental impacts. Furthermore, additional energy and indirect emissions, associated with the reduction of the thermal energy requirements (fossil NG consumption) in the melting process, are avoided for various reasons: (i) the purged CaO, which leaves the system at very high temperature (700 °C), serves to preheat the batch; (ii) the raw material flow decreases, as 1 kg of CaO is equivalent to 1.79 kg of $CaCO_3$; and (iii) the indirect emissions related to fuel combustion required for $CaCO_3$ decomposition are avoided.

In Case 3 the oxygen by-produced in the PEM electrolyzer is used for oxy-combustion in the fining and annealing furnaces, reducing natural gas consumption and $CO_2$ emissions. The electrolyzer is sized to produce the $H_2$ required in methanation, producing enough oxygen for that purpose. The oxy-combustion in the melting furnace is not considered in this work, since not enough oxygen is produced in the electrolyzer and the use of an air-separation unit would result in additional economic and energetic costs.

Finally, Case 4 pursues a reduction in the net electricity consumption, adding a Rankine Power plant in which waste heat is recovered from methanation and capture systems. The waste heats from glass-making process are not considered for electricity generation as they are used for pre-heating of batch, air or natural gas (Zier et al., 2021). Three turbines and 4 pressure levels have been included. A Pinch analysis is carried out to determine the optimal configuration of heat exchangers that have to be incorporated.

Regarding the economic analysis, two scenarios have been analyzed. In the first one, electricity is purchased from the grid, while in the second one a photovoltaic (PV) power station is included with the purpose of generating electricity for self-consumption.

### 3.2. Modelling procedure

The base case study (Case 0), representing a conventional container glass plant, as well as the low-carbon concepts (Cases 1–4), have been modelled and simulated in Aspen Plus v.11, under steady-state conditions. The modelling procedure is based on mass and energy balances applied to each process. The glassmaking plant model has been implemented using the PENG-ROB property method, the electrolyzer using ELECNRTL, the methanation reactor with SRK, the CaL system with SOLIDS and the Rankine Power Plant using PENG-ROB (Aspen, 2019). All the thermal and physical properties were provided by the Aspen Plus integrated database.

#### 3.2.1. Glassmaking plant model

The stages represented in Fig. 1 have been implemented in the Aspen model for the conventional glass plant. The model is initially developed and validated with data from the literature. Specifically, for Case 0, electricity consumption and input mass flows of raw material and cullet ratios (Table 1) have been taken from bibliography (Papadogeorgos and Schure, 2019), while NG consumption is obtained from mass and energy balances. The external and domestic cullet composition is assumed to be identical to the final product. The composition of outlet glass is identical for Cases 0–4 and keeps constant from the melting furnace up to the plant exit after the inspection stage. It has to be noticed that only the main components ($SiO_2$, $Na_2O$, CaO and MgO) have been considered, as they roughly summarize 96 % of real content (Table 1) (Madivate, 1998).

After integration with the low-carbon technologies, certain inputs are adapted to keep constant the proper outputs in the different equipment. The mass flow of raw material is maintained in Cases 0–1 and 3–4. So, the quantity and composition of the flue gases in the melting furnace is the same for those cases (replacing NG by SNG leads to negligible differences). In Case 2, the limestone mass flow is reduced according to the CaO recirculation to obtain the same glass composition. Operating conditions in the melting furnace change due to the different input mass flows. However, outlet flue gas temperature after going through the regenerative heat exchanger has been considered the same as in Case 1. In Case 3, the NG needed for oxy-combustion in the fining and the annealing furnaces is calculated assuming that the temperatures and the heat absorbed by the glass is the same than in Case 0. Finally, in Case 4 no changes are introduced, since the Rankine Power Plant works independently from the rest of the system.

Melting, fining and annealing furnaces have been modelled as stoichiometric reactors. The required thermal energy in those processes is provided by the complete combustion of either the fossil NG or the SNG generated in the methanation (94.77 % $CH_4$, 3.96 % $H_2$ and 1.27 % $CO_2$, LHV = 48,986 kJ/kg). The excess air is set to 10 % for the combustion in the three furnaces, as it is a typical value in the industry. The decomposition process reactions, Eqs. (1)–(4), are considered complete (100 % conversion) in the melting furnace. The temperatures of melting and fining furnaces have been set to 1500 °C. Typical temperature figures have been assumed for the regenerative heat exchanger. Air is preheated before melting furnace with the outlet flue gases, which reduce their temperature from 1500 °C to 850 °C. Atmospheric pressures have been considered in every stage.

$$Na_2CO_3(s) \rightarrow Na_2O(s) + CO_2(g) \quad \Delta H_{298} = 273.3\ kJ/mol \tag{1}$$

$$CaMg(CO_3)_2(s) \rightarrow CaCO_3(s) + CO_2(g) + MgO\ (s) \quad \Delta H_{298} = 68.9\ kJ/mol \tag{2}$$

$$CaCO_3(s) \rightarrow CaO\ (s) + CO_2(g) \quad \Delta H_{298} = 473.7\ kJ/mol \tag{3}$$

$$Na_2SO_4(s) \rightarrow Na_2O\ (s) + SO_3(g) \quad \Delta H_{298} = 522.4\ kJ/mol \tag{4}$$

Finally, the temperature after the forming process has been fixed at 500 °C, which offers a satisfactory validation regarding the energy expenditure of the annealing furnace.

Oxy-combustion in the fining and annealing furnaces of the SNG produced in the PtG system is considered in Case 3, reducing thermal losses and $NO_x$ emissions derived from the presence of nitrogen. As other studies suggest (Kim et al., 2016), SNG is introduced at 450 °C while oxygen is introduced at 650 °C in this case. Combustion is considered complete and in stoichiometric conditions, with no oxygen dilution.

#### 3.2.2. Calcium-Looping capture system

CaL technology is used to capture the $CO_2$ present in the flue gases that leave the melting furnace. The carbon capture model has been implemented according to the scheme shown in Fig. 3. The main equipment of the CaL system are the calciner and the carbonator, which have been modelled in Aspen Plus as stoichiometric reactors with 90 % (to $CO_2$) and 100 % conversion, respectively (Sánchez-Biezma et al., 2013; Ortiz et al., 2017). The operation parameters, such as mass ratios and temperatures assumed for modelling are gathered in Table 2.

The exothermic carbonatation reaction takes place in the carbonator: the $CO_2$ contained in the flue gas stream coming from the glass melting furnace reacts with the CaO to produce $CaCO_3$. The resulting limestone ($CaCO_3$) is driven to the calciner to release a $CO_2$-rich stream. The endothermic decomposition of $CaCO_3$ regenerates the CaO and liberates the $CO_2$ ($\Delta H_{298K}$ = 177.9 kJ/mol). The required thermal energy is provided by the oxy-combustion of a part SNG produced in the PtG system. A $CO_2$ recirculation loop at the exit of the calciner prevents the appearance of hot spots at the entrance that could damage the process. The amount of $CO_2$ recirculated is set to obtain 21 % $O_2$ at the entrance of the calciner, emulating air conditions. Oxygen is introduced in stoichiometric quantities and complete combustion is considered. Since this carbon dioxide is already at 950 °C, no additional preheating has been considered for oxygen or fuel.

Gases, primarily $CO_2$ and steam, are separated through a cyclone model from the pure CaO stream that heads back to the carbonator. A flash separator has been included before compressing the exiting $CO_2$ stream in order to condense the remaining water.

A sorbent purge is usually included to prevent excessive amounts of sintered CaO, formed because of the high temperatures, which reduces

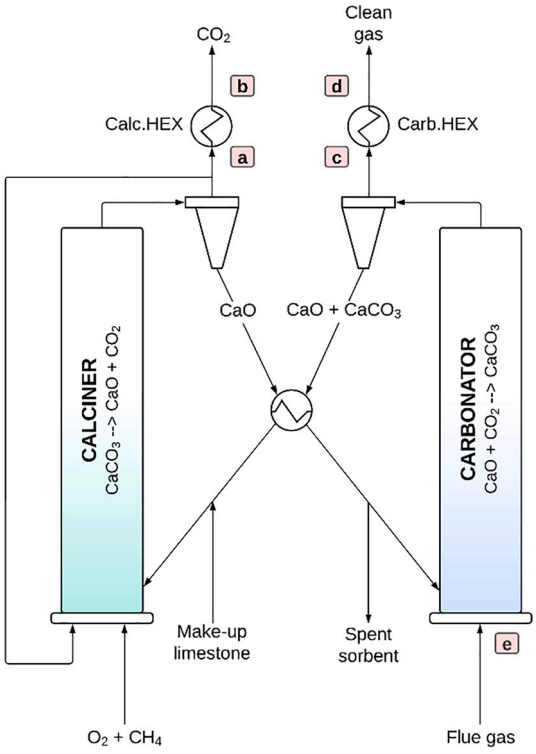


**Fig. 3.** CaL system scheme.

**Table 2**
Input data of CaL system (Domínguez, 2018).

| Variable | Units | Case 1 |
|---|---|---|
| Ratios | | |
| Introduced limestone/introduced $CO_2$ | $mol_{CaCO3}/mol_{CO2}$ | 0.05 |
| Recirculated CaO/introduced $CO_2$ | $mol_{CaO}/mol_{CO2}$ | 10 |
| Purged CaO (Pascual et al., 2021) | % | 4 |
| Streams | | |
| Calciner Exit (a) | °C | 950 |
| $CO_2$ Exit (b) | °C | 50 |
| Carbonator Exit (c) | °C | 650 |
| Clean Gas Exit (d) | °C | 90 |
| Carbonator Entry (e) | °C | 700 |

the efficiency of the CaL system. The CaO purge has been modelled as a separator in Aspen Plus which is located before the entrance of the carbonator, with the purpose of easing the CaO transport to the melting furnace in Case 2.

In order to improve the thermal efficiency of the process, heat exchangers have been included at the exit of each reactor. Those heat exchangers offer the possibility of using their residual heats as a way of achieving different purposes. For instance, they have been used to heat some water streams in the Rankine Power Plant considered in Case 4. Additionally, a solid-particle heat exchanger preheats the limestone before entering the calciner, recovering the thermal energy of the CaO from the exit (Table 2, notation of streams is referred to Fig. 3).

### 3.2.3. Power-to-gas system

The PEM electrolyzer produces hydrogen (0.002 % $O_2$) and oxygen (0.02 % $H_2$) operating at 1.5 bar and 80 °C, with 3.8 $kWh_e/Nm^3_{H2}$ energy consumption (NEL Electrolysers, 2022). The water enters at ambient conditions (25 °C and 1 atm). Thermal losses are assumed negligible.

The methanation system (Fig. 4) consists of two isothermal fixed-bed reactors, reaching higher yields than for adiabatic conditions (Izumiya and Shimada, 2021; Rönsch et al., 2016). The methanation reactors operate at 5 bar and temperatures of 350 °C and 300 °C, respectively, and GHSV (Eq. (5)) of 5000 $h^{-1}$ is considered (Perpiñán et al., 2022). The main reactions are shown in Eqs. (6)–(7). The $H_2$ is compressed and mixed in stoichiometric ratio (4:1) with the $CO_2$ stream coming from CaL system. The gas mixture is preheated up to 250 °C and driven to the first methanation stage, modelled as a Gibbs reactor to simulate equilibrium conditions. The outlet flow is cooled up to 100 °C in a flash separator to condensate the water, and then heated up to 250 °C before entering the second reactor. The resulting SNG stream is separated from water at 25 °C in a second flash separator.

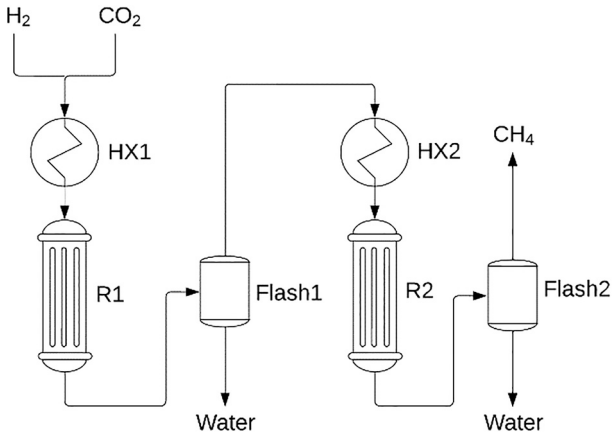


**Fig. 4.** Methanation system scheme.

$$GHSV = \dot{V}_{gas}/V_{catalyst} \quad (5)$$

$$CO_2 + 4H_2 \Leftrightarrow CH_4 + 2H_2O \quad \Delta H_{298} = -113.6\ kJ/mol \quad (6)$$

$$CO + 3H_2 \Leftrightarrow CH_4 + H_2O \quad \Delta H_{298} = -485.2\ kJ/mol \quad (7)$$

### 3.2.4. Power Plant

In Case 4, a Rankine cycle with three evaporators (EV1, EV2 and EV3 of low, intermediate and high pressure), three turbines (T1–T3) and four pressure levels is considered for power generation from waste heat recovered from the CaL system and the first methanation reactor (see Fig. 5). The main design parameters are gathered in Table 3 (Manzolini et al., 2020). The power plant is sized through a Pinch analysis where the number of heat exchangers is optimized (see Supplementary material for further details).

### 3.2.5. Economic analysis

Two different scenarios have been compared from the economic point of view: electricity purchase and self-consumption through a photovoltaic plant. The nominal power of the solar system has been sized to cover the electricity consumption needed for the 4 different cases.

The economic analysis has been conducted by using the correlations gathered in Table 4, with parameters based on September 2022 data. Although the glass industry operates under continuous production, service and maintenance stops are also considered, rendering an equivalent of 8000 h of production per year. For the reference case, 77 €/$MWh_e$ electricity cost (Trading Economics A, 2022), 80 €/$t_{O2}$ selling price of oxygen (Hurskainen, 2017), 90 €/$t_{CO2}$ $CO_2$ tax (EUA, 2022), 0.787 €/$kg_{NG}$ natural gas price (Trading Economics B, 2022), and 10 €/$t_{CaCO3}$ limestone price (Ortiz et al., 2019) are considered. A time horizon of 20 years with an annual interest of 4 % is assumed. Regarding methanation, in order to calculate the necessary catalyst mass, a GHSV of 5000 $h^{-1}$ has been considered, assuming the bed occupies 60 % of the volume of the reactors. As for PV farm, an initial investment of 620 €/kW and an a typical utilization factor in Spain of 25 % (1990 h/year) are

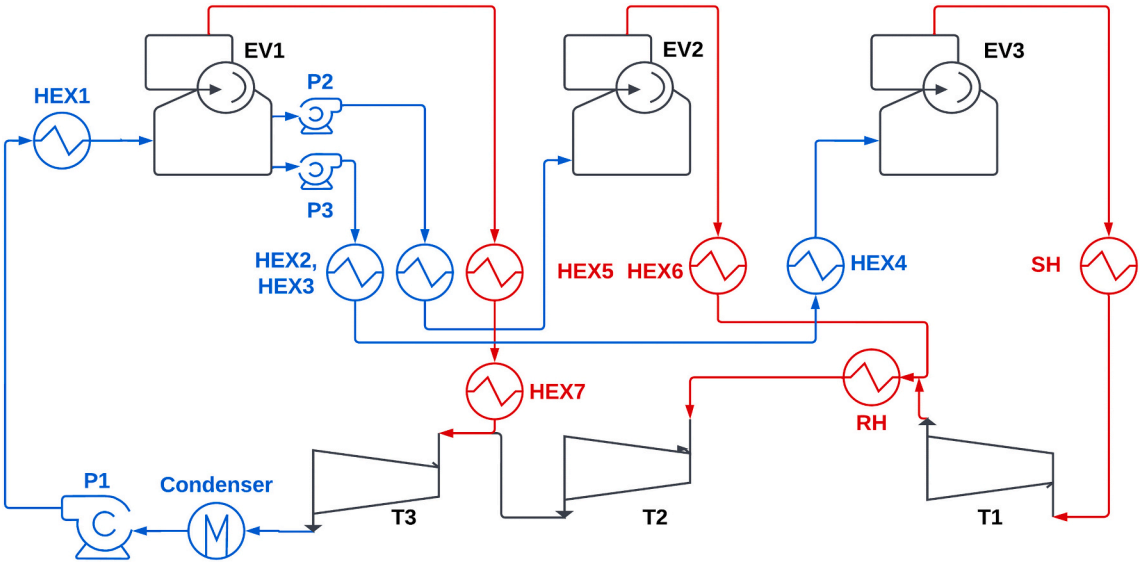


**Fig. 5.** Rankine power plant scheme.

**Table 3**
Input data of Rankine Power Plant (Manzolini et al., 2020).

| Variable | Units | Case 4 |
|---|---|---|
| Condenser pressure | kPa | 4.8 |
| Condenser temperature | °C | 32 |
| LP evaporator quality (EV1) | – | 0.2 |
| IP/HP evaporator quality (EV2/EV3) | – | 1 |
| EV3/EV2/EV1 pressure | bar | 130/28/4 |
| EV3/EV2/EV1 temperature | °C | 331/230/144 |
| SH and RH temperature | °C | 565 |
| Adiabatic efficiencies in T1/T2/T3 (HP/IP/LP) | % | 92/94/88 |

considered (RDL14/2010).

#### 3.2.6. Key Performance Indicators (KPIs)

A total of 17 KPIs are assessed in order to evaluate the obtained results. KPIs 1 to 7 refer to CaL, PtG and Rankine cycle. KPIs 1 and 2 refer to the calciner (cal) and carbonator (car) volume, respectively. KPIs 3 and 4 are the amount of thermal energy necessary in both reactors with respect to the $CO_2$ captured and the glass produced, respectively. KPI 5 considers the amount of synthetic natural gas produced in the methanation system, while KPI 6 addresses the sum of volumes of the methanation reactors. Finally, KPI 7 amounts the electricity generated in the power plant per glass mass unit, only included in Case 4. KPIs 8 to 10 refer, respectively, to the NG consumption, $CO_2$ emissions and electricity consumption per glass mass produced, while KPI 11 refers to the energy penalty incurred. KPIs 12 to 17 focus on the economic assessment. KPI 12 references the 20-year balance of the case. For its calculation, KPI 13 (CAPEX incurred), KPI 14 (OPEX) and KPI 15 (yearly annual benefits, calculated as the difference between incomes and OPEX) are considered. KPI 16 represents the carbon abatement cost per ton of $CO_2$ and KPI 17 the specific implementation cost of the PtG system per ton of glass.

## 4. Results and discussion

The modelling validation and the results obtained for the conventional glass plant are discussed in Section 4.1. The Pinch analysis required for the integration of the power plant is presented in Section 4.2, providing the configuration finally simulated in Case 4. The potential profits and drawbacks of the proposed low-carbon concepts are discussed and compared from energy and $CO_2$ emission points of view in Section 4.3. The economic analysis is finally discussed in Section 4.4.

### 4.1. Conventional glass plant

The Aspen model of the conventional glass plant has been validated with bibliographic data (Papadogeorgos and Schure, 2019; Manzolini et al., 2020). Deviation values of the main mass flows, gathered in Tables 5 and 2, are below 3.5 % except for MgO, which is a minority compound that weighs <3 wt% of the final glass composition. The specific glass composition is variable depending on the manufacturer, the color and quality of the produced glass what may justify the observed deviations with respect to reference (Papadogeorgos and Schure, 2019). Nevertheless, these deviations have little effect in the global mass and energy balances, as it is shown in Table 5. According to that, the presented Aspen model can be considered representative of container glassmaking process.

### 4.2. Pinch analysis

The Pinch method performed in Case 4 allows for an efficient integration of the power plant. The analysis considers the residual heats of Calcium Looping (solids heat exchanger, calciner and carbonator) and reactor R1 of methanation (see Fig. 4) in order to feed the Rankine cycle. The optimal configuration obtained from this analysis is shown in Figs. 6 and 7. Fig. 6 shows the temperature profiles of the streams considered in the Pinch analysis as a function of their net energy content. Meanwhile Fig. 7 shows the inlet-outlet temperatures of the hot (red) and cold (blue) mass flows in the optimal heat exchanger network proposed by Aspen Plus. The heat streams with low enough energy content have not been considered (specifically, the heat exchangers integrated in the electrolyzer and the glassmaking plant). HP Steam Generation at 249 °C and Cooling Water at 15 °C have been used as utility streams, increasing their temperatures up to 250 °C and 25 °C, respectively. The resulting water mass flow circulating in the system is 800 kg/$t_{glass}$ to reach a compromise between the complexity of the heat exchanger network and a reasonable power output (further details in the Supplementary material). The optimal configuration includes 11 heat exchangers which is a feasible number to be implemented in the industry.

### 4.3. Technical comparison of low-carbon concepts

The SNG stream obtained from the methanation system reaches a

**Table 4**
Data for the economic analysis of the PtG integration in the glass industry.

| | Cost eq. (M€ or M€/y) | Parameters $\alpha;\beta$ [units] | Ref |
|---|---|---|---|
| CAPEX | | | |
| Methanation | | | |
| $H_2$ compressor | $0.267 * (\alpha/445)^{0.65}$ | Power [$kW_e$] | (De Saint Jean et al., 2015) |
| $CO_2$ compressor | $0.267 * (\alpha/445)^{0.65}$ | Power [$kW_e$] | (De Saint Jean et al., 2015) |
| Reactors | $300 * 10^{-6} * \alpha$ | SNG power [$kW_{SNG}$] | (Lehner et al., 2014) |
| Catalyst | $0.1875 * \alpha$ | Volume of catalyst [m3] | (De Saint Jean et al., 2015) |
| Electrolysis | | | |
| Overall cost | $400 * 10^{-6} * \alpha$ | Power [$kW_e$] | (Proost, 2019) |
| Calcium looping | | | |
| Calciner | $0.193 * \alpha^{0.65}$ | Thermal power [$MW_t$] | (De Lena et al., 2019) |
| Carbonator | $0.217 * \alpha + 3.83$ | Low heating value [$MW_t$] | (De Lena et al., 2019) |
| Heat exchangers | Aspen Energy Analyzer | | |
| Overall cost | $(9016.3 + 721.3 * \alpha^{0.8}) * 10^{-6}$ | Area [$m^2$] | – |
| Rankine | | | |
| Steam turbine | $3880.5 * \alpha^{0,7} * (1+\frac{0.05}{1-\beta}^{3})(1 + \exp(\frac{\gamma - 593}{10.42})) * 10^{-6}$ | Power [kW]; Efficiency; Entry Temperature [K] | (Mohammadi et al., 2018) |
| Pump | $549.13 * \alpha^{0.71} * 1.41 * (1 + \frac{0.2}{1-\beta}) * 10^{-6}$ | Power [kW]; Efficiency | (Mohammadi et al., 2018) |
| Condenser | $1773 * \alpha$ | | |
| Evaporator | $34.9 * \alpha$ | Area [$m^2$] | (Mohammadi et al., 2018) |
| Superheater | $96.2 * \alpha$ | Area [$m^2$] | (Mohammadi et al., 2018) |
| Other direct costs | | | |
| Installation | 10 % * α | Total equipment costs [€] | (Abu-Zahra et al., 2007) |
| Instrumentation and control | 4 % * α | Total equipment costs [€] | (Abu-Zahra et al., 2007) |
| Piping | 16 % * α | Total equipment costs [€] | (Abu-Zahra et al., 2007) |
| Electrical | 5 % * α | Total equipment costs [€] | (Abu-Zahra et al., 2007) |
| Building | 5 % * α | Total equipment costs [€] | (Abu-Zahra et al., 2007) |
| Land | 1 % * α | Total equipment costs [€] | (Abu-Zahra et al., 2007) |
| Indirect costs | | | |
| Engineering | 7 % * α | Total direct costs [€] | (Abu-Zahra et al., 2007) |
| Legal expenses | 2 % * α | Total CAPEX [€] | (Abu-Zahra et al., 2007) |
| Construction expenses | 4 % * α | Total CAPEX [€] | (Abu-Zahra et al., 2007) |
| Contingency | 7 % * α | Total CAPEX [€] | (Abu-Zahra et al., 2007) |
| OPEX | | | |
| Catalyst renovation | 15 % * α | Initial catalyst cost [€] | (Bailera et al., 2017) |
| Electricity | $7.7 * 10^{-8} * \alpha * \beta$ | Electricity consumption [$kW_e$]; Operating hours [h/y] | – |
| Water | $1.47 * 10^{-6} * \alpha$ | Water consumption [$m^3$/y] | (Benjaminsson et al., 2013) |
| Limestone | $10^{-5} * \alpha$ | Limestone consumed [t/y] | (Ortiz et al., 2019) |
| O&M | 3 % * α | Total CAPEX [€] | (Abu-Zahra et al., 2007) |
| INCOMES | | | |
| Oxygen selling | $80 * 10^{-6} * \alpha$ | $O_2$ generated [$t_{O2}$/y] | (Hurskainen, 2017) |
| $CO_2$ taxes | $89 * 10^{-6} * \alpha$ | $CO_2$ consumed [$t_{CO2}$/y] | (EUA, 2022) |
| NG reduction | $7.87 * 10^{-4} * \alpha$ | NG consumed [$t_{NG}$/y] | (Trading Economics B, 2022) |

**Table 5**
Output data of the Aspen Plus models.

| Variable | Units | Reference (Papadogeorgos and Schure, 2019) | Model | Deviation (%) |
|---|---|---|---|---|
| Important streams | | | | |
| External cullet | $kg/t_{glass}$ | 733 | 744 | 1.5 |
| $CO_2$ (melting) | $kg/t_{glass}$ | 308 | 317.5 | 3.1 |
| $CO_2$ (refining) | $kg/t_{glass}$ | 25 | 25.04 | 0.16 |
| $CO_2$ (annealing) | $kg/t_{glass}$ | 12 | 12.01 | 0.083 |
| Glass composition | | | | |
| $SiO_2$ | %wt | 73.26 | 74.74 | 2 |
| CaO | %wt | 9.92 | 9.31 | −6.1 |
| $Na_2O$ | %wt | 12.61 | 13.04 | 3.4 |
| MgO | %wt | 2.55 | 2.91 | 14.1 |
| Input thermal energy | | | | |
| Melting | $GJ/t_{glass}$ | 4.77 | 4.74 | −0.63 |
| Refining | $GJ/t_{glass}$ | 0.51 | 0.50 | −2 |
| Annealing | $GJ/t_{glass}$ | 0.25 | 0.26 | 4 |

purity of 94.77 % $CH_4$ (3.96 % $H_2$, 0.77 % $CO_2$ and 0.50 % $H_2O$) and a conversion of 99.2 %, with a mass flow of 133.3 $kg/t_{glass}$. Regarding the PEM electrolyzer, a mass flow of 66 $kg_{H2}/t_{glass}$ is considered, which results in an electricity consumption of 30 $MW_e$ for a glass plant of 250 tglass per day, with only minor variations among Cases 1–4 (2.17 %).

This figure is within the current state of the art of electrolysis plants, as the current largest PEM electrolyzer achieves 20 MW (Air Liquid, 2020) and new plants of higher capacity are under construction (Linde, 2022; Plug Power Inc, 2022).

KPIs 1 to 7 are presented in Table 6 and in Fig. 8. KPIs 1–6 are identical in Cases 1, 3 and 4. The only differences are obtained in Case 2, for which calciner and carbonator volumes are slightly bigger (KPIs 1 and 2). No substantial differences are obtained in the specific thermal consumption of the calciner (KPI 3). Thermal demand in the melting stage, and therefore the SNG required, decreases in Case 2, resulting in smaller amounts of thermal energy consumption in CaL per ton of glass produced (KPI 4). Accordingly, the reduction of the SNG to be produced in the methanation reactor for melting and CaL carbon capture (KPI 5) results in a smaller reactor volume (KPI 6).

The NG consumption per glass mass produced (KPI 8) and the $CO_2$ emissions (KPI 9) are significantly reduced for the proposed PtG concepts (Cases 1–4), with respect to the conventional plant for which this figures are 111 and 355 $kg/t_{glass}$, respectively (Fig. 8). Specifically, the substitution of NG by SNG in the melting stage reduces the fossil fuel consumption and the specific $CO_2$ emissions to 13.51 $kg_{NG}/t_{glass}$ and 72.28 $kg_{CO2}/t_{glass}$, respectively, in Case 1. On the contrary, the electricity consumption (KPI 10) increases about ten times with respect to the conventional glass plant (216 $kWh_e/t_{glass}$). The electricity

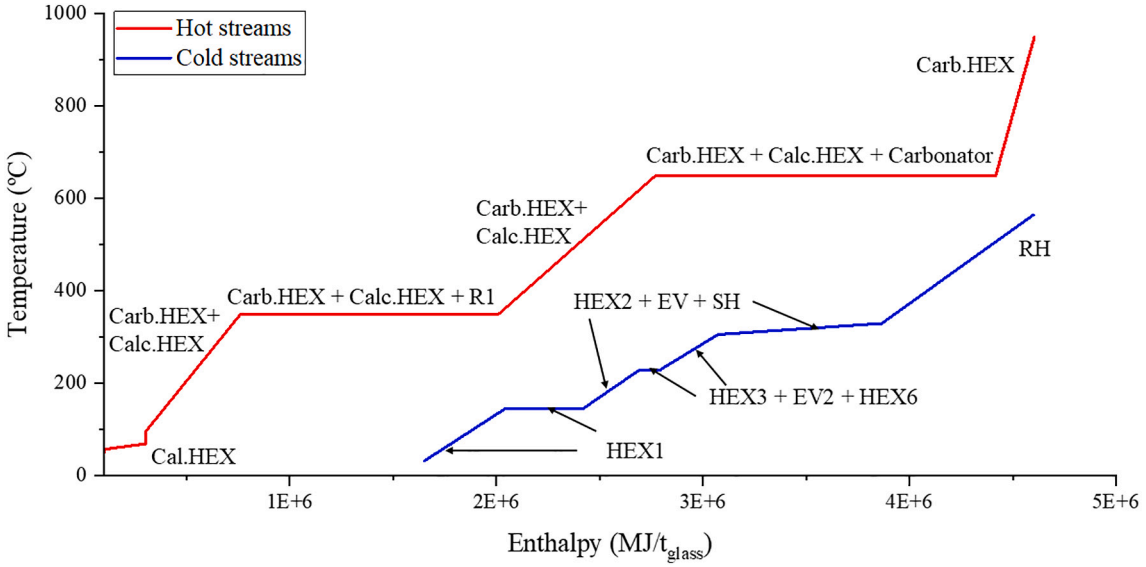


**Fig. 6.** Hot streams vs cold streams considered in the Pinch analysis. Notation is defined in Figs. 3 and 5.

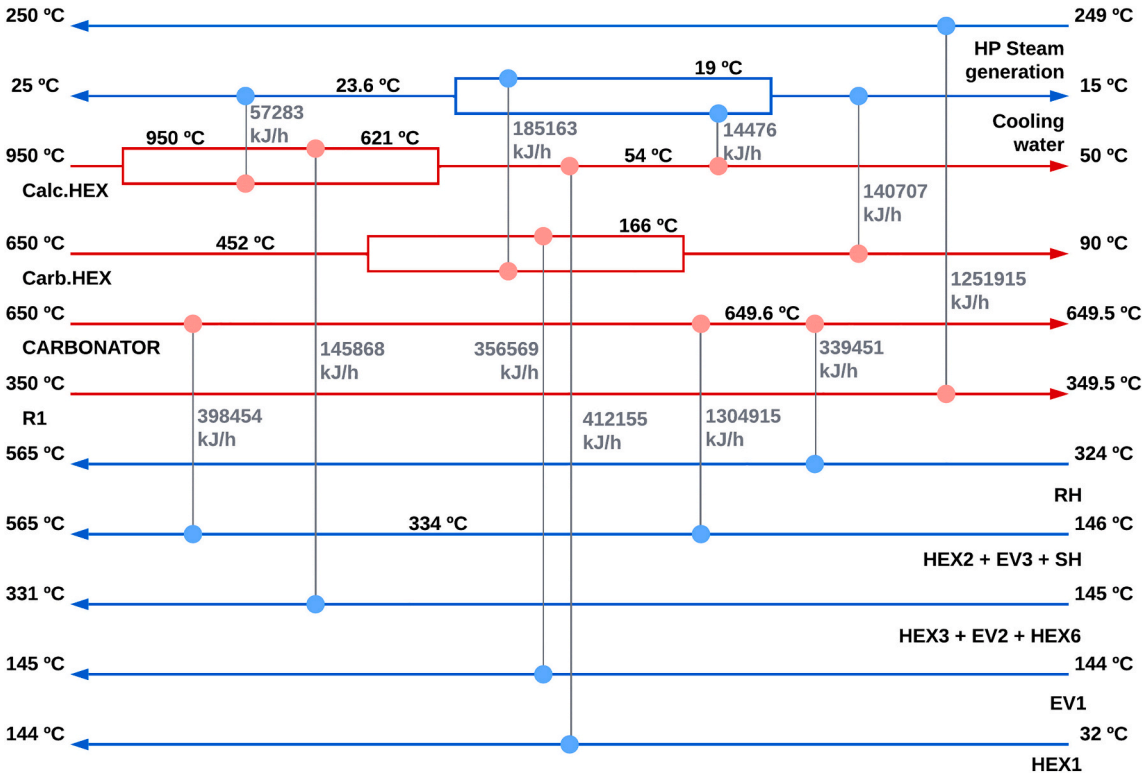


**Fig. 7.** Optimal network resulting from the Pinch analysis.

consumption increases up to 3026.38 kWh$_e$/t$_{glass}$, which implies an energy penalty (KPI 11) of 35.83 MJ$_e$/kg$_{CO2}$. This result is double to that encountered by Perpiñán et al. (Perpiñán et al., 2022) in a similar integration of Power to Gas with the steel industry. The difference in thermal demand is caused by the different carbon capture technology, which was amine scrubbing in that work. It has to be noticed that previous studies only includes the energy penalty associated to the carbon capture, but the electrolyzer consumption to recycle the captured $CO_2$ or the penalty related to transport and geological storage is not considered (Gärtner et al., 2021).

Significant benefits are achieved in Cases 2–4 because of the improvement strategies added to Case 1 (see Section 2.2). The recirculation of CaO in Case 2, which reduces the thermal demand in the melting furnace, provides further reductions in $CO_2$ emissions (−2.27 % with respect to Case 1), specific electricity consumption (−2.12 %) and energy penalty of carbon capture (−5.53 %). Regarding NG savings, no additional benefits are obtained, since the melting furnace in Case 1 uses 100 % SNG, as also occurs in Case 2 and 4.

The implementation of oxy-combustion in fining and annealing stages (Case 3) results in additional savings, with respect to Case 1, of specific $CO_2$ emissions and NG consumption of 6 and 7 percentual points (p.p.), respectively, reaching NG consumption as low as 5.79 kg$_{NG}$/t$_{glass}$.

**Table 6**
Comparison of KPIs for the low-carbon concepts (P: purchased; S-C: self-consumption).

| KPI | Related to | Description | Units | Case 1 | Case 2 | Case 3 | Case 4 |
|---|---|---|---|---|---|---|---|
| 1 | CaL | Calciner volume | $m^3_{cal}/kg_{CO2}$ | 4.26 | 4.25 | 4.26 | 4.26 |
| 2 | CaL | Carbonator volume | $m^3_{car}/kg_{CO2}$ | 16.36 | 16.71 | 16.35 | 16.35 |
| 3 | CaL | $CO_2$ energy requirements | $kWh_t/kg_{CO2}$ | 1.21 | 1.22 | 1.21 | 1.21 |
| 4 | CaL | CaL energy requirements | $kWh_t/t_{glass}$ | 456.77 | 450.33 | 456.77 | 456.77 |
| 5 | PtG | SNG production | $kg_{SNG}/t_{glass}$ | 133.29 | 130.48 | 133.29 | 133.29 |
| 6 | PtG | Reactor volume | $m^3_{reactor}/t_{glass}$ | 468.3 | 458.31 | 468.25 | 468.25 |
| 7 | Rankine | Electricity generation | $kWh_e/t_{glass}$ | – | – | – | 346.89 |
| 8 | Operation | NG consumption | $kg_{NG}/t_{glass}$ | 13.5 | 13.5 | 5.8 | 13.5 |
| 9 | Operation | $CO_2$ emissions | $kg_{CO2}/t_{glass}$ | 72 | 62 | 51 | 72 |
| 10 | Operation | Electricity consumption | $kWh_e/t_{glass}$ | 3026 | 2967 | 3026 | 2681 |
| 11 | Operation | Energy penalty | $MJ/kg_{CO2}$ | 35.8 | 33.9 | 33.3 | 31.4 |
| 12 | Economics | 20-year balance | M€ | *P:* −151.3<br>*S-C:* −139.2 | *P:* −136.0<br>*S-C:* −123.0 | *P:* −133.5<br>*S-C:* −121.4 | *P:* −123.1<br>*S-C:* −105.5 |
| 13 | Economics | CAPEX | M€ | *P:* −36.8<br>*S-C:* −68.3 | *P:* −32.9<br>*S-C:* −63.7 | *P:* −33.4<br>*S-C:* −64.9 | *P:* −41.0<br>*S-C:* −68.6 |
| 14 | Economics | OPEX | M€/y | P: −151.3<br>S-C:−139.2 | P: −136.0<br>S-C. −123.0 | P: −133.5<br>S-C: −121.4 | P:-123.1<br>S-C: −105.0 |
| 15 | Economics | Annual benefits | M€/y | *P:* −8.4<br>*S-C:* −5.2 | *P:* −7.6<br>*S-C:* −4.4 | P: −7.4<br>*S-C:* −4.2 | *P:* 6.0<br>*S-C:* −2.7 |
| 16 | Economics | Carbon Abatement Cost | $€/t_{CO2}$ | *P:* 436.5<br>*S-C:* 367.0 | *P:* 378.9<br>*S-C:* 344.8 | *P:* 357.4<br>*S-C:* 292.7 | *P:* 343.9<br>*S-C:* 261.2 |
| 17 | Economics | Spec. Implementation Cost | $€/t_{glass}$ | *P:* 164.8<br>*S-C:* 138.6 | *P:* 140.1<br>*S-C:* 127.5 | *P:* 134.9<br>*S-C:* 110.5 | *P:* 129.9<br>S-C: 98.6 |

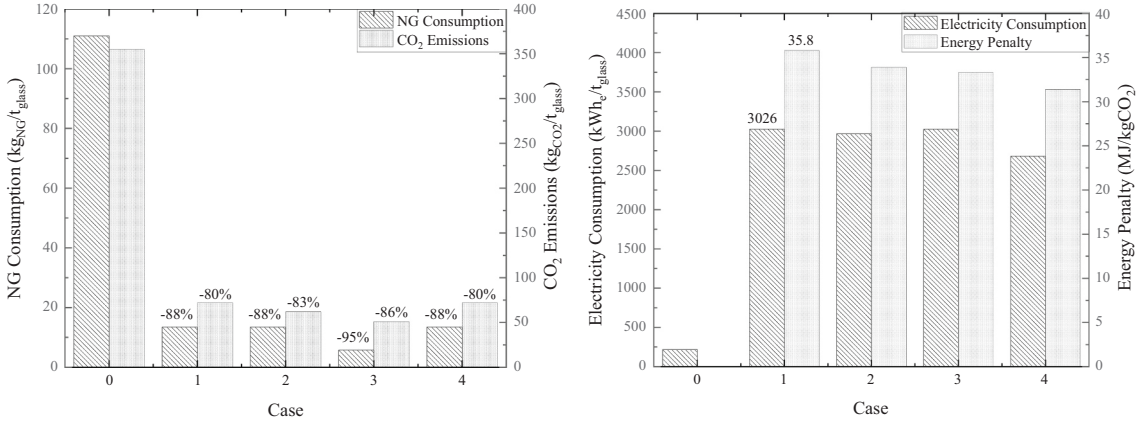


**Fig. 8.** Left: Fossil natural gas consumption ($kg_{NG}/t_{glass}$) and $CO_2$ emissions ($kg_{CO2}/t_{glass}$) and their relative reductions with respect to Case 0. Right: Electricity consumption ($kWh_e/t_{glass}$) and energy penalty ($MJ_e/kg_{CO2}$).

Electricity consumption does not vary with respect to Case 1 (Fig. 8), while energy penalty is reduced by 6.9 %. This decrease is directly related to the increase in energy efficiency through oxy-combustion.

Finally, the only effect of the inclusion of a power plant in Case 4 is the reduction in electricity consumption and energy penalty by 11.4 % and 12.3 % regarding Case 1. Considering a net glass production of 250 $t_{glass}$/day, the size of the Rankine cycle is of 3.6 $MW_e$.

### 4.4. Economic analysis

The 20-year capital expenditure (CAPEX) and operation expenditure (OPEX) of the new equipment with respect to the reference case (Case 0), as well as the annual benefits are summarized in Table 6 (KPI 12–15) for eight economic scenarios, corresponding to Cases 1–4 with (S—C) and without (P) self-production of electricity and considering Case 0 as the reference scenario. In all cases the annual benefit (KPI 15, considered as the difference between income and OPEX) is negative, which means the system is not profitable, being Case 3 with PV self-consumption the most favourable situation. Although the CAPEX is higher due to the PV plant, the four self-consumption scenarios show lower annual losses.

Similar trend is obtained from the comparison of carbon abatement costs: from 261 to 367 $€/t_{CO2}$ considering PV self-supply, versus 344–437 $€/t_{CO2}$ for scenarios with electricity purchase. If the current situation of high energy prices is maintained, the self-consumption option will be the most competitive in the future. These figures are similar to that obtained in previous industrial integrations of Power to Gas (Perpiñán et al., 2022).

Two sensitivity analyses (Figs. 9 and 10) have been conducted for Case 4 with self-consumption, corresponding to the best carbon abatement costs. Case 4 with self-consumption was chosen for the sensitivity analyses because it is the most favourable scenario in economic terms. In the first one, electricity prices as well as $CO_2$ tax prices are varied to find profitable future scenarios. The analysis considers a range of 0 to 100 €/MWh for electricity prices, which encompasses the standard price for industrial electricity consumption. Similarly, the $CO_2$ tax range is set from 0 to 700 $€/t_{CO2}$, covering scenarios without any tax, the current price tax, and a plausible maximum limit of 700 $€/t_{CO2}$ for future $CO_2$ price tax. In order to be cost-effective, the electricity price should be obtained at cost of production, or even have subsidies, while the $CO_2$ tax price should increase substantially. To put these figures in context, two reference points associated with the costs of solar and wind generation have been included in the graph. Considering the electricity price to be equal to the cost of production of solar energy (51 $€/MWh_e$), and $CO_2$ tax

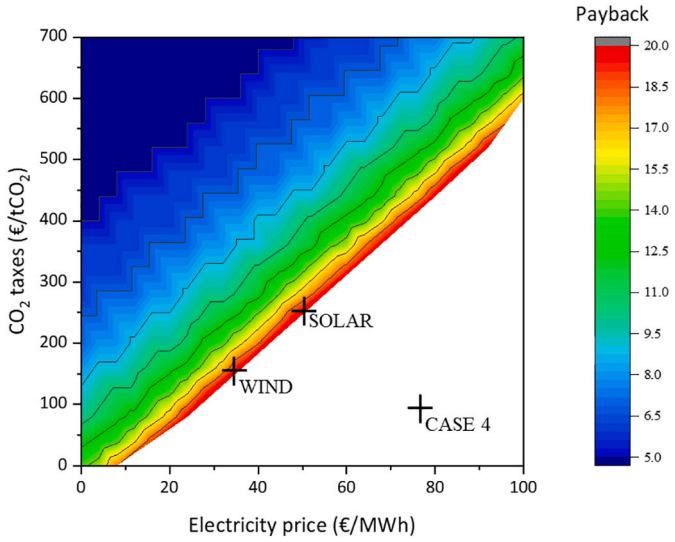


**Fig. 9.** Sensitivity analysis of payback varying $CO_2$ tax prices and electricity prices, for Case 4 with PV self-consumption.

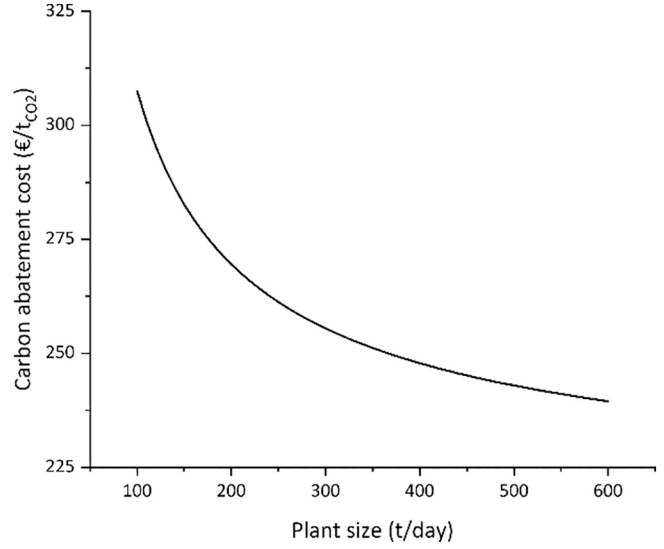


**Fig. 10.** Sensitivity analysis varying the plant size with reference to carbon abatement costs.

price of 250 €/$t_{CO2}$, the PtG integration would be economically profitable with a payback of 20 years. If electricity was obtained via wind power with a generation cost of 35 €/$MWh_e$, a price of 150 €/$t_{CO2}$ would be enough to obtain actual benefits. Although these values are far from the current prices, Strefler et al. (Strefler et al., 2021) suggest that $CO_2$ tax prices will rise in the following years, reaching 128 €/$t_{CO2}$ by 2050 and between 384 and 907 €/$t_{CO2}$ by 2100.

For the second sensitivity analysis, the plant size has been varied from 100 to 600 t/day. Tts effect on the carbon abatement cost are presented in Fig. 10. An asymptotic decreasing behavior is obtained as expected, caused by a cost advantage related to scale economy. The larger the size of the plant, the lower the weight of the CAPEX with respect to the OPEX. If the plant were infinitely large, a minimum carbon abatement cost of 202 €/$t_{CO2}$ achievable, equivalent to 77 €/$t_{glass}$.

## 5. Conclusions

The present work constitutes the first complete study on the integration of Power to Gas technology in the glassmaking industry, simulating and interconnecting every subsystem in Aspen Plus. Fossil natural gas (NG) is substituted by synthetic natural gas (SNG), produced within the bounds of the industry in a methanation reactor, forming a closed loop. This is achieved by combination of the $CO_2$ captured through a Calcium Looping system and the green $H_2$ produced in a PEM electrolyzer. The capture system and the electrolyzer are sized according to the SNG required, which feeds the melting furnace and the calciner reactor. A part of the $O_2$ produced in the electrolyzer is used in the calciner to achieve oxy-combustion, while the excess can be sold or used for different purposes.

One of the main advantages of the proposed concept is its versatility, as it does not change the current glassmaking process. Although the container industry has been considered as a case study because it covers the largest market worldwide, the application of our model to other types of glass industries may be quite straightforward.

Four low-carbon concepts based in Power to Gas have been simulated to separately assess the effects on energy penalty and carbon abatement with respect to the conventional plant. It should be noted that the improvements analyzed here separately can be combined to optimize the system. Further research will be done to this respect, as well as to assess other capture systems and other hydrogen sources. In addition, the economic analysis has considered both full purchase of electricity and self-consumption.

Reductions from 88 % to 95 % in NG consumption and from 80 % to 86 % in $CO_2$ emissions have been reached. The corresponding energy penalty ranges from 32 to 35 MJ/$kg_{CO2}$, mainly due to the electricity consumption in the electrolyzer (29 $MW_e$ for a 250 $t_{glass}$/day plant). From the economic point of view, the self-consumption scenarios are more advantageous. The carbon abatement costs are in the line of other industrial integrations of Power to Gas, ranging from 261 to 367 €/$t_{CO2}$. In spite of these high figures, the proposed concepts may be profitable under future scenarios with high carbon taxes, high prices of fossil fuels and low prices of renewable electricity.

To sum up, this study shows that this concept is promising from the $CO_2$ mitigation perspective and from a medium-term economic point of view. The deployment of renewable power will generate surplus of electricity that Power to Gas may convert to decarbonize the energy-intensive industry. According to that, the proposed concept may contribute both to mitigate $CO_2$ emissions and to balance the electricity generation and demand.

## CRediT authorship contribution statement

Conceptualization, J.P. and B·P.; methodology, J.P. and B.P.; model, C.B., J.P. and M.B.; formal analysis, C.B., J.P. and B.P.; writing—original draft preparation, C.B. and B.P; writing—review and editing, M.B., B.P. and J.P.; supervision, J.P. and B.P.; project administration and funding acquisition, B.P. and M.B. All authors have read and agreed to the published version of the manuscript.

## Declaration of competing interest

The authors declare that they have no known competing financial interests or personal relationships that could have appeared to influence the work reported in this paper.

## Acknowledgements

This work is part of the R&D project TED2021-130000B-I00, funded by MCIN/AEI/10.13039/501100011033/ and by the “European Union NextGenerationEU/PRTR”. This work has also received funding from the European Union's Horizon 2020 research and innovation program under the Marie Sklodowska-Curie grant agreement no. 887077.

## Appendix A. Supplementary data

Supplementary data to this article can be found online at https://doi.org/10.1016/j.spc.2023.07.029.

## References


Abu-Zahra, M.R.M., Niederer, J.P.M., Feron, P.H.M., Versteeg, G.F., 2007. $CO_2$ capture from power plants: part II. A parametric study of the economical performance based on mono-ethanolamine. Int. J. Greenhouse Gas Control 1, 135–142. https://doi.org/10.1016/S1750-5836(07)00032-1.

Air Liquid, 2020. PEM Electrolyzer in Bécancour, Canada. https://es.airliquide.com/soluciones/transicion-energetica (accessed Sept. 13, 2023).

Aspen Technology Inc, 2019. Aspen Physical Property Methods - Reference Manual.

Bailera, M., Espatolero, S., Lisbona, P., Romeo, L.M., 2017. Power to gas-electrochemical industry hybrid systems: a case study. Appl. Energy 202, 435–446. https://doi.org/10.1016/J.APENERGY.2017.05.177.

Beerkens, R., 2008. Analysis of elementary process steps in industrial glass melting tanks - some ideas on innovations in industrial glass melting. Ceramics-Silikáty 52 (4), 206–217.

Benjaminsson, G., Benjaminsson, J., Rudberg, R.B., 2013. Power-to-gas-a technical review (El-till-Gas-System, ekonomi och teknik) SGC rapport. In: Catalyzing Energy Gas Development for Sustainable Solutions, 284 n.d. www.sgc.se.

Conradt, R., 2019. Prospects and physical limits of processes and technologies in glass melting. J. Asian Ceram. Soc. 7, 377–396. https://doi.org/10.1080/21870764.2019.1656360.

Council GMI, Ross, C.P., Tincher, G.L., 2004. Glass Melting Technology - A Technical and Economic Assessment. Ed. Glass Manufacturing Industry Council, ISBN 9780976128304.

Danieli, P., Rech, S., Lazzaretto, A., 2019. Supercritical $CO_2$ and air Brayton-Joule versus ORC systems for heat recovery from glass furnaces: performance and economic evaluation. Energy. 168, 295–309. https://doi.org/10.1016/j.energy.2018.11.089.

De Lena, E., Spinelli, M., Gatti, M., Scaccabarozzi, R., Campanari, S., Consonni, S., Cinti, G., Romano, M.C., 2019. Techno-economic analysis of calcium looping processes for low $CO_2$ emission cement plants. Int. J. Greenhouse Gas Control 82, 244–260. https://doi.org/10.1016/j.ijggc.2019.01.005.

De Saint Jean, M., Baurens, P., Bouallou, C., Couturier, K., 2015. Economic assessment of a power-to-substitute-natural-gas process including high-temperature steam electrolysis. Int. J. Hydrog. Energy 40, 6487–6500. https://doi.org/10.1016/J.IJHYDENE.2015.03.066.

Deng, W., Backhouse, D.J., Kabir Kazi, F., Janani, R., Holcroft, C., Magallanes, M., Marshall, M., Jackson, C.M., Bingham, P.A., 2023. Alternative raw material research for decarbonization of UK glass manufacture. Int. J. Appl. Glas. Sci. 14, 341–365. https://doi.org/10.1111/ijag.16637.

Domínguez, C., Ortiz, 2018. The Calcium-looping Process for Advancing in the Development of both $CO_2$ Capture and Thermochemical Energy Storage Systems. Universidad de Sevilla. PhD Thesis.

Dowell, Niall Mac, Fennell, Paul S., Shah, Nilay, Maitland, Geoffrey C., 2017. The role of $CO_2$ capture and utilization in mitigating climate change. Nat. Clim. Change 7, 243–249. https://doi.org/10.1038/NCLIMATE3231.

EUA, 2022. ICE - EUA Futures. https://www.theice.com/products/197/EUA-Futures/data?marketId=7100229 (accessed Sep. 2022).

Fiehl, M., Leicher, J., Giese, A., Görner, K., Fleischmann, B., Spielmann, S., 2017. Biogas as a co-firing fuel in thermal processing industries: implementation in a glass melting furnace. In: Energy Procedia. Elsevier Ltd, pp. 302–308. https://doi.org/10.1016/j.egypro.2017.07.221.

Flammatec, 2020. Hydrogen carbon free burner. In: Burners/Injectors: Gaseous Fuels. FlammaTec. https://www.flammatec.com/services-products/burners/gaseous-fuels/hydrogen-carbon-free/. (Accessed 8 May 2023).

Furszyfer Del Rio, D.D., Sovacool, B.K., Foley, A.M., Griffiths, S., Bazilian, M., Kim, J., Rooney, D., 2022. Decarbonizing the glass industry: a critical and systematic review of developments, sociotechnical systems and policy options. Renew. Sust. Energ. Rev. 155, 111885 https://doi.org/10.1016/j.rser.2021.111885.

Gärtner, S., Rank, D., Heberl, M., Gaderer, M., Dawoud, B., Haumer, A., Sterner, M., 2021. Simulation and techno-economic analysis of a power-to-hydrogen process for oxyfuel glass melting. Energies (Basel) 14. https://doi.org/10.3390/en14248603.

Gärtner, S., Marx-Schubach, T., Gaderer, M., Schmitz, G., Sterner, M., 2023. Techno-economic analysis of carbon dioxide separation for an innovative energy concept towards low-emission glass melting. Energies (Basel). 16 https://doi.org/10.3390/en16052140.

Hu, P., Li, Y., Zhang, X., Guo, Z., Zhang, P., 2018. $CO_2$ emission from container glass in China, and emission reduction strategy analysis. Carbon Manag. 9, 303–310. https://doi.org/10.1080/17583004.2018.1457929.

Hujová, M., Vernerová, M., 2017. Influence of fining agents on glass melting: a review, part 1. Ceramics-Silikaty. 61, 119–126. https://doi.org/10.13168/cs.2017.0006.

Hurskainen, M., 2017. Industrial Oxygen Demand in Finland. Research Report VTT-R-06563-17. VTT Technical Research Center of Finland Ltd.. https://publications.vtt.fi/julkaisut/muut/2017/VTT-R-06563-17.pdf

HyGlass, 2020. IN4climate.NRW. https://www.in4climate.nrw/best-practice/2020/hyglass/. (Accessed 11 June 2020).

Izumiya, K., Shimada, I., 2021. Methane producing technology from $CO_2$ for carbon recycling. In: The First Symposium on Carbon Ultimate Utilization Technologies for the Global Environment. CUUTE-1, pp. 34–35.

Jonson, B., Zethrasus, B., Beerkens, R., Lankhorst, A., 2008. $CO_2$ neutral glass manufacturing?- A study of the possibilities. Adv. Mat. Res. 39–40. https://doi.org/10.4028/www.scientific.net/amr.39-40.425, 425–430.

Kim, H., Kang, T., Kaiser, K., S.R. Liedel Air Liquide, U. Luc Jarry Air Liquide Metal, G. Market, C. Xavier Paubel Air Liquide ALTEC, F.R. Youssef Jumani Air Liquide, Kaya, F. Levent, 2016. Heat Oxy-combustion: An Innovative Energy Saving Solution for Glass Industry.

Kopernikus, 2022. Kopernikus Project: P2X. https://www.kopernikus-projekte.de/en/projects/p2x. (Accessed 5 August 2023).

Lehner, M., Tichler, R., Steinmüller, H., Koppe, M., 2014. Power-to-Gas: Technology and Business Models. Springer Briefs in Energy. https://doi.org/10.1007/978-3-319-03995-4 (ISBN: 978-3-319-03994-7).

Linde, 2022. Announce of Builing of a 35 MW PEM Electrolyzer in Niagara Falls. https://www.linde.com/. (Accessed 13 September 2023).

Madivate, C., 1998. Calculation of the theoretical energy requirement for melting technical silicate glasses. J. Am. Ceram. Soc. 81, 3300–3306.

Manzolini, G., Giuffrida, A., Cobden, P.D., van Dijk, H.A.J., Ruggeri, F., Consonni, F., 2020. Techno-economic assessment of SEWGS technology when applied to integrated steel-plant for $CO_2$ emission mitigation. Int. J. Greenhouse Gas Control 94, 102935. https://doi.org/10.1016/j.ijggc.2019.102935.

Mohammadi, A., Ashouri, M., Ahmadi, M.H., Bidi, M., Sadeghzadeh, M., Ming, T., 2018. Thermoeconomic analysis and multiobjective optimization of a combined gas turbine, steam, and organic Rankine cycle. Energy Sci. Eng. 6, 506–522. https://doi.org/10.1002/ese3.227.

Morris, G., 2020. NSG to Test Hydrogen Fuel for Glassmaking at St Helens Site. Glass International. https://www.glass-international.com/news/. (Accessed 8 May 2023).

NEL Electrolysers, 2022. https://nelhydrogen.com/. (Accessed 3 February 2022).

Ortiz, C., Valverde, J.M., Chacartegui, R., Benítez-Guerrero, M., Perejón, A., Romeo, L. M., 2017. The Oxy-CaL process: a novel $CO_2$ capture system by integrating partial oxy-combustion with the calcium-looping process. Appl. Energy 196, 1–17. https://doi.org/10.1016/j.apenergy.2017.03.120.

Ortiz, C., Valverde, J.M., Chacartegui, R., Perez-Maqueda, L.A., Giménez, P., Romeo, L. M., 2019. The Calcium-Looping ($CaCO_3$/CaO) process for thermochemical energy storage in Concentrating Solar Power plants. Renew. Sust. Energ. Rev. 113, 109252 https://doi.org/10.1016/j.rser.2019.109252.

Papadogeorgos, I., Schure, K.M., 2019. Decarbonisation options for the dutch container and tableware glass industry. In: Manufacturing Industry Decarbonisation Data Exchange Network PBL-ECN part of TNO|2-A MIDDEN report. www.pbl.nl/en.

Pascual, S., Lisbona, P., Bailera, M., Romeo, L.M., 2021. Design and operational performance maps of calcium looping thermochemical energy storage for concentrating solar power plants. Energy. 220, 119715 https://doi.org/10.1016/j.energy.2020.119715.

Pellegrino, J.L., 2002. Energy and Environmental Profile of the U.S. Glass Industry. Energetics Incorporated Columbia, Maryland, and U.S. Department of Energy, Office of Industrial Technologies. Technical Report DOE/GO-102002-1590. https://www.nrel.gov/docs/fy02osti/32135.pdf. (Accessed 8 May 2023).

Perpiñán, J., Bailera, M., Peña, B., Romeo, L.M., Eveloy, V., 2022. Technical and Economic Assessment of Iron and Steelmaking Decarbonisation via Power to Gas and Amine Scrubbing. Under review. Available at SSRN. https://doi.org/10.2139/ssrn.4213148.

Perpiñán, J., Peña, B., Bailera, M., Eveloy, V., Kannan, P., Raj, A., Lisbona, P., Romeo, L. M., 2023. Integration of carbon capture technologies in blast furnace based steel making: a comprehensive and systematic review. Fuel 336, 127074. https://doi.org/10.1016/j.fuel.2022.127074.

Pili, R., García Martínez, L., Wieland, C., Spliethoff, H., 2020. Techno-economic potential of waste heat recovery from German energy-intensive industry with organic Rankine cycle technology. Renew. Sust. Energ. Rev. 134 https://doi.org/10.1016/j.rser.2020.110324.

Plug Power Inc, 2022. Lhyfe Secures Deal with Plug to Provide 50MW of PEM Electrolyzers for Renewable Green Hydrogen Production. https://www.ir.plugpower.com/. (Accessed 13 September 2023).

Proost, J., 2019. State-of-the art CAPEX data for water electrolysers, and their impact on renewable hydrogen price settings. Int. J. Hydrog. Energy 44, 4406–4413. https://doi.org/10.1016/J.IJHYDENE.2018.07.164.

Real Decreto-ley 14/2010, 2010. de 23 de diciembre, por el que se establecen medidas urgentes para la corrección del déficit tarifario del sector eléctrico. BOE núm. 312 de 24 de diciembre de 2010.

Rozendaal, N., Habraken, A., Beerkes, R., 2017. Steam generation from flue gases. https://optimumenvitech.nl/wp-content/uploads/2017/10/glassworld.pdf. (Accessed 25 September 2020).

Rönsch, S., Schneider, J., Matthischke, S., Schlüter, M., Götz, M., Lefebvre, J., Prabhakaran, P., Bajohr, S., 2016. Review on methanation – from fundamentals to current projects. Fuel. 166, 276–296. https://doi.org/10.1016/J.FUEL.2015.10.111.

Sánchez-Biezma, A., Paniagua, J., Diaz, L., Lorenzo, M., Alvarez, J., Martínez, D., Arias, B., Diego, M.E., Abanades, J.C., 2013. Testing postcombustion $CO_2$ capture with CaO in a 1.7 MW t pilot facility. In: Energy Procedia. Elsevier Ltd, pp. 1–8. https://doi.org/10.1016/j.egypro.2013.05.078.

Schmitz, A., Kamiński, J., Maria Scalet, B., Soria, A., 2011. Energy consumption and $CO_2$ emissions of the European glass industry. Energy Policy 39, 142–155. https://doi.org/10.1016/j.enpol.2010.09.022.

Strefler, J., Kriegler, E., Bauer, N., Luderer, G., Pietzcker, R.C., Giannousakis, A., Edenhofer, O., 2021. Alternative carbon price trajectories can avoid excessive carbon removal. Nat. Commun. 12 (1), 2264. https://doi.org/10.1038/s41467-021-22211-2.

Subramani, V., Basile, A., Nejat Veziro, T., 2015. Energy: Number 83 Compendium of Hydrogen Energy Volume 1: Hydrogen Production and Purification. Woodhead Publishing Series. http://store.elsevier.com/.

The Paris Agreement, 2015. UNFCCC. In: https://unfccc.int/process-and-meetings/theparis-agreement/the-paris-agreement.

Tiozzo, S., Battaglia, W., Migatta, A., 2017. Optimization of combustion settings: an energy efficient approachto the reduction of emissions by glass melting furnaces. In: Sundaram, S.K. (Ed.), Ceramic Engineering and Science Proceedings. John Wiley & Sons Inc, Hoboken, NJ, USA, pp. 103–112.

Trading Economics A, 2022. Spanish Electricity Price. https://tradingeconomics.com/spain/electricity-price (accessed Sep. 2022).

Trading Economics B, 2022. Natural Gas Prices. https://tradingeconomics.com/commodity/natural-gas (accessed Sep. 2022).

Westbroek, C.D., Bitting, J., Craglia, M., Azevedo, J.M.C., Cullen, J.M., 2021. Global material flow analysis of glass: from raw materials to end of life. J. Ind. Ecol. 25, 333–343. https://doi.org/10.1111/jiec.13112.

Yu, F., Hughes, T., Krause, B., 2014. Dry Batch Optimizer–Gain All Benefits of Waterwetting While Reducing the Drawbacks, pp. 93–100. https://doi.org/10.1002/9781118932964.ch9.

Zier, M., Stenzel, P., Kotzur, L., Stolten, D., 2021. A review of decarbonization options for the glass industry. Energy Convers. Manag. X 10, 100083. https://doi.org/10.1016/j.ecmx.2021.100083.

energies

MDPI

*Article*

# $CO_2$ Recycling in the Iron and Steel Industry via Power-to-Gas and Oxy-Fuel Combustion

**Jorge Perpiñán [1], Manuel Bailera [1,2], Luis M. Romeo [1,*], Begoña Peña [1] and Valerie Eveloy [3]**

[1] Escuela de Ingeniería y Arquitectura, Universidad de Zaragoza, María de Luna 3, 50018 Zaragoza, Spain; jorge.perpinan@unizar.es (J.P.); mbailera@unizar.es (M.B.); bpp@unizar.es (B.P.)
[2] Graduate School of Creative Science and Engineering, Waseda University, Tokyo 169-8555, Japan
[3] Department of Mechanical Engineering, Khalifa University, Abu Dhabi P.O. Box 127788, United Arab Emirates; valerie.eveloy@ku.ac.ae
* Correspondence: luismi@unizar.es

**Abstract:** The iron and steel industry is the largest energy-consuming sector in the world. It is responsible for emitting 4–5% of the total anthropogenic $CO_2$. As an energy-intensive industry, it is essential that the iron and steel sector accomplishes important carbon emission reduction. Carbon capture is one of the most promising alternatives to achieve this aim. Moreover, if carbon utilization via power-to-gas is integrated with carbon capture, there could be a significant increase in the interest of this alternative in the iron and steel sector. This paper presents several simulations to integrate oxy-fuel processes and power-to-gas in a steel plant, and compares gas productions (coke oven gas, blast furnace gas, and blast oxygen furnace gas), energy requirements, and carbon reduction with a base case in order to obtain the technical feasibility of the proposals. Two different power-to-gas technology implementations were selected, together with the oxy blast furnace and the top gas recycling technologies. These integrations are based on three strategies: (i) converting the blast furnace (BF) process into an oxy-fuel process, (ii) recirculating blast furnace gas (BFG) back to the BF itself, and (iii) using a methanation process to generate $CH_4$ and also introduce it to the BF. Applying these improvements to the steel industry, we achieved reductions in $CO_2$ emissions of up to 8%, and reductions in coal fuel consumption of 12.8%. On the basis of the results, we are able to conclude that the energy required to achieve the above emission savings could be as low as 4.9 MJ/kg $CO_2$ for the second implementation. These values highlight the importance of carrying out future research in the implementation of carbon capture and power-to-gas in the industrial sector.

**Keywords:** ironmaking; power-to-gas; iron and steel industry; methanation; oxy-fuel combustion; top gas recycling

check for updates

**Citation:** Perpiñán, J.; Bailera, M.; Romeo, L.M.; Peña, B.; Eveloy, V. $CO_2$ Recycling in the Iron and Steel Industry via Power-to-Gas and Oxy-Fuel Combustion. *Energies* **2021**, *14*, 7090. https://doi.org/10.3390/en14217090

Academic Editor: Attilio Converti

Received: 27 September 2021
Accepted: 22 October 2021
Published: 29 October 2021

**Publisher's Note:** MDPI stays neutral with regard to jurisdictional claims in published maps and institutional affiliations.

**Copyright:** © 2021 by the authors. Licensee MDPI, Basel, Switzerland. This article is an open access article distributed under the terms and conditions of the Creative Commons Attribution (CC BY) license (https://creativecommons.org/licenses/by/4.0/).

## 1. Introduction

The iron and steel sector is one of the most energy- and carbon-intensive in the world. Iron and steel making processes are still mostly coal-based and thus highly dependent on fossil fuels, releasing a substantial amount of $CO_2$ [1]. According to the Intergovernmental Panel on Climate Change (IPCC), the steel industry accounts for 4–5% of the total world $CO_2$ emission. It is the second largest consumer of industrial energy, consuming around 616 Mtoe (25.8 EJ) [2].

The iron and steel industry has a complex structure. However, only a limited number of processes are used worldwide that use similar energy resources and raw materials. Globally, steel is produced using two main routes, the blast furnace–basic oxygen furnace route (BF-BOF) and the direct scrap smelting route (electric arc furnace (EAF)). The BF-BOF route uses mainly iron ore, and depending on the facility, up to 30% scrap. The EAF route mainly uses scrap, and depending on the facility, up to 30% iron and iron ore [2–4].

Another fundamental difference between the two routes is the nature of the energy input. In the case of the BF-BOF, mainly coke is used as fuel, while the EAF route produces

steel using mainly recycled steel and electricity. The overall process of the two main steel production routes is depicted in Figure 1.

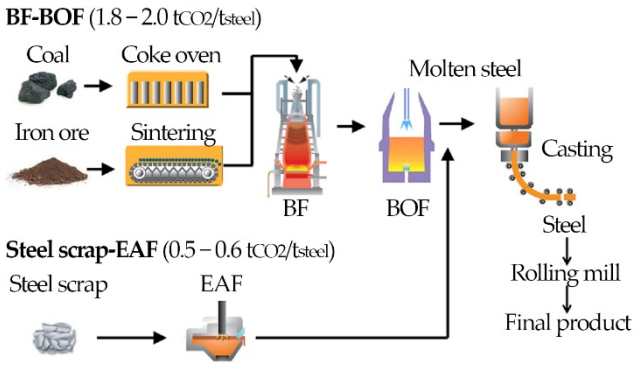


**Figure 1.** Main routes of steel production [4].

The BF-BOF route consists of several processes: sintering, coke oven, blast furnace, basic oxygen furnace, and the final stage of casting and rolling. The sintering is used to agglomerate iron ore. The coke oven allows for the obtaining of coke from coal by pyrolysis. In the BF, the iron ore is reduced by coke obtaining pig iron, then the BOF lowers the carbon content of the iron thus obtaining steel, and finally the hot metal passes through casting and rolling to obtain the final desired form. Along this processes, different waste exhaust fuel gases are obtained, which can be used in the steel plant (coke oven gas (COG), blast furnace gas (BFG), and basic oxygen furnace gas (BOFG)). All of them contain $CO_2$, which is emitted into the atmosphere unless the waste gas is recycled and/or treated.

A third iron and steel production route, the direct reduced iron (DRI)-EAF route, uses natural gas or coal-based syngas as reducing agent in combustion-free reactors to directly reduce the iron ore into metallic iron, which is processed in EAFs to produce steel. DRI processes differ in terms of the iron source (fine ore or pellets) and reactor type (fluidized bed, fixed bed, or shaft furnace). Among them, the commercially available Energiron and Midrex concepts, which use iron pellets in shaft furnaces with countercurrent moving beds, are the best options from an environmental point of view. Although representing significantly smaller steel production market shares than either the BF-BOF or EAF routes, DRI-EAF has the potential for significant carbon abatement.

Aiming for solutions that substantially reduce $CO_2$ while providing additional benefits, power-to-gas (PtG) stands out as a promising candidate [5]. The PtG concept converts renewable electricity into valuable gases using an electrolysis stage and uses $CO_2$ that may come from industrial processes. Conventionally, the conversion of electricity is carried out by water electrolysis, which produces $H_2$. The consumption of this $H_2$ together with $CO_2$ (or CO), through the Sabatier reaction (Equation (1) or Equation (2)), produces methane, water, and heat [6].

$$CO_2 + 4H_2 \leftrightarrow CH_4 + 2H_2O \; \Delta H_{298K} = -164.9 \text{ kJ/mol} \quad (1)$$

$$CO + 3H_2 \leftrightarrow CH_4 + H_2O \; \Delta H_{298K} = -206.4 \text{ kJ/mol} \quad (2)$$

When the electrolyser is fed from a renewable energy source, the obtained synthetic natural gas (SNG) can be considered neutral in $CO_2$ emissions. The amount of $CO_2$ that is emitted by this SNG is the same as that is required for its own formation [7]. To make the most of this technology, one can use it with oxy-fuel combustion, since it produces a pure stream of $CO_2$ for the methanation, while electrolysis provides pure $O_2$ for the oxy-fuel combustion [7–10].

In the case of the iron and steel industry, electrolysis can be performed as usual on water to produce $H_2$ or on the $CO_2$ emissions of the industry to obtain syngas ($CO_2$

electrolysis). Both the syngas and the $H_2$ produced can be used in a methanation process to obtain methane (power-to-methane) [11].

Power-to-$H_2$ can be integrated in ironmaking in two ways. The first method consists in injecting the $H_2$ as auxiliary reducing agent in conventional BFs to reduce the carbon content of the fossil reducing gas, while the second technique uses the $H_2$ as reducing agent in DRI reactors. Studies assessing the injection of $H_2$ in BFs show the potential of reducing $CO_2$ emissions by approximately 20%, barely affecting the overall energy demand of the process. In this case, the injected flow of $H_2$ should be around 30 kg $H_2$/t pig iron, to not significantly modify the operating conditions inside the furnace. Regarding the second method, i.e., DRI, integration of power-to-$H_2$ has the potential to lead to the low energy consumption (3.5–3.7 MWh/t steel) and net-zero $CO_2$ emissions (if carbon-free electricity is used, corresponding to 97–100% emission reduction). Still, to make the power-to-$H_2$-DRI route competitive, carbon allowances should reach approximately EUR 62 per t $CO_2$ and electricity price should be below EUR 40 per $MWh_e$ [11]. The subsequent process following the DRI, i.e., the EAF, can also benefit from power-to-methane integrations, as partial substitution of electrical energy by natural gas in EAF may be beneficial for $CO_2$ reduction, thanks to the increment in the efficiency of the process [12].

Since 95% of the world's iron production is coal-based, it is important to focus on the BF-BOF route, which is the focus of this study. Power-to-syngas and power-to-methane can supply a useful fuel to be injected in a conventional BF, acting as a renewable reducing agent (recycled $CO_2$) [11]. Recent studies have concluded that $CO_2$ emission reduction in power-to-syngas, compared to conventional ironmaking, could be in the range of 11% to 22%, with typical electrolysis capacities of 100–900 MW. In the case of power-to-methane, the $CO_2$ reduction would be between 13% and 19%, requiring water electrolysis power capacities of about 880 MW [11,13].

The objective of this paper was to study a novel concept that integrates power-to-gas technology in the iron and steel industry, together with oxy-fuel combustion and top gas recycling. Two types of integration, which differ in the source of the $H_2$ (water electrolysis or COG), were studied and compared to a reference iron and steel plant in terms of energy requirement and emission reduction. The main novelty of the study relied on the reduction of energy penalties thanks to the combination of power-to-gas and oxy-fuel combustion, which has not been quantified so far in the literature specifically for the iron and steel industry.

## 2. Description of Case Studies

Three case studies were undertaken to evaluate the energy requirements and carbon emission reductions of power-to-gas (PtG) integrated with blast furnace-basic oxygen furnace (BF-BOF) plants relative to a conventional reference BF-BOF process. The reference plant is described in Section 2.1. The proposed power-to-methane integration in ironmaking with oxy-fuel combustion and top gas recycling (TGR) is described in Section 2.2, and methanation of coke oven gas (COG) integration in ironmaking with oxy-fuel combustion and TGR in Section 2.3.

### *2.1. Case 0: Reference Plant for BF-BOF Ironmaking*

The plant consists of a sintering process, coke oven, hot stoves, BF, air separation unit (ASU), BOF, and casting and rolling. The block diagram of the reference ironmaking plant is shown in Figure 2, for which an average production of 2.8 million $t_{steel}$/year (7.7 kt/day) was assumed [14]. For the sake of simplicity, secondary processes were neglected (e.g., material recirculation in sintering), such as in similar studies [15,16]. The relevance of these processes to this study is minor since the objective was to conduct a first assessment of the novel integration under overall energy and mass balances.

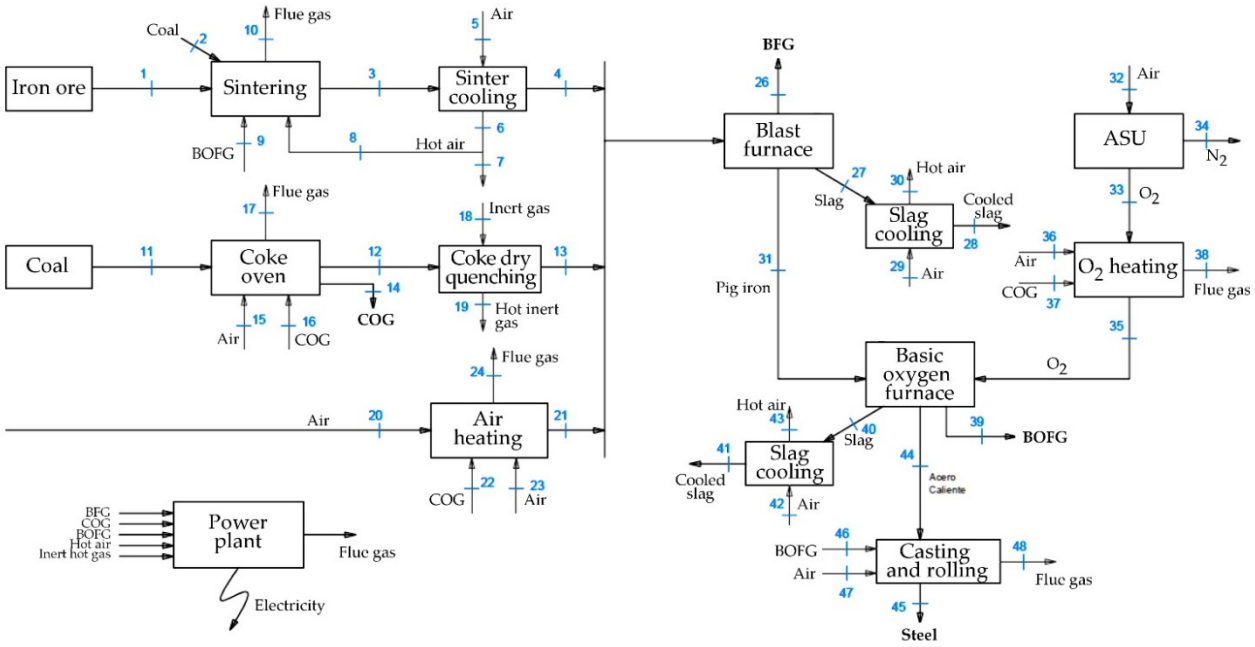


**Figure 2.** Block diagram of the reference ironmaking plant (Case 0).

The main input mass flows were iron ore, coal (converted to pure C in the coke oven), and air (for combustion in BF and for oxygen production in the ASU), as shown in Figure 2. Regarding the inputs to the BOF, we assumed that only pig iron was used (without scrap metal), as in others studies [3,4,15,16]. Those processes requiring heat at high temperature were supplied with thermal energy by consuming part of the fuel gases by-produced in the coke oven, BF and BOF (Table 1) instead of using additional fossil fuels.

**Table 1.** Elemental composition considered for the fuel gases produced as by-products in the ironmaking plant (vol %), according to the ranges reported in [3].

| | Natural Gas | COG | BFG | BOFG |
|---|---|---|---|---|
| $H_2$ | 0 | 56 | 4 | 1.5 |
| $CH_4$ | 100 | 30 | 0 | 0 |
| CO | 0 | 10 | 25 | 66.5 |
| $CO_2$ | 0 | 5 | 20 | 20 |
| $O_2$ | 0 | 1 | 0 | 2 |
| $N_2$ | 0 | 5 | 51 | 10 |

In addition, there was a power plant for the utilization of the remaining COG, BFG, and BOFG, as well as for gas streams at high temperature coming from cooling processes (sinter, slag, and coke cooling).

### *2.2. Case 1: Power-to-Methane Integration in Ironmaking with Oxy-Fuel Combustion and TGR*

The modified ironmaking plant integrated with power-to-methane in Case Study 1 is depicted in Figure 3. The BF was here operated under oxy-fuel regime, and coke input to the BF was partially replaced by synthetic methane (stream 140, Figure 3). Part of the blast furnace gas (BFG) (stream 157) was recirculated (top gas recycling (TGR)), and the other was diverted to the power-to-gas plant (stream 157). Here, the emissions of the BF were used to obtain synthetic methane again by combining them with the $H_2$ from a low temperature electrolyser (stream 182). Thus, a continuous recycling of $CO_2$ was established. Moreover, the $O_2$ from the electrolyser (stream 183) was used for the oxy-fuel combustion in the BF, which allowed us to significantly reduce the ASU energy consumption. In addition

to the above new equipment necessary for the power-to-gas integration, new preheating blocks ($O_2$ + BFG preheating and $CH_4$ preheating) were also included.

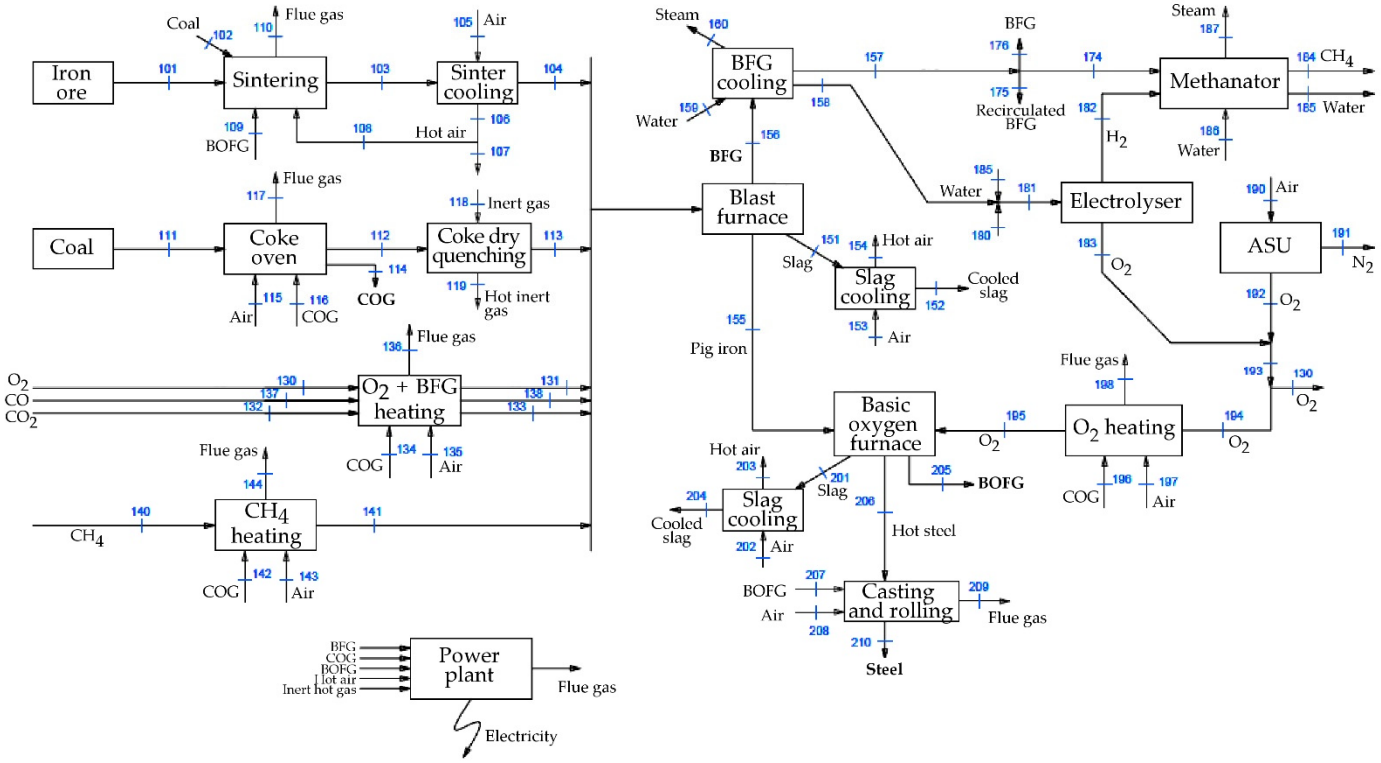


**Figure 3.** Block diagram of the integration of power-to-methane in ironmaking with oxy-fuel combustion and TGR (Case 1).

The oxy-blast furnace chosen for this case study ran in a nitrogen-free atmosphere. A pure stream of oxygen was introduced through the tuyeres instead of hot air, in order to obtain exhaust gases that were also nitrogen-free (composed only of $CO_2$ and CO). This concept is closely related to the top gas recycling. The TGR technology consists of recirculating the exhaust gases (mainly $CO_2$, CO, and $H_2$) back to the BF to reduce the coke (and consequently the air) consumption, which made the final BFG contain less $N_2$. In the present case, both oxyfuel and TGR technologies were simultaneously applied. The reason for applying TGR was that introducing a reducing gas (CO) diminished the coke consumption, while separating CO and $CO_2$ would have an energy penalization. The selected proportion between $O_2$ and $CO_2$ in the oxy-blast furnace was 40% $O_2$–60% $CO_2$.

The gas introduced in the methanation reactor was BFG, since it contains no nitrogen and large proportions of CO, which reduced the methanator $H_2$ requirement.

### *2.3. Case 2: Methanation of COG Integration in Ironmaking with Oxy-Fuel Combustion and TGR*

The modified ironmaking plant for power-to-methane integration for Case Study 2 is depicted in Figure 4. In this case, the ironmaking worked in the same oxy-fuel regime with TFG as in Case 1, but here the COG (stream 114/382) was used as $H_2$ source in the methanation process instead of pure $H_2$. Since COG does not contain nitrogen, and has large contents of $CH_4$, $H_2$, and CO, it completely avoided the need for an electrolyser and its associated investment cost, unlike in Case 1. The rest of the operating conditions and assumptions remained the same as in the Case Study 1.

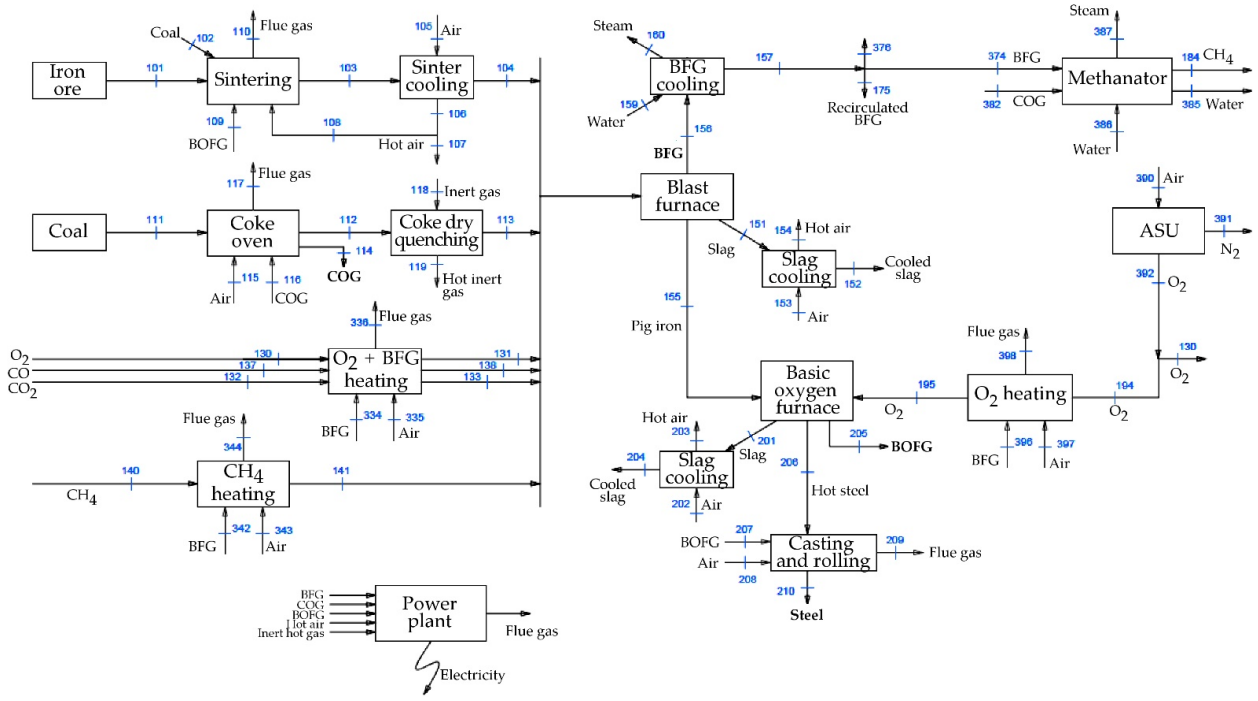


**Figure 4.** Block diagram of the integration of COG methanation in ironmaking with oxy-fuel combustion and TGR (Case 2).

In summary, in terms of produced gas utilization, Case 1 recycled BFG to the methanator and SNG to the BF, while Case 2 recycled both BFG and COG to the methanator and SNG to the BF.

## 3. Methodology

The modelling assumptions common to the analyses of Cases 0–2 plant concepts included steady-state conditions, ideal gases, and adiabatic reactions. Further case-specific assumptions are documented in Section 3.1.

The modelling methodology is based on overall mass balance (Equation (3)) and energy balance (Equation (4)) in steady state, applied to each equipment in Case 0, Case 1, and Case 2 plant layouts (Figures 2–4).

$$0 = \sum m_i - \sum m_o \tag{3}$$

$$0 = Q - W + \sum m_i h_i - \sum m_o h_o \tag{4}$$

where $m$ is the mass flow, $h$ the specific enthalpy, $W$ the network, and $Q$ the net heat transfer. Enthalpy can be written as Equation (5), where $\Delta_f h^{T_{ref}}$ is the enthalpy of formation at the reference temperature and $c_p$ is the temperature-dependent specific heat.

$$h_i = \Delta_f h_i^{T_{ref}} + \int_{T_{ref}}^{T} c_{p,i} dT \tag{5}$$

When necessary, data from the literature were used. The specific assumptions for the subsystems (ironmaking, power plant, and power-to-gas) are described in the following subsections.

### *3.1. Iron and Steel Plant*

For Case 0, in the ironmaking process (BF), instead of fixing the input mass flows of iron ore (Stream 1, Figure 2), coal (Stream 11, Figure 2), and hot blast (Stream 20, Figure 2), we calculated them from the mass balance by assuming a final composition of the steel and the BFG, taken from [17] and [3], respectively. The mass fraction of iron was set at 96% in

pig iron and 99.7% in steel, with carbon as the remaining component (other elements such as Si or Mn were neglected) [17]. The mole fraction of the BFG was fixed according to data from [3] in Table 1. The mass flows of the pig iron (Stream 31, Figure 2), BFG (Stream 26, Figure 2), and slag (Stream 27, Figure 2) were also calculated in the BF's mass and energy balances. The air for the hot blast was heated to 1200 °C by means of COG (Stream 22, Figure 2) [18].

The coal added to the sintering process was set at 5 wt % of the amount of iron treated [19]. The temperature of the sintered iron at the exit of this sintering process was assumed at 800 °C (Stream 3, Figure 2), which was later reduced to 150 °C (Stream 4, Figure 2) [16]. The amount of BOFG (Stream 9, Figure 2) and the cooling air (Stream 5, Figure 2) were calculated with the mass and energy balances for each block.

The coke produced in the coke oven was assumed as pure carbon, and the mole fraction of the COG was fixed as shown in Table 1. The coke temperatures before and after the coke dry quenching (CDQ) were 1100 °C (Stream 13, Figure 2) and 150 °C (Stream 13, Figure 2), respectively [2]. The mass flow of COG was calculated in a mass balance between the input coal and the output coke. The self-consumed COG and the inert gas needed for the CDQ were calculated in mass and energy balances for each block.

Regarding the air separation unit required for the BOF, we assumed that it produced pure streams of $O_2$ (Stream 33, Figure 2) and $N_2$ (Stream 34, Figure 2). The electricity consumption of the ASU was set at 1440 kJ per kilogram of oxygen produced [20]. The pure stream of oxygen was heated up to 1650 °C [3] by burning COG (Stream 37, Figure 2).

In the BOF, the amount of hot steel produced was assumed as a unit reference (1 kg of steel). The composition of the BOFG was again fixed according to Table 1, and the mass flows of slags (Stream 40, Figure 2), BOFG (Stream 39, Figure 2), and $O_2$ (Stream 35, Figure 2) were calculated by a mass and energy balance in the BOF.

For Cases 1 and 2, the assumptions and methodology explained for Case 0 were the same, with some minor changes. In the BF's mass balance, not only the iron ore, coal, BFG, and pig iron mass flows were calculated, but also the $O_2$ (Stream 130, Figure 3), $CH_4$ (Stream 140, Figure 3), and BFG (recirculated) (Stream 175, Figure 3). The $O_2$ demand for the BOF remained the same (Stream 195, Figure 2), but the amount of $O_2$ produced by the ASU was lower (Stream 192, Figure 2), since a by-product stream of $O_2$ from the electrolyser was used (Stream 183, Figure 3) (only for Case 1).

### *3.2. Power Plant*

This plant produces electricity for self-consumption from the energetic gases of the steel plant (i.e., COG, BFG, BOFG) and from heat streams from other heat recovery processes (i.e., coke dry quenching and slag cooling). An overall efficiency of 17.9% was assumed for the power plant [16], because of the low temperatures of the heat recovery flows, the gas treatment before entering the boiler, and the limited calorific value of the gases (due to the high $CO_2$ content and the dilution in the $N_2$ present in the air).

### *3.3. Power-to-Gas Plant*

In Case Study 1, the $H_2$ was produced from water electrolysis, while in Case Study 2, the $H_2$ came from the COG, which was directly diverted to methanation. The COG contained enough $H_2$ to produce all the necessary methane, but lacked $CO_2$. Therefore, some BFG was also diverted to methanation to fulfil the stoichiometric requirements of reactions (1) and (2). It is important to note that in Case 2, no electrolyser was needed. The methanation plant worked at 300 °C and 30 bar [7].

For the sake of simplicity, the electrolyser was assumed to produce pure streams of $O_2$ and $H_2$, while the methanation was set to produce a pure stream of methane. By these assumptions, as well as reactions Equations (1) and (2), we can easily solve the mass balance. Regarding electricity, the energy consumption of the low-temperature electrolyser was fixed at 4.5 kWh/$Nm^3$ [7,8,21].

## 4. Results and Discussion

The modelling results obtained for Cases 0, 1, and 2 are presented and discussed in Sections 4.1–4.3, respectively. In addition, the corresponding stream data for each Case are presented in the Appendix A.

### *4.1. Case 0: Reference Plant for BF-BOF Ironmaking*

The mass flows of Case 0 are summarized in Table 2, where the main calculated variables are compared to data from the literature [3,11,15–17]. All results lay within reasonable limits, thus validating the results of the reference case, which was the basis for the rest of the analyses. As already stated in the methodology section, the input streams were calculated as a function of a desired steel output composition.

**Table 2.** Mass flows (kg/t steel) of the main streams calculated for Case 0, Case 1, and Case 2. Bibliographic data were taken from [3,11,15–17]. * Input data for solving mass and energy balances.

| | Stream | Bibl. | Case 0 | Case 1 | Case 2 |
|---|---|---|---|---|---|
| Raw materials | Iron ore | 1550 | 1430 | 1430 | 1430 |
| | Coal | 560 | 520 | 460 | 460 |
| Coke oven | COG | 90 | 110 | 90 | 90 |
| Blast furnace (BF) | Sinter | 1550 | 1430 | 1430 | 1430 |
| | Coke | 400 | 420 | 370 | 370 |
| | Air (hot blast) | 1210 | 1280 | - | - |
| | $O_2$ (hot blast) | - | - | 310 | 310 |
| | BFG (hot blast) | - | - | 1060 | 1060 |
| | $CH_4$ (hot blast) | - | - | 65 | 65 |
| | BFG | 2420 | 2080 | 2190 | 2190 |
| | Slag | 280 * | 280 | 280 | 280 |
| | Pig iron | 1040 * | 1040 | 1040 | 1040 |
| Basic oxygen furnace (BOF) | $O_2$ | 70 | 90 | 90 | 90 |
| | Steel | 1000 | 1000 | 1000 | 1000 |
| | Slag | 80 * | 80 | 80 | 80 |
| | BOFG | 130 * | 130 | 130 | 130 |
| Power-to-gas (PtG) | $O_2$ | - | - | 210 | - |
| | $H_2$ | - | - | 27 | - |
| | BFG | - | - | 139 | 14 |
| | COG | - | - | - | 91 |
| | $CH_4$ | - | - | 65 | 65 |

The total electricity consumption of the ironmaking process was 874 MJ/t steel, and the electricity produced by the power plant was 1260 MJ/t steel (Table 3); therefore, the overall process was self-sufficient (typical power productions were about 1300 MJ/t steel in on-site power plants [15]). Regarding the thermal energy consumption, the BF was the largest consumer, representing 55% of the overall process when the air heating was accounted for (in the literature, the energy consumption of the blast furnace (BF) process can reach 70% of the total plant [3]). The heat removed by cooling the stoves of the BF was fixed at 1260 MJ/t pig iron, according to [22].

**Table 3.** Main energy streams (MJ/t steel) calculated for Case 0, Case 1, and Case 2. * From: [15].

| | Process | Case 0 | Case 1 | Case 2 |
|---|---|---|---|---|
| Thermal energy consumption | Sintering | 523 | 523 | 523 |
| | Coke oven | 1631 | 1442 | 1442 |
| | Air (hot blast) | 1814 | - | - |
| | $O_2$ + BFG (hot blast) | - | 1239 | 1239 |
| | $CH_4$ (hot blast) | - | 431 | 431 |
| | Blast furnace | 2915 | 3900 | 3900 |
| | $O_2$ heating | 170 | 170 | 170 |
| | BOF | 1228 | 1228 | 1228 |
| | Casting, rolling | 300 | 300 | 300 |
| | Total | 8581 | 9233 | 9233 |
| Electricity consumption | Sintering * | 180 | 180 | 180 |
| | Coke oven * | 42 | 42 | 42 |
| | Blast furnace * | 376 | 376 | 376 |
| | ASU | 128 | 252 | 568 |
| | BOF * | 128 | 128 | 128 |
| | Electrolyser | - | 4991 | - |
| | $H_2$ compressor | - | 96 | 32 |
| | $CO_2$ compressor | - | 51 | 36 |
| | Other * | 20 | 20 | 20 |
| | Total | 874 | 6136 | 1382 |
| Electricity production | Power plant | 1260 | 1443 | 652 |

The percentage of utilization of COG, BFG, and BOFG by type of process is presented in Table 4, together with their energy density and mass flow production. In overall terms, the 46.5% energy content of these gases was used in internal processes of the plant, while the rest was used in the power plant (Figure 5). The total $CO_2$ emissions of the plant were 1718 kg/t steel (Figure 6), with BFG as the major emitting source (1368 kg/t steel). According to the literature, BF $CO_2$ emissions may range between 1270 and 1550 kg/t steel, and total emissions up to 2200 kg/t steel [16,23].

### *4.2. Case 1: Power-to-Methane Integration in Ironmaking with Oxy-Fuel Combustion and TGR*

In Case 1, the installation included an oxygen blast furnace with top gas recycling and a power-to-gas (PtG) plant. The latter converted the $CO_2$ emissions into synthetic methane to be reinjected in the blast furnace, thus replacing some fossil fuel. The power capacity of the power-to-gas plant was sized to produce a SNG amount enough to replace 50 kg coke/t steel. According to the simulation, the replacement ratio was 1.3 kg SNG/kg coke, and therefore the necessary $H_2$ was 27 kg $H_2$/t steel. Assuming a steel production of 7.7 kt/day, we found the electrolysis power capacity to be installed was 431.9 $MW_e$ if working continuously (4.5 kWh/$Nm^3$ $H_2$ electricity consumption). Currently, the world's largest planned electrolyser farm has a power capacity of 100 MW [24], which is within the same order of magnitude as the PtG capacity required for the proposed case study.

**Table 4.** Mass flow, energy content, and use of the fuel gases produced in the ironmaking process.

| | | Case 0 | | | Case 1 | | | Case 2 | | |
|---|---|---|---|---|---|---|---|---|---|---|
| | | COG | BFG | BOFG | COG | BFG | BOFG | COG | BFG | BOFG |
| Utilization of the energy content of the gases by type of process (%) | Mass flow (kg/t steel) | 110 | 2080 | 130 | 90 | 2140 | 130 | 90 | 2140 | 130 |
| | Energy content (MJ/kg) | 40.0 | 2.7 | 6.3 | 40.0 | 5.7 | 6.3 | 40.0 | 5.7 | 6.3 |
| | Internal use | 99.1 | 0 | 99.0 | 0 | 42.2 | 99.0 | 0 | 43.6 | 99.0 |
| | Power plant | 0.9 | 100 | 1.0 | 100 | 1.6 | 1.0 | 0.3 | 6.0 | 1.0 |
| | Methanation | - | - | - | 0 | 6.5 | 0 | 99.7 | 0.6 | 0 |
| | TGR | - | - | - | 0 | 49.7 | 0 | 0 | 49.7 | 0 |

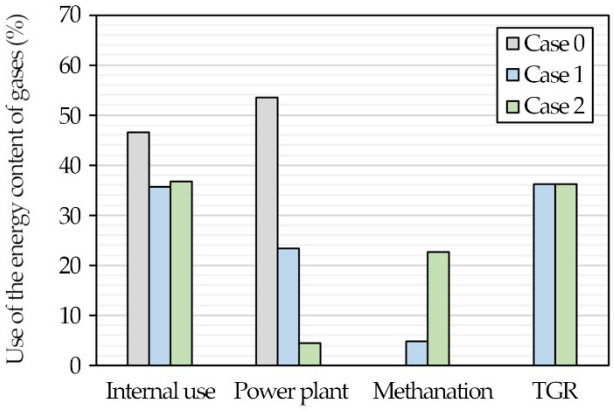


**Figure 5.** Use of the energy content of the total gases (COG, BFG, and BOFG) by type of process for each plant layout (i.e., Case 0–2).

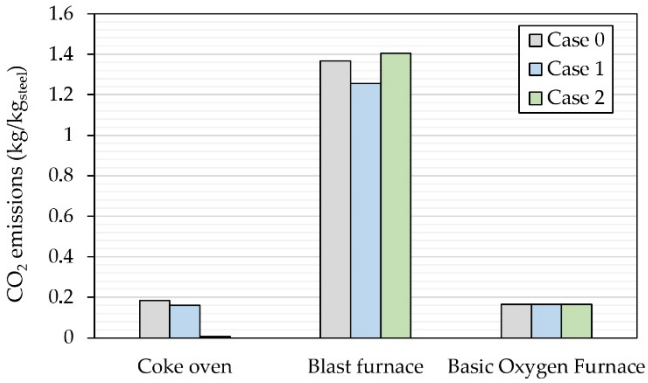


**Figure 6.** $CO_2$ emissions by process for each plant layout (i.e., Case 0–2).

The total electricity consumption of the overall plant was 6.1 MJ/t steel, which means an increment of 702% with respect to the base case scenario (Table 3). The electricity demand of those processes already existing in the base simulation was kept constant [15], and the new electricity consumptions corresponding to the PtG plant were added (the production of $H_2$ represents 81% of the total electricity consumption). Despite the power plant now producing 14.5% more power (1.4 MJ/t steel), the overall process is no longer self-sufficient. The remaining electricity (4.7 MJ/t steel) should come from renewable sources to avoid further emissions. Within this framework, a renewable facility working continuously of 417 $MW_e$ is required to satisfy this electricity demand.

Regarding thermal energy consumption (Table 3), the largest consumer is still the blast furnace (60.3% of the total needs). Its energy consumption increased by 9.4% due to oxy-fuel combustion. However, the coke oven consumption decreased by 11.6% due to the reduction of fossil fuel input. In the air heating furnace, we had to heat $CO_2$ for the oxy-combustion instead of air, resulting in a slight reduction of the thermal energy consumption.

In this integration, BFG was used in top gas recycling and methanation, and therefore the percentage of utilization of fuel gases by type of process remarkably changed (Table 4). Here, only 35.7% of the energy content of these gases was used in the internal processes of ironmaking and 21.4% in the power plant (Figure 5). The remaining was mostly recirculated to the blast furnace (36.1%), and a small fraction was diverted to methanation (4.7%).

Regarding $CO_2$, the BF was still the larger emitting source, producing 1255 kg/t steel. In total, the $CO_2$ emissions were 1582 kg/t steel, which was 8% less than in the reference case (Case 0, Figure 6). Thus, 136 kg $CO_2$/t steel were avoided by consuming 5079 MJ/t steel additional electrical energy, and a saving of 3.34 MJ/kg $CO_2$ by means of coke reduction was achieved, which means a $CO_2$ avoidance penalization of 34 MJ/kg

$CO_2$. Comparing this penalization with those in other processes, such as power-to-syngas (4.8–10.8 MJ/kg $CO_2$ [11]) and amine scrubbing (3–4 MJ/kg $CO_2$ [25,26]), indicates that Case 1 configuration does not present any energy advantage.

### *4.3. Case 2: Methanation of COG Integration in Ironmaking with Oxy-Fuel Combustion and TGR*

In this case, the ironmaking process worked under oxy-fuel regime with top gas recycling as in Case 1. However, here, the $H_2$ source for the methanation process was the coke oven gas instead of pure $H_2$.

The total electrical consumption of this plant was 1382 MJ/t steel. This was well below Case 1 (77% lower) since electrolysis was no longer used, but still above Case 0 (58% higher) because of the gas compression in the methanation process and the production of $O_2$ for the oxy-fuel blast furnace. Moreover, since COG was here used in methanation, the power plant only produced 652 MJ/t steel (47% of the total electricity consumption, i.e., not self-sufficient). To supply the missing electricity, we required a renewable facility of 65 $MW_e$ working continuously, assuming a steel production of 7.7 kt/day. Regarding thermal energy consumption, the requirements are the same than those of Case 1 (Table 3).

In terms of gas utilization (Table 4), the COG was used entirely in methanation instead of in internal plant processes. For this reason, 43.6% of the BFG had to be allocated to this end. The BOFG was also used in the internal processes of the plant (as in the two previous cases). With this implementation, 36.8% of the energy from these gases was used in the internal processes, 4.5% in the power plant, 22.6% in methanation, and 36.1% in top gas recycling (Figure 5).

Regarding emissions, the $CO_2$ that was avoided remained the same as for Case 1 (136 kg $CO_2$/t steel) because the same amount of methane was produced, and therefore the amount of $CO_2$ that was recycled in closed loop did not change. Then, total emissions were 1582 kg/t steel (the BF accounted for 1405 kg $CO_2$/t steel, while the coke oven barely emitted $CO_2$ because COG was used in methanation). Since the electricity consumption increased by 1116 MJ/t steel, the $CO_2$ avoidance penalization was 4.9 MJ/kg $CO_2$. This penalization is in the range of other processes such as power-to-syngas or amine scrubbing, and therefore is energetically competitive.

### *4.4. Discussion*

Figure 7 depicts a Sankey diagram of the energetic gases of the steel industry for the three scenarios: Case 0, Case 1, and Case 2. It can be seen that the energy flow to the power plant was increasingly reduced for each case, thus explaining why a renewable facility is needed. The internal energy use increased in Cases 1 and 2 due to the blocks that were added to the diagram (e.g., $CH_4$ heating). In the methanation section, the same energy was consumed in both Cases 1 and 2, and therefore the main difference was the $H_2$ source, either an electrolyser or the COG. The TGR was not changed in the two integrations, obtaining the energy from the BFG.

Although integrating oxy-fuel combustion in the BF is an interesting option in terms of $CO_2$ mitigation, the technology is not commercial yet (current TRL is 6–7) [27]. Thus far, Zuo and Hirsch [28] reported experimental results from a 9 $m^3$ TGR-BF, combined with a vacuum pressure swing adsorption carbon capture method for removing $CO_2$ of the top gas. They found 24% savings in carbon consumption and 76% reduction in $CO_2$ emissions when assuming underground storage of the corresponding captured $CO_2$ [29]. On average, the carbon input decreased from 470 kg/t pig iron to 350 kg/t pig iron [27]. It is worth mentioning that oxy-fuel combustion is already applied commercially in secondary processes in ironmaking plants, such as during the preheating of ladles and converter, or during the steel reheating and heat treatment. Since the oxy-fuel technology is familiar to the industry, its adoption in BFs is a reasonable option [11]. In fact, the topic is being studied widely in the literature to solve remaining technical issues related to the smoothness of operation (non-linear behavior of the feedback induced by the top gas recycle) [30].

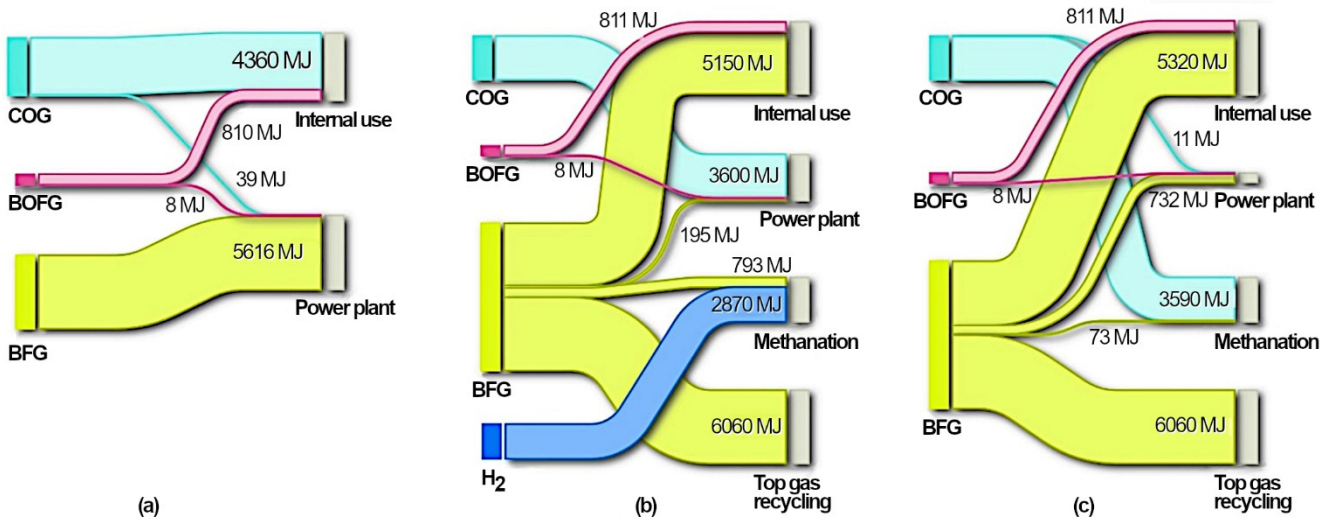


**Figure 7.** Sankey diagram of the change in the energy utilization inside the ironmaking plant of the energetic gases COG, BOFG, and BFG: (**a**) Case 0, (**b**) Case 1, and (**c**) Case 2.

## 5. Conclusions

A novel concept integrating power-to-gas technology in the ironmaking process, together with oxy-fuel combustion and top gas recycling, was presented. Two integration options were analyzed, differing in the source of $H_2$ for the methanation process ($H_2$ from water electrolysis, Case 1, or syngas from the coke oven, Case 2). In both cases, synthetic natural gas from methanation was injected into the blast furnace to reduce the coke consumption, thus recycling $CO_2$ in a closed loop. The power-to-gas plant was sized to reduce the coke content by 50 kg/t steel. Both Cases 1 and 2 were compared with a conventional ironmaking process (Case 0).

The base case simulation included the sintering process, coke oven, hot stoves, blast furnace, air separation unit, basic oxygen furnace, casting, and power plant. For the power-to-gas (PtG) integrations, an electrolyser (only in Case 1) and methanation plant were added to the simulation, and the blast furnace was run under oxy-fuel conditions with top gas recycling. Mass flows, compositions, and thermal and electricity consumptions were calculated through mass and energy balances.

Savings in $CO_2$ emissions with either of the two PtG implementations were 8%, with a reduction in coal fuel of 12.8%. The energy required to avoid these emissions was 34 MJ/kg $CO_2$ for Case 1 and 4.9 MJ/kg $CO_2$ for Case 2. This remarkable difference was because the first PtG integration required a 431.9 MW electrolyser to produce the $H_2$, while the second used the $H_2$ content of coke oven gas (COG) and therefore an electrolyser was not needed. Under this framework, the only competitive option is Case 2, whose energy penalization is in the range of conventional amine carbon capture [31]. Moreover, it has the advantage of reducing the fuel consumption and reducing geological storage, which are additional benefits regarding economic costs compared to conventional carbon capture and storage.

The energy content of the gases generated in the industry (COG, BFG, and BOFG) are normally used in internal processes, but mainly in the production of electricity. The implementation of the PtG implies a greater consumption of these gases in the internal processes of the plant, as well as in the methanation and recirculation processes. This means that only a small percentage of the gases are diverted to the thermal power plant, making necessary a renewable facility to fulfil the electricity demand (in Case 1 and Case 2, the plant is no longer self-sufficient). Case 1 requires a renewable-based power production 5.2 times larger than Case 2 (417 MW vs 65 MW), due to electrolysis.

This study shows good technical prospects for the future in terms of reducing steel-making industry emissions. An economic analysis of the proposed alternative processes will be performed in future work.

**Author Contributions:** Conceptualization, J.P., M.B., L.M.R. and B.P.; methodology, J.P. and M.B.; model, J.P. and M.B.; validation, J.P. and M.B.; formal analysis, J.P.; writing—original draft preparation, J.P. and M.B.; writing—review and editing, V.E.; visualization, J.P. and M.B.; supervision, M.B., L.M.R., B.P. and V.E.; project administration, M.B., L.M.R., B.P. and V.E.; funding acquisition, M.B., L.M.R. and V.E. All authors have read and agreed to the published version of the manuscript.

**Funding:** The work described in this paper has been supported by both the University of Zaragoza under the project UZ2020-TEC-06 and Khalifa University project CIRA-2020-080. This work has also received funding from the European Union's Horizon 2020 research and innovation program under the Marie Sklodowska-Curie grant agreement no. 887077.

**Institutional Review Board Statement:** Not applicable.

**Informed Consent Statement:** Not applicable.

**Data Availability Statement:** Not applicable.

**Conflicts of Interest:** The authors declare no conflict of interest.

## Abbreviations

| | |
|---|---|
| ASU | air separation unit |
| BAT | best available technology |
| BF | blast furnace |
| BFG | blast furnace gas |
| BOF | basic oxygen furnace |
| BOFG | basic oxygen furnace gas |
| CDQ | coke dry quenching |
| CO | coke oven |
| COG | coke oven gas |
| PtG | power-to-gas |
| SNG | synthetic natural gas |
| TGR | top gas recycling |

## Appendix A. Stream Data

**Table 1.** Specific heat, mass flows, and temperatures for Cases 0, 1 and 2.

| Stream | cp | m | T | Stream | cp | m | T | Stream | cp | m | T |
|---|---|---|---|---|---|---|---|---|---|---|---|
| | (kJ/kg.K) | (kg/kgsteel) | (°C) | | (kJ/kg.K) | (kg/kgsteel) | (°C) | | (kJ/kg.K) | (kg/kgsteel) | (°C) |
| **1** | 0.473 | 1.426 | 25 | **49** | 0.907 | 0.085 | 25 | **180** | 4.18 | 0.08955 | 25 |
| **2** | 0.835 | 0.0713 | 25 | **101** | 0.473 | 1.426 | 25 | **181** | 4.18 | 0.2414 | 25 |
| **3** | 0.473 | 1.426 | 800 | **102** | 0.835 | 0.0713 | 25 | **182** | 14.34 | 0.02701 | 25 |
| **4** | 0.473 | 1.426 | 150 | **103** | 0.473 | 1.426 | 800 | **183** | 0.914 | 0.2144 | 25 |
| **5** | 1.005 | 0.6232 | 25 | **104** | 0.473 | 1.426 | 150 | **184** | 2.239 | 0.06506 | 25 |
| **6** | 1.126 | 0.6232 | 650 | **105** | 1.005 | 0.6232 | 25 | **185** | 4.18 | 0.1016 | 25 |
| **7** | 1.126 | 0.4762 | 650 | **106** | 1.126 | 0.6232 | 650 | **186** | 4.18 | 2.665 | 25 |
| **8** | 1.126 | 0.147 | 650 | **107** | 1.126 | 0.4762 | 650 | **187** | 4.18 | 2.665 | 80 |
| **9** | 1.426 | 0.08527 | 25 | **108** | 1.126 | 0.147 | 650 | **190** | 1.005 | 0.7772 | 25 |
| **10** | 1.012 | 0.2374 | 500 | **109** | 1.426 | 0.08527 | 25 | **191** | 1.038 | 0.5938 | 25 |
| **11** | 0.835 | 0.5238 | 25 | **110** | 1.012 | 0.2374 | 500 | **192** | 0.914 | 0.1803 | 25 |
| **12** | 0.836 | 0.4191 | 1100 | **111** | 0.835 | 0.4568 | 25 | **193** | 0.914 | 0.3947 | 25 |
| **13** | 0.836 | 0.4191 | 150 | **112** | 0.836 | 0.3654 | 1100 | **194** | 0.914 | 0.08873 | 25 |
| **14** | 9.035 | 0.1048 | 1350 | **113** | 0.836 | 0.3654 | 150 | **195** | 1.179 | 0.08873 | 1650 |
| **15** | 1.005 | 0.668 | 25 | **114** | 9.035 | 0.09136 | 1350 | **196** | 1.117 | 0.04026 | 25 |
| **16** | 9.035 | 0.04969 | 25 | **115** | 1.005 | 0.4562 | 25 | **197** | 1.005 | 0.05914 | 25 |
| **17** | 1.012 | 0.7408 | 500 | **116** | 1.117 | 0.3105 | 25 | **198** | 1.012 | 0.104 | 600 |
| **18** | 1.038 | 0.3646 | 25 | **117** | 1.012 | 0.8021 | 500 | **200** | 0.907 | 0.085 | 25 |
| **19** | 1.178 | 0.3646 | 800 | **118** | 1.038 | 0.318 | 25 | **201** | 0.749 | 0.085 | 1650 |
| **20** | 1.005 | 1.278 | 25 | **119** | 1.178 | 0.318 | 800 | **202** | 1.005 | 0.06183 | 25 |
| **21** | 1.208 | 1.278 | 1200 | **130** | 0.914 | 0.3059 | 25 | **203** | 1.154 | 0.06183 | 800 |
| **22** | 9.035 | 0.05062 | 25 | **131** | 1.142 | 0.3059 | 1200 | **204** | 0.749 | 0.085 | 460 |
| **23** | 1.005 | 0.6805 | 25 | **132** | 0.842 | 0.5324 | 25 | **205** | 1.426 | 0.1346 | 1650 |
| **24** | 1.012 | 0.7547 | 300 | **133** | 1.323 | 0.5324 | 1200 | **206** | 0.5 | 1 | 1650 |

**Table 1.** *Cont.*

| Stream | cp | m | T | Stream | cp | m | T | Stream | cp | m | T |
|---|---|---|---|---|---|---|---|---|---|---|---|
| **25** | 0.907 | 0.283 | 25 | **134** | 1.117 | 0.4782 | 25 | **207** | 1.412 | 0.04795 | 25 |
| **26** | 1.412 | 2.084 | 200 | **135** | 1.005 | 0.7025 | 25 | **208** | 1.005 | 0.08269 | 25 |
| **27** | 0.749 | 0.283 | 1200 | **136** | 1.012 | 1.235 | 600 | **209** | 1.012 | 0.1335 | 850 |
| **28** | 0.749 | 0.283 | 460 | **137** | 1.037 | 0.53 | 25 | **210** | 0.5 | 1 | 25 |
| **29** | 1.005 | 0.1754 | 25 | **138** | 1.254 | 0.53 | 1200 | **334** | 1.412 | 0.4782 | 25 |
| **30** | 1.154 | 0.1754 | 800 | **140** | 2.239 | 0.06506 | 25 | **335** | 1.005 | 0.7025 | 25 |
| **31** | 0.48 | 1.039 | 1200 | **141** | 5.632 | 0.06506 | 1200 | **336** | 1.012 | 1.235 | 600 |
| **32** | 1.005 | 0.3825 | 25 | **142** | 1.117 | 0.1019 | 25 | **342** | 1.412 | 0.1019 | 25 |
| **33** | 0.914 | 0.08873 | 25 | **143** | 1.005 | 0.1498 | 25 | **343** | 1.005 | 0.1498 | 25 |
| **34** | 1.038 | 0.2922 | 25 | **144** | 1.012 | 0.2633 | 600 | **344** | 1.012 | 0.2633 | 600 |
| **35** | 1.179 | 0.08873 | 1650 | **150** | 0.907 | 0.283 | 25 | **374** | 1.412 | 0.01384 | 25 |
| **36** | 1.005 | 0.07301 | 25 | **151** | 0.749 | 0.283 | 1200 | **376** | 1.098 | 1.059 | 25 |
| **37** | 9.035 | 0.00543 | 25 | **152** | 0.749 | 0.283 | 460 | **382** | 9.035 | 0.09106 | 25 |
| **38** | 1.012 | 0.08096 | 600 | **153** | 1.005 | 0.1754 | 25 | **385** | 4.18 | 0.00883 | 25 |
| **39** | 1.426 | 0.1346 | 1650 | **154** | 1.154 | 0.1754 | 800 | **386** | 4.18 | 0.8714 | 25 |
| **40** | 0.749 | 0.085 | 1650 | **155** | 0.48 | 1.039 | 1200 | **387** | 4.18 | 0.8714 | 80 |
| **41** | 0.749 | 0.085 | 460 | **156** | 1.117 | 2.186 | 200 | **390** | 1.005 | 1.701 | 25 |
| **42** | 1.005 | 0.0847 | 25 | **157** | 1.098 | 2.136 | 25 | **391** | 1.038 | 1.3 | 25 |
| **43** | 1.154 | 0.0847 | 800 | **158** | 4.18 | 0.05031 | 25 | **392** | 0.914 | 0.3947 | 25 |
| **44** | 0.5 | 1 | 1650 | **159** | 4.18 | 2.352 | 25 | **396** | 1.412 | 0.04026 | 25 |
| **45** | 0.5 | 1 | 25 | **160** | 4.18 | 2.352 | 80 | **397** | 1.005 | 0.05914 | 25 |
| **46** | 1.426 | 0.04795 | 25 | **174** | 1.098 | 0.1389 | 25 | **398** | 1.012 | 0.104 | 600 |
| **47** | 1.005 | 0.08269 | 25 | **175** | 1.098 | 1.062 | 25 | | | | |
| **48** | 1.012 | 0.1335 | 850 | **176** | 1.098 | 0.9343 | 25 | | | | |

## References


1. Huitu, K.; Helle, H.; Helle, M.; Kekkonen, M.; Saxén, H. Optimization of steelmaking using fastmet direct reduced iron in the blast furnace. *ISIJ Int.* **2013**, *53*, 2038–2046. [CrossRef]
2. Quader, M.A.; Ahmed, S.; Ghazilla, R.A.R.; Ahmed, S.; Dahari, M. A comprehensive review on energy efficient $CO_2$ breakthrough technologies for sustainable green iron and steel manufacturing. *Renew. Sustain. Energy Rev.* **2015**, *50*, 594–614. [CrossRef]
3. He, K.; Wang, L. A review of energy use and energy-efficient technologies for the iron and steel industry. *Renew. Sustain. Energy Rev.* **2017**, *70*, 1022–1039. [CrossRef]
4. Ariyama, T.; Takahashi, K.; Kawashiri, Y.; Nouchi, T. Diversification of the Ironmaking Process Toward the Long-Term Global Goal for Carbon Dioxide Mitigation. *J. Sustain. Metall.* **2019**, *5*, 276–294. [CrossRef]
5. Lisbona, P.; Bailera, M.; Peña, B.; Romeo, L.M. Integration of $CO_2$ capture and conversion. In *Advances in Carbon Capture*; Rahimpour, M.R., Farsi, M., Makarem, M.A., Eds.; Woodhead Publishing: Cambridge, UK, 2020; pp. 503–522. ISBN 9780128196571.
6. Gao, J.; Wang, Y.; Ping, Y.; Hu, D.; Xu, G.; Gu, F.; Su, F. A thermodynamic analysis of methanation reactions of carbon oxides for the production of synthetic natural gas. *RSC Adv.* **2012**, *2*, 2358–2368. [CrossRef]
7. Bailera, M.; Lisbona, P.; Romeo, L.M. Power to gas-oxyfuel boiler hybrid systems. *Int. J. Hydrog. Energy* **2015**, *40*, 10168–10175. [CrossRef]
8. Romeo, L.M.; Bailera, M. Design configurations to achieve an effective $CO_2$ use and mitigation through power to gas. *J. $CO_2$ Util.* **2020**, *39*, 1–10. [CrossRef]
9. Bailera, M.; Hanak, D.P.; Lisbona, P.; Romeo, L.M. Techno-economic feasibility of power to gas–oxy-fuel boiler hybrid system under uncertainty. *Int. J. Hydrog. Energy* **2019**, *4*, 9505–9516. [CrossRef]
10. Eveloy, V. Hybridization of solid oxide electrolysis-based power-to-methane with oxyfuel combustion and carbon dioxide utilization for energy storage. *Renew. Sustain. Energy Rev.* **2019**, *108*, 550–571. [CrossRef]
11. Bailera, M.; Lisbona, P.; Peña, B.; Romeo, L.M. A review on $CO_2$ mitigation in the Iron and Steel industry through Power to X processes. *J. $CO_2$ Util.* **2021**, *46*, 101456. [CrossRef]
12. Kirschen, M.; Risonarta, V.; Pfeifer, H. Energy efficiency and the influence of gas burners to the energy related carbon dioxide emissions of electric arc furnaces in steel industry. *Energy* **2009**, *34*, 1065–1072. [CrossRef]
13. Rosenfeld, D.C.; Böhm, H.; Lindorfer, J.; Lehner, M. Scenario analysis of implementing a power-to-gas and biomass gasification system in an integrated steel plant: A techno-economic and environmental study. *Renew. Energy* **2020**, *147*, 1511–1524. [CrossRef]
14. Steelmaking Technologies. CISDI Ingeniering CO. LTD. Available online: http://www.cisdigroup.com/4-steelmaking.html (accessed on 15 September 2021).
15. He, H.; Guan, H.; Zhu, X.; Lee, H. Assessment on the energy flow and carbon emissions of integrated steelmaking plants. *Energy Rep.* **2017**, *3*, 29–36. [CrossRef]
16. Wu, J.; Wang, R.; Pu, G.; Qi, H. Integrated assessment of exergy, energy and carbon dioxide emissions in an iron and steel industrial network. *Appl. Energy* **2016**, *183*, 430–444. [CrossRef]
17. Geerdes, M.; Chaigneau, R.; Lingiardi, O.; Molenaar, R.; van Opbergen, R.; Sha, Y.; Warren, P. *Modern Blast Furnace Ironmaking an Introduction*; IOS Press: Amsterdam, The Netherlands, 2020; ISBN 978-1-64368-123-8.

18. Ariyama, T.; Sato, M.; Nouchi, T.; Takahashi, K. Evolution of blast furnace process toward reductant flexibility and carbon dioxide mitigation in steel works. *ISIJ Int.* **2016**, *56*, 1681–1696. [CrossRef]
19. Fisher, L.V.; Barron, A.R. The recycling and reuse of steelmaking slags—A review. *Resour. Conserv. Recycl.* **2019**, *146*, 244–255. [CrossRef]
20. Darde, A.; Prabhakar, R.; Tranier, J.P.; Perrin, N. Air separation and flue gas compression and purification units for oxy-coal combustion systems. *Energy Procedia* **2009**, *1*, 527–534. [CrossRef]
21. Rönsch, S.; Schneider, J.; Matthischke, S.; Schlüter, M.; Götz, M.; Lefebvre, J.; Prabhakaran, P.; Bajohr, S. Review on methanation—From fundamentals to current projects. *Fuel* **2016**, *166*, 276–296. [CrossRef]
22. Biswas, A.K. *Principles of Blast Furnace Ironmaking. Theory and Practice*; Cootha Publishing House: Brisbane, Australia, 1981.
23. IAE—Iron & Steel Roadmap. 2020. Available online: https://www.iea.org/reports/iron-and-steel-technology-roadmap (accessed on 24 October 2021).
24. ITM Power to study feasibility of 100 MW P2G energy storage. *Fuel Cells Bull.* **2018**, *2018*, 11. [CrossRef]
25. Arasto, A.; Tsupari, E.; Kärki, J.; Pisilä, E.; Sorsamäki, L. Post-combustion capture of $CO_2$ at an integrated steel mill—Part I: Technical concept analysis. *Int. J. Greenh. Gas Control* **2013**, *16*, 271–277. [CrossRef]
26. Tobiesen, F.A.; Svendsen, H.F.; Mejdell, T. Modeling of blast furnace $CO_2$ capture using amine absorbents. *Ind. Eng. Chem. Res.* **2007**, *46*, 7811–7819. [CrossRef]
27. Keys, A.; van Hout, M.; Daniels, B. *Decarbonisation Options for the Dutch Steel Industry*; PBL Netherlands Environmental Assessment Agency: The Hague, The Netherlands, 2019.
28. Zuo, G.; Hirsch, A. The trial of the Top Gas Recycling Blast Furnace at LKAB's EBF and Scale-Up. *Rev. Métallurgie* **2009**, *2*, 255. [CrossRef]
29. Danloy, G.; Berthelemot, A.; Grant, M.; Borlée, J.; Sert, D.; van der Stel, J.; Jak, H.; Dimastromatteo, V.; Hallin, M.; Eklund, N.; et al. ULCOS—Pilot testing of the low-$CO_2$ Blast Furnace process at the experimental BF in Lulea. *Rev. Metall. Cah. D'Inform. Technol.* **2009**, *106*, 1–8. [CrossRef]
30. Zhang, W.; Dai, J.; Li, C.; Yu, X.; Xue, Z.; Saxén, H. A Review on Explorations of the Oxygen Blast Furnace Process. *Steel Res. Int.* **2021**, *92*, 202000326. [CrossRef]
31. Bailera, M.; Lisbona, P.; Peña, B.; Romeo, L.M. *Energy Storage*; Springer International Publishing: Cham, Switzerland, 2020; ISBN 978-3-030-46526-1.

Fuel 336 (2023) 127074

Contents lists available at ScienceDirect

Fuel

journal homepage: www.elsevier.com/locate/fuel

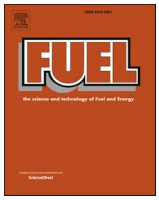

# Integration of carbon capture technologies in blast furnace based steel making: A comprehensive and systematic review

Jorge Perpiñán [a,*], Begoña Peña [a], Manuel Bailera [a,b], Valerie Eveloy [c], Pravin Kannan [c], Abhijeet Raj [d,e], Pilar Lisbona [a], Luis Miguel Romeo [a]

[a] Escuela de Ingeniería y Arquitectura, Universidad de Zaragoza, María de Luna 3, Zaragoza 50018, Spain
[b] Graduate School of Creative Science and Engineering, Waseda University, Okubo, Shinjuku-ku, Tokyo 169-8555, Japan
[c] Department of Mechanical Engineering, Khalifa University, Abu Dhabi P.O. Box 127788, United Arab Emirates
[d] Department of Chemical Engineering, Khalifa University, Abu Dhabi P.O. Box 127788, United Arab Emirates
[e] Department of Chemical Engineering, Indian Institute of Technology Delhi, New Delhi 110016, India

ARTICLE INFO

*Keywords:*
Steel industry
Ironmaking
Carbon capture
Technical comparison
Systematic review

ABSTRACT

Decarbonization of the iron and steel industry, which accounts for 7–9% of global annual emissions, is a strategic objective to achieve carbon emissions reduction targets in line with climate change policies, while maintaining economic competitiveness. Carbon capture (CC) technologies are of critical importance to achieve these goals. This work presents the first systematic review of the integration of CC technologies in the blast furnace-basic oxygen furnace (BF-BOF) steelmaking route, which is expected to maintain a dominant market share over the coming decades. Integration options for post-combustion, looping cycles, oxy-combustion and pre-combustion are described and compared in terms of energy penalty, carbon emissions abatement potential, cost, technology readiness level, and practical deployment considerations. The review yielded 188 studies from peer-reviewed articles and technical papers. Research is mainly focused on chemical absorption, physical adsorption, and oxy-blast furnace technologies, but other carbon capture methods including calcium looping, Sorption Enhanced Water Gas Shift, and membranes appear promising in terms of cost and carbon emission reduction. This article provides an in-depth analysis of the current state of the art and crucial considerations for future decision making in the techno-economic selection and integration of CC technologies. Barriers to overcome for practical implementation are also identified and discussed in this article.

## 1. Introduction

Decarbonisation of energy-intensive industries is a strategic objective in European and National policies to accomplish the ambitious target posed in the European Green Deal (2020): to reach a Europe climate neutral in 2050 [1]. The iron and steel (I&S) industry is one of the major industrial contributors to global $CO_2$ emissions, and is responsible for 5 % of total global greenhouse gas emissions (GHG) [2], mainly due to the current dependency on coal-based processes [3]. In addition, it is a relevant economic sector embedded in strategic value chains that involve 1.3 % of GDP and 330,000 direct employments in Europe with an expected increase in production [4]. Current policies, together with the significant rise in the price of electricity, natural gas (NG) and $CO_2$ allowances in the past years, is fostering the interest of the sector in the development of low-emission technologies.

Globally, steel is produced through three main routes (Fig. 1): the blast furnace-basic oxygen furnace route (BF-BOF), the scrap-based electric arc furnace (EAF), and the direct reduced iron-electric arc furnace (DRI-EAF). The BF-BOF route consumes mainly iron ore, coal and coke, to cover the 70 % of the global steel demand [2]. Iron ore and coal are processed on a sinter strand and a coke oven, respectively. Then, the hot metal (HM) formed in the blast furnace is send to the basic oxygen furnace to reduce the carbon content and form molten steel.

The scrap-based EAF route uses recycled steel scrap and electricity, encompassing 23 % of the global production, but the expansion of this technology depends on the scrap availability [2]. This process consists only of one stage, the EAF, where the scrap is melted to form new steel. The emerging DRI-EAF route, accounting for 7 % production share [2], includes a shaft furnace, where iron ore is directly reduced by using

* Corresponding author.
*E-mail addresses:* jorge.perpinan@unizar.es (J. Perpiñán), bpp@unizar.es (B. Peña), mbailera@unizar.es (M. Bailera), valerie.eveloy@ku.ac.ae (V. Eveloy), pravin.kannan@ku.ac.ae (P. Kannan), abhijeet.raj@ku.ac.ae, raj@iitd.ac.in (A. Raj), pilarlm@unizar.es (P. Lisbona), luismi@unizar.es (L.M. Romeo).

https://doi.org/10.1016/j.fuel.2022.127074
Received 21 September 2022; Received in revised form 15 November 2022; Accepted 4 December 2022
Available online 15 December 2022
0016-2361/© 2022 The Author(s). Published by Elsevier Ltd. This is an open access article under the CC BY-NC license (http://creativecommons.org/licenses/by-nc/4.0/).

**Nomenclature**

| *Abbreviation* | *Meaning* |
|---|---|
| BF-BOF | Blast Furnace-Basic Oxygen Furnace |
| BFG | Blast Furnace Gas |
| BOFG | Basic Oxygen Furnace Gas |
| CC | Carbon Capture |
| CCUS | Carbon Capture Utilization and Storage |
| CaL | Calcium Looping |
| ChL | Chemical Looping |
| COG | Coke Oven Gas |
| DRI-EAF | Direct Reduced Iron-Electric Arc Furnace |
| EUA | European Union Allowance |
| FSCM | Fixed Site Carrier Membrane |
| GWP | Global Warming Potential |
| HM | Hot Metal |
| I&S | Iron and Steel |
| IEA | International Energy Agency |
| NGCC PP | Natural Gas Combined Cycle Power Plant |
| OBF | Oxygen Blast Furnace |
| Oxy-TGR | Oxy-Top Gas Recycling |
| OtherL | Other Looping Processes |
| Pre-adsor | Pre-combustion CC with physical adsorption |
| Post-chem | Post-combustion CC with chemical absorption |
| Pre-chem | Pre-combustion CC with chemical absorption |
| Post-memb | Post-combustion CC with membranes |
| Pre-memb | Pre-combustion CC with membranes |
| SPECCA | Specific Primary Energy Consumption for $CO_2$ Avoided |
| SEWGS | Sorption Enhanced Water Gas Shift |
| TRL | Technology Readiness Level |
| TGR | Top Gas Recycling |
| TSA | Temperature Swing Adsorption |
| VPSA | Vacuum Pressure Swing Adsorption |
| WGS | Water Gas Shift |

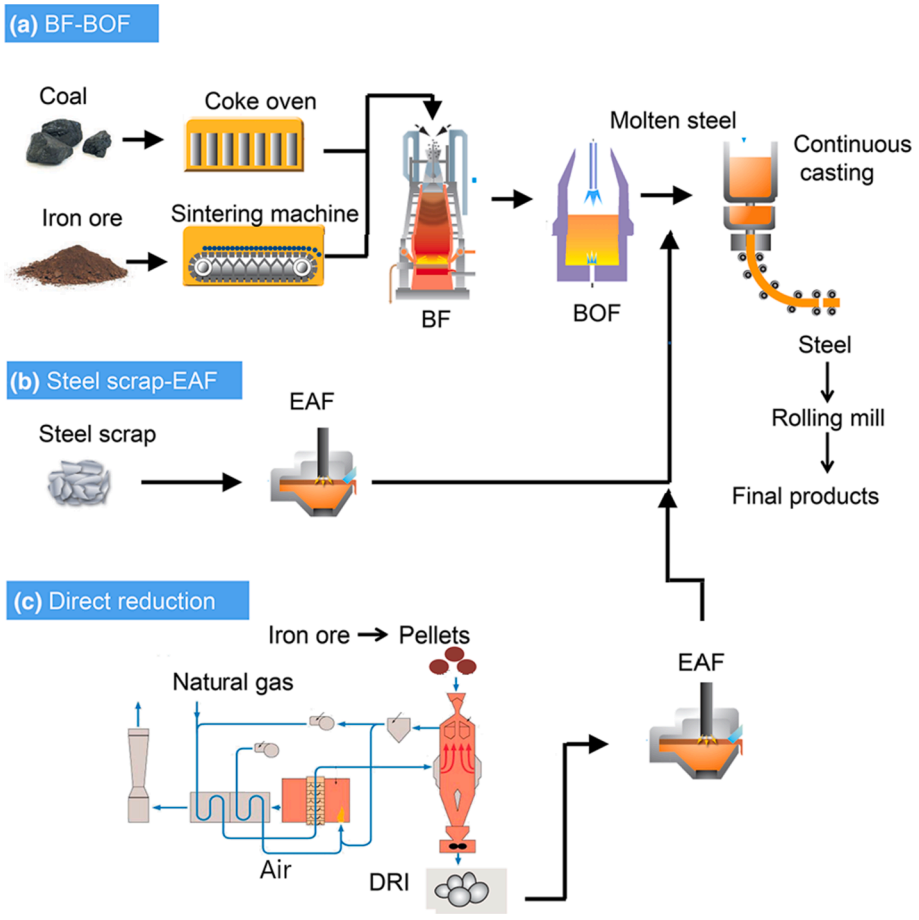


**Fig. 1.** The main routes of steel production. .
Adapted from [7]

reducing gases such as natural gas, coal syngas, or hydrogen. The resulting direct reduced iron (DRI) is melted, together with scrap, in an EAF. MIDREX [5] and ENERGIRON [6] are commercial-scale processes for DRI production.

Specific energy consumption and $CO_2$ emissions are very different for each route, and contrasted in Table 1. The BF-BOF process is clearly the most energy intensive one because of the energy needs associated with iron ore reduction in the blast furnace and with the conditioning of the raw materials, iron ore agglomeration and coking processes. The main energy inputs come from coal, giving rise to very high GHG emissions. Despite its high emissions, the BF-BOF route is still under expansion. In China, the I&S industry has developed rapidly over the past two decades, producing almost half of the current global production. Approximately 90 % of China's steel is produced via BF-BOF route [8]. Since the

**Table 1**
Main steelmaking production routes: BF-BOF, Scrap-EAF and DRI-EAF [2].

| Steelmaking production route | BF-BOF | Scrap-EAF | DRI-EAF |
|---|---|---|---|
| Steel world production | 70 % | 23 % | 7 % |
| Main inputs | Iron ore, coal and coke | Scrap and electricity | Iron ore, NG, coal syngas, $H_2$, scrap and electricity. |
| Energy consumption (GJ/tHM) | 13–14 | 4–6 | 10 |
| $CO_2$ emissions ($tCO_2$/tHM) | 2.0–2.2 | 0.3–0.5 | 0.7–1.3 |

global steel demand cannot be covered through recycled scrap, the BF-BOF route is expected to maintain its dominance in the market, despite its high emissions. Besides, blast furnaces are only phased-out at relining, which typically takes places every 20–35 years, or up to 40 years for newly commissioned plants. Thus, at least 20 % of today's blast furnaces are anticipated to still be in operation by year 2050 [9].

The reduction of greenhouse gas emissions from steel production has been the topic of extensive research worldwide. Several alternative ultra-low-$CO_2$ steel production technologies are under development to replace existing carbon-based steel manufacturing. The project Carbon2Chem [10] studies possible uses for steel gases, while ULCORED [11], ULCOWIN [11], ULCOLYSIS [11], COREX [12], HIsmelt [13], and FINEX [14] are projects and programmes aiming at the development of new routes for steel production. ULCOS-BF [11] and COURSE50 [15] are the only projects focused on capturing $CO_2$ in the BF-BOF route through physical adsorption and chemical absorption methods from the BFG.

Carbon capture technologies will be necessary to achieve significant carbon emission reduction in the I&S industry. Because of the much larger steel production and specific emissions of integrated steel mills (BF-BOF route) compared to EAF or DRI-EAF, the integrated mills have been the main focus of capture technology development and cost analysis. Besides the huge carbon volume to be captured, another major drawback to integrate $CO_2$ capture in steel mills is the number of different point sources (Fig. 2). The largest single point source is the blast furnace, from which 70 % of the emissions can be captured, followed by the power plant and the sinter strand. Apart from these processes, other sources emit smaller $CO_2$ amounts including the coke oven, the basic oxygen furnace or the casting and rolling. Since the emission rate and the mole fraction of $CO_2$ are very different among the various sources, multiple carbon capture plants or combining flue streams would be needed for each large mill in order to capture a large proportion of the total emissions. I&S gases, unlike flue gases from power production, have the particularity that besides $CO_2$ and $N_2$, other gas species are present at important concentrations, notably CO, $H_2$ and $CH_4$ (Table 2). However, steel gases have a higher $CO_2$ concentration than flue gases from power production.

Previous reviews related to low carbon ironmaking have not focused on CC or the BF-BOF route [18–21]. The main objective of this article is to present a systematic review of the state of the art related to carbon capture (CC) within the I&S industry, with special focus on the BF-BOF route. A global and holistic picture is presented to assist decision making regarding the most promising CC technology for the BF-BOF steelmaking route, by evaluating and comparing the technologies in terms of energy penalisation, economic cost, efficiency, Technology Readiness Level (TRL) [22], and the volume of $CO_2$ captured.

The paper is organised as follows: Section 2 presents the methodology of the systematic review; Section 3 comprises the post-combustion carbon capture systems; Section 4 include the looping carbon capture

**Table 2**
Typical composition for steel gases [17] and power plant flue gases (%vol).

| | Units | BFG | COG | BOFG | Coal PP | NGCC PP |
|---|---|---|---|---|---|---|
| $H_2$ | %vol | 4 | 45–64 | 1.5 | – | – |
| $CH_4$ | %vol | – | 20–30 | – | – | – |
| CO | %vol | 22–25 | 5–10 | 60–70 | – | – |
| $CO_2$ | %vol | 20–22 | 2–5 | 15–20 | 13 | 4 |
| $O_2$ | %vol | – | 1–4 | 2 | 5 | 14 |
| $N_2$ | %vol | 49–54 | 0–5 | 10 | 82 | 82 |
| LHV | $MJ/Nm^3$ | 3–3.8 | 16–19.3 | 7.5–8 | – | – |

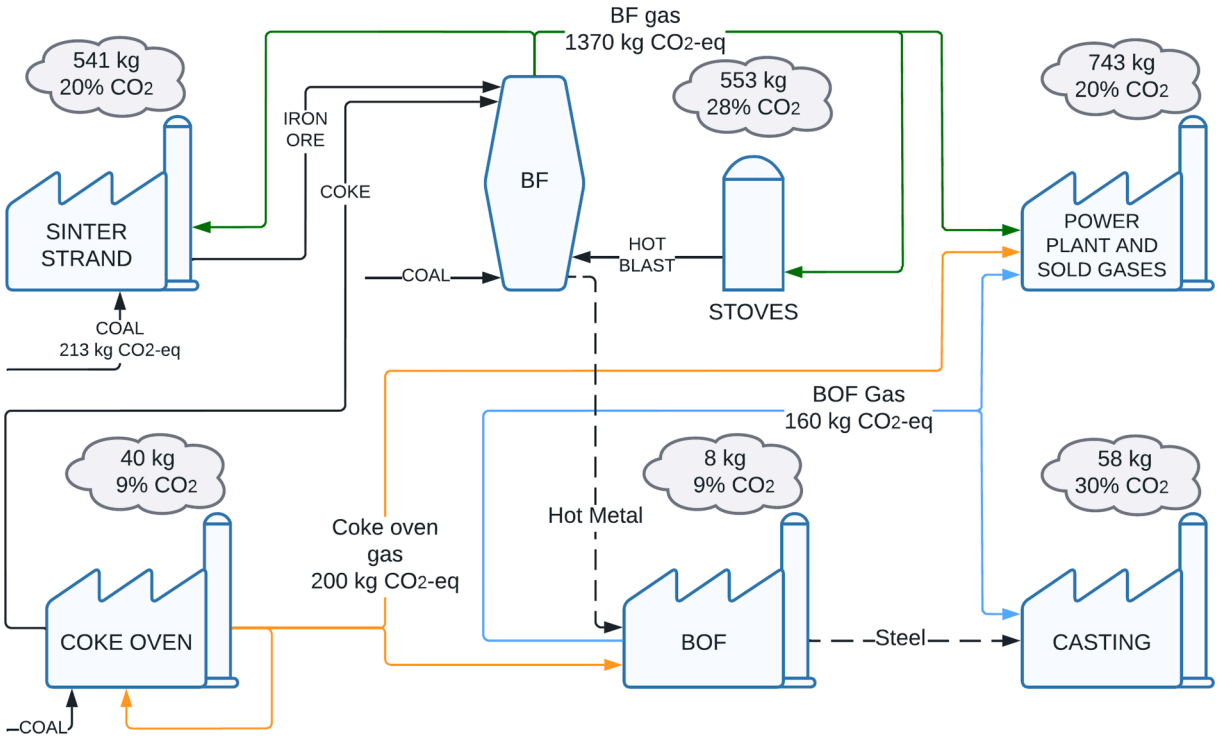


**Fig. 2.** Simplified flow sheet of an integrated steel mill, showing $CO_2$ emissions (kg/t steel) and concentration in flue gas (volume %) [16].

**Table 3**
Search terms, number of hits returned and number of papers reviewed.

| N° | Search term | Hits | Reviewed |
|---|---|---|---|
| 0 | ("Iron plant" OR "Iron industry" OR "Ironworks" OR "Ironmaking" OR "Iron-making" OR "Iron production" OR "Iron refining" OR "Steel plant" OR "Steel industry" OR "Steelworks" OR "Steelmaking" OR "Steel-making" OR "Steel production" OR "Steel refining" OR "Blast furnace" OR "Basic oxygen furnace" OR "Coke Oven" OR "Sinter plant" OR "Sinter strand") | Common I&S terms for all the CC searches | |
| 1 | ("Carbon capture" OR "Carbon dioxide capture" OR "CO2 capture" OR "CC" OR "Carbon utilization" OR "Carbon dioxide utilization" OR "CO2 utilization" OR "Carbon utilisation" OR "Carbon dioxide utilization" OR "CO2 utilisation" OR "CCU" OR "CCUS" OR "Carbon recycling" OR "Carbon dioxide recycling" OR "CO2 recycling" OR "Carbon reduction" OR "Carbon dioxide reduction" OR "CO2 reduction" OR "Carbon mitigation" OR "Carbon dioxide mitigation" OR "CO2 mitigation" OR "Low carbon" OR "Decarbonization" OR "Decarbonisation" OR "Emission reduction" OR "Emission mitigation" OR "Emission recycling") | 971 | 35 |
| 2 | ("Amine gas treating" OR "Amine scrubbing" OR "Amines" OR "MEA" OR "DEA" OR "MDEA") | 92 | 15 |
| 3 | ("Oxy combustion" OR "Oxycombustion" OR "Oxy-combustion" OR "Oxyfuel" OR "Oxy-fuel" OR "Oxy-fuel combustion") | 44 | 3 |
| 4 | ("Top gas recycling" OR "TGR" OR "Top gas injection" OR "BFG injection" OR "Hot Reducing Gases" OR "HRG") | 118 | 37 |
| 5 | ("Precombustion capture" OR "Pre-combustion capture" OR "Pre combustion capture" OR "CO2/H2 separation" OR "Partial oxidation") | 130 | 2 |
| 6 | ("Membranes" OR "Membrane separation" OR "Membrane-based separation" OR "Membrane technology") | 84 | 7 |
| 6 | ("Calcium looping" OR "Calcium-looping" OR "Ca-Looping" OR "CaL" OR "Carbonate looping" OR "Chemical looping" OR "Chemical-looping" OR "Combustion looping" OR "Oxygen carrier") | 68 | 15 |
| 8 | ("Pressure Swing Adsorption" OR "PSA" OR "Temperature Swing Adsorption" OR "TSA" OR "Vacuum Swing Adsorption" OR "VSA" OR "VPSA" OR "PTSA") | 62 | 6 |
| | Total | 1569 | 120 |

systems; Section 5 contain the oxygen blast furnaces and top gas recycling technologies; Section 6 comprises pre-combustion carbon capture systems; and Section 7 presents a carbon capture technologies comparison.

## 2. Systematic review approach

To identify the most relevant literature on the topic, a systematic review approach was adopted. Web of Science was selected as the search engine because of its advanced search capabilities and wide range of databases. The search is limited to studies presented in scientific journals and conferences included in the selected search engine. A set of 7 searches were performed, returning a total of 1569 entries (Table 3). Each search combined a term related to the I&S process (N° 0) and another term concerning carbon capture and storage (N° 1 to 7). The hits returned from the search were screened based on their abstract, and selected for review when applying any type of CC on the BF-BOF route of the I&S industry, leading to a total of 120 articles.

The 120 research articles were reviewed and classified into four different topics, according to the typical CC technology classification: post-combustion, looping cycles, oxy-combustion, and pre-combustion [23]. Fig. 3 illustrates the different options available for each CC technology. Each type of technology, if applicable, is divided according to the specific CC technology applied within the category: chemical absorption, physical adsorption, membranes, calcium looping, chemical looping and sorption enhanced water gas shift (SEWGS). For example, for oxy-combustion CC technology, only oxygen blast furnace technology was found (i.e., oxy-combustion CC technology of BOFG or other gases were not found in the literature).

Articles purely related to the improvement of energy efficiency, fuel consumption reduction, $H_2$ production without carbon capture, injection of hot reducing agents in the BF without carbon capture, steam methane reforming, and carbon dioxide reforming of methane were not included in this review since $CO_2$ is not captured or used directly. Articles related to CC in other steelmaking routes (i.e., DRI or EAF) were also not considered.

## 3. Post-combustion CC in BF-BOF

Post-combustion technologies include those systems where $CO_2$ is captured from the flue gases. This section reviews chemical absorption and membrane separation techniques for carbon capture in the I&S industry, and is focused on those previous works related to decarbonization of gas streams with no presence of combustible gases or including a stage of water-gas shift reactor to convert CO into $CO_2$. Research works, where the resulting cleaned gas is considered as a useful fuel, are classified in Section 6 as pre-combustion capture.

### 3.1. Post-combustion $CO_2$ capture by chemical absorption

Chemical absorption systems are based on chemical solvents that react reversibly with a certain target species. This method allows for a very selective separation compared to other technologies, and high purities and recoveries. Difficulties arise from the handling of the solvent systems, often exhibiting corrosive or volatile characteristics, as well as from the regeneration process of the saturated absorbent, usually endothermic, necessary for the economical operation of the separation.

The typical operation of industrial absorption consists of two stages: absorber to capture the $CO_2$ from the acid gas, and stripper to release the captured $CO_2$, as shown in Fig. 4. In the latter, the rich solution (amine + $CO_2$) is heated up to 110 °C in order to recover the $CO_2$ in a concentrated gas stream. The lean solution exiting the stripper is recycled back to the absorber. The global efficiency is increased by including a heat exchanger, where the rich solution is pre-heated before entering the stripper using the outgoing lean solution.

#### 3.1.1. Solvents and associated energy penalizations

In the context of the I&S industry, chemical absorption has been investigated for carbon capture from the flue gases of BF hot stoves [24–28], power plants [29–32], and coke ovens [24,33]. Concurrent carbon capture from different sources has been also studied in other works, aiming for a bigger $CO_2$ emission reduction [34,35,44,36–43].

The most widely used chemical solvents are single-component alkanolamines in an aqueous solution. These are classified into three categories depending on the type of the amine functional group: primary such as monoethanolamine (MEA) and diglycolamine (DGA), secondary such as diethanolamine (DEA), isopropylaminoethanol (IPAE) and aminoethylethanolamine (AEEA), and tertiary such as piperazine (PZ) and methyldiethanolamine (MDEA). They exhibit different behaviour with regards to reaction rates, heats of reaction, and corrosion. Primary amines are the most reactive, possess the highest heat of reaction, and are usually the most corrosive. These properties are less pronounced for secondary and tertiary amines. In addition to single-component amines, some multi-component solvents (RITE-A and RITE-B) have been developed by the Research Institute of Innovative Technology for the Earth (RITE) [28]. These novel solvents are IPAE-based mixtures of amines.

The most commonly used amine solvent is monoethanolamine (MEA), while other solvents have barely been studied in the literature (see Table 8). The high heat of reaction results in energy penalties ranging from 2.9 MJ/kg$CO_2$ to 6.5 MJ/kg$CO_2$ for MEA (30 %wt MEA) [24,25,34,36–38,40,42,43,45,26–33] and between 2.9 MJ/kg$CO_2$ and 3.1 MJ/kg$CO_2$, for MDEA (50 %wt MDEA) [35,39]. Yang et. al. [44]

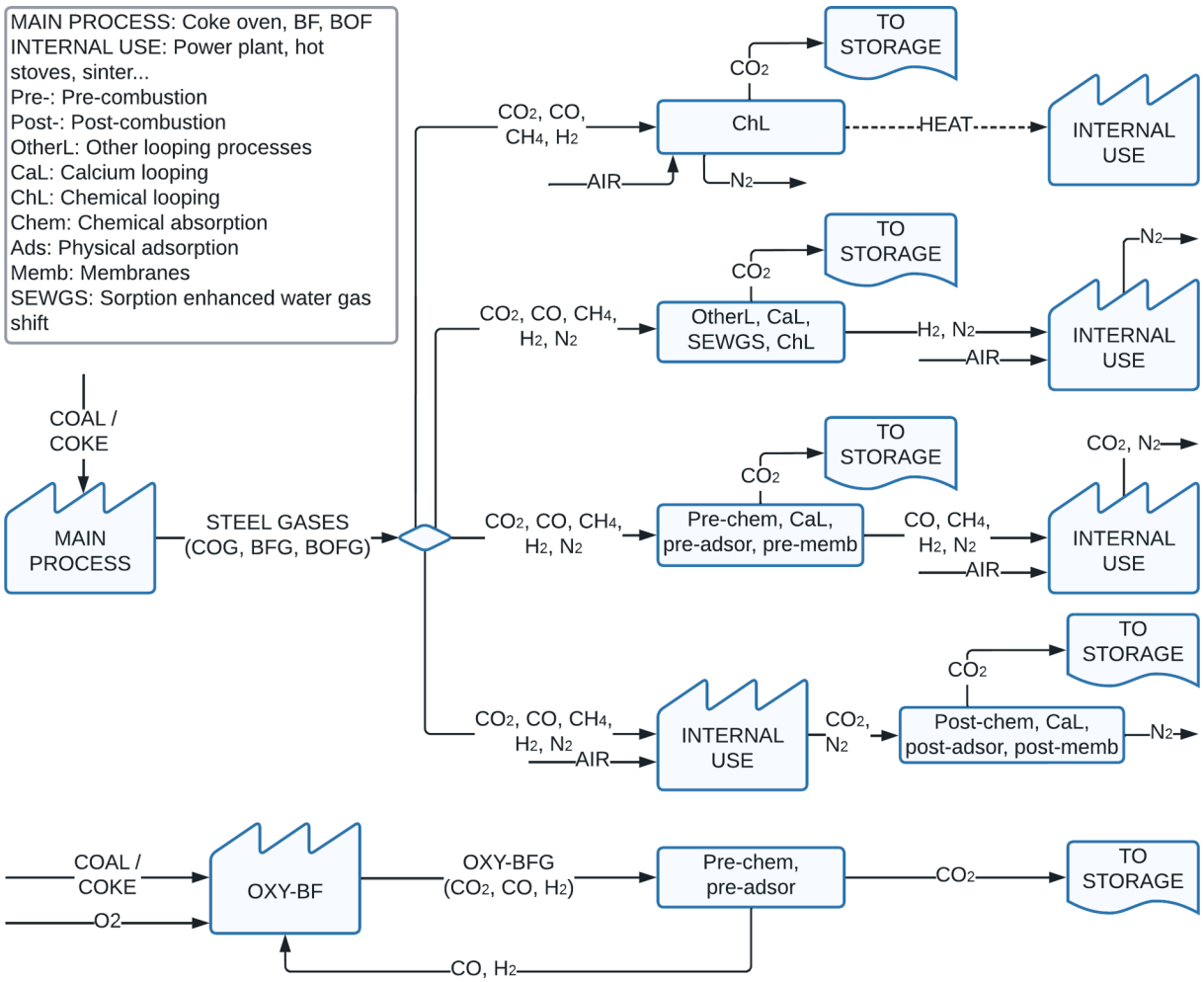


**Fig. 3.** Carbon capture routes in the Iron and Steel industry (BF-BOF route).

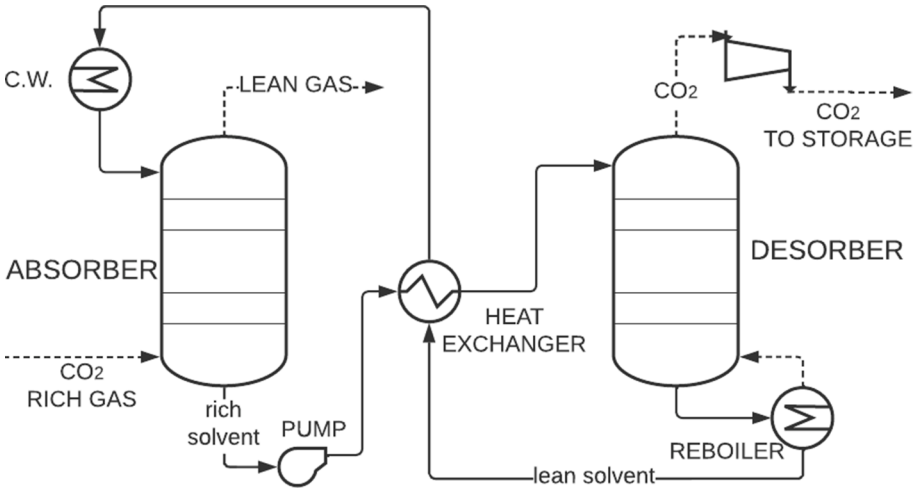


**Fig. 4.** $CO_2$ capture with chemical absorption.

investigated a mixture of 40 % MDEA with 10 % PZ obtaining a thermal consumption of 2.3 MJ/kg$CO_2$. For the solvents RITE-A and RITE-B, the standard thermal penalizations are 3.3 MJ/kg$CO_2$ and 3.1 MJ/kg$CO_2$, respectively, but after optimization for RITE-B, 2.5 MJ/kg$CO_2$ can be achieved. [28]. Cheng et. al. [25] compared the heat of reaction for MEA, AEEA, PZ, and their mixtures with respect to $CO_2$ capture in the hot stove flue gas. The study showed 10 % less consumption for PZ than for MEA and AEEA, which exhibit similar thermal penalization (3.7 MJ/kg$CO_2$).

Among these articles, only a few works [26,30,37,38,42–44] studied the electricity consumption of carbon capture, ranging from 0.28 to 1.5 MJ/kg$CO_2$. This electricity consumption is related to the required $CO_2$

**Table 4**
Main KPIs for pre-combustion CC with membranes in the I&S industry.

| Source | Baker (2018) [59] | | Luca (2021) [41] | Yun (2021) [42] | | | | | | | | |
|---|---|---|---|---|---|---|---|---|---|---|---|---|
| Membrane | Polaris | | PVAm | Polyimide | | | | | | | | |
| Permeab. (gpu) | 1500 | | 371 | 500 | | | | | | | | |
| Selectivity $CO_2/N_2$ | 25 | | 200 | 20 | | | | | | | | |
| Membrane configuration | Two-stage A | Two-stage B | Two-series | Two-stage B | | | | | | Two-stage A | | |
| $CO_2$ Source | BF stoves | BF stoves | BOFG | BF stoves | | Utility PP | | Lime | | Coke | | Sintering | |
| Inlet $\%CO_2$ | 25,0 | 28,0 | 21,1 | 27,3 | | 26,4 | | 19,4 | | 14,8 | | 4,8 | |
| Purification and compression | Cond + rec | Mem + Cond + rec | - | - | Cond + Mem + rec | - | Cond + Mem + rec | - | Cond + Mem + rec | - | Cond + Mem + rec | - | Cond + Mem + rec |
| Pressure of $CO_2$ stream (bar) | 150 | 150 | 120 | 1–2 | 152 | 1–2 | 152 | 1–2 | 152 | 1–2 | 152 | 1–2 | 152 |
| Spec. Consump. ($kWh_e/tCO_2$) | 286 | 235 | 327 | 207 | 318 | 235 | 320 | 302 | 393 | 330 | 473 | 1063 | 1220 |
| Spec. Consump. ($MJ/kgCO_2$) | 1,03 | 0,846 | 1,18 | 0,745 | 1,15 | 0,846 | 1,15 | 1,09 | 1,42 | 1,19 | 1,7 | 3,83 | 4,39 |
| Membrane area ($m^2/(tCO_2/h)$) | 3400 | 2780 | 5114 | 2543 | 1953 | 3079 | 2659 | 4080 | 4515 | 4724 | 5504 | 37,894 | 13,321 |
| $CO_2$ inlet ($tCO_2/h$) | 41,7 | 220 | 6,8 | 189 | 189 | 448 | 448 | 32,7 | 32,7 | 87,4 | 87,4 | 15,3 | 15,2 |
| Captured $CO_2$ ($tCO_2/h$) | 33,3 | 176 | 6,4 | 171 | 170 | 404 | 404 | 29,5 | 29,5 | 78,4 | 78,4 | 13,7 | 13,7 |
| Capture rate of $CO_2$ (%) | 80 | 80 | 94 | 90 | 90 | 90 | 90 | 90,1 | 90,1 | 89,7 | 89,7 | 89,7 | 90 |
| $CO_2$ purity in outlet stream (%) | 99 | 99 | 95,5 | 90 | | | | | | | | | |
| CapEx ($/($kgCO_2$/h) | 1482 | 1248 | | 1325 | 1651 | 1537 | 1709 | 2119 | 2932 | 2319 | 3094 | 9190 | 8912 |
| Cost of electricity ($cS/kWh_e$) | 5 | 5 | | 6 | | | | | | | | | |
| Plant life (y) | | | | 30 | | | | | | | | | |
| Membrane life (y) | 3 | 3 | 5 | 5 | | | | | | | | | |
| Capacity factor (%) | | | 93 | 85 | | | | | | | | | |
| Cost of capture ($/$tCO_2$) | 47 | 36 | | 41,7 | 52,5 | 46,6 | 54 | 64,7 | 83,3 | 70,7 | 91,2 | 271,7 | 252,7 |

compression work for transport and storage. Both consumptions, thermal and electrical, give an overall equivalent electricity penalization between 1.1 $MJ/kgCO_2$ and 3.8 $MJ/kgCO_2$ for this specific technology.

### 3.1.2. $CO_2$ emission reduction, technology readiness level and costs

The $CO_2$ capture process by amine solvents is mature (TRL 9) and already commercialized in natural gas or fertilizers processing plants [46]. Nevertheless, no large-scale project has been found in the literature regarding post-combustion capture with chemical absorption in the I&S industry. This could be due to the large $CO_2$ amounts, the high costs, and the geological storage difficulties. Most of the published works are theoretical studies. The reported emission reductions range between 11 % and 77 %,corresponding to 230 $kgCO_2/tHM$ and 1700 $kgCO_2/tHM$, respectively [24,26,36–45,27,29–35].

Only two experimental studies were identified. Cheng et al. [25] investigated the $CO_2$ capture in a rotating packed bed from a hot stove flue gas flow of 33 l/min containing 30 vol% $CO_2$. The research was focused on thermal energy consumption with different solvents (MEA, AEEA, PZ and their mixtures), but the $CO_2$ emission reduction was not assessed. The alkanolamine solutions with 10 %wt PZ and 20 %wt MEA or AEEA were found to be the most effective absorbents to capture $CO_2$. Goto et al. [28] presented a pilot plant of 1 $tCO_2$/day installed at the Kimitsu works of Nippon Steel Co. The CC plant was fed with the blast furnace flue gas and tested with MEA, RITE-A, and RITE-B. RITE solvents were developed with IPAE, and the best regeneration energy calculated was 2.5 $MJ/kgCO_2$ for an ideal operation with RITE-B.

Since post-combustion carbon capture does not offer any technological or economical advantage (such as increased energy efficiency or fuel-saving), it will always result in a financial burden. The key factor for the installation of a carbon capture stage is the $CO_2$ tax price. If this price is higher than the carbon capture cost, capturing the $CO_2$ will be profitable as compared to emitting it into the atmosphere. Until 2018, the European Union Allowance (EUA) price was always below 16 $/$tCO_2$, but since then, it has increased to reach 91 $/$tCO_2$ in February 2022 [47]. According to the literature, capture costs are between 38.2 $/$tCO_2$ and 204 $/$tCO_2$ for MEA solvent (with an average of 77.4 $/$tCO_2$) [24,26,32,36–38,40,42,43], 76–81 $/$tCO_2$ for MDEA [35,39], and about 97 $/$tCO_2$ for a mixture of MDEA and PZ [44]. Therefore, based on the current scenario of EUA prices, establishing a carbon capture stage is profitable in most cases.

## 3.2. Post-combustion $CO_2$ capture with membranes

Membrane is a cost-effective emerging technology for carbon capture in power plants and energy intensive industries. Gas separation with membranes takes advantage from the different permeation rates of certain materials to specific species, when both sides of the membrane are subjected to a differential pressure. The few theoretical works published in the literature related to I&S industry (TRL-2) are reviewed in this section.

### 3.2.1. Materials and characterization of membranes

Different materials including polymers [48], inorganic compounds [49,50], metal-organic frameworks [51], zeolite imidazolate

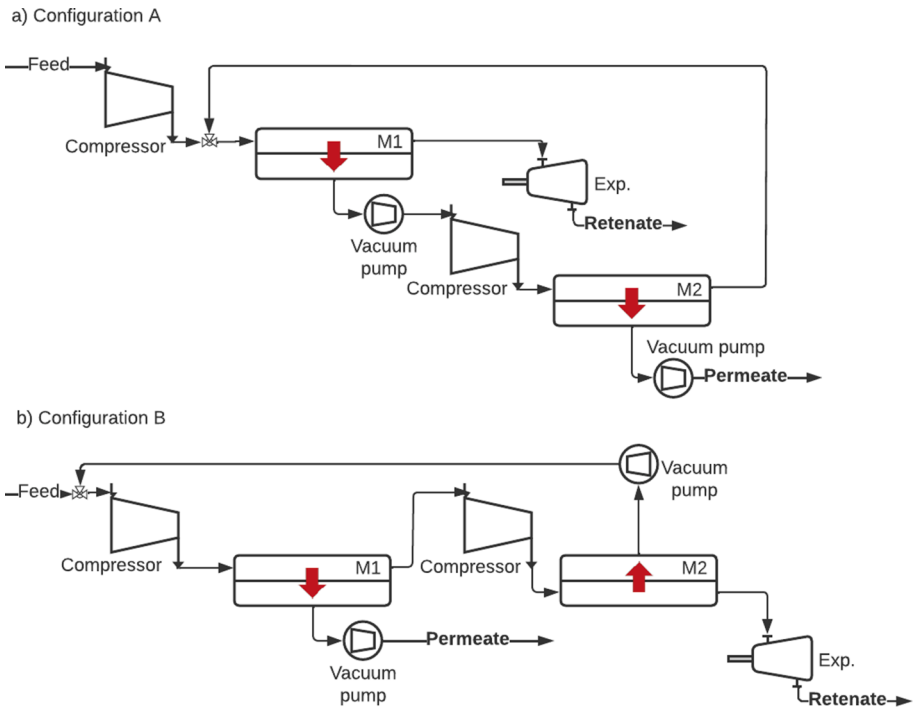


**Fig. 5.** Configuration of two-stage membrane-based $CO_2$ capture. .
Adapted from [42]

frameworks [52,53], graphene oxide [54], and micro porous hollow fibers [55] have been investigated for $CO_2$ separation. Membrane performance is mainly assessed through the properties of selectivity and permeability, which traditionally have involved a trade-off among them. The gas permeance is the permeated flow per membrane area and per differential pressure across the membrane (gas permeance unit: $1gpu = 2.7 \bullet 10^{-3} m^3(STP)/(m^2 \bullet h \bullet bar)$). Permeability is the product of permeance and membrane thickness, while the selectivity is the ratio of permeability coefficients of two gases defined greater than unity [56]. Other important characteristics to be considered are stability, mechanical resistance, and easy and cost-effective manufacturing.

Gas transport mechanism mainly consists of three steps: dissolution, diffusion, and desorption of permeate (solution-diffusion transfer mechanism). Additionally, the presence of reactive carriers in the membrane may enhance mass transfer and selectivity (facilitated transfer mechanism). Accordingly, selectivity and permeability of a membrane to a certain gas depend on the relative size of molecules with respect to pore size and on the difference in the solubility, diffusivity and/or reactivity with certain mass carriers as compared to that of other species present in the gas stream. Solubility selectivity increases with the critical temperature, while diffusivity selectivity favors small molecules [48]. Higher permeability results in lower differential pressure and membrane area, and therefore lower costs, while higher selectivity produces higher purity in the permeate, but higher costs.

Commercially available membranes already exist for the separation of $H_2$ and $CO_2$ [57], i.e. Polaris$^{TM}$ (MTR, Inc.), the first commercial membrane developed specifically for post-combustion. Nevertheless, this capture technology is currently under development stage (TRL-6), with only one small pilot plant operating in Norcem Cement at Brevik (Norway), where 70 mol% $CO_2$ purity was achieved with a single membrane stage [58]. Current developments are mainly focused on power plants because of the global volume of the involved emissions [59]. However, since the costs of CC strongly decrease with $CO_2$ concentration in the inlet flow, steel and cement plant gases (20–30 vol%) are favored with respect to power plant gases (12–15 vol%) [59]. In the presence of CO, it is desirable to include a stage of water-gas shift reactor to increase $CO_2$ concentration. Additionally, since membranes are easily poisoned by sulphur components, a previous desulphurization stage is required to lower the $SO_2$ concentration to levels of 10–25 ppmv [57].

### 3.2.2. *Configurations and KPIs*

There is no experimental study published in the literature related to the integration of membrane-based $CO_2$ capture systems in the I&S industry. Only a few theoretical research works can be found. Membranes operation is based on a sufficient partial pressure difference between the feed and the permeate stream sides. Since the BFG is at ~3 bar, there are two options: (i) to pressurize the BFG before entering the separation system [57], or (ii) to install a vacuum pump on permeate-side [59]. The latter option is preferred as it consumes less energy.

Given that the optimal range for a low-cost capture based on membranes is that where the rate of $CO_2$ capture is from 50 to 70 % in the first step [59], at least two membrane stages are needed for higher capture rates. Different configurations have been simulated for the principal $CO_2$ emission sources in I&S industry. The main results found in the literature are summarized in Table 4. Luca & Petrescu [41] investigated a $CO_2$ capture system with two spiral wound membranes connected in series with recirculation of 30 % and 5 % of permeate and pressure ratios of 100 and 80 for the first and second stage, respectively. The flue gas stream contained 21.1 vol% $CO_2$, while the output $CO_2$ stream reached a purity of 95.5 %. The capture rate was 94 % with a specific energy consumption of 327 kWh/t$CO_2$.

The two-stage concepts of Fig. 5 have been also explored in [42,59]. Retentate or permeate after the second membrane is recycled in configurations A and B, respectively. The former is more suitable for 20–25 vol% $CO_2$, while streams containing more than 25 % are better treated by the latter. Baker et al. [59] used Polaris$^{TM}$ membrane [60] in both cases including a $CO_2$ condensation column for purification (>99 %, 30 bar, −25 °C) and the subsequent compression up to 150 bar. Configuration A was applied to a stream of 1000 $t_{CO2}$/day with a typical composition of cement industry (25 vol% $CO_2$), which is similar to that of the flue gas of BF stove or of utility power plant in I&S industry. The first stage increases $CO_2$ concentration up to 40 vol%, capturing about 60 % of incoming $CO_2$. The second stage enriches permeate gas above 75 vol%, reaching a global capture rate of 80 %. The electric

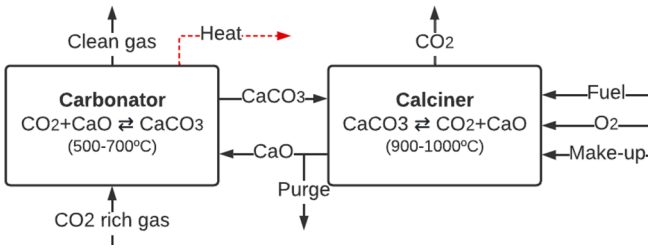


**Fig. 6.** Configuration of a Calcium Looping-based $CO_2$ capture process.

consumption is 286 kWh/$tCO_2$, the required membrane area is 3400 $m^2$/($t_{CO2}$/h) and the total cost of capture is 47 \$/$tCO_2$. Configuration B was applied to a typical composition of BF stoves flue gas [61] with 28.5 vol % $CO_2$. The first and second membranes reduce $CO_2$ concentration from 28 % to 17 % and 8 %, respectively, representing a global capture of 80 % of incoming $CO_2$. The resulting permeate stream is further enriched (above 80 %) through a third membrane module before the condensation column. The electric consumption is 235 kWh/$tCO_2$ and a membrane interface of 2780 $m^2$/($t_{CO2}$/h) is required. The total cost of capture is 36 \$/$tCO_2$.

Yun et al. [42] used a polyimide membrane in both the configurations of Fig. 5, analyzing separately the effect of purification (dehydration and stripping column) and final compression up to 152.7 bar. For the sake of comparison, the capture rate and the mole fraction of $CO_2$ were set to 90 %. Configuration A was applied to sinter strand (4.81 vol %) and coke oven (14.77 vol%) gases, while configuration B was implemented for flue gases of lime production (19.41 vol%), power plant (26.43 vol%) and BF stoves (27.3 vol%). Electricity consumption and the required membrane surface area sharply increase below 10 vol% $CO_2$ in the inlet stream. Carbon capture costs increase with lower $CO_2$ incoming content from 42 \$/$tCO_2$ in the latter case (BF stoves) to 272 \$/$tCO_2$ in the former case (sintering process).

According to these theoretical results, membrane-based capture systems could be a competitive solution for $CO_2$ rich streams. Nevertheless, further experimental research is required for such systems to become available at commercial scale.

## 4. Looping processes for CC in BF-BOF

Carbon capture with looping processes include those systems where $CO_2$ is captured either in combustible gases or in flue gases. This section review calcium looping (CaL), chemical looping (ChL) and other looping processes (OtherL), including Ca-Fe or Ca-Cu for carbon capture in the I&S industry.

### 4.1. Calcium looping

Calcium looping (CaL) is a CC technology where calcium oxide (CaO) is reacted with $CO_2$ to form calcium carbonate ($CaCO_3$), and $CaCO_3$ is then heated to regenerate CaO and $CO_2$ in a calciner (see Fig. 6). The calcination process in endothermic, and a fuel input to the process is required. The captured $CO_2$ can then be used or transported for storage. The few theoretical works published in the literature related to I&S industry (TRL 2–3) are revised in this section.

Cormos performed a technoeconomic evaluation of a Calcium Looping (CaL) carbon capture process in post-combustion as the alternative to decarbonise an integrated steel mill [35]. A conventional integrated steel mill (4 million tonnes Hot Rolled Coil per year output) with CaL carbon capture was analysed under two scenarios which accounted for the most important $CO_2$ emission sources within the steel mill (e.g., power plant, hot stoves, lime plant, coke ovens). The carbon capture efficiency, specific $CO_2$ emissions, and $CO_2$ capture investment costs of the integrated steel mill with CaL capture process were evaluated (see Table 8). The evaluated captive power plants and the carbon capture process were thermally integrated using pinch method. Heat integration is of importance considering the multiple heat sources within the steel plant to be used to cover the energy duties. Heat integration is especially critical for CaL processes to quantify the high temperature heat recovery potential. Chisalita et al. explored the environmental aspects of this configuration through a Life Cycle Assessment using the functional unit of 1 tHRC [34]. Global warming potential (GWP) of the integrated steel mill was reduced by 64–75 % when CaL was coupled (emitting 516–754 kg $CO_2$ eq/tHRC). The GWP even shows negative values given the negative $CO_2$ emissions allocated to the exported electricity. Nevertheless all other environmental indicators (acidification potential or eutrophication potential) have a more or less significant increase compared to the benchmark case, associated to the extraction and transportation of the natural gas required in the calciner (71.8–119 kg of natural gas/tHRC). The economic penalty of CaL capture leads to a 6 % increase of specific capital investment and a 12 % increase of steel production cost [39].

CaL capture process can be also applied in precombustion for the production of hydrogen from raw coke oven gas (COG) by means of $CO_2$ sorption enhanced steam reforming using CaO as $CO_2$ sorbent (CaL-SESR). Xie et al. thermodynamically analysed this process, and estimated equilibrium compositions, energy consumption, and $CO_2$ emissions [62]. This configuration can lead to concentrations over 95 vol% $H_2$ in the reforming gas while reducing the temperature of the reforming processes, the $CO_2$ emission, and the total energy demand per unit of generated hydrogen in comparison to conventional reforming. The CaL-SESR process avoids 99 % of $CO_2$ generated from the COG after a conventional reforming.

Halmann and Steinfeld also studied the enhanced reforming of blast furnace gas ($CO_2$, CO, $N_2$ and $H_2$) through CaL capture process from a thermodynamic modelling approach. Partial or complete carbon capture can be achieved depending on the operating conditions of the SESR reactor and a relatively pure $CO_2$ produced. The implications of such reactions with respect to hydrogen production, $CO_2$ emission avoidance and process efficiency are presented in this work [63].

Liu et al. experimentally explored the sorption enhanced water gas shift (SEWGS) reaction to improve the carbon capture from BFG. The CO in the BFG was first converted to $CO_2$ and, then, captured through carbonation reaction. The lab-scale experimental results from this study highlighted the importance of the sorbent type on the SEWGS reaction, with both CaO and MgO in the sorbent catalyzing the reaction. WGS reaction becomes the rate limiting step for calcined limestone, while for calcined dolomite, WGS reaction is not a limiting step and most of the $CO_2$ for the CaO carbonation comes from WGS reaction on MgO surface. Besides, it was observed that not only CaO but also MgO experienced the decay in the catalytic reactivity after multiple cycles [64]. Tian et al. deepen the study of this concept combining CaL $CO_2$ capture and waste recycling into I&S production. The sorbents used in this experimental study were CaO-based, 90 wt% CaO, obtained from steel slag which showed better reactivity and slower deactivation than commercial CaO. The preparation of steel slag as sorbents co-produces high-quality iron ore with iron content of 55.1–70.6 % which compensate the larger costs when compared to naturally derived CaO. The cost of the steel slag-derived $CO_2$ sorbent achieves 57.7 €/t, which makes this material a cost-effective option for $CO_2$ removal in I&S industry. [65].

Tian et al. also performed a techno-economic study of this CaL decarbonisation concept for steelmaking showing a substantial and cost-effective $CO_2$ emission reduction and the superiority of CaL in comparison to other technologies [66]. The cost of avoided tonne of $CO_2$ is reduced down to 12.5–15.8 €/$tCO_2$ (below one third the cost obtained using amine scrubbing technology) while the emissions can be reduced up to an 80 %.

Calcium looping technology has a demonstrated TRL 6, achieved through experimental experimentation with fluidized bed reactors at significant scale and relevant operating conditions for industrial applications [67–69]. Over fourteen CaL experimental plants of different

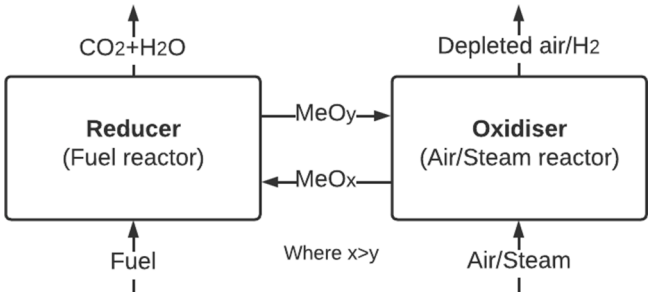


**Fig. 7.** Configuration of a Chemical Looping-based $CO_2$ capture process.

sizes from few kWth to MWth have been constructed and operated worldwide [70] while its feasibility at 1–2 MWth scale has been demonstrated through the operation of two large pilot plants [71–73]. The concept itself has been completely demonstrated and its applications to industry has been explored at lower TRLs through the integration with power and cement plants [69,70]. Several ongoing projects target to demonstrate the technical feasibility of industrial integration of CaL capture processes at large scale in relevant environments. CLEANKER project aims at demonstrating at TRL 7 the CaL concept with 90 % of $CO_2$ capture in a fully integrated configuration with a cement production process. Instead of fluidized beds, this project proposes the use of entrained flow reactors which are well-known equipment in the cement industry [74]. C4U project also targets to elevate two modified CaL carbon capture processes, DISPLACE and CASOH, from TRL 5 to 7 and to design for optimal integration in the steel industry [75].

### 4.2. *Chemical looping*

The Chemical Looping (ChL) concept is based on the transfer of oxygen from air to the fuel by means of a metal oxygen carrier, avoiding direct contact between fuel and air (see Fig. 7).Fig. 8.

The utilisation of chemical looping (ChL) as an option of $CO_2$ capture in the I&S industry has focused on the development of alternatives for the combustion coke oven gases (COG) without $CO_2$ emissions, or $H_2$ production for the steel process or other uses such as $NH_3$ production.

In the case of power production with steel gases, a chemical looping combustion (CLC) combined cycle using COG as fuel was proposed in [76]. Low TRL levels (2–3) are reached as the technology concept has been just formulated using ASPEN simulation considering Ni-based oxygen carriers $NiO/NiAl_2O_4$ (60:40 wt%) due to good results for $CO_2$ capture applications [76]. Nevertheless, others oxygen carriers composed of $Fe_2O_3$/CuO and MgAl2O4 have been investigated using thermogravimetric analysis (TGA) and a laboratory pressurised circulating fluidised bed system for this specific applications in a 3–10 kWth test rig [77].

$H_2$ production based on CLC has been also suggested for decarbonising I&S production. For Chemical-looping water-splitting (CLWS), an additional reactor is required in a three-stage process that combines the concepts of CLC and steam-iron process [7879]. In this new stage, compared with CLC, steam reactor, the oxygen carrier is partially oxidised by steam to yield $H_2$ that provides a decarbonised fuel source for producing direct reduced iron (DRI) [78]. Low TRL are also suggested (2/3), with the concept formulated and some integration schemes analysed to improve state-of-the-art options by reducing the amount of coke used in the sintering plant, increasing thermal energy efficiency, $CO_2$ capture ratio [80] and exergy efficiency [79]. Moreover, some researchers have also proposed to use $H_2$ generated to produce ammonia, integrating this scheme with pressure swing adsorption technology [81]. In all these alternatives, 100 % direct $CO_2$ capture efficiency and improved economic figures, compared to the present technologies, could be achieved.

Regarding CLC, there is a general consensus that the maturity of the technology has reached a TRL of approximately 6 [46,82–84]. At least 46 CLC pilot rectors have been successfully constructed and operated with gaseous, liquid, and solid fuels [85,86]. Although the CLC concept and its performance has been completely demonstrated, its applications to industry remain unexplored. Fortunately, recent planned research projects have been proposed to fill this gap. CHEERS project is going to develop a CLC system, with inherent carbon capture, to increase CLC TRL to 7 [87]. The system is designed for deployment in a refinery environment, with petroleum coke as fuel, and to produce high temperature steam. It will have a thermal power of 3 MW and will combine oxygen polisher, a heat recovery steam generator, $CO_2$ capture, as well as compression and purification of the $CO_2$ in compliance with

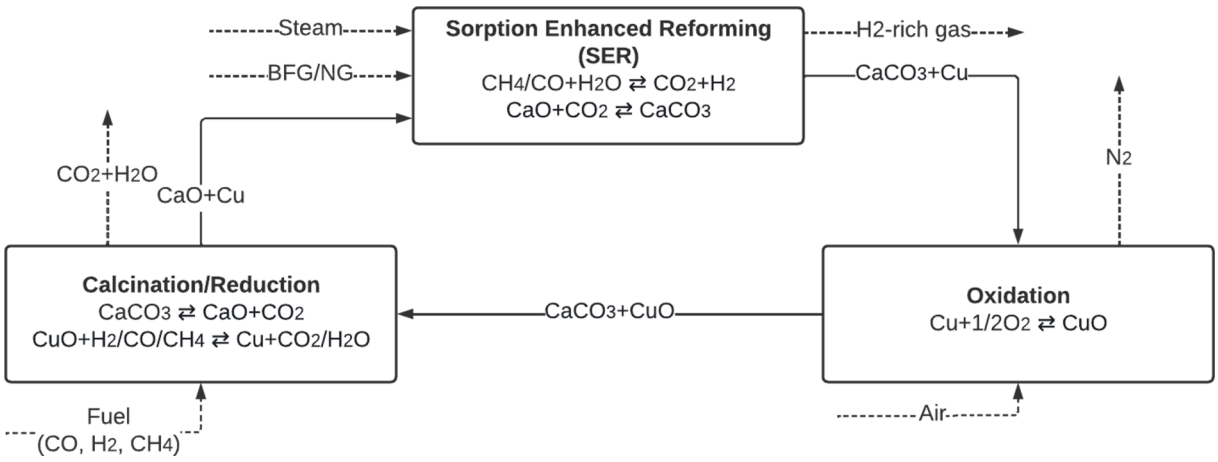


**Fig. 8.** Configuration of a Ca-Cu based $CO_2$ capture process, .
adapted from [90,91]

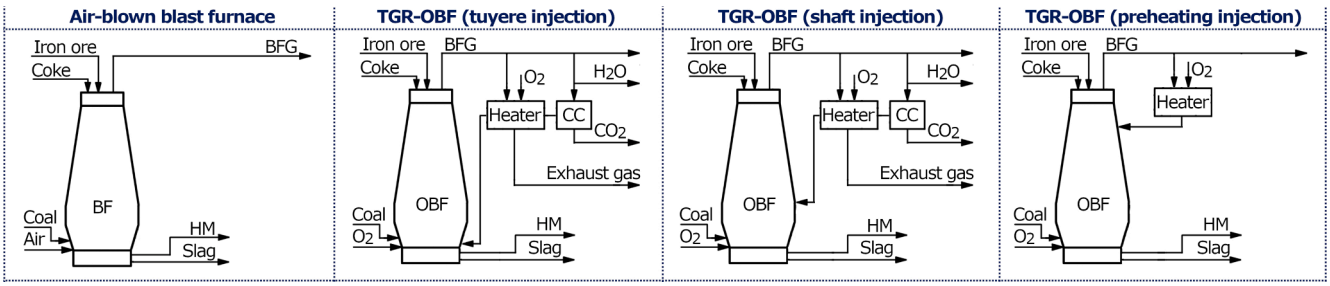


**Fig. 9.** Process flow diagrams of oxygen blast furnaces with top gas recycling, compared to an air-blown blast furnace.

specifications for enhanced oil recovery [88]. Also, LOUISE project [89] aims to demonstrate CLC of solid refuse fuels using ilmenite as the oxygen carrier at a TRL 6 (150 kWth and 1 MWth) and to accelerate the deployment of CLC by providing the basic design of a 10 MWth CLC demonstration plant (TRL 7) for waste-derived fuels. There are no specific projects or applications of CLC for the steel sector, but the challenges that ongoing projects have to face would be similar to those of CLC in the steel sector.

### 4.3. Other looping processes

The combination of calcium Looping (CaL) and chemical looping combustion (CLC) has also been proposed for the blast furnace gas (BFG) utilisation. There are two main routes for this process depending on the metal that is combined with calcium: Ca-Fe or Ca-Cu. Both alternatives are promising and have similar level of development (TRL 2/3).

Combined CaL processes have been investigated by Tian et al., who developed a new material to be used in a combined Ca-Fe chemical loop using steel slag as feedstock. In the case of iron, using steel slag as feedstock, the CaO-based, Fe-functionalized $CO_2$ sorbent ($Fe_2O_3$ and CaO) have shown promising potential with stable cyclic $CO_2$ uptaking 10 realistic combined Ca–Fe looping cycles [92]. This is also a three-stage process, where the heat released due to FeO oxidation provides the heat to drive the endothermic $CaCO_3$ decomposition reaction.

For the copper alternative, there are two schemes proposed. The first one, based on packed-bed, converts mainly blast furnace gas (BFG) into $H_2/N_2$ together with the release of a large amount of high temperature heat [8]. Around 30 % of the BFG can be upgraded via calcium looping-assisted water gas shift (WGS). Decarbonised fuel gas could be used for onsite power generation or to obtain sponge iron by a Direct Reduced Iron (DRI) process, thus increasing the overall capacity of the steel plant and avoiding the $CO_2$ emissions. Low values for the specific energy consumption of around 1.5 MJLHV/kg$CO_2$ and $CO_2$ capture efficiencies higher than 95 % support the further development of the proposed Ca-Cu looping [91]. The second scheme uses a sorption enhanced water gas shift (SEWGS) reactor with blast furnace gas (BFG) of steel mills. $CO_2$ is simultaneously removed from the gas using a CaO based sorbent. A Cu/CuO chemical loop supplies the energy required for the regeneration of the sorbent via the exothermic reduction of CuO with coke oven gas (COG) [93]. Approximately 27 % of the BFG can be decarbonised in the SEWGS reactor while also producing $H_2$. A $CO_2$ capture ratio of 31 % ($CO_2$ capture efficiencies of up to 95 %) with respect to the total carbon emissions in the steel mill can be achieved. More than 60 % of the thermal input can be recovered as high-temperature heat, which could be efficiently recovered for producing electricity [93]. This represents a clear improvement when compared with a steelmaking plant with a post-combustion MEA absorption system [31] and allows the utilisation of the excess of $H_2$-rich gas in the Ca-Cu steel plant to produce additional iron through a direct reduction iron (DRI) process. It has been demonstrated that the production capacity of the steel plant can be increased by around 10.5 % without installing a purpose-built and high-cost NG reforming plant [31,90].

Sun et al. proposed a system for coupled decarbonisation and desulfurization of BFG via a magnesium-molybdenum looping process [94]. The system includes a desulfurization-decarbonization reactor and a regenerator. Four carbon-sulfur carriers were screened, highlighting MgO-$MoO_3$ as the most capable sorbent for decarbonisation and desulfurization. Results showed that temperatures over 240 °C decrease in carbon capture efficiency. Carbon removal efficiency reached values up to 99.70 % and complete sulfur removal.

## 5. Oxygen blast furnaces and top gas recycling for CC in BF-BOF

The most spread strategies for carbon mitigation in the I&S industry are the oxy-fuel combustion in the oxygen blast furnace (OBF) and the top gas recycling (TGR). The former uses $O_2$-enriched air as hot blast for the combustion of coke and the auxiliary fuels, producing a top gas with very little content of nitrogen [95], while the latter recirculates part of the top gas to the blast furnace, usually after a carbon capture stage. Both strategies are usually combined to make use of the synergies among them.

### 5.1. Type of configurations and associated penalties

The difference between oxy-fuel systems for power production, and oxygen blast furnaces, is that the former performs complete combustion (i.e., exhaust gas mainly composed by $CO_2$ and $H_2O$) [96]. In oxygen blast furnaces there is incomplete combustion to obtain CO and $H_2$, which are then used to reduce the iron oxides (i.e., top gas composed mainly of CO, $CO_2$, $H_2$, and $H_2O$) [97].

Conventionally, in oxy-fuel combustion, a part of the exhaust gas is recirculated to palliate the lack of nitrogen and its sensible heat, aiming for keeping similar fluid- and thermo-dynamic behavior than in air-blown combustion [98,99]. However, injecting $CO_2$ or $H_2O$ to the blast furnace is not desirable as it increases the coke consumption and hinders the reduction of iron oxides because of displacing the chemical equilibrium. Therefore, a carbon capture stage is usually included before recycling the top gas, in order to reject the 90 % to 100 % of the $CO_2$ [100–105] (water is also typically removed through condensation stages). Moreover, recirculating CO and $H_2$ (reducing agents) diminishes the required amount of coke in the blast furnace, what lowers the $CO_2$ emissions. Typical capture technologies are vacuum pressure swing adsorption (VPSA) and amine scrubbing. The VPSA presents lower electricity consumption 0.5–0.6 GJ/t$CO_2$ [103,106], but the $CO_2$ streams obtained is not of sufficient purity for permanent storage, thus requiring additional cryogenic distillation to reach 99 % purity (cooling necessities of 0.1 GJ/t$CO_2$) [106]. In the case of amine scrubbing, the main disadvantages are the degradation/replacement of the amines, and the requirement of a non-negligible amount of steam to desorb the $CO_2$ (2.0–4.0 GJ/t$CO_2$ of thermal energy, equivalent to 0.7–1.4 GJ/t$CO_2$ of electricity penalty) [100,107].

In blast furnaces, the top gas can be recirculated not only at the combustion region (i.e., raceways, at the lower tuyeres zone), but also at the beginning of the indirect reduction zone (i.e., shaft, mid zone), at the preparation zone (i.e., preheating, upper zone), or at a combination of them (Fig. 9). Injecting the recirculated gas at the lower tuyeres allow

**Table 5**
Range of values found in the literature for the inlet and outlet streams that can be considered in a typical TGR-OBF process boundary. Not all the inlet streams will necessarily exist in a given process flow diagram.

| TGR-OBF process flow diagram | Flow | Temp. (°C) | References |
|---|---|---|---|
| Iron ore (kg/thm) | 1450–1730 | 25 | [100,103,106,111,112,127,139] |
| Coke (kg/thm) | 159–468 | 25 | [100,102,103,106,108,112,113,136] |
| Auxiliary tuyere injections | | | |
| PCI (kg/thm) | 50–320 | 25 | [100,102,103,106,112,114,136,141] |
| Natural gas (kg/thm) | 42–150 | 25 | [100,109] |
| COG ($Nm^3$/thm) | 140 | 25 | [112] |
| Recycled top gas ($Nm^3$/thm) | | | |
| Injected in the preparation zone (after combustion) | 200–294 | 1000 | [100,109] |
| Injected in the shaft (after $CO_2$ separation) | 82–600 | 900–1000 | [100,103,108,111,112,114,117] |
| Injected in the tuyeres (after $CO_2$ separation) | 60–620 | 25–1250 | [100,103,106,108,111–116] |
| $O_2$/Enriched-air | | 25–1150 | [105,108,112] |
| $O_2$ ($Nm^3$/thm) | 183–353 | | [100,106,111–114,116,117,136] |
| $H_2O$ (g/$Nm^3$) | 2–60 | | [100,108,111,140,142] |
| $N_2$ ($Nm^3$/thm) | 0–118 | | [100,106,111–113,117] |
| Hot metal production (thm/h) | 150–570 | 1350–1500 | [21,100,143,102,105,106,108,112,114,116,140] |
| Slag (kg/thm) | 189–364 | | [100,105,108,111,142] |
| BFG (before recycling) ($Nm^3$/thm) | 1030–1447 | 100–326 | [100,102,136,139,103,105,106,109,111,112,116,128] |
| CO (%vol) | 23–52 | | [102,103,137,105,106,109,111,112,114,116,136] |
| $CO_2$ (%vol) | 22–48 | | [102,103,137,105,106,109,111,112,114,116,136] |
| $H_2$ (%vol) | 8–26 | | [102,103,137,105,106,109,111,112,114,116,136] |
| $H_2O$ (%vol) | 4–6 | | [103,111,112,116,136,137] |
| $N_2$ (%vol) | 1–15 | | [102,103,105,106,109,111,112,136] |
| Operating hours (h) | 8600 | | [106] |

for a proper interaction between the reducing gas and the solids, but it decreases the flame temperature. Contrarily, injections at mid shaft avoids decreasing the flame temperature, but the peripheral injection leads to a limited penetration and diffusion of the gas to the center of the descending burden (poor solid-gas interaction) [100]. In the case of upper injections, the role of the recirculated gas is only to preheat the descending solids, mitigating the lack of sensible heat that would provide $N_2$. As the gas is not aimed to be used as a reducing agent, the diffusion of the gas towards the center is not critical, and the presence of $CO_2$ is not a problem [100]. Depending on the configuration, the recirculating ratio of the top gas may vary between 30 % and 100 % [100,103,104]. It implies a decrease in the available gases downstream for the I&S plant, and therefore a penalization of 1.5–4.0 GJ/thm in terms of available thermal energy (or 0.5–1.4 GJ/thm in terms of electricity) [100,108]. A potential strategy to palliate this effect is to replace pulverized coal by natural gas, what will increase the $H_2$ content of the BFG and its calorific value [100]. Typical calorific value of top gas in OBF is 5.7–9.2 MJ/$Nm^3$, while in conventional BF is around 3.0 MJ/$Nm^3$ [102,103,109,110].

To fulfill its role as provider of sensible heat, the recirculated gas is normally injected at 900–1250 °C (in the case of mid and upper injections, at 1000 °C maximum to avoid coke gasification) [100,103,115–117,105,106,108,109,111–114]. To preheat the recirculated gas, pebble-heaters fueled by top gas itself are used (typical heat losses to the ambient are around 5 %) [106]. About 7 % to 12 % of the BFG is used as fuel in the preheating, mixed with other fuels if necessary (e.g., liquefied petroleum gas, natural gas, and/or COG) [103,104,106,110,114]. Hence, this implies an additional decrease on the available thermal energy downstream for the I&S plant of 0.5 GJ/thm (equivalent to 0.17 GJ/thm of electricity) [106]. Another option could be to heat the $O_2$-enriched blast instead of the recirculated top gas, but this solution is not adopted in practice due to technical limitations in the hot stoves (maximum 32 %vol $O_2$ in the stoves, in order to avoid equipment damage by oxidation), so the $O_2$ is injected cold at 25 °C [118]. Furthermore, it was shown that at high recycling ratios, is more cost-effective to heat the recycled gas rather than the oxygen blast [118].

In addition to the impact on the available gases (less energy available for self-sufficiency), oxygen blast furnaces also imply greater electricity consumptions in the air separation unit (ASU). The volume fraction of $O_2$ in the enriched hot blast changes from 0 % to 5 % in conventional BF to 70 % – 100 % in OBF [100,104–106,110–113,117], so the $O_2$ produced in the ASU increases by 150–280 $Nm^3$/thm [106,109,116,119]. Depending on how modern is the technology of the steel plant, the ASU consumption may vary between 260 and 400 kWh/t$O_2$ [106,109], meaning increments of 0.2 to 0.6 GJ/thm in the electricity consumption.

In total, accounting for all the penalizations ($CO_2$ separation stage, top gas recycled in the OBF, top gas consumed for heating, and ASU consumption), the thermal energy penalization is 2.0–8.6 GJ/thm, and the electricity penalization is 0.7–1.2 GJ/thm (both combined give an overall equivalent electricity penalization of 1.4–4.2 GJ/thm). Taking into account that integrated steel mills produce only 8.6 to 10.7 GJ/thm of thermal energy in the form of COG and BFG, and that they use between 3.9 and 8.0 GJ/thm of this thermal energy in internal processes (i.e., in coke oven, hot stoves and power plant) [95,109,120–126], the fact of having penalizations associated to OBF of 2.0 to 8.6 GJ/thm may lead to situations of non-self-sufficiency. Therefore, the shortage of available gases is one of the main handicaps of this technology.

### 5.2. $CO_2$ emission reduction

Besides providing sensible heat, the recycled top gas acts as reducing agent inside the blast furnace as it is mainly composed by CO and $H_2$. This allows to reduce the coke consumption by 14–150 kg/thm, at coke replacement ratios of 0.17–0.25 $kg_{coke}$/$Nm^3$ (5–34 % decrease with respect to conventional BF) [11,108,110,112,114,127,128]. Although

**Table 6**
Range of values found in literature for different characteristic data of oxygen blast furnaces.

| | Value | Reference |
|---|---|---|
| Characteristic data of TGR-OBF | | |
| Volume fraction of $O_2$ in enriched air (%) | 70–100 | [100,104–106,110–113,117] |
| Percentage of BFG recycled into BF (%) | 30–100 | [100,103,104] |
| Percentage of $CO_2$ captured from the recycled gas (%) | 90–100 | [100–105] |
| Percentage of BFG used for heating the recycled gas (%) | 7–12 | [103,104,106,110,114] |
| Calorific value of top gas (MJ/$Nm^3$) | 5.7–9.2 | [102,103,109,110] |
| Thermal reserve zone temperature (°C) | 700–950 | [100,103,108,127,140] |
| Chemical efficiency (-) | 0.94–0.98 | [100,109] |
| Heat losses (MJ/thm) | 230–630 | [100,108,110,111,127,137,139] |
| Percentage of direct reduction (%) | 4–19 | [103,109,110,129,135,136] |
| Minimum flame temperature (°C) | 1800 | [100,108,113,137,138] |
| Decrease in flame temperature by the recycled gas (°C/$Nm^3$) | 1.4–5.0 | [108,110,114] |
| Replacement ratio (kg/$Nm^3$) | 0.17–0.25 | [11,108,110,112,114,127,128] |
| Gas utilization (%) | 47.7–54.3 | [109,112] |
| Furnace inner volume ($m^3$) | 2500–2800 | [103,109,140] |
| Productivity (t/$m^3$d) | 1.6–8.1 | [100,108,112,113,116,135,140,141,144] |
| Technology Readiness Level (TRL) | 2–6 | [7,113,131,135,141,144,145] |
| Cost of retrofitting (M€) | 900 | [102] |
| Pay-back (y) | 20–30 | [146] |
| Change in performance with respect to air-blown BF | | |
| Increase in $O_2$ production ($Nm^3$/thm) | 150–280 | [106,109,116,119] |
| Decrease in coke consumption (kg/thm) | 14–150 | [11,108,110,112,114,127,128] |
| Decrease in $CO_2$ emissions (kg/thm) | | |
| Due to recycling | 100–500 | [100,106,108,112,114,119,129,130] |
| Due to permanent storage | 700–770 | [105,106,108,119,131] |
| Increase in electricity consumption (GJ/thm) | | |
| Due to ASU | 0.2–0.6 | [106,109,116,119] |
| Due to carbon capture (VPSA) | 0.5–0.6 | [103,106] |
| Decrease in available thermal energy downstream (GJ/thm) | | |
| Due to recycling itself | 1.5–4.0 | [100,108] |
| Due to heating the recycled gas | 0.5 | [106] |
| Due to carbon capture (amines) | 2.1–4.1 | [100,107] |
| Increase in productivity (%) | 25–75 | [100,108,112,143,147] |
| Increase in CAPEX (incl. carbon capture) (M€/(thm/h)) | 1.25 | [146] |
| Increase in OPEX (€/thm) | 76 | [146] |

some studies report coke consumptions as low as 159 kg/thm, experimentation in prototype-scale oxygen blast furnaces showed 200–230 kg/thm as the minimum feasible coke rate [111].

A direct consequence of this coke saving is the cut in $CO_2$ emissions. This decrease is inherent to the TGR-OBF technology, and it is in the range 100 to 500 kg$CO_2$/thm (typically, 10 % – 40 % reduction with respect to BF) [100,106,108,112,114,119,129,130]. On average, the $CO_2$ emission reduction found in the literature is around 20 % (Table 8). Additionally, as $CO_2$ is rejected from the recycled top gas via a capture stage, a non-negligible amount of highly-concentrated $CO_2$ gas is available for underground storage. Considering that this $CO_2$ is sent to permanent storage, the total $CO_2$ emissions reduction can be as high as 800–1270 kg/thm (i.e., up to 86 % reduction) [105,106,108,119,131]. It is worth to mention that all the $CO_2$ emissions presented in this section are calculated after complete combustion of the gas (i.e., the CO content is accounted as equivalent $CO_2$).

An alternative option to take advantage of the captured $CO_2$ is to combine OBF with Power to Gas (PtG) [121]. PtG technology consumes renewable electricity to produce $H_2$ via water electrolysis, which is then combined with the $CO_2$ emissions of the ironmaking process to obtain synthetic methane [132,133]. This synthetic fuel is used in the blast furnace to keep carbon in a closed loop and avoid geological storage [120,134]. The amount of $CO_2$ that can be avoided through this method is limited by the mass flow of natural gas that can be injected in the blast furnace, which depends on the flame temperature. About 70–90 kg/thm of $CO_2$ could be kept in closed loop and prevented from being permanently stored, which represents 5–7 % of the emissions of a conventional BF. However, it implies additional electricity penalizations of 1.3–2.1 GJ/thm, because of the production of renewable $H_2$ [121].

### 5.3. Operating parameters in OBF

In addition to the process mass flows (Table 5), the operation of a blast furnace is characterized by the percentage of direct reduction, the flame temperature, the heat losses, the temperature of the thermal reserve zone, the chemical efficiency, and the gas utilization (Table 6). All of them present some differences between oxygen blast furnaces and air-blown blast furnaces.

The percentage of direct reduction is between 4 % and 19 % in OBF (in air-blown BF is between 20 % and 40 %) [103,109,110,129,135,136]. The higher the $O_2$ concentration in the blast, the lower the direct reduction. To a lesser extent, increasing the volume of recycled gas also diminishes the percentage of direct reduction [103]. Moreover, for each $Nm^3$ of recycled top gas injected at the tuyeres, the flame temperature will be reduced by 1.4–5.0 °C, depending on the temperature of the injected gas [108,110,114]. The amount of gas

**Table 7**
Physical dimensions of experimental oxygen blast furnaces [7,113,131,135,141,144,145].

| Institution | JFE Steel | Minmetals | LKAB | Baowu | Tulachermet |
|---|---|---|---|---|---|
| Height (m) | 5.1 | n/a | 6.0 | n/a | n/a |
| Hearth diameter (m) | 0.95 | 1.0 | 1.4 | n/a | n/a |
| Throat diameter (m) | 0.7 | n/a | 1.0 | n/a | n/a |
| Inner volume ($m^3$) | 3.9 | 8.0 | 8.2 | 430 | 1033 |
| Productivity ($t/m^3d$) | 5.1 | 5.4–8.1 | 4.4 | n/a | 1.6 |

injected will be limited by the minimum adiabatic flame temperature (AFT) that allows keeping the proper operation of the furnace. The AFT assumed in the OBF studies found in literature is between 1900 and 2800 °C [100,108,137]. This range is actually taken from conventional BF experiences, whose minimum AFT is traditionally assumed at 2000 °C [97]. However, in practice, the lower the percentage of direct reduction, the lower the minimum limit for the flame temperature can be [138]. In fact, some actual blast furnaces have been successfully operated with 1600–1900 °C flame temperatures [113,138]. Since OBFs present remarkably lower percentages of direct reduction than BFs, 1800 °C could be considered as a more realistic technical limit for the flame temperature in OBF [113]. Heat losses for OBF reported in literature are in the range 230–630 MJ/thm [100,108,110,111,127,137,139], which are lower than for BF thanks to the higher productivity and smaller size of the furnace [109]. The temperature of the thermal reserve zone in OBF (700–950 °C) is usually assumed lower than for conventional BF (850–1000 °C), in literature [100,103,108,127,140]. The chemical efficiency used for OBF in the literature is between 0.94 and 0.98 [100], which is higher than that for conventional BF (0.85–0.95) [114] thanks to the downsized hearth diameter, what makes gas channeling effect less relevant [109]. Lastly, the gas utilization for OBF is in the range 47.7 % to 54.3 %, for the studies reviewed [109,112].

### 5.4. Size and productivity

The productivity of a blast furnace is usually restricted by the flooding phenomena, which limits the downward mass flow of a liquid in a bed of solid particles with countercurrent gases. The liquid will stop flowing downwards (or will even rise upwards as reflux), when the gas exerts a limiting force in the opposite direction to the descent of the liquid [148]. Since the OBF presents lower bosh gas flows than conventional BFs, the flooding limitation is less restrictive. In the literature, productivities in the range of 1.6 to 8.1 $t/m^3d$ are reported (thm per $m^3$ of inner volume per day) [100,108,112,113,116,135,140,141,144]. In general, the productivity of the OBF is 25 % to 75 % greater than those for conventional BF, what allows to downsize the furnace while keeping the same production rate [100,108,112,143,147]. Conventional BFs have 5000 $m^3$ inner volume, so OBFs are expected to have around 2500–2800 $m^3$ inner volume [103,109,140]. Despite of the smaller diameter of the shaft, analysis based on discrete element method showed that the compressive stress on the solids is similar or even lower than in conventional BF [109].

### 5.5. Technology readiness level, and costs

The TGR-OBF technology is not yet commercial. Most of studies found in the literature are TRL 2, and only a few articles mention experimental tests between TRL 3 and TRL 6 (Table 7; note that commercial OBF should have 2500 $m^3$ inner volume). Institutions that have performed experimental research on OBF include (in the ascending order of size) JFE Steel [7,141], the State Key Laboratory of Advanced Steel Processes and Products of China in cooperation with Minmetals Yingkou Medium Plate [135,144], the ULCOS project at LKAB's experimental blast furnace [7], the Baowu Group [135], and Tulachermet [113,135].

The viability of future research and investments in OBF is ruled by the cost of producing 1 ton of steel [146]. The price of steel (without accounting $CO_2$ taxes) was around 500 €/t during the last decade, but it rose to 1400–1800 €/t last year due to the global scenario [149]. According to the studies based on pre-pandemic scenarios, the price of steel under OBF technology equals the price of conventional steel when the $CO_2$ taxes are in the range 40–150 €/$tCO_2$, depending on the price of electricity and the carbon capture technology (VPSA or amine scrubbing) [102,104,118,146,150]. It should be noted that the electricity price and the $CO_2$ taxes are correlated, and therefore, it is recommended to consider that electricity price increases by 0.85 €/MWh per each 1 €/$tCO_2$ increase in the $CO_2$ price [146].

Retrofitting BF to OBF is barely considered in literature [102], since the required size of the blast furnace decreases, and $O_2$-enrichment above 30 % causes equipment damage in hot air blowing systems (oxidation of metallic pipes, lances, etc.) [100]. Nevertheless, the cost of retrofitting the furnace and piping is estimated at approximately 900 M€ (cost of the carbon capture plant not included) [102]. The investment cost for a new standalone OBF may be smaller than that for a new conventional BF because of its smaller dimensions. However, it implies additional costs related to the larger ASU, compressors, and carbon capture stage. Hence, the overall investment for OBF may be 1.25 M€ greater than that for conventional BF, per thm/h (including carbon capture) [146]. Pay-back on blast furnace investments is assumed to be between 20 and 30 years in the literature [146].

Regarding operating costs, the major differences between the OBF and BF are the amount of coke consumed (up to 150 kg/thm less) and the electricity consumption (up to 4.2 GJ/thm more). Typical costs for coke and electricity are 300 €/t and 80 €/MWh, respectively [146]. Thus, the OPEX would decrease by up to 45 €/thm because of coke savings, but increase by up to 93 €/thm due to the electricity consumption (extreme values). Moreover, the transportation and permanent storage of $CO_2$ can be assumed as an additional cost of 27 \$/$tCO_2$ [146] what translates into 28 €/thm. In total, the net increase in OPEX is 76 €/thm. At the current price of steel, this represents a 5 % increment in the price of steel (one decade ago, it would correspond to a 15 % increment in the price).

## 6. Pre-combustion CC in BF-BOF

Pre-combustion technologies for carbon capture in the I&S industry can be applied to the CO2 emissions from raw materials preparation, blast furnace, and blast oxygen furnace. The resulting gas stream after CC can be used as fuel in internal combustion processes. The design and integration of chemical absorption, physical adsorption, membrane separation, and sorption enhanced water gas shift (SEWGS) technology

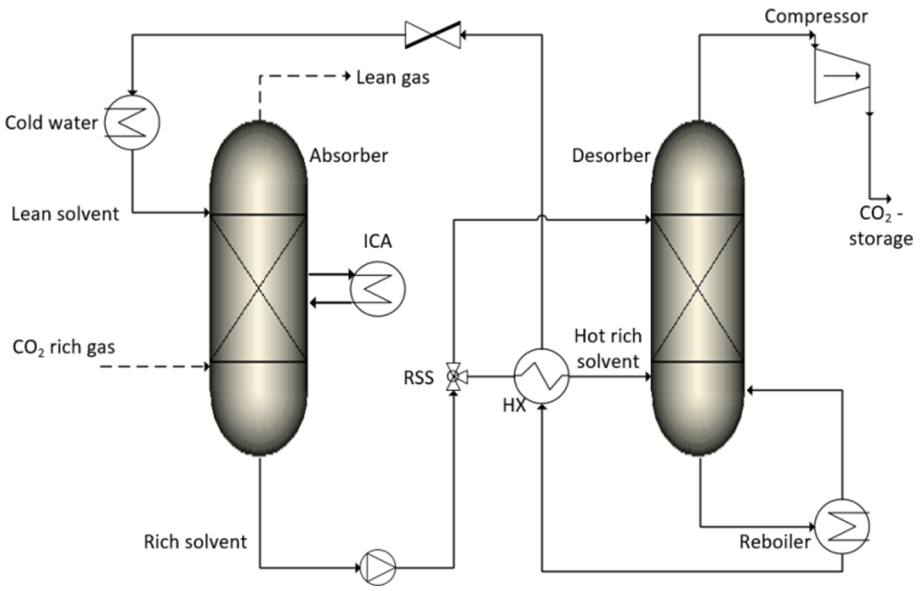


**Fig. 10.** $CO_2$ absorption with intercooled absorber (ICA) and rich solvent splitting (RSS), . adapted from [30]

for pre-combustion CC in the BF-BOF route are reviewed in this section.

### 6.1. *Pre-combustion with chemical absorption*

Certain chemical solvents, such as amine-based (presented in Section 4.1) or aqueous ammonia, can be used for pre-combustion carbon capture. Tobiesen et al. [151] presents one of the early studies based on modelling $CO_2$ absorption from the off-gases of conventional and oxygen-based blast furnaces using monoethanolamine (MEA), methyldiethanolamine (MDEA)/piperazine (Pz), and 2-amino-2-methyl-1-propanol (AMP) as primary, tertiary/secondary mixture, and sterically-hindered primary amine solvents, respectively. It is unclear why secondary amines were not tested despite both primary and secondary amines undergo hydrolysis and carbamate mechanisms for $CO_2$ absorption, as shown in reactions (1) to (7), while tertiary amines only undergo slow hydrolysis reaction with $CO_2$ [152].

*Hydrolysis mechanism:*

$$CO_2 + H_2O \leftrightarrow H_2CO_3 (CO_2 hydrolysis) \quad (1)$$

$$H_2CO_3 \leftrightarrow HCO_3^- + H^+ (Bicarbonate formation) \quad (2)$$

$$H^+ + R_1 - \underset{\underset{R_3}{|}}{\overset{\overset{R_2}{|}}{N}} \leftrightarrow R_1 - \underset{\underset{R_3}{|}}{\overset{\overset{R_2}{|}}{N^+}} - H (Acid - base reaction) \quad (3)$$

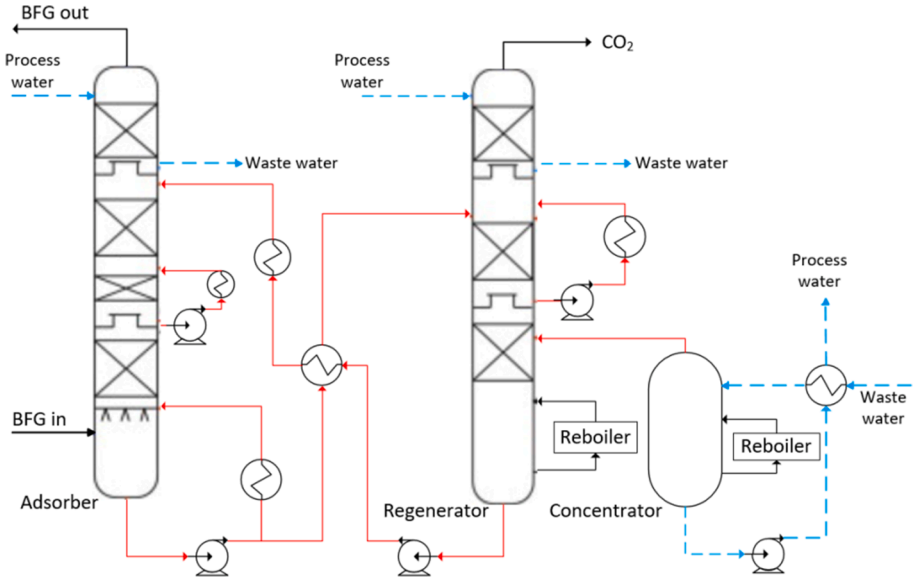


**Fig. 11.** Aqueous ammonia-based $CO_2$ capture from the blast furnace off-gas (BFG) . adapted from [155]

$$CO_2 + H_2O + R_1 - \underset{\underset{R_3}{|}}{\overset{\overset{R_2}{|}}{N}} \leftrightarrow R_1 - \underset{\underset{R_3}{|}}{\overset{\overset{R_2}{|}}{N^+}} - H + HCO_3^- \,(Overall reaction) \quad (4)$$

Carbamate mechanism:

$$CO_2 + R_1 - \underset{\underset{H}{|}}{\overset{\overset{R_2}{|}}{N}} \leftrightarrow R_1 - \underset{\underset{H}{|}}{\overset{\overset{R_2}{|}}{N^+}} - \underset{\underset{O}{||}}{\overset{\overset{.}{.}}{C}} - O^- \,(Amine salt formation) \quad (5)$$

$$R_1 - \underset{\underset{H}{|}}{\overset{\overset{R_2}{|}}{N^+}} - \underset{\underset{O}{||}}{\overset{\overset{.}{.}}{C}} - O^- + R_1 - \underset{\underset{H}{|}}{\overset{\overset{R_2}{|}}{N}} \leftrightarrow R_1 - \underset{\underset{.}{|}}{\overset{\overset{R_2}{|}}{N}} - \underset{\underset{O}{||}}{\overset{\overset{.}{.}}{C}} - O^- + R_1 - \underset{\underset{H}{|}}{\overset{\overset{R_2}{|}}{N^+}} - H \;(Carbamate\ formation) \quad (6)$$

$$CO_2 + 2R_1 - \underset{\underset{H}{|}}{\overset{\overset{R_2}{|}}{N}} \leftrightarrow R_1 - \underset{\underset{.}{|}}{\overset{\overset{R_2}{|}}{N}} - \underset{\underset{O}{||}}{\overset{\overset{.}{.}}{C}} - O^- + R_1 - \underset{\underset{H}{|}}{\overset{\overset{R_2}{|}}{N^+}} - H (Overall\ reaction) \quad (7)$$

Moreover, AMP also does not favour fast $CO_2$ absorption, as it hinders carbamate reaction. Since absorption process has high efficiency at low temperature and high pressure, $CO_2$ capture typically involves four steps: (a) gas pretreatment to reduce temperature and increase pressure through compression, (b) gas absorption with intercooling using alkaline solvent, (c) solvent regeneration by separating $CO_2$, and (d) $CO_2$ compression and drying for transportation. According to the process simulations [151], about 80–90 % of the total energy is needed for steam generation for desorber reboiler, while the remaining 10–20 % drives the gas compressors, blower, and the solvent recirculation pumps. Based on the regeneration energy requirement and the solvent recirculation rate, AMP was the most suitable solvent (reboiler steam consumption: 2.6 MJ/$kg_{CO2}$ with AMP, 2.9 MJ/$kg_{CO2}$ with MDEA/Pz, and 3.7 MJ/$kg_{CO2}$ with MEA), although it would require a large absorber size due to its slow reaction with $CO_2$.

To enhance process efficiency and energy savings, heat recovered from BFG or from flue gas of power plant can cover the thermal needs of the amine capture system [30,153]. As it is shown in Fig. 10, an intercooled absorber (ICA) and rich solvent splitting (RSS) was included in the simulation model. The maximum $CO_2$ capture from BFG was 5 % lower than that from flue gas stream due to the lower $CO_2$ content in the former. The effect of feed split ratio for minimising solvent regeneration energy and the implications of such designs on the capital cost were not investigated.

Different published works [19,21,154] present overviews of various $CO_2$ breakthrough programs, including ultra-low carbon dioxide steel making (ULCOS-2004) program in the EU (also discussed in [11]), $CO_2$ Ultimate Reduction in Steelmaking Process for Cool Earth 50 (COURSE50-2008) in Japan, Pohang Iron and Steel Company (POSCO-2020) program in South Korea, and American Iron and Steel Institute (AISI-2011) program in USA. The ULCOS program focused on the amine scrubbing using MDEA, though it suffers from high energy requirements (about 3.2 GJ/t$CO_2$) and further research is needed to reduce the CC energy penalties [11]. The COURSE50 program investigated $CO_2$ absorption with amines or amines mixed with alcohols/additives. Under this program, Onoda et al. [107] studied 21 solvents such as MEA, MDEA, 2-amino-2-methyl-1-propanol (AMP), 2-Piperidineethanol (2-PPE), diethanolamine (DEA), 2-(ethylamino) ethanol (EAE), *N*-isopropyldiethanolamine (IPDEA), and 4-piperidineethanol (4PPE). The temperature of adsorbent regeneration was optimised through two pilot plant tests to reduce the CC energy penalty from about 4 to 2 GJ/t$CO_2$. However, further studies are needed to understand their degradation and vaporisation losses in the presence of gas contaminants and high temperature over an extended period of time.

The POSCO program recommends aqueous ammonia as solvent for absorption process (see Eq. (8)-(12)). A pilot-scale ammonia-based absorption process for $CO_2$ capture was integrated in an actual I&S plant (Fig. 11) [155].

Aqueous ammonia captures $CO_2$ through the following reactions:

$$NH_3 + CO_2 + H_2O \leftrightarrow NH_4HCO_3 \quad (8)$$

$$2NH_3 + CO_2 + H_2O \leftrightarrow (NH_4)_2CO_3 \quad (9)$$

$$2NH_3 + CO_2 \leftrightarrow NH_2COOH + NH_3 \leftrightarrow NH_4COONH_2 \quad (10)$$

$$(NH_4)_2CO_3 + CO_2 + H_2O \leftrightarrow 2NH_4HCO_3 \quad (11)$$

$$NH_4HCO_3 + NH_3 \leftrightarrow NH_4COONH_2 + H_2O \quad (12)$$

To avoid ammonia loss with the gas exiting the absorber, the treated gas is water-washed. The $CO_2$-loaded solution is regenerated using a reboiler (maintained near 80 °C). The $CO_2$-rich stream from the regenerator is also water-washed to remove ammonia escaping with it. The regenerated ammonia solution is sent to the absorber for its reuse. The regeneration of washing water takes place in the concentrator, where water is separated from ammonia. Through the comparison of $CO_2$ absorption by amines, ammonia, and $K_2CO_3$, it was argued that ammonia would require lowest regeneration energy and absorbent cost with less risk of corrosion and solvent thermal degradation. With a blast furnace off-gas flow rate of 1000 $Nm^3$/h, the process was shown to absorb over 95 % $CO_2$ (about 10 $t_{CO2}$/day), and produced a gas stream from the regenerator with nearly 99 % $CO_2$. However, an economic analysis and the feasibility of a full-scale plant implementation (with high off-gas flow rate) should be evaluated since the slow rate of $CO_2$ absorption by ammonia may require a significantly large column size and a high solvent recirculation rate.

Ho et al. [26] studied the retrofitting of existing I&S plants in Australia with $CO_2$ capture using MEA for $CO_2$ absorption. Feed pretreatment involved selective catalytic reduction (SCR) to reduce $NO_x$ concentration below 20 ppm, particulate filter to remove solids, and flue gas desulfurization (FGD) to reduce $SO_x$ concentration below 20 ppm.

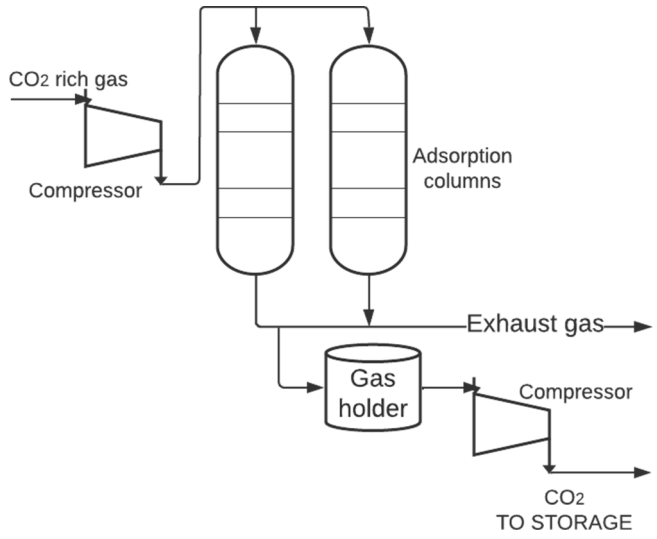


**Fig. 12.** Process flow diagram of a simple PSA technology, . adapted from [158]

For off-gas with low $CO_2$ partial pressure, water-gas shift reactor was considered to convert CO to $CO_2$, and thereafter, Selexol (physical solvent) was used for $CO_2$ absorption [26]. For MEA-based $CO_2$ capture, the capital and operating cost represented 20–30 % and 70–80 % of the total cost, respectively. Overall, the costs of $CO_2$ capture were A$74/t$CO_2$ for the blast furnace and A$56/t$CO_2$ for the Corex process. The $CO_2$ capture cost for the Corex process could be further reduced to A$39/t$CO_2$, if the inlet gas was compressed to about 20 bar and the water-gas shift reactor was used to enrich the gas with $CO_2$ so that a physical solvent (Selexol) could be used. Ho et al. [102] extended study [26] by investigating $CO_2$ capture from Hismelt, Midrex, and mini mill processes. To be cost-effective, it was recommended to capture $CO_2$ only from main emission sources (for example, from onsite power plant with cost estimate of A$76/t$CO_2$, coke ovens and stoves with a cost of A$80/t$CO_2$, and sinter plant with a cost of A$90/t$CO_2$) that can achieve $CO_2$ emission reduction by about 80 % from an I&S industry. Moreover, the use of vacuum pressure swing adsorption (VPSA) with concentrated gas was found to involve lower cost of $CO_2$ capture than MEA absorption due to lower regeneration energy requirements.

Some studies in the literature provide the comparison of different techniques for $CO_2$ capture. Quadar et al. [156] compared the efficiency and energy requirements of some $CO_2$ capture studies from the literature from blast furnace/stove off-gas using aqueous ammonia [155], MEA [26,38], and MDEA/MEA [157], and VPSA [106]. Since the efficiency of $CO_2$ capture and energy requirements depend on the gas composition, temperature, pressure, and flow rate, a direct comparison of the results from studies utilizing different feed parameters is difficult. Quadar et al. [156] noted that both absorption and adsorption are suitable for $CO_2$ capture. Kim et al. [158] simulated PSA and MEA-based absorption processes for $CO_2$ capture from furnace off-gas. The MEA-based absorption process suffered from solvent degradation and loss and equipment corrosion. The absorption process led to a $CO_2$ stream with higher purity than the PSA process with a difference of 9.95 mol%, but the energy required in the absorption process was 224.78 MW higher than that for PSA. While PSA required lower regeneration energy than the absorption process, its adsorption efficiency was high only when $CO_2$ was present in high concentrations. Gazzani et al. [29] studied $CO_2$ capture from an iron & steel plant in the pre-combustion and post-combustion stages using MEA and MDEA solvents, and with sorption-enhanced-water–gas-shift (SEWGS) reactors. The results were presented in terms of specific primary energy consumption for $CO_2$ avoided (SPECCA, MJ/kg$_{CO2}$) versus % of $CO_2$ avoided. The pre-combustion $CO_2$ capture process involved compressing the off-gas, passing it through a water saturator, sending the resultant gas to water-gas shift reactors, and finally, using MDEA-based absorption unit to capture $CO_2$ and send the $H_2$-rich gas to the onsite power plant for combustion. This process, with heat integration, achieved a $CO_2$ avoidance of 89 % with a SPECCA of about 3 MJ/kg$_{CO2}$. In comparison, the processes requiring passing the off-gas from the iron & steel plant to a water saturator and water-gas shift reactors, and thereafter, capturing $CO_2$ using adsorbents and sending the $H_2$-rich gas to the onsite power plant, achieved a $CO_2$ avoidance of 78–89 % with a low SPECCA of about 2.2–2.95 MJ/kg$_{CO2}$.

Onarheim et al. [159] compared the processes involving $CO_2$ capture using a chemical (MEA) and a physical (Selexol) solvent. A process with a blast furnace using oxygen-enriched air (40 % $O_2$) and a basic oxygen furnace was simulated, where the off-gas was passed through a water-gas shift reactor. In comparison to the reference base process (without CCS) with $CO_2$ emission of 81.6 kg/s, the absorption processes with MEA and Selexol reduced the $CO_2$ emissions to 34.7 and 24.8 kJ/mol, respectively. The study did not present an economic analysis to understand if the cost associated with physical absorption was lower than that with MEA, as they involved different process equipment.

Chung et al. [160] studied $CO_2$ capture from the blast furnace off-gas through amine (piperazine) absorption, membrane separation, and hybrids of absorption and membrane separation. A hybrid process required lowest utility and capital costs with operating cost change of $77 M/year, capital cost of $66 M, highest rate of $CO_2$ avoided (69.4 %), and lowest $CO_2$ avoidance cost ($30.4/t$CO_2$). Their calculations suggest that the membrane separation unit has a better rate of $CO_2$ avoided (66.4 %) and a lower $CO_2$ avoidance cost ($34.4/t$CO_2$) as compared to the amine

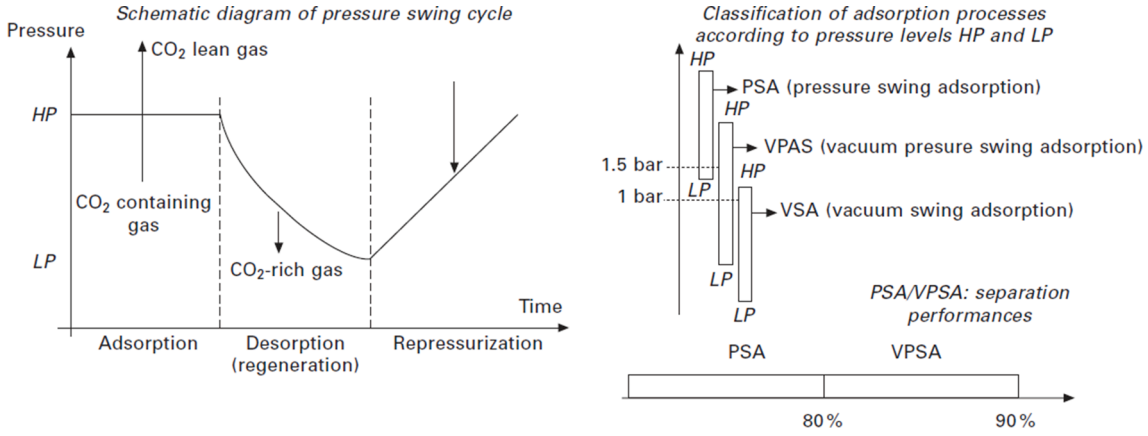


**Fig. 13.** Principle of the PSA CO2-scrubbing techniques (left) and various domains of application and performances of the variant techniques, PSA, VPSA and VSA . adapted from [163]

absorption unit (with their respective values of 61.3 % and $40.6/t$CO_2$). However, only one amine (piperazine) was tested to reach this conclusion.

The above studies indicate that $CO_2$ absorption by amines may be a well-established technique, but VPSA is more suitable for iron & steel plants with less energy demand and lower cost of $CO_2$ avoidance. This has motivated several adsorption studies, such as by Arasto et al. [106] and Tsupari et al. [146], on $CO_2$ capture from the oxygen blast furnace, and by Hisashige et al. [161] on $CO_2$ capture from the smelter off-gas, as discussed in Section 6.2.

The technologies for $CO_2$ absorption using chemical solvents (e.g., MEA, MDEA) are widely deployed in industries (e.g., for removal of $H_2S$ and $CO_2$ from sour gas in natural gas processing facilities), and thus exhibits high TRL (9). However, their application and demonstration to carbon capture from BFG, BOFG, and COG streams at industrial scale has been limited to date. Thus the majority of pre-combustion-based CC technologies reviewed in Section 6.1 are found to be of low TRL (2–4), and to have been investigated solely through simulation rather than experiments, with the exception of a few pilot scale studies conducted as part of either COURSE50, ULCOS, and STEPWISE projects [87,111,144,148,157] for technologies (carbon capture using various amines) or in an independent study [134] for technology (carbon capture using ammonia).

### 6.2. Pre-combustion CC with adsorption processes

In physical adsorption, the main interacting force is the Van der Waals force. In this system, there is no chemical reaction between the gases and the adsorbents, as the gas is physically bonded to the surface of the solid. There are four different ways of regenerating the adsorbent: pressure swing adsorption (PSA), vacuum-pressure swing adsorption (VPSA), temperature swing adsorption (TSA) and electrical swing adsorption (ESA).

A key finding from the ULCOS project indicated that the chemisorption methods such as amine scrubbing, physisorption technologies such as VPSA or PSA, and cryogenics have different domains of optimality, with the concentration of $CO_2$ in the gas stream to be treated being one of the most critical determining factors [162]. The physisorption schemes are the best in terms of technical performance and cost, both operational and capital, at the concentration levels reported in the BF instance and the TGR–BF scenarios [163]. The technologies for $CO_2$ capture and separation in the pre-combustion stage with adsorption can be categorized in terms of the adsorbent type (such as alumina, zeolite & MOFs, and activated carbon), regeneration method (such as pressure swing, temperature swing, electric swing, and washing), and type of monolith molecular sieve (*e.g.*, carbon coated substrate and carbon/carbon fiber monolith) [101]. Among these, pressure swing adsorption (PSA)-based techniques have been the most advanced adsorption techniques reported till date. A typical PSA technology involves two stages that could be either operated as a single stage (as shown in Fig. 12) or as dual stage, wherein CO and $N_2$ are first separated from $CO_2$ in the first unit packed with a $CO_2$ adsorbent, such as Zeolite 13X [158] or Zeolum F-9 [164]. Thereafter, the off-gas from the first PSA, consisting mainly of $N_2$ and CO, is introduced to the second unit which accomplishes the separation of CO and $N_2$ using a CO adsorbent [165]. Under plant conditions, the total energy required to recover about 90 % $CO_2$ with a purity of 91 % is ca. 36.9 MW [158]. In addition, a highly-concentrated combustible gas (with 72 mol% of CO and $H_2$) is obtained as an exhaust gas byproduct that could be utilized in power generation boilers [158].Fig. 13.

Although high $CO_2$ recoveries (>90 %) have been reported [158], the purity of $CO_2$ in the recovered stream is relatively low with PSA technology compared to other $CO_2$ separation processes. Rao et al. [166] employed a PSA for recovering $CO_2$ from coke oven gas. The final $CO_2$ recovered stream contained as much as 24 % moisture, making it unsuitable for compression and storage without further purification. To overcome this demerit, advances in PSA technology have resulted in a combination of other $CO_2$ mitigation or separation processes with PSA [167]. Another similar technique to PSA is the Vacuum Pressure Swing Adsorption (VPSA) wherein adsorption is carried out at ca. 1.5 bar and desorption is performed under vacuum conditions at 0.05 bar. As the exhaust gas from BF contains moderately high partial pressure of $CO_2$ (>0.2 bar), VPSA has been shown to be more economical in reducing the $CO_2$ capture costs [168]. A detailed economic analysis by Ho et al. [102] has shown that VPSA has the potential to reduce $CO_2$ capture costs by 25–40 % compared to MEA solvent absorption technology.

Two of the key concepts of a top gas recycling blast furnace (TGR-BF) are the removal of $CO_2$ from the top gas to enhance recycling and injection of oxygen into the furnace in the place of air [169]. In general, the oxygen blast furnace has the benefits of substantially lowering the $CO_2$ emissions compared to the traditional blast furnace [135]. The net $CO_2$ emissions from an integrated steel mill combined with a TGR-OBF is about 1.17 t/t crude steel compared to 1.75 t/t crude steel for a process without CCS. Arasto et al. [106] evaluated a VPSA-based $CO_2$ capture process configuration from the oxygen blast furnace, based on an existing steel facility in Finland. $CO_2$ emissions are estimated to be reduced between 1.2 and 1.4 Mt/year (from over 4 Mt/year) when CCS is applied to the oxygen blast furnace with and without $CO_2$ storage, respectively.

TGR-OBF equipped with VPSA for $CO_2$ capture has also been beneficial for reducing energy consumption of an integrated steel mill (ISM). This technology significantly decreases generation of metallurgy gas in the coking and ironmaking processes (by ca. 53.4 %) which might consequently decrease the electricity output of the power plant. Moreover, the electricity demand of the ISM is ca. 60 % higher than that of the conventional process due to increased consumption by VPSA and oxygen generation plants [103,119]. Thus, additional electricity may have to be generated or purchased for the ISM with TGR-OBF compared with conventional ISM. On the other hand, the energy input to the ISM with TGR-OBF process decreases substantially from 17.89 to 14.67 GJ/t owing to decreased coking coal consumption. It has been demonstrated in the literature that compared to a traditional air blast furnace equipped with TGR, the utilization of a lean grade burden with pulverized coal injection (PCI) and high blast oxygen enrichment (medium, 50 %; enriched 98 %) can curtail carbon consumptions by 14.1 % and 20.2 %, respectively [110,135]. Nevertheless, various strategies for overcoming issues related to low gas volume have been addressed in the literature [130]. Sen [142] proposed a $CO_2$ accounting procedure based on a carbon balance, which can facilitate evaluation of the recovery of surplus gases to reduce emissions. Carbon capture using VPSA with top exhaust gas recycling was identified as a promising emissions reduction approach. The analysis based on an oxygen blast furnace with top gas recycle configuration developed by ULCOS indicated ca. 90 % reduction in $CO_2$ content with a $CO_2$ purity of 87.7 % in the recovered stream. On a commercial scale, VPSA has been successfully implemented in combination with top gas recycling of blast furnace effluent gases [11,111]. While mitigation measures resulted in a 24 % $CO_2$ emission reduction, nearly 52 % reduction was accomplished with the VPSA technology [11,102]. However, an unsteady state analysis of the TGR-OBF blast furnace have indicated a slightly lower $CO_2$ emissions reduction (ca. 69 %), and the deviations have been attributed to the differences in $CO_2$ emission calculation method [128]. Nevertheless, the amount of treated gas recycled into the blast furnace determines the $CO_2$ reduction levels in the system. For example, at a gas injection rate of 600 $Nm^3$/thm, the level of $CO_2$ emission reduction that could be attained is ca. 1000 kg/thm. However, when the feed rate is increased to 1100 $Nm^3$/thm, the reduction levels increase to about 1200 kg/thm [131].

In addition, the coupling of a cryogenic system with the VPSA results in further purification to attain a higher level of purity (ca. 96.2 % on dry basis) in $CO_2$ stream, thus making it favourable for transport and storage. In comparison, the level of $CO_2$ purity attained with PSA and VPSA is about 79.7 % and 87.2 %, respectively. However, the energy

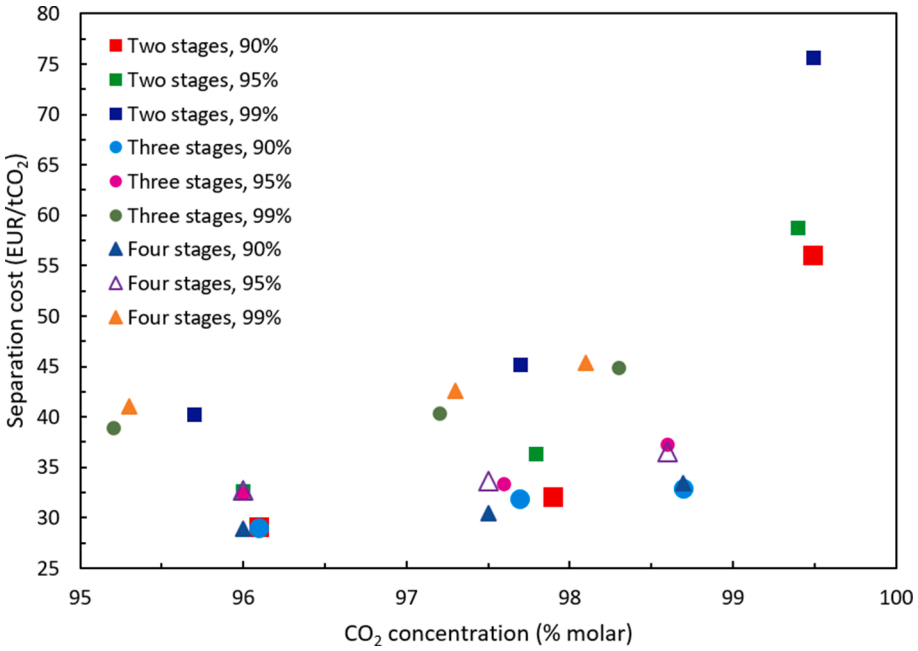


**Fig. 14.** Separation cost vs $CO_2$ product purity for the optimal configurations with two, three and four stages (% values in the legend refer to $CO_2$ recovery). Data from left to right on each series correspond to $N_2$ residual contents of 1%, 0.5% and 0.1% respectively, .
adapted from [162]

consumption for the combined VPSA and cryogenic technique is ca. 2.9 times higher than those for PSA or VPSA systems that could be directly attributed to the energy requirements for $CO_2$ compression [11]. Another interesting option is the combination of PSA with cryogenic distillation compression that is capable of delivering a 99–100 % pure $CO_2$ stream [106], with a total energy consumption of 1.12 GJ/t$CO_2$ compared to 1.05 GJ/t$CO_2$ for a VPSA + compression and cryogenic system.

An in-situ method for capturing $CO_2$ by adsorption during the process of COG gasification was proposed by Wang et al. [170]. By integrating the sub-processes of SMR, WGSR, and carbonation in an adsorption enhanced hydrogen amplification reactor (AEHAR), $CO_2$ was captured using calcium oxide packed in the reactor and later released during the regeneration process. In order to remove other desorbed gases from the recovered $CO_2$ stream, a hot potassium carbonate process was applied in the downstream section. Since this study focused on maximizing hydrogen recovery, the details on $CO_2$ recovery and efficiencies were not reported.

Generally, higher adsorption pressure results in a higher recovery ratio, but also in higher blower power consumption. Simultaneously, a lower desorption pressure results in a larger recovery ratio and higher vacuum pump power usage. In an attempt to minimize the recovery cost, Saima et al. [164] experimentally investigated the effects of cycle time and $CO_2$ concentration in the exhaust blast furnace gas on the efficiency of pressure swing adsorption (PSA) to extract CO and $CO_2$. Increasing the $CO_2$ feed concentration from 22 % to 33 % increases $CO_2$ recovery by ca. 1.6 times. However, the effect of process cycle time on $CO_2$ recovery levels was found to be negligible and an optimum time of 225 s was recommended. These findings were further demonstrated at a bench scale setup that recovered about 6.3 $t_{CO2}$/day resulting in an overall reduction in capture cost by 63 % [164].

The primary carbon capture technology by adsorption relies on the pressure swing adsorption or vacuum pressure swing adsorption technique. The adsorption process using solid sorbents such as Selexol, alumina, zeolites, and activated carbon, has been demonstrated for several industrial applications (TRL = 9), including hydrogen production in refineries, nitrogen production, and dehydration applications [171]. Most of the studies listed in section 6.2 employ various sorbents in PSA/VPSA with top gas recycling for carbon capture from steel plant off-gases. Nevertheless, since these studies are simulation-based without actual pilot- or plant-scale demonstration, their TRL has been characterized as low (2).

### 6.3. *Pre-combustion with membranes*

Hasan et al. [172] found that membrane separation is preferable to amine scrubbing when $CO_2$ concentration in the flue gas is higher than 36 %, which is true for blast furnace off-gas. A wide variety of membrane

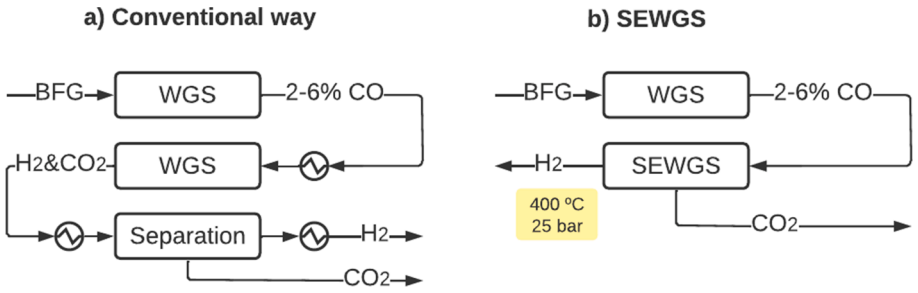


**Fig. 15.** Process flow diagram of a) conventional WGS and b) SEWGS technology, .
adapted from [179]

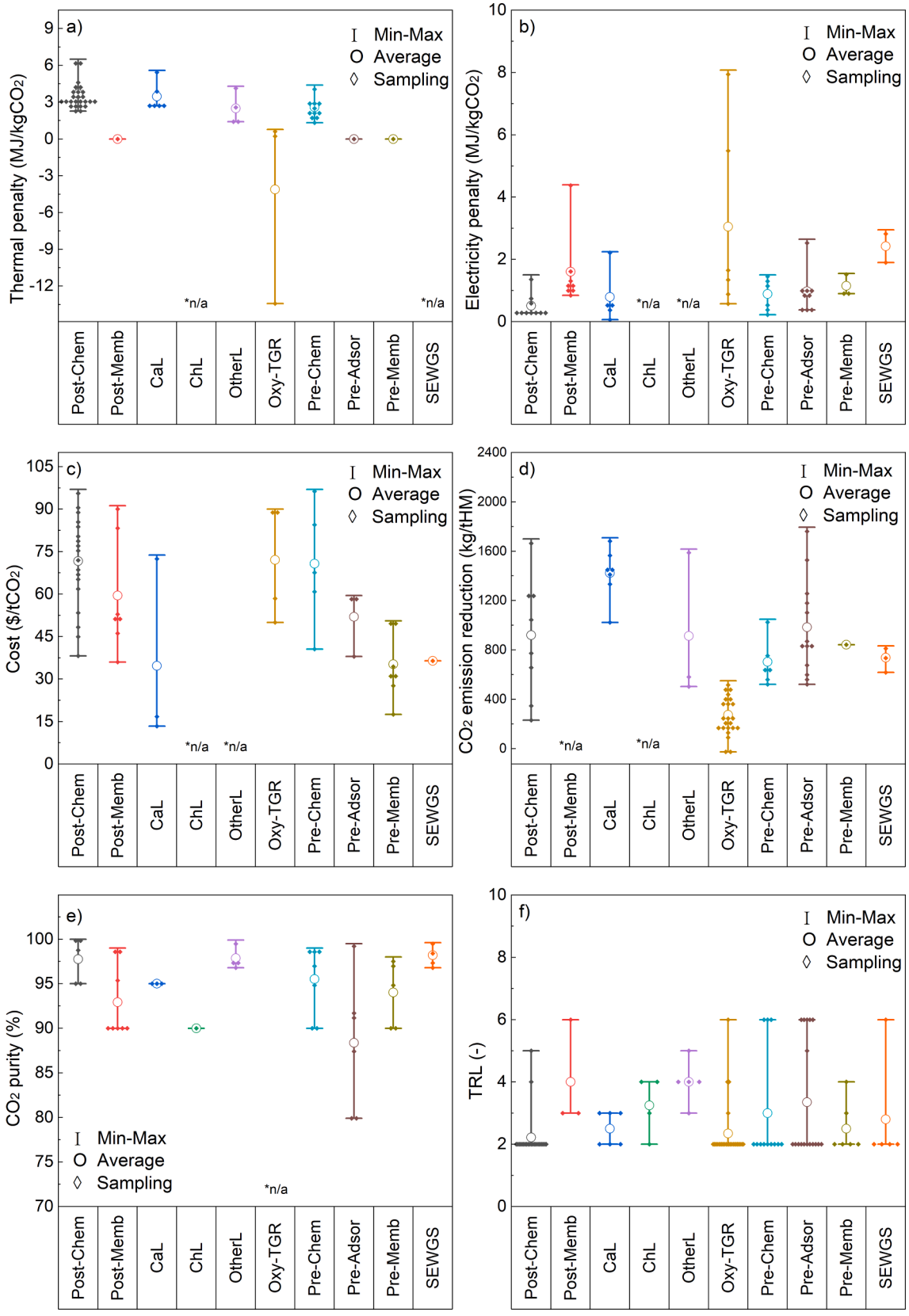


**Fig. 16.** KPI comparison for different carbon capture technologies: a) termal penalty (MJ/tHM), b) electricity penalty (MJ/tHM) c) cost ($/t$CO_2$), d) $CO_2$ emission reduction (kg/tHM), e) $CO_2$ purity (%) and f) TRL (-). Nomenclature: Post-Chem is postcombustion carbon capture (CC) by chemical absorption; Post-Memb is postcombustion CC by membranes; CaL is calcium looping; ChL is chemical looping; OthL is other looping processes; Oxy-TGR is oxy-blast furnace with top gas recycling (TGR); Pre-Chem is precombustion CC by chemical absorption; Pre-Adsor is precombustion CC by adsorption; Pre-Memb is is precombustion CC by membranes and SEWGS is sorption enhanced water gas shift.

materials including polymers [160,162,173–175] and zeolites [176] have been employed for $CO_2$ recovery from various industrial waste gases, among which polymeric membranes are largely preferred for coke oven gas and blast furnace gas. Lie et al. [174] compared the performance of a fixed site carrier membrane (FSCM), comprised of amine groups in the polymeric backbone, with carbon based membranes. The results showed that aminated polymeric membranes exhibited enhanced permeability and selectivity in favour of $CO_2$. Moreover, while the presence of moisture in the blast furnace top gas stream is detrimental for carbon-based membranes, it is beneficial for FSCM as the active amine groups act as carriers for $CO_2$-water complex. Membrane Technology Research (MTR)'s Polaris© membrane has been the most widely employed one in lab and pilot-scale $CO_2$ capture studies as it possesses the highest $CO_2$ Gas permeance unit (GPU) of 1000, $CO_2$-$N_2$ selectivity of 50, and $CO_2$-CO selectivity of more than 67 measured at 10 °C [177] in addition to higher stability. Such improvements in membrane selectivity have enabled development of novel $CO_2$ capture concepts in sub-ambient conditions using membrane-hybrid cryogenic processes. However, simulation studies have demonstrated that such hybrid techniques are economically suitable only for high-$CO_2$ content flue gas, and not significant for lean $CO_2$ streams like BF and COG [178].

CCU from BF or BOF process off-gas by polymeric membranes typically requires multi-staged operation to meet the desired $CO_2$ recovery and purity levels, owing to the inherent limitations of the solution-diffusion separation mechanism [162]. An advanced superstructure design with unrestricted stream connections and interlooping proposed by Santos et al (2018) [162] demonstrates the feasibility to minimise overall $CO_2$ recovery cost by optimising numerous membrane architectures parameters, including number of stages, downstream pressure, membrane surface area, and stream connections.

The effect of $CO_2$ recovery and residual $N_2$ constraints on separation cost has been reported in a few studies [160,162,173–175]. The desired $CO_2$ product purity is significantly higher for MTR's Polaris membrane due to its high $CO_2$-$N_2$ selectivity. $CO_2$ concentration and recovery are also influenced sharply by the number of membrane stages considered in the study. In fact, even with a high $CO_2$/CO selectivity, a high level of $CO_2$ purity (>95 %) cannot be achieved by a single membrane unit. A three-staged membrane reactor setup connected in series could reduce CO concentration in the exit gas below 0.2 % [160]. Further, it is possible to achieve product streams with very low $N_2$ content (0.1–1 %) using a superstructure design as demonstrated by Santos et al 2018 [162]. Nevertheless, it has been shown that at fixed recoveries, decreasing $N_2$ residual content, say from 1 % to 0.1 % in the $CO_2$-rich product stream would increase separation cost, although the reverse (increasing recovery at constant purity) has a less pronounced effect [162].

It could be expected that increasing the number of membrane stages may increase the overall $CO_2$ separation cost. Based on a global optimisation procedure employing a non-linear programming formulation of the multistage superstructure design, the influence of $CO_2$ purity and number of membrane stages on separation costs was investigated and has been illustrated in Fig. 14 [162]. It can be noted that when high recovery and/or purity are required, three-stage setups were optimum in reducing separation costs and projected to be in the range of 32–50 $/t$CO_2$. The third stage is utilised to collect $CO_2$ from the retentate of the first stage for $CO_2$ recoveries of 95–99 % and 0.5 % $N_2$ concentration. In the 90–99 % recovery range, a three-stage cascade was the optimum arrangement for a 0.1 % $N_2$ content. Separation costs were not significantly reduced in process designs with four membrane stages.Fig. 15.

The effect of effluent gas composition on $CO_2$ recovery and associated costs could be analyzed from the works of Lie et al. [174] and Chung et al. [160]. The variations in the furnace off-gas composition could result from the type of reducing gas (air or oxygen) used for combustion reactions. Generally, a decreased nitrogen content in the feed stream (oxygen as RG) improves the $CO_2$ flux through the membrane that results in increased recovery percentages. However, the resulting increased $CO_2$ handling volume increases the membrane section duty by about 66 % relative to the conventional air-driven blast furnace [174]. On the other hand, considering the expander energy and other associated costs involved in the two processes, the difference in overall $CO_2$ recovery costs remains quite similar. The relatively higher recovery cost (ca. 34.4 $/t$CO_2$) reported by Chung et al. in comparison to Lie et al. is due to the higher $CO_2$ purity levels considered in the product stream. In addition, the presence of impurities ($NO_x$, $SO_x$ and $H_2S$) in the effluent stream tends to deteriorate the membrane performance with time. Sensitivity studies on the membrane permeability values and $CO_2$ selectivity ratio indicated that a 50 % reduction in overall membrane permeability resulted in a 10 % increase in separation cost, whereas a 50 % reduction in $CO_2$ selectivity resulted in a 34 % increase [160].

Among all membranes including polymers and zeolites, Membrane Technology Research (MTR)'s Polaris© membrane has been widely tested for carbon capture in lab and pilot-scale studies. Technology development for pre-combustion CC with membranes has mainly focused on the optimization of the number of stages and process configuration in a superstructure-staged membrane process. While the single-staged process has been validated at lab-scale (TRL = 4) [175], most of the multistage processes have been investigated using modelling and simulation (TRL = 2) [160,162,173,174]. The technology for other concepts including membrane process coupled with cryogenics [178] has also been demonstrated only in simulations.

### 6.4. Pre-combustion with SEWGS

Sorption enhanced water gas shift (SEWGS) technology combines pre-combustion carbon capture via adsorption and hydrogen production from syngas via WGS reaction in a single process capsule [179]. The catalyst used for the WGS reaction also serves to adsorb the $CO_2$ generated by the WGS reaction. Among various catalytic materials, potassium carbonate hydrotalcite-based materials are the most common [29,45,179] and technically advanced in terms of dual efficiency. While other commercial iron-based high-temperature catalysts have been tested for WGS reaction, $CO_2$ adsorptive performance has not been assessed [180]. However, regeneration of the sorbents is highly energy-intensive and thus necessitates efficient thermal integration techniques, like Ca-Cu chemical looping [93] and pressure release followed by steam purging using a PSA approach [29,32]. The demand for steam by the WGS reaction and SEWGS rinse/purge is responsible for the $CO_2$ capture energy penalty. Hence different configurations, such as expander layout, and saturator layout, focusing on heat integration between steam cycle and SEWGS have been investigated in the literature [32,45].

A common method to provide the SEWGS reactor with the precise wet gas composition and reduce steam purge during regeneration is incorporating a pre-shift WGS reactor prior to the SEWGS unit [45,179]. For the pre-shift reactor, a Johnson Matthey catalyst has been proven to reduce CO concentration in the BFG effluent stream from 20 % to 5 % [179]. It has been demonstrated that integrating SEWGS for both exhaust gas recycling and power generation section reduces overall $CO_2$ plant emissions by nearly 85 % compared to only 50 % for power generation section of steel industry [32]. In particular, the treatment of effluent gases (BFG, BOFG, and COG) using SEWGS could curtail $CO_2$ emissions by 80–90 % [29,32,93]. Furthermore, sorbent reusability studies estimated a 12 % decrease in $CO_2$ avoidance efficiency between fresh and thousands of cycles-old material [29], which is negligible considering the lifetime and cost of the material. In comparison to other amine-based technologies, SEWGS exhibits the highest energy efficiency (ca. 37.7 %) and lowest specific primary energy consumption ca. 2.2 $MJ/kg_{CO2}$) [29].

The technology for pre-combustion CC with SEWGS has been demonstrated in a pilot-scale facility (14 t/d $CO_2$ removal rate) using BFG as part of the STEPWISE project (TRL = 6) [157, [181]. However, investigations focused on either process modification to SEWGS or their

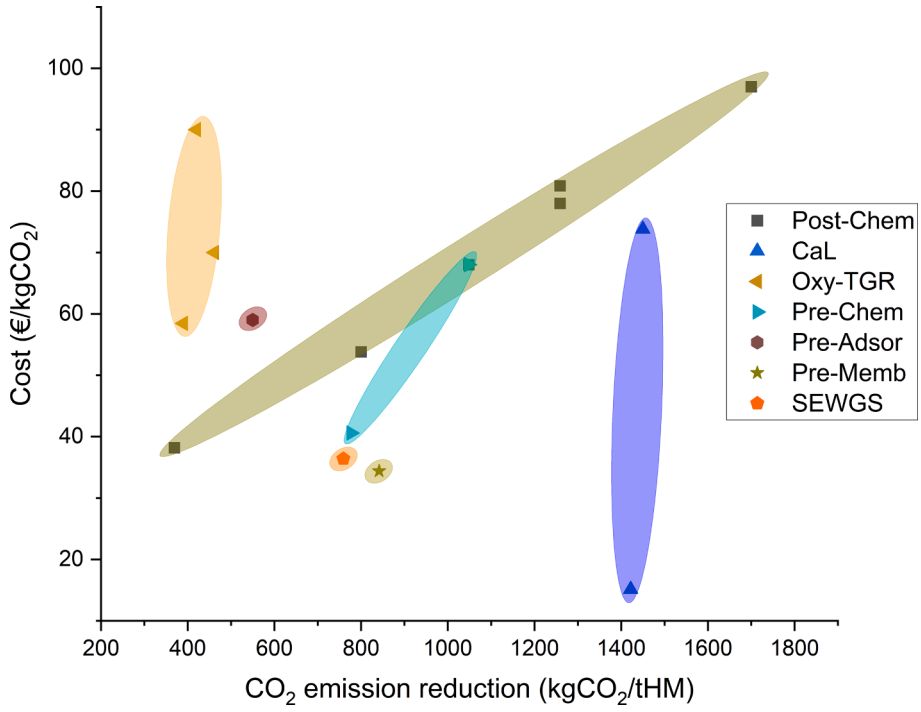


**Fig. 17.** Cost of CC as a function of $CO_2$ emission reduction, by carbon capture technology. Nomenclature identical to Fig. 16.

applications to other steel plant off-gases (i.e., other than BFG) [30,43,27,74] is currently at low TRL (2).

## 7. Carbon capture technologies comparison

A comparison of all carbon capture technologies is presented here with respect to 6 different KPIs: thermal penalty (MJ/kg$CO_2$), electrical penalty (MJ/kg$CO_2$), economic cost (\$/t$CO_2$), $CO_2$ emission reduction (kg$CO_2$/tHM), $CO_2$ purity (%) and TRL (-). The results of this comparison are compiled in Fig. 16. In order to provide a holistic insight, the minimum and maximum values, as well as the average and all the sampling found from all the reviewed scientific works, are included in Fig. 16. Such a representation highlights differences in the presence of each technology in the bibliography.

For oxy blast furnaces with top gas recycling (oxy-TGR) technology, only the decrease of $CO_2$ because of injecting TGR is accounted for, and not the decrease that would be achieved by storing underground the pure $CO_2$ from the CC stage. However, pre-combustion with adsorption (pre-adsor) technology is usually coupled with oxy-BF and TGR, and the combined benefit is taken into account for this technology.

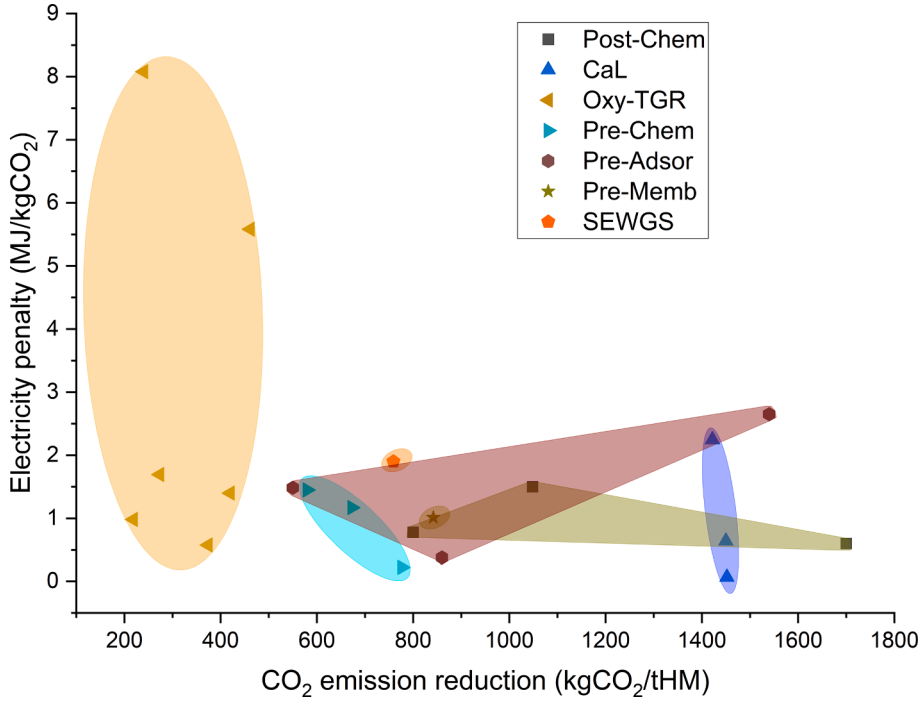


**Fig. 18.** Electricity penalty as a function of $CO_2$ emission reduction, by carbon capture technology. Nomenclature identical to Fig. 16.

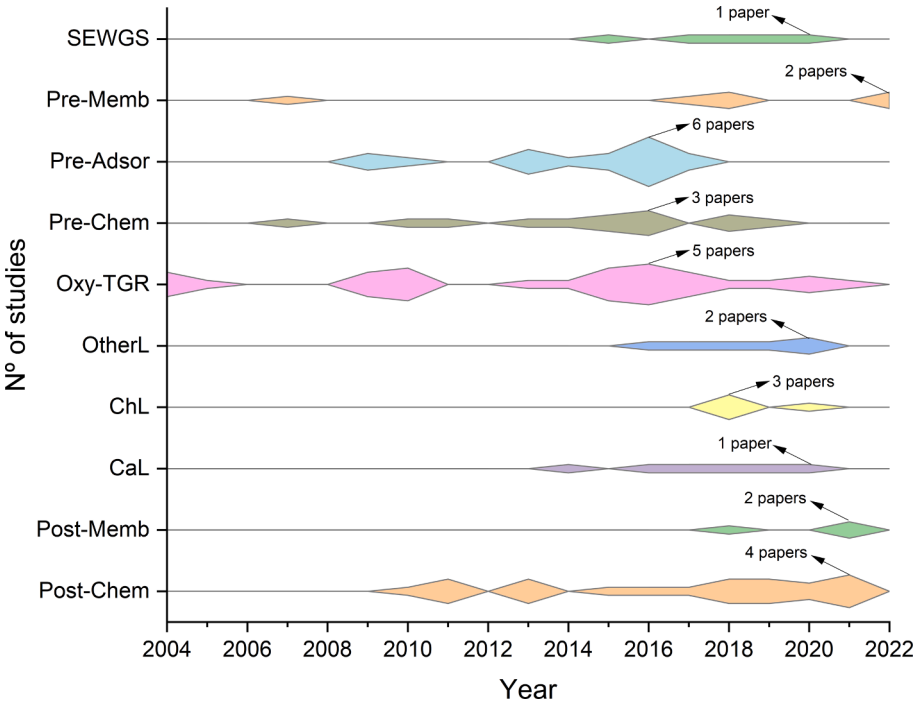


**Fig. 19.** Number of scientific papers published, organised by year and technology. Nomenclature identical to Fig. 16.

The thermal penalty ranges between 1.3 and 6.2 MJ/kg$CO_2$ for post-combustion chemical absorption (post-chem), calcium looping (CaL), other looping processes (OtherL) and pre-combustion chemical absorption (pre-chem); in contrast oxy-TGR stands out with 0.3–0.8 MJ/kg$CO_2$ of thermal energy consumption. Even more, Jin et. Al. [119] calculates a negative penalty (i.e. there is an excess of available energy) of −13.4 MJ/kg$CO_2$. Other technologies such as post- and pre-combustion with membranes (post-memb and pre-memb), chemical looping (ChL), pre-adsor and sorption enhanced water gas shift (SEWGS) do not have thermal consumption or the data was not available (n/a).

Regarding the electricity penalty, the ranges are wider. Post-chem, CaL and pre-chem are the technologies with the lower electricity consumption, with less than 1 MJ/kg$CO_2$ on an average. This is due to the process energy consumption being mainly thermal, with a marginal electricity consumption related to the $CO_2$ compression (up to 100–150 bar). Post-memb, pre-memb, SEWGS and pre-adsor are technologies that compress the gases to capture $CO_2$, and therefore have a higher electricity penalty between 1 and 3 MJ/kg$CO_2$ on an average. Post-memb has an outliner data much higher than the rest (4.4 MJ/kg$CO_2$, when the average is 1.8 MJ/kg$CO_2$). This study corresponds to sinter flue gas capture, which has a very low $CO_2$ content that provokes higher compression consumptions. Oxy-TGR has the wider range of electricity penalty of all technologies due to the great variety of configurations available to implement this technology, from less than 1 MJ/kg$CO_2$ to more than 8 MJ/kg$CO_2$.

The bulk of published economic analyses have focused on post-chem technology, with more than 19 samplings compared to other technologies that combine less than 7 samplings. This technology as well as oxy-TGR and pre-chem have the higher average economic cost, with approximately 70 \$/t$CO_2$, while other technologies range between 30 and 60 \$/t$CO_2$. It is important to notice that only three studies have performed economic analyses for CaL technology, only one study for SEWGS technology, and none for ChL and OtherL. This highlights a lack of economic analyses in this area. The potential $CO_2$ mitigation is very high, especially if it is considered that typical emissions from the BF-BOF route range between 2000 and 2200 kg$CO_2$/tHM. Nevertheless, most of the published works are simulations with a low TRL, and therefore they do not take into account the physical or economical constraints of actual facilities. So far, the maximum $CO_2$ amount captured has been 1270 kg$CO_2$/tHM, reached under TRL 6 in a pilot plant in Lulea (Sweeden), within ULCOS project [131]. They focused on an experimental oxy-blast furnace with top gas recycling and VPSA to capture the $CO_2$.

Only one technology achieves a $CO_2$ purity lower than 90 %, which is the pre-adsor, with an average of 88 % and a minimum of 80 %. From the remaining technologies, only membranes have an average value lower than 95 % for economic reasons. Many of the technologies analysed have a TRL 6, such as post-memb, oxy-TGR, pre-chem, pre-adsor and SEWGS; nevertheless, most studies are simulations with TRL 2. Thus, only 11 published works belong to TRL 6, 5 belong to TRL 5, and 101 belong to TRL 2–4.

In order to clarify the interrelations between specific economic costs and $CO_2$ mitigation potential, both KPIs are represented in Fig. 17. Additionally, the space defining the range for each KPI in the reviewed works is highlighted. Firstly, the shape of the coloured regions allows distinguishing the most investigated technologies from those with scarce data. Specifically, the natural trend should be the lower $CO_2$ reduction, the lower specific cost. Such behaviour is only exhibited by the pre- and post-chem technologies. This is an expected result as it is the only commercial technology of carbon capture, at least in the power sector. Secondly, the two works related to CaL present very different specific costs. This difference is due to the consideration or not of different issues, i.e. Tian et. al. [66] considers retrofitting of an existing lime kiln, cutting costs and directly capturing calcination $CO_2$, while Cormos et. al. [39] considers natural gas as a fuel in the calciner instead of coal. Therefore, it can be concluded that it could be a very promising and competitive technology, but further research is needed to corroborate the results. According to the available data, oxy-TGR is expensive and the $CO_2$ mitigation potential is limited, which is because the $CO_2$ decrease accounted only takes into account oxy and TGR, and not the $CO_2$ from the carbon capture stage. Finally, further research is required for pre-adsor, pre-memb and SEWGS to generate sufficient and reliable data, as only one published data is available for each one. Also, post-memb, ChL and OtherL need further research, because no study was found that carried out a technical and economic analysis in the same paper.

The interrelation between electricity penalty and $CO_2$ mitigation

**Table 8**
Main KPIs for reviewed CC technologies.

| Method/ Technology | Source | Thermal Penalty | Electrical Penalty | Cost | $CO_2$ emission reduction | Total $CO_2$ produced [c)] | $CO_2$ purity | TRL | Year | Country | Ref. |
|---|---|---|---|---|---|---|---|---|---|---|---|
| – | – | MJt/ $kgCO_2$ | MJe/ $kgCO_2$ | $/t$CO_2$ | $kgCO_2$/tHM | $kgCO_2$/tHM | % | – | – | – | – |
| 3.1. Post combustion CC with chemical absorption | | | | | | | | | | | |
| MEA | BF flue gas | n/a | n/a | 78.5 [a)] | n/a | n/a | n/a | 2 | 2011 | Australia | [24] |
| MEA | Coke oven | n/a | n/a | 85.6 [a)] | n/a | n/a | n/a | 2 | 2011 | Australia | [24] |
| MEA | Hot Stoves, Power plant, Coke oven, Lime kiln | 3.0–6.2 | n/a | n/a | n/a | n/a | greater than95 | 2 | 2019 | Romania | [34] |
| MEA. AEEA and PZ | Hot stoves | 3.7 | n/a | n/a | n/a | n/a | n/a | 4 | 2010 | Taiwan | [25] |
| MEA | Power plant | 3.8–4.1 | n/a | n/a | n/a | n/a | n/a | 2 | 2015 | Switzerland | [29] |
| MEA | BF flue gas | n/a | 1.5 [a)] | 68 [a)] | 2.7 Mt/year | n/a | n/a | 2 | 2011 | Australia | [26] |
| MEA | BF flue gas | 4.5–6.5 | n/a | n/a | n/a | n/a | n/a | 2 | 2017 | Taiwan | [27] |
| MEA | BF flue gas | 4.2 | n/a | n/a | 1 t/day | n/a | n/a | 5 | 2011 | Japan | [28] |
| RITE-A | BF flue gas | 3.3 | n/a | n/a | 1 t/day | n/a | n/a | 5 | 2011 | Japan | [28] |
| RITE-B | BF flue gas | 3.1 | n/a | n/a | 1 t/day | n/a | n/a | 5 | 2011 | Japan | [28] |
| MEA | Power plant | 3.1 | 0.4 [a)] | n/a | n/a | n/a | n/a | 2 | 2018 | Sweden | [30] |
| MDEA | Hot Stoves, Power plant, Coke oven, Lime kiln | 2.9 | n/a | 76–80 [a)] | 1259 | 2093 | greater than95 | 2 | 2016 | Romania | [35] |
| MEA | Power plant, Hot stoves, BFG | 3.2 | n/a | 48.8 [a)] | n/a | 1700 | n/a | 2 | 2019 | Sweden | [36] |
| MEA | Power plant | 3.0 | n/a | n/a | 688 | 1625 | n/a | 2 | 2018 | Spain | [31] |
| MEA | | | n/a | n/a | 230 | 2093 | n/a | 2 | 2019 | Romania | [45] |
| MEA | Hot Stoves, Power plant | 3.4 | 0.4 [a)] | 92–204 [a)] | n/a | n/a | n/a | 2 | 2013 | Finland | [37 38] |
| MEA | Coke Oven | 4.1 | n/a | n/a | n/a | n/a | n/a | 2 | 2018 | UK | [33] |
| MDEA | Hot Stoves, Power plant, Coke oven, Lime kiln | 3.1 | n/a | 80.9 [a)] | 1259 | 2093 | n/a | 2 | 2020 | Romania | [39] |
| MEA | Power plant | 4.8 | n/a | 38.2 [a)] | 369 | 2016 | 100 | 2 | 2020 | Italy | [32] |
| MEA | Hot Stoves, Power plant | n/a | n/a | 46–90 [a)] | n/a | n/a | n/a | 2 | 2013 | Finland | [40] |
| MDEA | Coke oven, Lime kiln, BOF | n/a | n/a | n/a | n/a | n/a | 98.8 | 2 | 2021 | Romania | [41] |
| MEA | Sintering | 3.5 | 0.28 [a)] | 84.9 [a)] | n/a | n/a | n/a | 2 | 2021 | S. Korea | [42] |
| MEA | Coke oven | 3.3 | 0.28 [a)] | 69.9 [a)] | n/a | n/a | n/a | 2 | 2021 | S. Korea | [42] |
| MEA | Lime kiln | 3.3 | 0.28 [a)] | 72.2 [a)] | n/a | n/a | n/a | 2 | 2021 | S. Korea | [42] |
| MEA | Power plant | 2.9 | 0.28 [a)] | 63 [a)] | n/a | n/a | n/a | 2 | 2021 | S. Korea | [42] |
| MEA | Hot stoves | 2.9 | 0.28 [a)] | 65.6 [a)] | n/a | n/a | n/a | 2 | 2021 | S. Korea | [42] |
| MEA | – | 4.4 | 0.78 [a)] | 53.8 [a)] | 800 | 1800 | n/a | 2 | 2021 | The Nether. | [43] |
| MDEA/PZ | Hot Stoves, Power plant, Coke oven, Lime kiln | 2.3 | 0.6 [a)] | 97 [a)] | 1700 | 2200 | n/a | 2 | 2021 | The Nether. | [44] |
| 3.2. Post combustion CC with membranes | | | | | | | | | | | |
| Polaris | Power plant, Hot stoves | n/a | 0.9–1.0 [a)] | 36–47 [a)] | n/a | n/a | 99 | 6 | 2018 | USA | [59] |
| PVAm | Power plant, Hot stoves | n/a | 1.2 [a)] | | n/a | n/a | 95.5 | 3 | 2021 | Romania | [41] |
| Polyimide | Sintering | n/a | 4.4 [a)] | 252.7 [a)] | n/a | n/a | 90 | 3 | 2021 | S. Korea | [42] |
| Polyimide | Coke oven | n/a | 1.7 [a)] | 91.2 [a)] | n/a | n/a | 90 | 3 | 2021 | S. Korea | [42] |
| Polyimide | Lime kiln | n/a | 1.4 [a)] | 83.3 [a)] | n/a | n/a | 90 | 3 | 2021 | S. Korea | [42] |
| Polyimide | Power plant | n/a | 1.2 [a)] | 54 [a)] | n/a | n/a | 90 | 3 | 2021 | S. Korea | [42] |
| Polyimide | Hot stoves | n/a | 1.2 [a)] | 52.5 [a)] | n/a | n/a | 90 | 3 | 2021 | S. Korea | [42] |
| 4.1. Looping CC with calcium looping | | | | | | | | | | | |
| CaO-CaCO3 | BFG, BOFG, hot stoves, lime kilns, COG | 2.9 | 0.5 | 60.2 €/tHRC | 1023–1709 | 2090 | 95 | 2 | 2016 | Romania | [35] |
| CaO-CaCO3 | Hot stoves, BFG, BOFG, COG, lime kiln | 2.7 | 0.1 [a)] | N.A. | 1337–1567 | 2090 | 95 | 2 | 2019 | Romania | [34] |
| CaO-CaCO3 | Hot stoves, BFG, BOFG, COG, lime kiln | n.a. | 0.6 | 73.8 [a)] | 1450 | 2090 | 95 | 2 | 2020 | Romania | [39] |

(*continued on next page*)

**Table 8** (*continued*)

| Method/ Technology | Source | Thermal Penalty | Electrical Penalty | Cost | $CO_2$ emission reduction | Total $CO_2$ produced [c)] | $CO_2$ purity | TRL | Year | Country | Ref. |
|---|---|---|---|---|---|---|---|---|---|---|---|
| – | – | MJt/ $kgCO_2$ | MJe/ $kgCO_2$ | $/$tCO_2$ | $kgCO_2$/tHM | $kgCO_2$/tHM | % | – | – | – | – |
| 3.1. Post combustion CC with chemical absorption | | | | | | | | | | | |
| CaO-CaCO3 | COG | 4.2–5.6 | n.a. | n.a. | 68071 t/year | 68400 t/ year | high-purity | 3 | 2017 | China | [62] |
| CaO-CaCO3 | BFG | n.a. | n.a. | n.a. | n.a. | n.a. | high-purity | 3 | 2014 | Israel | [63] |
| CaO-CaCO3 | BFG, COG | 2.7 | 2.5 [a)] | 13–17 [a)] | 1422 | 1800 | high-purity | 3 | 2018 | China – UK | [66] |
| 4.2. Looping CC with chemical looping | | | | | | | | | | | |
| Fe2O3-FeO | COG | n/a | n/a | n/a | n/a | n/a | n/a | 2 | 2018 | China | [81] |
| Fe2O3-FeO | Sinter plant | n/a | n/a | n/a | n/a | n/a | n/a | 3 | 2020 | UK | [80] |
| Fe2O3-FeO | COG | n/a | n/a | n/a | 1771–2280 kmol/h | n/a | 90 | 4 | 2018 | China | [79] |
| NiO-Ni | COG | n/a | n/a | n/a | n/a | n/a | n/a | 4 | 2018 | China | [76] |
| 4.3. Looping CC with other looping processes | | | | | | | | | | | |
| Ca-Cu | BFG | 1.4–1.7 | n/a | n/a | n/a | n/a | 57–99.9 | 4 | 2020 | Spain | [91] |
| Ca-Cu | | n/a | n/a | n/a | n/a | n/a | n/a | | 2019 | Spain | [90] |
| Ca-Cu. (COG) | BFG, COG | 2.6 | n/a | n/a | 502 | 1619 | 97.4 | 4 | 2018 | Spain | [31] |
| Ca-Cu. (COG + NG) | BFG, COG | 4.3 | n/a | n/a | 1618 | 1619 | 97.4 | 4 | 2018 | Spain | [31] |
| CaCO3/FeO-CaO/Fe2O3 | BFG | n/a | n/a | n/a | n/a | n/a | n/a | 4 | 2016 | China | [92] |
| MgO/MoO3-MgCO3/ MoS2 | BFG | n/a | n/a | n/a | n/a | n/a | n/a | 3 | 2020 | China | [94] |
| Ca-Cu + SEWGS | BFG, BOFG, COG | n/a | n/a | n/a | 617 | 1922 | 96.8 | 5 | 2017 | Spain | [93] |
| 5. CC with Oxy-blast furnace with TGR | | | | | | | | | | | |
| Oxy-BF + TGR | BFG | 0.3 | 5.6 | 50–90 | 462[b)] | 1244 | n/a | 2 | 2014 | Finland | [106 146] |
| Oxy-BF + TGR | BFG | n/a | n/a | n/a | 550[b)] | 1320 | n/a | 2 | 2004 | Japan | [108] |
| Oxy-BF + TGR | BFG | 0.8 | 1.7 | n/a | 273[b)] | 1367 | n/a | 4 | 2015–2016 | Japan | [100109 111] |
| Oxy-BF + TGR + PtG | BFG | n/a | n/a | n/a | 176[b)] | 1330 | n/a | 2 | 2021 | Spain | [121] |
| Oxy-BF + TGR | BFG | n/a | 0.6 | n/a | 374[b)] | 1338 | n/a | 2 | 2004 | Korea | [182] |
| Oxy-BF + TGR | BFG | n/a | 1.4 | 90 | 420[b)] | 2420 | n/a | 2 | 2013 | Australia | [102] |
| Oxy-BF + TGR | BFG | n/a | 0.98 | n/a | 218[b)] | 1377 | n/a | 2 | 2016 | China | [112] |
| Oxy-BF + TGR | BFG | n/a | n/a | n/a | 489[b)] | 1429 | n/a | 2 | 2016 | China | [103] |
| Oxy-BF + TGR | BFG | −13.4 | 8.1 | n/a | 240[b)] | 2066 | n/a | 2 | 2015 | China | [119] |
| Oxy-BF + TGR | BFG | n/a | n/a | n/a | n/a | n/a | n/a | 2 | 2019 | Japan | [161] |
| Oxy-BF + TGR | BFG | n/a | n/a | n/a | 181[b)] | 1267 | n/a | 2 | 2010 | China | [127] |
| Oxy-BF + TGR | BFG | n/a | n/a | n/a | n/a | n/a | n/a | 4 | 2018 | China | [139] |
| Oxy-fuel coke oven | COG | n/a | n/a | n/a | n/a | n/a | n/a | 3 | 2020 | China | [183] |
| Oxy-BF + TGR | BFG | n/a | n/a | n/a | 184 | 1397 | n/a | 2 | 2020 | China | [184] |
| Oxy-BF + TGR | BFG | n/a | n/a | n/a | 167[b)] | 1450 | n/a | 2 | 2010 | Finland | [104] |
| Oxy-BF + TGR | BFG | n/a | n/a | 58.5 | 390 | 1600 | n/a | 2 | 2010 | Finland | [105] |
| Oxy-BF + TGR | BFG | n/a | n/a | n/a | 100 | n/a | n/a | 2 | 2015 | Finland | [114] |
| Oxy-BF + TGR | BFG | n/a | n/a | n/a | 367[b)] | 1547 | n/a | 2 | 2015 | India | [110] |
| Oxy-BF + TGR | BFG | n/a | n/a | n/a | 401[b)] | 1670 | n/a | 6 | 2009 | Sweden | [169131 115] |
| Oxy-BF + TGR | BFG | n/a | n/a | n/a | 506[b)] | 1701 | n/a | 2 | 2017 | China | [129] |

(*continued on next page*)

**Table 8** (*continued*)

| Method/ Technology | Source | Thermal Penalty | Electrical Penalty | Cost | $CO_2$ emission reduction | Total $CO_2$ produced [c)] | $CO_2$ purity | TRL | Year | Country | Ref. |
|---|---|---|---|---|---|---|---|---|---|---|---|
| – | – | MJt/ $kgCO_2$ | MJe/ $kgCO_2$ | $/t$CO_2$ | $kgCO_2$/tHM | $kgCO_2$/tHM | % | – | – | – | – |
| 3.1. Post combustion CC with chemical absorption | | | | | | | | | | | |
| Oxy-BF + TGR | BFG | n/a | n/a | n/a | 166[b)] | 1305 | n/a | 2 | 2016 | China | [128] |
| Oxy-BF + TGR | BFG | n/a | n/a | n/a | 159[b)] | 1330 | n/a | 2 | 2017 | China | [130] |
| Oxy-BF + TGR | BFG | n/a | n/a | n/a | 279[b)] | 1305 | n/a | 2 | 2017 | China | [185] |
| Oxy-BF + TGR | BFG | n/a | n/a | n/a | −7.5 [b)] | 1436 | n/a | 2 | 2004 | Japan | [137] |
| Oxy-BF + TGR | BFG | n/a | n/a | n/a | −27[b)] | 1408 | n/a | 2 | 2005 | Japan | [116] |
| Oxy-BF + TGR | BFG | n/a | n/a | n/a | 247[b)] | 1379 | n/a | 2 | 2010 | Japan | [186] |
| 6.1. Pre combustion CC with chemical absorption | | | | | | | | | | | |
| TGR-BF + PZ | BFG | 2.4 | 0.2 [a)] | 40.6 [a)] | 777 | 1268 | 95 | 2 | 2018 | Korea | [160] |
| unspecified | BFG | 2 | n/a | n/a | n/a | n/a | 90 | 6 | 2016 | Japan | [165] |
| MEA | BFG, BOFG, COG | 3.1 | 0.4 [a)] | 62 [a)] | 130 t/h | 141 t/h | 99 | 2 | 2015 | Korea | [158] |
| NH3 | BFG | 2.5 | n/a | n/a | 9.3 t/day | 10.3 t/day | 99 | 6 | 2014 | Korea | [155] |
| TGR-BF + MEA | BFG | n/a | 1.4–1.5 [a)] | 86–97 [a)] | 520–640 | n/a | n/a | 2 | 2013 | Australia | [102] |
| ULCOS-MDEA | BFG | 3.2 | 0.61 [a)] | n/a | n/a | n/a | n/a | – | 2010 | France | [163] |
| MEA | BFG | n/a | n/a | n/a | 564 | n/a | n/a | 2 | 2019 | Sweden | [153] |
| MEA | BFG | 3 | 0.4 [a)] | n/a | n/a | n/a | n/a | 2 | 2018 | Sweden | [30] |
| unspecified | BFG | 2 | n/a | n/a | n/a | n/a | n/a | 6 | 2016 | Japan | [107] |
| MEA | BFG, BOFG | 1.3 | 1.2 [a)] | n/a | 673 | 961 | n/a | 2 | 2016 | Finland | [159] |
| MDEA | BFG, BOFG, COG | 2.9 | n/a | n/a | 1192 g/kWel | 1339 g/ kWhe | 98.6 | 2 | 2015 | Italy | [29] |
| MEA | BFG | 4.4 | n/a | 68 [a)] | 1048 | 1188 | n/a | 2 | 2011 | Australia | [26] |
| MEA, MDEA/ PZ and AMP | BFG | 2.2–2.4 | n/a | n/a | n/a | n/a | 90–97 | 2 | 2007 | Norway | [151] |
| 6.2. Pre combustion CC with adsorption | | | | | | | | | | | |
| TGR + VPSA | OBFG | n/a | 0.4 [a)] | n/a | 860 | 1650 | n/a | 2 | 2016 | Malaysia | [101] |
| PSA | BFG | n/a | n/a | n/a | 3 t/day | 3.8 t/day | 99.5 | 6 | 2016 | Japan | [165] |
| PSA | BFG, BOFG, COG | n/a | 1.0 [a)] | 38 [a)] | 130 t/h | 141 t/h | 91.2 | 2 | 2015 | S. Korea | [158] |
| TGR-VPSA | BFG | n/a | 0.9–1.0 [a)] | 59–60 [a)] | 520–580 | n/a | n/a | 2 | 2013 | Australia | [102] |
| VPSA | BFG | n/a | 1.1 [a)] | n/a | n/a | n/a | n/a | 2 | 2010 | France | [163] |
| TGR + VPSA | OBFG | n/a | 0.9 | n/a | 2.7 Mt/a | 3.2 Mt/a | 92 | 2 | 2014 | Finland | [106] |
| TGR + VPSA | BFG | n/a | n/a | n/a | 1794 | 1900 | 87.7 | 2 | 2013 | India | [142] |
| PSA | BFG | n/a | 0.4 [a)] | n/a | 6.3 t/day | 7.8 t/day | n/a | 5 | 2013 | Japan | [187] |
| TGR + VPSA | BFG | n/a | n/a | n/a | 1270 | 1671 | n/a | 6 | 2009 | Sweden | [131] |
| TGR + VPSA | OBFG | n/a | n/a | n/a | n/a | n/a | n/a | 2 | 2017 | China | [130] |
| TGR + VPSA | OBFG | n/a | 2.7 [a)] | n/a | 1540 | 2080 | n/a | 2 | 2017 | China | [119] |
| TGR + VPSA | OBFG | n/a | 10.4 kJ/ thm | n/a | 701 | 1485 | n/a | 2 | 2016 | China | [103] |
| TGR + VPSA | OBFG | n/a | 0.4 [a)] | n/a | 860 | 1650 | | 6 | 2016 | Malaysia | [11] |
| TGR + VPSA | BFG | n/a | n/a | n/a | 1200 | n/a | 79.9 | 2 | 2016 | Japan | [111] |
| TGR + VPSA | OBFG | n/a | n/a | n/a | 906–1117 | 1313 | n/a | 2 | 2016 | China | [128] |
| TGR + VPSA | OBFG | n/a | n/a | n/a | 607 | n/a | 79.9 | 2 | 2015 | India | [110] |
| TGR + VPSA | BFG | n/a | n/a | n/a | n/a | n/a | n/a | 6 | 2009 | Sweden | [169] |
| 6.3. Pre combustion CC with membranes | | | | | | | | | | | |
| 2-stage memb. | BFG | n/a | n/a | 32.5–50.6 | n/a | n/a | 90–98 | 2 | 2018 | France | [162] |
| TGR + 2-stage memb. | BFG | n/a | 1.0 [a)] | 34.4 [a)] | 842 | 1268 | 95 | 2 | 2018 | Korea | [160] |
| 2-stage memb. | BFG | n/a | n/a | 32.5–50.6 | n/a | n/a | n/a | 2 | 2017 | France | [173] |
| 2-stage memb. | BFG | n/a | 0.9 [a)] | 17.5 [a)] | 407 t/h | 420 t/h | 90 | 3 | 2007 | Norway | [174] |
| 1-stage memb. | BOFG | n/a | n/a | n/a | n/a | n/a | 55 | 4 | 2022 | Korea | [175] |
| membrane + cryogenic | BFG | n/a | 1.6 [a)] | 28.8 [a)] | n/a | n/a | 97.1 | 2 | 2022 | China | [178] |
| 6.4. Pre combustion CC with SEWGS | | | | | | | | | | | |

(*continued on next page*)

**Table 8** (*continued*)

| Method/ Technology | Source | Thermal Penalty | Electrical Penalty | Cost | $CO_2$ emission reduction | Total $CO_2$ produced [c)] | $CO_2$ purity | TRL | Year | Country | Ref. |
|---|---|---|---|---|---|---|---|---|---|---|---|
| – | – | MJt/ $kgCO_2$ | MJe/ $kgCO_2$ | $/t$CO_2$ | $kgCO_2$/tHM | $kgCO_2$/tHM | % | – | – | – | – |
| 3.1. Post combustion CC with chemical absorption | | | | | | | | | | | |
| SEWGS | BFG | n/a | n/a | n/a | 14 t/day | n/a | n/a | 6 | 2018 | The Nether. | [179] |
| WGS + SEWGS | BFG, BOFG, COG | n/a | 1.9 [a)] | 36.4 [a)] | 759 | 2016 | 97.6–99.6 | 2 | 2020 | Italy | [32] |
| SEWGS w/ saturator | BFG, BOFG, COG | n/a | n/a | n/a | 833 | 1422 | n/a | 2 | 2019 | Romania | [45] |
| SEWGS w/ saturator | BFG, BOFG, COG | n/a | 2.9 [a)] | n/a | 149 g/kWhe | 1339 g/ kWhe | 98.85 | 2 | 2015 | Italy | [29] |
| SEWGS + Ca-Cu | BFG, BOFG, COG | n/a | n/a | n/a | 617 | 1922 | 96.8 | 2 | 2017 | Spain | [93] |

[a)] Electricity penalty and cost includes $CO_2$ compression to 100–150 bar.
[b)] It is only accounted the decrease of $CO_2$ because of injecting TGR and making oxy-blast furnace, and not the decrease that would be achieved by storing underground the pure $CO_2$ from the CC stage.
[c)] Typical $CO_2$ emissions in an integrated steel plant are 1900–2200 $kgCO_2$/tHM. When lower than this value, the total $CO_2$ produced in the industry refers to the steel plant without the power plant, or refers only to the blast furnace.

potential is represented in Fig. 18, where the space representing the rage of each KPI values in the reviewed works is highlighted for each category of technologies. The highest electricity penalty with lower $CO_2$ emission reduction is obtained with oxy-TGR, but as noted above, the $CO_2$ decrease depends on how it is measured, and the high electricity penalty is due to the high demand of pure oxygen (high ASU consumption). For post-chem, CaL, pre-chem and pre-adsor, three studies per technology were identified that analysed both KPIs. Post-chem and pre-adsor have a wide range of $CO_2$ reduction while maintaining the electricity penalty at reasonable levels. CaL and pre-chem have less sparse range of values obtaining similar electricity penalty, with the former achieving higher $CO_2$ emission reduction. Finally, the technologies with scarce data are pre-memb and SEWGS, while for post-memb, ChL and OtherL no scientific studies analysing both KPIs were identified, which highlights the necessity for further research in this field.

With the aim of highlighting the most studied or novel technologies, Fig. 19 shows the number of scientific papers organised by year and technology. Oxy-TGR is the most studied technology, with 30 published papers, with the first one from 2004. Other well studied and known technologies are post-chem, pre-chem and pre-adsor, with 22, 13 and 17 published papers, respectively, starting between 2007 and 2010. Among the most novel technologies, pre- and post-memb, SEWGS, CaL, ChL and OtherL can be found. Investigation of these novel technologies in the I&S industry began between 2014 and 2016, and therefore, none of them have more than 6 published papers.

For a rapid development of all CC technologies, the high costs and the availability of underground storage are the main bottlenecks. For new promising technologies, such as membranes, CaL or otherL, the low TRL and the lack of pilot plants can also be considered as a bottleneck, which slow down the development of these technologies. Besides, another technical limitation appears for pre-combustion CC technologies. These technologies capture $CO_2$ from energetic streams such as BFG, COG and BOFG, which also have significant amounts of CO and $CH_4$. The two latter components will be combusted, converted to $CO_2$ and emitted to the atmosphere. This means that this pre-combustion technologies will never be able to capture all the $CO_2$, and a significant amount of it will be released to the atmosphere. However, this problem can be partially solved if the CO is injected to the BF (i.e., TGR or hot reducing gases) as a reducing agent, as it will be oxidised to $CO_2$ and captured from the BFG in the pre-combustion CC stage. This partial solution is limited by the amount of CO that can be injected in the BF. Other possible solution to this problem is implementing a water gas shift (WGS) prior the pre-combustion CC stage, shifting all the CO to $CO_2$ and generating additional $H_2$. However, this solution arises other economic and technical limitations regarding the use of pure $H_2$, such as different combustion behaviour, high volatility, and higher compression energy.

## 8. Conclusions

In this article, we have presented the first systematic review of the state of the art related to carbon capture (CC) technologies investigated to date for the blast furnace-basic oxygen furnace route of the I&S industry, in terms of energy penalisation, economic cost, efficiency, TRL and volume of $CO_2$ captured. These technologies can capture $CO_2$ from different streams, producing a concentrated stream of $CO_2$ that can subsequently be stored or used.

Based on a systematic review procedure, 120 research articles were identified and reviewed. The reported carbon capture technologies were classified into four different groups: post-combustion, looping cycles, oxy-combustion and pre-combustion. Each group of technologies was further divided according to the specific CC technology applied: chemical absorption, physical adsorption, membranes, calcium looping, chemical looping and sorption enhanced water gas shift (SEWGS). For oxy-combustion CC technology, only oxy-blast furnace technology was found to be reported (i.e. oxy-combustion of BOFG or other gases were not found in literature, in relation to CC technology). When the capture is allocated in streams with combustible species such as BFG, BOFG or COG, it is considered a pre-combustion system, while when applied to flue gases, it is a post-combustion system. No study related to pre-combustion CC systems was identified for the solid fuels employed in the I&S industry (i.e., coal and coke).

An in-depth review of each carbon capture (CC) technology was carried out individually, as well as a detailed comparison of the technologies considering 6 KPIs: thermal penalty ($MJ/kgCO_2$), electrical penalty ($MJ/kgCO_2$), economic cost ($/t$CO_2$), $CO_2$ emission reduction (kg/tHM), $CO_2$ purity (%) and TRL.

Calcium looping (CaL), precombustion CC by adsorption (pre-adsor) and postcombustion CC by chemical absorption (post-chem) are the three technologies that have lower electricity penalty when capturing high amounts of $CO_2$. CaL technology achieves the highest $CO_2$ emission reduction at a lower cost, but other technologies such as post-chem, other looping processes (otherL) and pre-adsor achieve similar carbon capture rates. Precombustion CC by membranes (pre-memb) has the lowest economic costs, but with lower potential of carbon capture to date.

None of the technologies investigated for carbon capture are yet commercially available in the I&S industry, but some have achieved TRL 6, including postcombustion CC by membranes (post-memb), oxy-blast furnace with top gas recycling (oxy-TGR), precombustion CC by chemical absorption (pre-chem), pre-adsor and sorption enhanced water gas

shift (SEWGS). The latter stands out as a promising alternative because, despite its high penalty, it has a low cost and very high $CO_2$ purity.

In the I&S industry, as the main $CO_2$ streams have a similar $CO_2$ content (i.e., 15–28 %vol) and a similar pressure (atmospheric to 2 bar), it is not of significant importance where the CC stage is implemented, the capture will behave similarly. Taking into account the 6 KPIs analysed, pre-adsor is found to be the most promising technology for capturing $CO_2$ in the I&S industry, according to its high TRL and $CO_2$ emission reduction at reasonable cost and penalty. The only drawback of this technology is the level of $CO_2$ purity (88 % on an average), that is lower than for other technologies.

There are substantial opportunities for further investigation to characterise the actual potential of those technologies for decarbonisation of the I&S industry. Future research must reaffirm technologies with demonstrated positive outcomes such as pre-adsor, and also focus on new promising technologies such as membranes, CaL or otherL. Furthermore, the currently high costs of this kind of systems must be tackled, and there is a necessity to optimize the thermal and electrical penalties associated with carbon capture.

## Declaration of Competing Interest

The authors declare that they have no known competing financial interests or personal relationships that could have appeared to influence the work reported in this paper.

## Data availability

Data will be made available on request.

*Acknowledgements*

The work presented in this paper has been supported by both the University of Zaragoza under the project UZ2020-TEC-06 and Khalifa University project CIRA-2020-080. This work has also received funding from the European Union's Horizon 2020 research and innovation program under the Marie Sklodowska-Curie grant agreement no. 887077. This work is part of the R&D project PID2021-126164OB-I00, funded by MCIN/AEI/10.13039/501100011033/ and by the "ERDF A way of making Europe".

## *Annex A. Main KPIs for reviewed CC technologies*

The KPI data (i.e., thermal and electrical penalties ($MJ/kgCO_2$), economic cost ($/tCO_2$), $CO_2$ emission reduction ($kgCO_2/tHM$), $CO_2$ purity (%) and TRL) extracted from the 120 studies reviewed and analysed in Section 7, is compiled in Table A for each technology, namely post combustion CC with either chemical absorption or membranes, Looping CC with calcium, chemical or other looping process, CC with oxy-blast furnace and TGR, and pre combustion CC with either chemical absorption, adsorption, membranes or SEWGS.

## References

[1] "European Commission." https://energy.ec.europa.eu/index_es (accessed Apr. 26, 2022).
[2] "International Energy Agency, Iron and Steel Technology Roadmap, 2020." https://www.iea.org/reports/iron-and-steel-technology-roadmap (accessed Apr. 26, 2022).
[3] Huitu K, Helle H, Helle M, Kekkonen M, Saxén H. Optimization of steelmaking using fastmet direct reduced iron in the blast furnace. ISIJ Int 2013;53(12): 2038–46. https://doi.org/10.2355/isijinternational.53.2038.
[4] Larrea and García-Berezo. Economía Industrial 406 (2017) 139-150.
[5] "Midrex Technologies, 2022. The Midrex (R) Process." https://www.midrex.com/technology/midrex-process/(accessed May 10, 2022).
[6] "Energiron, DRI technology by Tenova and Danieli." https://www.energiron.com/(accessed Jun. 08, 2022).
[7] Ariyama T, Takahashi K, Kawashiri Y, Nouchi T. Diversification of the Ironmaking Process Toward the Long-Term Global Goal for Carbon Dioxide Mitigation. J Sustain Metall 2019;5(3):276–94. https://doi.org/10.1007/s40831-019-00219-9.
[8] He H, Guan H, Zhu X, Lee H. Assessment on the energy flow and carbon emissions of integrated steelmaking plants. Energy Rep 2017;3:29–36. https://doi.org/10.1016/j.egyr.2017.01.001.
[9] J. von Scheele, "Decarbonization of Ironmaking," 2021.
[10] Deerberg G, Oles M, Schlögl R. The Project Carbon2Chem®. Chem-Ing-Tech 2018;90(10):1365–8. https://doi.org/10.1002/cite.201800060.
[11] Abdul Quader M, Ahmed S, Dawal SZ, Nukman Y. Present needs, recent progress and future trends of energy-efficient Ultra-Low Carbon Dioxide (CO2) Steelmaking (ULCOS) program. Renew Sustain Energy Rev Mar. 2016;55:537–49. https://doi.org/10.1016/J.RSER.2015.10.101.
[12] X. L. Zhou and Z. N. Du, "The introduction of COREX process development," *Adv. Mater. Res.*, vol. 774–776, no. November 1995, pp. 1430–1433, 2013, doi: 10.4028/www.scientific.net/AMR.774-776.1430.
[13] N. Goodman, "Operation of the First HIsmelt Plant in China," 2017. [Online]. Available: https://www.researchgate.net/publication/298065259_Hismelt_Plant_Ramp-Up.
[14] Yi SH, Choi ME, Kim DH, Ko CK, Il Park W, Kim SY. FINEX® as an environmentally sustainable ironmaking process. Ironmak Steelmak 2019;46(7): 625–31. https://doi.org/10.1080/03019233.2019.1641682.
[15] Tonomura S. Outline of course 50. Energy Procedia 2013;37:7160–7. https://doi.org/10.1016/j.egypro.2013.06.653.
[16] J. Perpiñán, M. Bailera, B. Peña, L. M. Romeo, and V. Eveloy, "Technical and economic assessment of iron and steelmaking decarbonisation via power to gas and amine scrubbing," 2022, [Online]. Available: Under Revision.
[17] K. He and L. Wang, "A review of energy use and energy-efficient technologies for the iron and steel industry," *Renew. Sustain. Energy Rev.*, vol. 70, no. September 2016, pp. 1022–1039, 2017, doi: 10.1016/j.rser.2016.12.007.
[18] Leeson D, Mac Dowell N, Shah N, Petit C, Fennell PS. A Techno-economic analysis and systematic review of carbon capture and storage (CCS) applied to the iron and steel, cement, oil refining and pulp and paper industries, as well as other high purity sources. Int J Greenh Gas Control 2017;61:71–84. https://doi.org/10.1016/j.ijggc.2017.03.020.
[19] Zhao J, Zuo H, Wang Y, Wang J, Xue Q. Review of green and low-carbon ironmaking technology. Ironmak Steelmak 2020;47(3):296–306. https://doi.org/10.1080/03019233.2019.1639029.
[20] Fan Z, Friedmann SJ. Review Low-carbon production of iron and steel: Technology options, economic assessment, and policy. Joule 2021:1–34. https://doi.org/10.1016/j.joule.2021.02.018.
[21] Quader MA, Ahmed S, Ghazilla RAR, Ahmed S, Dahari M. A comprehensive review on energy efficient CO2 breakthrough technologies for sustainable green iron and steel manufacturing. Renew Sustain Energy Rev 2015;50:594–614. https://doi.org/10.1016/j.rser.2015.05.026.
[22] "European Commission. Research and innovation. Horizon 2020. Work programme 2014-2015, general annexes." https://ec.europa.eu/research/participants/data/ref/h2020/wp/2014_2015/annexes/h2020-wp1415-annex-g-trl_en.pdf (accessed Nov. 15, 2022).
[23] W. Y. Hong, "A techno-economic review on carbon capture, utilisation and storage systems for achieving a net-zero CO2 emissions future," *Carbon Capture Sci. Technol.*, vol. 3, no. December 2021, p. 100044, 2022, doi: 10.1016/j.ccst.2022.100044.
[24] Wiley DE, Ho MT, Bustamante A. Assessment of opportunities for CO2 capture at iron and steel mills: An Australian perspective. Energy Procedia 2011;4:2654–61. https://doi.org/10.1016/j.egypro.2011.02.165.
[25] Cheng H, Shen J, Tan C. CO2 capture from hot stove gas in steel making process. Int J Greenh Gas Control 2010;4(3):525–31. https://doi.org/10.1016/j.ijggc.2009.12.006.
[26] Ho MT, Allinson GW, Wiley DE. Comparison of MEA capture cost for low CO2 emissions sources in Australia. Int J Greenh Gas Control 2011;5(1):49–60. https://doi.org/10.1016/j.ijggc.2010.06.004.
[27] Chamchan N, et al. Comparison of rotating packed bed and packed bed absorber in pilot plant and model simulation for CO2 capture. J Taiwan Inst Chem Eng 2017;73:20–6. https://doi.org/10.1016/j.jtice.2016.08.046.
[28] Goto K, Okabe H, Chowdhury FA, Shimizu S, Fujioka Y, Onoda M. Development of novel absorbents for CO2 capture from blast furnace gas. Int J Greenh Gas Control 2011;5(5):1214–9. https://doi.org/10.1016/j.ijggc.2011.06.006.
[29] Gazzani M, Romano MC, Manzolini G. CO2 capture in integrated steelworks by commercial-ready technologies and SEWGS process. Int J Greenh Gas Control 2015;41:249–67. https://doi.org/10.1016/j.ijggc.2015.07.012.
[30] M. Sundqvist, M. Biermann, F. Normann, M. Larsson, and L. Nilsson, "Evaluation of low and high level integration options for carbon capture at an integrated iron and steel mill," *Int. J. Greenh. Gas Control*, vol. 77, no. July 2017, pp. 27–36, 2018, doi: 10.1016/j.ijggc.2018.07.008.
[31] Martínez I, Fernández JR, Abanades JC, Romano MC. Integration of a fluidised bed Ca–Cu chemical looping process in a steel mill. Energy 2018;163:570–84. https://doi.org/10.1016/j.energy.2018.08.123.
[32] G. Manzolini, A. Giuffrida, P. D. Cobden, H. A. J. van Dijk, F. Ruggeri, and F. Consonni, "Techno-economic assessment of SEWGS technology when applied to integrated steel-plant for CO2 emission mitigation," *Int. J. Greenh. Gas Control*, vol. 94, no. February 2019, p. 102935, 2020, doi: 10.1016/j.ijggc.2019.102935.
[33] Oko E, Zacchello B, Wang M, Fethi A. Process analysis and economic evaluation of mixed aqueous ionic liquid and monoethanolamine (MEA) solvent for CO2 capture from a coke oven plant. Greenh Gases Sci Technol 2018;8(4):686–700. https://doi.org/10.1002/ghg.1772.

[34] Chisalita DA, Petrescu L, Cobden P, H. A. J. (Eric. van Dijk, A. M. Cormos, and C. C. Cormos,. Assessing the environmental impact of an integrated steel mill with post-combustion CO2 capture and storage using the LCA methodology. J Clean Prod 2019;211:1015–25. https://doi.org/10.1016/j.jclepro.2018.11.256.

[35] Cormos CC. Evaluation of reactive absorption and adsorption systems for post-combustion CO2 capture applied to iron and steel industry. Appl Therm Eng 2016;105:56–64. https://doi.org/10.1016/j.applthermaleng.2016.05.149.

[36] Biermann M, Ali H, Sundqvist M, Larsson M, Normann F, Johnsson F. Excess heat-driven carbon capture at an integrated steel mill – Considerations for capture cost optimization. Int J Greenh Gas Control 2019;vol. 91, no. September:102833. https://doi.org/10.1016/j.ijggc.2019.102833.

[37] Arasto A, Tsupari E, Kärki J, Pisilä E, Sorsamäki L. Post-combustion capture of CO2 at an integrated steel mill - Part I: Technical concept analysis. Int J Greenh Gas Control 2013;16:271–7. https://doi.org/10.1016/j.ijggc.2012.08.018.

[38] Tsupari E, Kärki J, Arasto A, Pisilä E. Post-combustion capture of CO2 at an integrated steel mill - Part II: Economic feasibility. Int J Greenh Gas Control 2013;16:278–86. https://doi.org/10.1016/j.ijggc.2012.08.017.

[39] Cormos A-M, Dragan S, Petrescu L, Sandu V, Cormos C-C. Techno-Economic and Environmental Evaluations of Decarbonized Fossil-Intensive Industrial Processes by Reactive Absorption & Adsorption CO2 Capture Systems. Energies 2020;no. 13. https://doi.org/10.3390/en13051268.

[40] Arasto A, Tsupari E, Kärki J, Sihvonen M, Lilja J. Costs and potential of carbon capture and storage at an integrated steel mill. Energy Procedia 2013;37:7117–24. https://doi.org/10.1016/j.egypro.2013.06.648.

[41] Luca AV, Petrescu L. Membrane technology applied to steel production: Investigation based on process modelling and environmental tools. J Clean Prod 2021;294:126256. https://doi.org/10.1016/j.jclepro.2021.126256.

[42] Yun S, Jang MG, Kim JK. Techno-economic assessment and comparison of absorption and membrane CO2 capture processes for iron and steel industry. Energy 2021;229:120778. https://doi.org/10.1016/j.energy.2021.120778.

[43] F. Yang, J. C. Meerman, and A. P. C. Faaij, "Carbon capture and biomass in industry: A techno-economic analysis and comparison of negative emission options," *Renew. Sustain. Energy Rev.*, vol. 144, no. June 2020, p. 111028, 2021, doi: 10.1016/j.rser.2021.111028.

[44] Yang F, Meerman H, Faaij A. Harmonized comparison of virgin steel production using biomass with carbon capture and storage for negative emissions. Int J Greenh Gas Control 2021;112(April). https://doi.org/10.1016/j.ijggc.2021.103519.

[45] Petrescu L, Chisalita DA, Cormos CC, Manzolini G, Cobden P, van Dijk HAJ. Life cycle assessment of SEWGS technology applied to integrated steel plants. Sustain 2019;11(7):pp. https://doi.org/10.3390/su11071825.

[46] D. Kearns, H. Liu, and C. Consoli, "Technology Readiness and Costs of CCS - Global CCS Institute," *Glob. CCS Insitute*, no. March, p. 50, 2021, [Online]. Available: https://www.globalccsinstitute.com/wp-content/uploads/2021/03/Technology-Readiness-and-Costs-for-CCS-2021-1.pdf.

[47] Sendeco2, "sendeco2." https://www.sendeco2.com/es/precios-co2%0A (accessed Mar. 02, 2022).

[48] Han Y, Ho WSW. Recent advances in polymeric membranes for CO2 capture. Chinese J Chem Eng 2018;26(11):2238–54. https://doi.org/10.1016/j.cjche.2018.07.010.

[49] Lei L, Lindbråthen A, Hillestad M, Sandru M, Favvas EP, He X. Screening Cellulose Spinning Parameters for Fabrication of Novel Carbon Hollow Fiber Membranes for Gas Separation. Ind Eng Chem Res 2019;58(29):13330–9. https://doi.org/10.1021/acs.iecr.9b02480.

[50] Cao Y, Zhang K, Sanyal O, Koros WJ. Carbon Molecular Sieve Membrane Preparation by Economical Coating and Pyrolysis of Porous Polymer Hollow Fibers. Angew Chemie - Int Ed 2019;58(35):12149–53. https://doi.org/10.1002/anie.201906653.

[51] Elsaidi SK, et al. Custom Formulation of Multicomponent Mixed-Matrix Membranes for Efficient Post-combustion Carbon Capture. Cell Reports Phys Sci 2020;1(7):100113. https://doi.org/10.1016/j.xcrp.2020.100113.

[52] Cacho-Bailo F, et al. On the molecular mechanisms for the H2/CO2 separation performance of zeolite imidazolate framework two-layered membranes. Chem Sci 2017;8(1):325–33. https://doi.org/10.1039/c6sc02411d.

[53] Huang A, Dou W, Caro J. Steam-stable zeolitic imidazolate framework ZIF-90 membrane with hydrogen selectivity through covalent functionalization. J Am Chem Soc 2010;132(44):15562–4. https://doi.org/10.1021/ja108774v.

[54] Kim HW, et al. Selective Gas Transport Through Few-Layered Graphene and Graphene Oxide Membranes. Science 2013;80-.), 342(October:91–5.

[55] Lei L, Bai L, Lindbråthen A, Pan F, Zhang X, He X. Carbon membranes for CO2 removal: Status and perspectives from materials to processes. Chem Eng J 2020;vol. 401, no. June:126084. https://doi.org/10.1016/j.cej.2020.126084.

[56] Freeman BD. Basis of permeability/selectivity tradeoff relations in polymeric gas separation membranes. Macromolecules 1999;32(2):375–80. https://doi.org/10.1021/ma9814548.

[57] N. McQueen, C. M. Woodall, P. Psarras, and J. Wilcox, "Chapter 11: CCS in the iron and steel industry," in *RSC Energy and Environment Series*, vol. 2020-Janua, no. 26, 2020, pp. 353–391. doi: 10.1039/9781788012744-00353.

[58] Hägg MB, Lindbråthen A, He X, Nodeland SG, Cantero T. Pilot Demonstration-reporting on CO2 Capture from a Cement Plant Using Hollow Fiber Process. Energy Procedia 2017;114(1876):6150–65. https://doi.org/10.1016/j.egypro.2017.03.1752.

[59] Baker RW, Freeman B, Kniep J, Huang YI, Merkel TC. CO2 Capture from Cement Plants and Steel Mills Using Membranes. Ind Eng Chem Res 2018;57(47):15963–70. https://doi.org/10.1021/acs.iecr.8b02574.

[60] White LS, Amo KD, Wu T, Merkel TC. Extended field trials of Polaris sweep modules for carbon capture. J Memb Sci 2017;542(August):217–25. https://doi.org/10.1016/j.memsci.2017.08.017.

[61] Global CCS Institute Toshiba, "Applying carbon capture and storage to a Chinese steel plant." 2015.

[62] Xie H, Yu Q, Zhang Y, Zhang J, Liu J, Qin Q. New process for hydrogen production from raw coke oven gas via sorption-enhanced steam reforming: Thermodynamic analysis. Int J Hydrogen Energy 2017;42(5):2914–23. https://doi.org/10.1016/j.ijhydene.2016.12.046.

[63] Halmann M, Steinfeld A. Reforming of blast furnace gas with methane, steam, and lime for syngas production and CO2 capture: A thermodynamic study. Miner Process Extr Metall Rev 2015;36(1):7–12. https://doi.org/10.1080/08827508.2013.793682.

[64] Liu Y, Li Z, Xu L, Cai N. Effect of sorbent type on the sorption enhanced water gas shift process in a fluidized bed reactor. Ind Eng Chem Res 2012;51(37):11989–97. https://doi.org/10.1021/ie301100y.

[65] Tian S, Jiang J, Yan F, Li K, Chen X, Manovic V. Highly efficient CO2 capture with simultaneous iron and CaO recycling for the iron and steel industry. Green Chem 2016;18(14):4022–31. https://doi.org/10.1039/c6gc00400h.

[66] Tian S, Jiang J, Zhang Z, Manovic V. Inherent potential of steelmaking to contribute to decarbonisation targets via industrial carbon capture and storage. Nat Commun 2018;9(1):1–8. https://doi.org/10.1038/s41467-018-06886-8.

[67] Arias B, et al. Demonstration of steady state CO2 capture in a 1.7 MWth calcium looping pilot. Int J Greenh Gas Control Oct. 2013;18:237–45. https://doi.org/10.1016/J.IJGGC.2013.07.014.

[68] Kremer J, Galloy A, Ströhle J, Epple B. Continuous CO2 Capture in a 1-MWth Carbonate Looping Pilot Plant. Chem Eng Technol 2013. https://doi.org/10.1002/ceat.201300084.

[69] M. Hornberger, R. Spörl, and G. Scheffknecht, "Calcium Looping for CO2 Capture in Cement Plants - Pilot Scale Test," *Energy Procedia*, vol. 114, no. November 2016, pp. 6171–6174, 2017, doi: 10.1016/j.egypro.2017.03.1754.

[70] Hanak DP, Anthony EJ, Manovic V. A review of developments in pilot-plant testing and modelling of calcium looping process for CO2 capture from power generation systems. Energy Environ Sci 2015;8(8):2199–249. https://doi.org/10.1039/c5ee01228g.

[71] Arias B, et al. Operating Experience in la Pereda 1.7 MWth Calcium Looping Pilot. Energy Procedia 2017;114:149–57. https://doi.org/10.1016/j.egypro.2017.03.1157.

[72] Ströhle J, Junk M, Kremer J, Galloy A, Epple B. Carbonate looping experiments in a 1 MWth pilot plant and model validation. Fuel Jul. 2014;127:13–22. https://doi.org/10.1016/J.FUEL.2013.12.043.

[73] M. Helbig, J. Hilz, M. Haaf, A. Daikeler, J. Ströhle, and B. Epple, "Long-term Carbonate Looping Testing in a 1 MWth Pilot Plant with Hard Coal and Lignite," *Energy Procedia*, vol. 114, no. November 2016, pp. 179–190, 2017, doi: 10.1016/j.egypro.2017.03.1160.

[74] "CLEANKER, CLEAN clinKER production by calcium looping process (2022)." http://www.cleanker.eu/the-project/project-contents (accessed Nov. 08, 2022).

[75] "C4U, Advanced Carbon Capture for steel industries integrated in CCUS Clusters (2022)." https://c4u-project.eu/work-packages/(accessed Nov. 08, 2022).

[76] Luo M, Wang C, Yi Y, Liu K, Cai J, Wang Q. Power Generation from Coke Oven Gas Using Chemical Looping Combustion: Thermodynamic Simulation. Chem Eng Technol 2018;41(3):524–31. https://doi.org/10.1002/ceat.201700322.

[77] Wang S, Wang G, Jiang F, Luo M, Li H. Chemical looping combustion of coke oven gas by using Fe2O 3/CuO with MgAl2O4 as oxygen carrier. Energy Environ Sci 2010;3(9):1353–60. https://doi.org/10.1039/b926193a.

[78] Bahzad H, Katayama K, Boot-Handford ME, Mac Dowell N, Shah N, Fennell PS. Iron-based chemical-looping technology for decarbonising iron and steel production. Int J Greenh Gas Control 2019;vol. 91, no. June:102766. https://doi.org/10.1016/j.ijggc.2019.06.017.

[79] Xiang D, Zhao S. Parameter optimization and thermodynamic analysis of COG direct chemical looping hydrogen processes. Energy Convers Manag 2018;172(July):1–8. https://doi.org/10.1016/j.enconman.2018.07.007.

[80] Katayama K, Bahzad H, Boot-Handford M, Patzschke CF, Fennell PS. Process Integration of Chemical Looping Water Splitting with a Sintering Plant for Iron Making. ACS Appl Mater Interfaces 2020. https://doi.org/10.1021/acs.iecr.9b05945.

[81] Xiang D, Zhou Y. Concept design and techno-economic performance of hydrogen and ammonia co-generation by coke-oven gas-pressure swing adsorption integrated with chemical looping hydrogen process. Appl Energy 2018;229(April):1024–34. https://doi.org/10.1016/j.apenergy.2018.08.081.

[82] Kevin J Whitty JoAnn S Lighty, "Development of Enabling Technologies for Chemical Looping Combustion and Chemical Looping with Oxygen Uncoupling.," *NETL Transform. Power Gener. Proj. Rev. Meet. 28 Sept. 2020.*, [Online]. Available: https://netl.doe.gov/sites/default/files/netl-file/20TPGVPR_Whitty.pdf.

[83] I. Gogolev, A. H. Soleimanisalim, C. Linderholm, and A. Lyngfelt, "Commissioning, performance benchmarking, and investigation of alkali emissions in a 10 kWth solid fuel chemical looping combustion pilot," *Fuel*, doi: 10.1016/j.fuel.2020.119530.

[84] Adánez J, Abad A, Mendiara T, Gayán P, de Diego LF, García-Labiano F. Chemical looping combustion of solid fuels. Prog Energy Combust Sci 2018;65:6–66. https://doi.org/10.1016/j.pecs.2017.07.005.

[85] Lyngfelt A, Brink A, Langørgen Ø, Mattisson T, Rydén M, Linderholm C. 11,000 h of chemical-looping combustion operation—Where are we and where do we want to go? Int J Greenh Gas Control 2019;88(May):38–56. https://doi.org/10.1016/j.ijggc.2019.05.023.

[86] Di Giuliano A, Capone S, Anatone M, Gallucci K. Chemical Looping Combustion and Gasification: A Review and a Focus on European Research Projects. Ind Eng Chem Res 2022. https://doi.org/10.1021/acs.iecr.2c02677.

[87] "IFP. 2021. BUILDING OF THE LARGEST CHEMICAL LOOPING COMBUSTION (CLC) FACILITY TO DRIVE DOWN THE COST OF CARBON CAPTURE." https://www.ifpenergiesnouvelles.com/article/building-largest-chemical-looping-combustion-clc-facility-drive-down-cost-carbon-capture (accessed Nov. 08, 2022).

[88] "INEA. INNOVATION AND NETWORKS EXECUTIVE AGENCY. CHEERS project. 2021." https://ec.europa.eu/inea/en/horizon-2020/projects/h2020-energy/carbon-capture-storage-power-plants/cheers (accessed Nov. 08, 2022).

[89] "SINTEF. 2021. LOUISE – Low-cost CO2 capture by chemical looping combustion of waste-derived fuels." https://www.sintef.no/en/projects/2021/louise-low-cost-co2-capture-by-chemical-looping-combustion-of-waste-derived-fuels/ (accessed Nov. 08, 2022).

[90] Martínez I, et al. Recent progress of the Ca-Cu technology for decarbonisation of power plants and carbon intensive industries. Int J Greenh Gas Control Jun. 2019; 85:71–85. https://doi.org/10.1016/j.ijggc.2019.03.026.

[91] Fernández JR, Spallina V, Abanades JC. Advanced Packed-Bed Ca-Cu Looping Process for the CO2 Capture From Steel Mill Off-Gases. Front Energy Res 2020;8 (July):1–13. https://doi.org/10.3389/fenrg.2020.00146.

[92] Tian S, Li K, Jiang J, Chen X, Yan F. CO2 abatement from the iron and steel industry using a combined Ca-Fe chemical loop. Appl Energy 2016;170:345–52. https://doi.org/10.1016/j.apenergy.2016.02.120.

[93] Fernández JR, Martínez I, Abanades JC, Romano MC. Conceptual design of a Ca–Cu chemical looping process for hydrogen production in integrated steelworks. Int J Hydrogen Energy 2017;42(16):11023–37. https://doi.org/10.1016/j.ijhydene.2017.02.141.

[94] Sun Z, Liu J, Sun Z. Synergistic decarbonization and desulfurization of blast furnace gas via a novel magnesium-molybdenum looping process. Fuel 2020;vol. 279, no. May:118418. https://doi.org/10.1016/j.fuel.2020.118418.

[95] M. Bailera, P. Lisbona, B. Peña, and L. M. Romeo, "A review on CO2 mitigation in the Iron and Steel industry through Power to X processes," *J. CO2 Util.*, vol. 46, no. November 2020, p. 101456, 2021, doi: 10.1016/j.jcou.2021.101456.

[96] Lisbona P, Bailera M, Peña B, Romeo LM. Integration of CO2 capture and conversion. In: Rahimpour MR, Farsi M, Makarem MA, editors. Advances in Carbon Capture. Woodhead Publishing; 2020. p. 503–22. https://doi.org/10.1016/B978-0-12-819657-1.00022-0.

[97] Geerdes M, Chaigneau R, Lingiardi O, R. van O. Molenaar, S. Y. R., and J. Warren,. Modern Blast Furnace Ironmaking An Introduction. IOS Press; 2020.

[98] Bailera M, Hanak DP, Lisbona P, Romeo LM. Techno-economic feasibility of power to gas–oxy-fuel boiler hybrid system under uncertainty. Int J Hydrogen Energy 2019;4:9505–16. https://doi.org/10.1016/j.ijhydene.2018.09.131.

[99] Díez LI, Lupiáñez C, Guedea I, Bolea I, Romeo LM. Anthracite oxy-combustion characteristics in a 90 kWth fluidized bed reactor. Fuel Process Technol 2015; 139:196–203. https://doi.org/10.1016/j.fuproc.2015.07.021.

[100] Sato M, Takahashi K, Nouchi T, Ariyama T. Prediction of next-generation ironmaking process based on oxygen blast furnace suitable for CO2 mitigation and energy flexibility. ISIJ Int 2015;55(10):2105–14. https://doi.org/10.2355/isijinternational.ISIJINT-2015-264.

[101] Quader MA, Ahmed S, Raja Ghazilla RA, Ahmed S, Dahari M. Evaluation of criteria for CO2 capture and storage in the iron and steel industry using the 2-tuple DEMATEL technique. J Clean Prod May 2016;120:207–20. https://doi.org/10.1016/J.JCLEPRO.2015.10.056.

[102] Ho MT, Bustamante A, Wiley DE. Comparison of CO2 capture economics for iron and steel mills. Int J Greenh Gas Control Nov. 2013;19:145–59. https://doi.org/10.1016/J.IJGGC.2013.08.003.

[103] Jin P, Jiang Z, Bao C, Lu Y, Zhang J, Zhang X. Mathematical Modeling of the Energy Consumption and Carbon Emission for the Oxygen Blast Furnace with Top Gas Recycling. Steel Res Int 2016;87(3):320–9. https://doi.org/10.1002/srin.201500054.

[104] Helle H, Helle M, Pettersson F, Saxén H. Multi-objective Optimization of Ironmaking in the Blast Furnace with Top Gas Recycling. ISIJ Int 2010;50(10): 1380–7. https://doi.org/10.2355/isijinternational.50.1380.

[105] Helle H, Helle M, Saxén H, Pettersson F. Optimization of Top Gas Recycling Conditions under High Oxygen Enrichment in the Blast Furnace. ISIJ Int 2010;50 (7):931–8. https://doi.org/10.2355/isijinternational.50.931.

[106] Arasto A, Tsupari E, Kärki J, Lilja J, Sihvonen M. Oxygen blast furnace with CO2 capture and storage at an integrated steel mill-Part I: Technical concept analysis. Int J Greenh Gas Control 2014;30:140–7. https://doi.org/10.1016/j.ijggc.2014.09.004.

[107] Onoda M, Matsuzaki Y, Chowdhury FA, Yamada H, Goto K, Tonomura S. Sustainable Aspects of Ultimate Reduction of CO2 in the Steelmaking Process (COURSE50 Project), Part 2: CO2 Capture. J Sustain Metall 2016;2(3):209–15. https://doi.org/10.1007/s40831-016-0067-3.

[108] Murai R, Sato M, Ariyama T. Design of Innovative Blast Furnace for Minimizing CO2 Emission Based on Optimization of Solid Fuel Injection and Top Gas Recycling. ISIJ Int 2004;44(12):2168–77. https://doi.org/10.2355/isijinternational.44.2168.

[109] Takahashi K, Nouchi T, Sato M, Ariyama T. Perspective on Progressive Development of Oxygen Blast Furnace for Energy Saving. ISIJ Int 2015;55(9): 1866–75. https://doi.org/10.2355/isijinternational.ISIJINT-2015-196.

[110] Sahu RK, Roy SK, P. K. Sen Ã,. "Applicability of Top Gas Recycle Blast Furnace with Downstream Integration and Sequestration in an. Integrated Steel Plant" 2015;1(5):502–16. https://doi.org/10.1002/srin.201400196.

[111] Ariyama T, Sato M, Nouchi T, Takahashi K. Evolution of blast furnace process toward reductant flexibility and carbon dioxide mitigation in steel works. ISIJ Int 2016;56(10):1681–96. https://doi.org/10.2355/isijinternational.ISIJINT-2016-210.

[112] Wang H, et al. Mathematical Simulation on Blast Furnace Operation of Coke Oven Gas Injection in Combination with Top Gas Recycling. Steel Res Int 2016;87(5): 539–49. https://doi.org/10.1002/srin.201500372.

[113] Tseitlin MA, Lazutkin SE, Styopin GM. A Flow-chart for Iron Making on the Basis of 100% Usage of Process Oxygen and Hot Reducing Gases Injection. ISIJ Int 1994;34(7):570–3. https://doi.org/10.2355/isijinternational.34.570.

[114] Helle M, Saxén H. Operation windows of the oxygen blast furnace with top gas recycling. ISIJ Int 2015;55(10):2047–55. https://doi.org/10.2355/isijinternational.ISIJINT-2015-083.

[115] van der Stel J, Louwerse G, Sert D, Hirsch A, Eklund N, Pettersson M. Top gas recycling blast furnace developments for 'green' and sustainable ironmaking. Ironmak Steelmak Oct. 2013;40(7):483–9. https://doi.org/10.1179/0301923313Z.000000000221.

[116] Nogami H, Chu M, Yagi J-I. Numerical analysis of blast furnace operations with top gas recycling. Rev Métallurgie Mar. 2005;102(3):189–97. https://doi.org/10.1051/metal:2005132.

[117] Zhou Z, Yi Q, Wang R, Wang G, Ma C. Numerical Investigation on Coal Combustion in Ultralow CO2 Blast Furnace: Effect of Oxygen Temperature. Processes Jul. 2020;8(7):877. https://doi.org/10.3390/pr8070877.

[118] Helle H, Helle M, Saxén H. Nonlinear optimization of steel production using traditional and novel blast furnace operation strategies. Chem Eng Sci Dec. 2011; 66(24):6470–81. https://doi.org/10.1016/j.ces.2011.09.006.

[119] Jin P, Jiang Z, Bao C, Hao S, Zhang X. The energy consumption and carbon emission of the integrated steel mill with oxygen blast furnace. Resour Conserv Recycl 2017;117:58–65. https://doi.org/10.1016/j.resconrec.2015.07.008.

[120] Perpiñán J, Bailera M, Romeo LM, Peña B, Eveloy V. CO2 Recycling in the Iron and Steel Industry via Power-to-Gas and Oxy-Fuel Combustion. Energies 2021;14 (21):7090. https://doi.org/10.3390/en14217090.

[121] M. Bailera, T. Nakagaki, and R. Kataoka, "Revisiting the Rist diagram for predicting operating conditions in blast furnaces with multiple injections," 2021, doi: 10.12688/openreseurope.14275.1.

[122] Oda J, Akimoto K, Sano F, Tomoda T. Diffusion of energy efficient technologies and CO2 emission reductions in iron and steel sector. Energy Econ 2007;29(4): 868–88. https://doi.org/10.1016/j.eneco.2007.01.003.

[123] M. A. A.-M. Rainer Remus and L. D. S. Serge Roudier, *Best Available Techniques (BAT) Reference Document for Iron and Steel Production*. 2013. doi: doi:10.2791/98516.

[124] Wu J, Wang R, Pu G, Qi H. Integrated assessment of exergy, energy and carbon dioxide emissions in an iron and steel industrial network. Appl Energy 2016;183: 430–44. https://doi.org/10.1016/j.apenergy.2016.08.192.

[125] Suzuki K, Hayashi K, Kuribara K, Nakagaki T, Kasahara S. Quantitative evaluation of CO2 emission reduction of active carbon recycling energy system for ironmaking by modeling with aspen plus. ISIJ Int 2015;55(2):340–7. https://doi.org/10.2355/isijinternational.55.340.

[126] A. F. Prego *et al.*, "Operación de hornos altos con inyección de carbón pulverizado en diferentes condiciones tecnológicas," *Rev. Metal.*, vol. 37, pp. 423–436, 2001, doi: 10.3989/revmetalm.2001.v37.i3.50810.3989/revmetalm.2001.v37.i3.508.

[127] Zhang H, Li H, Tang Q, Bao W. Conceptual design and simulation analysis of thermal behaviors of TGR blast furnace and oxygen blast furnace. Sci China Technol Sci 2010;53(1):85–92. https://doi.org/10.1007/s11431-010-0029-0.

[128] Zhang W, Zhang J, Xue Z, Zou Z, Qi Y. Unsteady Analyses of the Top Gas Recycling Oxygen Blast Furnace. ISIJ Int 2016;56(8):1358–67. https://doi.org/10.2355/isijinternational.ISIJINT-2016-090.

[129] She X, An X, Wang J, Xue Q, Kong L. Numerical analysis of carbon saving potential in a top gas recycling oxygen blast furnace. J Iron Steel Res Int Jun. 2017;24(6):608–16. https://doi.org/10.1016/S1006-706X(17)30092-4.

[130] Zhang W, Xue Z, Zhang J, Wang W, Cheng C, Zou Z. Medium oxygen enriched blast furnace with top gas recycling strategy. J Iron Steel Res Int Aug. 2017;24(8): 778–86. https://doi.org/10.1016/S1006-706X(17)30117-6.

[131] Danloy G, et al. ULCOS - Pilot testing of the low-CO2 Blast Furnace process at the experimental BF in Lulea. Rev Metall Cah D'Informations Tech 2009;106(1):1–8. https://doi.org/10.1051/metal/2009008.

[132] Bargiacchi E, Candelaresi D, Valente A, Spazzafumo G, Frigo S. Life Cycle Assessment of Substitute Natural Gas production from biomass and electrolytic hydrogen. Int J Hydrogen Energy 2021;46(72):35974–84. https://doi.org/10.1016/j.ijhydene.2021.01.033.

[133] Faria DG, Carvalho MMO, Neto MRV, de Paula EC, Cardoso M, Vakkilainen EK. Integrating oxy-fuel combustion and power-to-gas in the cement industry: A process modeling and simulation study. Int J Greenh Gas Control Feb. 2022;114: 103602. https://doi.org/10.1016/j.ijggc.2022.103602.

[134] M. Bailera, T. Nakagaki, and R. Kataoka, "Limits on the integration of power to gas with blast furnace ironmaking," *J. Clean. Prod.*, p. 134038, Sep. 2022, doi: 10.1016/J.JCLEPRO.2022.134038.

[135] W. Zhang, J. Dai, C. Li, X. Yu, Z. Xue, and H. Saxén, "A Review on Explorations of the Oxygen Blast Furnace Process," *Steel Res. Int.*, vol. 92, no. 1, 2021, doi: 10.1002/srin.202000326.

[136] Lan R, Wang J, Han Y, She X, Wang L, Qing-guo X. Reduction Behavior of Sinter Based on Top Gas Recycling-Oxygen Blast Furnace. J Iron Steel Res Int Sep. 2012; 19(9):13–9. https://doi.org/10.1016/S1006-706X(13)60003-5.

[137] Chu M, Nogami H, Yagi J. Numerical Analysis on Blast Furnace Performance under Operation with Top Gas Recycling and Carbon Composite Agglomerates

Charging. ISIJ Int 2004;44(12):2159–67. https://doi.org/10.2355/isijinternational.44.2159.
[138] Babich A. Blast furnace injection for minimizing the coke rate and CO2 emissions. Ironmak Steelmak Jul. 2021;48(6):728–41. https://doi.org/10.1080/03019233.2021.1900037.
[139] Li Z, et al. Numerical Investigation of Novel Oxygen Blast Furnace Ironmaking Processes. Metall Mater Trans B Aug. 2018;49(4):1995–2010. https://doi.org/10.1007/s11663-018-1259-y.
[140] R. Kumar Sahu, C. Halder, and P. K. Sen, "Optimization of Top Gas Recycle Blast Furnace Emissions with Implications of Downstream Energy," *steel Res. Int.*, vol. 87, no. 9, pp. 1190–1202, Sep. 2016, doi: 10.1002/srin.201500312.
[141] Ohno Y, Matsuura M, Mitsufuji H, Furukawa T. Process Characteristics of a Commercial-scale Oxygen Blast Furnace Process with Shaft Gas Injection. ISIJ Int 1992;32(7):838–47. https://doi.org/10.2355/isijinternational.32.838.
[142] Sen PK. Co2 Accounting and Abatement: An Approach for Iron and Steel Industry. Trans Indian Inst Met Dec. 2013;66(5–6):711–21. https://doi.org/10.1007/s12666-013-0285-3.
[143] Liu L, et al. Effects of top gas recycling on in-furnace status, productivity, and energy consumption of oxygen blast furnace. Energy Nov. 2018;163:144–50. https://doi.org/10.1016/j.energy.2018.08.114.
[144] Qi Y, Yan D, Gao J, ZHANG J, LI M. Study on Industrial test of the Oxygen Blast Furnace. Iron Steel 2011;3:6–8. https://doi.org/10.13228/j.boyuan.issn0449-749x.2011.03.013.
[145] Zuo G, Hirsch A. The trial of the Top Gas Recycling Blast Furnace at LKAB's EBF and Scale-Up. La Rev Métallurgie 2009;2(5):255.
[146] Tsupari E, Kärki J, Arasto A, Lilja J, Kinnunen K, Sihvonen M. Oxygen blast furnace with CO2 capture and storage at an integrated steel mill - Part II: Economic feasibility in comparison with conventional blast furnace highlighting sensitivities. Int J Greenh Gas Control 2015;32:189–96. https://doi.org/10.1016/j.ijggc.2014.11.007.
[147] Austin PR, Nogami H, Yagi J. Prediction of Blast Furnace Performance with Top Gas Recycling. ISIJ Int 1998;38(3):239–45. https://doi.org/10.2355/isijinternational.38.239.
[148] D. H. B. Andrade, R. P. Tavares, A. C. B. Quintas, V. E. de S. Moreira, A. O. Viana, and V. M. Gasparini, "Evaluation of the permeability of the dripping zone and of flooding phenomena in a blast furnace," *J. Mater. Res. Technol.*, vol. 8, no. 1, pp. 134–139, Jan. 2019, doi: 10.1016/j.jmrt.2017.10.001.
[149] Marketwatch. NYSE American, Steel Index 2022.
[150] Kuramochi T, Ramírez A, Turkenburg W, Faaij A. Comparative assessment of CO2 capture technologies for carbon-intensive industrial processes. Prog Energy Combust Sci Feb. 2012;38(1):87–112. https://doi.org/10.1016/j.pecs.2011.05.001.
[151] Tobiesen FA, Svendsen HF, Mejdell T. Modeling of blast furnace CO2 capture using amine absorbents. Ind Eng Chem Res 2007;46(23):7811–9. https://doi.org/10.1021/ie061556j.
[152] Kidnay AJ, Paarish WR, Mccartney DG. Fundamentals of Natural Gas Processing. 3rd ed. Boca Raton: CRC Press; 2019.
[153] Martinez Castilla G, Biermann M, Montañés RM, Normann F, Johnsson F. Integrating carbon capture into an industrial combined-heat-and-power plant: performance with hourly and seasonal load changes. Int J Greenh Gas Control Mar. 2019;82:192–203. https://doi.org/10.1016/J.IJGGC.2019.01.015.
[154] xun Fu J, hao Tang G, jie Zhao R, sing Hwang W. Carbon Reduction Programs and Key Technologies in Global Steel Industry. J Iron Steel Res Int Mar. 2014;21(3):275–81. https://doi.org/10.1016/S1006-706X(14)60042-X.
[155] Han K, Ahn CK, Lee MS. Performance of an ammonia-based CO2 capture pilot facility in iron and steel industry. Int J Greenh Gas Control 2014;27:239–46. https://doi.org/10.1016/j.ijggc.2014.05.014.
[156] Quader MA, Ahmed S, Ghazilla RAR, Ahmed S. CO2 Capture and Storage for the iron and steel manufacturing industry: Challenges and Opportunities. J Appl Sci Agric 2014;9(21):60–7.
[157] Farla JCM, Hendriks CA, Blok K. Carbon dioxide recovery from industrial processes. Clim Change 1995;29(4):439–61. https://doi.org/10.1007/BF01092428.
[158] Kim H, Lee J, Lee S, Lee IB, J. hyoung Park, and J. Han,. Economic process design for separation of CO2 from the off-gas in ironmaking and steelmaking plants. Energy Aug. 2015;88:756–64. https://doi.org/10.1016/J.ENERGY.2015.05.093.
[159] Onarheim K, Arasto A. Staged implementation of alternative processes in an existing integrated steel mill for improved performance and reduced CO2 emissions – Part I: Technical concept analysis. Int J Greenh Gas Control Feb. 2016;45:163–71. https://doi.org/10.1016/J.IJGGC.2015.12.008.
[160] Chung W, Roh K, Lee JH. Design and evaluation of CO2 capture plants for the steelmaking industry by means of amine scrubbing and membrane separation. Int J Greenh Gas Control Jul. 2018;74:259–70. https://doi.org/10.1016/J.IJGGC.2018.05.009.
[161] Hisashige S, Nakagaki T, Yamamoto T. CO2 emission reduction and exergy analysis of smart steelmaking system adaptive for flexible operating conditions. ISIJ Int 2019;59(4):598–606. https://doi.org/10.2355/isijinternational.ISIJINT-2018-355.
[162] Ramírez-Santos ÁA, Bozorg M, Addis B, Piccialli V, Castel C, Favre E. Optimization of multistage membrane gas separation processes. Example of application to CO2 capture from blast furnace gas. J Memb Sci 2018;566. https://doi.org/10.1016/j.memsci.2018.08.024.
[163] J.-P. Birat, "Carbon dioxide (CO2) capture and storage technology in the iron and steel industry," *Dev. Innov. Carbon Dioxide Capture Storage Technol.*, pp. 492–521, 2010, doi: 10.1533/9781845699574.5.492.
[164] Saima WH, Mogi Y, Haraoka T. Development of PSA System for the Recovery of Carbon Dioxide and Carbon Monoxide from Blast Furnace Gas in Steel Works. Energy Procedia 2013;37:7152–9. https://doi.org/10.1016/j.egypro.2013.06.652.
[165] Y. Ujisawa, S. Tonomura, N. Ishiwata, Y. Nabeshima, and K. Saito, "Topic: CO2 breakthrough program by COURSE50 in Japanese steel industry sector," in *Energy Technology Roadmaps of Japan: Future Energy Systems Based on Feasible Technologies Beyond 2030*, 2016. doi: 10.1007/978-4-431-55951-1_29.
[166] Rao M, Fernandes A, Pronk P, Aravind PV. Design, modelling and techno-economic analysis of a solid oxide fuel cell-gas turbine system with CO2 capture fueled by gases from steel industry. Appl Therm Eng 2019;148. https://doi.org/10.1016/j.applthermaleng.2018.11.108.
[167] A. B. Rao, E. S. Rubin, and M. B. Berkenpas, "AN INTEGRATED MODELING FRAMEWORK FOR CARBON MANAGEMENT TECHNOLOGIES," Pittsburg, PA, 2004.
[168] Ho MT, Allinson GW, Wiley DE. Reducing the Cost of CO2 Capture from Flue Gases Using Pressure Swing Adsorption. Ind Eng Chem Res Jul. 2008;47(14):4883–90. https://doi.org/10.1021/ie070831e.
[169] Zuo G, Hirsch A. The trial of the top gas recycling blast furnace at LKABsEBF and scale-up. Rev Metall Cah D'Informations Tech 2009;106(9):pp. https://doi.org/10.1051/metal/2009067.
[170] Wang X, Wang T. Hydrogen amplification from coke oven gas using a CO 2 adsorption enhanced hydrogen amplification reactor. Int J Hydrogen Energy 2012;37(6):pp. https://doi.org/10.1016/j.ijhydene.2011.12.018.
[171] Siqueira RM, et al. Carbon Dioxide Capture by Pressure Swing Adsorption. Energy Procedia Jul. 2017;114:2182–92. https://doi.org/10.1016/J.EGYPRO.2017.03.1355.
[172] Hasan MMF, Baliban RC, Elia JA, Floudas CA. Modeling, Simulation, and Optimization of Postcombustion CO2 Capture for Variable Feed Concentration and Flow Rate. 1. Chemical Absorption and Membrane Processes. Ind Eng Chem Res Dec. 2012;51(48):15642–64. https://doi.org/10.1021/ie301571d.
[173] Ramírez-Santos ÁA, Castel C, Favre E. Utilization of blast furnace flue gas: Opportunities and challenges for polymeric membrane gas separation processes. J Memb Sci 2017;526. https://doi.org/10.1016/j.memsci.2016.12.033.
[174] Lie JA, Vassbotn T, Hägg MB, Grainger D, Kim TJ, Mejdell T. Optimization of a membrane process for CO2 capture in the steelmaking industry. Int J Greenh Gas Control 2007;1(3):pp. https://doi.org/10.1016/S1750-5836(07)00069-2.
[175] Jeon J-Y, Park B-R, Kim J-H. Numerical Simulation and Optimization of 4-Component LDG Separation in the Steelmaking Industry Using Polysulfone Hollow Fiber Membranes. Membranes 2022;12(1):pp. https://doi.org/10.3390/membranes12010097.
[176] Roy P, Das N. A lithium–aluminosilicate zeolite membrane for separation of CO2 from simulated blast furnace gas. J Porous Mater 2020;27(3):pp. https://doi.org/10.1007/s10934-019-00849-0.
[177] Baker RW, Freeman B, Kniep J, Wei X, Merkel T. CO2 capture from natural gas power plants using selective exhaust gas recycle membrane designs. Int J Greenh Gas Control 2017;66:35–47. https://doi.org/10.1016/j.ijggc.2017.08.016.
[178] Li R, Lian S, Zhang Z, Song C, Han R, Liu Q. Techno-economic evaluation of a novel membrane-cryogenic hybrid process for carbon capture. Appl Therm Eng 2022;200. https://doi.org/10.1016/j.applthermaleng.2021.117688.
[179] Van Dijk HAJ, et al. "Stepwise project: Sorption-enhanced water-gas shift technology to reduce carbon footprint in the iron and steel industry", *Johnson Matthey*. Technol Rev 2018;62(4):pp. https://doi.org/10.1595/205651318X15268923666410.
[180] Lukashuk L, et al. A new application of the commercial high temperature water gas shift catalyst for reduction of CO2 emissions in the iron and steel industry: Lab-scale catalyst evaluation. Int J Hydrogen Energy 2021;46(79):39023–35. https://doi.org/10.1016/j.ijhydene.2021.09.203.
[181] "Stepwise Project." https://www.stepwise.eu/project/.
[182] Choi JO, Kim JG. CO2 reduction by blast furnace top gas recycling combined with waste hydrocarbon gasification. Stud Surf Sci Catal 2004;153:125–30. https://doi.org/10.1016/s0167-2991(04)80230-1.
[183] Li Z, et al. Numerical study and design strategy for a low emission coke oven system using oxy-fuel combustion of coke oven gas. J Clean Prod 2020;vol. 252, no. x:119656. https://doi.org/10.1016/j.jclepro.2019.119656.
[184] Qie Y, Lyu Q, Lan C, Zhang S. Energy Conservation and CO2 Abatement Potential of a Gas-injection Blast Furnace. High Temp Mater Process 2020;39(1):96–106. https://doi.org/10.1515/htmp-2020-0031.
[185] Zhang W, Zhang J, Xue Z. Exergy analyses of the oxygen blast furnace with top gas recycling process. Energy 2017;121:135–46. https://doi.org/10.1016/j.energy.2016.12.125.
[186] Chu M, Yagi JI. Numerical evaluation of blast furnace performance under top gas recycling and lower temperature operation. Steel Res Int 2010;81(12):1043–50. https://doi.org/10.1002/srin.201000103.
[187] H. Takashi, Y. Mogi, and H. Saima, "PSA System for the Recovery of Carbon Dioxide from Blast Furnace Gas in Steel Works The Influence of Operation Conditions on CO2 Separation," 2013, doi: 10.1252/kakoronbunshu.39.439.

Energy 276 (2023) 127616

Contents lists available at ScienceDirect

Energy

journal homepage: www.elsevier.com/locate/energy

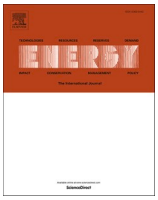

# Technical and economic assessment of iron and steelmaking decarbonization via power to gas and amine scrubbing

Jorge Perpiñán [a,*], Manuel Bailera [a,b], Begoña Peña [a], Luis M. Romeo [a], Valerie Eveloy [c]

[a] Escuela de Ingeniería y Arquitectura, Universidad de Zaragoza, María de Luna 3, 50018, Zaragoza, Spain
[b] Graduate School of Creative Science and Engineering, Waseda University, Tokyo, 169-8555, Japan
[c] Khalifa University, Department of Mechanical Engineering, United Arab Emirates

ARTICLE INFO

Handling Editor: Krzysztof (K.J.) Ptasinski

*Keywords:*
Ironmaking
Power-to-gas
Iron and steel industry
Methanation
CO2 capture
Decarbonization

ABSTRACT

The iron and steel industry is one of the most energy-intensive industries, emitting 5% of the total anthropogenic carbon dioxide ($CO_2$). The control of $CO_2$ emissions has become increasingly stringent in the European Union (EU), resulting in EU allowance above 90 €/$t_{CO2}$. Carbon capture will be required to achieve $CO_2$ emissions control, and carbon utilization via power-to-gas could significantly increase interest in carbon capture in the iron and steel sector. This paper presents a new concept that combines amine scrubbing with power-to-gas to reduce emissions in blast furnace-basic oxygen furnace steelmaking plants. Synthetic natural gas (SNG) is produced using green hydrogen from water electrolysis and $CO_2$ from steelmaking. The synthetic natural gas is later used as a reducing agent in the blast furnace, constantly recycling carbon in a closed loop and avoiding geological storage. The oxygen by-produced via electrolysis eliminates the necessity of an air separation unit. By applying these innovations to steelmaking, a reduction in $CO_2$ emissions of 9.4% is obtained with an energy penalty of 16.2 MJ/$kg_{CO2}$, and economic costs of 52 €/$t_{HM}$ or 283 €/$t_{CO2}$. A sensitivity analysis with respect to electricity and the $CO_2$ allowances prices is also performed.

## 1. Introduction

The current European targets on global warming include the reduction of greenhouse gas (GHG) emissions by 80–95%, compared to 1990 levels, by the year 2050 [1]. One of the largest industrial emitters of GHG emissions, in particular $CO_2$, is the steel sector. Iron and steel making processes are still highly dependent on fossil fuels, thereby releasing a substantial amount of $CO_2$ [2]. These emissions accounted for 223 $Mt_{CO2\text{-}eq}$ in the European Union in 2010 [3], i.e. 5% of the total GHG emissions of the EU-27 [4]. Steel is mainly produced by two routes: (i) blast furnace–basic oxygen furnace (BF–BOF) with 70% market share, and (ii) electric arc furnace (EAFs) with 30% market share [4].

The BF-BOF route, which uses coal as the main primary energy resource, mainly consists of the following processes: sinter strand, coke oven, blast furnace (BF), basic oxygen furnace (BOF), and the final stage of casting and rolling. The sintering is used to agglomerate iron ore. The coke oven allows obtaining coke from coal. In the BF, the iron ore is reduced by coke, obtaining hot metal (HM). Then, the BOF lowers the carbon content of the molten iron to produce crude steel (CS) which finally passes through casting and rolling stages to obtain the desired product. Along the involved processes, different exhaust gases are obtained, which can be used as fuel in the steel plant (coke oven gas - COG, blast furnace gas - BFG, and basic oxygen furnace gas - BOFG). BF-BOF is highly energy- and carbon-intense, resulting in a net energy consumption of 13–14 GJ per ton of crude steel (GJ/$t_{CS}$) and specific emissions of 2200 $kg_{CO2}/t_{CS}$ [5].

The EAF route produces steel by melting recycled scrap using electricity. When the availability of scrap is limited, direct reduced iron (DRI) can also be used as feedstock. The DRI contains >90% metallic iron, and it is produced in combustion-free reactors by using natural gas or coal-based syngas as reducing agents. The dominant commercially available technologies, Energiron and Midrex [6], use iron pellets in shaft furnaces with countercurrent moving beds. Depending on the scrap-metallic iron share in the DRI-EAF, the energy consumption and $CO_2$ emissions are significantly lower, 4–10 GJ/$t_{CS}$ and 400–1300 $kg_{CO2}/t_{CS}$, respectively, than for the BF-BOF route [5]. Substitution of natural gas or coal-based syngas with hydrogen can further abate DRI-EAF emissions significantly [7].

However, since the global steel demand cannot be covered through

* Corresponding author. Escuela de Ingeniería y Arquitectura, Universidad de Zaragoza, María de Luna 3, 50018, Zaragoza, Spain.
*E-mail addresses:* jorge.perpinan@unizar.es (J. Perpiñán), mbailera@unizar.es (M. Bailera), bpp@unizar.es (B. Peña), luismi@unizar.es (L.M. Romeo), valerie.eveloy@ku.ac.ae (V. Eveloy).

https://doi.org/10.1016/j.energy.2023.127616
Received 2 September 2022; Received in revised form 19 April 2023; Accepted 20 April 2023
Available online 21 April 2023
0360-5442/© 2023 The Authors. Published by Elsevier Ltd. This is an open access article under the CC BY-NC-ND license (http://creativecommons.org/licenses/by-nc-nd/4.0/).

**Nomenclature**

| *Abbreviation* | *Meaning* |
|---|---|
| AFT | Adiabatic Flame Temperature |
| ASU | Air Separation Unit |
| AHF | Air Heating Furnace |
| BF-BOF | Blast Furnace-Basic Oxygen Furnace |
| BFG | Blast Furnace Gas |
| BOFG | Basic Oxygen Furnace Gas |
| CC | Carbon Capture |
| CCUS | Carbon Capture Utilization and Storage |
| COG | Coke Oven Gas |
| DRI | Direct Reduced Iron |
| EAF | Electric Arc Furnace |
| GHG | Green House Gas |
| HM | Hot Metal |
| I&S | Iron and Steel |
| IEA | International Energy Agency |
| IRR | Internal Rate of Return |
| MDEA | Methyldiethanolamine |
| PtG | Power to Gas |
| PCI | Pulverised Coal Injection |
| PFD | Process Flow Diagram |
| PPAs | Power purchase agreements |
| SNG | Synthetic Natural Gas |
| tHM | Ton of Hot Metal |
| tCS | Ton of Crude Steel |

recycled scrap, the BF-BOF route will maintain its dominance in the market, despite its high emissions. Besides, blast furnaces will only phased-out at relining, which typically takes place every 20–35 years, or up to 40 years for newly commissioned plants. Thus, it is expected that at least 20% of today's blast furnaces will still be in operation by year 2050 [8].

The need to reduce greenhouse gas emissions from steel production has gained significant attention globally, leading to widespread research into the development of alternative ultra-low-$CO_2$ steel production technologies. To this end, numerous projects and programs have been launched, such as Carbon2Chem [9], which explores potential uses for steel gases, and ULCORED [10], ULCOWIN [10], ULCOLYSIS [10], COREX [11], HIsmelt [12], and FINEX® [13], which focus on the creation of new pathways for steel production. In addition to these projects, MIDREX® [5] and ENERGIRON® [6] processes are also being developed as alternative methods for steel production that emit fewer greenhouse gases. These processes utilize direct reduction technology to reduce iron ore (DRI) and eliminate the need for coke in the production process. Despite the challenges associated with developing these new technologies, the potential benefits to the environment and the steel industry are considerable, and these initiatives hold great promise for the future of sustainable steel production. However, out of all these projects, only ULCOS-BF [10] and COURSE50 [14] are dedicated to capturing $CO_2$ in the BF-BOF route through physical adsorption and chemical absorption methods from the BFG.

Carbon capture with amines is a well-established technology used in many industries to reduce greenhouse gas emissions. In the iron and steel industry, amine scrubbing is widely considered one of the most effective and practical approach for capturing $CO_2$ emissions from blast furnace gases. Despite its effectiveness, the use of amine scrubbing for carbon capture in the iron and steel industry still faces several challenges. One of the main challenges is the high energy consumption associated with the regeneration of the solvent, ranging between 2.9 MJ/kg$CO_2$ and 6.5 MJ/kg$CO_2$ [10], which can significantly increase the overall energy consumption of the process. Although the $CO_2$ capture process using amine solvents is well-established (TRL 9) and commercially available for use in natural gas and fertilizer processing plants [11], it has not been fully deployed in the iron and steel industry, resulting in a TRL2-TRL6 level [10].

Power to Gas (PtG) stands out as a promising solution to substantially reduce $CO_2$ emissions while providing additional benefits [12]. The Power to X concept involves processes that convert renewable electricity into valuable products, using an electrolysis stage to obtain renewable $H_2$ as an intermediate or final energy carrier. The hydrogen produced can be combined with captured $CO_2$ in a methanation reactor to obtain methane (Power to Methane, PtM). This synthetic natural gas can substitute a fraction of the currently consumed coke as a reducing agent in the blast furnace [13,14]. The application of Power to Gas to the Iron and Steel industry can result in benefits accompanying the energy penalty of carbon capture, contrarily to other carbon reduction measures such as chemical absorption or physical adsorption. When comparing with CCS alone, underground geological storage would be required, along with transportation and compression. Furthermore, geological storage requires available site near the CO2 source, but the suitable locations are very scarce. In addition, this is a controversial issue and the social acceptance is quite low.

Only a few studies have been found in the literature on PtG and carbon capture integration to reduce steelmaking emissions. Hisashige et al. [15] studied a shaft furnace coupled with a pressure swing adsorption stage (for carbon capture and $CH_4$ separation) and a $CH_4$ synthesis reactor (at 300 °C and 5.3 bar), injecting 33 $kg_{SNG}/t_{HM}$ in the BF. Hisashige et al. found a 13% of $CO_2$ emission reduction in the blast furnace. Rosenfeld et al. [16] analysed the integration of Power to Methane, together with biomass gasification (mainly for further $H_2$ supply), concluding with a 14–19% of $CO_2$ emission reduction in the blast furnace. Perpiñán et al. [13] investigated the combination of power to gas, top gas recycling and oxy-blast furnace, achieving an 8% decrease in $CO_2$ emissions for the whole BF-BOF plant, accounting for 65 $kg_{SNG}/t_{CS}$ injected in the BF. Bailera et al. [14,17,18] developed a detailed model of the blast furnace according to the Rist Diagram and studied a new concept proposal that combines oxygen blast furnaces with Power to Gas technology. The reduction of $CO_2$ emission obtained in that study ranged between 6% and 7% in the blast furnace, with an injection of 22 $kg_{SNG}/t_{HM}$.

The objective of this paper is to assess from the technical and economic point of view a novel concept that integrates PtM with amine scrubbing in the iron and steel industry to reduce the emission intensity of the conventional BF-BOF process. This is achieved using detailed process models of a complete conventional BF-BOF process plant and of the proposed PtG-based concept developed using Aspen Plus and validated using reference data. Both the conventional steelmaking process and the novel process that integrates PtM and amine scrubbing are compared in terms of demand for coal, overall energy consumption and $CO_2$ emissions. The influence of the amount of synthetic natural gas (SNG) injected to the BF on the adiabatic flame temperature (AFT) is analysed. Sankey diagrams for the energy and carbon flows are also presented and discussed to quantify the contribution of each process to energy consumption and carbon emission/recycling. Lastly, the economic feasibility of the proposed PtM and carbon capture integration is evaluated, to identify technical and economic conditions to reach reasonable pay-back periods and internal rate of returns (IRR) for the proposed steelmaking emission abatement process. The process models developed in this study can also be used to evaluate alternative emission reduction strategies for BF-BOF steelmaking processes.

Both the novel and conventional steelmaking processes are described in Section 2, and their modelling methodology in Section 3.

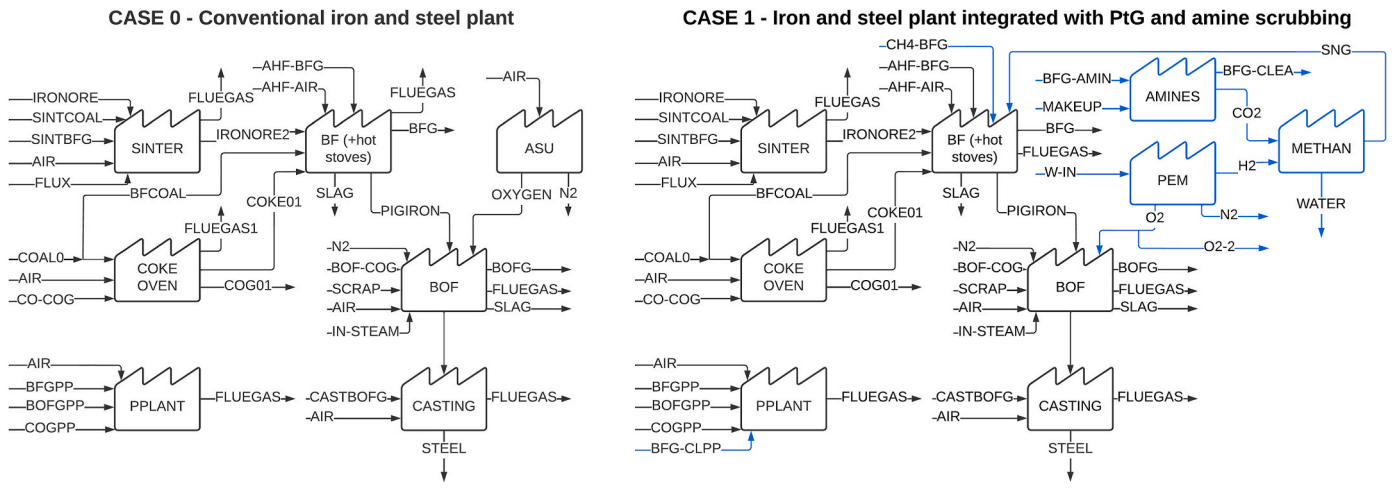


**Fig. 1.** Process flow diagram in Aspen Plus: (left) conventional iron and steel plant (Case 0), (right) its integration with power to gas and carbon capture (Case 1). Sub-systems drawn using blue coloured lines are the main innovations of the modified process (Case 1).

**Table 1**
Input and Output data of the Aspen Plus models for the proposed low-carbon steelmaking process concept and conventional BF-BOF process. Stream ID corresponding to Fig. 1.

| Hierarchy | Stream ID | Composition | Flow | Temperature |
|---|---|---|---|---|
| SINTER | Iron ore | Input | Output | Input |
| SINTER | Coal | Input | Output | Input |
| SINTER | Flux | Input | Input | Input |
| SINTER | Iron ore (out) | Input | Output | Input |
| COKE OVEN | Coal | Input | Output | Input |
| COKE OVEN | Coke | Output | O/I[a)] | Input |
| COKE OVEN | COG (out) | Output | Output | Output |
| BF | Coal | Input | Input | Input |
| BF | Air | Input | Output | Input |
| BF | BFG | Output | Output | Output |
| BF | Slag | Output | Output | Output |
| BF | Pig iron | Input | Input | Input |
| BOF | Scrap | Input | Input | Input |
| BOF | Oxygen | Output | Output | Input |
| BOF | N2 | Input | Input | Input |
| BOF | Slag | Output | Output | Input |
| BOF | BOFG | Input | Output | Input |
| CASTING | Steel | Input | Output | Input |
| AMINES | BFG | Output | Output | Input |
| AMINES | BFG-CLEAN | Output | Output | Input |
| AMINES | CO2 | Output | Output | Input |
| PEM | Water | Input | Output | Input |
| PEM | H2 | Output | Output | Input |
| ASU/PEM | O2 | Output | Output | Input |
| METHAN | SNG | Output | Output | Input |

[a)] O/I: Output/Input. Coke is calculated as an output in Case 0 and is maintained as an input in Case 1.

## 2. Process description

A conventional iron and steel plant producing 320 $t_{HM}$/h [19] is assumed as base case (Case 0) according to the process flow diagram (PFD) of Fig. 1. This reference plant consists of a sinter strand, coke oven, blast furnace (BF, including hot stoves), air separation unit (ASU), basic oxygen furnace (BOF), the casting-rolling stage and a combined cycle power plant. The mass flow inputs to the system are iron ore, coal, air, scrap, and flux, Fig. 1. Some processes are supplied also with COG, BFG, or BOFG for producing heat at high temperatures (streams *BFG* in the sinter strand, *COG* in the coke oven, *BFG* in the hot stoves, and *COG* in the basic oxygen furnace). The power plant generates electricity to be self-sufficient, consuming part of the available COG, BFG and BOFG (100 $MW_e$ net power [20]). The remaining gases are supposed to be sold to nearby industries.

The second analysed concept is a PtG-steelmaking plant (Case 1) which adds an amine scrubbing to capture $CO_2$ from the BFG, a PEM electrolyser to produce $H_2$, and a methanation plant to produce synthetic natural gas. The SNG is injected into the BF to continuously recycle the $CO_2$ and to reduce coal consumption. The $O_2$ from the electrolyser is used in part to cover the demand in the BOF, avoiding the expensive ASU, while the surplus is sold to interested industries. The resulting clean gas from the amine scrubbing (stream BFG-CLEAN) is derived to the power plant for power production. In this paper, Case 1 is assessed in comparison with Case 0 in terms of energy requirements, $CO_2$ emission reduction and economic feasibility.

The use of PtG (SNG) as opposed to $PtH_2$ in the proposed process concept (Case 1) offers the following advantages. Although the addition of the methanation step to water electrolysis in general process incurs additional energy losses, the injection of methane is a demonstrated technology in the iron and steel sector [21,22], whereas the injection of $H_2$ in the BF is relatively new. Additionally, $H_2$ injection has been found to reduce the adiabatic flame temperature (AFT) of the BF at a much faster rate than $CH_4$ injection does [18], which means that for the same AFT, more $CH_4$ than $H_2$ can be injected, thereby achieving higher coke consumption reductions. Furthermore, $H_2$ has also a lower coke replacement ratio than $CH_4$, which means that less coke can be saved by injecting $H_2$. Moreover, when adopting the SNG route, part of the $CO_2$ is converted to SNG, instead of being emitted into the atmosphere, achieving also higher $CO_2$ reductions. Furthermore, thanks to the heat integration applied in this study, the energy rejected by the methanation process can provide the heat requirement of the carbon capture system (amine scrubbing), with no extra fuel requirement.

## 3. Modelling methodology

Models of Case 0 and Case 1 were implemented in Aspen Plus v11 using the PENG-ROB property method for iron and steel processes and the ASU, the ELECNRTL property method for amines and electrolyser, the PR-BM property method for the combined cycle power plant, and the SRK property method for methanation [23]. In the case of non-conventional solids (i.e., coal), HCOALGEN and DCOALIGT property models were used with the following correlations [24]: (i) Revised IGT correlation for the heat of combustion [25], (ii) Direct correlation for the heat of formation, (iii) Kirov correlation for the specific heat capacity, and (iv) IGT correlations for density on a dry basis. In addition, user-defined heat capacities from NIST database were used for different chemical components (instead of the data provided by the Aspen Plus database) to increase the valid range of application up to 2700 K. Simulations were performed under steady-state conditions, chemical

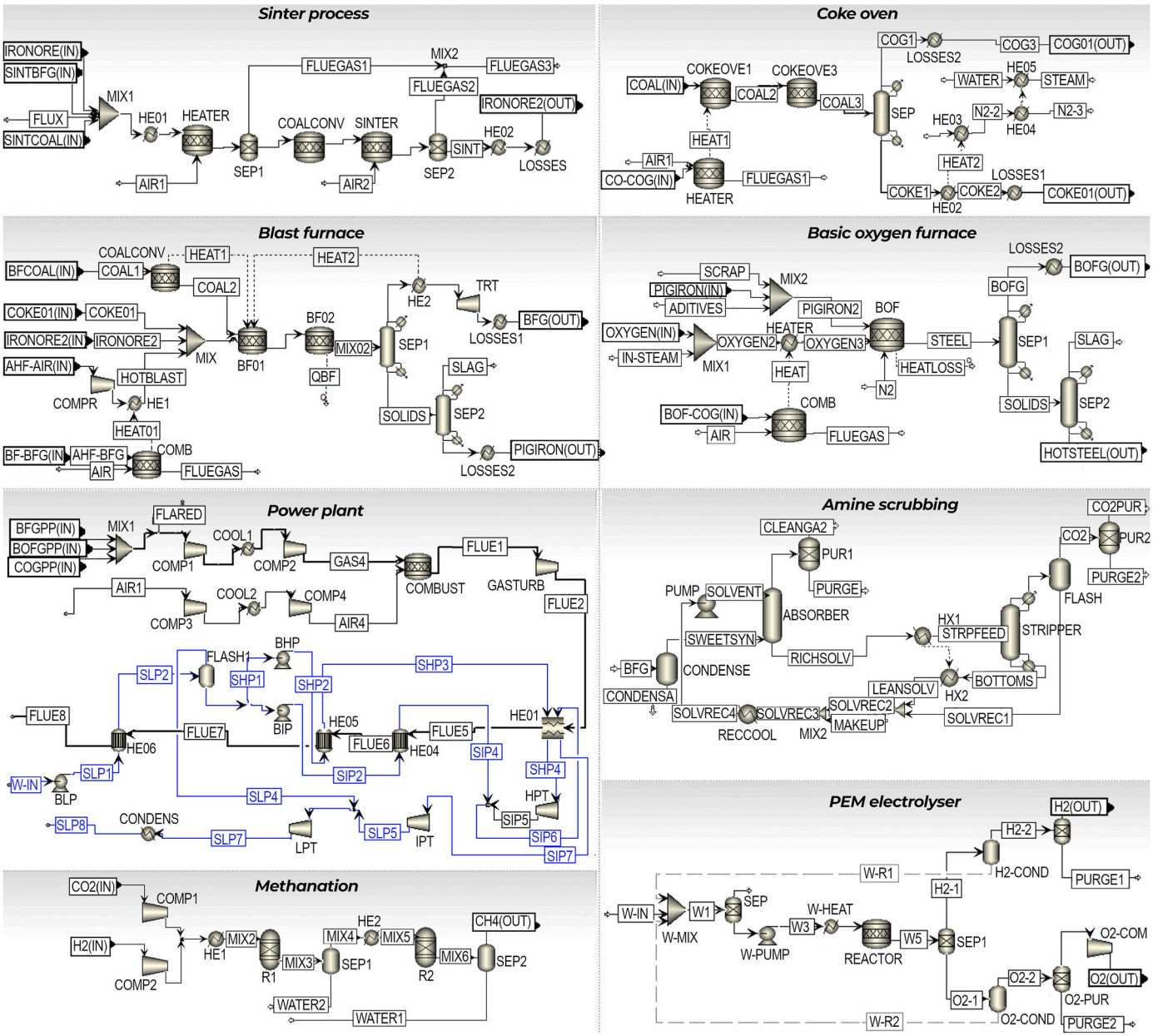


**Fig. 2.** Process flow diagrams of the Hierarchy blocks. Blue lines in Power Plant section represent the steam cycle. The nomenclature of each block can be found at the bottom of the figure. Further details about each block can be found in Annex A.

**Table 2**
Proximate and ultimate analysis of the coal [26].

| Proximate Analysis | % | Ultimate Analysis | % |
|---|---|---|---|
| MOISTURE | 1.20 | ASH | 10.89 |
| FC | 71.59 | CARBON | 77.73 |
| VM | 17.42 | HYDROGEN | 4.20 |
| ASH | 10.89 | NITROGEN | 1.59 |
| | | SULFUR | 0.43 |
| | | OXYGEN | 5.16 |

equilibrium, and complete combustion assumption. Table 1 details modelling input and outputs for stream compositions flows and temperature, for main streams of both the proposed low-carbon steelmaking process concept and conventional BF-BOF process.

The process modelling methodology for the iron and steel plant, amine scrubbing and power-to-gas sub-systems is described in Sections 3.1 to 3.3, respectively. The approaches used to evaluate the energy and economic penalties associated with carbon emission abatement are described in Sections 3.4 and 3.5, respectively.

### 3.1. Iron and steel making processes for both conventional and PtG-amine scrubbing based BF-BOF processes

The PFD of Fig. 1 shows the Hierarchy blocks that model the different stages of Case 0 and Case 1. Each Hierarchy block gathers the necessary sub-models of the involved processes, as shown in Fig. 2 (further details in Appendix A). The SINTER Hierarchy represents the agglomeration of fine ore particles, which takes place through an incipient fusion caused by the combustion of coal (see Fig. 2. Process flow diagrams of the Hierarchy blocks. Blue lines in Power Plant section represent the steam cycle. The nomenclature of each block can be found at the bottom of the figure. Further details about each block can be found in Annex A.

Table 2) [2]. First, a mixture of iron ore, coal (5%wt) and limestone

**Table 3**
Mass flows (kg/$t_{HM}$) of the main streams for the conventional I&S plant (Case 0) and the PtG-amine scrubbing bases I&S integration (Case 1). Stream ID corresponding to Fig. 1.

| Hierarchy | Stream ID | Typical values [12,20,29,44,45] | Case 0 | Case 1 |
|---|---|---|---|---|
| SINTER | Iron ore | 1315–1510 | 1464 | 1464 |
| SINTER | Coal | 45–75 | 75 | 75 |
| SINTER | Iron ore (out) | 1315–1510 | 1555 | 1555 |
| COKE OVEN | Coal | 380–534 | 443 | 443 |
| COKE OVEN | Coke | 300–400 | 332 | 332 |
| COKE OVEN | COG (out) | 100–140 | 111 | 111 |
| BF | Coal | 150–200 | 150 | 89 |
| BF | Air | 1100–1600 | 1449 | 1520 |
| BF | BFG | 1800–2420 | 2216 | 2242 |
| BF | Slag | 260–298 | 261 | 261 |
| BF | Pig iron | 1000 | 1000 | 1000 |
| BOF | Scrap | 150 | 150 | 150 |
| BOF | Oxygen | 60–90 | 87 | 87 |
| BOF | N2 | 29 | 9 | 9 |
| BOF | BOFG | 90–130 | 128 | 128 |
| CASTING | Steel | 1000–1100 | 1079 | 1079 |
| AMINES | BFG | – | – | 604 |
| AMINES | BFG-CLEAN | – | – | 461 |
| AMINES | CO2 | – | – | 145 |
| PEM | Water | – | – | 245 |
| PEM | H2 | – | – | 26 |
| ASU/PEM | O2 | – | 87 | 207 |
| METHAN | SNG | – | – | 54 |

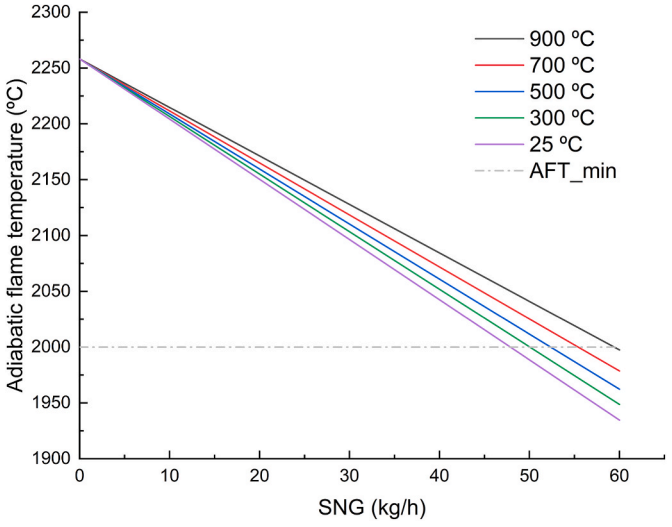


**Fig. 3.** Adiabatic flame temperature of the BF as a function of the SNG flow rate and temperature, when replacing coal by SNG for the proposed plant with PtG and amine scrubbing (Case 1).

is heated up to 800 °C using BFG as fuel, and then the coal of the mixture is burnt to form the sinter [20,21]. The COKEOVEN Hierarchy simulates the coke-making process from coal under anaerobic conditions. Temperature increases up to 1100 °C by burning COG (indirect heat exchange), producing coke as the target product and coke oven gas as a by-product. Then, the coke is cooled to 150 °C in the coke dry quenching (CDQ).

The BF Hierarchy comprises hot stoves and a simplified version of a blast furnace. In the hot stoves, the air is compressed up to 5 bar and indirectly heated up to 1200 °C. In the blast furnace, a first reactor reduces iron oxides to metallic iron, and a second reactor adjusts the BFG composition as a function of the CO and $H_2$ utilization (Eq. (1) and Eq. (2), respectively). The pulverised coal rate in the BF is initially fixed at 150 kg/$t_{HM}$, the $H_2$ utilization at 0.47, and the carbon content in hot metal at 4.5 wt% [21,22]. The rest of the necessary parameters (BFG temperature and composition, air and coke flow rates, and flame temperature) were externally calculated through a revised Rist diagram [14,17,27]. These data were introduced into the Aspen Plus model as inputs. When injecting SNG to the BF (Case 1), the coal rate is decreased to keep the same total coke input.

$$\mu_{CO} = CO_2 / (CO_2 + CO) \quad (1)$$

$$\mu_{H2} = H_2O / (H_2O + H_2) \quad (2)$$

The BOF Hierarchy converts the hot metal (4.5 wt% C) to steel (0.267 wt% C) by blowing pure $O_2$ to react with carbon, producing CO and $CO_2$. This reaction is highly exothermal, so 150 kg/$t_{HM}$ of scrap (0.267 wt% C) are added to take advantage of this energy [28,29]. The scrap melts and dissolves with the rest of the hot metal, increasing the total steel production and controlling the temperature of the process (1650 °C [19,30]). Also, some nitrogen is added from the bottom of the BOF to stir the mixture [19]. Part of the BOFG is used to preheat the oxygen inlet stream up to 1650 °C. This $O_2$ is produced in the ASU Hierarchy, which is based on the Hampson-Linde cycle. The ASU model was directly taken from the Aspen Plus repository (example block Power, Coal gasification, IGCC [31]), so it is not included in Fig. 2. This process separates the oxygen at −189 °C by liquefaction with 94% purity [32–34].

The PPLANT Hierarchy models a combined cycle power plant fuelled by unused BFG, COG and BOFG (100 MWe net power, [20]) [29,35]. The gas power cycle (stream in black in Fig. 2) consists of two stage air compression with intercooling before the combustion chamber and one expansion turbine for the flue gas. The turbine inlet pressure and temperature are 27 bar and 1389 °C, respectively [36]. The HRSG block is formed by four heat exchangers in counter-current mode that transfer the energy from the flue gases to the steam (stream in blue in Fig. 2), being the highest steam temperature 560 °C [36]. The steam power cycle consists of three expansion stages, corresponding to high, intermediate and low pressure turbines (blocks HPT, IPT and LPT).

### 3.2. Amine scrubbing processes

The amine scrubbing model was elaborated from a pre-defined Example File (Reactor and process design in Ref. [37]). It has been modified to capture 90% of the inlet $CO_2$, using methyldiethanolamine (MDEA) as solvent (50 wt% MDEA and 50 wt% water). Before diverting BFG to the capture plant, water is condensed. The absorption column has been modelled with 15 stages, the gas enters at the bottom (stage 15) while the lean solvent enters at the top (stage 1). The clean gas exits the absorber at atmospheric pressure and 42 °C through the top, while the rich solvent exits through the bottom at 43 °C and 1.1 bar (load of 0.2 $kmol_{CO2}/kmol_{MDEA}$). Then, the rich solvent is heated up to 100 °C in a heat recovery exchanger that cools the lean solvent exiting the stripper from 112 °C to 56 °C before entering again to the absorber [37]. The stripper column has 19 stages, including condenser and reboiler stages. The reflux ratio of the condenser is 0.01, and the boil-up ratio of the reboiler is 0.1 [37]. In the stripper, the rich solvent enters at the second stage, and it descends along the reactor as the $CO_2$ is released (the lean solvent leaves the stripper through the last stage, and the $CO_2$ through the first stage). A condenser separates the remaining solvent by cooling the $CO_2$-rich stream from 85 °C to 35 °C, achieving 95 vol% $CO_2$ purity. The condensed solvent is recirculated back to the absorber with the lean solvent [37]. Finally, a makeup stream, also mixed with the lean solvent before the absorber, is necessary to compensate for the water and MDEA lost in the clean gas and the $CO_2$ streams.

**Table 4**
Molar composition and lower heating value for gas streams in both the conventional process plant (Case 0) and proposed plant with PtG and amine scrubbing (Case 1).

| Composition (vol%) | Case 0 – Conventional I&S | | | | | Case 1 – I&S plant integrated with PtG and amine scrubbing | | | | | | | | |
|---|---|---|---|---|---|---|---|---|---|---|---|---|---|---|
| | COG | BOFG | BFG | $O_2$ | Sold gases | COG | BOFG | BFG | Clean BFG | $O_2$ | $H_2$ | $CO_2$ | SNG | Sold gases |
| $O_2$ | 0.07 | 1.93 | – | 95.00 | 0.15 | 0.07 | 3.31 | – | – | 99.98 | – | – | – | 0.23 |
| $N_2$ | 2.26 | 8.00 | 55.10 | 0.8 | 39.95 | 2.26 | 8.00 | 54.52 | 64.67 | – | – | 0.02 | 0.02 | 44.94 |
| CO | 9.37 | 66.00 | 21.98 | – | 22.10 | 9.37 | 66.00 | 21.21 | 25.01 | – | – | 0.79 | – | 23.41 |
| $CO_2$ | 2.34 | 19.35 | 19.37 | – | 15.51 | 2.34 | 20.69 | 17.30 | 2.05 | – | – | 95.82 | 0.99 | 7.51 |
| $H_2$ | 57.31 | 2.00 | 2.25 | – | 14.70 | 57.31 | 2.00 | 5.67 | 6.72 | 0.02 | 100.0 | 0.00 | 3.86 | 17.51 |
| $H_2O$ | – | – | 1.3 | – | 0.92 | – | – | 1.30 | 1.55 | – | – | 3.37 | 0.50 | – |
| $CH_4$ | 28.65 | – | – | – | 6.49 | 28.65 | – | – | – | – | – | – | 94.65 | 6.41 |
| Ar | – | 2.72 | – | 4.2 | 0.18 | – | – | – | – | – | – | – | – | – |
| LHV (MJ/kg) | 39.27 | 6.18 | 2.23 | – | 5.81 | 39.27 | 6.18 | 2.53 | 3.29 | – | 119.9 | – | 48.73 | 6.69 |

### 3.3. Power to gas processes

The PEM Hierarchy stands for the water electrolysis process. The input stream is water at ambient conditions (25 °C and 1 atm), and the energy consumption is set to 3.8 kWh/$Nm^3_{H2}$ [38]. The outlet hydrogen stream drags 2 mol of $H_2O$ per mole of $H_2$ (which are condensed and recirculated), and 0.1% of $O_2$ (which is purified). The outlet oxygen flow has only traces of hydrogen (0.01%) [38,39].

The METHAN Hierarchy contains the methanation plant where the $CO_2$ from the amine scrubbing reacts with the $H_2$ from the electrolyser to produce SNG, under stoichiometric conditions [40]. The plant uses two isothermal fixed-bed reactors working at 5 bar [41,42]. The temperature of the gas entering to the first reactor is 250 °C, while the reactor is kept isothermal at 350 °C. The outlet stream is cooled up to 100 °C to condensate the water, and then heated up to 250 °C before being diverted to the second stage. The second reactor operates at 300 °C. After this reactor, water is condensed at 25 °C to reach a SNG of 95 vol% $CH_4$.

### 3.4. Energy penalty assessment

The energy penalty associated with carbon emission reduction relative to the conventional BF-BOF process is defined as the net energy consumed per kilogram of $CO_2$ avoided through Power to Gas and amines carbon capture integration (Eq. (3)).

$$E_{penalty} = \frac{\left(E_{cons}^{Case1} - E_{prod}^{Case1}\right) - \left(E_{cons}^{Case0} - E_{prod}^{Case0}\right) - \left(\dot{m}_{coal}^{Case0} - \dot{m}_{coal}^{Case1}\right) * Q_{coal} * \mu_{elec} - \left(\dot{m}_{gases}^{Case1} * Q_{gases}^{Case1} - \dot{m}_{gases}^{Case0} * Q_{gases}^{Case0}\right) * \mu_{elec}}{CO_2^{Case0} - CO_2^{Case1}} \quad (3)$$

Where $E_{cons}$ is the electricity consumed in the industry (MJ/$t_{HM}$), $E_{prod}$ is the electricity produced by the owned power plant (MJ/$t_{HM}$), $\dot{m}_{coal}$ is the coal consumption (kg/$t_{HM}$), $Q_{coal}$ is the coal heating value (MJ/kg), $\dot{m}_{gases}$ is the steel gases sold (kg/$t_{HM}$), $Q_{gases}$ is the steel gases heating value (MJ/kg) and $\mu_{elec}$ is the energy conversion factor from coal to electricity (0.33).

### 3.5. Economic analysis

The cash flow statement was analysed for the investment required to integrate power to gas and amine scrubbing in the I&S plant (i.e., passing from Case 0 to Case 1), assuming 4% interest (i) for discount coefficient ($D_{coeff}$, defined in Eq. (4), where n is the year). The power to gas system is assumed to operate 8000 h per year [43], with electricity purchased from the grid if needed with renewable electricity assumed. The annual OPEX with regards to the reference plant are the amine renovation, the catalyst renovation, the purchased electricity, the water consumed by the electrolyser and the operation and maintenance (O&M). The annual incomes are the saved coal, the saved $CO_2$ taxes, the sold oxygen and the sold fuel gases to other industries.

$$D_{coeff} = \frac{1}{(1+i)^n} \quad (4)$$

## 4. Results and discussion

The comparative energy analysis of the proposed integrated PtG and amine scrubbing based steelmaking process (Case 1), and conventional BF-BOF steelmaking process (Case 0), is presented in Section 4.1 based on the simulation results. Coal and emissions savings associated with the novel PtG-amine scrubbing based process are presented and discussed in Section 4.2. The heat integration analysis performed to reduce the energy penalty of the proposed low-carbon steelmaking process concept is presented in Section 4.2. The economic viability of the proposed PtG and amine scrubbing based process concept is analysed in Section 4.3.

### 4.1. Simulation of conventional I&S plant (case 0) and PtG integration (case 1)

The conventional I&S plant (Case 0) was simulated considering the literature data summarized in Table 3. In the base case, 1079 kg/$t_{HM}$ of steel are produced by consuming 1464 kg/$t_{HM}$ of iron ore, 668 kg/$t_{HM}$ of coal, and 150 kg/$t_{HM}$ of scrap. After fulfilling the internal energy consumption, the remaining gases are mixed and used for electricity production in the power plant or sold to other industries (490 kg/$t_{HM}$ and 438 kg/$t_{HM}$ respectively).

When integrating power to gas (Case 1), the injection of SNG allows for replacing a fraction of fossil fuel, but it leads to a decrease of the adiabatic flame temperature (AFT) at the raceways. Since the AFT should not be dropped below 2000 °C for technical reasons [46–49], the amount of SNG that can be injected is limited, as well as the size of the power to gas plant. Since replacing coke with SNG leads to a greater reduction in AFT, the substitution of coal (PCI) instead is considered to allow for greater PtG plant size. Fig. 3 shows the dependence of AFT on the SNG flow rate and on its inlet temperature when replacing coal. The preheat temperature is fixed at 700 °C (red line) according to the literature [47], so the maximum SNG flow rate to be injected is 53.6 $kg_{SNG}/t_{HM}$. It corresponds to a coal replacement ratio of 1.14 $kg_{Coal}/kg_{SNG}$, and a reduction in AFT of 4.3 °C/$kg_{SNG}$.

In order to obtain 53.6 $kg_{SNG}/t_{HM}$, a production of 26.1 $kg_{H2}/t_{HM}$ in the electrolyser is needed. This corresponds to a PEM electrolyzer of 335

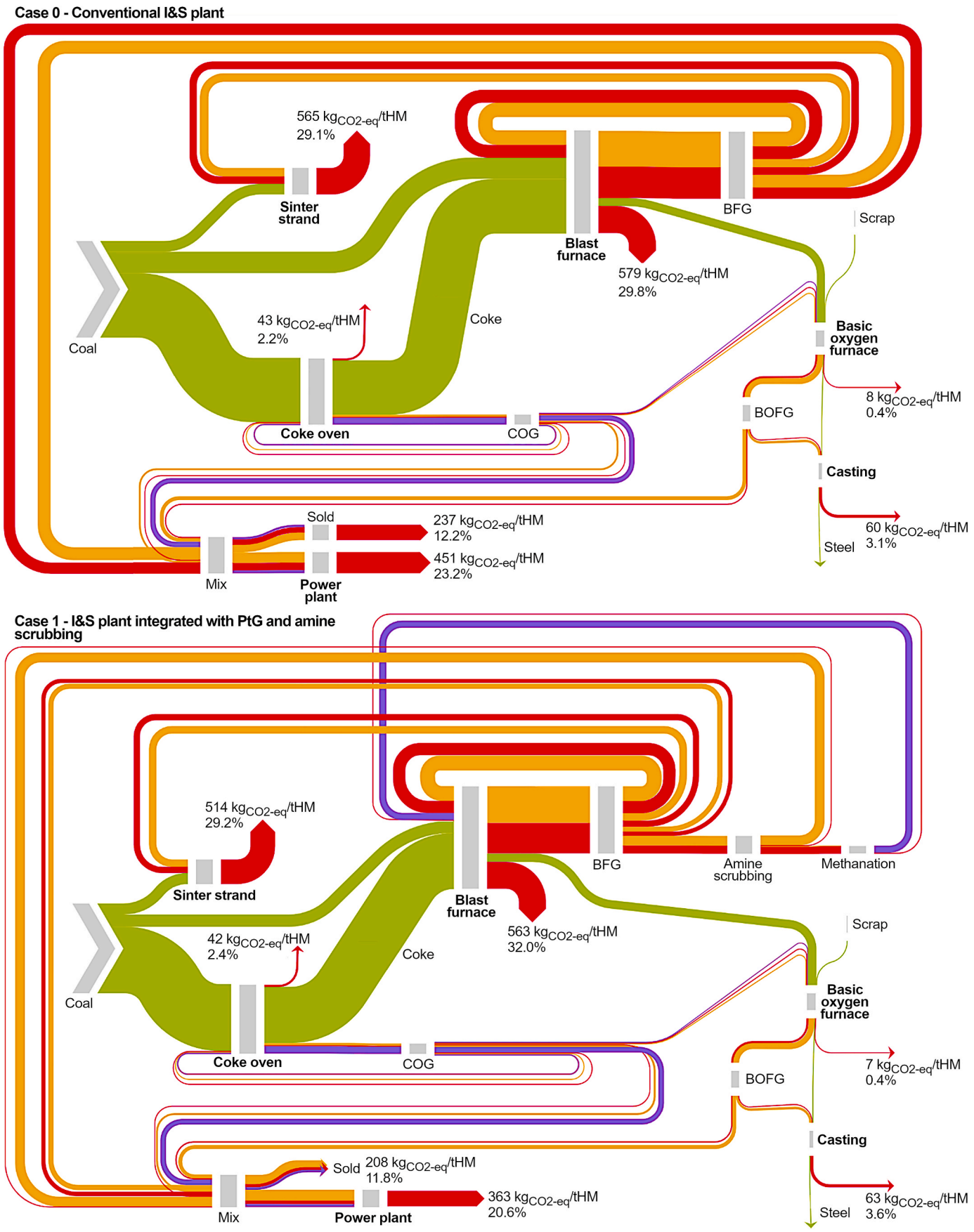


**Fig. 4.** Sankey diagram of the carbon mole flows ($kg_{CO2\text{-}eq}/t_{HM}$) in both the conventional process plant (Case 0) and proposed plant with PtG and amine scrubbing (Case 1). Green: C; Orange: CO; Red: $CO_2$; Purple: $CH_4$.

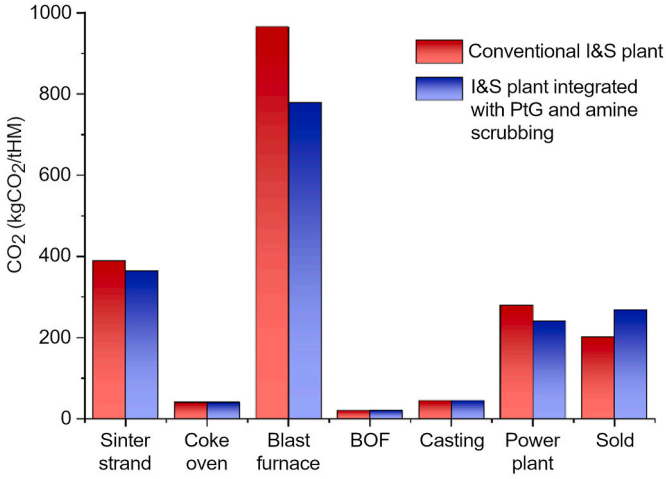


**Fig. 5.** $CO_2$ production by process ($kg_{CO2}/t_{HM}$) for the conventional I&S plant (Case 0) and its integration with PtG and amine scrubbing (Case 1).

**Table 5**
Process temperature and heat released and absorbed by each block of the amine and methanation system for the PtG and amine scrubbing based process (Case 1).

| Block ID | Type | Load ($MJ/t_{HM}$) | T in (°C) | T out (°C) |
|---|---|---|---|---|
| R1 | ↙ Cooling | −500.6 | 350 | 350 |
| R2 | ↙ Cooling | −12.0 | 300 | 300 |
| SEP1 | ↙ Cooling | −324.1 | 350 | 100 |
| SEP2 | ↙ Cooling | −103.9 | 300 | 25 |
| Stripper | ↗ Heating | +542.3 | 110 | 130 |
| HE1 | ↗ Heating | +28.5 | 193 | 250 |
| HE2 | ↗ Heating | +28.8 | 100 | 250 |

MW, assuming a hot metal production of 320 $t_{HM}$/h. According to the simulation, the total electricity consumption of the electrolysis plant is 4021 $MJ/t_{HM}$ (3981 $MJ/t_{HM}$ in the stack, 39.8 $MJ/t_{HM}$ in the compressors and 0.06 $MJ/t_{HM}$ in the pump). The $O_2$ by-produced in the electrolyser amounts to 207 $kg_{O2}/t_{HM}$, which is enough to replace the ASU, and sell the excess to other industries. The water consumption accounts for 245 $kg_{H2O}/t_{HM}$, but the most part can be supplied internally by recycling water streams from the I&S plant and the PtG plant.

The carbon capture plant is also sized according to the SNG requirements (to obtain 53.6 $kg_{SNG}/t_{HM}$, 145 $kg_{CO2}/t_{HM}$ are needed). Since amine scrubbing captures 90% of the inlet $CO_2$, and the BFG has 17.3 vol % of $CO_2$ (Table 4), the total mass flow of BFG that has to be treated in the amine plant is 604 $kg_{BFG}/t_{HM}$, in order to obtain a $CO_2$ stream of 145 $kg_{CO2}/t_{HM}$ for the methanation plant. Results show a specific heat consumption of 3.74 $MJ/kg_{CO2}$ (i.e., 542.3 $MJ/t_{HM}$) for the amine scrubbing process (which is in agreement with literature, 3.1–3.64 $MJ/kg_{CO2}$ [50]). The electricity consumption in the amine plant is 29 $kJ/kg_{CO2}$ (i.e., 4.2 $MJ/t_{HM}$) [50].

In the methanation plant, there is only electricity consumption, which amounts to 2.09 $MJ/kg_{SNG}$ (i.e., 112 $MJ/t_{HM}$). The heat released by the exothermic reaction was 16.3 $MJ/kg_{SNG}$ (i.e. 874 $MJ/t_{HM}$), which is enough to satisfy the methanation preheaters as well as the thermal demand of the amine scrubbing process.

### 4.2. $CO_2$ emissions and coal saving

The total operational $CO_2$-equivalent emissions of the conventional I&S plant are 1943 $kg_{CO-eq}/t_{HM}$ which is in agreement with the literature, 1800–2500 $kg_{CO2-eq}/t_{HM}$ [30,51–53]. These emissions can be diminished to 1760 $kg_{CO2-eq}/t_{HM}$ by integrating power to gas, representing a 9.4% reduction in $CO_2$-equivalent emissions. The cut in $CO_2$-equivalent emissions is directly related to the saving in coal consumption. The amount of pulverised coal substituted by SNG in the BF is 65 $kg/t_{HM}$ (56.7% replacement), which represents 9.6% of the total coal consumed in the whole I&S plant accounting sinter strand, coke oven and BF (680 $kg/t_{HM}$ in the base case).

The Sankey diagrams (Fig. 4) show how these equivalent emissions are distributed through the BF-BOF plant by type of component (green: C, orange: CO, red: $CO_2$, and purple: $CH_4$). The equivalent $CO_2$ released in the sinter strand is reduced by 9% when integrating PtG because the BFG burnt in the preheating of the sinter has a higher energy content and lower $CO_2$ volume fraction. Therefore, less BFG mass flow rate is needed

**Table 6**
Heat exchanger network of the pinch analysis for the PtG and amine scrubbing based process (Case 1).

| HEX | Block ID | Load ($MJ/t_{HM}$) | Area ($cm^2/(t_{HM}/h)$) | Area ($m^2$)[a] | ΔT min Hot (°C) | ΔT min Cold (°C) |
|---|---|---|---|---|---|---|
| HE-A | R1 to HE1 | 28.5 | 20319 | 650 | 99.5 | 153.8 |
| HE-B | R1 to HE2 | 28.8 | 16970 | 543 | 100.0 | 249.5 |
| HE-C | SEP1 to STRIPPER | 84.2 | 6104 | 195 | 220.0 | 175.1 |
| HE-D | R1 to STRIPPER | 443.3 | 23778 | 761 | 220.0 | 239.5 |
| HE-E | SEP1 to WATER | 239.9 | 22315 | 714 | 265.1 | 85.0 |

[a] Assuming a BF of 320 $t_{HM}$/h.

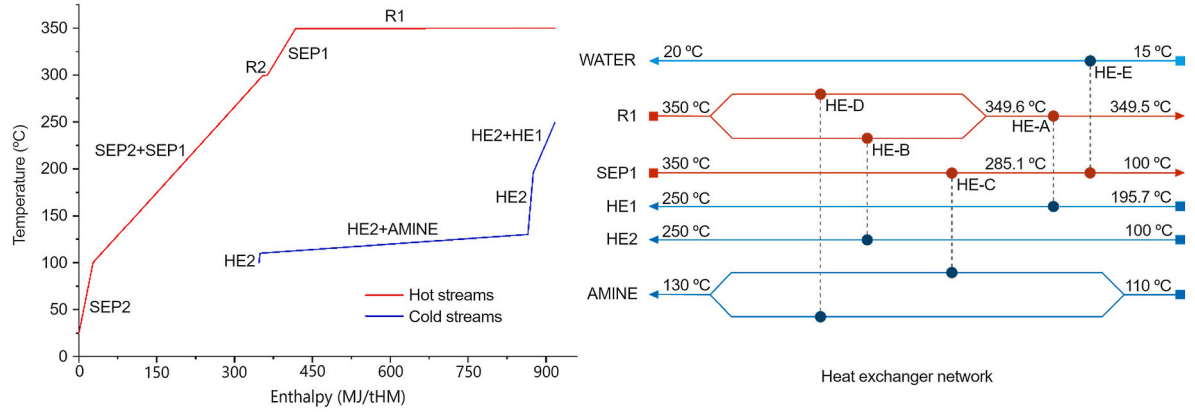


**Fig. 6.** Heat integration through pinch analysis of the amine plant and the methanation plant for the PtG and amine scrubbing based process (Case 1). Left: Composite curve; Right: Heat exchanger network.

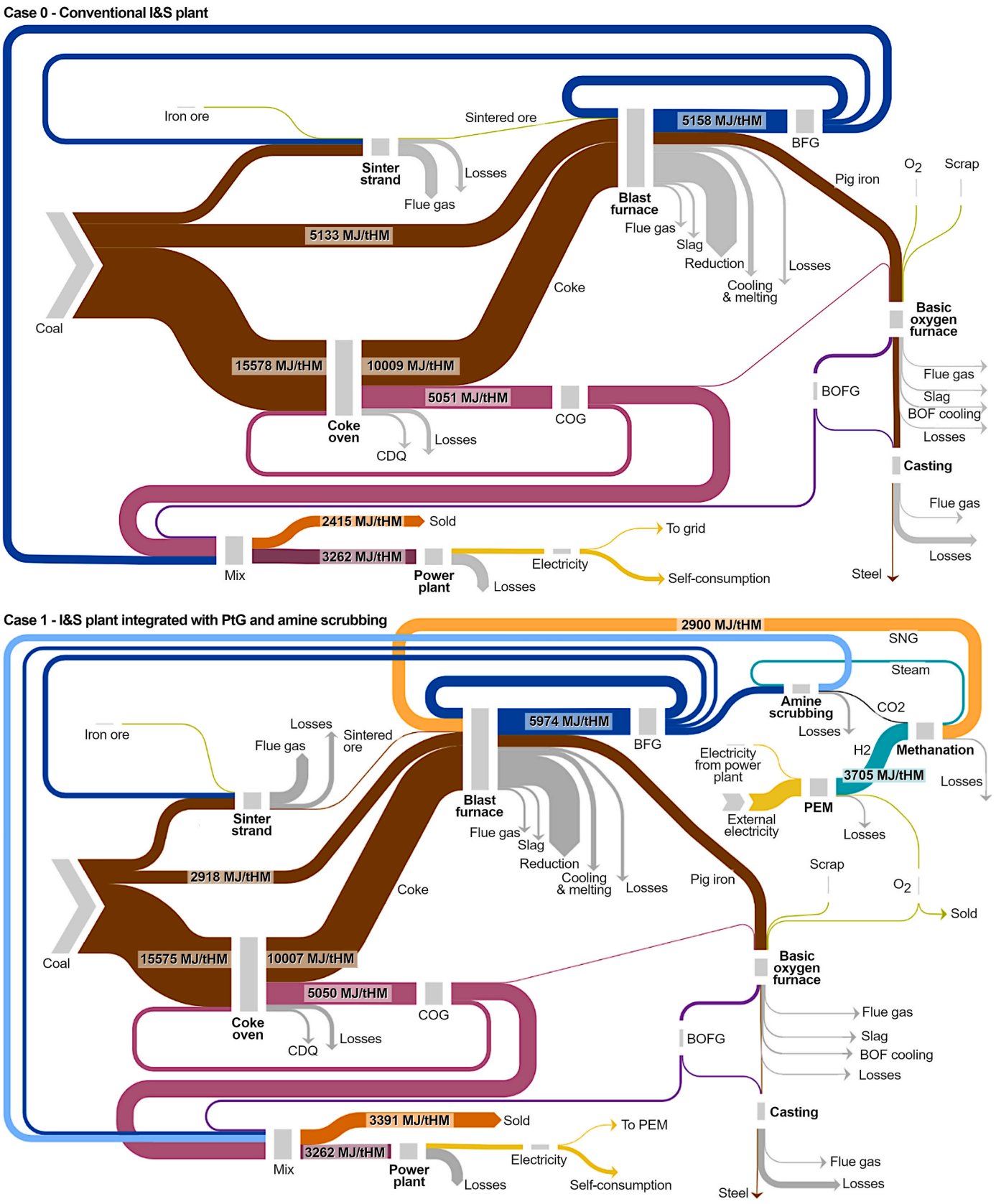


**Fig. 7.** Sankey diagram of the energy flows in both the conventional process plant (Case 0) and proposed plant with PtG and amine scrubbing (Case 1).

**Table 7**
Main electrical consumptions and productions ($MJ/t_{HM}$) calculated for the conventional I&S plant (Case 0) and its integration with PtG and amine scrubbing (Case 1).

| | Case 0 | Case 1 |
|---|---|---|
| Electricity consumption | | |
| Sintering [29] | 180 | 180 |
| Coke oven [29] | 42 | 42 |
| Blast Furnace [29] | 376 | 376 |
| ASU | 119 | – |
| PEM | – | 4021 |
| Amines | – | 5 |
| Methanation | – | 108 |
| BOF [29] | 128 | 128 |
| Other [29] | 105 | 105 |
| Total | 950 | 4965 |
| Electricity production | | |
| Power plant | 1122 | 1122 |
| Power plant efficiency | 34.4% | 34.4% |

to provide the same energy. This effect also occurs in the BF block, whose direct emissions are related to the BFG consumed to preheat the hot blast. However, in this case the reduction in $CO_2$-equivalent emissions is lower (3%) because the effect is counterbalanced by the higher amount of hot blast required and by the necessity of preheating the SNG to 700 °C (i.e., more BFG is consumed). The major reduction in $CO_2$-equivalent emissions takes place in the power plant (19.5% reduction), since most of the $CO_2$ that was being diverted (because of the BFG) is now recycled into methane. This can be seen in the red line which is now captured by the amine scrubbing and converted to methane (purple line). Other sub-processes such as the coke oven, the BOF, and the casting step, are barely affected by the PtG integration.

Despite the $CO_2$-equivalent emissions are similar in the hot stoves, the sintering process and the downstream gases (power plant and sold gases), most of the $CO_2$ released was originally generated in the blast furnace. Fig. 5 depicts the $CO_2$ actually generated in each process of the I&S plant (not the $CO_2$-equivalent emissions), including the conversion shown in the Sankey diagram for C (green colour), CO (yellow colour) or $CH_4$ (purple colour). The $CO_2$ pre-existing in the input stream is accounted into the stage where is generated (e.g., in the sintering process it is not accounted for the $CO_2$ coming from the BFG, since it was actually generated and considered in the BF). Under this framework, it can be seen in Figs. 4 and 5 that the BF actually produces 966 $kg_{CO2}/t_{HM}$ in Case 0, but these emissions are later diverted in the form of BFG and emitted in other processes (sintering and power plant mainly). When integrating power to gas, the production of $CO_2$ in the BF is decreased by 19% (to 780 $kg_{CO2}/t_{HM}$), but it is still the major producer of $CO_2$ in the I&S plant. The reduction is due to the recycling of $CO_2$ (carbon closed loop) and the utilization of fuel with greater hydrogen content ($CH_4$ instead of coal). It can be seen that the $CO_2$ generated in the sinter strand and in the power plant barely changes, since both processes keep producing the same amount of energy (heat or electricity), which means the same conversion of CO into $CO_2$. The little decrease is due to the greater $H_2$ content and lower $CO_2$ content in the BFG which in turn reduces the CO consumption as less inert gas has to be heated. The processes in coke oven, BOF and casting produce small amounts of $CO_2$, since their outlet gases are mainly composed of CO and $CH_4$.

### 4.3. Heat integration and energy penalty

When integrating Power to Gas and amine scrubbing (Case 1), new thermal streams arise in the process flow diagram. The methanation process provides heat at 300–350 °C, while the $CO_2$ desorption requires heat at 110–130 °C. Moreover, additional preheating and condensation stages come into operation. Therefore, the proposed concept was thermally integrated using Pinch analysis to reduce the energy penalty. The overall cooling and heating needs of the PtG plant are 940.6 $MJ/t_{HM}$ and 599.6 $MJ/t_{HM}$, respectively (Table 5). The main heating requirement (solvent regeneration in Stripper) can be satisfied by the cooling needs of methanation process. The analysis with Aspen Energy Analyser tool provided 11 different possible configurations, being the feasible number of heat exchangers between 5 and 9. Fig. 6 shows the composite curve of the Pinch analysis and the selected network of five heat exchangers. Assuming a BF producing 320 $t_{HM}/h$, the major heat exchanger would require an effective area of 8.8 $m^2$ (Table 6).

The selected configuration does not recover heat from reactor 2 (block R2) because of the low amount of energy available, nor from the separator 2 (SEP2) because of the low temperature level. Producing steam with the remaining heat is also not worth it because of the low energy flow recoverable compared with the energy available from other processes within the steel plant (investment in additional pipes for this steam distribution would not be reasonable). Another alternative to heat integration would be to increase the size of the $CO_2$ capture plant to match the heat available in methanation. However, this option is discarded because it would imply the need for geological storage for the extra $CO_2$, which is not considered in Case 1.

Thanks to the heat integration, we avoid using part of the BFG in the heat requirements of the amine scrubbing and in the preheating of the methanation plant. Thus the total energy that can be sold in the form of fuel gases is 3391 $MJ/t_{HM}$ for Case 1 (I&S integrated with PtG), which is

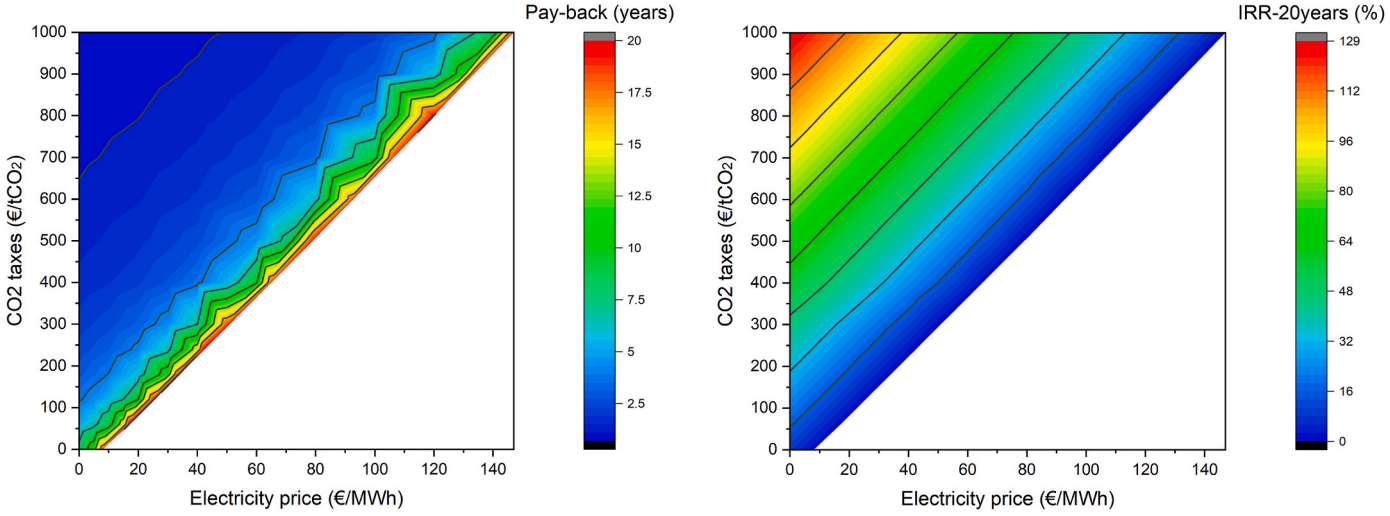


**Fig. 8.** Pay-back and Internal rate of return (IRR) as a function of electricity price and CO2 taxes for the proposed plant with PtG and amine scrubbing (Case 1).

**Table 8**
Economic analysis for PtG and amine scrubbing integration in the iron and steel industry (Case 1).

| | Cost (M€) or (M€/y) | Cost equation (M€) or (M€/y) | Parameters α, β, γ | Ref. |
|---|---|---|---|---|
| CAPEX | | | | |
| Amine Plant | | | | |
| Overall Cost | 7.40 | $26.094 \cdot (\alpha/408)^{0.65}$ | $CO_2$ captured [t/h] | [57] |
| Electrolysis | | | | |
| Overall Cost | 142 | $400 \cdot 10^{-6} \cdot \alpha$ | Power [kW] | [58] |
| Methanation | | | | |
| H2 compressor | 0.036 | $0.267 \cdot (\alpha/445)^{0.67}$ | Power [kW] | [59] |
| CO2 compressor | 0.017 | $0.267 \cdot (\alpha/445)^{0.67}$ | Power [kW] | [59] |
| Reactors | 0.245 | $300 \cdot 10^{-6} \cdot \alpha$ | SNG power [kWSNG] | [60] |
| Catalyst | 4.391 | $0.1875 \cdot \alpha$ | Volume of catalyst [$m^3$] | [59] |
| Heat exchangers | | Aspen Energy Analyzer | | |
| HE-A | 0.137 | $(9016.3 + 721.3 \cdot (\alpha^{0.8})) \cdot 10^{-6}$ | Area [$m^2$] | – |
| HE-B | 0.120 | $(9016.3 + 721.3 \cdot (\alpha^{0.8})) \cdot 10^{-6}$ | Area [$m^2$] | – |
| HE-C | 0.058 | $(9016.3 + 721.3 \cdot (\alpha^{0.8})) \cdot 10^{-6}$ | Area [$m^2$] | – |
| HE-D | 0.155 | $(9016.3 + 721.3 \cdot (\alpha^{0.8})) \cdot 10^{-6}$ | Area [$m^2$] | – |
| HE-E | 0.147 | $(9016.3 + 721.3 \cdot (\alpha^{0.8})) \cdot 10^{-6}$ | Area [$m^2$] | – |
| Other direct costs | | | | |
| Installation | 15.47 | $10\% \cdot \alpha$ | Total equipment costs [€] | [57] |
| Instrumentation & control | 6.19 | $4\% \cdot \alpha$ | Total equipment costs [€] | [57] |
| Piping | 24.75 | $16\% \cdot \alpha$ | Total equipment costs [€] | [57] |
| Electrical | 7.74 | $5\% \cdot \alpha$ | Total equipment costs [€] | [57] |
| Building | 7.74 | $5\% \cdot \alpha$ | Total equipment costs [€] | [57] |
| Land | 1.55 | $1\% \cdot \alpha$ | Total equipment costs [€] | [57] |
| Indirect costs | | | | |
| Engineering | 15.27 | $7\% \cdot \alpha$ | Total direct costs [€] | [57] |
| Legal expenses | 5.37 | $2\% \cdot \alpha$ | Total CAPEX | [57] |
| Construction expenses | 10.73 | $4\% \cdot \alpha$ | Total CAPEX | [57] |
| Contingency | 18.78 | $7\% \cdot \alpha$ | Total CAPEX | [57] |
| TOTAL CAPEX | 268.3 | | | |
| OPEX | | | | |
| Amine renovation | 0.16 | $3204 \cdot 10^{-6} \cdot \alpha$ | MDEA renovation [$t_{CO2}$/y] | [61] |
| Catalyst renovation | 0.66 | $15\% \cdot \alpha$ | Initial catalyst cost [M€] | [43] |
| Electricity | 210.97 | $342.5 \cdot 10^{-6} \cdot \alpha \cdot \beta$ | Electricity cost [€/MWh], Operating hours [h/y] | – |
| Water | 0.87 | $1.47 \cdot 10^{-6} \cdot \alpha$ | Water consumption [$m^3$/y] | [62] |
| O&M | 8.05 | $3\% \cdot \alpha$ | Total CAPEX | [57] |
| TOTAL OPEX | 220.71 | | | |
| INCOMES | | | | |
| Coal | 20.42 | $130.43 \cdot 10^{-6} \cdot \alpha$ | Coal generated [$t_{Coal}$/y] | [63] |
| Oxygen | 25.13 | $80 \cdot 10^{-6} \cdot \alpha$ | $O_2$ generated [$t_{O2}$/y] | [55] |
| CO2 taxes | 39.59 | $84.28 \cdot 10^{-6} \cdot \alpha$ | $CO_2$ consumed [$t_{CO2}$/y] | [54] |
| Steel gases | 16.83 | $(15 + \alpha \cdot \beta/13) \cdot 10^{-6} \cdot \gamma$ | Natural gas price [€/MWh]<br>Steel gases LHV [kWh/kg]<br>Steel gases generated [MWh/y] | – |
| TOTAL INCOMES | 101.97 | | | |
| ANNUAL BENEFIT | −127.73 | | | |
| PAY-BACK | >20 years | | | |
| CARBON AVOIDANCE COST | 52 €/$t_{HM}$ or 283 €/$t_{CO2}$ | | | |

greater than the energy sold in the base case scenario, 2415 MJ/$t_{HM}$. The increase in the energy sold is due to the higher energy content of the BFG when injecting SNG into the blast furnace (higher $H_2$ content and lower $CO_2$ content). This leads to more efficient processes when BFG is used (sintering, BF and power plant), namely, less BFG is consumed for the same energy production. Approximately, in Case 0, 10% of the total energy input is just sold to other industries nearby, while in Case 1 it is sold the 14% (Fig. 7).

The opposite situation it is found in the case of electricity. In the conventional I&S plant (Case 0), the total electricity consumption is 950 MJ/$t_{HM}$, and the electricity produced by the power plant is 1122 MJ/$t_{HM}$ (34.4% efficiency), hence being a self-sufficient industry (Table 7). When integrating PtG, the electrical consumption remarkably increases to 4965 MJ/$t_{HM}$, mainly due to the electrolyser (4021 MJ/$t_{HM}$). The electrical production in the power plant is assumed to remain constant, as greater productions (by consuming the sold gases) would require investing in a new power plant or retrofitting the existing one. Therefore, the industry is no longer self-sufficient, and 3843 MJ/$t_{HM}$ of green electricity from a renewable source are needed in Case 1. The net energy penalty of the PtG integration is 16.2 $MJ_e/kg_{CO2}$.

### 4.4. Economic analysis

The economic analysis of the PtG integration in the iron and steel industry together with the cost equations are presented in Fig. 8, using economic parameters for year 2022. An operation of 8000 equivalent hours is considered [43], with an electricity cost of 77 €/MWh, a $CO_2$ allowances price of 84 €/$t_{CO2}$ [54], a selling price for $O_2$ of 80 €/$t_{O2}$ [55] and a variable selling price for the steel gases depending on its heating value and the natural gas price (see Table 8). The amortization of the loan is considered to happen in 20 years with an annual interest of 4%. Moreover, the volume of the reactors is calculated assuming a GHSV of 5000 $h^{-1}$ [56], and the catalyst is supposed to occupy 60% of that volume. Under the current scenario, the annual benefit of the PtG integration is negative (128 M€/y annual loss), which implies that the loan cannot be amortized. Therefore, the carbon abatement cost is 52 €/$t_{HM}$ or 283 €/$t_{CO2}$.

An economic parametric study was performed looking for those combinations of electricity prices and $CO_2$ allowances that allow the Power to Gas to be economically viable for the proposed solution. The calculated pay-back and internal rate of return (IRR) are presented in Fig. 8. It can be seen that even at electricity prices of 40 €/MWh, a minimum of 240 €/$t_{CO2}$ is required to amortize the investment (14.6

years of pay-back and 2.6% of IRR). This economic analysis suggests that profitable scenarios would require that either the electricity is obtained at the cost of production (i.e., the renewable park belongs to the I&S industry) or subsidies are given to the purchased electricity or power purchase agreements (PPAs) are signed in order to fight against global warming. For example, assuming an electricity cost of 51 €/MWh (i.e., cost production for solar panels in 2022 [64]), the PtG integration would be profitable when the $CO_2$ taxes are above 294 €/$t_{CO2}$. If the cost of the electricity is 35 €/MWh (i.e., cost of production for wind power in 2022 [64]), profits are obtained for $CO_2$ taxes greater than 177 €/$t_{CO2}$. Furthermore, for the current scenario of $CO_2$ allowances prices (84 €/$t_{CO2}$) and grid's electricity prices (77 €/MWh), the minimum subsidy to make PtG integration profitable would be 54.6 €/MWh. If the $CO_2$ taxes increases to 128 €/$t_{CO2}$ in the coming years (estimated price by 2050 by Strefler et al. [65]), the necessary subsidy would be reduced to 49 €/MWh. By 2100, Strefler estimates $CO_2$ taxes between 384 €/$t_{CO2}$ and 907 €/$t_{CO2}$, needing a 13.7 €/MWh subsidy and no subsidy respectively. In the last evaluation (907 €/$t_{CO2}$) the pay-back would be 2 years and the IRR 52%.

## 5. Conclusions

A novel concept of integrating power-to-gas (PtG) technology in the ironmaking process is presented. Synthetic natural gas (SNG) from methanation is injected into the blast furnace to reduce the pulverised coal consumption, thus recycling $CO_2$ in a closed loop. The PtG plant is sized to inject as much SNG as possible, as long as the AFT does not fall below 2000 °C, accounting for 53.6 $kg_{SNG}/t_{HM}$. The electrolyser and the amine scrubbing plants are sized according to the SNG flow rate. This concept is compared with a conventional blast furnace – basic oxygen furnace (BF-BOF) steelmaking plant (Case 0).

The base case model includes the sintering, coke oven, blast furnace, ASU, basic oxygen furnace, casting and power plant. For PtG integration, an electrolyser, amine scrubbing and methanation plant are added to the reference model, and the blast furnace is run under SNG injection. The SNG injection replaces pulverised coal injection (PCI) with a ratio of 1.14 $kg_{Coal}/kg_{SNG}$. Mass flows, compositions and thermal and electricity consumptions are calculated through Aspen Plus® software simulations.

Optimization of the heat integration between the amine plant (endothermic) and the PtG (exothermic) was carried out through the pinch analysis method. In this way, no extra heat is needed for the amine plant, which means no energy penalisation is added for capturing the $CO_2$.

Savings achieved in $CO_2$ emissions with the PtG integration are 9.4% (equivalent to $4.7{\cdot}10^5$ $t_{CO2}$/year), with a reduction in coal fuel of 9.2% (61 $kg_{Coal}/t_{HM}$, representing a 41% replacement of the PCI). The electric energy required to avoid these emissions is 16.2 $MJ/kg_{CO2}$ of renewable power for electrolysis. This significant energy penalty is mainly due to a 355 MW electrolyser.

Under the current economic situation, the concept is not economically feasible, reaching a carbon abatement cost of 52 €/$t_{HM}$ or 283 €/$t_{CO2}$. However, sensitivity analyses have shown that the concept would become economically feasible under certain conditions, depending on the $CO_2$ taxes, the electricity price or the subsidy amount.

A limitation of the economic analysis presented is the uncertainty in future electricity and carbon prices, as these parameters have a significant impact on the payback period and IRR of the proposed process concept. With regard to potential technical limitations, each steelmaking process plant has unique equipment/space layouts that can impact the practical implementation of energy integration, including heat integration.

In general, this novel concept has the advantage of reducing fuel consumption and eliminating geological storage of the recirculated $CO_2$, which are additional economic and practical benefits compared to conventional carbon capture and storage. This PtG configuration also allows the industry to be indirectly electrified since fossil fuel is replaced by synthetic natural gas, which is derived from hydrogen produced by renewable sources. Other concepts of PtG integration in the blast furnace ironmaking will be considered in future work to reduce energy penalties and costs.

## Credit author statement

Conceptualization, **J.P., M.B., and B.P.**; methodology, **J.P., M.B. and B.P.**; model, **J.P. and M.B.**; formal analysis, **J.P.**; writing—original draft preparation, **J.P. and M.B.**; writing—review and editing, M.B., B. P., L.M.R., and V.E.; visualization, **J.P. and M.B.**; supervision, **M.B. and B.P.**; project administration, **M.B. and L.M.R.**; funding acquisition, **M. B. L.M.R. and V.E.** All authors have read and agreed to the published version of the manuscript.

## Declaration of competing interest

The authors declare the following financial interests/personal relationships which may be considered as potential competing interests: Luis Miguel Romeo reports financial support was provided by University of Zaragoza. Luis Miguel Romeo and Valerie Eveloy report financial support was provided by Khalifa University. Manuel Bailera reports financial support was provided by EU Framework Programme for Research and Innovation Marie Sklodowska-Curie Actions.

## Data availability

Data will be made available on request.

## Acknowledgements

The work presented in this paper has been supported by both the University of Zaragoza under the project UZ2020-TEC-06 and Khalifa University project CIRA-2020-080. This work has also received funding from the European Union's Horizon 2020 research and innovation program under the Marie Sklodowska-Curie grant agreement no. 887077. This work is part of the R&D project PID2021-126164OB-I00, funded by MCIN/AEI/10.13039/501100011033/and by the "ERDF A way of making Europe"

## Appendix A. Aspen Plus modelling blocks considered in hierarchies

The main modelling blocks are listed in Table 9, showing the hierarchy, the block ID, the type of block (for Aspen Plus modelling), the description and the reactions.

**Table 9**
List of main Aspen Plus modelling blocks.

| Hierarchy | Block ID | Type | Description | Reactions |
|---|---|---|---|---|
| Sinter | HE01 | Heater | Preheats the mix and the BF off-gas (BFG) | n/a |
| Sinter | HEATER | RStoic | Heats the raw mix by burning the BFG with air (stream AIR1) to 800 °C | $H_2 + 0.5O_2 \rightarrow H_2O$<br>$CO + 0.5O_2 \rightarrow CO_2$ |
| Sinter | SEP1/SEP2 | Sep | Separates the flue gases from the solid phase | n/a |
| Sinter | COAL-CONV | RStoic | Converts the nonconventional coal to the individual components | $Coal \rightarrow C + H_2 + O_2 + N_2 + Ash$ |
| Sinter | SINTER | RStoic | Burns the coal creating the sinter | $C + O_2 \rightarrow CO_2$<br>$H_2 + 0.5O_2 \rightarrow H_2O$ |
| Sinter | HE02 | Heater | Recovers heat from the sintered ore to preheat the inlet (HE01) | n/a |
| Coke oven | HEATER | RStoic | Indirectly heats the coal by burning COG, until the COAL3 stream reaches 1100 °C | $H_2 + 0.5O_2 \rightarrow H_2O$<br>$CO + 0.5O_2 \rightarrow CO_2$<br>$CH_4 + 2O_2 \rightarrow CO_2 + 2H_2O$ |
| Coke oven | COKEOVE1 | RStoic | Converts the nonconventional coal to the individual components | $Coal \rightarrow C + H_2 + O_2 + N_2 + Ash$ |
| Coke oven | COKEOVE3 | RStoic | Converts the initial components obtained from coal decomposition in COKEOVE1 to the desired COG components | $C + 0.5O_2 \rightarrow CO$<br>$C + O_2 \rightarrow CO_2$<br>$C + 2H_2 \rightarrow CH_4$ |
| Coke oven | SEP | Sep | Separates the gases from the solid phase | n/a |
| BF | COALCONV | RStoic | Converts the nonconventional coal to the individual components | $Coal \rightarrow C + H_2 + O_2 + N_2 + Ash$ |
| BF | COMPR | Turbine | Compresses the inlet air to 5 bar | n/a |
| BF | HE1 | Heater | Heats the hot blast up to 1200 °C | n/a |
| BF | COMB | RStoic | Indirectly heats the hot blast by burning BFG | $H_2 + 0.5O_2 \rightarrow H_2O$<br>$CO + 0.5O_2 \rightarrow CO_2$ |
| BF | BF01 | RStoic | Reduces the iron ore to pure iron | $Fe_2O_3 + 3CO \rightarrow 2Fe + 3CO_2$<br>$Fe_2O_3 + 3C \rightarrow 2Fe + 3CO$ |
| BF | BF02 | RStoic | Reacts the coal and gases to form the BFG | $C + 0.5O_2 \rightarrow CO$<br>$CO + 0.5O_2 \rightarrow CO_2$<br>$CH_4 + 0.5O_2 \rightarrow CO + 2H_2$<br>$H_2 + 0.5O_2 \rightarrow H_2O$ |
| BF | SEP1 | Sep | Separates the gases from the solid phase | n/a |
| BF | SEP2 | Sep | Separates the slag from the pig iron | n/a |
| BF | TRT | Turbine | Top Recovery Turbine: Recovers energy from the BFG | n/a |
| BF | HE2 | Heater | Heat exchange between the BFG and the solids on the top | n/a |
| BF | LOSSES1 | Heater | Thermal losses to the ambient temperature | n/a |
| BF | LOSSES2 | Heater | Thermal losses of the pig iron out of the BF | n/a |
| BOF | COMB | RStoic | Indirectly heats the $O_2$ stream by burning COG | $H_2 + 0.5O_2 \rightarrow H_2O$<br>$CO + 0.5O_2 \rightarrow CO_2$<br>$CH_4 + 2O_2 \rightarrow CO_2 + 2H_2O$ |
| BOF | HEATER | Heater | Heats the $O_2$ stream to 1650 °C | n/a |
| BOF | BOF | RStoic | Reduces the C content and forms the BOFG | $C + 0.5O_2 \rightarrow CO$<br>$CO + 0.5O_2 \rightarrow CO_2$<br>$H_2O \rightarrow H_2 + 0.5O_2$ |
| BOF | SEP1 | Sep | Separates the gases from the solid phase | n/a |
| BOF | SEP2 | Sep | Separates the slag from the hot steel | n/a |
| BOF | LOSSES2 | Heater | Thermal losses to the ambient temperature | n/a |
| Power plant | SPLIT1 | FSplit | Separates excess gases | n/a |
| Power plant | COMP1-4 | Compr | Compresses the air and the energetic gases | n/a |
| Power plant | COOL1-2 | HeatX | Cools down the air and the gas streams | n/a |
| Power plant | COMBUST | RStoic | Burns the mixed gases | $H_2 + 0.5O_2 \rightarrow H_2O$<br>$CO + 0.5O_2 \rightarrow CO_2$<br>$CH_4 + 2O_2 \rightarrow CO_2 + 2H_2O$ |
| Power plant | GASTURB | Compr | Turbines the flue gases producing electricity | n/a |
| Power plant | HE01 | MHeatX | Heats two steam flows | n/a |
| Power plant | HE04-06 | HeatX | Vaporizes water streams | n/a |
| Power plant | FLASH1 | Flash2 | Separates the steam from the water | n/a |
| Power plant | BLP/BIP/BHP | Pump | Pumps water to low, intermediate and high pressure | n/a |
| Power plant | HPT/IPT/LPT | Compr | Turbines the steam to high, intermediate and low pressure | n/a |
| Power plant | CONDENS | Heater | Cools the steam condensing the water | n/a |
| Amine plant | CONDENSE | Flash2 | Condenses the water in the inlet stream | n/a |
| Amine plant | ABSORBER | RadFrac | Reacts the MDEA with the $CO_2$, forming the rich solvent | n/a |
| Amine plant | HX1 | Heater | Heats the rich solvent by cooling the lean solvent | n/a |
| Amine plant | STRIPPER | RadFrac | Heats the rich solvent releasing the $CO_2$ | n/a |
| Amine plant | FLASH | Flash2 | Condenses the water and MDEA in the $CO_2$ stream at 25 °C | n/a |
| Amine plant | HX2 | Heater | Cools the lean solvent by heating the rich solvent | n/a |
| Amine plant | RECCOOL | Heater | Cools the lean solvent to 40 °C | n/a |
| Amine plant | PUMP | Pump | Pumps the solvent to 1.5 bar | n/a |
| PEM | W-PUMP | Pump | Pumps the inlet water to 1.5 bar | n/a |
| PEM | W-HEAT | Heater | Heats the water to 80 °C | n/a |
| PEM | REACTOR | RStoic | Splits the water into $H_2$ and $O_2$ | $H_2O \rightarrow H_2 + 0.5O_2$ |
| PEM | SEP1 | Sep2 | Separates the $H_2$ and $O_2$ in two different streams | n/a |
| PEM | H2-COND | Flash2 | Condensates the water dragged by the $H_2$ | n/a |

(*continued on next page*)

**Table 9** (*continued*)

| Hierarchy | Block ID | Type | Description | Reactions |
|---|---|---|---|---|
| PEM | O2-COND | Flash2 | Condensates the water dragged by the $O_2$ | n/a |
| PEM | O2-COM | Compr | Compresses the $O_2$ to 5 bar | n/a |
| Methanation | COMP1 | Compr | Compresses the $CO_2$ to 5 bar | n/a |
| Methanation | COMP2 | Compr | Compresses the $H_2$ to 5 bar | n/a |
| Methanation | HE1 | Heater | Heats the gases to 250 °C | n/a |
| Methanation | R1 | RGibbs | Reacts the inlet gases to form SNG at 350 °C | $4H_2 + CO_2 \rightarrow CH_4 + 2H_2O$ |
| Methanation | SEP1 | Flash2 | Condensates the water formed in R1 at 100 °C | n/a |
| Methanation | HE2 | Heater | Heats the gases to 250 °C | n/a |
| Methanation | R2 | RGibbs | Reacts the inlet gases to form SNG at 300 °C | $4H_2 + CO_2 \rightarrow CH_4 + 2H_2O$ |
| Methanation | SEP2 | Flash2 | Condensates the water formed in R2 at 25 °C | n/a |

## References


[1] European Commission 2022. https://energy.ec.europa.eu/index_es. [Accessed 26 April 2022].
[2] Huitu K, Helle H, Helle M, Kekkonen M, Saxén H. Optimization of steelmaking using fastmet direct reduced iron in the blast furnace. ISIJ Int 2013;53:2038–46. https://doi.org/10.2355/isijinternational.53.2038.
[3] Wörtler M, Dahlmann P, Schuler F, Lüngen HB, Voigt N. Steel's contribution to a low-carbon Europe 2050-Technical and economic analysis of the sector's CO2 abatement potential. 2013. https://www.bcg.com/de-de/. [Accessed 26 April 2022]. accessed.
[4] EUROFER. A steel roadmap for a low carbon europe 2050, the European Steel Association EUROFER. 2013. Brussels, Belgium, https://www.eurofer.eu/assets/publications/archive/archive-of-older-eurofer-documents/2013-Roadmap.pdf. [Accessed 26 February 2023].
[5] International Energy Agency. Iron and steel technology roadmap. 2020. https://www.iea.org/reports/iron-and-steel-technology-roadmap. [Accessed 26 April 2022]. accessed.
[6] Midrex Technologies. The Midrex (R) Process. n.d. 2022. https://www.midrex.com/technology/midrex-process/. [Accessed 10 May 2022]. accessed.
[7] Elsheikh H, Eveloy V. Assessment of variable solar- and grid electricity-driven power-to-hydrogen integration with direct iron ore reduction for low-carbon steel making. Fuel 2022. https://doi.org/10.1016/j.fuel.2022.124758.
[8] Scheele J von. Decarbonization of ironmaking. MM Steel Club; 2021.
[9] Deerberg G, Oles M, Schlögl R. The project Carbon2Chem. Chem-Ing-Tech 2018; 90:1365–8. https://doi.org/10.1002/cite.201800060.
[10] Perpiñán J, Peña B, Bailera M, Eveloy V, Kannan P, Raj A, et al. Integration of carbon capture technologies in blast furnace based steel making: a comprehensive and systematic review. Fuel 2022. https://doi.org/10.1016/j.fuel.2022.127074.
[11] Kearns D, Liu H, Consoli C. Technology readiness and costs of CCS - global CCS institute. Glob CCS Insitute 2021:50.
[12] Bailera M, Lisbona P, Peña B, Romeo LM. A review on CO2 mitigation in the Iron and Steel industry through Power to X processes. J CO2 Util 2021;46:101456. https://doi.org/10.1016/j.jcou.2021.101456.
[13] Perpiñán J, Bailera M, Romeo LM, Peña B, Eveloy V. CO2 recycling in the iron and steel industry via power-to-gas and oxy-fuel combustion. Energies 2021;14:7090. https://doi.org/10.3390/en14217090.
[14] Bailera M, Nakagaki T, Kataoka R. Revisiting the Rist diagram for predicting operating conditions in blast furnaces with multiple injections. 2021. https://doi.org/10.12688/openreseurope.14275.1.
[15] Hisashige S, Nakagaki T, Yamamoto T. CO2 emission reduction and exergy analysis of smart steelmaking system adaptive for flexible operating conditions. ISIJ Int 2019;59:598–606. https://doi.org/10.2355/isijinternational.ISIJINT-2018-355.
[16] Rosenfeld DC, Böhm H, Lindorfer J, Lehner M. Scenario analysis of implementing a power-to-gas and biomass gasification system in an integrated steel plant: a techno-economic and environmental study. Renew Energy 2020;147:1511–24. https://doi.org/10.1016/j.renene.2019.09.053.
[17] Bailera M, Nakagaki T, Kataoka R. Extending the operating line methodology to consider shaft and preheating injections in blast furnaces. ISIJ Int 2022;62:1–12. https://doi.org/10.2355/isijinternational.ISIJINT-2022-111.
[18] Bailera M, Nakagaki T, Kataoka R. Limits on the integration of power to gas with blast furnace ironmaking. J Clean Prod 2022:134038. https://doi.org/10.1016/J.JCLEPRO.2022.134038.
[19] Steelmaking technologies. CISDI ingeniering CO. LTD; 2022. http://www.cisdigroup.com/4-steelmaking.html. [Accessed 26 April 2022].
[20] Wu J, Wang R, Pu G, Qi H. Integrated assessment of exergy, energy and carbon dioxide emissions in an iron and steel industrial network. Appl Energy 2016;183:430–44. https://doi.org/10.1016/j.apenergy.2016.08.192.
[21] Babich A, Senk D, Gudenau KTM HW. IRONMAKING 2008:402.
[22] Biswas AK. Principles of blast furnace ironmaking. Theory and practice. Cootha Publishing house; 1981.
[23] Aspen Technology Inc. Aspen physical property methods - reference manual. 2019.
[24] Aspen Technology Inc. Physical property models - reference manual. 2019.
[25] Green DW, Southard MZ. Perry's chemical engineers' handbook. ninth ed. McGraw-Hill Education; 2019.
[26] Babich AI, Gudenau HW, Mavrommatis KT, Froehling C, Formoso A, Cores A, et al. Choice of technological regimes of a blast furnace operation with injection of hot reducing gases. Rev Metal (Madr) 2002;38:288–305. https://doi.org/10.3989/revmetalm.2002.v38.i4.411.
[27] Bailera M. DISIPO project. Personal communication (mbailera@unizar.es). 2022.
[28] Fisher LV, Barron AR. The recycling and reuse of steelmaking slags — a review. Resour Conserv Recycl 2019;146:244–55. https://doi.org/10.1016/j.resconrec.2019.03.010.
[29] He H, Guan H, Zhu X, Lee H. Assessment on the energy flow and carbon emissions of integrated steelmaking plants. Energy Rep 2017;3:29–36. https://doi.org/10.1016/j.egyr.2017.01.001.
[30] Pasquale Cavaliere. Clean ironmaking and steelmaking processes. Efficient technologies for greenhouse emissions abatement n.d. https://doi.org/https://doi.org/10.1007/978-3-030-21209-4.
[31] Aspen Technology Inc. Aspen examples - reference manual. 2019.
[32] Alsultanny YA, Al-Shammari NN. Oxygen specific power consumption comparison for air separation units. Eng J 2014;18:67–80. https://doi.org/10.4186/ej.2014.18.2.67.
[33] Darde A, Prabhakar R, Tranier JP, Perrin N. Air separation and flue gas compression and purification units for oxy-coal combustion systems. Energy Proc 2009;1:527–34. https://doi.org/10.1016/j.egypro.2009.01.070.
[34] Aneke M, Wang M. Improving the energy efficiency of cryogenic air separation units (ASU) through compressor waste heat recovery using direct binary heat engine cycle, vol. 37. Elsevier; 2015. https://doi.org/10.1016/B978-0-444-63576-1.50090-X.
[35] Manzolini G, Giuffrida A, Cobden PD, van Dijk HAJ, Ruggeri F, Consonni F. Techno-economic assessment of SEWGS technology when applied to integrated steel-plant for CO2 emission mitigation. Int J Greenh Gas Control 2020;94:102935. https://doi.org/10.1016/j.ijggc.2019.102935.
[36] Kehlhofer R, Bachmann R, Nielsen H, Warner J. Combined-cycle gas & steam turbine power plants-PennWell. 1999.
[37] Shi F. Reactor and process design in sustainable energy technology. Elsevier; 2014.
[38] NEL Hydrogen 2019. https://nelhydrogen.com/. [Accessed 2 March 2022].
[39] Zaccara A, Petrucciani A, Matino I, Branca TA, Dettori S, Iannino V, et al. Renewable hydrogen production processes for the off-gas valorization in integrated steelworks through hydrogen intensified methane and methanol syntheses. Metals 2020;10:1–24. https://doi.org/10.3390/met10111535.
[40] Gao J, Wang Y, Ping Y, Hu D, Xu G, Gu F, et al. A thermodynamic analysis of methanation reactions of carbon oxides for the production of synthetic natural gas. RSC Adv 2012;2:2358–68. https://doi.org/10.1039/c2ra00632d.
[41] Izumiya K, Shimada I. K2- methane producing technology from CO 2 for carbon recycling. 2021. p. 34. –5.
[42] Rönsch S, Schneider J, Matthischke S, Schlüter M, Götz M, Lefebvre J, et al. Review on methanation - from fundamentals to current projects. Fuel 2016;166:276–96. https://doi.org/10.1016/j.fuel.2015.10.111.
[43] Bailera M, Espatolero S, Lisbona P, Romeo LM. Power to gas-electrochemical industry hybrid systems: a case study. Appl Energy 2017;202:435–46. https://doi.org/10.1016/j.apenergy.2017.05.177.
[44] He K, Wang L. A review of energy use and energy-efficient technologies for the iron and steel industry. Renew Sustain Energy Rev 2017;70:1022–39. https://doi.org/10.1016/j.rser.2016.12.007.
[45] Geerdes M, Chaigneau R, Lingiardi O, Molenaar R van O, SY R, Warren J. Modern blast furnace ironmaking an introduction. IOS Press; 2020.
[46] Abdel Halim KS, Andronov VN, Nasr MI. Blast furnace operation with natural gas injection and minimum theoretical flame temperature. Ironmak Steelmak 2009;36:12–8. https://doi.org/10.1179/174328107X155240.
[47] Halim KSA. Theoretical approach to change blast furnace regime with natural gas injection. J Iron Steel Res Int 2013;20:40–6. https://doi.org/10.1016/S1006-706X(13)60154-5.
[48] Abdel Halim KS. Effective utilization of using natural gas injection in the production of pig iron. Mater Lett 2007;61:3281–6. https://doi.org/10.1016/j.matlet.2006.11.053.
[49] Peacey JG, Davbenport WG. The iron blast furnace. Theory and practice. 1979. 1979. ISBN 0-08-023258-2.
[50] Farla JCM, Hendriks CA, Blok K. Carbon dioxide recovery from industrial processes. Clim Change 1995;29:439–61. https://doi.org/10.1007/BF01092428.
[51] Quader MA, Ahmed S, Ghazilla RAR, Ahmed S, Dahari M. A comprehensive review on energy efficient CO2 breakthrough technologies for sustainable green iron and

steel manufacturing. Renew Sustain Energy Rev 2015;50:594–614. https://doi.org/10.1016/j.rser.2015.05.026.
[52] Ariyama T, Takahashi K, Kawashiri Y, Nouchi T. Diversification of the ironmaking process toward the long-term global goal for carbon dioxide mitigation. J Sustain Metall 2019;5:276–94. https://doi.org/10.1007/s40831-019-00219-9.
[53] IEA - iron & steel roadmap. https://www.iea.org/reports/iron-and-steel-technology-roadmap. [Accessed 26 April 2022].
[54] Sendeco2. sendeco2. https://www.sendeco2.com/es/precios-co2%0A. [Accessed 2 March 2022].
[55] Hurskainen M. Industrial oxygen demand in Finland. 2017.
[56] Götz M, Lefebvre J, Mörs F, McDaniel Koch A, Graf F, Bajohr S, et al. Renewable Power-to-Gas: a technological and economic review. Renew Energy 2016;85:1371–90. https://doi.org/10.1016/j.renene.2015.07.066.
[57] Abu-Zahra MRM, Niederer JPM, Feron PHM, Versteeg GF. CO2 capture from power plants. Part II. A parametric study of the economical performance based on monoethanolamine. Int J Greenh Gas Control 2007;1:135–42. https://doi.org/10.1016/S1750-5836(07)00032-1.
[58] Proost J. State-of-the art CAPEX data for water electrolysers, and their impact on renewable hydrogen price settings. Int J Hydrogen Energy 2019;44:4406–13. https://doi.org/10.1016/j.ijhydene.2018.07.164.
[59] De Saint Jean M, Baurens P, Bouallou C, Couturier K. Economic assessment of a power-to-substitute-natural-gas process including high-temperature steam electrolysis. Int J Hydrogen Energy 2015;40:6487–500. https://doi.org/10.1016/j.ijhydene.2015.03.066.
[60] Lehner M, Tichler R, Steinmüller H, Koppe M. Power-to-Gas: technology and business models. 2014.
[61] Kohl AL, Nielsen RB. Gas purification. 1997. https://doi.org/10.1016/B978-0-88415-220-0.X5000-9.
[62] Benjaminsson G, Benjaminsson J, Rudberg RB. Power-to-Gas - a technical review. 2013.
[63] Quarterly coal report july–September 2021. U.S. Department of Energy; 2021.
[64] IRENA 2022. https://www.irena.org/costs/Power-Generation-Costs. [Accessed 10 May 2022]. accessed.
[65] Strefler J, Kriegler E, Bauer N, Luderer G, Pietzcker RC, Giannousakis A, et al. Alternative carbon price trajectories can avoid excessive carbon removal. Nat Commun 2021;12:1–8. https://doi.org/10.1038/s41467-021-22211-2.

Journal of Cleaner Production 405 (2023) 137001

Contents lists available at ScienceDirect

Journal of Cleaner Production

journal homepage: www.elsevier.com/locate/jclepro

# High oxygen and SNG injection in blast furnace ironmaking with Power to Gas integration and $CO_2$ recycling

Jorge Perpiñán [a,*], Manuel Bailera [a], Begona Peña [a], Luis M. Romeo [a], Valerie Eveloy [b]

[a] Escuela de Ingeniería y Arquitectura, Universidad de Zaragoza, María de Luna 3, 50018, Zaragoza, Spain
[b] Khalifa University, Department of Mechanical Engineering, United Arab Emirates

ARTICLE INFO

Handling Editor: Panos Seferlis

*Keywords:*
Steel industry
Oxygen blast furnace
Power-to-Gas
Amine scrubbing
Decarbonization

ABSTRACT

In the last years, reduction of $CO_2$ emissions from the steel industry has been of great importance. Carbon capture, oxygen blast furnaces and top gas recycling technologies, among others, have been deeply studied as low carbon solutions. In this paper, a novel integration of carbon capture and power to gas technologies in the steelmaking industry is presented. Green hydrogen via proton exchange membrane (PEM) electrolysis and $CO_2$ via methyldiethanolamine (MDEA) scrubbing from the blast furnace gas (BFG) are used to produce synthetic natural gas in an isothermal fixed bed methanation plant. The latter gas is injected into the blast furnace, closing a carbon loop and reducing coal consumption. The oxygen by-produced in the electrolyser covers the entire oxygen demand of the steelmaking plant and avoids the need for an air separation unit (ASU). The novelty of this work relies on the variation of the oxygen enrichment and its temperature in the hot blast, and how it influences the power to gas integration concept. This power to gas integration is compared with a conventional BF-BOF plant from a technical, economic, energy and environmental point of view. Both plant process configurations were implemented in Aspen Plus simulations, assessing the fossil fuel demand, energy penalty, cost and $CO_2$ emissions. Emission reduction up to 34% can be achieved with power to gas integration, with an energy penalty of 17 MJ/$t_{HM}$ and a cost of 352 €/$t_{CO2}$.

## 1. Introduction

An essential goal in the transition toward a sustainable energy system is to decarbonize conventional energy systems. The Paris Agreement in 2015 targets a maximum increase of the world average temperature of 1.5–2.0 °C compared with the pre-industrial revolution period, and 80–95% cut in greenhouse gas (GHG) emissions in Europe compared with the level in 1990 (*European Commission*, 2022).

The industry accounts for 40% of global $CO_2$ emissions, according to (Intergovernmental Panel on Climate Change (IPCC), 2022), and the iron and steel (I&S) sector for up to 27% of the global manufacturing sectors (International Energy Agency, Iron and Steel Technology Roadmap., 2020). Consequently, improving overall energy efficiency and reducing primary energy consumption should be high priorities of the I&S sector, especially in times of high energy competitiveness and energy dependency.

Steel is mainly produced by three routes: (i) blast furnace-basic oxygen furnace (BF-BOF), with 70% share of steel world production; (ii) scrap-electric arc furnace (scrap-EAF), with 23% share; and (iii) direct reduced iron-electric arc furnace (DRI-EAF), with 7% share. Among the three routes, the BF-BOF is the largest specific energy consumer (21–23 GJ/$t_{HM}$) and the largest $CO_2$ emitter (2.0–2.2 $t_{CO2}$/$t_{HM}$) (International Energy Agency, Iron and Steel Technology Roadmap., 2020). Regarding the fuel consumed by each route, the BF-BOF is mainly based on coal, while the DRI-EAF consumes NG, $H_2$ and electricity, and the scrap-EAF consumes mostly electricity.

Reduction of $CO_2$ emissions from the BF-BOF route in the I&S industry has been the topic of extensive research. The transition to low carbon BFs started in the 1960s, combining oil injection and oxygen enrichment, hitting today's advanced oxygen blast furnaces (OBFs). Throughout this transition, different technologies have been used, such as pulverised coal injection (PCI), hot reducing gas derived from the reforming of COG or oil, OBFs with massive PCI, low-temperature BF, high reactivity coke BF, charcoal blast furnace (Andrade de Castro et al., 2005), top gas recycling (TGR), and advanced OBF. The TGR process is commonly studied in an OBF and includes $CO_2$ sequestration prior to reusing the top gas, in order to get rid of the $N_2$ and $CO_2$ before the

* Corresponding author.
*E-mail addresses:* jorge.perpinan@unizar.es (J. Perpiñán), mbailera@unizar.es (M. Bailera), bpp@unizar.es (B. Peña), luismi@unizar.es (L.M. Romeo), valerie.eveloy@ku.ac.ae (V. Eveloy).

https://doi.org/10.1016/j.jclepro.2023.137001
Received 24 November 2022; Received in revised form 7 March 2023; Accepted 26 March 2023
Available online 30 March 2023
0959-6526/© 2023 The Authors. Published by Elsevier Ltd. This is an open access article under the CC BY-NC-ND license (http://creativecommons.org/licenses/by-nc-nd/4.0/).

**Nomenclature**

| *Abbreviation* | *meaning* |
|---|---|
| AFT | Adiabatic Flame Temperature |
| ASU | Air Separation Unit |
| AHF | Air Heating Furnace |
| BF-BOF | Blast Furnace-Basic Oxygen Furnace |
| BFG | Blast Furnace Gas |
| BOFG | Basic Oxygen Furnace Gas |
| CC | Carbon Capture |
| CCUS | Carbon Capture Utilization and Storage |
| COG | Coke Oven Gas |
| DRI | Direct Reduced Iron |
| EAF | Electric Arc Furnace |
| GHG | Green House Gas |
| HM | Hot Metal |
| I&S | Iron and Steel |
| IEA | International Energy Agency |
| LHV | Lower Heating Value |
| MDEA | Methyldiethanolamine |
| PEM | Proton Exchange Membrane |
| PtG | Power to Gas |
| PCI | Pulverised Coal Injection |
| PFD | Process Flow Diagram |
| SNG | Synthetic Natural Gas |
| tHM | Ton of Hot Metal |
| tCS | Ton of Crude Steel |
| α, β, γ | Parameters for Economic Analysis |

tuyere or shaft injection. The concept of advanced OBF (Sato et al., 2015). takes advantage of a preheated gas injection in the upper shaft, allowing for reductant flexibility, i.e. intensified natural gas injection, high PCI or other reducing agents (Ariyama et al., 2016). Additionally, the nitrogen-free condition in the OBF contributes to the acceleration of the reduction rate and increased productivity. International projects such as ULCOS-BF (Abdul Quader et al., 2016) and COURSE50 (Tonomura, 2013) aim to apply carbon capture (CC) from the blast furnace gas (BFG) through physical adsorption and chemical absorption, where the $CO_2$ is sent to storage, and the clean gas is recycled to the OBF (TGR). Most OBF-TGR studies focus on CO recycling, leading to a marked reduction of energy content for downstream gases for plant use (Sahu et al., 2015), and although great emission reduction can be achieved, it may not fulfil downstream energy requirement needs, which is one of the main challenges presented for this kind of configurations.

Some drawbacks of CC technology are the need for geological storage (Perpiñán et al., 2022a,b) or the need for large-scale and long-term carbon utilization (Mac Dowell et al., 2017). Recent steel roadmaps refer to smart carbon avoidance or carbon capture and re-use (CCU) as one of the routes to lower carbon emissions (ArcelorMittal, 2023). This is where Power to Gas (PtG) stands out as a promising alternative, as reduces $CO_2$ emissions while providing additional benefits (Bailera et al., 2017a; 2017b, 2021a, b). The PtG concept involves processes that convert renewable electricity into synthetic gaseous fuels, primarily $H_2$. This green gas can be an intermediate or a final energy carrier. If combined with $CO_2$ in a methanation reactor, synthetic natural gas (SNG) is obtained (i.e., Power to Methane) (Romeo et al., 2020). If this SNG is used again in the I&S industry, the $CO_2$ is being recycled and used constantly, thus not being emitted to the atmosphere or stored underground. Another additional benefit of PtG technology is the reduction of fossil fuel consumption since it is substituted by SNG.

Only a few studies have been found in the literature on Power to Gas and carbon capture integration in the BF-BOF route (Bailera et al., 2022a,b; Bailera et al., 2021a,b, 2022a,b; Perpiñán et al., 2022a,b). Different configurations have been approached while integrating PtG technology, such as biomass methanation (Rosenfeld et al., 2020), OBF (Perpiñán et al., 2021), TGR and SOEC electrolysis (Hisashige et al., 2019), obtaining a wide range of results. $CO_2$ emission reduction in the BF varies from 6% to 21%, injecting up to 115 $kg_{SNG}/t_{HM}$ in the BF.

The present work assesses the performance and cost of a PtG-steelmaking integration, where green $H_2$ is produced in a PEM electrolyser, $CO_2$ is captured by amine scrubbing from the BFG, and SNG is produced via catalytic isothermal methanation from the two previous components. The SNG is injected into the BF, keeping the $CO_2$ in a closed loop, reducing emissions and avoiding geological storage. This configuration focuses on $CO_2$ recycling instead of on CO recycling (TGR), thus ensuring enough energy content for downstream processes. The oxygen by-produced in the electrolyser covers the oxygen demand of the industry, eliminating the air separation unit (ASU). This PtG-steelmaking integration is studied by varying the oxygen enrichment in the hot blast and its temperature, and the results are compared with a conventional BF-BOF plant in terms of fossil fuel demand, energy penalty and $CO_2$ emissions. Both simulations, the conventional and the PtG integration, have been undertaken using Aspen Plus software. Lastly, an economic evaluation of the PtG-steelmaking integration is carried out to determine the specific costs of this novel integration.

## 2. Case studies

In order to assess the improvement of the proposed low-carbon concept, a conventional steelmaking plant with a production of 320 $t_{HM}/h$ (Steelmaking Technologies. CISDI Ingeniering CO. LTD, 2022)is assumed as a base case of Fig. 1a. Conventional BF-BOF plants consist of a coke oven, blast furnace and hot stoves, sinter strand, basic oxygen furnace, ASU, the casting and rolling stage and a combined cycle power plant. The inputs to the system are the iron ore in the sinter strand; the coal in the sintering, coke oven and blast furnace; and scrap in the BOF. The by-produced energetic gases of the industry (COG, BFG and BOFG) are used as fuel in different processes. The power plant is sized with 100 MWe net power (Wu et al., 2016), consuming part of the available COG, BOFG and BFG, generating enough electricity for the industry, making it self-sufficient. The remaining gases not used in the power plant or other processes are supposed to be sold to nearby industries.

The proposed PtG-steelmaking integration is shown in Fig. 1b. This case adds a PEM electrolyser to produce $H_2$, an amine scrubbing to capture $CO_2$, and a methanation plant to produce synthetic natural gas. The $CO_2$ is captured from the BFG, and the SNG is continuously injected into the BF, recycling the $CO_2$ and closing a carbon loop. It is expected that enough energy content meets the needs of the downstream processes, $CO_2$ emissions are lowered, and geological storage is not needed. The $O_2$ by-produced in the electrolyser is used to feed the BOFG demand, avoiding the ASU, and is also used to enrich the blast furnace's hot blast. The excess of oxygen is supposed to be sold. The hot blast enrichment is studied gradually, from 21 vol% $O_2$ to 95 vol% $O_2$ in the hot blast, obtaining an oxygen blast furnace (OBF) as a result. The influence of the oxygen temperature has also been studied, at 25 °C and 1200 °C. With this technology, we are able to indirectly electrify the BF-BOF steel industry to some extent.

## 3. Methodology

The process models of the conventional I&S plant and the PtG-steelmaking integration were implemented in Aspen Plus v11. The process flow diagrams in Fig. 1 show the hierarchy blocks for the conventional I&S industry and the PtG-steelmaking integration. Each hierarchy block combined the necessary sub-models to faithfully reproduce

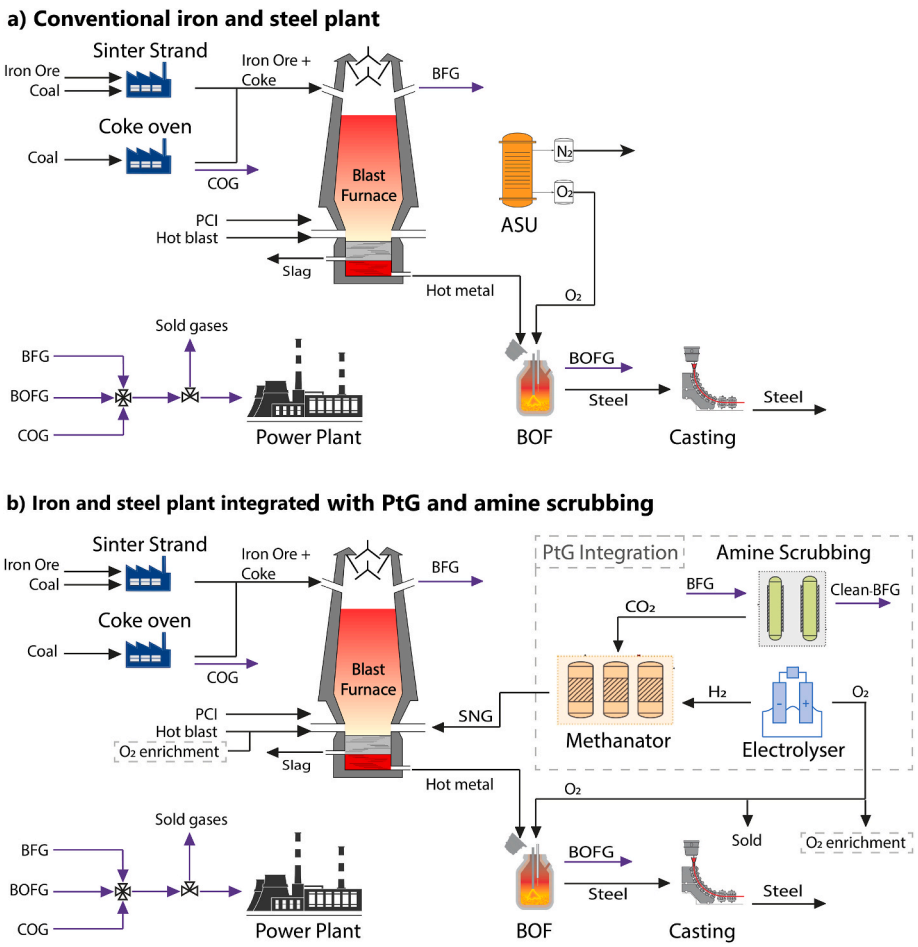


**Fig. 1.** Process flow diagram for a) conventional iron and steel plant and b) its integration with power to gas and carbon capture (dashed rectangle).

every process and works with its own Aspen property method (Aspen Technology Inc, 2019c). The sinter strand represents the agglomeration of fine ore particles. The coke oven simulates the coke-making process, with COG as a by-product. The blast furnace hierarchy comprises a simplified version of a blast furnace process that reduces the iron ore forming hot metal and BFG. The hot blast temperature is 1200 °C. Some additional parameters of the BF, such as top gas composition and temperature, air and coke flow rates, CO utilization (Eq. (1)) and the AFT, were externally calculated through a revised Rist diagram (Bailera et al., 2021a,b). The $H_2$ utilization is fixed at 0.47 (Eq. (2)) (A. Babich, D. Senk, H. W. Gudenau, 2008) and the efficiency of the furnace stack is 0.9. The BOF converts the hot metal to steel, reducing the carbon content from 4.5 wt% C to 0.267 wt% C. The ASU was directly taken from the Aspen repository (example block Power, Coal gasification, IGCC (Aspen Technology Inc, 2019b)). For the I&S production blocks and the ASU, the PENG-ROB property method was used. The power plant is a combined cycle sized at 100 MWe net power (Wu et al., 2016), modelled using the PR-BM property method. The amine scrubbing model captures 90% of the inlet $CO_2$, using methyldiethanolamine (MDEA) as solvent. The PEM electrolyser generates $O_2$ and $H_2$ with an energy consumption assumed at 3.8 kWh/Nm$^3$ (Salehmin et al., 2022). Both the amine scrubbing and the electrolyser use the ELECNRTL property method. The methanation plant consists of two isothermal fixed-bed reactors working at 300–350 °C and 5 bar (Izumiya and Shimada, 2021; Rönsch et al., 2016) that reach a SNG purity of 95 vol% $CH_4$, with the SRK property method. Stoichiometric conditions are considered for the methanation reaction, with a H2:CO2 ratio of 4. More details about the methodology, the simulation processes and the Aspen Plus model of the base case can be found in (Perpiñán et al., 2022).

$$\mu_{CO} = CO_2 / (CO_2 + CO) \quad (1)$$

$$\mu_{H2} = H_2O / (H_2O + H_2) \quad (2)$$

Although secondary processes (i.e., hot blast heating (also called hot stoves), SNG heating, other heating and combustion processes and CO2 emission streams) are not represented in Fig. 1, they are taken into account and modelled in the Aspen model. Sub-sections 3.1 to 3.6 state the fundamental changes compared to previous works (Perpiñán et al., 2022a,b).

### 3.1. Preheating gas injection

The decreased bosh gas volume in the OBF, caused by the lack of nitrogen, causes that preheating of the burden in the upper part tends to be insufficient in comparison with the conventional BF, which leads to low BFG temperature. If this temperature drops below 100 °C, this can generate significant problems regarding water condensation. In order to compensate for the insufficient heat supply in the shaft, it is necessary to inject preheating gas into the upper shaft. A fuel (usually BFG) is burned with pure oxygen and the flue gas is injected at 1000 °C in the upper part of the BF. Fig. 2 (Ariyama et al., 2016; Sato et al., 2015) shows the evolution of the blast furnace towards reductant flexibility and carbon dioxide mitigation, from a conventional BF to an advanced OBF with pure oxygen and preheating gas injection.

### 3.2. Distribution of energetic gases

The energetic gases (BOFG, COG and BFG) are distributed in

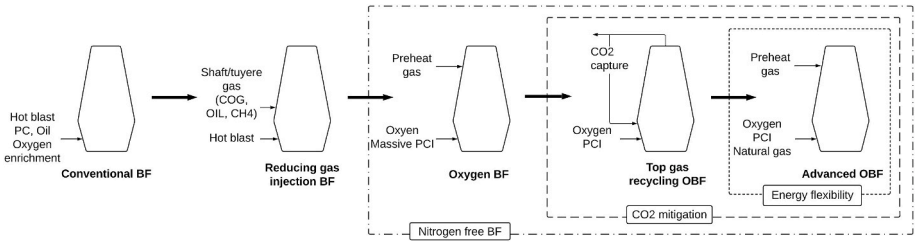


**Fig. 2.** Evolution of blast furnace for reducing coke rate and $CO_2$ emissions. Adapted from (Ariyama et al., 2016).

different processes. BFG is supplied to the sinter strand, the hot stoves and the power plant, BOFG is supplied to the casting stage and the power plant, and the COG is supplied to the coke oven, BOF and the power plant. As mentioned before, a certain amount of these gases is sold to nearby industries.

For the PtG-steelmaking integration, the distribution of the energetic gases remains almost the same, but with some changes in the BFG distribution, see Fig. 3. The raw BFG is used as preheating gas in the BF and the amine scrubbing stage. After this stage, the clean-BFG is mixed with the rest of the BFG, and is used in the processes mentioned before (sinter strand, hot stoves and power plant) but also to heat the SNG to 700 °C before injecting it into the BF (Perpiñán et al., 2022a,b).

### 3.3. Oxygen temperature for hot blast enrichment

Oxygen injection in blast furnaces is usually heated together with the atmospheric air in the hot stoves for concentrations up to 30% $O_2$. This temperature is around 1200 °C. For higher enrichments, the oxygen is injected after the hot stoves, at atmospheric temperature (25 °C) (R. Li et al., 2022; Tsupari et al., 2015). Nie et al. (2021) and Sato et al. (2015) describe that oxygen enrichment exceeding 30% can cause safety problems and equipment damage in conventional existing hot stoves.

However, Sahu et al. (2015) preheats a 45% oxygen-enriched hot blast to 1200 °C, Zhang et al. (2017) simulates 98% pure oxygen at 500 °C, and Kim et al. (2016) experimentally preheats pure oxygen to 650 °C (in the glass industry), but none of this works clarifies if higher temperatures can be reached.

Since the temperature limit of pure oxygen is not clear, and no information was found regarding potential technical limitations in new equipment, two different cases are investigated in this study: oxygen enrichment at atmospheric temperature (25 °C), and oxygen enrichment preheated to 1200 °C.

### 3.4. Sizing of the PtG plant

For the PtG-steelmaking integration, the oxygen enrichment in the hot blast increases from 21% (atmospheric air) to 95%. For each point, the maximum amount of SNG is injected, firstly to reduce the pulverised coal injection (PCI) and once it is over, to substitute the coke rate. The amount of SNG is limited by the adiabatic flame temperature (AFT), which should not be dropped below 2000 °C for technical reasons (Peacey and Davbenport, 1979). Consequently, the oxygen enrichment increases the AFT and the SNG injection lowers it, reaching an equilibrium of 2000 °C in the AFT for each point of the oxygen enrichment. Then, the AFT (2000 °C), the oxygen enrichment (21–95%) and the oxygen temperature (25 or 1200 °C) are inputs to the model, while SNG, coal, coke and BFG mass flow rates are outputs to the model. Thus, knowing the amount of SNG required for each point, the methanation plant, the amine scrubbing plant and the PEM electrolyser can be sized. The oxygen by-produced in the electrolyser is used to eliminate the ASU and to feed the BOF and hot blast enrichment necessities.

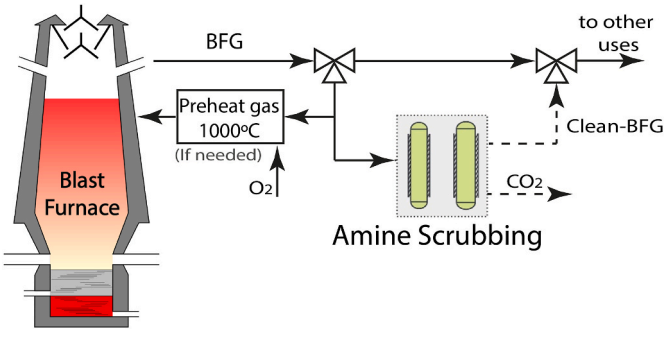


**Fig. 3.** Process flow diagram for BFG distribution in the PtG-steelmaking integration.

### 3.5. Coal-equivalent replacement ratio (coal-e RR) and energy penalty

The coal-e RR is defined as the net coal replaced by the synthetic natural gas (SNG) injected (Eq. (3)). The net coal is the sum of the PCI and the coking coal needed for coke making.

$$Coal-e\ RR = \frac{\Delta \dot{m}_{PCI} + \Delta \dot{m}_{CokingCoal}}{\Delta \dot{m}_{SNG}} \left[kg_{Coal} / kg_{SNG}\right] \quad (3)$$

The energy penalty is defined as the net energy consumed in the industry per kg of $CO_2$ avoided with the PtG-steelmaking integration (Eq. (4)).

$$E_{penalty} = \frac{\Delta E_{cons} - \Delta E_{coal} \bullet \eta_{elec} - \Delta E_{gases} \bullet \eta_{elec}}{\Delta \dot{m}_{CO2}} \left[MJ / kg_{CO_2}\right] \quad (4)$$

Where $\Delta E_{cons}$ is the electricity consumed in the industry (MJ/$t_{HM}$), $\Delta E_{coal}$ is the coal energy avoided (MJ/$t_{HM}$), $\Delta E_{gases}$ is the excess of gases sold to nearby industries, $\eta_{elec}$ is the energy conversion factor from coal to electricity (0.33) and $\Delta \dot{m}_{CO2}$ is the amount of $CO_2$ avoided $kg_{CO2}/t_{HM}$). All these parameters are concerning the conventional iron and steel plant and the PtG-steelmaking integration.

### 3.6. Economic analysis

The economic analysis was performed for the investment required for the PtG-steelmaking integration, i.e., implementing the PEM, methanation stage and amine scrubbing. A 4% interest for the discount factor is assumed (Eq. (5)), with a loan amortization of 20 years. The PtG system is assumed to operate 8000 h per year (Bailera et al., 2017a; 2017b), a carbon tax value of 84.28 €/$t_{CO2}$ (Sendeco2, 2022) and a renewable electricity consumption cost of 77 €/MWh are assumed. The initial capital expenditure (CAPEX) for the PtG integration is composed of the amine, electrolysis and methanation plants, the heat exchangers network, the BF retrofitting, and other direct and indirect costs. The annual operational expenditure (OPEX) is composed of the catalyst renovation, the water consumed by the electrolyser, the amine renovation, the purchased electricity and the operation and maintenance (O&M). The annual incomes are the saved $CO_2$ taxes and coal, and the sold steel gases (BFG, BOFG and COG) and oxygen, see Table 1. The specific cost, in €/$t_{CO2}$ and €/$t_{HRC}$, is shown in Eq. (6) and Eq. (7).

**Table 1**
Data for the economic analysis of the PtG integration in the iron and steel industry.

| | Cost equation (M€) or (M€/y) | Parameters α, β, γ | Ref. |
|---|---|---|---|
| **CAPEX** | | | |
| Amine Plant | | | |
| Overall Cost | $26.094 \cdot (\alpha/408)^{0.65}$ | α = $CO_2$ captured [t/h] | Abu-Zahra et al. (2007) |
| Electrolysis | | | |
| Overall Cost | $400 \cdot 10^{-6} \cdot \alpha$ | α = Power [kW] | TURNER (2022) |
| Methanation | | | |
| $H_2$ compressor | $0.267 \cdot (\alpha/445)^{0.67}$ | α = Power [kW] | De Saint Jean et al. (2015) |
| $CO_2$ compressor | $0.267 \cdot (\alpha/445)^{0.67}$ | α = Power [kW] | De Saint Jean et al. (2015) |
| Reactors | $300 \cdot 10^{-6} \cdot \alpha$ | α = SNG power [$kW_{SNG}$] | Lehner et al. (2014) |
| Catalyst | $0.1875 \cdot \alpha$ | α = Volume of catalyst [$m^3$] | De Saint Jean et al. (2015) |
| Heat exchangers | $(9016.3 + 721.3 \cdot (\alpha^{0.8})) \cdot 10^{-6}$ | α = Area [$m^2$] | (Aspen Technology Inc, 2019a) |
| BF retrofitting | $0.5 \cdot \alpha$ | α = BF construction cost | (IEA - Iron & Steel Roadmap, 2020) |
| Other direct costs | | | |
| Installation | $10\% \cdot \alpha$ | α = Total equipment costs [M€] | Abu-Zahra et al. (2007) |
| Instrumentation & control | $4\% \cdot \alpha$ | α = Total equipment costs [M€] | Abu-Zahra et al. (2007) |
| Piping | $16\% \cdot \alpha$ | α = Total equipment costs [M€] | Abu-Zahra et al. (2007) |
| Electrical | $5\% \cdot \alpha$ | α = Total equipment costs [M€] | Abu-Zahra et al. (2007) |
| Building | $5\% \cdot \alpha$ | α = Total equipment costs [M€] | Abu-Zahra et al. (2007) |
| Land | $1\% \cdot \alpha$ | α = Total equipment costs [M€] | Abu-Zahra et al. (2007) |
| Indirect costs | | | |
| Engineering | $7\% \cdot \alpha$ | α = Total direct costs [M€] | Abu-Zahra et al. (2007) |
| Legal expenses | $2\% \cdot \alpha$ | α = Total CAPEX [M€] | Abu-Zahra et al. (2007) |
| Construction expenses | $4\% \cdot \alpha$ | α = Total CAPEX [M€] | Abu-Zahra et al. (2007) |
| Contingency | $7\% \cdot \alpha$ | α = Total CAPEX [M€] | Abu-Zahra et al. (2007) |
| **OPEX** | | | |
| Amine renovation | $3204 \cdot 10^{-6} \cdot \alpha$ | α = MDEA renovation [$t_{CO2}$/y] | Kohl and Nielsen (1997) |
| Catalyst renovation | $15\% \cdot \alpha$ | α = Initial catalyst cost [M€] | Bailera et al., 2017a; 2017b |
| Electricity | $\alpha \cdot \beta \cdot \gamma \cdot 10^{-6}$ | α = Electricity purchased [MWh/$t_{HM} \cdot h^{-1}$], β = Operating hours [h/y], γ = Electricity cost [€/MWh] | – |
| Water | $1.47 \cdot 10^{-6} \cdot \alpha$ | α = Water consumption [$m^3$/y] | Benjaminsson et al. (2013) |
| O&M | $3\% \cdot \alpha$ | α = Total CAPEX [M€] | Abu-Zahra et al. (2007) |
| **INCOMES** | | | |
| Coal | $130.43 \cdot 10^{-6} \cdot \alpha$ | α = Coal saved [$t_{Coal}$/y] | (Quarterly Coal Report July–September 2021. U.S. Department of Energy, 2021) |
| Oxygen | $80 \cdot 10^{-6} \cdot \alpha$ | α = $O_2$ generated [$t_{O2}$/y] | Hurskainen (2017) |
| $CO_2$ taxes | $84.28 \cdot 10^{-6} \cdot \alpha$ | α = $CO_2$ saved [$t_{CO2}$/y] | (Sendeco2, 2022) |
| Steel gases | $(15 + \alpha \cdot \beta/13) \cdot 10^{-6} \cdot \gamma$ | α = Natural gas price [€/MWh] β = Steel gases LHV [kWh/kg] γ = Steel gases generated [MWh/y] | – |

$$D_{coeff} = \frac{1}{(1+i)^n} \tag{5}$$

$$Specific\ Cost = \frac{\left(\frac{Capex}{Loan\ amortization} + Opex - Incomes\right) \cdot 10^6}{CO_2\ avoided \cdot Operating\ hours} \left[\frac{€}{t_{CO_2}}\right] \tag{6}$$

$$Specific\ Cost = \frac{\left(\frac{Capex}{Loan\ amortization} + Opex - Incomes\right) \cdot 10^6}{Steel\ Production \cdot Operating\ hours} \left[\frac{€}{t_{HRC}}\right] \tag{7}$$

## 4. Results and discussion

### 4.1. Conventional I&S plant results

The conventional I&S plant model was validated with literature data. Assuming a 320 $t_{HM}$/h production plant, the main consumptions are 1464 kg/$t_{HM}$ of iron ore, 668 kg/$t_{HM}$ of coal, and 150 kg/$t_{HM}$ of scrap. The coal is derived to the coke oven for coke production (443 kg/$t_{HM}$), the sintering (75 kg/$t_{HM}$) and the blast furnace as PCI (150 kg/$t_{HM}$). The AFT in the BF is 2258 °C and the energetic gases sold to other industries account for 2400 MJ/$t_{HM}$.

The $CO_2$ emissions and their concentration in flue gases for the conventional steel plant simulated in Aspen are shown in Fig. 4. The total $CO_2$ emissions are 1943 kg$CO_2$/$t_{HM}$, and the most contaminant stream is the BFG, with 1370 kg$CO_2$-eq/$t_{HM}$ in form of CO and $CO_2$. Table 2 shows the main mass flow streams for the conventional I&S plant simulated in Aspen, where all results agree with bibliography data, validating the conventional I&S plant model. More details about stream results and validation data can be found in (Perpiñán et al., 2022a,b).

### 4.2. PtG-steelmaking integration: Blast furnace results

The amount of reducing agents injected in the BF (coke, PCI and SNG), as well as the total $CO_2$ emissions from the I&S plant, are analysed as a function of the oxygen enrichment and its temperature in Fig. 5. With low oxygen injection, there is a drastic increase in SNG injection, being more pronounced when injecting $O_2$ at 1200 °C. With higher oxygen enrichments, the same benefits are found but less pronounced, achieving a maximum injection of 192 $kg_{SNG}$/$t_{HM}$ for $O_2$ at 1200 °C. This result agrees with that obtained by Pistorius et al. (Sato et al., 2015), who simulated injections of 180 $kg_{SNG}$/$t_{HM}$, with an oxygen enrichment of 39%. At this point, all PCI has been substituted along with 53.5 kg/$t_{HM}$ of coke. When injecting 40% $O_2$ at 1200 °C, the PCI is completely substituted, but when injecting oxygen at 25 °C, the PCI is never fully substituted. For all cases analysed, the AFT is set to 2000 °C.

For the case of 95% of hot oxygen enrichment, the coke consumption is 278.5 kg/tHM, with no PCI injection. In order to put these results into perspective, Sahu et al. (2015) investigated the impact of the nature of the fuel and burden of the OBF process with top gas recycling, obtaining 323–342 $kg_{coke}$/$t_{HM}$ and 200 $kg_{PCI}$/$t_{HM}$. Zhang et al. (2017) studied the

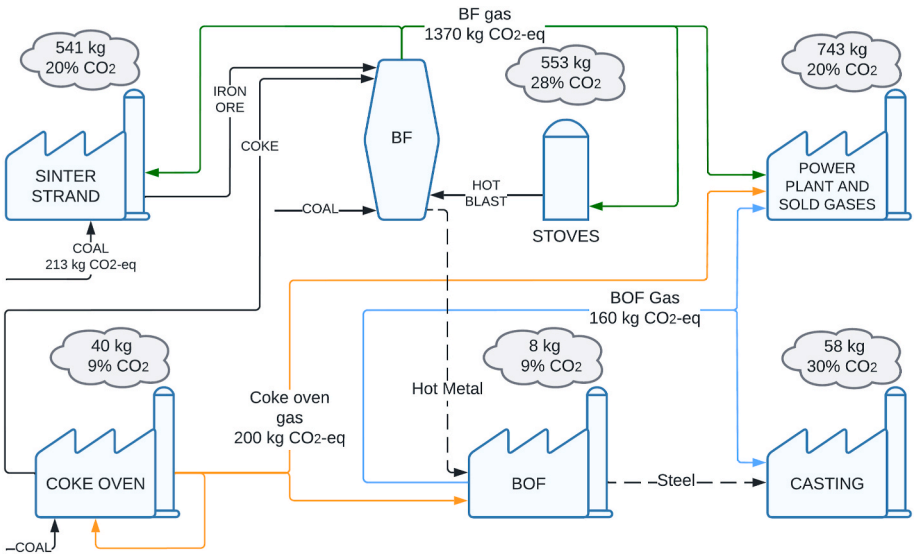


**Fig. 4.** Distribution of energetic gases for the conventional I&S plant: BF gas green line, Coke oven gas orange line, BOF gas blue line; and energetic content of each energetic gas in MJ/$t_{HM}$. $CO_2$ emissions, expressed in volume (kg/$t_{HM}$) and concentration in flue gas (volume %) are also shown in the Aspen model. (For interpretation of the references to colour in this figure legend, the reader is referred to the Web version of this article.)

**Table 2**
Mass flows (kg/tHM) of the main streams for the conventional I&S plant simulated in Aspen compared to typical values from (A. Babich, D. Senk, H. W. Gudenau, 2008; He and Wang, 2017).

| Material | Typical values | Present model |
|---|---|---|
| Iron ore | 1315–1510 | 1464 |
| Coal (Sinter) | 45–75 | 75 |
| Coal (Coke Oven) | 380–534 | 443 |
| Coal (BF) | 150–200 | 150 |
| Coke | 300–400 | 332 |
| COG | 100–140 | 111 |
| Hot blast | 1100–1600 | 1449 |
| BFG | 1800–2420 | 2216 |
| BF Slag | 260–298 | 261 |
| Pig iron | 900-1000 | 1000 |
| Scrap (BOF) | 150 | 150 |
| $O_2$ (BOF) | 60–90 | 87 |
| BOFG | 90–130 | 128 |
| Final Steel | 1000–1100 | 1079 |

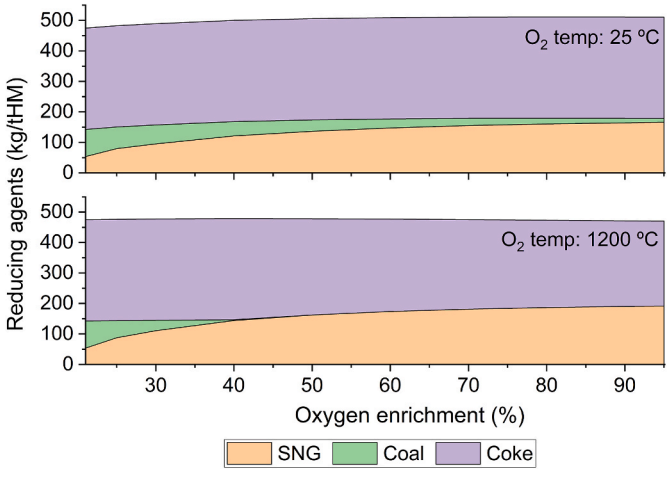


**Fig. 5.** Reducing agents in BF (orange area: SNG; green area: coal; purple area: coke) as a function of the oxygen temperature and its percentage in the hot blast. (For interpretation of the references to colour in this figure legend, the reader is referred to the Web version of this article.)

medium (50% O2) and full (98% O2) oxygen enriched blast furnace with top gas recycling, reaching a consumption of 300 $kg_{coke}/t_{HM}$ and 126 $kg_{PCI}/t_{HM}$ for medium OBF and 200 $kg_{coke}/t_{HM}$ and 205 $kg_{PCI}/t_{HM}$ for full OBF. A similar study with similar results was performed by Li et al. (C. L. Li et al., 2019), with 337 $kg_{coke}/t_{HM}$ and 150 $kg_{PCI}/t_{HM}$ for medium OBF and 200 $kg_{coke}/t_{HM}$ and 205 $kg_{PCI}/t_{HM}$ for full OBF. However, further studies that use data-driven analyses with actual long term plant data are required (Zhai and Chen, 2023).

The coal-e RR and the SNG injection are shown in Fig. 6. The coal-e RR is among 1.05–1.15 $kg_{Coal}/kg_{SNG}$ when $O_2$ is preheated at 1200 °C, with a slight decrease at low oxygen enrichment. It can get as low as 0.81 $kg_{Coal}/kg_{SNG}$ if cold oxygen is injected. This difference is because cold oxygen lowers the AFT and therefore less SNG can be injected and less PCI can be substituted. Dashed lines in Fig. 6 and following figures mean

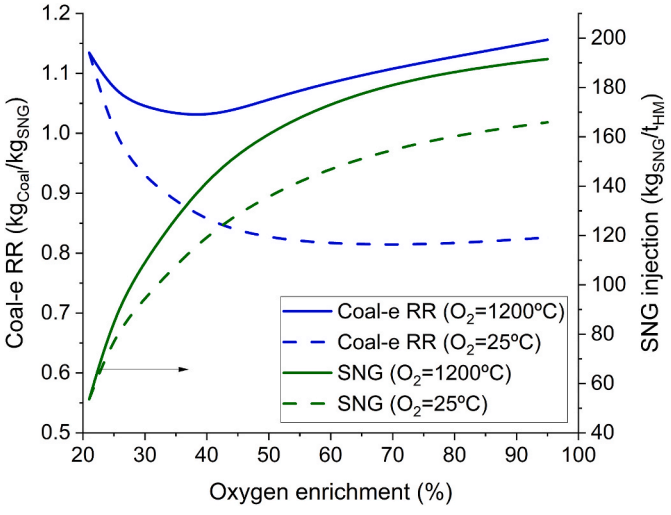


**Fig. 6.** Coal equivalent replacement ratio (Coal-e RR, blue lines) and SNG injection (green lines) as a function of the oxygen temperature (1200 °C in solid lines and 25 °C in dashed lines) and its percentage in the hot blast. Where SNG is the synthetic natural gas injected in the BF tuyeres and Coal-e RR is the sum of the pulverised coal injection and the coking coal replaced by the SNG. (For interpretation of the references to colour in this figure legend, the reader is referred to the Web version of this article.)

low temperature (25 °C) oxygen enrichment.

When increasing the oxygen enrichment in the hot blast, more SNG can be injected, hence less $N_2$ and more $CO_2$, CO and $H_2$ can be found in the BFG, see Fig. 7. Moreover, these percentages are not significantly dependent on temperature. When 95% $O_2$ is used, $H_2$ percentage contents of 23–28% are found, in agreement with Sato et al. (2015) who simulate an OBF with high NG injection, reaching 25% $H_2$ in BFG). The increasing contribution of CO and $H_2$ promotes a higher BFG LHV ($MJ/kg_{BFG}$), but the decreasing contribution of $N_2$ promotes a lower BFG mass flow rate ($kg_{BFG}/t_{HM}$). Fig. 7 joins the two parameters showing the BFG energy content ($MJ/t_{HM}$), which can achieve 8086 $MJ/t_{HM}$, compared with the 4930 $MJ/t_{HM}$ obtained in the conventional I&S plant. This value is in accordance with the literature, specifically Pistorius et al. (2017) inject similar amounts of NG resulting in 7000–8000 $MJ/t_{HM}$.

Fig. 8 shows the amount of preheating gas injection needed to keep the BFG temperature above 150 °C, and the CO utilization ($\mu_{CO}$) in the BF, as a function of the oxygen enrichment and its temperature. The BFG temperature decreases clearly when increasing the $O_2$ percentage in the hot blast and when injecting high amounts of SNG, as explained before. Thus, preheating gas injection is needed when the oxygen enrichment is above 30%, achieving a maximum value of 233 $kg_{BFG}/t_{HM}$, which agrees with Sato et al. (2015) who simulates an OBF with high NG injection, injecting 213 $kg_{BFG}/t_{HM}$ as preheating gas. The CO utilization exhibits a minimum at 30% oxygen enrichment, but then increases with the preheating gas injection, being in a range of 42–52%. This is mainly because of the large $CO_2$ content of the injected preheated gas (which ends up in the BFG), and the definition of Eq. (1) for the CO utilization, which was referred to the final BFG composition.

### 4.3. PtG-steelmaking heat integration and energy penalty

Table 3 shows the molar composition and the lower heating value (LHV) of the main gaseous streams for both the conventional I&S plant and the PtG-steelmaking integration. Note that BFG, clean-BFG and sold gases have a wide range of data which depend on the $O_2$ enrichment of the hot blast, as it lowers the $N_2$ content in the BFG. Considering all compositions and impurities in Table 3, the total $CO_2$ and $H_2$ streams needed in the methanation plant are 2.7 $kg_{CO2}/kg_{SNG}$ and 0.49 $kg_{H2}/kg_{SNG}$, respectively.

The heat consumption in amine scrubbing can be covered by the exothermic heat of the methanation. A pinch analysis validating this amine-methanation heat integration was undertaken via Pinch analysis using Aspen Energy Analyzer tool when using atmospheric air (i.e., no oxygen enrichment in the hot blast). The methanation temperature ranges between 300 and 350 °C, while the amine scrubbing is between 110 and 130 °C. A minimum of five different heat exchangers are needed to fulfil the thermal needs. More details about the pinch analysis when using atmospheric air can be found in (Perpiñán et al., 2022a,b).

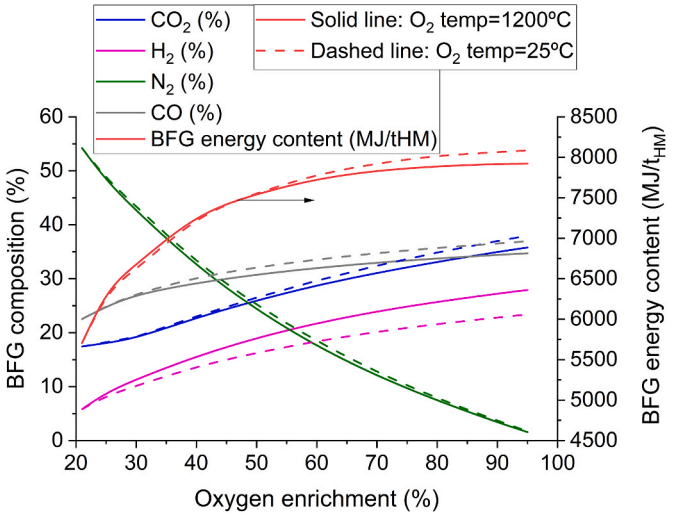


**Fig. 7.** BFG composition (blue lines: $CO_2$; pink lines: $H_2$; green lines: $N_2$; grey lines: CO) and BFG energy content (red lines) as a function of the oxygen temperature (1200 °C in solid lines and 25 °C in dashed lines) and its percentage in the hot blast. (For interpretation of the references to colour in this figure legend, the reader is referred to the Web version of this article.)

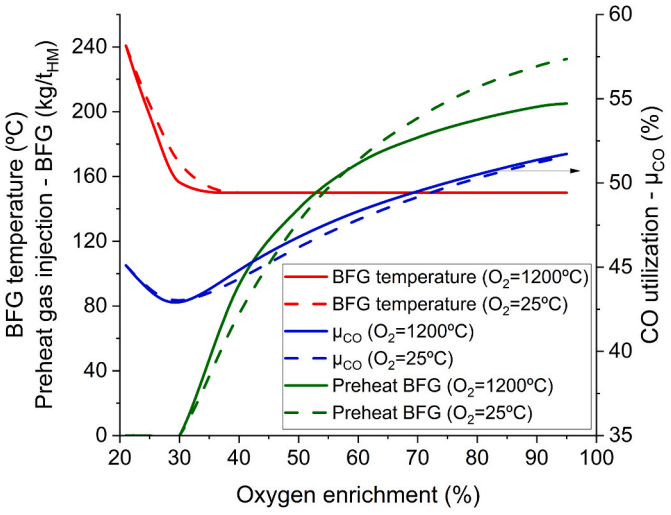


**Fig. 8.** BFG temperature (red lines), preheating gas injection (green lines) and CO utilization ($\mu_{CO}$, blue lines) as a function of the oxygen temperature (1200 °C in solid lines and 25 °C in dashed lines) and its percentage in the hot blast. (For interpretation of the references to colour in this figure legend, the reader is referred to the Web version of this article.)

When increasing the oxygen enrichment in the hot blast, the $CO_2$ content in the BFG increases, which implies a lower amine specific heat consumption (see Fig. 9). As the exothermic methanation heat remains constant (per kilogram of captured $CO_2$), it can be asserted that the amine heat demand can be covered by the methanation in all cases. This means that the amine heat consumption decreases from 3.7 to 3.1 $MJ/kg_{CO2}$, while the heat released by the methanation is always 6.1 $MJ/kg_{CO2}$.

The PEM size increases with the $O_2$ enrichment and its temperature (see Fig. 10). Higher $O_2$ enrichments and temperatures allow for higher SNG injections, which require higher $H_2$ production and therefore higher PEM sizes. The PEM size ranges from 355 MW when injecting air, to 1268 MW when injecting 95% $O_2$ at 1200 °C. The $O_2$ by-produced (red lines) grows proportionally up to 739 $kg/t_{HM}$, which is always above the $O_2$ consumed in the hot blast and the BOF (blue lines). It is important to highlight that for the same oxygen enrichment; more oxygen is needed when injecting cold oxygen. This is because, at lower oxygen temperatures, less coal can be substituted (see coal-e RR, Fig. 6), and therefore there is a greater amount of reducing agents in the BF (see Fig. 5), requiring more oxygen to burn them.

Fig. 11 shows the main streams with their $CO_2$-eq content, i.e., the $CO_2$ generated after burning the carbonaceous components (C, CO and $CH_4$), as well as the total $CO_2$ emissions for the PtG-steelmaking integration. Total $CO_2$ emissions can be calculated in three different ways (Eq. (8)): by adding the flue gases $CO_2$ emissions; by adding the $CO_2$-eq emissions from the input coal streams; or by adding the sintering coal, the intermediate gaseous streams (BFG, BOFG and COG) and the recirculated streams (SNG and preheating gas) $CO_2$-eq emissions.

The BOFG and the sintering coal $CO_2$-eq content are constant because the current integration does not influence these processes. The COG $CO_2$-eq content decreases slightly for the hot oxygen (1200 °C) integration, as part of the coking coal is replaced, but is constant in the cold oxygen (25 °C) integration. The BFG $CO_2$-eq content increases due to the high amount of SNG and preheating gas injected into the furnace.

**Table 3**
Molar composition and lower heating value for gas streams in both the conventional process plant and proposed plant with PtG and amine scrubbing.

| | Composition (vol %) | $O_2$ | $N_2$ | CO | $CO_2$ | $H_2$ | $H_2O$ | $CH_4$ | Ar | LHV (MJ/kg) |
|---|---|---|---|---|---|---|---|---|---|---|
| Conventional I&S | COG | 0.07 | 2.26 | 9.37 | 2.34 | 57.31 | – | 28.65 | – | 39.27 |
| | BOFG | 1.93 | 8.00 | 66.00 | 19.35 | 2.00 | – | – | 2.72 | 6.18 |
| | BFG | – | 55.10 | 21.98 | 19.37 | 2.25 | 1.3 | – | – | 2.23 |
| | $O_2$ | 95.00 | 0.8 | – | – | – | – | – | 4.2 | – |
| | Sold gases | 0.15 | 39.95 | 22.10 | 15.51 | 14.70 | 0.92 | 6.49 | 0.18 | 5.81 |
| PtG-steelmaking integration | COG | 0.07 | 2.26 | 9.37 | 2.34 | 57.31 | – | 28.65 | – | 39.27 |
| | BOFG | 3.31 | 8.00 | 66.00 | 20.69 | 2.00 | – | – | – | 6.18 |
| | BFG | – | 1.57–55.1 | 21.23–35.65 | 17.44–37.97 | 2.25–27.92 | 1.3–1.3 | – | – | 2.23–6.15 |
| | Clean BFG | – | 2.32–66.73 | 24.82–54.23 | 2.07–5.77 | 2.73–41.19 | 1.9–1.9 | – | – | 3.29–13.34 |
| | $O_2$ | 99.98 | – | – | – | 0.02 | – | – | – | – |
| | $H_2$ | – | – | – | – | 100.0 | – | – | – | 119.9 |
| | $CO_2$ | – | 0.02 | 0.79 | 95.82 | – | 3.36 | – | – | – |
| | SNG | – | 0.02 | – | 0.96 | 3.86 | 4.96 | 94.65 | – | 48.73 |
| | Sold gases | 0.23–0.35 | 2.7–44.94 | 23.41–42.36 | 7.51–10.33 | 17.51–39.44 | 1.00–1.46 | 4.81–6.41 | – | 6.69–13.47 |

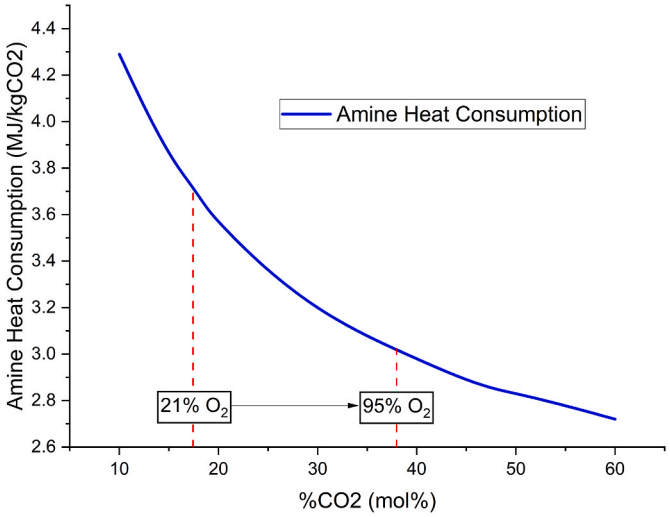


**Fig. 9.** Amine heat consumption as a function of the $CO_2$ percentage in the BFG. Red dashed lines represent the 21% oxygen content and the 95% oxygen content in the hot blast. (For interpretation of the references to colour in this figure legend, the reader is referred to the Web version of this article.)

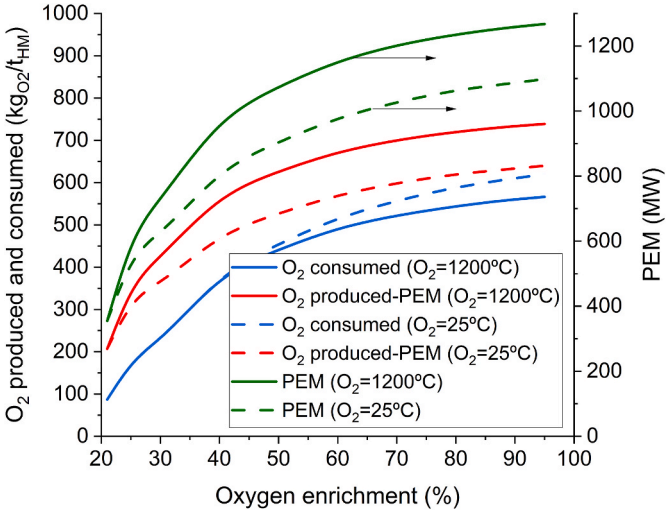


**Fig. 10.** Oxygen produced in the PEM (red lines), oxygen consumed in the industry (blue lines) and PEM capacity (green lines) as a function of the oxygen temperature (1200 °C in solid lines and 25 °C in dashed lines) and its percentage in the hot blast. (For interpretation of the references to colour in this figure legend, the reader is referred to the Web version of this article.)

The SNG and the preheating gas have negative values, as this $CO_2$-eq flow rate is not emitted into the atmosphere but recycled and constantly recirculated in the system. Regarding total $CO_2$ emissions, a linear dependency with the SNG injection is obtained. When injecting pure oxygen at 25 °C, 22% of $CO_2$ saving is achieved, but when preheating the oxygen to 1200 °C, 34% $CO_2$ savings are achieved, with respect to the conventional I&S plant.

$$\begin{aligned} Total\ CO_2\ emissions = \Sigma\ \text{Flue gases} &= Sint.Coal + Coking\ Coal + PCI \\ &= Sint.Coal + BFG + BOFG + COG \\ &\quad - SNG - Preheating\ gas \end{aligned} \tag{8}$$

The sold gases, electricity consumption and energy penalty are represented in Fig. 12. The sold gases (BFG, BOFG and COG) increase at first and then stabilize at 4500–5500 MJ/$t_{HM}$, being double than that obtained in the conventional I&S plant (2400 MJ/$t_{HM}$). This is caused by the increasing energy content of the BFG (see Fig. 7) counteracted by the BFG consumed in the preheating gas, 0–1313 MJ/$t_{HM}$ (see Fig. 8), and in the SNG heating, 111–271 MJ/$t_{HM}$.

The electricity consumption has a direct correlation with the PEM size, and therefore with the SNG injected in the BFG, since other electricity consumptions barely vary. The total electricity consumption rises from 5000 MJ/$t_{HM}$ when injecting air, to 15,600 MJ/$t_{HM}$ when injecting 95% $O_2$ at 1200 °C, compared to the 950 MJ/$t_{HM}$ obtained in the conventional I&S plant. The electricity production in the power plant has been kept constant at 1122 MJ/$t_{HM}$ (100 MW). Other minor electrical consumptions added are the pumps in the amine system and the $CO_2$ and $H_2$ compressors prior to methanation, accounting for 9–15 MJ/$t_{HM}$ and 231–400 MJ/$t_{HM}$ respectively. The energy penalty shows a great difference when using cold oxygen (21–25 MJ/$kg_{CO2}$) or hot oxygen (17–19 MJ/$kg_{CO2}$), being 16 MJ/$kg_{CO2}$ when using atmospheric air.

### 4.4. Economic analysis

When increasing the oxygen enrichment in the hot blast, the Capex and Opex increase, due to higher carbon capture and electrolysis plants, and higher electricity consumption (Table 4). Capex and Opex have values between 268 and 1157 M€ and 221–835 M€/year, respectively. The PEM electrolyser accounts for 44–53% of the Capex, and the renewable purchased electricity accounts for 94–96% of the Opex. However, when increasing the oxygen enrichment, the Incomes also increase, mainly due to higher coal saved and $CO_2$ taxes saved, ranging between 102 and 294 M€/year. The $CO_2$ taxes saved accounts for 39–49% of the Incomes.

The specific carbon capture (CC) cost, in €/$t_{CO2}$ and €/$t_{HRC}$, is shown in Fig. 13 as a function of the oxygen enrichment and its temperature.

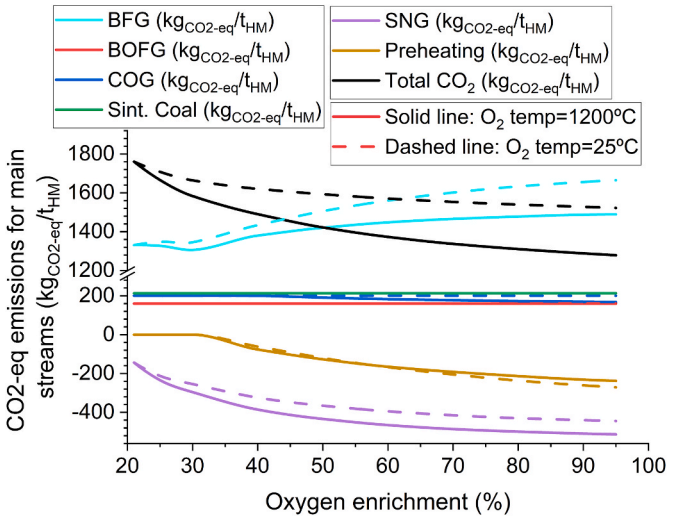


**Fig. 11.** $CO_2$ equivalent ($CO_2$-eq) emissions for the main streams: BFG in the blue line, BOFG in the red line, COG in the dark blue line, sinter coal in the green line, SNG in the purple line, preheating gas in the yellow line and total CO2 emissions in black line; as a function of the oxygen temperature (1200 °C in solid lines and 25 °C in dashed lines) and its percentage in the hot blast. (For interpretation of the references to colour in this figure legend, the reader is referred to the Web version of this article.)

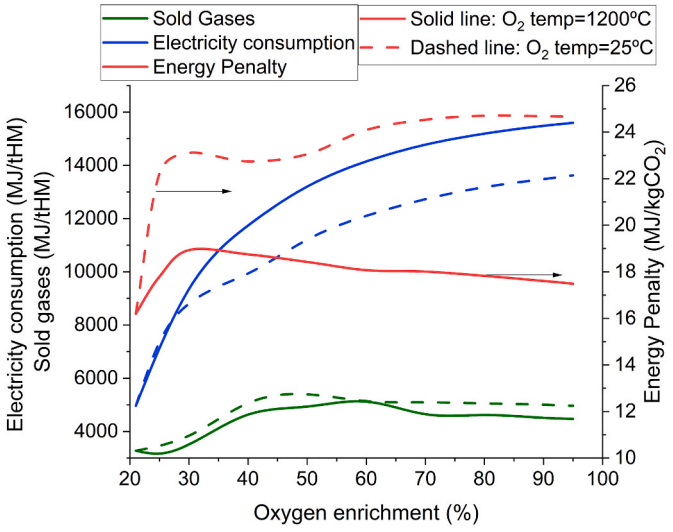


**Fig. 12.** Electricity consumption (blue line), sold gases (green line) and energy penalty (red line) as a function of the oxygen temperature (1200 °C for the solid line and 25 °C for the dashed line) and its percentage in the hot blast. (For interpretation of the references to colour in this figure legend, the reader is referred to the Web version of this article.)

Since the steel price is around 660–1400 €/$t_{HRC}$ in 2022 (*Marketwatch Web Page (HRC Steel)*, 2022), the specific CC cost –in €/$t_{HRC}$– represents 4–35% of the actual steel price, depending on the oxygen enrichment degree. Contrary to this variable, the specific CC cost regarding the $CO_2$ avoided (€/$t_{CO2}$) is highly dependent on the oxygen temperature, due to the lower $CO_2$ abatement when injecting cold oxygen. For illustration purposes, 30–95% of hot oxygen enrichment may be compared: the $CO_2$ abatement is 19–34% with a cost of 366-352 €/$t_{CO2}$, respectively; whereas for cold oxygen enrichment the $CO_2$ abatement is 14–22% with a cost of 466–539 €/$t_{CO2}$, respectively (see Figs. 5 and 13).

Regarding discounted pay-back period, two representative situations have been investigated: 21% $O_2$ in the hot blast (corresponding with a PEM size of 355 MW) and 95% $O_2$ at 1200 °C (corresponding to a PEM size of 1268 MW), both with a BF size of 320 $t_{HM}$/h, see Fig. 14. They correspond to the maximum $CO_2$ reduction and maximum profitability cases, respectively. The rest of cases are intermediate cases. The parametric analyses look for the most favourable combinations of $CO_2$ allowances and electricity prices that make the Power to Gas integration

**Table 4**
Main results for the economic analysis of the PtG integration in the iron and steel industry, for the data points of 21% $O_2$, 95% $O_2$ at 25 °C and 95% $O_2$ at 1200 °C.

| | 21% $O_2$ | 95% $O_2$ at 25 °C | 95% $O_2$ at 1200 °C |
|---|---|---|---|
| **CAPEX [M€]** | **267.8** | **1027.4** | **1156.7** |
| Amine Plant | | | |
| Overall Cost | 7.39 | 12.71 | 17.11 |
| Electrolysis | | | |
| Overall Cost | 141.92 | 439.26 | 507.04 |
| Methanation | | | |
| $H_2$ compressor | 0.036 | 0.077 | 0.084 |
| $CO_2$ compressor | 0.017 | 0.037 | 0.041 |
| Reactors | 0.245 | 0.760 | 0.877 |
| Catalyst | 4.39 | 13.59 | 15.68 |
| Heat exchangers | | | |
| BF retrofitting | 0.429 | 1.047 | 1.173 |
| Other direct costs | | | |
| Installation | 15.44 | 59.25 | 66.70 |
| Instrumentation & control | 6.18 | 23.70 | 26.68 |
| Piping | 24.71 | 94.80 | 106.72 |
| Electrical | 7.72 | 29.62 | 33.35 |
| Building | 7.72 | 29.62 | 33.35 |
| Land | 1.54 | 5.92 | 6.67 |
| Indirect costs | | | |
| Engineering | 15.24 | 58.48 | 65.83 |
| Legal expenses | 5.36 | 20.55 | 23.13 |
| Construction expenses | 10.71 | 41.10 | 46.27 |
| Contingency | 18.75 | 71.92 | 80.97 |
| **OPEX [M€/year]** | **220.69** | **722.14** | **835.38** |
| Amine renovation | 0.16 | 0.36 | 0.57 |
| Catalyst renovation | 0.66 | 2.04 | 2.35 |
| Electricity | 210.97 | 686.22 | 794.64 |
| Water | 0.87 | 2.69 | 3.11 |
| O&M | 8.03 | 30.82 | 34.70 |
| **INCOMES [M€/year]** | **101.69** | **191.43** | **293.94** |
| Coal | 20.36 | 45.88 | 74.12 |
| Oxygen | 24.59 | 4.15 | 35.42 |
| $CO_2$ taxes | 39.46 | 90.98 | 143.66 |
| Steel gases | 17.28 | 50.42 | 40.74 |

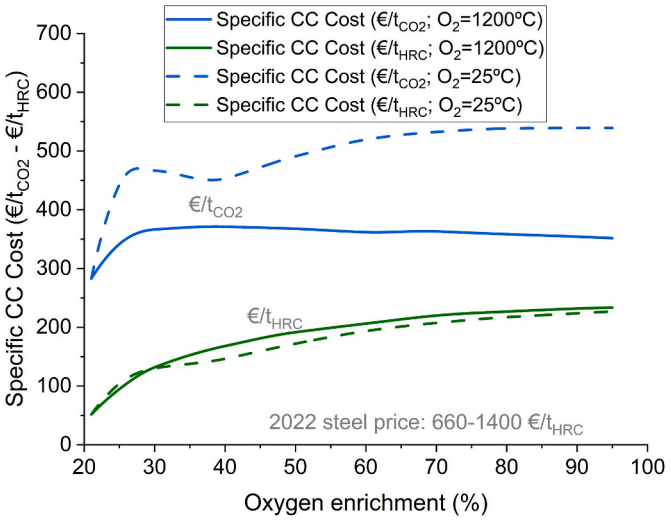


**Fig. 13.** Specific carbon capture (CC) cost in €/$t_{CO2}$ and €/$t_{HRC}$ as a function of the oxygen temperature (1200 °C for the solid line and 25 °C for the dashed line) and its percentage in the hot blast (2022 steel price (Marketwatch Web Page (HRC Steel), 2022)).

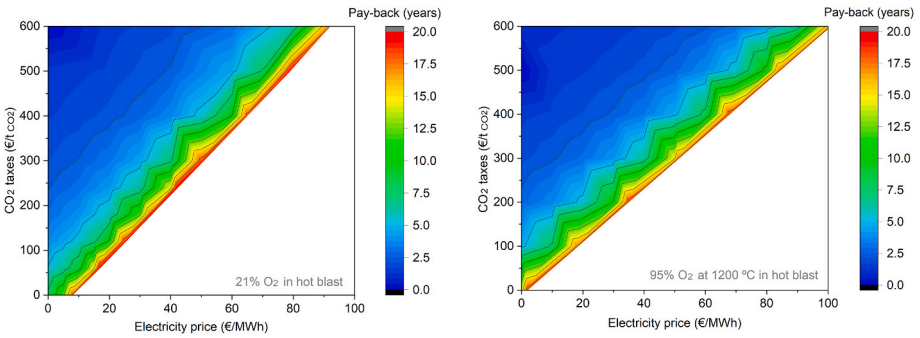


**Fig. 14.** Pay-back in years as a function of the $CO_2$ taxes and the electricity price, for the data points of 21% $O_2$ in the hot blast (left) and 95% $O_2$ at 1200 °C (right).

economically viable. A maximum of 20 years has been fixed as it is the replacement period of some important equipment as the blast furnace. This economic study indicates that profitable scenarios would require the supply of electricity at the cost of production or subsidies given to the industry.

It is important to highlight the exponential descent of the pay-back, as values higher than 13 years (red area) are in a very reduced area, values between 6 and 13 years (green area) are in a small area, and values lower than 6 years (blue area) cover most of the profitable price-tax mix. This means that for a given value of electricity price, e.g. 35 €/MWh (cost of production for wind power (*IRENA*, 2022)), the pay-back is 20 years when the $CO_2$ tax is 135 €/$t_{CO2}$ for the first data point and 200 €/$t_{CO2}$ for the second one; but the payback changes to 6 years when the $CO_2$ tax is 200 €/$t_{CO2}$ and 300 €/$t_{CO2}$, respectively.

## 5. Conclusions

A novel concept of integration of Power to Gas (PtG) technology in the steelmaking industry with oxygen enrichment of the hot blast was presented in this study. Renewable electricity is used to power a PEM electrolyser that produces green $H_2$, an MDEA amine plant captures $CO_2$ from the BFG, and a methanation reactor produces synthetic natural gas (SNG) from the two previous components. This SNG is injected into the blast furnace (BF), thus recycling $CO_2$ in a closed loop and reducing coal consumption. Along with this PtG integration, the oxygen enrichment has been studied at two different temperatures, 25 °C and 1200 °C, and its percentage in the hot blast ranges from 21% (atmospheric air) to 95%.

For all the parameters analysed, better results were found with hot oxygen (1200 °C) compared to that at ambient temperature (25 °C). Similarly, the oxygen enrichment analysis showed better technical results at higher oxygen percentages, but also higher costs, compared to that with low oxygen enrichment. Therefore, when injecting 95% $O_2$ at 1200 °C in the hot blast, 192 $kg_{SNG}/t_{HM}$ can be injected, substituting all the pulverised coal injection (PCI) and 16% of the coke, causing an overall $CO_2$ emission reduction of 34% (equivalent to 664 $kg_{CO2}/t_{HM}$). The overall coal reduction accounts for 221 $kg/t_{HM}$ (33% of current coal consumption).

The BFG increases its energy content from 4930 $MJ/t_{HM}$ when atmospheric air to 8086 $MJ/t_{HM}$ when 95% $O_2$, due to the reduced $N_2$ contribution and the high SNG injection that increases the $H_2$ contribution. Due to the increase in the BFG energy content, the energy needs for the downstream processes are covered, avoiding a problem that usually appears in TGR configurations. The BFG temperature decreases sharply when injecting oxygen, which makes necessary a preheating gas injection in the upper part of the shaft when the oxygen enrichment is above 30%.

The thermal integration between the amine heat consumption and the exothermic heat of the methanation has demonstrated that no extra energy is needed to cover the amine thermal demand. The PEM electrolyser is sized between 355 MW and 1268 MW depending on the oxygen enrichment and its temperature. The oxygen by-produced in the electrolyser is used to eliminate the ASU and to feed the BOF and hot blast enrichment necessities. The overall electricity consumption increases between 5 and 16 times compared to the conventional I&S plant, accounting the PEM for 92% of the total electricity consumption.

The energy penalty obtained is dependent on the oxygen temperature, likewise if using cold oxygen 25 $MJ/kg_{CO2}$ is achieved, but if using hot oxygen (1200 °C) 17 $MJ/kg_{CO2}$ is achieved. Under the current economic situation, the specific carbon capture (CC) cost is between 4 and 35% of the actual steel price. Economic profitability can be achieved with certain combinations of electricity price, $CO_2$ tax or economic subsidies.

The main economic limitation of this study is the uncertainty in future carbon and electricity prices, as these variables have a great influence on the specific carbon capture costs. Regarding the technical limitations, the feasibility of an OBF can be seen as the main concern, since these types of furnaces are still under development and have not yet reached the commercial stage. Additionally, each I&S industry has its unique equipment layouts, which can impact the practical implementation of this concept.

In general, this novel concept of PtG technology in the steelmaking industry with oxygen enrichment has the advantage of reducing fuel consumption and $CO_2$ emissions, while avoiding geological storage as the carbon is recycled. This PtG configuration consumes renewable electricity, producing green hydrogen and later SNG. More PtG integration concepts in the blast furnace ironmaking will be considered in future work to reduce energy penalties and costs.

## CRediT authorship contribution statement

**Jorge Perpiñán:** Conceptualization, Methodology, model, Formal analysis, Writing – original draft, Visualization. **Manuel Bailera:** Conceptualization, Methodology, model, Writing – review & editing, Visualization, Supervision, Project administration, Funding acquisition. **Begona Peña:** Conceptualization, Methodology, Writing – review & editing, Supervision, Project administration, Funding acquisition. **Luis M. Romeo:** Writing – review & editing, Project administration, Funding acquisition, All authors have read and agreed to the published version of the manuscript. **Valerie Eveloy:** Writing – review & editing, Project administration, Funding acquisition.

## Declaration of competing interest

The authors declare that they have no known competing financial interests or personal relationships that could have appeared to influence the work reported in this paper.

## Data availability

Data will be made available on request.

## Acknowledgements

The work presented in this paper has been supported by the Khalifa University project CIRA-2020-080. This work has also received funding from the European Union's Horizon 2020 research and innovation program under the Marie Sklodowska-Curie grant agreement no. 887077. This work is part of the R&D project TED2021-130000B–I00, funded by MCIN/AEI/10.13039/501100011033/and by the "European Union NextGenerationEU/PRTR". This research is co-funded by the University of Zaragoza, Fundación Bancaria Ibercaja, and Fundación CAI, through the program "Programa Ibercaja-Cai Estancias de Investigación", nº IT 16/12. Manuel Bailera acknowledges Waseda University, Tokyo, and K1-MET GmbH, Linz.

## Appendix ASupplementary data

Supplementary data to this article can be found online at https://doi.org/10.1016/j.jclepro.2023.137001.

## References

Abdul Quader, M., Ahmed, S., Dawal, S.Z., Nukman, Y., 2016. Present needs, recent progress and future trends of energy-efficient Ultra-Low Carbon Dioxide (CO2) Steelmaking (ULCOS) program. Renew. Sustain. Energy Rev. 55, 537–549. https://doi.org/10.1016/J.RSER.2015.10.101.

Abu-Zahra, M.R.M., Niederer, J.P.M., Feron, P.H.M., Versteeg, G.F., 2007. CO2 capture from power plants. Part II. A parametric study of the economical performance based on mono-ethanolamine. Int. J. Greenh. Gas Control 1 (2), 135–142. https://doi.org/10.1016/S1750-5836(07)00032-1.

Andrade de Castro, L.F., Tavares, R.P., Seshadri, V., 2005. Process control model for charcoal blast furnaces in Brazil. Mater. Manuf. Process. 20 (2), 287–298. https://doi.org/10.1081/amp-200042085.

ArcelorMittal, 2023. Technology Pathways to Net-Zero Steel. https://corporate.arcelormittal.com/climate-action/technology-pathways-to-net-zero-steel.

Ariyama, T., Sato, M., Nouchi, T., Takahashi, K., 2016. Evolution of blast furnace process toward reductant flexibility and carbon dioxide mitigation in steel works. ISIJ Int. 56 (10), 1681–1696. https://doi.org/10.2355/isijinternational.ISIJINT-2016-210.

Aspen Technology Inc, 2019a. Aspen Energy Analyzer. AspenTech.

Aspen Technology Inc, 2019b. Aspen Examples - Reference Manual. AspenTech.

Aspen Technology Inc, 2019c. Aspen Physical Property Methods - Reference Manual. AspenTech.

Babich, A., Senk, D., Gudenau, H.W., K. T. M, 2008. IRONMAKING, p. 402.

Bailera, M., Espatolero, S., Lisbona, P., Romeo, L.M., 2017a. Power to gas-electrochemical industry hybrid systems: a case study. Appl. Energy 202, 435–446. https://doi.org/10.1016/j.apenergy.2017.05.177, 2017.

Bailera, M., Lisbona, P., Romeo, L.M., Espatolero, S., 2017b. Power to Gas projects review: lab, pilot and demo plants for storing renewable energy and CO2. Renew. Sustain. Energy Rev. 69 (November 2016), 292–312. https://doi.org/10.1016/j.rser.2016.11.130.

Bailera, M., Lisbona, P., Pena, B., Romeo, L.M., 2021a. A review on CO2 mitigation in the Iron and Steel industry through Power to X processes. J. CO2 Util. 46 (November 2020), 101456 https://doi.org/10.1016/j.jcou.2021.101456.

Bailera, M., Nakagaki, T., Kataoka, R., 2021b. Revisiting the Rist Diagram for Predicting Operating Conditions in Blast Furnaces with Multiple Injections. https://doi.org/10.12688/openreseurope.14275.1.

Bailera, M., Lisbona, P., Pena, B., Alarcon, A., Guilera, J., Perpinan, J., Romeo, L.M., 2022a. Synthetic natural gas production in a 1 kW reactor using Ni-Ce/Al2O3 and Ru-Ce/Al2O3: kinetics, catalyst degradation and process design. Energy 256. https://doi.org/10.1016/j.energy.2022.124720.

Bailera, M., Nakagaki, T., Kataoka, R., 2022b. Limits on the integration of power to gas with blast furnace ironmaking. J. Clean. Prod., 134038 https://doi.org/10.1016/J.JCLEPRO.2022.134038.

Benjaminsson, G., Benjaminsson, J., Rudberg, R.B., 2013. Power-to-Gas - A Technical Review. http://sgc.camero.se/ckfinder/userfiles/files/SGC284_eng.pdf.

De Saint Jean, M., Baurens, P., Bouallou, C., Couturier, K., 2015. Economic assessment of a power-to-substitute-natural-gas process including high-temperature steam electrolysis. Int. J. Hydrogen Energy 40 (20), 6487–6500. https://doi.org/10.1016/j.ijhydene.2015.03.066.

European Commission, 2022. https://energy.ec.europa.eu/index_es.

He, K., Wang, L., 2017. A review of energy use and energy-efficient technologies for the iron and steel industry. Renew. Sustain. Energy Rev. 70 (September 2016), 1022–1039. https://doi.org/10.1016/j.rser.2016.12.007.

Hisashige, S., Nakagaki, T., Yamamoto, T., 2019. CO2 emission reduction and exergy analysis of smart steelmaking system adaptive for flexible operating conditions. ISIJ Int. 59 (4), 598–606. https://doi.org/10.2355/isijinternational.ISIJINT-2018-355.

Hurskainen, M., 2017. Industrial Oxygen Demand in Finland. https://www.vttresearch.com/sites/default/files/julkaisut/muut/2017/VTT-R-06563-17.pdf.

IEA - iron & steel roadmap. https://www.iea.org/reports/iron-and-steel-technology-roadmap, 2020.

Intergovernmental, 2022. Panel on climate change (IPCC). https://www.ipcc.ch/.

International Energy Agency, 2020. Iron and steel technology roadmap. https://www.iea.org/reports/iron-and-steel-technology-roadmap.

IRENA, 2022. https://www.irena.org/costs/Power-Generation-Costs.

Izumiya, K., Shimada, I., 2021. K2- Methane Producing Technology from CO 2 for Carbon Recycling, pp. 34–35.

Kim, H., Kang, T., Kaiser, K., Liedel, S., Jarry, L., Paubel, X., Jumani, Y., Kaya, L., 2016. Heat Oxy-Combustion: An Innovative Energy Saving Solution For Glass Industry. 76th Conference on Glass Problems Edited by S . K . Sundaram 1, 185–191.

Kohl, A.L., Nielsen, R.B., 1997. Gas purification. https://doi.org/10.1016/B978-0-88415-220-0.X5000-9.

Lehner, M., Tichler, R., Steinmuller, H., Koppe, M., 2014. Power-to-Gas: technology and business models. https://link.springer.com/book/10.1007/978-3-319-03995-4?noAccess=true.

Li, C.L., Xue, Q.G., Liu, Y.L., Dong, Z.S., Wang, G., Wang, J.S., 2019. Comprehensive analysis on material and exergy balances of oxygen blast furnace. Ironmak. Steelmak. 46 (8), 761–770. https://doi.org/10.1080/03019233.2017.1410947.

Li, R., Lian, S., Zhang, Z., Song, C., Han, R., Liu, Q., 2022. Techno-economic evaluation of a novel membrane-cryogenic hybrid process for carbon capture. Appl. Therm. Eng. 200 https://doi.org/10.1016/j.applthermaleng.2021.117688.

Mac Dowell, N., Fennell, P.S., Shah, N., Maitland, G.C., 2017. The role of CO2 capture and utilization in mitigating climate change. Nat. Clim. Change 7 (4), 243–249. https://doi.org/10.1038/nclimate3231.

Marketwatch Web Page (HRC Steel), 2022. https://www.marketwatch.com/investing/index/steel?countryCode=XX.

Nie, H., Li, Z., Kuang, S., Yan, L., Zhong, W., Yu, A., Mao, X., Xu, H., 2021. Numerical investigation of oxygen-enriched operations in blast furnace ironmaking. Fuel 296. https://doi.org/10.1016/j.fuel.2021.120662. July 2020.

Peacey, J.G., Davbenport, W.G., 1979. The Iron Blast Furnace. Theory and Practice, 1979.

Perpiñán, J., Bailera, M., Romeo, L.M., Pena, B., Eveloy, V., 2021. CO2 recycling in the iron and steel industry via power-to-gas and oxy-fuel combustion. Energies 14 (21), 7090. https://doi.org/10.3390/en14217090.

Perpinan, J., Bailera, M., Pena, B., Romeo, L.M., Eveloy, V., 2022a. Technical and economic assessment of iron and steelmaking decarbonisation via power to gas and amine scrubbing. ReVision.

Perpiñán, J., Pena, B., Bailera, M., Eveloy, V., Kannan, P., Raj, A., Lisbona, P., Romeo, L. M., 2022b. Integration of Carbon Capture Technologies in Blast Furnace Based Steel Making: a Comprehensive and Systematic Review. https://doi.org/10.1016/j.fuel.2022.127074.

Pistorius, P.C., Gibson, J., Jampani, M., 2017. Natural gas utilization in blast furnace ironmaking: tuyere injection, shaft injection and prereduction. Minerals, Metals and Materials Series 9783319510903, 283–292. https://doi.org/10.1007/978-3-319-51091-0_26.

Quarterly Coal Report July–September 2021, 2021. U.S. Department of Energy. https://www.eia.gov/coal/production/quarterly/pdf/qcr-all.pdf.

Romeo, L.M., Pena, B., Bailera, M., Lisbona, P., 2020. Reducing cycling costs in coal fired power plants through power to hydrogen. Int. J. Hydrogen Energy 45 (48), 25838–25850. https://doi.org/10.1016/j.ijhydene.2020.04.095.

Ronsch, S., Schneider, J., Matthischke, S., Schluter, M., Gotz, M., Lefebvre, J., Prabhakaran, P., Bajohr, S., 2016. Review on methanation - from fundamentals to current projects. Fuel 166, 276–296. https://doi.org/10.1016/j.fuel.2015.10.111.

Rosenfeld, D.C., Bohm, H., Lindorfer, J., Lehner, M., 2020. Scenario analysis of implementing a power-to-gas and biomass gasification system in an integrated steel plant: a techno-economic and environmental study. Renew. Energy 147, 1511–1524. https://doi.org/10.1016/j.renene.2019.09.053.

Sahu, R.K., Roy, S.K., Sen, P.K., 2015. Applicability of top gas recycle blast furnace with downstream integration and sequestration in an integrated steel plant. Steel Res. Int. 1 (5), 502–516. https://doi.org/10.1002/srin.201400196.

Salehmin, M.N.I., Husaini, T., Goh, J., Sulong, A.B., 2022. High-pressure PEM water electrolyser: a review on challenges and mitigation strategies towards green and low-cost hydrogen production. Energy Convers. Manag. 268 (June), 115985 https://doi.org/10.1016/j.enconman.2022.115985.

Sato, M., Takahashi, K., Nouchi, T., Ariyama, T., 2015. Prediction of next-generation ironmaking process based on oxygen blast furnace suitable for CO2 mitigation and energy flexibility. ISIJ Int. 55 (10), 2105–2114. https://doi.org/10.2355/isijinternational.ISIJINT-2015-264.

Sendeco2, 2022. sendeco2. https://www.sendeco2.com/es/precios-co2%0A.

Steelmaking Technologies, 2022. CISDI ingeniering CO. LTD. http://www.cisdigroup.com/4-steelmaking.html

Tonomura, S., 2013. Outline of course 50. Energy Proc. 37, 7160–7167. https://doi.org/10.1016/j.egypro.2013.06.653.

Tsupari, E., Karki, J., Arasto, A., Lilja, J., Kinnunen, K., Sihvonen, M., 2015. Oxygen blast furnace with CO2 capture and storage at an integrated steel mill - Part II: economic feasibility in comparison with conventional blast furnace highlighting sensitivities. Int. J. Greenh. Gas Control 32, 189–196. https://doi.org/10.1016/j.ijggc.2014.11.007.

Turner, L.A., 2022. OpenForum2022 (bloomberg (BNEF) report: 1H 2022 hydrogen market outlook). https://www.rechargenews.com/energy-transition/will-us-and-european-green-hydrogen-markets-soon-be-flooded-by-cheap-chinese-electrolysers-/2-1-1165966.

Wu, J., Wang, R., Pu, G., Qi, H., 2016. Integrated assessment of exergy, energy and carbon dioxide emissions in an iron and steel industrial network. Appl. Energy 183, 430–444. https://doi.org/10.1016/j.apenergy.2016.08.192.

Zhai, X., Chen, M., 2023. Comparison of data-driven prediction methods for comprehensive coke ratio of blast furnace. High Temp. Mater. Process. 42 (1), 16–19. https://doi.org/10.1515/htmp-2022-0261.

Zhang, W., Zhang, J., Xue, Z., 2017. Exergy analyses of the oxygen blast furnace with top gas recycling process. Energy 121, 135–146. https://doi.org/10.1016/j.energy.2016.12.125.

Journal of CO2 Utilization 78 (2023) 102634

Contents lists available at ScienceDirect

Journal of CO2 Utilization

journal homepage: www.elsevier.com/locate/jcou

# Power to gas and top gas recycling integration in an oxygen blast furnace steelmaking industry

Jorge Perpiñán [a,*], Manuel Bailera [a], Begoña Peña [a], Pravin Kannan [b], Valerie Eveloy [b], Luis M. Romeo [a]

[a] Escuela de Ingeniería y Arquitectura, Universidad de Zaragoza, María de Luna 3, 50018 Zaragoza, Spain
[b] Khalifa University, Department of Mechanical Engineering, United Arab Emirates

ARTICLE INFO

*Keywords:*
Low-carbon steel
Power-to-Gas
Methanation
Amine scrubbing
Decarbonization

ABSTRACT

A new process concept integrating power to methane with top gas recycling in an oxygen blast furnace (BF) is investigated to reduce the emission intensity of steelmaking. Power to gas produces synthetic methane using hydrogen ($H_2$) generated by an electrolyser operated with renewable electricity, and $CO_2$ captured from the BF gas by amine scrubbing supplied with heat from the methanation process. The clean gas from the amine scrubbing is recycled and injected in the BF (via top gas recycling), together with synthetic methane. A parametric analysis is performed to vary the amount of top gas recycled (from 0 kg/tHM to 270 kg/tHM). Based on the results, $CO_2$ equivalent emissions can decrease by 34% using power to gas technology, and by 30% with power to gas and top gas recycling (compared to conventional BFs). Nevertheless, if both integrations are present, additional benefits on the specific energy consumption (12.0 MJ/$t_{HM}$), and specific cost (130 €/$t_{HM}$) are achieved, compared to only applying power to gas (17.5 MJ/$t_{HM}$ and 233 €/$t_{HM}$). In all cases, the downstream thermal energy needs of the steel plant are fulfilled, contrarily to conventional top gas recycling concepts. The main conclusion is that top gas recycling should be considered together with PtG technology, and vice versa, when integrated in blast furnace ironmaking, in order to both abate emissions while supplying downstream energy needs.

## Nomenclature

| | |
|---|---|
| AFT | Adiabatic Flame Temperature |
| ASU | Air Separation Unit |
| AHF | Air Heating Furnace |
| BF-BOF | Blast Furnace-Basic Oxygen Furnace |
| BFG | Blast Furnace Gas. |
| BOFG | Basic Oxygen Furnace Gas |
| CC | Carbon Capture |
| CCS | Carbon Capture Storage |
| COG | Coke Oven Gas |
| DRI | Direct Reduced Iron |
| EAF | Electric Arc Furnace |
| GHG | Green House Gas |
| HM | Hot Metal |
| I&S | Iron and Steel |
| IEA | International Energy Agency |
| LHV | Lower Heating Value |
| MDEA | Methyldiethanolamine |
| PEM | Proton Exchange Membrane |
| PtG | Power to Gas |
| PCI | Pulverised Coal Injection |
| PFD | Process Flow Diagram |
| SNG | Synthetic Natural Gas |
| tHM | Ton of Hot Metal |
| tCS | Ton of Crude Steel |
| TGR | Top Gas Recycling |
| α,β,γ | Parameters for Economic Analysis |

## 1. Introduction

Annual $CO_2$ emissions from the iron and steel (I&S) industry have increased over the past decade by ~31% [1], primarily due to increased demand for steel production, and currently represent almost 25% of all

* Corresponding author.
*E-mail address:* jorge.perpinan@unizar.es (J. Perpiñán).

https://doi.org/10.1016/j.jcou.2023.102634
Received 5 May 2023; Received in revised form 25 October 2023; Accepted 23 November 2023
Available online 28 November 2023
2212-9820/© 2023 The Authors. Published by Elsevier Ltd. This is an open access article under the CC BY-NC-ND license (http://creativecommons.org/licenses/by-nc-nd/4.0/).

industrial emissions (~2.6 Gt of $CO_2$) [2]. In order to limit global warming to below 1.5 °C, the I&S industry will require a portfolio of low-carbon technologies, including renewable electricity, hydrogen ($H_2$), and carbon capture (CC), especially in the medium term, when direct abatement technologies not yet deployed at sufficient scales [2].

The blast furnace-basic oxygen furnace (BF-BOF) is the dominant primary steel production route [3] and the most energy-intensive, utilizing 20–30 GJ/$t_{LS}$ [1]. Conventional coal/coke-based BF-BOF processes utilize ~800 kg of coal and emit ~1.8–2.2 $t_{CO2}/t_{LS}$ [2], with two thirds of these emissions incurred in the BF [4]. Molten metal is formed in the BF through reduction of iron and accompanying elements from their oxides, and refined in the BOF to produce crude liquid steel [5]. Typical reducing agents include coke formed after carbonization of coal in coke oven, pulverized coal (PC), and natural gas (NG). Complete reduction of iron ore (mainly hematite $Fe_2O_3$ and magnetite $Fe_3O_4$) is accomplished by a combination of indirect reduction with CO and $H_2$ and direct reduction with carbon [6,7] (Table 1).

The evolution of the BF process, illustrated in Fig. 1, is characterized initially by a decrease in coke rate utilization, followed by several technology improvements, especially on the composition of the blast, to reduce carbon consumption [8], [9]. In the early years (1960's), the traditional blast furnace (BF) employed a combined blast of hot air and oil to supply energy for iron ore reduction reactions. Following the subsequent oil crisis, the blast oil was substituted with PC and enriched $O_2$ towards coke-only operation. During the transition period, approaches to reduce coke consumption using reducing gas produced by reforming either oil or NG, or using coke oven gas were explored. Although these process modifications did not lead to commercialization, they enabled the development of various oxygen blast furnace (OBF) variants during the 1980's that sought to significantly reduce carbon consumption. These variants employed a combination of pre-heat gas and blast furnace gas (BFG) exhaust injection back into the BF after $CO_2$ capture, using various process configurations. Subsequently, an advanced OBF process utilizing intensified NG injection in a downsized BF, was proposed to reduce carbon input and energy penalty. Among notable OBF variants, the oxygen BF with top gas recycling (OBF-TGR) using carbon capture and storage (CCS), and the advanced OBF, have enabled a coke rate reduction to 200–300 kg/$t_{HM}$, from 330 to 400 kg/$t_{HM}$ in the traditional BF process, and thus have been considered a significant technological improvement for energy savings and emission reductions [10], [11]. Key research efforts that have addressed OBF development, OBF integration with TGR, OBF integration with CCS, and OBF integration with Power to Gas (PtG) are reviewed as follows.

The OBF involves injection of either medium $O_2$-enriched (30–60% $O_2$) or full-oxygen (>90% $O_2$) blast furnace, instead of slightly-rich $O_2$ blast in the traditional BF (<30%). The $O_2$-enriched air enhances partial combustion of coke and auxiliary fuels, thereby generating a $N_2$-deficit top gas, comprising mainly of CO, $CO_2$, $H_2$ and $H_2O$ [12]. A higher $O_2$ content in the blast enables injection of large amounts of PC [9], and thus increases productivity. On the other hand, gas injection as a supplementary reducing agent lowers the direct reduction ratio, and promotes low carbon consumption. Among the different gaseous injectants tested, NG has been found to be the most effective in significantly curtailing coke rate for a specified injection volume [9]. Zhang et al. [11]

**Table 1**
Typical reduction reactions of iron ore in a blast furnace [6,7].

| Reaction | Equation | No. |
|---|---|---|
| Indirect reduction by CO | $3Fe_2O_3(s) + CO(g) \rightarrow 2Fe_3O_4(s) + CO_2(g)$ | (1) |
| | $Fe_3O_4(s) + CO(g) \rightarrow 3FeO(s) + CO_2(g)$ | (2) |
| | $Fe_3O_4(s) + 4CO(g) \rightarrow 3Fe(s) + 4CO_2(g)$ | (3) |
| | $FeO(s) + CO(g) \rightarrow Fe(s) + CO_2(g)$ | (4) |
| Indirect reduction by $H_2$ | $3Fe_2O_3(s) + H_2(g) \rightarrow 2Fe_3O_4(s) + H_2O(g)$ | (5) |
| | $Fe_3O_4(s) + H_2(g) \rightarrow 3FeO(s) + H_2O(g)$ | (6) |
| | $FeO(s) + H_2(g) \rightarrow Fe(s) + H_2O(g)$ | (7) |
| Direct reduction of liquid FeO | $FeO(l) + C(s) \rightarrow Fe(l) + CO(g)$ | (8) |

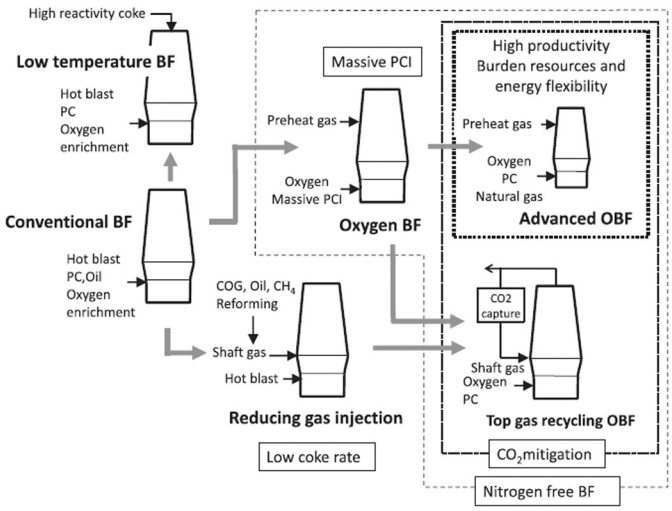


**Fig. 1.** Evolution of BF technology for diminishing coke rate and $CO_2$ emissions. PC – Pulverized coal.
Adapted from [8].

reviewed the evolution of OBF with particular focus on gas injection point and process characteristics. OBF development has particularly focused on minimizing spatial temperature gradients between the upper and lower regions of the OBF.

The concept of integrating the OBF with TGR has been studied comprehensively in recent years [8,9,11,13–19]. The primary goal of TGR is to decrease the carbon input by partially substituting PC with unused CO and/or $H_2$ in the top gas after $CO_2$ capture. In this context, different OBF-TGR process designs have been proposed depending on the point where recycled gas is introduced into the BF, or whether $CO_2$ is captured from the exhaust before recycling the top gas [8,9,11,15,16,19]. The recycled gas could be introduced back into the BF either through the hearth tuyeres, mid shaft, upper tuyeres, or a combination of these [20]. The first industrial trial of the OBF process (NKK-OBF) employed TGR without $CO_2$ sequestration [11]. In this process, a part of the recycle stream was split between hearth tuyeres and mid-shaft, and the remaining exported for utilization. The results demonstrated a significant decrease in coke rate (and thus total fuel rate) due to the increase in the amount of PC injected [11]. Another industrial Tula-OBF process employed $CO_2$ capture before a part of treated blast furnace gas (BFG) was preheated and introduced into the hearth tuyeres along with full $O_2$ blast [11]. Although successful in reducing the coke injection rate, technical difficulties were encountered in the process due to prolonged operation of the OBF with low coke flowrate and low $O_2$ blast velocity. In a more recently developed TGR-OBF process within ULCOS project, recycling of $CO_2$-deprived top gas at both hearth and shaft sections of the BF was considered, after preheating the recycled gas to different temperatures using a blast mixture of cold $O_2$ and PC [11], [18]. The results showed that combined injection of recycle gas into hearth led to lower coal and coke consumption compared to injection at hearth alone. Also, 76% reduction in $CO_2$ emissions (24% mitigation by gas recycling, and 52% by $CO_2$ extraction) was found to be potentially achievable using the proposed configuration [21]. Other studies that have investigated similar process designs have proposed combusting a part (~10%) of raw BFG to supply heat for pre-heating the recycled shaft or tuyere gas stream [19], [22], [23]. Some alternative OBF design features include a pre-heated injection stream, wherein a fraction of raw BFG is pre-heated to ~1000 °C and introduced into the upper shaft of the BF [24]. The results showed that the auxiliary stream assisted in improving the heat distribution throughout the upper shaft, and the pre-heating gas composition and flow had minimal impact on the reduction reactions in the lower shaft [24].

Integration of the OBF and TGR can synergetic act towards carbon

mitigation. For instance, an integrated steel mill operated with the OBF-TGR process was found to significantly curtail $CO_2$ emissions (ca. 43%) relative to a traditional BF steel mill [22], [23]. Other benefits over the OBF-TGR include: high productivity, reduced fuel rate (due to increase in indirect reduction degree), improved top gas calorific value (and thus reduced energy demand), improved bed fluidization (and thus productivity), reduced environmental impact, and improved PC injection rate (and thus reduced dependence on metallurgical coke) [11], [21], [24], [25]. Although $O_2$ consumption in the OBF is significantly higher than in the traditional BF process (220 $Nm^3/t_{HM}$ vs. 70 $Nm^3/t_{HM}$ [22]), the additional $O_2$ supply could be sourced from the existing air separation unit in traditional BF. One of the main challenges in deploying TGR in OBF is unavailability of sufficient energy for downstream processes due to top gas recycling and subsequent reduced carbon input [9], [14]. Depending on the recirculating ratio of the top gas, which typically ranges between 30% and 100% [20], the process would incur a thermal energy penalization of 1.5–4 $GJ/t_{HM}$ [9]. Integrating the TGR process with a low-carbon source such as NG instead of PC has been found to increase the calorific value of the BFG by ~2 times relative to traditional BF [8], and thus has been recommended as a potential solution [9].

It should be noted that recycling part of the BFG exhaust with high $CO_2$ and $H_2O$ content into the tuyeres would not be desirable, as this tends to increase coke consumption and impedes reduction reactions of iron oxides [20]. Thus, the TGR process is usually accompanied by CC and steam condensation prior to recycling the gases into the furnace. The benefits of integrating CCS with an OBF-TGR steel mill has been realized in industrial trials [19], [22], [23]. In comparison to the traditional BF, the overall $CO_2$ emissions reduction was estimated to reach ~88%, and thus the integration has been envisaged as the only technological pathway for reducing on-site emissions from integrated steel mills [22]. Quader et al. [13] evaluated different criteria for CCS technology selection for a specific iron and steel process, and identified energy for capture and storage, and $CO_2$ removal efficiency as the two key factors. Vacuum pressure swing adsorption (VPSA) and amine scrubbing are the most common $CO_2$ capture techniques employed in BF-BOF processes based on previous works by [26–34]. The primary drawbacks of amine scrubbing are degradation of the solvent (which thus requires replacement), and the need for a significant amount of steam for solvent regeneration, ~2–4 $GJ/t_{CO2}$ of thermal energy (equivalent electricity penalty of ~0.7–1.4 $GJ/t_{CO2}$) [9], [35]. However, as the BFG contains minimal amounts of $O_2$, the amines would be less susceptible to degradation, making amine absorption technique suitable for $CO_2$ capture from the BF top gas. Among the solvents tested for $CO_2$ absorption performance, monoethanolamine (MEA) has been found to be the ideal candidate, despite the high regeneration energy [26,28]. This is due to the ability of MEA to regenerate at a lower temperature using low exergy heat that is widely available in steel site. Moreover, the differences in $CO_2$ recovery ratio between MEA and advanced solvents were not found to be significant. Although some solvent blends have been found to exhibit improved performance [32], the results have been limited to simulation studies.

Combining OBF and PtG has been recently proposed to promote carbon recycling within steel production facilities [36]. Rosenfeld et al. [37] and Medved [38] analysed different configurations of PtG with biomass methanation, and Hisashige et al. [39] studied a combination of TGR with a SOEC electrolyser. Other authors injected pure $H_2$ in the furnace, either from a low temperature electrolyser (PEM or Alkaline) [40] or from a high temperature electrolyser (SOEC) [41]. Utilizing renewable energy for water electrolysis, PtG technology generates $H_2$ that is combined with either carbon-rich exhaust gases [42], [43] or treated BFG [17], [20], [44] from the ironmaking process to generate synthetic methane or SNG and effectively replace NG. Following a comprehensive analysis of various PtG options, it has been concluded that PtG using treated BFG offers the highest $CO_2$ reduction potential [42]. The amount of $CO_2$ emissions that can be avoided by PtG integration is limited by the maximum volume of SNG that can be injected in the BF, which depends on the flame temperature. Approximately, up to 200–500 $kg/t_{HM}$ of $CO_2$ (equivalent to 15–40% of the emissions of a traditional BF) could be retained in closed loop recycling and avoided from being permanently stored [42], [45]. However, this approach implies an additional electricity penalization of ~1.3–2.1 $GJ/t_{HM}$ for the production of renewable $H_2$ [36].

In previous work, we developed and validated a reference model for the conventional iron and steel plant [43]. Building on this foundation, in this paper, we present a novel integration model that combines Power to Gas technology in the iron and steel industry. Specifically, while our previous work focused on Power to Gas in an air-blown blast furnace (9.4% of carbon avoidance and 283 €/$t_{CO2}$ of carbon avoidance cost) [43], and on the influence of the oxygen enrichment and its temperature in the hot blast (34% of carbon avoidance and 352 €/$t_{CO2}$ of carbon avoidance cost) [45], the new integration model operates with Top Gas Recycling in an oxygen blast furnace, to achieve lower energy consumption and costs while maintaining a high carbon avoidance rate.

Therefore, the present work seeks to assess the performance and cost of a power to gas installation in an oxygen blast furnace ironmaking plant and its coupling with top gas recycling technology. The novelty of the study relies on the synergetic injection of $CO_2$-free top gas (clean-BFG or TGR gas) and intensified SNG in an advanced OBF process, which has not been explored earlier. Moreover, the effects of complete substitution of the PC with SNG on the techno-economic performance of an OBF, for which understanding is at present limited, are investigated. Accordingly, through the present investigation, we intend to develop an improved "closed-loop" strategy for carbon recycling within BF operation based on an integrated PtG and OBF-TGR process model. The outcome of this study will detail the significance of integration and assess the influence of the top gas recycling ratio, and recycling gas composition on the specific energy consumption and cost of steel production.

## 2. Process configurations

In this study, a new process configuration that integrates Power to Gas technology with the steelmaking process is investigated having the potential to lead to significant reductions in energy consumption and costs, without compromising the high carbon avoidance rate. This configuration is compared with a reference case that serves as a baseline for comparison, and has been previously detailed, modelled and validated [43].

The proposed PtG-steelmaking integration with top gas recycling (TGR) and oxy-BF is presented in Fig. 2, where the dashed lines represent the additional streams and blocks needed to carry out the PtG integration. This case includes several blocks, such as the PEM electrolyser for $H_2$ production, amine scrubbing for $CO_2$ capture, and methanation plant for synthetic natural gas (SNG) production. Moreover, it modified the BF to an oxy-BF (i.e., pure oxygen is supplied instead of air). The $H_2$ is produced in the electrolyser, and diverted to the methanation plant, while the $O_2$ co-produced is used to alleviate the ASU demand, that feeds the BOF and the oxy-BF. The amine scrubbing stage captures $CO_2$ from the BFG, and sends it to the methanation plant, while the clean-BFG is presented with two options (TGR-Split block): it can be blended again with the remaining BFG, or be injected in the tuyeres of the oxy-BF as reducing agent. The methanation plant produces SNG from $CO_2$ and $H_2$, and injects it as reducing agent in the oxy-BF. The BF now operates under oxy-fuel conditions, which means that pure oxygen is injected instead of air. Other heating blocks were represented with the conventional heat exchanger icon (e.g., $O_2$, Clean-BFG or SNG heating), together with the required temperature and the fuel used. The modelling details and methodology for the PtG-steelmaking blocks, as well as for the conventional I&S blocks, were fully explained in Section 3. The main differences between the conventional I&S plant, OBF with SNG injection, and OBF with SNG and TGR injection are shown in Table 2.

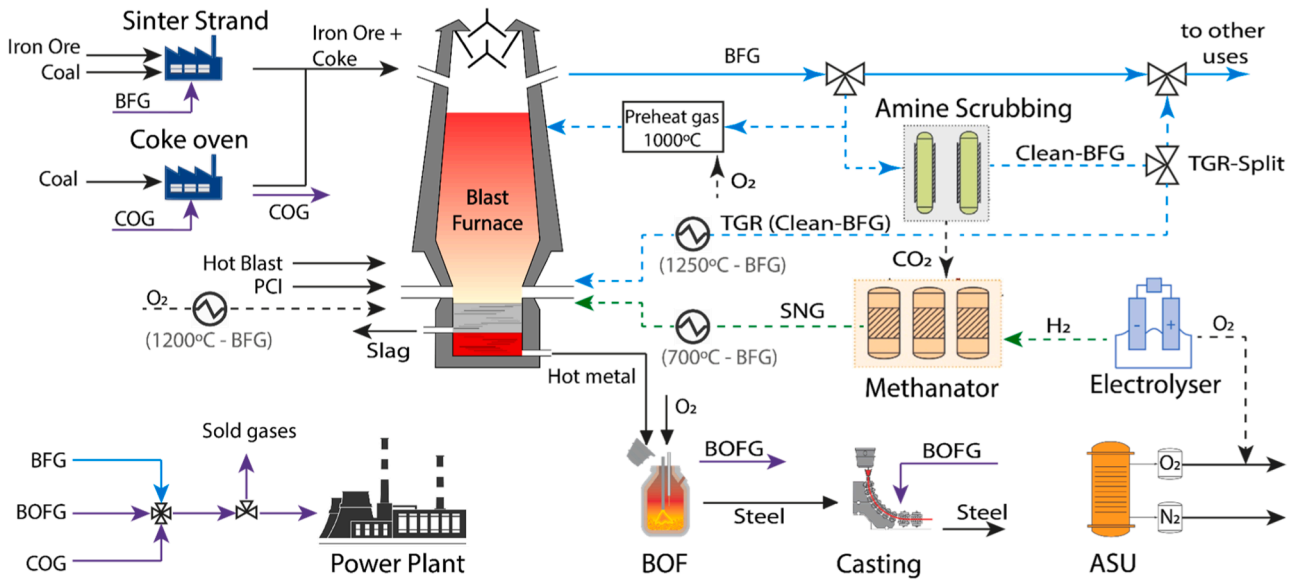


**Fig. 2.** Process flow diagram for conventional iron and steel plant (solid lines) and the integration of power to gas and top gas recycling in an oxygen blast furnace (dashed lines).

**Table 2**
Main data for the description of the conventional I&S plant, OBF with SNG injection, and OBF with SNG and TGR injection.

| | Conventional I&S, serving as benchmark and for Aspen validation [43] | OBF with SNG injection (no TGR) | OBF with SNG and TGR injection |
|---|---|---|---|
| Blast furnace | Conventional BF | Oxygen BF | Oxygen BF |
| Hot blast | Air at 1200 °C | $O_2$ 1200 °C | $O_2$ 1200 °C |
| Auxiliary fuels (tuyeres) | ·Coal | ·SNG: fixed to have 2000 °C AFT | ·TGR: varied from 0 kg/$t_{HM}$ (base case) to 270 kg/$t_{HM}$ (maximum clean-BFG available, which depends on the amine plant size)<br>·SNG: fixed to have 2000 °C AFT (as more TGR is injected, less SNG can be injected) |
| Additional equipment | n/a | ·Methanator: sized to produce the SNG required in the OBF<br>·Electrolyser: sized to produce the $H_2$ required in the methanator<br>·Amine scrubbing; sized to capture the $CO_2$ required in the methanator | ·Methanator: sized to produce the SNG required in the OBF (the higher the TGR injected, the lower the SNG, and the smaller the methanator)<br>·Electrolyser: sized to produce the $H_2$ required in the methanator<br>·Amine scrubbing; sized to capture the $CO_2$ required in the methanator |

## 3. Methodology

The process models for both the conventional I&S and the PtG-steelmaking integration were modelled in Aspen Plus v11. Fig. 2 shows the hierarchy blocks for both case studies, where each block consists of different sub-models and works with its own Aspen property method [46], in order to faithfully reproduce each process. Mass and energy balances of the system are calculated by the software Aspen Plus.

### 3.1. Conventional I&S plant

Solid lines in Fig. 2 represent the conventional I&S plant. The conventional I&S plant serves as a reference model, which has been previously detailed in [43]. The reference case includes several hierarchies, such as the sinter strand, coke oven, blast furnace, basic oxygen furnace, and power plant hierarchies, and the model considers a simplified version of the process (table Table 3). Additional parameters, such as BFG composition and air and coke flow rates, are externally calculated using the extended operating line methodology [36], [44]. CO and $H_2$ utilization are computed using Eqs. (9) and (10), respectively, with each component representing the content present in the blast furnace gas. The utilization of $H_2$ varies widely in the literature, with reported values ranging from 0.3 to 0.54 [47], [48]. In our study, we have opted for a value of 0.47 (if we do not take into account in Eq. (10) the steam from the upper injection, because this $H_2O$ does not come from the reduction of iron oxides, the utilization of $H_2$ is 0.42).

**Table 3**
Input data for the conventional I&S plant modelling.

| Variable | Value | Units |
|---|---|---|
| Coke oven temperature | 1100 | °C |
| $H_2$ utilization (Eq. (10)) | 0.47 | - |
| Carbon content in hot metal | 4.5 | wt% |
| Carbon content in final steel | 0.267 | wt% |
| Power plant size | 100 | MW |

$$\mu_{CO} = CO_2/(CO_2 + CO) \quad (9)$$

$$\mu_{H2} = H_2O/(H_2O + H_2) \quad (10)$$

#### 3.1.1. Model validation

The results and validation of the reference case were previously performed in [43] and can also be found in the supplementary data. The plant was assumed to have a 320 $t_{HM}$/h production rate and the total $CO_2$ emissions of the plant were found to be 1943 $kg_{CO2}/t_{HM}$. The main mass flow rates for the conventional I&S plant simulated in Aspen were compared to typical values from bibliography, and all results agreed

with the literature data, validating the conventional I&S plant model.

### 3.2. PtG-steelmaking integration with TGR

Following subsections show the assumptions made for the oxygen blast furnace (3.2.1), the modelling methodology for the PtG plant (3.2.2), the distribution of combustible gases (3.2.3), the sizing of the PtG plant (3.2.4), the techno-economic indicators (3.2.5).

#### 3.2.1. Oxy-BF

When injecting pure $O_2$ instead of air in the BF, the total bosh gas volume decreases due to the absence of nitrogen, what causes an insufficient preheat of the burden and a low BFG temperature. If the BFG temperature decreases below 100 °C, problems regarding water condensation and oxidation may appear. To solve this problem, a preheating gas injection in the upper part of the furnace was necessary. As preheating gas, it is commonly used BFG which is burned with pure oxygen at 1000 °C [8], [9].

The temperature at which the $O_2$ should be injected in the oxy-BF was already discussed in [45], concluding that hot oxygen injection (1200 °C) obtains greater benefits than cold oxygen injection (25 °C), both technical and economically.

#### 3.2.2. PtG modelling

The power to gas plant considered in this integration consists of a PEM electrolyser, an amine scrubbing and a methanation plant. The amine scrubbing model captures 90% of the inlet $CO_2$, using methyldiethanolamine (50 wt% MDEA and 50 wt% water) as solvent. The absorber column was modelled with 15 stages, and the stripper column with 19 stages. There is also a heat exchanger to recover heat between the lean and rich streams, and a condenser in the $CO_2$ stream exiting the stripper to recover water and solvent dragged in the gas. For the PEM electrolyser, water was fed at ambient conditions and the energy consumption was set to 3.8 kWh/$Nm^3$ [49]. PEM technology was chosen over SOEC (solid oxide electrolysis cell) due to its higher level of commercial development (TRL-7 vs. TRL-5). Additionally, PEM technology was preferred over AEL (alkaline) because it offers greater flexibility in load-following operations with renewable sources [50]. The methanation plant was supplied with green $H_2$ from the electrolyser and $CO_2$ from the amine scrubber, in stoichiometric proportion ($H_2/CO_2$ ratio of 4). Two isothermal fixed-bed reactors worked at 350 and 300 °C respectively, and at constant pressure of 5 bar [51], [52]. An intermediate condensation removed the water at 100 °C. The final SNG was delivered at 25 °C and 5 bar. Additional information on the methodology and validation of the PtG system can be found in [43].

#### 3.2.3. Distribution of combustible gases

The distribution for the combustible gases (BFG, BOFG and COG) remained almost the same, compared with the base case. However, there were noticeable differences, especially for the BFG, as its energy content increased when shifting from BF to oxy-BF.

First, part of the raw BFG was diverted to the preheating gas burner, where it was combusted with pure oxygen and injected at 1000 °C in the upper part of the oxy-BF. Then, part of the BFG passed through the amine scrubbing stage, where the $CO_2$ that feeds the methanation plant is captured. The clean-BFG is divided into two streams (TGR-split block, see Fig. 2): the first one was used as reducing agent in the oxy-BF (i.e., TGR), and the second one was blended with the remaining BFG. The latter was used to feed the remaining thermal needs (sinter strand, $O_2$ heater, clean-BFG heater and SNG heater).

The distribution of the remaining combustible gases, the COG and BOFG, was kept the same, feeding the coke oven and the casting stage. Excess BFG, COG and BOFG were mixed and fed to the power plant or sold to industries nearby, as in the base case.

#### 3.2.4. Sizing of the PtG plant

For the PtG-steelmaking integration with TGR and oxy-BF, several data points were analysed. In all of these data points, the adiabatic flame temperature (AFT) of the furnace should be kept above 2000 °C for technical reasons [53–56], which is a limiting factor when injecting SNG and TGR gases. The first point corresponded to 0 $kg_{TGR}/t_{HM}$, i.e., 0 kg of clean-BFG were directed to the oxy-BF through the TGR-split valve. The gas injected was increased until a maximum is found, corresponding to all the clean-BFG available.

In the first point, the amount of SNG injected was maximum, due to the absence of TGR gas. Thus, the methanation plant, the amine scrubbing and the PEM electrolyser were sized. At this point, the TGR-split valve sent all clean-BFG flow rate to blend with the remaining BFG.

For the next data points, the TGR-split valve divided the clean-BFG flow and sent a certain amount of clean-BFG to the oxy-BF. In order not to drop the AFT below 2000 °C, the SNG flow rate had to be reduced, what also decreased the size of the methanation plant, amine scrubbing and PEM electrolyser. This also meant that, for a given flow rate of TGR gas (i.e., a given flow of clean-BFG derived to the oxy-BF), less clean-BFG was produced in the first place in the amine scrubbing. The last data point studied corresponded to the one where the maximum amount of TGR could be injected, and therefore no clean-BFG was left to be blended with the BFG. At this point, some SNG was also injected, as the $CO_2$ produced in the amine scrubbing was consumed in the methanation stage.

The results in Section 4 were all presented as a function of the TGR mass flow rate (X-axis), where 0 $kg_{TGR}/t_{HM}$ means no TGR was considered, and 270 $kg_{TGR}/t_{HM}$ means that all the clean-BFG was injected in the oxy-BF as reducing agent.

#### 3.2.5. Techno-economic indicators

The technical indicators are the coal-equivalent replacement ratio (coal-e RR) and the energy penalty. The former was defined as the sum of the pulverized coal and coking coal replaced by the SNG and the TGR (Eq. (11)). The latter was defined as the net energy consumed in the industry per kg of $CO_2$ avoided with the PtG-steelmaking integration (Eq. (12)). Units and description of equation variables are in Table 4.

$$Coal-e \quad RR = \frac{\Delta\dot{m}_{PCI} + \Delta\dot{m}_{CokingCoal}}{\Delta\dot{m}_{SNG} + \Delta\dot{m}_{TGR}} \quad \left[kg_{Coal}/kg_{ReducingGas}\right] \tag{11}$$

$$E_{penalty} = \frac{\Delta E_{cons} - \Delta E_{coal} \bullet \eta_{elec} - \Delta E_{gases} \bullet \eta_{elec}}{\Delta\dot{m}_{CO2}} \left[MJ \Big/ kg_{CO_2}\right] \tag{12}$$

The economic indicators are the specific costs, in in €/$t_{CO2}$ and €/$t_{HM}$, see Eq. (13) and Eq. (14). The analysis assumed a loan amortization period of 20 years, a PtG system operating for 8000 h per year [57], and

**Table 4**
Description of variables in Eqs. (9–12).

| Variable | Units | Description |
|---|---|---|
| $\Delta\dot{m}_{PCI}$ | $kg_{PCI}/t_{HM}$ | *Savings in PCI consumption* |
| $\Delta\dot{m}_{CokingCoal}$ | $kg_{CokingCoal}/t_{HM}$ | *Savings in coking coal consumption* |
| $\Delta\dot{m}_{SNG}$ | $kg_{SNG}/t_{HM}$ | *Increase in SNG injection* |
| $\Delta\dot{m}_{TGR}$ | $kg_{TGR}/t_{HM}$ | *Increase in TGR injection* |
| $\Delta E_{cons}$ | $MJ/t_{HM}$ | *Increase in electricity consumption in the industry* |
| $\Delta E_{coal}$ | $MJ/t_{HM}$ | *Savings in coal energy* |
| $\Delta E_{gases}$ | $MJ/t_{HM}$ | *Increase in excess sold gases* |
| $\eta_{elec}$ | - | *Energy conversion factor from coal to electricity (0.33)* |
| CAPEX | *M€* | *Capital Expenditure* |
| OPEX | *M€/year* | *Operational Expenditure* |
| Incomes | *M€/year* | *Operational Incomes* |
| Loan amortization | *Years* | *Process of paying off a loan over time* |
| $CO_2$ avoided | $t_{CO_2}/h$ | *$CO_2$ avoided per hour* |
| Operating hours | $h/year$ | *Operating hours per year* |

a renewable electricity price of 77 €/MWh. A detailed analysis on the CAPEX, OPEX and Incomes can be found in the supplementary data.

$$CO_2\ avoidance\ Cost = \frac{\left(\frac{Capex}{Loan\ amortization} + Opex - Incomes\right)\cdot 10^6}{CO_2\ avoided \cdot Operating\ hours}\ \left[\frac{€}{t_{CO_2}}\right] \quad (13)$$

$$Specific\ Implementatio\ Cost = \frac{\left(\frac{Capex}{Loan\ amortization} + Opex - Incomes\right)\cdot 10^6}{Iron\ Production \cdot Operating\ hours}\ \left[\frac{€}{t_{HRC}}\right] \quad (14)$$

It is worth noting that for the CO2 emission calculation all direct and indirect sources of CO2 have been considered. This includes CO2 emissions from the different processes for steelmaking (sintering, coke oven, etc), the power plant and the sold gases. The CO contained in the BFG is also computed, as it is used as fuel in the sintering or power plant and therefore transformed to CO2.

It's important to highlight that the $CO_2$ emission calculation encompasses all sources, both direct and indirect. This covers $CO_2$ emissions from various steelmaking processes (sintering, coke ovens, etc.), the power plant, and the sale of gases. It is also considered the CO and $CH_4$ within the BFG, BOFG and COG gases, as they are used as fuel in other processes, leading to its conversion into $CO_2$.

## 4. Results and discussion

Sections 4.1, 4.2 and 4.3 document the main results for the PtG-steelmaking integration with TGR and oxy-BF, where all the figures present the data as a function of the TGR mass flow rate ($kg_{clean\text{-}BFG}/t_{HM}$).

### 4.1. PtG integration in TGR-Oxygen blast furnace

Converting the BF to an oxy-BF allowed for higher inputs of reducing agents. In this simulation, SNG was fixed so that the flame temperature was 2000 °C (minimum technical limit). All the PCI and part of the coke were avoided thanks to the synthetic gas. At this operating point, we progressively shifted the SNG injection to TGR injection. Fig. 3 shows the amount of reducing agents injected in the oxy-BF (coke, SNG and TGR), and the coal-e RR of the gaseous reducing agents, as the SNG is replaced by TGR. The SNG consists mainly of methane (94.7% $CH_4$), with minor components comprising 3.9% $H_2$, 1.0% $CO_2$ and 0.4% $H_2O$. The total flow of reducing agents increased, while the coal-e RR decreased, with the TGR. This suggests that the TGR is not as good reducing agent as the SNG. Nevertheless, despite the coal-e RR decreased rapidly, it only resulted in a slight increase in the coke rate (279–300 $kg_{coke}/t_{HM}$). The reason can be found in Eq. (11), where the numerator barely changed, but the denominator increased remarkably (per each kg of SNG replaced, 3.1–3.4 kg of TGR were added).

When increasing the TGR gas, a drop in the $H_2$ content in the BFG was observed, compensated by an increase in the CO and $CO_2$ content (see Fig. 4). The reason is the lower H:C ratio of the TGR (approx. 0.5–0.8) compared to that of SNG (approx. 4). The decrease in the $H_2$ content, and the increase in the $CO_2$ content, made the lower heating value (LHV) of the BFG to diminish. However, the higher amount of reducing agents also led to a higher BFG mass flow rate. Both effects counterbalanced each other, resulting in a nearly constant BFG energy content (referred to the total energy content, before recirculations), as shown in Fig. 4.

Despite the increase in CO and $CO_2$ in the BFG, the CO utilization ratio (Eq. (9)) hardly varied, ranging between 50.0% and 51.7% for all data points. The preheating gas injected in the upper part of the oxy-BF was also considered, but its influence was very small since it remained constant at 205–207 $kg/t_{HM}$, allowing the BFG temperature to not fall below 150 °C.

### 4.2. Thermal energy integration and energy penalty

The amine scrubber captured 90% of the $CO_2$ contained in the BFG, with a $CO_2$ purity of 95%, and a specific heat consumption of 3.1 $MJ/kg_{CO2}$. The methanation plant produced SNG at 5 bar and with 95 vol% of $CH_4$, releasing 6.1 $MJ/kg_{CO2}$. No solid carbon deposition was found in the methanation plant.

When integrating the PtG technology, new thermal streams had to be considered. The isothermal methanation plant generated heat at 300–350 °C, while the stripper of the amine scrubber required heat at 110–130 °C, so the heat consumption of the amine scrubbing could be covered by the exothermal heat released by the methanation. Perpiñán et al. [43] demonstrated through a pinch analysis the technical feasibility of supplying the heat demand of an amine scrubbing plant (3.7 $MJ/kg_{CO2}$) with the exothermal heat of an isothermal methanation plant (6.1 $MJ/kg_{CO2}$). In this simulation, the same amount of heat was released by the methanation, and less thermal consumption was found in the amine scrubbing (3.1 $MJ/kg_{CO2}$), so the technical viability for this thermal integration is guaranteed.

As the TGR gas increased, less SNG was injected into the oxy-BF,

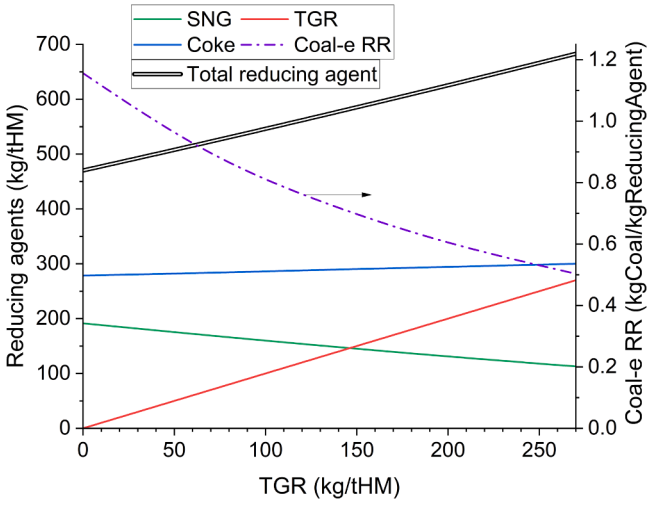


**Fig. 3.** Reducing agents in the OBF (SNG, green line; TGR, red line; coke, blue line; total reducing agents, black line) and coal-e RR (purple dashed line) as a function of the TGR mass flow injected in the OBF.

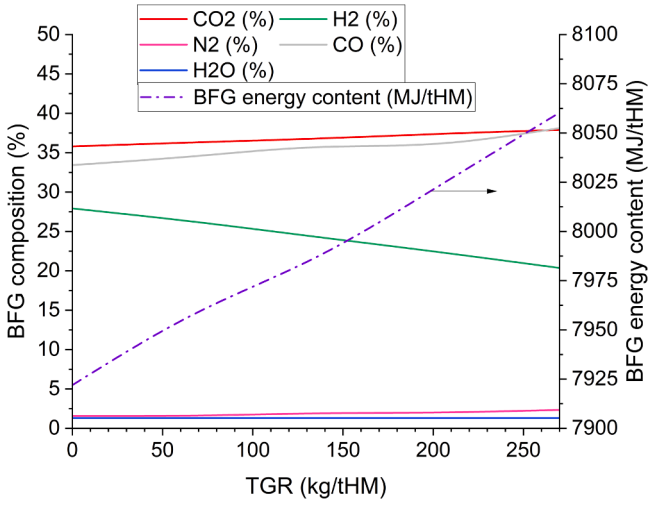


**Fig. 4.** BFG composition ($CO_2$, red line; $H_2$, green line; $N_2$, pink line; CO, grey line; $H_2O$, blue line) and BFG energy content (purple dashed line) as a function of the amount of TGR mass flow injected in the OBF.

what lowers the size of the methanation plant and the electrolyser. The PEM size decreased from 1268 MW to 741 MW when injecting 270 $kg_{TGR}/t_{HM}$. However, the lower the electrolyser size, the lower the oxygen by-produced, leading to an oxygen deficit for TGR flows higher than 190 $kg_{TGR}/t_{HM}$. This should be covered by an ASU plant (see Fig. 5).

The $CO_2$ emission reduction for the PtG-steelmaking integration ranged between 30% and 34% (Fig. 6). Higher emission reduction was found without TGR injection, due to the higher coal-e RR at this point (see Fig. 3). The total emissions decreased from 1943 $kg_{CO2}/t_{HM}$ to 1279 and 1361 $kg_{CO2}/t_{HM}$, compared to the conventional BF, when integrating PtG and TGR technologies, respectively. The $CO_2$ recycled through methanation ranged between 305 and 517 $kg_{CO2}/t_{HM}$, which would otherwise be emitted to the atmosphere.

The electricity consumption, sold gases and energy penalty are shown in Fig. 7. The electricity consumption had a mostly linear dependency on the PEM electrolyser, as its consumption accounted for 88–92% of all the electricity consumed in the industry. The maximum electricity consumption was 15,581 $MJ/t_{HM}$ (no TGR), which could be reduced to 9548 $MJ/t_{HM}$ if TGR gas was used. However, it still represented an increase of 16 times and 10 times in the total electricity consumption, respectively, compared to the conventional BF (950 $MJ/t_{HM}$). For TGR flow rates above 190 $kg_{TGR}/t_{HM}$, the ASU started working and consuming electricity, yet the total electricity consumption was barely affected and continued its decreasing trend. The ASU electricity consumption was very low compared to that of the electrolyser. The electricity production in the power plant was the same as for the conventional BF, 1122 $MJ/t_{HM}$ (100 MW).

The sold gases (BFG, COG and BOFG) decreased from 4471 to 1143 $MJ/t_{HM}$ when using TGR gas as reducing agent in the oxy-BF, because of the high fraction of BFG used as TGR (in the conventional I&S plant, the energy sold as combustible gases was 2400 $MJ/t_{HM}$). The energy penalty considers the increase in the electricity consumed, the sold gases and the coal savings. When injecting TGR gas, despite the less energy sold with the steel gases, and the lower coal savings, the energy penalty offered better results. This is because the electricity consumption of the electrolyser rules the energy penalty. The energy penalty was 17 $MJ/t_{HM}$ when injecting SNG alone, and 12 $MJ/t_{HM}$ when also injecting TGR gas.

### 4.3. Economic analysis

The specific carbon capture (CC) cost is shown in Fig. 8, where the red line represents the cost in terms of €/$t_{HM}$ and the black line represents the cost in terms of €/$t_{CO2}$. For higher TGR gas rates, lower CC costs

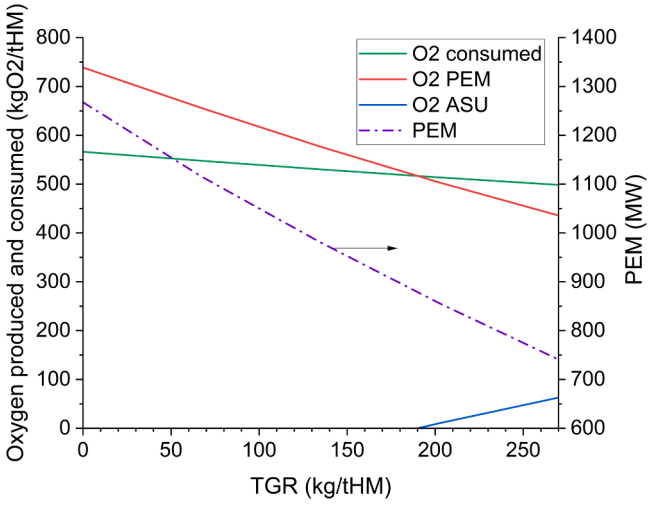


**Fig. 5.** Oxygen produced in the PEM (red line) and in the ASU (blue line), oxygen consumed in the industry (green line) and PEM capacity (purple dashed line) as a function of the amount of TGR mass flow injected in the OBF.

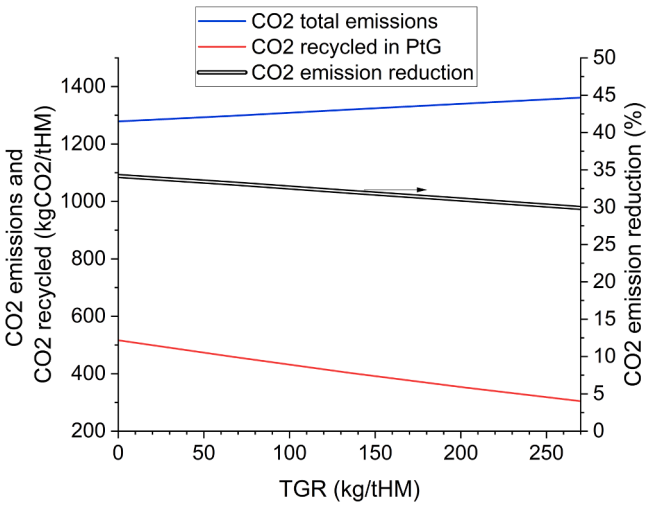


**Fig. 6.** Total $CO_2$ emissions (blue line), $CO_2$ recycled in the PtG system (red line), and percentage of $CO_2$ emission reduction compared to conventional BF (black line) as a function of the amount of TGR mass flow injected in the OBF.

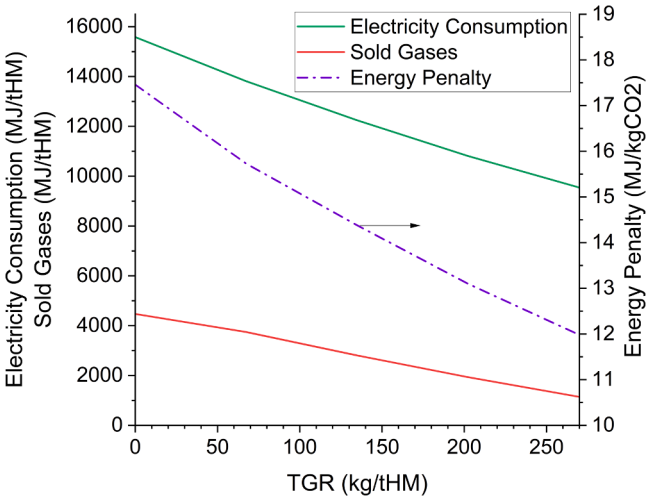


**Fig. 7.** Electricity consumption (green line), sold gases (red line) and energy penalty (purple dashed line) as a function of the amount of TGR mass flow injected in the OBF.

were found, because of the lower electrolyser size and the lower electricity consumption. The PEM accounted for 38–43% of the CAPEX and the electricity for 94–95% of the OPEX. The steel price in 2022 was between 660 and 1400 €/$t_{HRC}$, so the specific CC cost represents an increase of 9–35% in the final product.

For the operation with 270 $kg_{TGR}/t_{HM}$ injected in the oxy-BF, a sensitivity analysis of the specific CC costs (in €/$t_{CO2}$) was performed. The $CO_2$ taxes and the electricity price were varied, looking for those combinations that make the PtG-steelmaking integration economically viable (Fig. 9). Today, with an electricity price of 77 €/MWh and a $CO_2$ tax of 84 €/$t_{CO2}$, the specific CC cost is 216 €/$t_{CO2}$. Negative costs (i.e., actual benefits) could be achieved under some conditions. For a specific CC cost of 0 €/$t_{CO2}$, a maximum electricity price of 21 €/MWh should be paid, or a minimum $CO_2$ tax of 300 €/$t_{CO2}$ should apply. However, these prices or taxes do not guarantee a profitable investment, since the CAPEX should also be amortized. To amortize CAPEX in 20 years (i.e., total investment pay-back of 20 years), the electricity price should be 18 €/MWh, or the $CO_2$ tax 313 €/$t_{CO2}$, or an intermediate combination of both parameters, coinciding with a specific CC cost of − 13 €/$t_{CO2}$ or − 8 €/$t_{HM}$. With an electricity price of 35 €/MWh (cost of production for

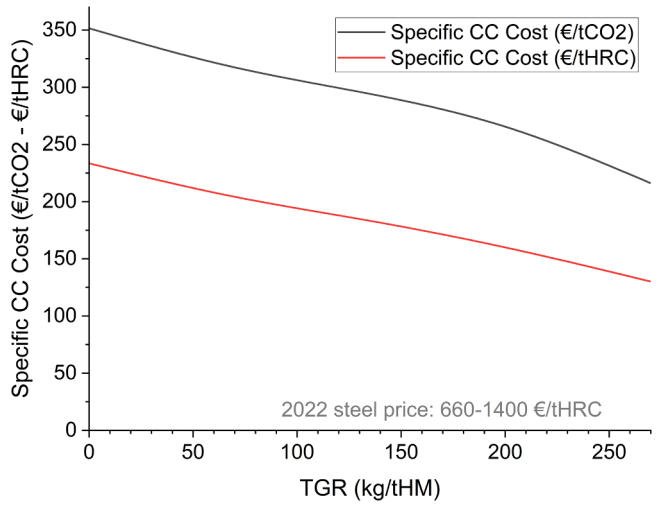


**Fig. 8.** Specific carbon capture (CC) cost in €/$t_{CO2}$ (black line) and €/$t_{HRC}$ (red line) as a function of the amount of TGR mass flow injected in the OBF (2022 steel price [58]).

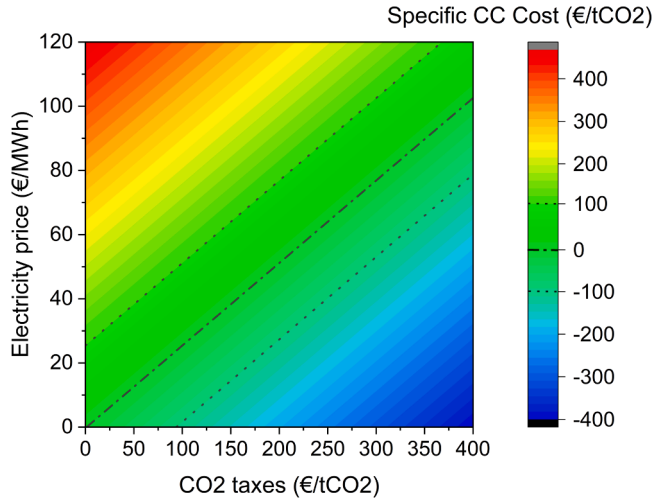


**Fig. 9.** Specific CC cost in €/$t_{CO2}$ as a function of the $CO_2$ taxes and the electricity price for an OBF with two auxiliary fuel injections (113 $kg_{SNG}/t_{HM}$ and 270 $kg_{TGR}/t_{HM}$), an electrolyser of 741 MW, and an amine scrubbing of 305 $kg_{CO2}/t_{HM}$.

wind power [59]), and a $CO_2$ tax of 150 €/$t_{CO2}$, the pay-back is 20 years and the investment would be profitable.

For illustration purposes, Table 5 compares results for two different data points: only SNG injection and maximum TGR gas injection. It can be seen that the first data point offered better environmental results, such as higher $CO_2$ emission reduction and lower coke rate in the OBF. However, similar environmental results were found in the second data point but offering further benefits, such as lower PEM size, energy penalty and costs. For these reasons, whenever possible, TGR is a technology that should be considered along with PtG technology.

## 5. Conclusions

A new concept integrating power to gas and BF top gas recycling with an oxy-BF was presented in this study for $CO_2$ emissions reduction and utilization in the iron and steel industry. Green $H_2$ was produced in an electrolyser with renewable electricity, $CO_2$ was obtained from the BFG through an amine scrubbing stage, and synthetic natural gas is produced from the two previous components in an isothermal methanation plant.

**Table 5**
Main results and comparison for (i) only SNG injection and (ii) maximum TGR gas injection, in an OBF.

| Variable | Units | OBF with SNG injection (no TGR) | OBF with SNG and TGR injection |
|---|---|---|---|
| SNG mass flow rate | $kg/t_{HM}$ | 192 | 113 |
| TGR mass flow rate | $kg/t_{HM}$ | 0 | 270 |
| Coke mass flow rate | $kg/t_{HM}$ | 288 | 300 |
| Total reducing agents | $kg/t_{HM}$ | 470 | 683 |
| PEM size | MW | 1115 | 741 |
| $CO_2$ emission reduction | % | 34.4 | 29.9 |
| Energy penalty | $MJ/t_{HM}$ | 17.5 | 12.0 |
| Cost | €/$t_{CO2}$ | 352 | 216 |
| Cost | €/$t_{HM}$ | 233 | 130 |

The synthetic methane was injected into the OBF on its own or mixed with some clean-BFG (recycled top gas, after $CO_2$ separation). This integration was compared with a conventional BF-BOF iron and steel process. Both simulations, the conventional and the PtG-integration, were modelled in Aspen Plus.

The oxygen by-produced in the electrolyser was almost sufficient to satisfy the oxygen demand in the plant, including the oxygen for the BOF, the preheating gas, and the oxy-BF. Only when the TGR gas was above 190 $kg_{TGR}/t_{HM}$ (i.e., when the PEM capacity was lower than 880 MW), the ASU had to produce a small portion of the overall oxygen demand. The LHV of the BFG decreased when injecting TGR gas, but the mass flow rate increased, resulting in a nearly constant BFG energy content (in $MJ/t_{HM}$).

When injecting SNG in the OBF, 34.4% and 33.1% of the total $CO_2$ emissions and coal consumption were saved, respectively. Due to the lower coal-e RR of the TGR compared to that of the SNG, less $CO_2$ and coal were saved when injecting both reducing agents in the OBF; 29.9% and 28.9% respectively. However, the joint injection of SNG and TGR offered other relevant advantages. For instance, the PEM electrolyser size was greatly reduced, from 1115 to 741 MW, providing additional benefits. As the PEM size decreased, the electricity consumed was also lower, diminishing the energy penalty and the costs, from 17.5 to 12.0 $MJ/t_{HM}$ and from 352 to 216 €/$t_{CO2}$, respectively. However, under certain combinations of $CO_2$ tax, electricity price or economic subsidies, economic profitability could be achieved.

This PtG-steelmaking configuration recycles $CO_2$ via methanation, and CO via TGR. Contrary to other studies that only recycle CO, this configuration is able to supply all downstream thermal energy needs of the steel plant (i.e., the sintering, power plant and other processes). As downstream energy needs were always covered, there was a certain amount of steel gases sold. These sold gases accounted for 4471 $MJ/t_{HM}$ when injecting SNG, and 1143 $MJ/t_{HM}$ when injecting both reducing agents (SNG and TGR).

Technical limitations for this PtG-integration with TGR include the feasibility of the OBF and the TGR, which are technologies still under development, along with the necessity for addressing dynamics and transient effects. Moreover, the on-site configuration of each specific industry may affect the practical implementation of the energy integration, including heat integration. Additionally, the integration of a GW scale electrolyser into the I&S industry raises concerns about various factors such as the availability of renewable electricity in the region or the feasibility of the supply line to the plant. Economic limitations include prices for the $CO_2$ tax and the electricity, as these two variables had a great impact on the specific CC costs and the pay-back. Future research should explore these aspects further to ensure the practicality and viability of large-scale implementation.

To sum up, this novel concept of PtG-integration with TGR in the I&S industry has the potential to recycle $CO_2$ via methanation and CO via TGR, thus reducing $CO_2$ emissions and coal consumption without the need for geological storage. Despite the slightly lower $CO_2$ and coal savings, injection of both SNG and TGR is preferred over the injection of SNG alone, because of the lower energy penalty and costs found. Additionally, the downstream energy needs are always covered, and a certain amount of steel gases are sold (what would not happen if only TGR is applied).

## CRediT authorship contribution statement

**Jorge Perpiñán:** Conceptualization, Methodology, Formal analysis, Visualization, Software, Writing - original draft. **Manuel Bailera:** Conceptualization, Methodology, Visualization, Supervision, Funding acquisition, Project administration, Software, Writing - review & editing. **Begoña Peña:** Conceptualization, Methodology, Supervision, Project administration, Funding acquisition, Writing - review & editing. **Pravin Kannan:** Writing - review & editing. **Valerie Eveloy:** Project administration, Funding acquisition, Writing - review & editing. **Luis M. Romeo:** Project administration, Funding acquisition, Writing - review & editing.

## Declaration of Competing Interest

The authors declare that they have no known competing financial interests or personal relationships that could have appeared to influence the work reported in this paper.

## Data Availability

Data will be made available on request.

## Acknowledgements

The work presented in this paper has been supported by the Khalifa University project CIRA-2020-080. This work has also received funding from the European Union's Horizon 2020 research and innovation program under the Marie Sklodowska-Curie grant agreement no. 887077. This work is part of the R&D project PID2021-126164OB-I00, funded by MCIN/AEI/10.13039/501100011033/ and by the "ERDF A way of making Europe". This research is co-funded by the University of Zaragoza, Fundación Bancaria Ibercaja, and Fundación CAI, through the program "Programa Ibercaja-Cai Estancias de Investigación", nº IT 16/12. Manuel Bailera acknowledges Waseda University, Tokyo, and K1-MET GmbH, Linz.

## Appendix A. Supporting information

Supplementary data associated with this article can be found in the online version at doi:10.1016/j.jcou.2023.102634.

## References

[1] IEA, 2022. "World Energy Outlook 2022," Paris. License: CC BY 4.0 (report); CC BY NC SA 4.0 (Annex A), 2022.
[2] World Steel Association, "WorldSteel." ⟨https://worldsteel.org/steel-topics/statistics/world-steel-in-figures-2022/⟩.
[3] World Economid Forum, "Report on 'The Net-Zero Industry Tracker.'" [Online]. Available: ⟨https://worldsteel.org/steel-topics/statistics/world-steel-in-figures-2022/⟩.
[4] EUROFER, 2023 "A steel roadmap for a low carbon europe 2050, the European Steel Association EUROFER. Brussels, Belgium.," 2013. ⟨https://www.eurofer.eu/assets/publications/archive/archive-of-older-eurofer-documents/2013-Roadmap.pdf⟩ (Accessed Feb. 26, 2023).
[5] M. Wörtler, P. Dahlmann, F. Schuler, H.B. Lüngen, and N. Voigt, 2023. "Steel's contribution to a low-carbon Europe 2050-Technical and economic analysis of the sector's CO2 abatement potential.," 2013. ⟨https://www.bcg.com/de-de/⟩ (Accessed Apr. 26, 2022).
[6] D. Fu, G. Tang, Y. Zhao, J. D'Alessio, C.Q. Zhou, Modeling of iron ore reactions in blast furnace, Int. J. Heat. Mass Transf. vol. 103 (2016) 77–86, https://doi.org/10.1016/j.ijheatmasstransfer.2016.06.060.
[7] H. Kildahl, L. Wang, L. Tong, Y. Ding, Cost effective decarbonisation of blast furnace – basic oxygen furnace steel production through thermochemical sector coupling, J. Clean. Prod. vol. 389 (March 2022) (2023), 135963, https://doi.org/10.1016/j.jclepro.2023.135963.
[8] T. Ariyama, M. Sato, T. Nouchi, K. Takahashi, Evolution of blast furnace process toward reductant flexibility and carbon dioxide mitigation in steel works, ISIJ Int vol. 56 (10) (2016) 1681–1696, https://doi.org/10.2355/isijinternational.ISIJINT-2016-210.
[9] M. Sato, K. Takahashi, T. Nouchi, T. Ariyama, Prediction of next-generation ironmaking process based on oxygen blast furnace suitable for $CO_2$ mitigation and energy flexibility, ISIJ Int. vol. 55 (10) (2015) 2105–2114, https://doi.org/10.2355/isijinternational.ISIJINT-2015-264.
[10] A. Babich and D. Senk, 2015. Recent developments in blast furnace iron-making technology, 2015, p. 505–547. doi:10.1016/B978–1-78242–156-6.00017–4.
[11] W. Zhang, J. Dai, C. Li, X. Yu, Z. Xue, H. Saxén, A review on explorations of the oxygen blast furnace process, Steel Res. Int. vol. 92 (1) (2021), https://doi.org/10.1002/srin.202000326.
[12] M. Bailera, P. Lisbona, B. Peña, L.M. Romeo, A review on $CO_2$ mitigation in the Iron and Steel industry through Power to X processes, J. $CO_2$ Util. vol. 46 (November 2020) (2021), 101456, https://doi.org/10.1016/j.jcou.2021.101456.
[13] M. Abdul Quader, S. Ahmed, S.Z. Dawal, Y. Nukman, Present needs, recent progress and future trends of energy-efficient Ultra-Low Carbon Dioxide ($CO_2$) steelmaking (ULCOS) program, Renew. Sustain. Energy Rev. vol. 55 (. 2016) 537–549, https://doi.org/10.1016/J.RSER.2015.10.101.
[14] R.K. Sahu, S.K. Roy, P.K. Sen, Applicability of top gas recycle blast furnace with downstream integration and sequestration in an integrated steel plant, Steel Res. Int. vol. 1 (5) (2015) 502–516, https://doi.org/10.1002/srin.201400196.
[15] W. Zhang, J. Zhang, Z. Xue, Exergy analyses of the oxygen blast furnace with top gas recycling process, Energy vol. 121 (2017) 135–146, https://doi.org/10.1016/j.energy.2016.12.125.
[16] W. Zhang, Z. Xue, J. Zhang, W. Wang, C. Cheng, Z. Zou, Medium oxygen enriched blast furnace with top gas recycling strategy, J. Iron Steel Res. Int. vol. 24 (8) (. 2017) 778–786, https://doi.org/10.1016/S1006-706X(17)30117-6.
[17] J. Perpiñán, M. Bailera, L.M. Romeo, B. Peña, V. Eveloy, $CO_2$ recycling in the iron and steel industry via power-to-gas and oxy-fuel combustion, Energies vol. 14 (21) (2021) 7090, https://doi.org/10.3390/en14217090.
[18] J. van der Stel, G. Louwerse, D. Sert, A. Hirsch, N. Eklund, M. Pettersson, Top gas recycling blast furnace developments for 'green' and sustainable ironmaking, Ironmak. Steelmak. vol. 40 (7) (. 2013) 483–489, https://doi.org/10.1179/0301923313Z.000000000221.
[19] P. Jin, Z. Jiang, C. Bao, S. Hao, X. Zhang, The energy consumption and carbon emission of the integrated steel mill with oxygen blast furnace, Resour. Conserv. Recycl. vol. 117 (2017) 58–65, https://doi.org/10.1016/j.resconrec.2015.07.008.
[20] J. Perpiñán, et al., Integration of carbon capture technologies in blast furnace based steel making: a comprehensive and systematic review, Fuel (2022), https://doi.org/10.1016/j.fuel.2022.127074.
[21] G. Danloy, et al., ULCOS - pilot testing of the low-$CO_2$ Blast Furnace process at the experimental BF in Lulea, Rev. Metall. Cah. D'Informations Tech. vol. 106 (1) (2009) 1–8, https://doi.org/10.1051/metal/2009008.
[22] A. Arasto, E. Tsupari, J. Kärki, J. Lilja, M. Sihvonen, Oxygen blast furnace with $CO_2$ capture and storage at an integrated steel mill-Part I: Technical concept analysis, Int. J. Greenh. Gas. Control vol. 30 (2014) 140–147, https://doi.org/10.1016/j.ijggc.2014.09.004.
[23] E. Tsupari, J. Kärki, A. Arasto, J. Lilja, K. Kinnunen, M. Sihvonen, Oxygen blast furnace with $CO_2$ capture and storage at an integrated steel mill - Part II: Economic feasibility in comparison with conventional blast furnace highlighting sensitivities, Int. J. Greenh. Gas. Control vol. 32 (2015) 189–196, https://doi.org/10.1016/j.ijggc.2014.11.007.
[24] Y. Ohno, M. Matsuura, H. Mitsufuji, T. Furukawa, Process characteristics of a commercial-scale oxygen blast furnace process with shaft gas injection, ISIJ Int. vol. 32 (7) (1992) 838–847, https://doi.org/10.2355/isijinternational.32.838.
[25] W. Zhang, J. Zhang, Z. Xue, Z. Zou, Y. Qi, Unsteady analyses of the top gas recycling oxygen blast furnace, ISIJ Int vol. 56 (8) (2016) 1358–1367, https://doi.org/10.2355/isijinternational.ISIJINT-2016-090.
[26] A. Arasto, E. Tsupari, J. Kärki, E. Pisilä, L. Sorsamäki, Post-combustion capture of $CO_2$ at an integrated steel mill - Part I: technical concept analysis, Int. J. Greenh. Gas. Control vol. 16 (2013) 271–277, https://doi.org/10.1016/j.ijggc.2012.08.018.
[27] A. Arasto, E. Tsupari, J. Kärki, M. Sihvonen, J. Lilja, Costs and potential of carbon capture and storage at an integrated steel mill, Energy Procedia vol. 37 (2013) 7117–7124, https://doi.org/10.1016/j.egypro.2013.06.648.
[28] E. Tsupari, J. Kärki, A. Arasto, E. Pisilä, Post-combustion capture of $CO_2$ at an integrated steel mill - Part II: economic feasibility, Int. J. Greenh. Gas. Control vol. 16 (2013) 278–286, https://doi.org/10.1016/j.ijggc.2012.08.017.
[29] D.E. Wiley, M.T. Ho, A. Bustamante, Assessment of opportunities for $CO_2$ capture at iron and steel mills: an Australian perspective, Energy Procedia vol. 4 (2011) 2654–2661, https://doi.org/10.1016/j.egypro.2011.02.165.
[30] M.A. Quader, S. Ahmed, R.A. Raja Ghazilla, S. Ahmed, M. Dahari, Evaluation of criteria for $CO_2$ capture and storage in the iron and steel industry using the 2-tuple DEMATEL technique, J. Clean. Prod. vol. 120 (2016) 207–220, https://doi.org/10.1016/J.JCLEPRO.2015.10.056.
[31] M. Biermann, H. Ali, M. Sundqvist, M. Larsson, F. Normann, F. Johnsson, Excess heat-driven carbon capture at an integrated steel mill – Considerations for capture

cost optimization, Int. J. Greenh. Gas. Control vol. 91 (September) (2019), 102833, https://doi.org/10.1016/j.ijggc.2019.102833.
[32] F.A. Tobiesen, H.F. Svendsen, T. Mejdell, Modeling of blast furnace $CO_2$ capture using amine absorbents, Ind. Eng. Chem. Res. vol. 46 (23) (2007) 7811–7819, https://doi.org/10.1021/ie061556j.
[33] H. Kim, J. Lee, S. Lee, I.B. Lee, J. hyoung Park, J. Han, Economic process design for separation of $CO_2$ from the off-gas in ironmaking and steelmaking plants, Energy vol. 88 (. 2015) 756–764, https://doi.org/10.1016/J.ENERGY.2015.05.093.
[34] S. Yun, M.G. Jang, J.K. Kim, Techno-economic assessment and comparison of absorption and membrane $CO_2$ capture processes for iron and steel industry, Energy vol. 229 (2021), 120778, https://doi.org/10.1016/j.energy.2021.120778.
[35] M. Onoda, Y. Matsuzaki, F.A. Chowdhury, H. Yamada, K. Goto, S. Tonomura, Sustainable aspects of ultimate reduction of $CO_2$ in the steelmaking process (COURSE50 Project), Part 2: $CO_2$ capture, J. Sustain. Metall. vol. 2 (3) (2016) 209–215, https://doi.org/10.1007/s40831-016-0067-3.
[36] M. Bailera, T. Nakagaki, and R. Kataoka, 2021. "Revisiting the Rist diagram for predicting operating conditions in blast furnaces with multiple injections," 2021, doi:10.12688/openreseurope.14275.1.
[37] D.C. Rosenfeld, H. Böhm, J. Lindorfer, M. Lehner, Scenario analysis of implementing a power-to-gas and biomass gasification system in an integrated steel plant: a techno-economic and environmental study, Renew. Energy vol. 147 (2020) 1511–1524, https://doi.org/10.1016/j.renene.2019.09.053.
[38] A.R. Medved, M. Lehner, D.C. Rosenfeld, J. Lindorfer, K. Rechberger, Enrichment of integrated steel plant process gases with implementation of renewable energy Integration of power-To-gas and biomass gasification system in steel production, Johns. Matthey Technol. Rev. vol. 65 (3) (2021) 453–465, https://doi.org/10.1595/205651321x16161444481140.
[39] S. Hisashige, T. Nakagaki, T. Yamamoto, $CO_2$ emission reduction and exergy analysis of smart steelmaking system adaptive for flexible operating conditions, ISIJ Int vol. 59 (4) (2019) 598–606, https://doi.org/10.2355/isijinternational.ISIJINT-2018-355.
[40] V. Shatokha, Modeling of the effect of hydrogen injection on blast furnace operation and carbon dioxide emissions, Int. J. Miner. Metall. Mater. vol. 29 (10) (2022) 1851–1861, https://doi.org/10.1007/s12613-022-2474-8.
[41] J. Kim, et al., An integrative process of blast furnace and SOEC for hydrogen utilization: techno-economic and environmental impact assessment, Energy Convers. Manag. vol. 250 (August) (2021), 114922, https://doi.org/10.1016/j.enconman.2021.114922.
[42] M. Bailera, T. Nakagaki, R. Kataoka, Limits on the integration of power to gas with blast furnace ironmaking, Elsevier, 2022, https://doi.org/10.1016/J.JCLEPRO.2022.134038.
[43] J. Perpiñán, M. Bailera, B. Peña, L.M. Romeo, V. Eveloy, Technical and economic assessment of iron and steelmaking decarbonization via power to gas and amine scrubbing, Energy vol. 276 (2023), https://doi.org/10.1016/j.energy.2023.127616.
[44] M. Bailera, T. Nakagaki, R. Kataoka, Extending the operating line methodology to consider shaft and preheating injections in blast furnaces, ISIJ Int vol. 62 (12) (2022) 1–12, https://doi.org/10.2355/isijinternational.ISIJINT-2022-111.
[45] J. Perpiñán, M. Bailera, B. Peña, L.M. Romeo, V. Eveloy, High oxygen and SNG injection in blast furnace steelmaking with power to gas integration and $CO_2$ recycling, J. Clean. Prod. (2023), https://doi.org/10.1016/j.jclepro.2023.137001.
[46] Aspen Technology Inc., 2019. "Aspen Physical Property Methods - Reference Manual." AspenTech, 2019.
[47] Y. Chen, H. Zuo, Review of hydrogen-rich ironmaking technology in blast furnace, Ironmak. Steelmak. vol. 48 (6) (2021) 749–768, https://doi.org/10.1080/03019233.2021.1909992.
[48] C. Lan, Y. Hao, J. Shao, S. Zhang, R. Liu, Q. Lyu, Effect of H2 on blast furnace ironmaking: a review, Metals vol. 12 (11) (2022), https://doi.org/10.3390/met12111864.
[49] "NEL Hydrogen", 2019. https://nelhydrogen.com/ (Accessed Mar. 02, 2022).
[50] M.N.I. Salehmin, T. Husaini, J. Goh, A.B. Sulong, High-pressure PEM water electrolyser: a review on challenges and mitigation strategies towards green and low-cost hydrogen production, Energy Convers. Manag. vol. 268 (June) (2022), 115985, https://doi.org/10.1016/j.enconman.2022.115985.
[51] K. Izumiya and I. Shimada, 2021. "K2- Methane Producing Technology from CO 2 for Carbon Recycling." pp. 34–35, 2021.
[52] S. Rönsch, et al., Review on methanation - From fundamentals to current projects, Fuel vol. 166 (2016) 276–296, https://doi.org/10.1016/j.fuel.2015.10.111.
[53] K.S. Abdel Halim, V.N. Andronov, M.I. Nasr, Blast furnace operation with natural gas injection and minimum theoretical flame temperature, Ironmak. Steelmak. vol. 36 (1) (2009) 12–18, https://doi.org/10.1179/174328107X155240.
[54] K.S.A. Halim, Theoretical approach to change blast furnace regime with natural gas injection, J. Iron Steel Res. Int. vol. 20 (9) (2013) 40–46, https://doi.org/10.1016/S1006-706X(13)60154-5.
[55] K.S. Abdel Halim, Effective utilization of using natural gas injection in the production of pig iron, Mater. Lett. vol. 61 (14–15) (2007) 3281–3286, https://doi.org/10.1016/j.matlet.2006.11.053.
[56] J.G. Peacey and W.G. Davbenport, 1979. The Iron Blast Furnace. Theory and Practice (1979). 1979. doi: ISBN 0–08-023258–2.
[57] M. Bailera, S. Espatolero, P. Lisbona, L.M. Romeo, Power to gas-electrochemical industry hybrid systems: a case study, Appl. Energy vol. 202 (2017) (2017) 435–446, https://doi.org/10.1016/j.apenergy.2017.05.177.
[58] "Marketwatch web page (HRC steel)," 2022. https://www.marketwatch.com/investing/index/steel?countryCode=XX (accessed Jul. 25, 2022).
[59] "IRENA," , 2022. ⟨https://www.irena.org/costs/Power-Generation-Costs⟩ (Accessed May 10, 2022).

Energy Conversion and Management 295 (2023) 117611

Contents lists available at ScienceDirect

Energy Conversion and Management

journal homepage: www.elsevier.com/locate/enconman

# Full oxygen blast furnace steelmaking: From direct hydrogen injection to methanized BFG injection

Jorge Perpiñán *, Manuel Bailera, Begoña Peña

*Escuela de Ingeniería y Arquitectura, Universidad de Zaragoza, María de Luna 3, 50018 Zaragoza, Spain*

ARTICLE INFO

*Keywords:*
Iron and steel industry
Power to Gas
Methanation
Hydrogen injection
Decarbonization
Electrification

ABSTRACT

This paper presents a novel concept of Power to Gas in an oxygen blast furnace, through blast furnace gas methanation and direct $H_2$ injection. The PEM electrolyser produces $H_2$, which reacts with the CO and $CO_2$ from the blast furnace gas forming synthetic natural gas. The latter gas is injected into the blast furnace, closing a carbon loop and avoiding $CO_2$ emissions. A parametric analysis is performed to vary the $H_2$:$CO_2$ ratio in the methanation reaction. Different ratios are simulated and compared, among of which the most representative are: (i) 2.5, where unreacted $CO_2$ is directly recycled with the synthetic natural gas; (ii) 4, where stoichiometric conditions are found and the synthetic gas is composed mostly by $CH_4$; and (iii) 8, where an excess of $H_2$ is found in the synthetic gas; and (iv) an infinite ratio, where only $H_2$ is injected in the blast furnace. In the latter, the methanation plant is not required, and no synthetic natural gas is produced. The results show that low $H_2$:$CO_2$ ratios perform poorly, involving high PEM sizes and high costs but only a 5% of $CO_2$ avoidance (compared to conventional blast furnaces). A $H_2$:$CO_2$ ratio of 4 and full $H_2$ injection results in higher reduction of $CO_2$ emissions (33.8 % and 28.6%) with carbon abatement costs of 260 and 245 €/$t_{CO2}$, respectively.

## 1. Introduction

The iron and steel (I&S) industry is one of the main contributors to global $CO_2$ emissions with up to 27% of the global manufacturing sector [1]. Over 70 % of these emissions are produced by ironmaking blast furnaces (BF), which also consume the largest amount of energy in the entire industry (13–14 GJ per ton of hot metal, $t_{HM}$ in the following) [1].

The dominant method of steel production worldwide is the blast furnace-basic oxygen furnace (BF-BOF) route, which accounts for over 70% of global output. This process involves the preparation of raw materials including iron ore, coke, and limestone. Iron ore is agglomerated through sintering, coke is produced from coal, and limestone is calcined to obtain lime [2,3]. These materials are then fed into the blast furnace (BF), where coke supplies heat and CO-reducing gas that reacts with iron oxides [4]. The resulting molten iron is further refined in the basic oxygen furnace (BOF) by injecting pure oxygen to reduce carbon content. Finally, the refined steel is cast into various shapes, cooled, and after that undergoes finishing techniques for its desired applications.

Given the current policies of the European Union focused on the ambitious target of zero emissions by 2050 [5], I&S industry is very interested in the development of low-carbon technologies [6–8]. Various strategies are being explored for $CO_2$ abatement in blast furnace ironmaking. These strategies include injecting low-carbon reducing agents like hydrogen, implementing Top Gas Recycling (TGR) in oxygen blast furnaces (OBF), employing Carbon Capture and Storage (CCS), and applying Power to X (PtX) technologies like Power to Methane. These approaches aim to reduce greenhouse gas emissions and contribute to the decarbonisation of the ironmaking industry.

Most efforts have focused on the development of alternatives to coke, such as pulverized coal injection, natural gas, coke oven gas, waste plastics or other hydrocarbon injections [4], and more also synthetic natural gas, bio-methane, syngas from biomass or hydrogen [9]. TGR has generated more attention over the past decades to achieve large $CO_2$ emissions reductions, usually applied in oxygen blast furnaces (OBF), such as in the pilot plant (TRL 6–7) developed in the ULCOS project in Luleå [10]. This not only reduces emissions (by up to 40–55% [11]) but also increases energy efficiency and can lead to cost savings.

In OBFs the absence of nitrogen decreases the total bosh gas volume, requiring a preheating gas injection in the upper part of the furnace to maintain the required operation temperature. This injection, usually burnt blast furnace gas (BFG) at 1000 °C [12,13], also increases flexibility, as other reducing agents, such as natural gas injection or $H_2$, may be used [12]. Additionally, the OBFs yield higher productivity rates than

* Corresponding author.
*E-mail addresses:* jorge.perpinan@unizar.es (J. Perpiñán), mbailera@unizar.es (M. Bailera), bpp@unizar.es (B. Peña).

https://doi.org/10.1016/j.enconman.2023.117611
Received 15 June 2023; Received in revised form 29 August 2023; Accepted 30 August 2023
Available online 4 September 2023
0196-8904/© 2023 The Authors. Published by Elsevier Ltd. This is an open access article under the CC BY-NC-ND license (http://creativecommons.org/licenses/by-nc-nd/4.0/).

**Nomenclature**

| Abbreviation | Meaning |
|---|---|
| AFT | Adiabatic Flame Temperature |
| ASU | Air Separation Unit |
| AHF | Air Heating Furnace |
| BF-BOF | Blast Furnace-Basic Oxygen Furnace |
| BFG | Blast Furnace Gas |
| BOFG | Basic Oxygen Furnace Gas |
| CC | Carbon Capture |
| CCUS | Carbon Capture Utilization and Storage |
| COG | Coke Oven Gas |
| DRI | Direct Reduced Iron |
| EAF | Electric Arc Furnace |
| GHG | Green House Gas |
| HM | Hot Metal |
| I&S | Iron and Steel |
| IEA | International Energy Agency |
| LHV | Lower Heating Value |
| MDEA | Methyldiethanolamine |
| PEM | Proton Exchange Membrane |
| PtG | Power to Gas |
| PCI | Pulverised Coal Injection |
| PFD | Process Flow Diagram |
| SNG | Synthetic Natural Gas |
| $t_{HM}$ | Ton of Hot Metal |
| $t_{CS}$ | Ton of Crude Steel |
| TGR | Top Gas Recycling |
| TRL | Technology Readiness Level |

traditional BFs, by 30–100% according to different estimates [11]. One of the best options within the TGR technology is to combine it with vacuum pressure swing adsorption (VPSA) and oxygen blast furnace (TGR-OBF, TRL 5–6). In this process, the $CO_2$ is captured from the top gas (or from the BFG), while the remaining gases, mainly CO and $H_2$, are recycled into the furnace [14–16]. $CO_2$ emissions of the blast furnace can be reduced between 26 % and 56 % with respect to conventional BFs [17], with capture costs ranging from 50 €/$t_{CO2}$ to 90 €/$t_{CO2}$ [18]. However, TGR-OBF concepts lead to a strong decrease in the available energy content for downstream processes, as they focus on CO recycling [19], being one of the main challenges presented for this kind of configurations.

Another potential low-carbon alternative is to apply carbon capture and storage (CCS) to conventional steelmaking plants (BF-BOF route). Among the available carbon capture technologies, the most promising are chemical absorption and physical adsorption. Both technologies have high TRL when applied in the I&S industry (TRL 6), being able to capture high amounts of $CO_2$ (up to 1700 $kg_{CO2}/t_{HM}$) with reasonable costs (38–97 \$/$t_{CO2}$) [18]. Other emerging carbon capture technologies that can be applied in the I&S industry are membranes and sorption enhanced water gas shift (SEWGS). Both technologies exhibit a low electricity penalty (1.2–2.4 $MJ_e/kg_{CO2}$) and relatively low costs (35–60 \$/$t_{CO2}$), but right now only TRL 2–4 has been achieved [18]. The main limitations of CCS technology encompass various aspects, including the requirements for geological storage or large-scale and long-term carbon utilization, as well as the crucial factor of the public's acceptance, which impacts its widespread implementation [20]. Geological storage necessitates identifying suitable and secure underground reservoirs for permanent $CO_2$ storage, ensuring their stability and integrity, and managing potential risks. Additionally, establishing the infrastructure and transportation systems for safe $CO_2$ transport adds complexity and cost [21]. Concerns related to safety, environmental impact, and the potential for $CO_2$ leakage can shape public attitudes and influence the acceptance of CCS initiatives [22].

To integrate PtX in the I&S industry stands out as a promising alternative for reducing $CO_2$ emissions while providing additional benefits [9]. PtX technologies allow the indirect electrification of industrial processes through the generation of valuable products from renewable electricity, such as e-fuels or chemicals. PtX also allow direct electrification through the Power to Iron technology, which is investigated in the project ULCOLYSIS, but is still in the laboratory phase (TRL 2) [23]. When the intermediate energy carrier is present in gaseous form, usually $H_2$, it is also called Power to Gas (PtG) [24]. The most common products of the PtG technology that can be applied in the steel industry are hydrogen (Power to Hydrogen) [25], methane (Power to Methane) [26,27] and syngas (Power to Syngas) [28]. Furthermore, hydrogen together with the top gas released from the BF can be utilized for methanol synthesis, thereby producing a valuable raw material for the production of synthetic fuels, plastics, and basic chemicals [29].

Feasibility evaluations for Power to Hydrogen (PtH2) integration have primarily focused on air-blown blast furnaces, with only one study found on oxygen blast furnaces. Experimental testing of hydrogen injection has also been limited. Simulation studies using alkaline and solid oxide electrolyzers in air-blown blast furnaces have injected 20–33 kg/tHM of preheated hydrogen at temperatures up to 1200 °C, resulting in CO2 emissions ranging from 1060 to 1182 kgCO2/tHM [25,27,30]. In an investigation by Bailera et al. [27], preheated hydrogen was injected into the tuyeres of an oxygen blast furnace with top gas recycling, using 24 kgH2/tHM and 321 kgTGR/tHM, leading to CO2 emissions of 905 kgCO2/tHM [27]. The study concluded that hydrogen injection was less polluting than synthetic natural gas injection but had a higher energy penalty due to the larger electrolyzer size. Thyssenkrupp [31] achieved the first hydrogen injection through one of the 28 tuyeres of blast furnace no. 9 in Duisburg in 2019, with plans to gradually expand the use of hydrogen to all tuyeres. The COURSE 50 project [32] conducted an experimental campaign from 2018 to 2020 using a 12 m3 experimental blast furnace, continuously injecting 32 kgH2/tHM and achieving a 16% reduction in CO2 emissions.

In the Power to Methane technology, methanation of carbonaceous compounds, such as CO and $CO_2$, is achieved with $H_2$, obtaining water as a by-product [33] through the Sabatier reaction. Few experimental studies were found regarding experimental methanation of steel gases (BFG, BOFG and COG) [34–37], reaching a TRL 4. Theoretical studies on the Power to Gas technology in the I&S industry have also been assessed, including configurations with biomass methanation [38], OBF [26,39], TGR and SOEC electrolysis [40]. These studies concluded that $CO_2$ avoidance ranging from 6% to 22% can be achieved, with energy penalties of approximately 18–34 $MJ/kg_{CO2}$. The primary cost associated with this process is the electricity consumption from the electrolyser.

In previous works, the authors conducted comprehensive research in the field of iron and steel production. They developed and validated a benchmark model for the traditional I&S industry. Additionally, they explored the integration of Power to Gas with amine scrubbing in an air-blown blast furnace, aiming to enhance its efficiency and reduce emissions [41]. Furthermore, the impact of oxygen enrichment and temperature on hot blast was analysed, providing valuable insights for improving the process [42]. The results of these studies revealed significant potential for $CO_2$ avoidance, with reductions ranging from 9% to 34% and related costs of 52 – 233 €/$t_{HM}$ and 283 – 352 €/$t_{CO2}$.

The present work assesses the technical performance and cost of a PtG-steelmaking integration, where the blast furnace gas is directly diverted to a methanation stage. Combined with renewable $H_2$ produced in a PEM electrolyser, the CO and $CO_2$ present in the BGF give rise to synthetic natural gas (SNG). Notably, this configuration eliminates the

need for a carbon capture stage since the blast furnace gas is directly methanized. The SNG is recycled back into the blast furnace, avoiding $CO_2$ emissions and geological storage. This PtG configuration focuses on both $CO_2$ and CO recycling via BFG methanation (contrary to the TGR configuration that only recycles CO), ensuring that all energy requirements of the downstream processes (sinter strand, power plant, etc.) are covered. This integration is studied by varying the $H_2$:$CO_2$ ratio in the methanation stage, from a ratio of 2.5 (where part of the $CO_2$ is not methanized and injected in the furnace), to an infinite ratio (where only $H_2$ is found and injected in the furnace). The results are compared with a conventional I&S plant in terms of $CO_2$ emissions, energy penalty and fossil fuel demand. Both simulations, the conventional plant and the PtG-steelmaking plant, have been modelled with Aspen Plus. An economic assessment of the PtG-steelmaking integration is made to identify the specific costs of the new integration.

## 2. Description of case studies

First, a conventional iron and steel (I&S) plant is considered as the reference case (Fig. 1, solid lines). The blast furnace (BF) is fed from the top with alternating layers of iron ore agglomerated in the sinter strand and coke produced in the corresponding oven. The hot metal results from the reduction process of iron in the BF with help of reducing agents, usually pulverized coal (PCI), which are injected from below together with the hot blast (air heated in the hot stoves). The hot metal (or pig iron) is mixed with scrap (recovered steel) and converted in crude steel after the excess of carbon is eliminated in the basic oxygen furnace (BOF). The required oxygen is provided by an air separation unit (ASU). The different process gases are used as fuels in different processes: blast furnace gas (BFG in cyan) in the sinter strand, hot stoves and power plant; basic oxygen furnace gas (BOFG, in brown) in the casting and power plant; and coke oven gas (COG in purple) in the coke oven, BOF and power plant. The integrated steelworks include a power plant to be electrically self-sufficient where the excess of process gases are burnt. The conventional I&S plant, which serves as a baseline for comparison in the present work, considers a 320 $t_{HM}$/h blast furnace [43] and a 100 MW [44] power plant. The conventional I&S plant was previously modelled in Aspen Plus and validated with literature data [41].

The low-carbon concept consists of an oxygen blast furnace (OBF) with PtG integration, see Fig. 1, where the dashed lines represents the changes regarding the base case. The main new blocks in this PtG-steelmaking integration are the PEM electrolyser for $H_2$ production ($O_2$ is also by-produced), and the methanation plant for synthetic natural gas (SNG) production (green lines). New streams (dashed lines) include pure oxygen in the OBF, some BFG as preheating gas injection, and some BFG diverted to the methanation. The two latter streams form a closed carbon loop, avoiding additional $CO_2$ emissions into the atmosphere. The oxygen from the PEM electrolyser is used to alleviate the ASU demand, feeding the OBF, the preheating gas injection and the BOF. The $H_2$:$CO_2$ ratio of the methanation stage is gradually varied, from 2.5 $mol_{H2}/mol_{CO2}$, going through 4 $mol_{H2}/mol_{CO2}$ (stoichiometric conditions), increasing the ratio to 8 $mol_{H2}/mol_{CO2}$, and reaching an infinite ratio (full $H_2$, no BFG). In the last case, only $H_2$ is injected in the OBF, therefore no methanation stage is required and no SNG is produced.

## 3. Methodology

For the modelling and simulation of the conventional I&S plant (Section 3.1) and the PtG-steelmaking integration concepts (Section 3.2), the software Aspen Plus is used. Fig. 1 shows all hierarchy blocks included in the simulation. Each block has different sub-models and its own Aspen property method [45] in order to reproduce the process. In all cases, steady-state conditions, complete combustion and chemical equilibrium is assumed. The different concepts are compared with respect to the techno-economic indicators explained in Section 3.3.

### 3.1. Conventional I&S plant

The detailed description of the Aspen Plus model of the conventional I&S plant (solid lines in Fig. 1) can be found in [41]. The reference case encompasses multiple levels in different hierarchies, and different blocks are used to accurately simulate each process (see Supplementary data). BFG composition, flame temperature and air and coke flow rates are calculated through the Rist model [39,46]. The BFG composition is calculated as function of the utilization factors of CO and $H_2$ (Eq. (1) and Eq. (2), respectively). The CO ($H_2$) utilization factor of a blast furnace refers to the ratio of CO ($H_2$) used in the process to the total amount of CO and $CO_2$ ($H_2$ and $H_2O$) gases produced. The power plant is a combined cycle with cooling between two air compression stages and three steam turbines. The ASU model is based in the cryogenic technology of

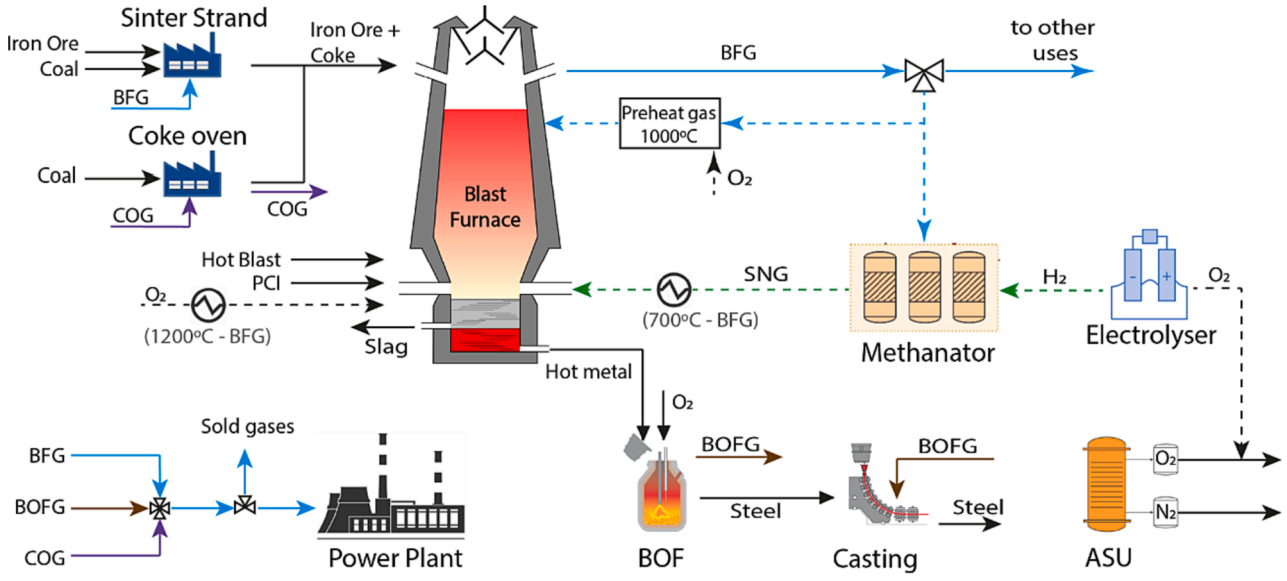


**Fig. 1.** Process flow diagram for conventional iron and steel plant (solid lines) and the integration of direct methanation through Power to Gas in an oxygen blast furnace (dashed lines). Blue line: blast furnace gas, BFG. Brown line: basic oxygen furnace gas, BOFG. Purple line: Coke oven gas, COG. Green line: synthetic gas, SNG.

Linde-Hampson model. The PENG-ROB property method is used for I&S processes and ASU, while PR-BM property method is used for the power plant.

$$\mu_{CO} = CO_2/(CO_2 + CO) \quad (1)$$

$$\mu_{H2} = H_2O/(H_2O + H_2) \quad (2)$$

The model represents a simplified version of a real I&S plant, considering the design parameters summarized in Table 1 [41].

### 3.2. PtG-steelmaking integration with direct BFG methanation

In the present work, the low-carbon I&S proposal integrates Power to Methane with an oxy blast furnace (OBF). The oxygen is injected in the OBF at 1200 °C, according to the better results obtained in our previous research [42] with respect to cold oxygen (25 °C) injection. As there is no nitrogen injected in the furnace, the insufficient preheat of the burden in the upper part of the furnace leads to BFG temperatures lower than 100 °C. To avoid problems related to oxidation and corrosion, a preheating gas injection in the upper part of the furnace is required. By doing so, the BFG temperature is maintained above 150 °C. The preheating gas consists of BFG burned with pure oxygen and injected at 1000 °C [12].

The distribution of the combustible gases remains the same as in the conventional I&S plant. The only differences are the absence of nitrogen in the BFG, resulting in lower mass flows, and that part of the BFG is now diverted to the preheating gas and the methanation plant (dashed blue lines in Fig. 1).

Regarding PtG technology, the PEM electrolyser is modelled with a specific energy consumption of 3.8 kWh/Nm$^3$, working at ambient temperature. The methanation plant consists of two isothermal fixed-bed reactors, operating at 5 bar and 350 °C (first reactor) and 300 °C (second reactor), with an intermediate condensation stage at 100 °C (Fig. 2), in order to achieve a methane concentration in the SNG of 95% with stoichiometric conditions, see Eq. (3) and Eq. (4).

$$CO_2 + 4H_2 \leftrightarrow CH_4 + 2H_2O \Delta H_{298K} = -164.9 kJ/mol \quad (3)$$

$$CO + 3H_2 \leftrightarrow CH_4 + H_2O \Delta H_{298K} = -206.4 kJ/mol \quad (4)$$

The PtG-steelmaking integration with direct BFG methanation is analysed under different operation conditions, obtained by varying the stoichiometry of the methanation reactor. Among others, $H_2$:$CO_2$ ratios of 2.5, 4 (stoichiometric conditions) and 8, to an infinite ratio (full $H_2$) are simulated. When directly injecting $H_2$, no methanation stage is required, and therefore no SNG is produced. In all cases, the amount of SNG injected is limited to have an adiabatic flame temperature (AFT) of 2000 °C, because the larger the amount of SNG injected, the lower the AFT is. If lower temperatures are found, productivity problems may arise [47]. The Power to Gas plant is sized according to the amount of SNG (or $H_2$) that can be injected in the blast furnace. Thus, knowing the amount of synthetic gas required for each $H_2$:$CO_2$ ratio, the methanation plant and the electrolyser can be sized. The oxygen by-produced in the electrolyser is used to eliminate the ASU and to feed the BOF and hot blast enrichment necessities.

**Table 1**
Input data for the conventional I&S plant modelling [41].

| Variable | Value | Units |
|---|---|---|
| Sintering temperature | 1262 | °C |
| Coke oven temperature | 1100 | °C |
| Hot blast pressure | 4.5 | bar |
| Hot blast temperature | 1200 | °C |
| Blast furnace top pressure | 2.0 | bar |
| $H_2$ utilization (Eq. (2)) | 0.47 | – |
| Carbon content in hot metal | 4.5 | wt% |
| Carbon content in final steel | 0.267 | wt% |
| Basic oxygen furnace temperature | 1650 | °C |
| Scrap flow rate | 150 | kg/$t_{HM}$ |
| Separation pressure levels in ASU | 6/1.5 | bar |
| Gas turbine pressure (Power Plant) | 27 | bar |
| Gas turbine inlet temperature (Power Plant) | 1389 | °C |
| Steam inlet temperature (Power Plant) | 560 | °C |
| Steam pressure levels (Power Plant) | 120/42/4 | bar |
| Power plant size | 100 | MW |

### 3.3. Techno-economic indicators

The comparison of the proposed low-carbon concepts with the conventional I&S plant is performed with regards to different techno-economic indicators.

The technical indicators are the coal-equivalent replacement ratio (coal-e RR) and the energy penalty. The former is defined as the sum of the coking coal and pulverized coal replaced by the SNG (Eq. (5)). The latter is the net energy consumed in the industry per kg of $CO_2$ avoided with the PtG-steelmaking integration (Eq. (6)). The involved magnitudes are detailed in Table 2.

$$Coal - eRR = \frac{\Delta \dot{m}_{PCI} + \Delta \dot{m}_{CokingCoal}}{\Delta \dot{m}_{SNG}} [kg_{Coal}/kg_{SNG}] \quad (5)$$

$$E_{penalty} = \frac{\Delta E_{cons} - \Delta E_{coal} \bullet \eta_{elec} - \Delta E_{gases} \bullet \eta_{elec}}{\Delta \dot{m}_{CO2}} [MJ/kg_{CO_2}] \quad (6)$$

The economic indicators are the specific costs per ton of $CO_2$ avoided (€/$t_{CO2}$) and per ton of hot metal (€/$t_{HM}$). The corresponding calculation is shown in Eq. (7) and Eq. (8), respectively, and the involved magnitudes are described in Table 2. The analysis assumed a loan amortization period of 20 years, a PtG system operating for 8000 h per year [48], and a renewable electricity price of 77 €/MWh. The detailed calculation of CAPEX, OPEX and Incomes can be found elsewhere [41], but for completeness purposes it has been summarized in the supplementary data.

$$CO_2 avoidance Cost = \frac{\left(\frac{Capex}{Loan amortization} + Opex - Incomes\right) \hat{A} \cdot 10^6}{CO_2 avoided \hat{A} \cdot Operating hours} \left[\frac{€}{t_{CO_2}}\right] \quad (7)$$

$$Specific Implementation Cost = \frac{\left(\frac{Capex}{Loan amortization} + Opex - Incomes\right) \hat{A} \cdot 10^6}{Iron Production \hat{A} \cdot Operating hours} \left[\frac{€}{t_{HRC}}\right] \quad (8)$$

## 4. Results and discussion

Results and discussion on the PtG-steelmaking integration with oxy blast furnace and its comparison with the conventional I&S plant are presented in Sections 4.1 and 4.2 with respect to technical and economic aspects, respectively. The figures depict data presented as a function of the $H_2$:$CO_2$ ratio in the methanation stage. The study includes a total of 12 data points, with the most significant ones being: 2.5 $mol_{H2}/mol_{CO2}$, 4 $mol_{H2}/mol_{CO2}$ (stoichiometric conditions), and an infinite ratio (full $H_2$).

### 4.1. PtG-steelmaking integration

In this section, we present the results of the integration of Power to Gas with steelmaking, specifically focusing on parameters like reducing agents, coal-e RR, SNG and BFG composition, PEM size, $CO_2$ emissions and energy penalty.

Switching from air-blown BF (conventional I&S) to an OBF (PtG-steelmaking integration) enables higher amounts of reducing agents maintaining the AFT above 2000 °C. This configuration allows the full replacement of PCI by synthetic natural gas. When stoichiometric conditions are taken in the methanation plant ($H_2$:$CO_2$ of 4), the minimum coke consumption in the OBF is obtained (280 kg/$t_{HM}$), see Fig. 3,

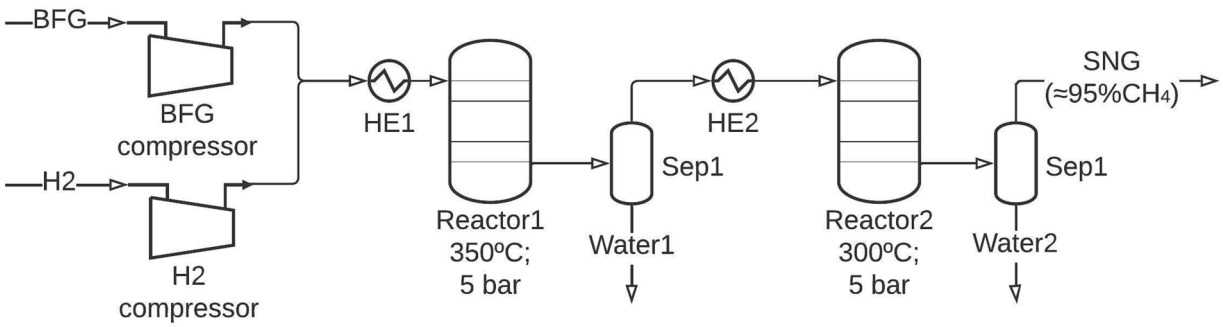


**Fig. 2.** Process flow diagram for the methanation plant (details in the text).

**Table 2**
Units and description of variables from equations (3)-(6).

| Variable | Units | Description |
|---|---|---|
| $\Delta\dot{m}_{PCI}$ | $kg_{PCI}/t_{HM}$ | Savings in PCI consumption |
| $\Delta\dot{m}_{CokingCoal}$ | $kg_{CokingCoal}/t_{HM}$ | Savings in coking coal consumption |
| $\Delta\dot{m}_{SNG}$ | $kg_{SNG}/t_{HM}$ | Increase in SNG injection |
| $\Delta E_{cons}$ | $MJ/t_{HM}$ | Increase in electricity consumption in the industry |
| $\Delta E_{coal}$ | $MJ/t_{HM}$ | Savings in coal energy |
| $\Delta E_{gases}$ | $MJ/t_{HM}$ | Increase in excess sold gases |
| $\eta_{elec}$ | – | Energy conversion factor from coal to electricity (0.33) |
| CAPEX | M€ | Capital Expenditure |
| OPEX | M€/year | Operational Expenditure |
| Incomes | M€/year | Operational Incomes |
| Loan amortization | y | Process of paying off a loan over time |
| $CO_2$ avoided | $t_{CO_2}/h$ | $CO_2$ avoided per hour |
| Operating hours | h/year | Operating hours per year |

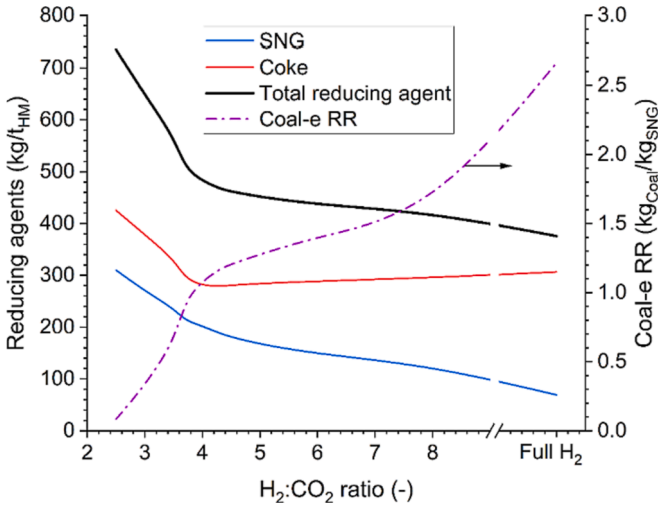


**Fig. 3.** Reducing agents in OBF (SNG, blue line; coke, red line; and total reducing agents, black line) and coal-e RR (purple dashed line) as a function of the $H_2$:$CO_2$ stoichiometry.

compared with that of the conventional I&S plant (332 $kg_{coke}/t_{HM}$ and 150 $kg_{PCI}/t_{HM}$). When increasing the ratio towards full $H_2$ injection, 69 $kg_{H2}/t_{HM}$ are injected, with a slight increase in the coke rate (307 kg/$t_{HM}$), but much less total reducing agent (376 kg/$t_{HM}$) is needed. This is due to the higher coal-e RR of the $H_2$ when compared to the SNG. These results are consistent with previous studies conducted by Yilmaz et al. [25] and Kim et al. [30] in an air-blown blast furnace. Yilmaz injected hydrogen produced by an alkaline electrolyser, achieving a coke consumption of 390 $kg_{coke}/t_{HM}$ and no use of PCI. Kim, on the other hand, utilized hydrogen produced by a SOEC electrolyser, resulting in a coke consumption of 327 $kg_{coke}/t_{HM}$ and a PCI consumption of 112 $kg_{PCI}/t_{HM}$. For $H_2$:$CO_2$ ratios below 4, poor results are found. The coal-e RR drops below 1 and the coke rate increases considerably. This is because large amounts of $CO_2$ are not methanized and therefore are injected into the blast furnace.

The BFG composition and the SNG composition are co-dependents of each other through the chemical reactions occurring in the blast furnace. The former gas is used in the methanation stage to form synthetic natural gas, which in turn is used as a reducing agent in the OBF, determining the BFG composition. The composition of both gases is also dependent on the $H_2$:$CO_2$ ratio used in the methanation stage.

At a $H_2$:$CO_2$ ratio of 4, the majority of the SNG consists of $CH_4$ (Fig. 4). As the ratio decreases, the $CO_2$ content increases, reaching 35.8 vol% at a ratio of 2.5, indicating direct recycling of $CO_2$. On the other hand, higher ratios lead to an increase in $H_2$ content, up to 100% (full $H_2$). The energy content of the SNG, shown by the purple dashed line in Fig. 4, takes into account both the lower heating value (LHV) of the gas ($MJ/kg_{SNG}$) and the mass flow rate ($kg_{SNG}/t_{HM}$), providing the energy content of this stream in $MJ/t_{HM}$. The maximum energy content of the SNG is observed at a $H_2$:$CO_2$ ratio of 4. As the ratio decreases, more SNG is injected into the OBF, but a significant portion consists of $CO_2$, resulting in lower energy content. Conversely, as the ratio increases, the concentration of $H_2$ increases, but the SNG flow rate decreases, again leading to less energy content.

When $CO_2$ is recycled through low $H_2$:$CO_2$ ratios, the BFG contains high amounts of CO and $CO_2$ (Fig. 5). However, injecting pure $H_2$ results in up to 45% hydrogen content in the gas. A stoichiometric $H_2$:$CO_2$ ratio results in 27% $H_2$, which is slightly higher compared to the 25%

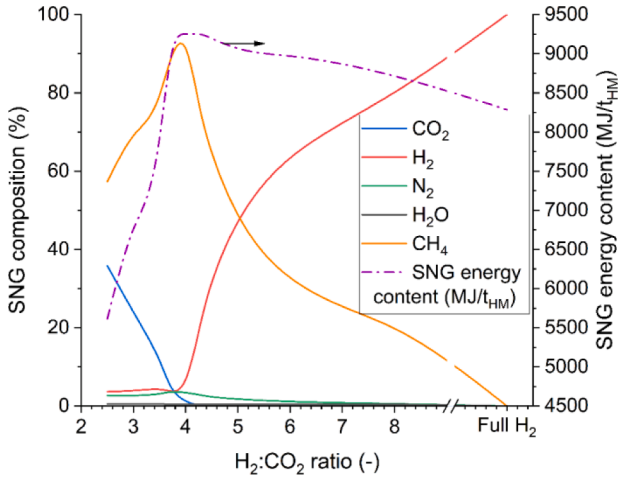


**Fig. 4.** SNG composition ($CO_2$, blue line; $H_2$, red line; $N_2$, green line; $H_2O$, grey line; $CH_4$, orange line) and SNG energy content (purple dashed line) as a function of the $H_2$:$CO_2$ stoichiometry.

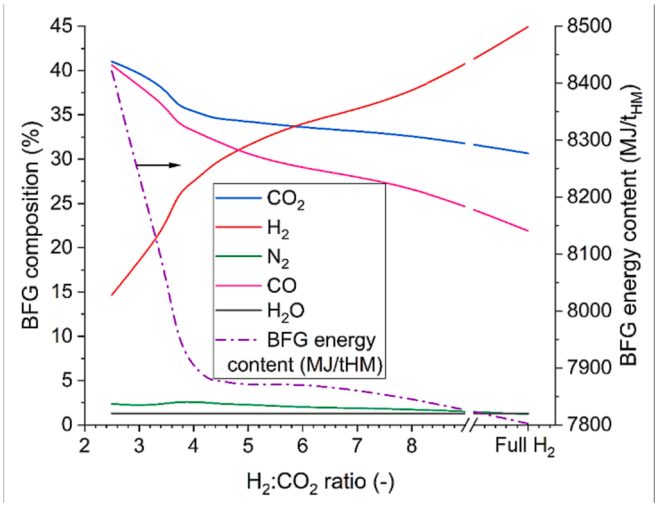


**Fig. 5.** BFG composition ($CO_2$, blue line; $H_2$, red line; $N_2$, green line; CO, pink line; $H_2O$, grey line) and BFG energy content (purple dashed line) as a function of the $H_2$:$CO_2$ stoichiometry.

reported by Sato et al. [13] in their simulation of an OBF with high natural gas injection. Despite the increase in $CO_2$ and decrease in $H_2$, a lower $H_2$:$CO_2$ ratio leads to a higher BFG energy content of 8424 MJ/$t_{HM}$. This is due to the blast furnace's increased coke rate, resulting in higher amounts of CO and larger BFG mass flow rates. For a stoichiometric $H_2$:$CO_2$ ratio and full $H_2$ injection, the BFG energy content ranges between 7800 and 7900 MJ/$t_{HM}$. In comparison to the conventional I&S plant's BFG energy content of 4930 MJ/$t_{HM}$, all cases show a significant increase. The CO utilization ratio (Eq. (1)) increases from 0.49 at a fixed $H_2$:$CO_2$ ratio of 2.5 to 0.52 at the stoichiometric ratio and further to 0.58 with full $H_2$ injection.

A low $H_2$:$CO_2$ ratio implies low $H_2$ demand, therefore the lowest PEM size is found at $H_2$:$CO_2$ ratio of 2.5 (Fig. 6). At this point, the $O_2$ by-produced in the PEM is not able to supply the full oxygen demand. The deficit of oxygen is covered by the ASU. For a stoichiometric ratio and full $H_2$, the PEM size ranges between 930 and 972 MW, being the lower size when pure hydrogen is injected in the OBF. The reason is that the $H_2$ cools the AFT to a larger degree, so less flow rate can be injected if compared with the SNG.

When the $H_2$:$CO_2$ ratio is decreased, there is an increase in the oxygen consumed by the industry (blue line) due to an increase in the oxy-hot blast mass flow rate (Fig. 6). When SNG is injected with $CH_4$ as the primary component, additional oxygen is required in the OBF to partially oxidize methane into CO and $H_2$. However, only additional oxygen from the ASU is necessary at $H_2$:$CO_2$ ratios lower than 4.

The integration of PtG with steelmaking shows that the optimum $CO_2$ emission reduction occurs at a stoichiometric $H_2$:$CO_2$ ratio, reaching 33.8% of carbon avoidance (Fig. 7). However, as the $H_2$:$CO_2$ ratio increases and full $H_2$ injection is employed, the percentage of $CO_2$ avoided decreases to 28.6%. This is primarily attributed to the coke rate, where higher carbon input in the form of coke leads to increased carbon output in the form of $CO_2$ emissions. In Fig. 7, the orange and green lines represent the $CO_{2\text{-eq}}$ recycled within a closed loop through the preheating BFG gas and the BFG diverted to methanation, respectively. With full $H_2$ injection, no BFG is diverted to methanation, resulting in no recycling of $CO_{2\text{-eq}}$ through the PtG system. To provide context for these results, it is important to consider other low-carbon methods used in oxygen blast furnace ironmaking production, such as top gas recycling. Studies have shown that top gas recycling can achieve $CO_2$ emissions ranging from 868 to 1180 $t_{CO2}/t_{HM}$ in the blast furnace [27,49]. In comparison, the $CO_2$ emissions emitted in the blast furnace of PtG concepts of the present study range from 747 to 833 $t_{CO2}/t_{HM}$ (not to be confused with the total emissions of the entire I&S industry, which range from 1286 to 1387 $t_{CO2}/t_{HM}$, shown in Fig. 7).

The sold gases, electricity consumption and energy penalty are shown in Fig. 8. The PEM electricity consumption accounts for 78–91% of the total electricity consumption, creating a linear dependency between the size of the electrolyser and the total electricity consumption. The maximum electricity consumption is 12163 MJ/$t_{HM}$ for a stoichiometric $H_2$:$CO_2$ ratio, compared with the 950 MJ/$t_{HM}$ in the conventional I&S plant. When decreasing the $H_2$:$CO_2$ ratio below 4, the ASU starts working, but its consumption is very low compared to that of the PEM electrolyser, barely affecting the results.

The amount of excess gases sold to nearby industries, including BFG, BOFG, and COG, decreases to 1828 MJ/$t_{HM}$ for a stoichiometric $H_2$:$CO_2$ ratio (Fig. 8). However, for a $H_2$:$CO_2$ ratio of 2.5 and full $H_2$ injection, the sold gases increase to over 4000 MJ/$t_{HM}$. This indicates that the industry's energetic gases are better utilized when a $H_2$:$CO_2$ ratio of 4 is employed. Lower $H_2$:$CO_2$ ratios result in higher BFG energy content, while higher $H_2$:$CO_2$ ratios lead to reduced BFG usage in the methanation process, resulting in larger quantities of gases available for sale.

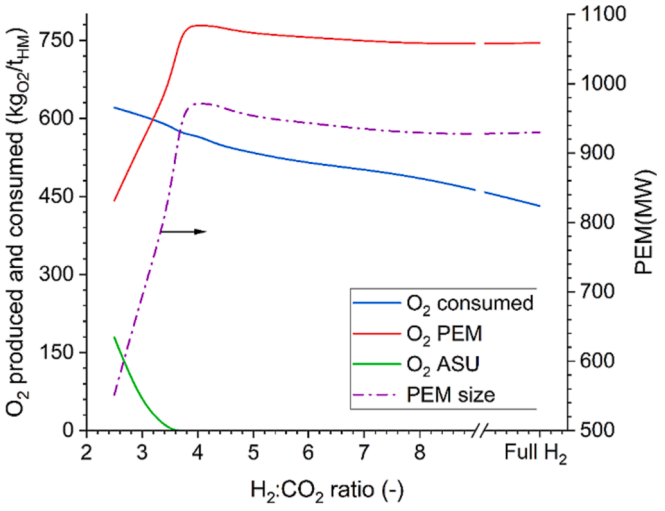


**Fig. 6.** Oxygen produced in the PEM (red line) and in the ASU (green line), oxygen consumed in the industry (blue line) and PEM capacity (purple dashed line) as a function of the $H_2$:$CO_2$ stoichiometry.

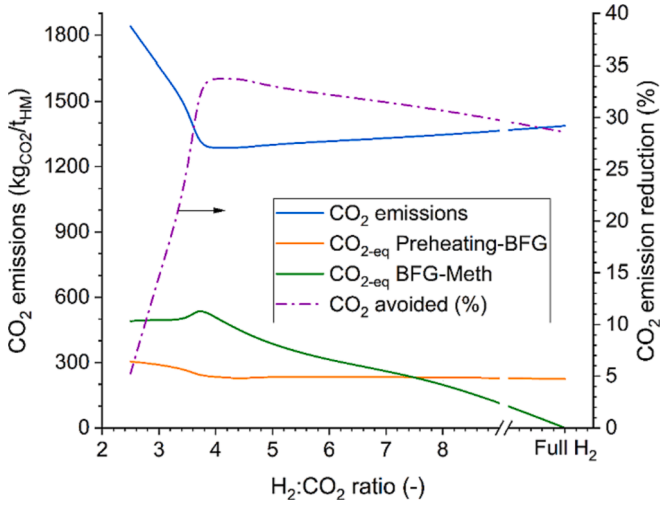


**Fig. 7.** $CO_2$ total emissions (blue line), CO2-eq in preheating BFG gas (orange line), CO2-eq in BFG diverted to methanation (green line) and percentage of $CO_2$ emission reduction (purple dashed line) as a function of the $H_2$:$CO_2$ stoichiometry. Orange and green lines represent the CO2-eq that is recycled in a closed loop.

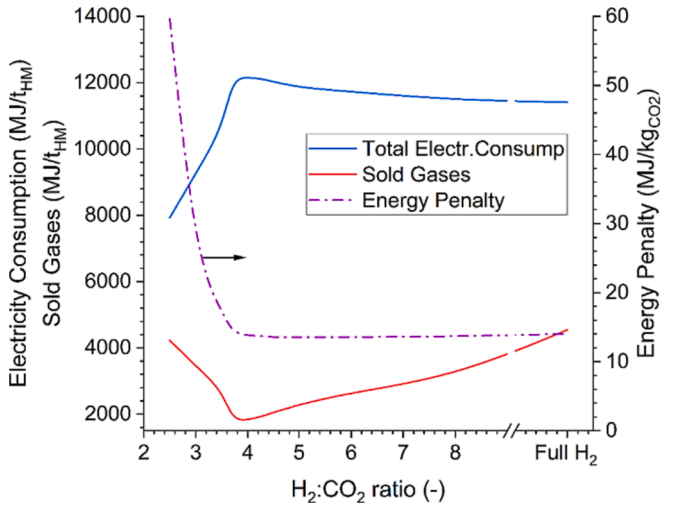


**Fig. 8.** Electricity consumption (blue line), sold gases (red line) and energy penalty (purple dashed line) as a function of the $H_2$:$CO_2$ stoichiometry.

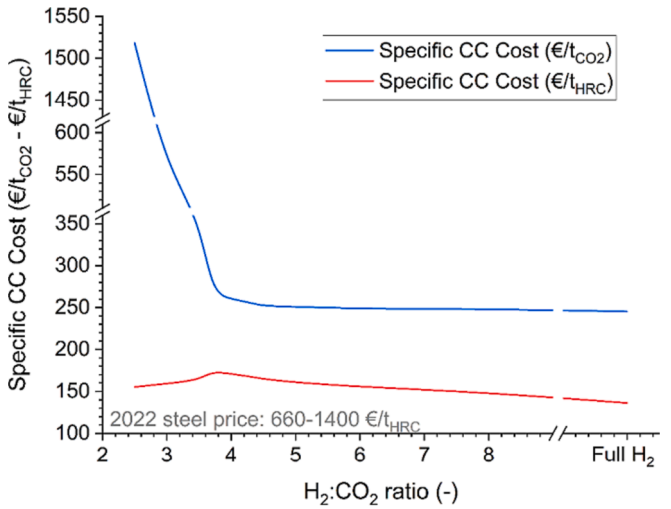


**Fig. 9.** Specific carbon capture (CC) cost in €/t$CO_2$ (blue line) and €/tHRC (red line) as a function of the $H_2$:$CO_2$ stoichiometry (2022 steel price [50]).

The energy penalty increases drastically for lower $H_2$:$CO_2$ ratios because only small amounts of $CO_2$ are avoided (Fig. 8). For stoichiometric ratio and full $H_2$ injection, the energy penalty is constant at 14 MJ/$kg_{CO2}$. For a $H_2$:$CO_2$ ratio of 4, higher PEM sizes and electricity consumptions are found, but also higher amounts of avoided $CO_2$, as opposed to full $H_2$ injection, leading to a constant energy penalty.

For illustration purposes, two configurations analysed in this paper, namely stoichiometric $H_2$:$CO_2$ ratio and full $H_2$ injection, are compared with OBF-TGR technology [27] (refer to Table 3). It's evident that the TGR configuration consumes 42–55% more fossil fuel (coke and PCI) than the other two configurations discussed. In terms of emissions from the blast furnace (BF) alone, the TGR setup exhibits higher $CO_2$ flow rates, but a significant portion can potentially be stored geologically. This implies that the environmental impact of the TGR configuration depends on the availability of storage. Furthermore, it's important to note that TGR technology often leads to a reduction in downstream process energy content, a drawback not observed in the other configurations explored here.

### 4.2. Economic analysis

In this section, we present the economic results of integrating Power to Gas with steelmaking, focusing on parameters such as CAPEX, OPEX, Incomes and specific carbon avoidance costs.

Full $H_2$ injection yields the best economic results, with a cost of 245 €/$t_{CO2}$ and 136 €/$t_{HRC}$ (Fig. 9), despite having a lower $CO_2$ capture rate. This configuration has better results than a $H_2$:$CO_2$ ratio of 4, which has a larger PEM size and costs 260 €/$t_{CO2}$ and 171 €/$t_{HRC}$. The CAPEX, OPEX, and Incomes for both full $H_2$ injection and stoichiometric conditions are very similar, ranging from 870 to 931 M€, 594–640 M€/year, and 248–288 M€/year, respectively. A $H_2$:$CO_2$ ratio of 2.5 shows lower values for these parameters, resulting in a cost of 155 €/$t_{HRC}$. However, due to poor $CO_2$ reduction, the specific carbon capture cost increases drastically to 1518 €/$t_{CO2}$.

In all cases, the PEM contributes the most to the CAPEX, accounting for 35–43% of the total cost. Purchased electricity is the largest contributor to the OPEX, comprising 94–95% of the expenses. The primary source of income comes from $CO_2$ taxes, ranging from 33 to 57%. It is worth noting that the steel price in 2022 was around 660–1400 €/$t_{HRC}$ [50], so the specific carbon capture cost represents a 10–26% increase in the actual steel price, depending on the $H_2$:$CO_2$ ratio. However, a recent study conducted by Subraveti et al. [51], published in January 2023, analysed CCS costs in a cement plant (90% capture with a 60% increase in cost) and a steel plant (47% capture with a 13% increase in cost), concluding that the cost increase in a bridge as the final product was only 1%. This implies that the costs incurred for implementing the PtG system in steelmaking, despite being significant, would have a limited impact on the final product competitiveness.

For the operation point with a stoichiometric $H_2$:$CO_2$ ratio of 4, a sensitivity analysis focusing on the specific CC cost in €/$t_{CO2}$ is performed (Fig. 10). In order to find the appropriate combinations of

**Table 3**
Comparison of analysed configurations in this paper and TGR [27].

| Variable | Units | Stoichiometric $H_2$:$CO_2$ ratio | Full $H_2$ injection | TGR in oxy-BF |
|---|---|---|---|---|
| Coke | kg/$t_{HM}$ | 280 | 307 | 235 |
| PCI | kg/$t_{HM}$ | 0 | 0 | 200 |
| Gaseous reducing agent (SNG, $H_2$ or TGR) | kg/$t_{HM}$ | 202 | 69 | 449 |
| $CO_2$ emitted in BF | $kg_{CO2}$/$t_{HM}$ | 747 | 833 | 1160 |
| $CO_2$ to geological storage | $kg_{CO2}$/$t_{HM}$ | 0 | 0 | 500 |

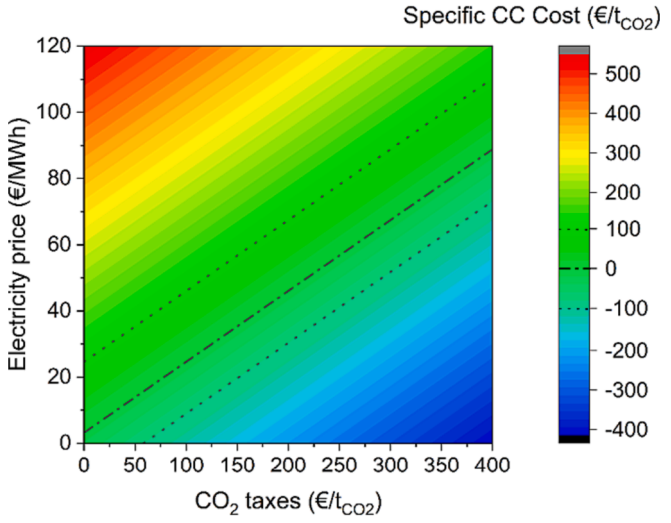


**Fig. 10.** Sensitivity analysis for stoichiometric ratio $H_2$:$CO_2$ of 4:1, representing specific CC cost in €/$t_{CO2}$ as a function of the $CO_2$ taxes and the electricity price.

electricity price and $CO_2$ tax that lead to a profitable scenario, these two parameters are analysed between 0 and 120 €/MWh and 0–400 €/$t_{CO2}$. With the current prices, the PtG-steelmaking integration is not profitable. However, under certain conditions negative values, e.g. actual benefits, can be obtained. For instance, 22 €/MWh or 345 €/$t_{CO2}$ is required to obtain a specific cost of 0 €/$t_{CO2}$. Nevertheless, with these conditions the CAPEX is not amortized. To have a payback of 20 years, a specific carbon capture cost of −13 €/$t_{CO2}$ is required (i.e., actual benefits). Given a $CO_2$ tax of 162 €/$t_{CO2}$ and an electricity price of 35 €/MWh (wind power cost of production [52]), the CC cost would be −13 €/$t_{CO2}$, the CAPEX would be amortized and the investment would be profitable.

## 5. Conclusions

A novel concept that integrates Power to Gas technology through direct methanation in an oxy-blast furnace (OBF) was presented in this study. First, a PEM electrolyser produces green $H_2$ with renewable electricity, later, this green gas is mixed with some BFG in a methanation stage (direct BFG methanation), producing synthetic natural gas (SNG). The synthetic gas is ultimately injected into the OBF as a reducing agent, closing the carbon loop, reducing $CO_2$ emissions, and avoiding the use of additional fossil fuels. A study on the stoichiometry of the methanation reactor was performed, varying the $H_2$:$CO_2$ ratio from 2.5 $mol_{H2}$/$mol_{CO2}$, going through 4 $mol_{H2}$/$mol_{CO2}$ (stoichiometric conditions), increasing the ratio to 8 $mol_{H2}$/$mol_{CO2}$, and reaching an infinite ratio (full $H_2$, no BFG).

For a low $H_2$:$CO_2$ ratio of 2.5 poor results are found. In this configuration, less $H_2$ than BFG is injected in the methanation stage, and as a result a certain amount of $CO_2$ is directly injected into the OBF. This results in a severe increase in the coke rate in the OBF, which leads to a very low $CO_2$ emission reduction of 5%. As less $H_2$ is needed, the PEM size is also smaller, and an ASU is required to produce additional oxygen. Despite the lower PEM size, the specific CC cost increases, reaching 1518 €/$t_{CO2}$. The specific CC cost referred to HRC production is still relatively high, with 155 €/$t_{HRC}$.

For a stoichiometric $H_2$:$CO_2$ ratio of 4, the SNG is composed mostly of $CH_4$ and is injected into the OBF. The coke rate decreases to 280 kg/$t_{HM}$ leading to a $CO_2$ emission reduction of 33.8 %. A total of 443 kg/$t_{HM}$ of BFG are diverted to the methanation stage, the PEM size is 972 $MW_e$ and no ASU is needed. The specific CC costs of this configuration are 260 €/$t_{CO2}$ and 171 €/$t_{HRC}$.

For full $H_2$ injection into the OBF, similar results are found with a stoichiometric $H_2$:$CO_2$ ratio of 4. The coke rate increases slightly to 307 kg/$t_{HM}$, resulting in a $CO_2$ emission reduction of 28.6 %. The PEM size is 930 MW and the $H_2$ produced is directly injected into the OBF, so no BFG is diverted to the methanation stage. The PEM also by-produces enough oxygen and the ASU is not required. The specific CC costs when full $H_2$ injection are 245 €/$t_{CO2}$ and 136 €/$t_{HRC}$.

This PtG integration in the steelmaking industry recycles $CO_2$ and CO via BFG methanation (except for full $H_2$ injection), and is able to supply all downstream energy requirements (the power plant, sintering, etc.), as opposed to some TGR configurations that only recycle CO.

In general, the PtG-steelmaking integration with direct BFG methanation and oxy-blast furnace had the advantage of reducing $CO_2$ emissions through carbon recycling. The use of low $H_2$:$CO_2$ ratios is not recommended, as poor results are obtained. $H_2$:$CO_2$ ratio of 4 and direct injection of $H_2$ obtain similar results, with higher capture ratios in the former and better economic results in the latter.

## CRediT authorship contribution statement

**Jorge Perpiñán:** Conceptualization, Methodology, Writing – original draft, Visualization. **Manuel Bailera:** Conceptualization, Methodology, Writing – review & editing, Supervision, Project administration, Funding acquisition. **Begoña Peña:** Conceptualization, Methodology, Writing – original draft, Writing – review & editing, Visualization, Supervision, Project administration, Funding acquisition.

## Declaration of Competing Interest

The authors declare that they have no known competing financial interests or personal relationships that could have appeared to influence the work reported in this paper.

## Data availability

Data will be made available on request.

## Acknowledgements

This work has received funding from the European Union's Horizon 2020 research and innovation program under the Marie Sklodowska-Curie grant agreement no. 887077. This work is also part of the R&D project TED2021-130000B-I00, funded by MCIN/AEI/ 10.13039/ 501100011033/ and by the "European Union NextGenerationEU/ PRTR", and PID2021-126164OB-I00, funded by MCIN/ AEI/10.13039/ 501100011033/ and by the "ERDF A way of making Europe". Manuel Bailera acknowledges Waseda University, Tokyo. Manuel Bailera and Jorge Perpiñán acknowledge K1-MET GmbH, Linz.

## Appendix A. Supplementary data

Supplementary data to this article can be found online at https://doi.org/10.1016/j.enconman.2023.117611.

## References

[1] International Energy Agency, Iron and Steel Technology Roadmap. 2020. https://www.iea.org/reports/iron-and-steel-technology-roadmap (accessed April 26, 2022).
[2] Remus R, Aguado-Monsonet Ma, Roudier S, Sancho LD. Best available techniques (BAT). In: Reference Document for Iron and Steel Production; 2013. https://doi.org/10.2791/98516.
[3] Piringer H, Bucher P, Wallimann R. Sustainable lime burning technology with shaft kilns. ZKG Cem Lime Gypsum 2021.
[4] A. Babich, D. Senk, H. W. Gudenau KTM. IRONMAKING 2008.
[5] Commission E. Delivering the European Green Deal 2021. https://commission.europa.eu/strategy-and-policy/priorities-2019-2024/european-green-deal/delivering-european-green-deal_en (accessed June 15, 2023).
[6] ArcelorMittal. ArcelorMittal Climate Action Report 2 2021.
[7] Thyssenkrupp. Thyssenkrupp (2020), Targeting a Future Without CO2 : Our Climate Strategy for Sustainable Steel Production 2020. https://www.thyssenkrupp-steel.com/en/company/sustainability/climate-strategy/?gclid=EAIaIQobChMIgL2O88zv6AIV1O5RCh2W2wacEAAYASAAEgI08PD_BwE.
[8] Voestalpine. Voestalpine (2023), Our path to carbon neutrality 2023. https://www.voestalpine.com/blog/en/commitment/our-path-to-carbon-neutrality/.
[9] Bailera M, Lisbona P, Peña B, Romeo LM. A review on CO2 mitigation in the iron and steel industry through power to X processes. J. CO2 Util. 2021;46:101456.
[10] Danloy G, Berthelemot A, Grant M, Borlée J, Sert D, van der Stel J, et al. ULCOS - Pilot testing of the low-CO2 blast furnace process at the experimental BF in lulea. Rev Metall Cah D'Informations Tech 2009;106:1–8. https://doi.org/10.1051/metal/2009008.
[11] Zhang W, Dai J, Li C, Yu X, Xue Z, Saxén H. A review on explorations of the oxygen blast furnace process. steel research int 2021;92(1).
[12] Ariyama T, Sato M, Nouchi T, Takahashi K. Evolution of blast furnace process toward reductant flexibility and carbon dioxide mitigation in steel works. ISIJ Int. 2016;56:1681–96. https://doi.org/10.2355/isijinternational.ISIJINT-2016-210.
[13] Sato M, Takahashi K, Nouchi T, Ariyama T. Prediction of next-generation ironmaking process based on oxygen blast furnace suitable for CO2 mitigation and energy flexibility. ISIJ Int. 2015;55:2105–14. https://doi.org/10.2355/isijinternational.ISIJINT-2015-264.
[14] Zhang W, Zhang J, Xue Z, Zou Z, Qi Y. Unsteady analyses of the top gas recycling oxygen blast furnace. ISIJ Int. 2016;56:1358–67. https://doi.org/10.2355/isijinternational.ISIJINT-2016-090.
[15] Zhang W, Xue Z, Zhang J, Wang W, Cheng C, Zou Z. Medium oxygen enriched blast furnace with top gas recycling strategy. J. Iron Steel Res. Int. 2017;24:778–86. https://doi.org/10.1016/S1006-706X(17)30117-6.
[16] Li J, Li C, Zhang W, Zhang J, Xue Z. Material, energy and exergy flows of the oxygen blast furnace process with sintering flue gas injection. J. Clean. Prod. 2022;371:133294. https://doi.org/10.1016/j.jclepro.2022.133294.

[17] Jin P, Jiang Z, Bao C, Hao S, Zhang X. The energy consumption and carbon emission of the integrated steel mill with oxygen blast furnace. Resour. Conserv. Recycl. 2017;117:58–65. https://doi.org/10.1016/j.resconrec.2015.07.008.
[18] Perpiñán J, Peña B, Bailera M, Eveloy V, Kannan P, Raj A, et al. Integration of carbon capture technologies in blast furnace based steel making: a comprehensive and systematic review. Fuel 2023;336:127074. https://doi.org/10.1016/j.fuel.2022.127074.
[19] Sahu RK, Roy SK, Sen PK. Applicability of top gas recycle blast furnace with downstream integration and sequestration in an integrated steel plant. Steel Res. Int. 2015;1:502–16. https://doi.org/10.1002/srin.201400196.
[20] Mac Dowell N, Fennell PS, Shah N, Maitland GC. The role of CO2 capture and utilization in mitigating climate change. Nat. Clim. Chang. 2017;7:243–9. https://doi.org/10.1038/nclimate3231.
[21] Svensson R, Odenberger M, Johnsson F, Strömberg L. Transportation systems for CO2 - Application to carbon capture and storage. Energy Convers Manag 2004;45:2343–53. https://doi.org/10.1016/j.enconman.2003.11.022.
[22] Waarum I-K, Blomberg AEA, Eek E, Brown J, Ulfsnes A, Carpenter M, et al. CCS leakage detection technology - Industry needs, government regulations, and sensor performance. Energy Procedia 2017;114:3613–27.
[23] Abdul Quader M, Ahmed S, Dawal SZ, Nukman Y. Present needs, recent progress and future trends of energy-efficient ultra-low carbon dioxide (CO2) steelmaking (ULCOS) program. Renew. Sustain. Energy Rev. 2016;55:537–49. https://doi.org/10.1016/J.RSER.2015.10.101.
[24] Bailera M, Lisbona P, Romeo LM, Espatolero S. Power to Gas projects review: Lab, pilot and demo plants for storing renewable energy and CO2. Renew. Sustain. Energy Rev. 2017;69:292–312. https://doi.org/10.1016/j.rser.2016.11.130.
[25] Yilmaz C, Wendelstorf J, Turek T. Modeling and simulation of hydrogen injection into a blast furnace to reduce carbon dioxide emissions. J. Clean. Prod. 2017;154:488–501. https://doi.org/10.1016/j.jclepro.2017.03.162.
[26] Perpiñán J, Bailera M, Romeo LM, Peña B, Eveloy V. CO2 recycling in the iron and steel industry via power-to-gas and oxy-fuel combustion. Energies 2021;14:7090. https://doi.org/10.3390/en14217090.
[27] Bailera M, Nakagaki T, Kataoka R. Limits on the integration of power to gas with blast furnace ironmaking. Elsevier 2022;374:134038. https://doi.org/10.1016/J.JCLEPRO.2022.134038.
[28] Bailera M. Comparing different syngas for blast furnace ironmaking by using the extended operating line methodology. Fuel 2023;333:126533. https://doi.org/10.1016/j.fuel.2022.126533.
[29] Deerberg G, Oles M, Schlögl R. The project Carbon2Chem®. Chem.-Ing.-Tech. 2018;90:1365–8. https://doi.org/10.1002/cite.201800060.
[30] Kim J, Lee H, Lee B, Kim J, Oh H, Lee I-B, et al. An integrative process of blast furnace and SOEC for hydrogen utilization: Techno-economic and environmental impact assessment. Energy Convers Manag 2021;250:114922.
[31] Thyssenkrupp. Thyssenkrupp launches hydrogen injection at blast furnace 2019. https://eurometal.net/thyssenkrupp-launches-hydrogen-injection-at-blast-furnace/.
[32] Kamijo C, Matsukura Y, Yokoyama H, Sunahara K, Kakiuchi K, Sakai H, et al. Influence of large amount of hydrogen containing gaseous reductant injection on carbon consumption and operation conditions of blast furnace - Development of low carbon blast furnace operation technology by using experimental blast furnace: part II. ISIJ Int. 2022;62(12):2433–41.
[33] Romeo LM, Bailera M. Design configurations to achieve an effective CO2 use and mitigation through power to gas. J CO2 Util 2020,;39:1–10. https://doi.org/10.1016/j.jcou.2020.101174.
[34] Qin Z, Zhao Y, Yi Q, Shi L, Li C, Yan X, et al. Methanation of coke oven gas over Ni-Ce/γ-Al2O3 catalyst using a tubular heat exchange reactor: Pilot-scale test and process optimization. Energy Convers Manag 2020;204:112302.
[35] Wolf-Zoellner P, Medved AR, Lehner M, Kieberger N, Rechberger K. In situ catalytic methanation of real steelworks gases. Energies 2021;14:8131. https://doi.org/10.3390/en14238131.
[36] Hauser A, Weitzer M, Gunsch S, Neubert M, Karl J. Dynamic hydrogen-intensified methanation of synthetic by-product gases from steelworks. Fuel Process. Technol. 2021:217. https://doi.org/10.1016/j.fuproc.2020.106701.
[37] Hauser A, Wolf-Zoellner P, Haag S, Dettori S, Tang X, Mighani M, et al. Valorizing steelworks gases by coupling novel methane and methanol synthesis reactors with an economic hybrid model predictive controller. Metals (Basel) 2022;12(6):1023.
[38] Rosenfeld DC, Böhm H, Lindorfer J, Lehner M. Scenario analysis of implementing a power-to-gas and biomass gasification system in an integrated steel plant: A techno-economic and environmental study. Renew. Energy 2020;147:1511–24. https://doi.org/10.1016/j.renene.2019.09.053.
[39] Bailera M, Nakagaki T, Kataoka R. Revisiting the rist diagram for predicting operating conditions in blast furnaces with multiple injections. Revisiting the Rist diagram for predicting operating conditions in blast furnaces with multiple injections 2021;1:141.
[40] Hisashige S, Nakagaki T, Yamamoto T. CO2 emission reduction and exergy analysis of smart steelmaking system adaptive for flexible operating conditions. ISIJ Int. 2019;59:598–606. https://doi.org/10.2355/isijinternational.ISIJINT-2018-355.
[41] Perpiñán J, Bailera M, Peña B, Romeo LM, Eveloy V. Technical and economic assessment of iron and steelmaking decarbonization via power to gas and amine scrubbing. Energy 2023:276. https://doi.org/10.1016/j.energy.2023.127616.
[42] Perpiñán J, Bailera M, Peña B, Romeo LM, Eveloy V. High oxygen and SNG injection in blast furnace steelmaking with Power to Gas integration and CO2 recycling. J. Clean. Prod. 2023. https://doi.org/10.1016/j.jclepro.2023.137001.
[43] Steelmaking technologies. CISDI ingeniering CO. LTD 2022. http://www.cisdigroup.com/4-steelmaking.html (accessed April 26, 2022).
[44] Wu J, Wang R, Pu G, Qi H. Integrated assessment of exergy, energy and carbon dioxide emissions in an iron and steel industrial network. Appl. Energy 2016;183:430–44. https://doi.org/10.1016/j.apenergy.2016.08.192.
[45] Aspen Technology Inc. Aspen Physical Property Methods - Reference Manual 2019.
[46] Bailera M, Nakagaki T, Kataoka R. Extending the operating line methodology to consider shaft and preheating injections in blast furnaces. ISIJ Int. 2022;62:1–12. https://doi.org/10.2355/isijinternational.ISIJINT-2022-111.
[47] Peacey JG, Davbenport WG. The iron blast furnace. Theory and Practice 1979.
[48] Bailera M, Espatolero S, Lisbona P, Romeo LM. Power to gas-electrochemical industry hybrid systems: A case study. Appl. Energy 2017;202:435–46. https://doi.org/10.1016/j.apenergy.2017.05.177.
[49] Kumar Sahu R, Halder C, Sen PK. Optimization of top gas recycle blast furnace emissions with implications of downstream energy. Steel Res. Int. 2016;87:1190–202. https://doi.org/10.1002/srin.201500312.
[50] Marketwatch web page (HRC steel) 2022. https://www.marketwatch.com/investing/index/steel?countryCode=XX (accessed July 25, 2022).
[51] Subraveti SG, Rodriguez E, Ramirez Ramirez A, Roussanaly S. Is CCS really so expensive? An analysis of cascading costs and CO2 emissions reduction of industrial CCS implementation applied to a bridge. Environ. Sci. Tech. 2022. https://doi.org/10.2139/ssrn.4278030.
[52] IRENA 2022. https://www.irena.org/costs/Power-Generation-Costs (accessed May 10, 2022).

Renewable and Sustainable Energy Reviews 201 (2024) 114605

Contents lists available at ScienceDirect

Renewable and Sustainable Energy Reviews

journal homepage: www.elsevier.com/locate/rser

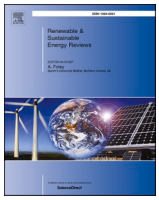

# Outline of all potential Power to Gas integrations in blast furnace ironmaking: A systematic review

Jorge Perpiñán *, Manuel Bailera, Begoña Peña

*Aragón Institute for Engineering Research (I3A), Energy and CO2. Escuela de Ingeniería y Arquitectura, Universidad de Zaragoza, María de Luna 3, 50018, Zaragoza, Spain*

A R T I C L E I N F O

*Keywords:*
Ironmaking
Power to gas
Decarbonisation
Technical comparison
Oxygen blast furnace
Systematic review

A B S T R A C T

This work presents the first systematic review analysis of potential Power to Gas integrations in blast furnace ironmaking. The primary objective of the paper is to evaluate the PtG technology implementation in both conventional air-blown and full oxygen blast furnaces, considering different BFG recycling routes (upper, shaft or tuyeres), and synthetic gases (SNG, H2 or syngas). Employing a systematic methodology, the paper compares all the studies using 14 Key Performance Indicators (KPI) and elaborates a discussion on the main findings and limitations, proposing areas for future research. PtG application enables air-blown blast furnaces to cut emissions to 1060 $kg_{CO2}/t_{HM}$. With PtG and top gas recycling, oxygen blast furnaces achieve a reduction to 747 $kg_{CO2}/t_{HM}$, and when combined with geological storage, the reduction further drops to 435 $kg_{CO2}/t_{HM}$. Additionally, the authors propose a novel PtG-ironmaking integration based on the findings of this paper.

Nomenclature

| Abbreviation | Meaning |
|---|---|
| AFT | Adiabatic Flame Temperature |
| ASU | Air Separation Unit |
| BF-BOF | Blast Furnace-Basic Oxygen Furnace |
| BFG | Blast Furnace Gas |
| BOFG | Basic Oxygen Furnace Gas |
| CC | Carbon Capture |
| CCUS | Carbon Capture Utilization and Storage |
| DRI | Direct Reduced Iron |
| HM | Hot Metal |
| I&S | Iron and Steel |
| IEA | International Energy Agency |
| PEM | Proton Exchange Membrane |
| PtG | Power to Gas |
| PCI | Pulverized Coal Injection |
| RA | Reducing agent |
| SNG | Synthetic Natural Gas |
| tHM | Ton of Hot Metal |
| tCS | Ton of Crude Steel |
| TGR | Top Gas Recycling |
| TRL | Technology Readiness Level |

## 1. Introduction

Iron and steel production is essential for modern society, providing a wide range of applications in construction, transportation, and manufacturing. However, due to the industry's heavy reliance on fossil fuels, it is also one of the largest emitters of greenhouse gases worldwide (1.8–2.0 $t_{CO2}/t_{steel}$), accounting for 7 % of global $CO_2$ emissions [1]. Reducing its carbon footprint is a significant challenge when aiming for the global climate change mitigation goals.

The blast furnace-basic oxygen furnace (BF-BOF) route is currently the dominant process for steel manufacturing, accounting for over 70 % of global production. The process starts with the preparation of raw materials (iron ore, coke, and limestone). The iron ore is first mined, then crushed into small pieces, and finally treated in the sinter strand. In sintering, iron ore fines are agglomerated with other fine materials (5–7 mm in size) by combusting coal, in order to obtain a 50 mm open-grained, consistent material with definite basicity optimal for the blast furnace [2]. Coke is made from coal in the coke ovens. Here, coal is heated to 1100 °C in an oxygen deficient atmosphere (carbonization process) to drive off the volatile products and leave a solid residue that mainly consists of carbon (i.e., coke). Coke is the most important raw material in blast furnaces since it is used to reduce the iron ore [3]. Lastly, limestone is calcined to obtain lime. Lime has different uses

* Corresponding author.
*E-mail addresses:* jorge.perpinan@unizar.es (J. Perpiñán), mbailera@unizar.es (M. Bailera), bpp@unizar.es (B. Peña).

https://doi.org/10.1016/j.rser.2024.114605
Received 14 June 2023; Received in revised form 8 March 2024; Accepted 24 May 2024
Available online 7 June 2024
1364-0321/© 2024 The Authors. Published by Elsevier Ltd. This is an open access article under the CC BY-NC-ND license (http://creativecommons.org/licenses/by-nc-nd/4.0/).

within the steel industry, such as binder in the production of sinter, desulfurizing agent in the blast furnace, slag forming component to remove impurities, and component to control melt chemistry to reduce the damage in furnace linings [4].

Once the raw materials are prepared, they are fed into the blast furnace at the top. The furnace is typically 34 m in height, 16 m in diameter, and lined with refractory materials [5,6]. At the lower part, hot air is blown into the furnace through tuyeres. The coke burns with the oxygen of the hot blast, thus providing the process with heat and CO-reducing gas (this gas reduces the iron oxides in counter-current while ascending). The molten iron is then tapped off from the bottom of the furnace and transported to a basic oxygen furnace (BOF) for further refining into steel. In the BOF, the carbon content of the molten iron is decreased by injecting pure oxygen, which oxidizes de carbon thus forming CO and $CO_2$. The heat released in this process is used to melt scrap, which is combined with the hot metal at the beginning of the BOF process. After the steel is refined, it is cast into various shapes and sizes, such as billets, slabs, or sheets, depending on the final application. The steel is then cooled and processed through various finishing techniques, such as rolling, cutting, and coating.

Despite the BF-BOF route has been optimized over the years to increase its efficiency and reduce its emissions, it still relies heavily on fossil fuels and is responsible for significant emissions of $CO_2$ and other greenhouse gases. To address the challenges posed by the BF-BOF process, alternative methods for steel production are being developed. One such method is the oxygen blast furnace (OBF), which uses pure oxygen instead of air to burn coke, reducing the amount of fuel required (lower emissions) and resulting in higher energy efficiency. Additionally, top gas recycling (TGR) can be used to further reduce emissions in the BF-BOF process. TGR involves the capture and recycling of the gases produced during the hot metal production, such as carbon monoxide and hydrogen, back into the process as reducing agent. This not only reduces emissions (by up to 40–55 % [7]) but also increases energy efficiency and can lead to cost savings.

Another promising technology that can contribute to decarbonizing the steel industry is power to gas (PtG) [8]. PtG technologies convert renewable electricity surplus into hydrogen, syngas or synthetic natural gas (SNG) using electrolysis and methanation processes. These gases can then be used as low-carbon fuels or feedstocks for the steel industry. PtG technologies can help to balance the intermittency of renewable electricity sources, to provide flexibility to the electricity grid, and to decarbonize the steel industry.

Few studies were found that apply power to gas technology in the blast furnace-basic oxygen furnace steel production route. Among them, only two papers have focused on substituting the fossil natural gas used in industry processes such as casting or reheating, rather than in the blast furnace. These studies injected synthetic gas into these specific processes, separate from the blast furnace. Rosenfeld [9] studied an electrolyzer and methanation systems coupled with a biomass gasification plant (105 $MW_{th}$), where the steel gases were used as the $CO_2$ source for methanation. Medved [10] studied different scenarios, including (i) methanation of all BFG and BOFG, (ii) substitution of fossil NG with BFG and BOFG methanation, and (iii) substitution of fossil NG with BOFG methanation, where the $H_2$ was produced in a PEM and a biomass gasification plant (100 $MW_{th}$).

A first approach of power to gas implemented in the blast furnace process was done by the Tokyo Institute of Technology, Japan. Throughout a series of studies [11–14], a novel process combining a nuclear HTGR (high-temperature gas-cooled reactor) with a SOEC electrolyser was proposed to reduce $CO_2$ into CO, which is later used to reduce the iron oxides. Hisashige et al. [15] performed an exergy analysis combining a PSR (Partial Smelting Reduction process) with top gas recycling, obtaining a maximum $CO_2$ emission decrease of 22 %.

Prior reviews in the field were overly broad, covering green and low-carbon ironmaking technologies [16], exclusively examining the impact of renewable gases without encompassing the entire Power to Gas chain [17,18], or investigating Power to X technologies within the I&S industry [8], rather than focusing specifically on Power to Gas in the blast furnace. Therefore, this review aims to fill that gap by summarizing information on this specific topic, presenting key findings, and suggesting future research directions.

This study outlines all the potential integrations of power to gas technology in blast furnace ironmaking. Firstly, it explains in detail different ways to implement the power to gas technology in both the conventional air-blown blast furnace and the full oxygen blast furnace, Section 3. These two options consider different BFG recycling routes (upper, shaft or tuyeres), and different synthetic gases (SNG, $H_2$ or syngas). Then, a systematic review is performed to find all the power to gas configurations studied in literature, Section 4. Finally, all the studies are compared using 14 Key Performance Indicators (KPI), Section 5. This work concludes with a discussion of the main findings and limitations, and proposes areas for future research, Section 6.

## 2. Methodology

### 2.1. Systematic review

To find the most relevant literature on Power to Gas integrations in blast furnace ironmaking, a systematic approach was implemented. Web of Science was selected as the search engine because of its advanced search capabilities and wide range of databases. The search is limited to studies presented in scientific journals and conferences included in the selected search engine. Two sets of words were used in the search (Table 1), the first one with terms related to blast furnaces, and the second one with terms related to Power to Gas. The search was done for the title, abstract and keywords, and returned a total of 78 entries, which were screened based on their abstract [19], and selected for examination when applying any type of Power to Gas on the blast furnace, leading a total of 14 articles.

Articles purely related to $CO_2$ emission reduction, fuel consumption reduction, methane production for sale or hydrogen production were not included in this analysis. Articles that does not recycle carbon through power to gas, or does not focus on the blast furnace, were also not considered.

### 2.2. Key performance indicators

The key performance indicators quantify the most important aspects that affect the overall performance of the system (Table 2). These serve to compare the different integrations of power to gas in blast furnace ironmaking. The first four KPIs are the fuel consumptions in the blast furnace (KPI01: coke; KPI02: pulverized coal; KPI03: total coal; and KPI04: synthetic gases). Characterizing the fuel consumption is essential as it affects both the economic and the environmental performance of the blast furnace. In the case of KPI03, Eq. (1) is used, where 1.33 kg of coking coal is typically required to produce 1 kg of coke [20].

$$KPI_{03} = Total\ coal\ consumption = PCI + Coke \times 1.33 \quad (1)$$

The KPI05 measures the amount of top gas that is recycled (at either tuyeres, shaft or upper part). Quantifying the gas recycled is important as it affects to the availability of fuel gas for self-consumption in the rest

**Table 1**
Search terms, number of hits returned and number of papers reviewed.

| Search term | Hits | Reviewed |
|---|---|---|
| (“Ironmaking” OR “steelmaking” OR “Iron and steel” OR “blast furnace” OR “steel industry”) | 325 | 14 |
| (“Power-to-Gas” OR “power to gas” OR “PtG” OR “power to methane” OR “synthetic natural gas” OR “power to H2″ OR “power to hydrogen” OR “PtH2″ OR “CO2 electrolysis” OR “power to syngas” OR “power-to-syngas” OR “H2 injection” OR “hydrogen injection” OR “methanation”) | | |

**Table 2**
Main KPIs for power to gas integrations in blast furnace ironmaking.

| KPI | Variable | Units |
|---|---|---|
| KPI01 | Coke rate | $kg_{Coke}/t_{HM}$ |
| KPI02 | PCI rate | $kg_{PCI}/t_{HM}$ |
| KPI03 | Total coal consumption (PCI + coking coal) | $kg_{Coal}/t_{HM}$ |
| KPI04 | Synthetic RA injected in BF (SNG, $H_2$, syngas) | $kg_{RA}/t_{HM}$ |
| KPI05 | Top gas recycled in BF | $kg_{TGR}/t_{HM}$ |
| KPI06 | Adiabatic Flame Temperature (AFT) | °C |
| KPI07 | $CO_2$ emissions (BF) | $kg_{CO2}/t_{HM}$ |
| KPI08 | $CO_2$ to geological storage | $kg_{CO2}/t_{HM}$ |
| KPI09 | Excess steel gases (sold or flared) | $MJ/t_{HM}$ |
| KPI10 | Energy Penalty | $MJ/kg_{CO2}$ |
| KPI11 | Electrolyser size | $MW/(t_{HM}/h)$ |
| KPI12 | $O_2$ produced in the ASU | $kg_{O2}/t_{HM}$ |
| KPI13 | $CO_2$ avoidance cost | $€/t_{CO2}$ |
| KPI14 | Specific implementation cost | $€/t_{HM}$ |

of the plant. It must be noted that when injecting top gas in the tuyeres or shaft (TGR), carbon capture is recommended in order to not inject $CO_2$. However, when injecting top gas in the upper part, raw BFG can be used since $CO_2$ has minor influence at this stage. The KPI06 considers the adiabatic flame temperature (AFT). This parameter is controlled to guarantee that it is 2000 °C or higher (technical constrain) [21]. The KPI07 and KPI08 are the $CO_2$ emissions exiting the blast furnace, and the $CO_2$ sent to geological storage, respectively. The former considers all $CO_{2\text{-eq}}$ out of the BF's limits, including the $CO_{2\text{-eq}}$ from the CO (assuming that it will be burned to $CO_2$ eventually) and the pure $CO_2$ for geological storage, but excluding the recycled $CO_{2\text{-eq}}$ through TGR and PtG, according to Fig. 1. The KPI09 quantifies the excess of fuel gases from the ironmaking processes, which could be sold (or should be flared). If this KPI is above 0, it means that there are enough steel gases to satisfy the energy requirements of the downstream processes (sintering, coke oven, power plant, etc.). However, if KPI09 is below 0, the ironmaking plant will not be self-sufficient in thermal energy consumption. For the calculation of KPI09, a power plant of 100 $MW_e$ and 36 % efficiency was assumed [22]. The KPI10 shows the energy penalty of the power to gas integration in blast furnace ironmaking, which is the additional energy consumed compared to the base case per kg of $CO_2$ avoided. This parameter is the basis for comparison between all the potential configurations and other technologies. The KPI11 is the maximum size of electrolysis that can be integrated (usually limited by the decrease in flame temperature, which is caused by the injection of synthetic gas). This value is given as a function of the size of the blast furnace, since scale-effects are not considered in the simulation. The KPI12 is the $O_2$ produced in the air separation unit to supply the different processes of the ironmaking plant (e.g., BF and BOF). When integrating power to gas, this value decreases thanks to taking advantage of the $O_2$ produced in the electrolyzer. If KPI12 drops to cero, it means that the ASU is no longer needed. Lastly, the KPI13 and KPI14 are the cost of integrating power to gas, per ton of $CO_2$ avoided (Eq. (2)) and per ton of hot metal produced (Eq. (3)), respectively.

$$CO_2\ avoidance\ cost = \frac{\left(\frac{Capex}{Loan\ amortization} + Opex - Incomes\right)\cdot 10^6}{CO_2\ avoided \cdot Operating\ hours} \quad \left[\frac{€}{t_{CO_2}}\right] \tag{2}$$

$$Specific\ Implementation\ cost = \frac{\left(\frac{Capex}{Loan\ amortization} + Opex - Incomes\right)\cdot 10^6}{Iron\ Production \cdot Operating\ hours} \quad \left[\frac{€}{t_{HM}}\right] \tag{3}$$

## 3. Outline of all potential power to gas integrations in blast furnace ironmaking

The outline of all potential integrations is the result of combining the different approaches that can be follow when integrating power to gas, in terms of (i) combustion regime, (ii) top gas recirculation, (iii) renewable gas produced, and (iv) location of the injection of the renewable gas:

- Combustion regime (2 options):
  - o Air-blown
  - o Oxy-fuel
- Type of top gas recirculation (8 options, see Fig. 2A):
  - o No recirculation
  - o Single, located at
    - Tuyeres
    - Shaft
    - Upper zone
  - o Double, located at
    - Tuyeres and shaft
    - Tuyeres and upper zone
    - Shaft and upper zone
  - o Triple, located at
    - Tuyeres, shaft and upper zone
- Type of renewable gas produced (5 options, see Fig. 2B):
  - o Synthetic natural gas from the methanation of
    - Pure $CO_2$ from amine scrubbing
    - Sweet gas from amine scrubbing
    - Blast furnace gas
  - o Hydrogen from electrolysis
  - o Syngas from $CO_2$ electrolysis
- Injection location of the renewable gas (3 options):

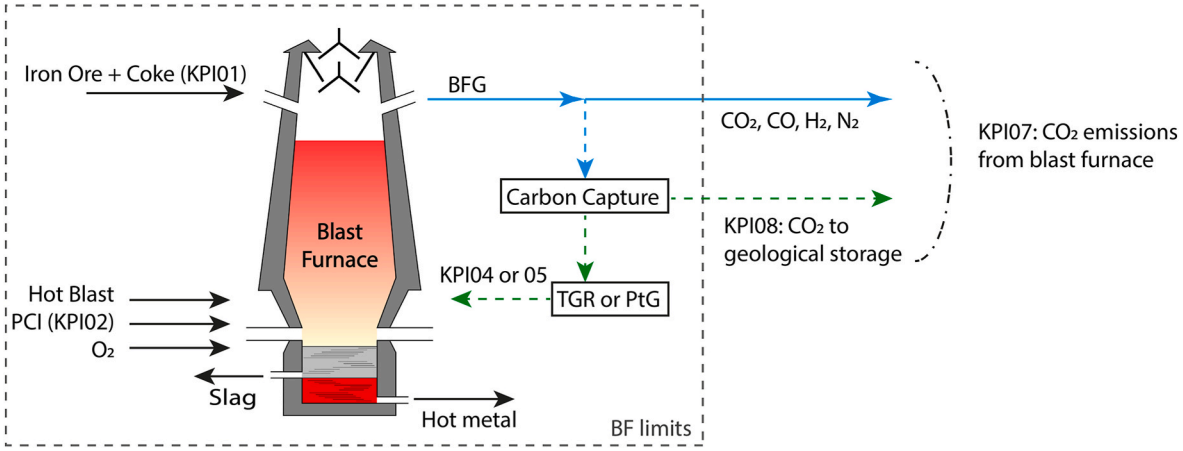


**Fig. 1.** Simplified process flow diagram of a blast furnace with top gas recycling (or power to gas), showing some of the KPIs considered for this analysis (Table 2).

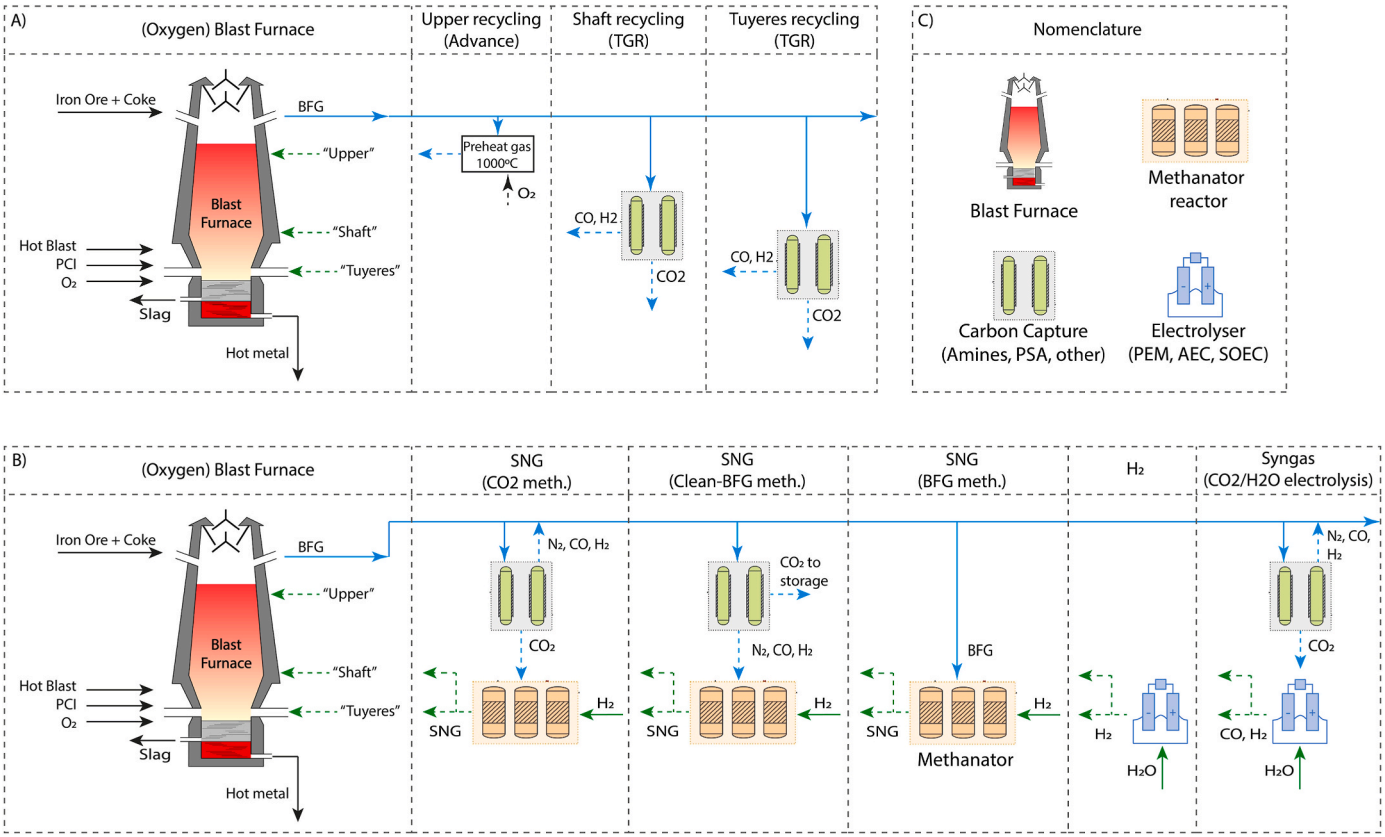


**Fig. 2.** Summary of the different options for blast furnace ironmaking when integrating power to gas, in terms of A) gas recycling, and B) renewable gas injection. Nomenclature appears in C).

- o Tuyeres
- o Shaft
- o Tuyeres and shaft

Considering all the options, the entire outline gathers 240 integration configurations (2 regimes × 8 top gas recyclings × 5 renewable gases × 3 injection locations). Table 3 summarises all these possible configurations, indicating the configurations that were already studied in literature, and identifying the configurations that are not worth studying because of the expected low performance. The latter are those that end up injecting large $N_2$ contents in the blast furnace, leading to remarkable drops in the adiabatic flame temperature and low fossil fuel replacement ratios, with the additional problem of the nitrogen build-up [23]. This happens under air-blown regimes when the top gas is recycled or when methanation consumes blast furnace gas without prior separation. Using oxy-fuel regimes prevents these problems, since the $N_2$ concentration of the BFG drops to 1 %–2 %. Moreover, the recirculation of $CO_2$ is not recommended for the same reasons. This may occur if methanation is carried out under sub-stiochiometric ratios ($H_2$:$CO_2$ < 4) [24], if $CO_2$ electrolysis has low conversion [6], or if top gas recycling is perfomed without prior carbon capture to reject the $CO_2$ from the BFG [25] (please note that none of these 3 possibilities are considered in the outline).

For many of the integrations presented in Table 3, readers may consider additional options, such as:

- Technology for $H_2$ production:
  - o PEM
  - o Alkaline
  - o SOEC
  - o Biomass gasification
- Fossil fuel replaced by the renewable gas:
  - o Coke
  - o Coal
- Temperature of the $O_2$ and renewable gases before injection:
  - o From 25 °C to 1250 °C
- Source of the electricity (and its price):
  - o Renewable
  - o Fossil
- Carbon capture technology:
  - o Amine scrubbing
  - o Calcium looping
  - o PSA
  - o Other

These are just a few examples of the differences that can be found when analysing a specific configuration, showing the vast knowledge gap, even for those cells of Table 3 that were already studied in literature. However, we do not deelve into these options, as the total outline would increase to more than 15,000 possibilities of integration. The comparison and discussion of the following sections is limited to those aspects that really brings innovation to the process. Still, some comments are worth to mention regarding these additional options.

Regarding the technology for renewable $H_2$ production, the most extended technologies are PEM and Alkaline electrolysis, but it can also be obtained from the gasification/pyrolysis of biomass. The main limitation of biomass is the availability of the resource, since power to gas requires large quantities of hydrogen. Another problem might be the presence of impurities in the $H_2$ or syngas obtained from the biomass, which could damage the methanation catalyst. An alternative to $H_2$ is the utilization of CO as reducing agent, obtained from the electrolysis of $CO_2$ supplied with renewable electricity. The limitation in this case is the

**Table 3**
Summary of the outline of all potential power to gas integrations in blast furnace ironmaking. The type of renewable gas produced is denoted by A (SNG from pure $CO_2$), B (SNG from sweet gas), C (SNG from BFG), D ($H_2$), and E (Syngas from $CO_2$ electrolysis). The configurations not recommended are marked with *. References are included for the configurations studied in literature.

| Combustion regime: Air-blown | | | |
|---|---|---|---|
| Type of top gas recirculation | Injection location of the renewable gas: | | |
| | Tuyeres | Shaft | Tuyeres & Shaft |
| No recirculation | A [20,26], B* [26], C* [26], D [26–28], E [6,29] | A, B*, C*, D, E | A, B*, C*, D, E |
| Single | | | |
| Tuyeres | A*, B*, C*, D*, E* | A*, B*, C*, D*, E* | A*, B*, C*, D*, E* |
| Shaft | A*, B*, C*, D*, E* | A*, B*, C*, D*, E* | A*, B*, C*, D*, E* [30] |
| Upper | A*, B*, C*, D*, E* | A*, B*, C*, D*, E* | A*, B*, C*, D*, E* |
| Double | | | |
| Tuyeres & shaft | A*, B*, C*, D*, E* | A*, B*, C*, D*, E* | A*, B*, C*, D*, E* |
| Tuyeres & upper | A*, B*, C*, D*, E* | A*, B*, C*, D*, E* | A*, B*, C*, D*, E* |
| Shaft & upper | A*, B*, C*, D*, E* | A*, B*, C*, D*, E* | A*, B*, C*, D*, E* |
| Triple | | | |
| Tuyeres & shaft & upper | A*, B*, C*, D*, E* | A*, B*, C*, D*, E* | A*, B*, C*, D*, E* |
| Combustion regime: Oxy-fuel | | | |
| Type of top gas recirculation | Injection location of the renewable gas: | | |
| | Tuyeres | Shaft | Tuyeres & Shaft |
| No recirculation | A, B, C, D, E | A, B, C, D, E | A, B, C, D, E |
| Single | | | |
| Tuyeres | A [26,31], B [26], C [25,26], D [26], E | A, B, C, D, E | A, B, C, D, E |
| Shaft | A, B, C, D, E | A, B, C, D, E | A, B, C, D, E |
| Upper | A [32], B, C [24], D [24], E | A, B, C, D, E | A, B, C, D, E |
| Double | | | |
| Tuyeres & shaft | A, B, C, D, E | A, B, C, D, E | A, B, C, D, E |
| Tuyeres & upper | A [33], B, C, D, E | A, B, C, D, E | A, B, C, D, E |
| Shaft & upper | A, B, C, D, E | A, B, C, D, E | A, B, C, D, E |
| Triple | | | |
| Tuyeres & shaft & upper | A, B, C, D, E | A, B, C, D, E | A, B, C, D, E |

high electricity consumption, the low TRL (5–6) and the limited $CO_2$ conversion (60 %–70 % [6,29]). Syngas production with low $CO_2$ conversion ratios leads to the direct injection of $CO_2$ into the blast furnace's tuyeres, what cools the adiabatic flame temperature rapidly [24]. Authors recommend in descending order of priority (i) the use of biomass as a hydrogen/syngas source when available, for direct injection (no methanation); (ii) the use of SOEC for $CO_2$ electrolysis coupled with a methanation stage (to fully convert the unreacted $CO_2$) if high TRL is reached; (iii) the use of a PEM/Alkaline electrolyser, for $H_2$ direct injection or SNG production.

In terms of fossil fuel replacement, the substitution ratio of coal is usually greater than for coke, so coal replacement allows injecting larger amounts of reducing agent. This leads to greater emission reductions and lower energy penalties [26]. Additionally, the temperature at which the oxygen and reducing gases are preheated affects to the amount of gas that can be injected. The higher the injection temperature, the higher the adiabatic flame temperature, and the greater the amount of reducing agent that can be used [32]. For instance, the ULCOS project injects the top gas recycled at 1250 °C [34]. Regarding carbon capture, the process is typically expensive and energy-consuming, independently of the technology chosen. Nevertheless, synergies are found in the case of amines, whose energy needs can be supplied with the exothermal heat from methanation [20]. Therefore, if carbon capture is required for the proper integration of power to gas, amine scrubbing should be chosen. Moreover, putting the cost in perspective, the capital expenditure of carbon capture is low compared with that of the electrolyser or cost of retrofitting a blast furnace. Therefore, despite there are a few configurations that do not need a carbon capture stage (e.g., those that use $H_2$, or that directly methanize the BFG), these should not be necessarily prioritized since they might not offer a significant advantage in terms of $CO_2$ avoidance or costs.

## 4. Review on power to gas integrations in blast furnace ironmaking

After applying the methodology of systematic review explained before, and classifying the different integrations according to the proposed outline, 14 different scientific papers were found dealing with the implementation of power to gas technology in the iron and steel industry (Table 4). These papers are summarized in the following subsections, distinguishing between air-blown and oxygen blast furnaces.

### 4.1. Power to gas integrations in air-blown blast furnaces

Six power to gas configurations were studied in literature for air-blown blast furnaces (Fig. 3). According to the outline, three of these integrations are not recommended because they recirculate large amounts of $N_2$ into the furnace. These are:

- No TGR, with SNG (from sweet gas) injected in tuyeres: Bailera et al. [26] studied four configurations within the air-blown blast furnace without recycling, including SNG production with $CO_2$ methanation, sweet BFG methanation, BFG methanation, and $H_2$ production as a reducing agent injected in the tuyeres. They focused on the blast furnace modelling and the influence of the SNG mass flow rate when replacing coal or coke, analysing up to 17 different KPIs as a function of the electrolysis power capacity (MW/($t_{HM}$/h)). For the case of

**Table 4**
Summary of the integration options for power to gas in ironmaking that were studied in literature, classified according to the outline of Table 3.

| | Air-blown blast furnace | Oxygen blast furnace |
|---|---|---|
| Not recommended integrations | 3 out of 111 | n/a |
| Recommended integrations | 3 out of 9 | 8 out of 120 |
| Total | 6 out of 120 | 8 out of 120 |

**Table 5**
Main KPIs for reviewed PtG integrations in blast furnaces (KPI definition in Table 2). Ref: Typical reference values.

| Combustion regime | Renewable gas | Type of top gas recirculation | KPI01 | KPI02 | KPI03 | KPI04 | KPI05 | KPI06 | KPI07 | KPI08 | KPI09 | KPI10 | KPI11 | KPI12 | KPI13 | KPI14 | Ref. |
|---|---|---|---|---|---|---|---|---|---|---|---|---|---|---|---|---|---|
| | | | $kg_{Coke}/t_{HM}$ | $kg_{PCI}/t_{HM}$ | $kg_{Coal}/t_{HM}$ | $kg_{RA}/t_{HM}$ | $kg_{TGR}/t_{HM}$ | °C | $kg_{CO2}/t_{HM}$ | $kg_{CO2}/t_{HM}$ | $MJ/t_{HM}$ | $MJ/kg_{CO2}$ | $MW/(t_{HM}/h)$ | $kg_{O2}/t_{HM}$ | $€/t_{CO2}$ | $€/t_{HM}$ | – |
| Air | – | No recirculation | 289–332 | 150–200 | 534–641 | 0 | 0 | 2258 | 1300–1400 | 0 | 2400–2700 | – | – | 87–95 | – | – | Ref. |
| Air | SNG ($CO_2$) | No recirculation | 332 | 88.8 | 531 | 53.6 | 0 | 2000 | 1187 | 0 | 3278 | 17.8 | 1.81 | 0 | 283 | 52 | [20] |
| | | | 289 | 115 | 500 | 65.2 | 0 | 2000 | 1100 | 0 | 3467 | 19.8 | 1.59 | 0 | – | – | [26] |
| Air | SNG (sweet gas) | No recirculation | 289 | 157 | 541 | 140 | 0 | 2000 | 1210 | 55 | 2567 | 12.8 | 0.61 | 0 | – | – | [26] |
| Air | SNG (BFG) | No recirculation | 289 | 141 | 526 | 133 | 0 | 2000 | 1190 | 0 | 3067 | 14.7 | 0.86 | 0 | – | – | [26] |
| Air | $H_2$ | No recirculation | 289 | 103 | 488 | 33.4 | 0 | 2000 | 1060 | 0 | 3517 | 18.5 | 1.67 | 0 | – | – | [26] |
| | | | 390 | 0 | 518 | 27.5 | 0 | 2150 | 1063 | 0 | – | – | 1.58 | 0 | – | – | [27] |
| | | | 327 | 112 | 546 | 20 | 0 | 2000 | 1182 | 0 | – | – | 0.88 | – | – | – | [28] |
| Air | Syngas | No recirculation | 288 | 85 | 467 | 140 | 0 | – | 1238 | 0 | – | – | – | – | – | – | [6] |
| | | | 359 | 101 | 579 | 89 | 0 | – | 1320 | 0 | – | 37.9 | 0.22 | – | – | – | [29] |
| Air | Syngas | Shaft recycling | 275 | 137 | 503 | 188 | 91 | – | 1129 | 216 | 3523 | – | 2.22 | 58 | – | – | [30] |
| Oxy-fuel | – | Tuyeres recycling | 150–367 | 0–400 | 470–655 | 0 | 449–950 | 2000–2400 | 868–1180 | 300–700 | −3300–767 | – | – | 250–350 | – | – | Ref. |
| Oxy-fuel | SNG ($CO_2$) | Tuyeres recycling | 235 | 120 | 432 | 61.5 | 408 | 2000 | 925 | 215 | 1267 | 17.8 | 1.50 | 100 | – | – | [26] |
| | | | 261 | 155 | 502 | 22 | 600 | 2014 | 1067 | 378 | – | 17.9 | 0.54 | 253 | – | – | [31] |
| Oxy-fuel | SNG (sweet gas) | Tuyeres recycling | 235 | 115 | 427 | 62.9 | 414 | 2000 | 925 | 490 | 267 | 10.0 | 0.98 | 180 | – | – | [26] |
| Oxy-fuel | SNG (BFG) | Tuyeres recycling | 235 | 115 | 427 | 62.2 | 411 | 2000 | 910 | 390 | 1057 | 12.5 | 1.18 | 150 | – | – | [26] |
| | | | 370 | 0 | 492 | 65 | 1022 | – | 1250 | 0 | 470 | 34.0 | 1.35 | 180 | – | – | [25] |
| Oxy-fuel | $H_2$ | Tuyeres recycling | 235 | 111 | 423 | 24.4 | 321 | 2000 | 905 | 340 | 887 | 13.6 | 1.22 | 90 | – | – | [26] |
| Oxy-fuel | SNG ($CO_2$) | Upper recycling | 279 | 0 | 370 | 192 | 205 | 2000 | 738 | 0 | 4470 | 17.5 | 3.96 | 0 | 352 | 233 | [32] |
| Oxy-fuel | SNG (BFG) | Upper recycling | 280 | 0 | 372 | 202 | 205 | 2000 | 747 | 0 | 1828 | 13.8 | 3.03 | 0 | 260 | 171 | [24] |
| Oxy-fuel | $H_2$ | Upper recycling | 307 | 0 | 408 | 69 | 205 | 2000 | 833 | 0 | 4542 | 14.0 | 2.90 | 0 | 245 | 136 | [24] |
| Oxy-fuel | SNG ($CO_2$) | Tuyeres & upper | 300 | 0 | 399 | 113 | 270&205 | 2000 | 811 | 0 | 1143 | 12.0 | 2.32 | 63 | 216 | 130 | [33] |

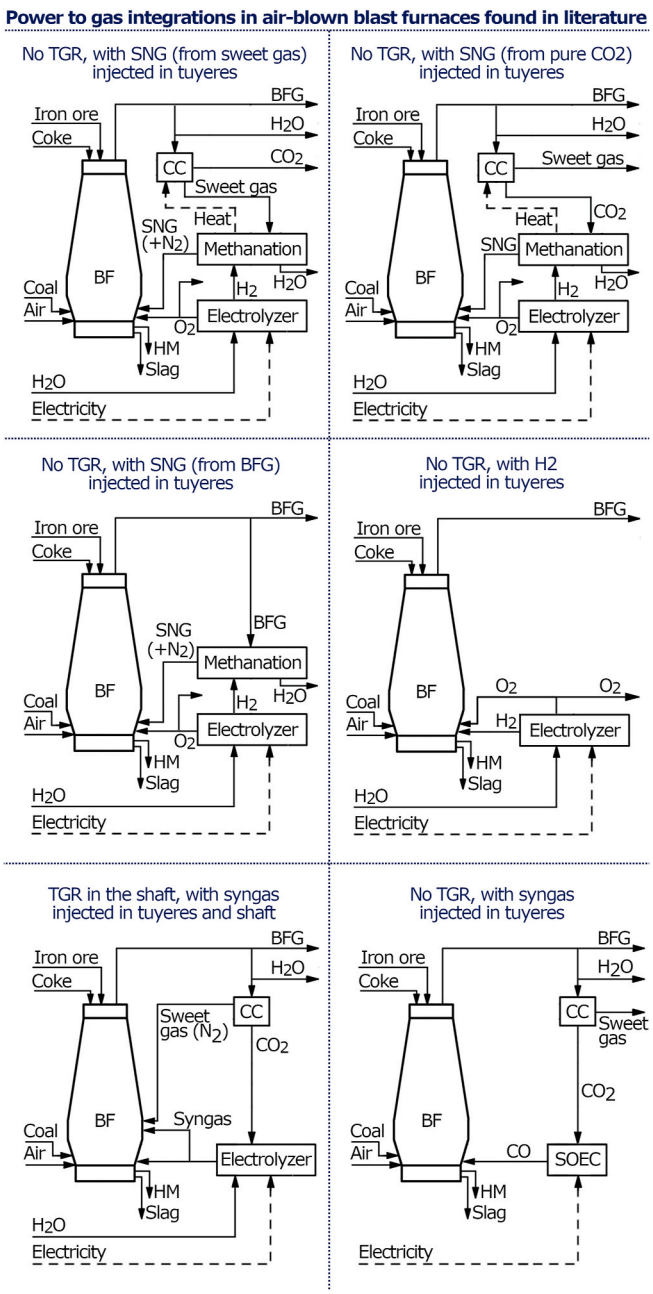


**Fig. 3.** Process flow diagrams of power to gas integrations in air-blown blast furnaces that have been studied in literature. The left column corresponds to the no recommended configurations because of the recirculation of large amounts of $N_2$ into the furnace.

sweet BFG methanation, they injected 140 $kg_{SNG}/t_{HM}$ at 900 °C, obtaining a total coal consumption of 541 $kg_{Coal}/t_{HM}$ and emitting 1210 $kg_{CO2}/t_{HM}$ in the blast furnace, see Table 5.

- No TGR, with SNG (from BFG) injected in tuyeres: As stated above, Bailera et al. [26] also analysed this specific configuration, obtaining a total coal consumption of 526 $kg_{Coal}/t_{HM}$ and emitting 1190 $kg_{CO2}/t_{HM}$.
- TGR in the shaft, with syngas injected in tuyeres and shaft: Hu et al. [30] assessed the opportunities to reduce $CO_2$ emissions from a conventional blast furnace by means of carbon capture, TGR (shaft injection) and syngas production with a SOEC electrolyser (tuyeres and shaft injection). They studied different cases, varying the proportion of BFG treated in $CO_2$ capture (from 85 to 100 %), the TGR ratio (from 0 to 15 %), and the $H_2$/CO selectivity of the SOEC (from 0 to 60 %). The optimum configuration to minimise $CO_2$ emissions from the BF was for a 100 % BFG capture, a 15 % of TGR ratio and a 60 % of SOEC selectivity. They obtained 1129 $kg_{CO2}/t_{HM}$ of $CO_2$ emissions in the blast furnace, of which up to 216.2 $kg_{CO2}/t_{HM}$ can be sent to storage.

The other three studied configurations, which not recirculate $N_2$ into the furnace, are:

- No TGR, with SNG (from pure $CO_2$) injected in tuyeres: Perpiñán et al. [20] explored a power to SNG integration ($CO_2$ methanation) in a conventional BF without TGR. They focused on the modelling of the complete iron and steel plant (including sintering, coke oven, power plant, etc.) and the influence of the SNG injection temperature, providing some Sankey diagrams (carbon mole flow, $kg_{CO2\text{-}eq}/t_{HM}$; energy flow, $MJ/t_{HM}$). Additionally, they performed a pinch analysis for the heat integration of the methanation exothermic heat and the amines endothermic heat demand, resulting in full coverage of the amine steam demand. An injection of 53.6 $kg_{SNG}/t_{HM}$ at 700 °C resulted in total coal consumption of 530.8 $kg_{Coal}/t_{HM}$ and total BF emissions of 1187 $kg_{CO2}/t_{HM}$. Perpiñán et al. [20] also obtained specific carbon avoidance costs of 283 €/$t_{CO2}$ and 52 €/$t_{HM}$. Bailera et al. [26] also studied this configuration, injecting the SNG at 900 °C and studying the replacement of coke or coal, achieving a total coal consumption of 500 $kg_{Coal}/t_{HM}$ and emitting 1100 $kg_{CO2}/t_{HM}$.
- No TGR, with $H_2$ injected in tuyeres: Yilmaz et al. [27] assessed the influence of hydrogen injection in a conventional blast furnace, using an alkaline electrolyser. They injected 27.5 $kg_{H2}/t_{HM}$ at 1200 °C, emitting 1063 $kg_{CO2}/t_{HM}$. However, the increase in energy consumption derived from hydrogen preheating led to an energy deficit of 109.7 $MJ/t_{HM}$. Kim et al. [28] analysed a conventional blast furnace with hydrogen injection from a SOEC electrolyser. They performed a techno-economic analysis, concluding that the optimum injection rate was 20 $kg_{H2}/t_{HM}$, leading to a specific blast furnace emission of 1182 $kg_{CO2}/t_{HM}$. Production costs of 8.8 US$/$kg_{H2}$ are calculated for the year 2021 but are expected to decrease to 1.4–4.0 US$/$kg_{H2}$ by 2050. Bailera et al. [26] injected preheated hydrogen in the tuyeres (33.4 $kg_{H2}/t_{HM}$ at 900 °C), emitting 1060 $kg_{CO2}/t_{HM}$. Among the four configurations studied by Bailera et al. [26] ($CO_2$ methanation, sweet BFG methanation, BFG methanation, and $H_2$) the $H_2$ configuration was the less contaminant one, but had a higher energy penalty than other SNG configurations, due to a larger electrolyser, see Table 5.
- No TGR, with syngas injected in tuyeres: Suzuki et al. [6] evaluated a power to syngas system integrated with a conventional blast furnace through the iACRES system (Active Carbon Recycling Energy System in ironmaking). Three different case studies were analysed: (i) SOEC with CCS, (ii) SOEC without CCS and (iii) reverse water-gas shift (RWGS) reactor with CCS. The heat and electricity source of the iACRES system is a high-temperature gas-cooled reactor. They concluded that the second case study was the one with lower emissions in the blast furnace, with 1238 $kg_{CO2}/t_{HM}$, injecting up to 140 $kg_{Syngas}/t_{HM}$, see Table 5. Hayashi et al. [29] studied the injection of syngas in a conventional blast furnace with two different syngas production systems: SOEC system, and RWGS with $H_2$ produced by the iodine-sulphur system. A high-temperature gas-cooled reactor was used in both cases as an energy source. They concluded that the latter system obtained greater $CO_2$ emission reduction, due to the excess $H_2$ not consumed in the RWGS that was used as a reducing agent in the BF. However, the former system (SOEC system) was able to obtain a higher $CO_2$ emission reduction per unit of heat, 5 $kg_{CO2}/MJ_{th}$, compared with that of the first system (9 $kg_{CO2}/MJ_{th}$).

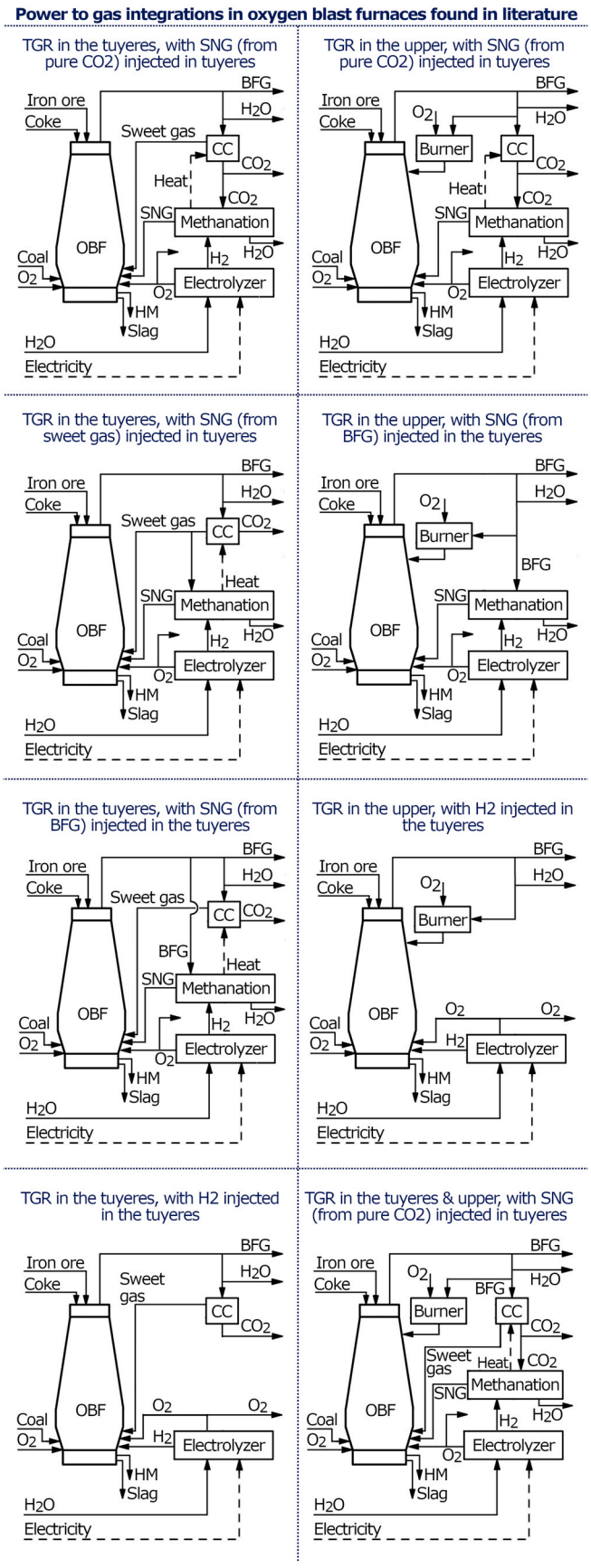


**Fig. 4.** Process flow diagrams of power to gas integrations in oxygen blast furnaces that have been studied in literature.

### 4.2. Power to gas integrations in oxygen blast furnaces

Eight power to gas configurations were studied in literature for oxygen blast furnaces (Fig. 4). This represents only the 7 % of the whole outline for the oxy-fuel regime (120 configurations). The work done by each researcher on the corresponding integrations is:

- TGR in the tuyeres, with SNG (from pure $CO_2$) injected in tuyeres: Bailera et al. revisited the Rist diagram [31], considering multiple injectants, and analysing with great detail for the first time the OBF-PtG integration under the operating diagram methodology. They provided six full data sets of different blast furnaces operations, stating temperatures, compositions and heats of the most relevant operating parameters. Bailera et al. completed this work by extending the operating line [35], to include shaft and preheating injections, and non-continuous oxidation profiles (presence of $H_2O$ and $CO_2$ in the injected gases). Bailera et al. [26] studied four configurations within the oxygen blast furnace with top gas recycling (tuyeres), including SNG production with $CO_2$ methanation, sweet BFG methanation, BFG methanation, and $H_2$ production as a reducing agent. They obtained similar results in the four configurations. For the case of pure $CO_2$ methanation, they injected 62 $kg_{SNG}/t_{HM}$ at 900 °C, obtaining a total coal consumption of 432 $kg_{Coal}/t_{HM}$ and emitting 925 $kg_{CO2}/t_{HM}$ in the blast furnace, see Table 5.

- TGR in the tuyeres, with SNG (from sweet gas) injected in tuyeres: As stated above, Bailera et al. [26] also analysed this specific configuration, obtaining a total coal consumption of 427 $kg_{Coal}/t_{HM}$ and emitting 925 $kg_{CO2}/t_{HM}$. This configuration allows for 490 $kg_{CO2}/t_{HM}$ to be sent to storage.
- TGR in the tuyeres, with SNG (from BFG) injected in the tuyeres: A first approach to an oxygen blast furnace-power to gas integration was developed by Perpiñán et al. [25], by using overall energy and mass balances. They considered BFG methanation and recirculation of BFG (tuyeres) without carbon capture. However, this study did not consider the adiabatic flame temperature and the endothermic effect of injecting $CO_2$ in the tuyeres, resulting in large amounts of BFG recirculated but low emission reductions, see Table 5. Perpiñán et al. [25] also studied BFG methanation with the coke oven gas as a hydrogen source, eliminating the need for an electrolyser. They obtained similar environmental results but great reductions in the energy penalty (from 34 to 4.9 MJ/$kg_{CO2}$). Bailera et al. [26] also studied this configuration, injecting the SNG at 900 °C and studying the replacement of coke or coal, achieving a total coal consumption of 427 $kg_{Coal}/t_{HM}$ and emitting 910 $kg_{CO2}/t_{HM}$.
- TGR in the tuyeres, with $H_2$ injected in the tuyeres: Bailera et al. [26] injected preheated hydrogen in the tuyeres (33.4 $kg_{H2}/t_{HM}$ at 900 °C), emitting 905 $kg_{CO2}/t_{HM}$, see Table 5.
- TGR in the upper, with SNG (from pure $CO_2$) injected in tuyeres: Perpiñán et al. [32] studied the influence of the oxygen injection (enrichment, %; temperature °C), on an advanced oxygen blast furnace when integrating a power to SNG system ($CO_2$ methanation). They concluded that higher enrichments and higher oxygen temperature (up to 1200 °C) led to an increase in the amount of SNG injected (191.5 $kg_{SNG}/t_{HM}$), which led to lower coal consumption and lower $CO_2$ emissions, see Table 5. With this configuration, Perpiñán concluded that the oxygen by-produced in the electrolyser could supply the oxygen demand, eliminating the need for the air separation unit. Specific costs of 352 €/$t_{CO2}$ and 233 €/$t_{HM}$ were achieved.
- TGR in the upper, with SNG (from BFG) injected in the tuyeres: Perpiñán et al. [24] performed a sensitivity analysis on an advanced oxygen blast furnace (upper recycling) by varying the $H_2$:$CO_2$ ratio of the BFG methanation stage. They studied from a ratio of 2.5 (insufficient $H_2$, direct $CO_2$ injection in the BF), through a ratio of 4 (SNG

with 95 % $CH_4$) to an infinite ratio (pure $H_2$ injection). For the case of SNG injection, the blast furnace emitted 747 $kg_{CO2}/t_{HM}$, see Table 5.

- TGR in the upper, with $H_2$ injected in the tuyeres: As stated above, Perpiñán et al. [24] also analysed this specific configuration, obtaining a total coal consumption of 408 $kg_{Coal}/t_{HM}$ and emitting 833 $kg_{CO2}/t_{HM}$. Similar results between SNG injection and $H_2$ injection were obtained, with better environmental results for the former, and improved economic results for the latter, see Table 5.
- TGR in the tuyeres & upper, with SNG (from pure $CO_2$) injected in tuyeres: Power to SNG integration ($CO_2$ methanation) in an advanced oxygen blast furnace was studied by Perpiñán et al. [33], analysing the influence of the TGR in this system. In this configuration, the preheating gas mass flow rate (upper recycling) was conditioned by the top gas temperature (150 °C), and a carbon capture stage fed the methanation stage while producing the top gas recycling (tuyeres), so no geological storage was needed. They injected simultaneously 299.9 $kg_{Coke}/t_{HM}$, 113 $kg_{SNG}/t_{HM}$, 207 $kg_{TGR}/t_{HM}$ (tuyeres) and 205 $kg_{PreheatingGas}/t_{HM}$ (upper) in the blast furnace, achieving a total $CO_2$ emission in the BF of 811 $kg_{CO2}/t_{HM}$.

## 5. Discussion and comparison of the different power to gas integrations

In this section, the 14 power to gas integrations found in literature (i.e., those summarized in the previous section) are compared using the 14 key performance indicators of Table 2. In order to provide a fair comparison, reference cases for the conventional blast furnace and the oxygen blast furnace with TGR are also included in the comparison.

The first aspect to discuss is the consumption of fuel and reducing agents in the blast furnace. This includes KPI01 (coke), KPI02 (pulverized coal), KPI03 (total coal), KPI04 (synthetic reducing agent: SNG, $H_2$ or syngas) and KPI05 (top gas recycling), which are presented in Fig. 5. The total coal consumption is 18 % lower in average for oxygen blast furnaces than for air-blown furnaces. Moreover, the total coal consumption decreases more sharply for upper recycling configurations, in comparison with tuyere recycling, thanks to the higher amount of synthetic gas that can be injected (69–202 $kg/t_{HM}$, instead of 22–63 $kg/t_{HM}$). The configuration that reaches the lower total coal consumption, 370 $kg/t_{HM}$, is the advanced oxygen blast furnace with SNG injection, from either $CO_2$ methanation or BFG methanation.

The adiabatic flame temperature (KPI06) is a technical limitation that influences the amount of reducing agent that can be injected through the tuyeres. These reducing agents decrease the adiabatic flame temperature, which should be above 2000 °C. Other injections such as shaft or upper does not influence this parameter, but are affected by other parameters like the thermal reserve zone or the volumetric flow rate through the blast furnace. Most of the studied reviewed considered this limitation, keeping this temperature between 2000 °C and 2100 °C. Only a few studies, especially those that are a first approach, did not consider this limitation, see Table 5. However further research is needed in this regard, due to the lack of studies assessing this issue.

Regarding the environmental performance, Fig. 6 presents the total BF's $CO_2$ emissions (KPI07) and the pure stream of $CO_2$ that can be sent to geological storage (KPI08, see Fig. 1). The most significant $CO_2$ savings in air-blown blast furnaces reach 1060–1100 $kg_{CO2}/t_{HM}$, which take place when injecting hydrogen or synthetic natural gas (from $CO_2$ methanation). This is quite limited since specific emissions remain always above 1000 $kg_{CO2}/t_{HM}$. Further $CO_2$ reductions are found for oxygen blast furnaces. In that sense, if geological storage is not an option, upper recycling with SNG injections provides the best results, 738–747 $kg_{CO2}/t_{HM}$, as it happened for KPI03 (total coal consumption). If geological storage is an option, examining the net $CO_2$ emissions becomes viable ($CO_2$ emissions of the BF minus the pure $CO_2$ sent to storage). Under this scenario, the best configuration is an oxygen blast furnace with top gas recycling (tuyeres) integrated with the methanation of sweet gas, with specific emissions of 435 $kg_{CO2}/t_{HM}$. Only those configurations that have a carbon capture stage and do not use the $CO_2$ for synthetic gas production are able to send pure $CO_2$ to storage (typically between 215 $kg_{CO2}/t_{HM}$ and 490 $kg_{CO2}/t_{HM}$).

In terms of energy, Fig. 7 quantifies the energy content of the steel gases that remain unused (KPI09) and the energy penalty of the power to gas integration (KPI10). The energy available in the form of steel gases

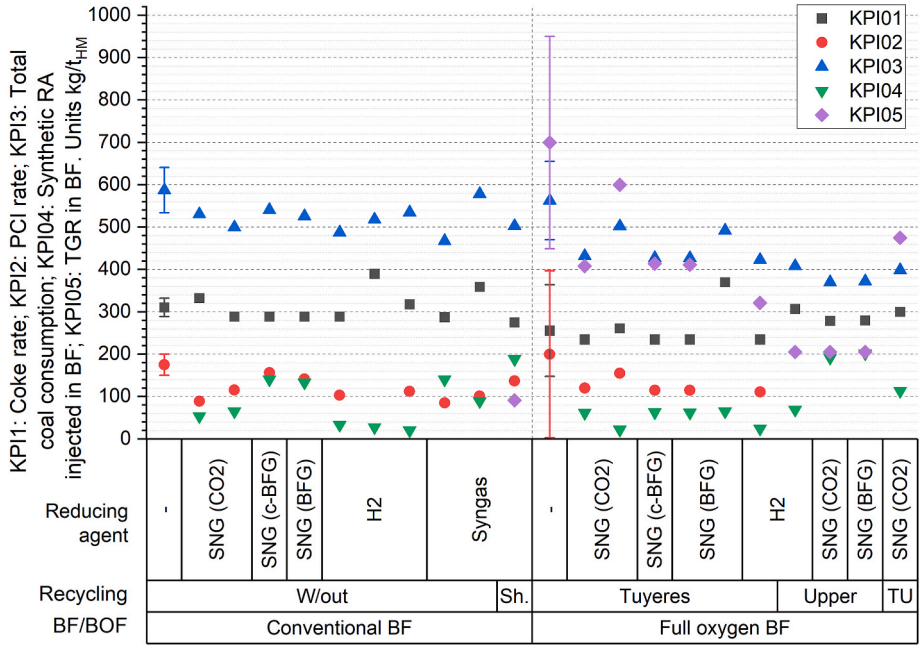


**Fig. 5.** KPI01: Coke rate ($kg_{Coke}/t_{HM}$), KPI02: PCI rate ($kg_{PCI}/t_{HM}$), KPI03: Total coal consumption (PCI + coking coal) ($kg_{Coal}/t_{HM}$), KPI04: Synthetic RA injected in BF (SNG, $H_2$, syngas) ($kg_{RA}/t_{HM}$) and KPI05: TGR in BF ($kg_{TGR}/t_{HM}$), as a function of the reducing agent production, the BFG recycling and the conventional or oxygen blast furnace. See Table 5. Nomenclature: SNG ($CO_2$) is synthetic natural gas with $CO_2$ methanation; SNG (c-BFG) is with clean-BFG methanation; SNG (BFG) is with BFG methanation; W/out is no BFG recycling; Sh is BFG recirculation (TGR) through the shaft; Tuyeres is BFG recirculation (TGR) through the tuyeres; Upper is BFG recirculation (Advanced) through the upper part of the furnace and TU is BFG recirculation through the tuyeres (TGR) and the upper part (Advanced).

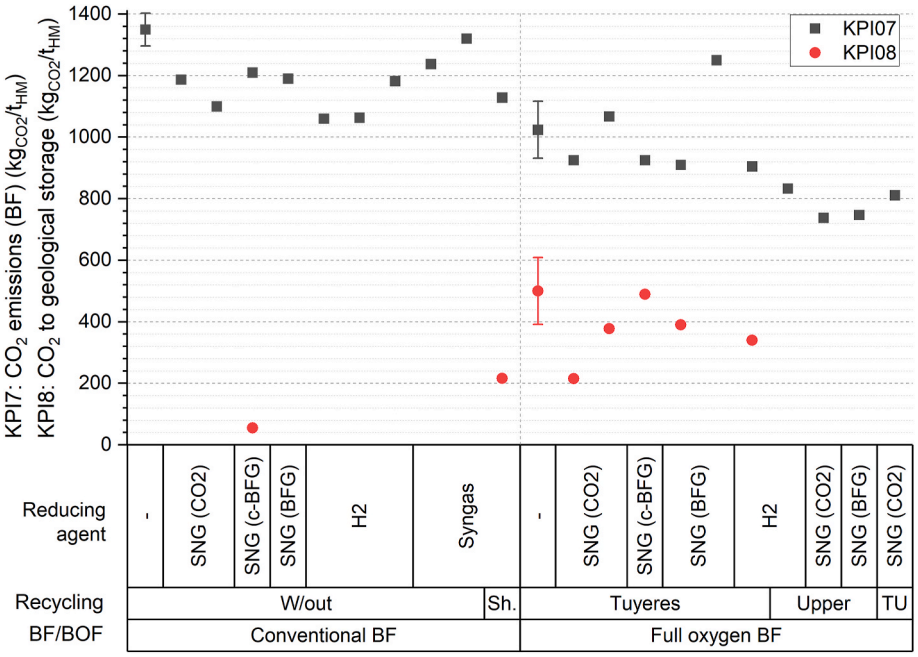


**Fig. 6.** KPI07: $CO_2$ emissions (BF) ($kg_{CO2}/t_{HM}$), KPI08: $CO_2$ to geological storage ($kg_{CO2}/t_{HM}$), as a function of the reducing agent production, the BFG recycling and the conventional or oxygen blast furnace. Nomenclature identical to Fig. 5.

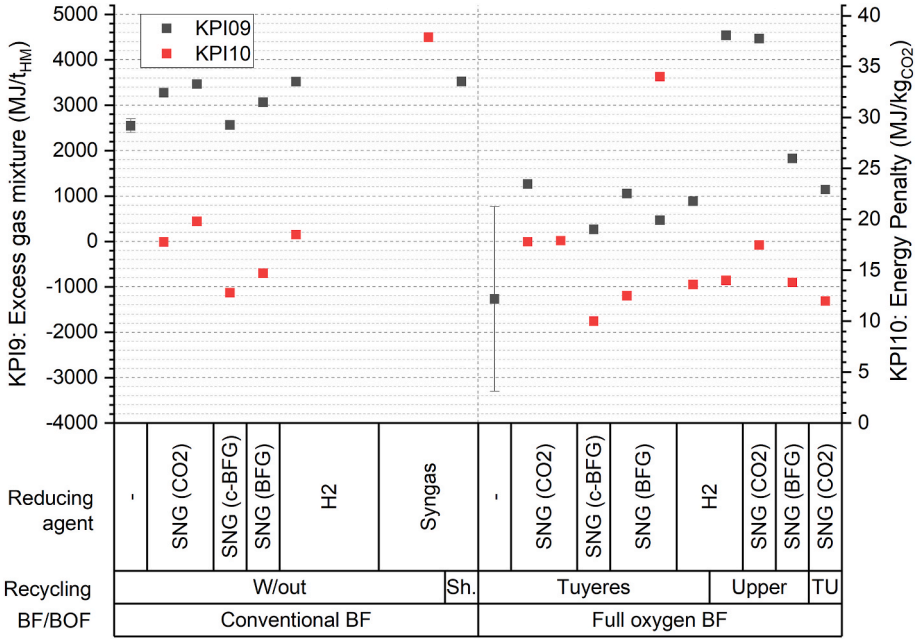


**Fig. 7.** KPI09: Excess gas mixture (sold or flared) (MJ/$t_{HM}$), KPI10: Energy Penalty (MJ/$kg_{CO2}$), as a function of the reducing agent production, the BFG recycling and the conventional or oxygen blast furnace. Nomenclature identical to Fig. 5.

increases by 27 % in average for air-blown blast furnaces because the synthetic reducing agents are not fully consumed in the furnace (the CO and $H_2$ utilization ratios are in the range from 0.25 to 0.55). This means that part of the synthetic gas from power to gas processes is just flared or sold to nearby industries. Contrarily, oxygen blast furnaces with top gas recycling often have issues with downstream energy supply because large amounts of BFG are recirculated, leading to insufficient steel gases diverted to other processes of the plant [36]. Nevertheless, this problem is solved when integrating power to gas thanks to the addition of energy provided by the electrolyser, thus being able to supply all downstream energy needs. The configurations with lower excess gases (i.e., less wasted energy), but still self-sufficient, are those with TGR in the tuyeres and SNG production. The excess energy in the form of steel gases ranges from 267 MJ/$t_{HM}$ to 4542 MJ/$t_{HM}$ in these oxygen blast furnaces.

The energy penalty of most power to gas integrations ranges between 10 MJ/$t_{HM}$ and 20 MJ/$t_{HM}$, whether it is an air-blown or oxygen blast furnace (Fig. 7). On average, the energy penalty in oxygen blast furnaces is slightly lower, compared with that of air-blown blast furnaces. When focusing on the SNG (from $CO_2$ methanation) injection in oxygen blast furnaces, similar energy penalties are found for tuyeres recycling and upper recycling (18 MJ/$kg_{CO2}$), but it greatly decreases if both tuyere and upper recycling injections are used simultaneously (12 MJ/$kg_{CO2}$).

The power to gas configuration with lower energy penalty is SNG injection (from sweet gas methanation) independently of the combustion regime (air-blown or oxygen). This is thanks to the lower electrolyser requirement per kg of synthetic gas injected, as some $H_2$ is already contained in the BFG.

The energy penalty is highly related with the specific electrolyser size required for each PtG integration (KPI11), which is shown in Fig. 8. These values are given in MW/($t_{HM}$/h) for illustration purposes, being scalable to any BF size (typical hot metal production is around 320 $t_{HM}$/h). On average, conventional blast furnaces have electrolyser sizes between 0.2 MW/($t_{HM}$/h) and 2.2 MW/($t_{HM}$/h), while for oxygen blast furnaces they range between 1.0 MW/($t_{HM}$/h) and 4.0 MW/($t_{HM}$/h). It must be noted that larger electrolysers do not necessarily mean higher injections of synthetic gas. In fact, in advanced oxygen BF injecting SNG (from $CO_2$ methanation), 3.96 MW/($t_{HM}$/h) are able to produce 191.5 $kg_{SNG}/t_{HM}$, but if SNG with BFG methanation is chosen, 3.03 MW/($t_{HM}$/h) are able to produce 202 $kg_{SNG}/t_{HM}$. This is due to the hydrogen content in the BFG, which relieves the electrolyser size. Another important factor not directly related to the electrolyser size is the $CO_2$ emitted. For instance, an oxygen blast furnace with sweet gas methanation and top gas recycling (tuyeres) needs only 0.98 MW/($t_{HM}$/h) of electrolysis capacity, but it can restrict the emission to the atmosphere to 435 $kg_{CO2}/t_{HM}$ (with other 490 $kg_{CO2}/t_{HM}$ sent to storage).

One of the advantages of integrating power to gas is the availability of $O_2$ coming from the water electrolysis, which can replace the oxygen produced in the ASU in the ironmaking plant (KPI12). This drops to cero in most cases, especially in air-blown blast furnaces, given their lower $O_2$ demand (Fig. 8). For oxygen blast furnaces, the configurations that implement TGR in tuyeres still need an ASU although smaller than in the case without PtG (62–250 $kg_{O2}/t_{HM}$ instead of 250–350 $kg_{O2}/t_{HM}$), while the configurations with upper injection do not need one. This is due to the higher synthetic gas production in the latter cases, which leads to higher oxygen availability.

Regarding the costs of implementing power to gas in the blast furnace ironmaking, only 5 of the 14 reviewed studies assessed the $CO_2$ avoidance cost (€/$t_{CO2}$; KPI13), and the specific implementation cost (€/$t_{HM}$; KPI14) (Fig. 9). Furthermore, only one study assessed the economic costs of power to gas in air-blown blast furnaces, resulting in 283 €/$t_{CO2}$ and 52 €/$t_{HM}$, for SNG injection with $CO_2$ methanation. The same configuration was studied for an advanced oxygen blast furnace, resulting in higher costs (352 €/$t_{CO2}$ and 233 €/$t_{HM}$); but if combined with TGR (upper and tuyeres), significant reductions can be found in the $CO_2$ avoidance cost (216 €/$t_{CO2}$), and a moderate increase in the specific implementation cost (130 €/$t_{HM}$). These results are in line with the expectations, since higher electrolyser sizes means higher costs (in both €/$t_{CO2}$ and €/$t_{HM}$), and higher $CO_2$ avoided means lower $CO_2$ avoidance cost (€/$t_{CO2}$). Other configurations show cost results that range in between, such as $H_2$ injection or SNG injection (from BFG methanation).

For comparison purposes, only one synthetic gas production configuration, SNG with $CO_2$ methanation, was assessed through three different BFG recirculation configurations, tuyeres, upper and both. The configuration with lower fossil fuel consumption is the one with upper recycling, as it is the one with higher synthetic gas injection. However, the configuration with lower $CO_2$ emissions is the one with tuyeres recycling, as part of the emissions are sent to storage. The latter is also the one with a smaller electrolyser, which allows for less purchased electricity and therefore lower costs, if compared with upper and both injections.

In summary, for air-blown blast furnaces, direct $H_2$ injection is the most promising option, followed by SNG from $CO_2$ methanation, due to its lower $CO_2$ emissions and similar energy penalty and electrolyser size. For oxygen blast furnaces, if geological storage is not available, the most viable configuration is SNG injection (from BFG methanation) and upper recycling of top gas (advanced OBF), as this option has the lowest fossil fuel consumption and blast furnace emissions, with moderate energy penalty and costs. If geological storage is available, the most attractive solution is SNG (from sweet gas methanation) and top gas recycling in tuyeres, thanks to the ultra-low $CO_2$ emissions to the atmosphere (435 $kg_{CO2}/t_{HM}$) and excess gas mixture available, and the moderate energy penalty and electrolyser size (Table 6).

## 6. Future trends on integrating power to gas with blast furnace ironmaking

Future research should focus on the configurations shown in Table 6, but also on their modifications. For instance, the performance of oxygen

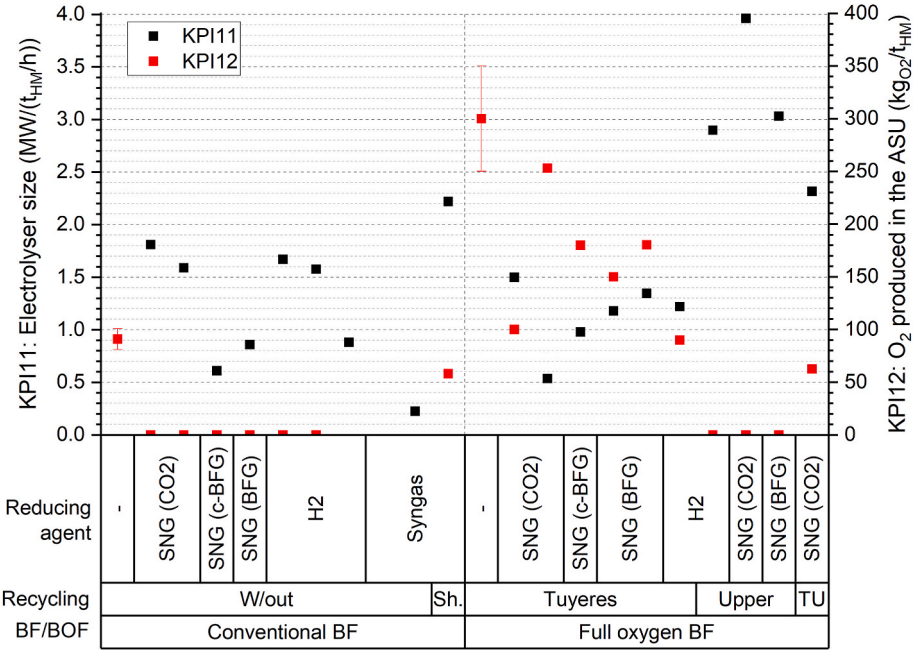


**Fig. 8.** KPI11: Electrolyser size (MW/($t_{HM}$/h)), KPI12: $O_2$ produced in the ASU ($kg_{O2}/t_{HM}$), as a function of the reducing agent production, the BFG recycling and the conventional or oxygen blast furnace. Nomenclature identical to Fig. 5.

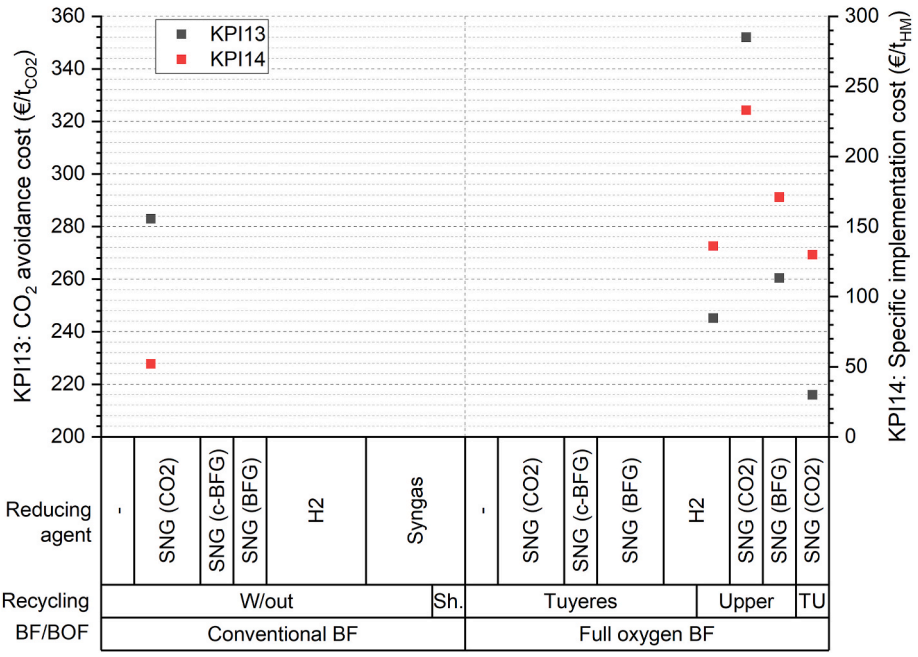


**Fig. 9.** KPI13: $CO_2$ avoidance cost (€/$t_{CO2}$), KPI14: Specific implementation cost (€/$t_{HM}$), as a function of the reducing agent production, the BFG recycling and the conventional or oxygen blast furnace. Nomenclature identical to Fig. 5.

**Table 6**
Most feasible configurations based on the articles found in literature for PtG implementation in blast furnace ironmaking.

| | Reducing agent | $H_2$ production | Recycling |
|---|---|---|---|
| **Conventional BF** | $H_2$ (tuyeres) | PEM | No |
| **Oxy-BF with CO2 storage** | SNG from sweet BFG methanation (tuyeres) | PEM | Top gas recycling (Tuyeres) |
| **Oxy-BF without CO2 storage** | SNG from BFG methanation (tuyeres) | PEM | Upper injection (Advanced) |

blast furnaces might be improved if the synthetic gas is injected not only in the tuyeres but also in the shaft. The possibility of recycling top gas through the shaft should be analysed too. Moreover, the ratio between the amount of top gas recycling and the amount of SNG injection is worth to be studied in detail. Alternative methods for $H_2$/CO production, based on SOEC ($CO_2$ electrolysis) or reverse water gas systems might lead to lower energy consumptions and costs. Besides, advance OBF based on upper recycling seems promising in terms of $CO_2$ avoidance.

Based on the results and discussion shown in previous sections, authors propose a novel configuration with the following characteristics (Fig. 10):

- Oxygen combustion regime: An oxygen blast furnace allows for larger injections of reducing gases, thanks to the higher temperatures in the tuyeres.
- Top gas recycled in the upper part: This technique regulates the BFG temperature at the top to avoid condensation. It is typically required

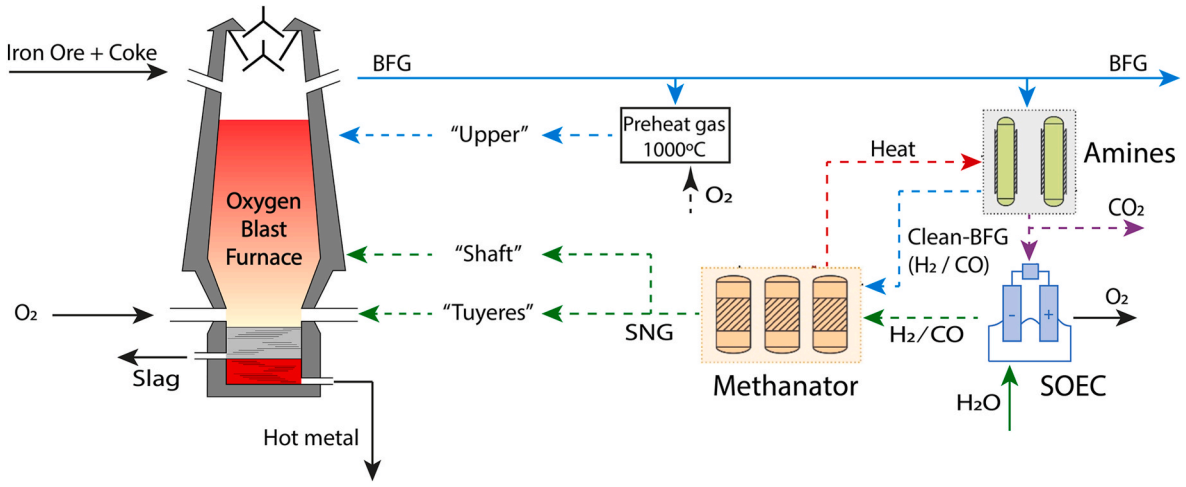


**Fig. 10.** Process flow diagram proposed by the authors for a novel PtG-ironmaking integration.

when there is no recycling at the tuyeres. In this novel configuration, recirculation at the tuyeres is not included in order to not diminish the flame temperature.

- $CO_2$ electrolysis as the source for $H_2$ and CO: This kind of SOEC electrolyser provides lower electricity consumptions, and therefore lower costs.
- Methanation stage for SNG production: An isothermal methanation stage is included to avoid the injection of unreacted $CO_2$ coming from the SOEC. In addition, sweet gas from amine scrubbing could be used in methanation to adjust stoichiometric ratios and decrease the electrolyser size.
- Amine scrubbing for $CO_2$ capture: Carbon capture is needed to derive the $CO_2$ to the SOEC (or storage). The carbon capture stage should be amines, as the heat for amine regeneration can be supplied by the methanation stage. The decision of sending the $CO_2$ to storage or the SOEC electrolyser depends on two parameters: (i) the availability of storage and (ii) the coverage of the downstream thermal energy needs, as sending $CO_2$ to the SOEC implies less sweet gas used in methanation, and therefore, more availability for downstream processes. The excess gases should be as close to zero as possible but never below it.
- SNG injected in both tuyeres and shaft: Distributing the gas injection among the tuyeres and the shaft allows increasing the amount of SNG injected, since shaft injections do not decrease the adiabatic flame temperature.
- Pulverized coal replacement: replacing the pulverized coal injection allows for larger SNG injections.

## 7. Conclusions

In summary, this study comprehensively outlined potential power-to-gas integrations in blast furnace ironmaking, evaluating and comparing relevant literature. Employing a systematic review methodology, 14 key performance indicators (KPIs) were established for comparison, encompassing various aspects such as coke rate, synthetic reducing agent rate, CO2 emissions, costs, and more.

The delineation of potential integrations considered (i) the combustion regime, (ii) the top gas recirculation, (iii) the renewable gas produced, and (iv) the location of the injection of the renewable gas, resulting in 240 possibilities, of which only 14 were studied in literature. Notably, not all configurations are recommended, especially those involving substantial $N_2$ or $CO_2$ recycling.

Examining literature, 6 studies were found on power-to-gas integration for air-blown blast furnaces and 8 for oxygen blast furnaces. Oxygen blast furnaces demonstrated an 18 % lower total coal consumption compared to air-blown furnaces, with upper recycling configurations further reducing consumption. While power-to-gas systems had limited impact on CO2 emissions for air-blown furnaces, significant reductions were observed for oxygen blast furnaces, especially when underground storage was available.

The surplus steel gases' energy content increased by 27 % in air-blown blast furnaces using power-to-gas. Oxygen blast furnace configurations combining tuyere gas recycling and power-to-gas minimized wasted energy, with excess energy ranging from 267 MJ/$t_{HM}$ to 4542 MJ/$t_{HM}$.

Electrolyser sizes depended on BFG's $H_2$ content and on the configuration analysed, in the range of 0.2 and 2.2 MW/($t_{HM}$/h). Additionally, the integration of electrolysis eliminated the need for an air separation unit in many cases, enhancing efficiency.

In terms of cost, only 5 out of 14 studies performed this analysis, with costs. Configurations with SNG injection using $CO_2$ methanation had lower costs for air-blown (283 €/$t_{CO2}$) than for advanced oxygen blast furnaces (352 €/$t_{CO2}$). Combined TGR in upper and tuyeres lead to important reductions in $CO_2$ avoidance cost (216 €/$t_{CO2}$).

Depending on the approach (air-blown BF, oxygen BF, or oxygen BF with $CO_2$ storage), the most feasible configurations among the already studied in literature are:

- Air-blown blast furnace: $H_2$ as a reducing agent (injected through the tuyeres), produced with a PEM electrolyser, and without top gas recycling. The $CO_2$ emissions to atmosphere are 1060 $kg_{CO2}/t_{HM}$.
- Oxygen blast furnace: SNG from BFG methanation as a reducing agent (injected through the tuyeres), produced with a PEM electrolyser and with top gas recycling in the upper part (advanced oxygen blast furnace). The $CO_2$ emissions to atmosphere are 747 $kg_{CO2}/t_{HM}$.
- Oxygen blast furnace combined with geological storage: SNG from sweet gas methanation as a reducing agent (injected through the tuyeres), produced with a PEM electrolyser and with top gas recycling in the tuyeres. The $CO_2$ emissions to atmosphere are 435 $kg_{CO2}/t_{HM}$. The $CO_2$ emissions sent to the storage are 490 $kg_{CO2}/t_{HM}$.

Future studies should validate successful technologies, particularly advanced oxygen blast furnaces with upper recycling. Addressing the current high expenses of these systems is crucial, and prioritizing efforts to reduce the energy penalty associated with green hydrogen production is essential.

## Author contributions

Conceptualization, J.P., M.B. and B.P.; methodology, J.P., M.B. and B.P.; formal analysis, J.P.; writing—original draft preparation, J.P. and M.B.; writing—review and editing, M.B. and B.P.; visualization, J.P. and M.B.; supervision, M.B., and B.P.; project administration and funding acquisition, M.B., and B.P. All authors have read and agreed to the published version of the manuscript.

## Declaration of competing interest

The authors declare that they have no known competing financial interests or personal relationships that could have appeared to influence the work reported in this paper.

## Data availability

Data will be made available on request.

## Acknowledgements

This work has received funding from the European Union's Horizon 2020 research and innovation program under the Marie Sklodowska-Curie grant agreement no. 887077. This work is also part of the R&D project TED2021-130000B–I00, funded by MCIN/AEI/10.13039/501100011033/and by the "European Union NextGenerationEU/PRTR", and PID2021-126164OB-I00, funded by MCIN/AEI/10.13039/501100011033/and by the "ERDF A way of making Europe". Grant RYC2022-038283-I funded by MICIU/AEI/10.13039/501100011033 and by "ESF+".

## References

[1] International energy agency, iron and steel technology roadmap. https://www.iea.org/reports/iron-and-steel-technology-roadmap. [Accessed 26 April 2022].
[2] Cores A, et al. Iron ore sintering. Part 3: automatic and control systems. DYNA May 2015;82(190):227–36. https://doi.org/10.15446/dyna.v82n190.44054.
[3] Remus R, Aguado-Monsonet Ma, Roudier S, Sancho LD. Best available techniques (BAT) reference document for iron and steel production. 2013. https://doi.org/10.2791/98516.
[4] Piringer H, Bucher P, Wallimann R. Sustainable lime burning technology with shaft kilns. ZKG Cem. Lime Gypsum 2021;(6).
[5] Babich A, Senk D, Gudenau H, Mavrommatis KT. Ironmaking textbook. RWTH Aachen University; 2008.
[6] Suzuki K, Hayashi K, Kuribara K, Nakagaki T, Kasahara S. Quantitative evaluation of CO2 emission reduction of active carbon recycling energy system for ironmaking by modeling with aspen plus. ISIJ Int 2015;55(2):340–7. https://doi.org/10.2355/isijinternational.55.340.

[7] Zhang W, Dai J, Li C, Yu X, Xue Z, Saxén H. A review on explorations of the oxygen blast furnace process. Steel Res Int 2021;92(1). https://doi.org/10.1002/srin.202000326.
[8] Bailera M, Lisbona P, Peña B, Romeo LM. A review on CO2 mitigation in the Iron and Steel industry through Power to X processes. J CO2 Util 2021;46(November 2020):101456. https://doi.org/10.1016/j.jcou.2021.101456.
[9] Rosenfeld DC, Böhm H, Lindorfer J, Lehner M. Scenario analysis of implementing a power-to-gas and biomass gasification system in an integrated steel plant: a techno-economic and environmental study. Renew Energy 2020;147:1511–24. https://doi.org/10.1016/j.renene.2019.09.053.
[10] Medved AR, Lehner M, Rosenfeld DC, Lindorfer J, Rechberger K. Enrichment of integrated steel plant process gases with implementation of renewable energy Integration of power-To-gas and biomass gasification system in steel production. Johnson Matthey Technol. Rev. 2021;65(3):453–65. https://doi.org/10.1595/205651321x16161444481140.
[11] Kato Y. Utilization of HTGR on active carbon recycling energy system. Nucl Eng Des 2014;271:79–83. https://doi.org/10.1016/j.nucengdes.2013.11.014.
[12] Kato Y, et al. Performance analysis of active carbon recycling energy system. Prog Nucl Energy 2011;53(7):1017–21. https://doi.org/10.1016/j.pnucene.2011.04.024.
[13] Dipu AL, Ryu J, Kato Y. Carbon dioxide electrolysis for a carbon-recycling iron-making system. ISIJ Int 2012;52(8):1427–32. https://doi.org/10.2355/isijinternational.52.1427.
[14] Dipu AL, Ujisawa Y, Ryu J, Kato Y. Carbon dioxide reduction in a tubular solid oxide electrolysis cell for a carbon recycling energy system. Nucl Eng Des 2014;271:30–5. https://doi.org/10.1016/j.nucengdes.2013.11.004.
[15] Hisashige S, Nakagaki T, Yamamoto T. CO2 emission reduction and exergy analysis of smart steelmaking system adaptive for flexible operating conditions. ISIJ Int 2019;59(4):598–606. https://doi.org/10.2355/isijinternational.ISIJINT-2018-355.
[16] Zhao J, Zuo H, Wang Y, Wang J, Xue Q. Review of green and low-carbon ironmaking technology. Ironmak Steelmak 2020;47(3):296–306. https://doi.org/10.1080/03019233.2019.1639029.
[17] Lan C, Hao Y, Shao J, Zhang S, Liu R, Lyu Q. Effect of H2 on blast furnace ironmaking: a review. Metals 2022;12(11). https://doi.org/10.3390/met12111864.
[18] Chen Y, Zuo H. Review of hydrogen-rich ironmaking technology in blast furnace. Ironmak Steelmak 2021;48(6):749–68. https://doi.org/10.1080/03019233.2021.1909992.
[19] Page MJ, et al. The PRISMA 2020 statement: an updated guideline for reporting systematic reviews. BMJ 2021;372. https://doi.org/10.1136/bmj.n71.
[20] Perpiñán J, Bailera M, Peña B, Romeo LM, Eveloy V. Technical and economic assessment of iron and steelmaking decarbonization via power to gas and amine scrubbing. Energy 2023;276. https://doi.org/10.1016/j.energy.2023.127616.
[21] Peacey JG, Davbenport WG. The Iron Blast Furnace. Theory and Practice 1979:1979. ISBN 0-08-023258-2.
[22] Wu J, Wang R, Pu G, Qi H. Integrated assessment of exergy, energy and carbon dioxide emissions in an iron and steel industrial network. Appl Energy 2016;183:430–44. https://doi.org/10.1016/j.apenergy.2016.08.192.
[23] European Commission. ULCOS top gas recycling blast furnace process (ULCOS TGRBF). Final Report; 2014. https://doi.org/10.2777/59481.
[24] Perpiñán J, Bailera M, Peña B. Full oxygen blast furnace steelmaking: from direct hydrogen injection to methanized BFG injection. Energy Convers Manag 2023. https://doi.org/10.1016/j.enconman.2023.117611.
[25] Perpiñán J, Bailera M, Romeo LM, Peña B, Eveloy V. CO2 recycling in the iron and steel industry via power-to-gas and oxy-fuel combustion. Energies 2021;14(21):7090. https://doi.org/10.3390/en14217090.
[26] Bailera M, Nakagaki T, Kataoka R. Limits on the integration of power to gas with blast furnace ironmaking. Elsevier; Sep. 2022. https://doi.org/10.1016/J.JCLEPRO.2022.134038.
[27] Yilmaz C, Wendelstorf J, Turek T. Modeling and simulation of hydrogen injection into a blast furnace to reduce carbon dioxide emissions. J Clean Prod 2017;154:488–501. https://doi.org/10.1016/j.jclepro.2017.03.162.
[28] Kim J, et al. An integrative process of blast furnace and SOEC for hydrogen utilization: techno-economic and environmental impact assessment. Energy Convers Manag 2021;250(August):114922. https://doi.org/10.1016/j.enconman.2021.114922.
[29] Hayashi K, et al. Process evaluation of use of high temperature gas-cooled reactors to an ironmaking system based on active carbon recycling energy system. ISIJ Int 2015;55(2):348–58. https://doi.org/10.2355/isijinternational.55.348.
[30] Hu Y, et al. Opportunities to reduce energy consumption and $CO_2$ emissions from ironmaking blast furnace using $CO_2$ electrolysis to CO for carbon recycling. J Clean Prod 2023;389(January):135997. https://doi.org/10.1016/j.jclepro.2023.135997.
[31] Bailera M, Nakagaki T, Kataoka R. Revisiting the Rist diagram for predicting operating conditions in blast furnaces with multiple injections. 2021. https://doi.org/10.12688/openreseurope.14275.1.
[32] Perpiñán J, Bailera M, Peña B, Romeo LM, Eveloy V. High oxygen and SNG injection in blast furnace steelmaking with Power to Gas integration and CO2 recycling. J Clean Prod 2023. https://doi.org/10.1016/j.jclepro.2023.137001.
[33] Perpiñán J, Bailera M, Peña B, Kannan P, Eveloy V, Romeo LM. Power to Gas and Top Gas Recycling integration in an oxygen blast furnace steelmaking industry. 2023. https://doi.org/10.1016/j.jcou.2023.102634.
[34] Danloy G, et al. Ulcos - pilot testing of the low-CO2 Blast Furnace process at the experimental BF in Lulea. Rev. Metall. Cah. D'Informations Tech. 2009;106(1):1–8. https://doi.org/10.1051/metal/2009008.
[35] Bailera M, Nakagaki T, Kataoka R. Extending the operating line methodology to consider shaft and preheating injections in blast furnaces. ISIJ Int 2022;62(12):1–12. https://doi.org/10.2355/isijinternational.ISIJINT-2022-111.
[36] Sahu RK, Roy SK, Sen PK. Applicability of top gas recycle blast furnace with downstream integration and sequestration in an integrated steel plant. Steel Res Int 2015;1(5):502–16. https://doi.org/10.1002/srin.201400196.

Energy 256 (2022) 124720

Contents lists available at ScienceDirect

Energy

journal homepage: www.elsevier.com/locate/energy

# Synthetic natural gas production in a 1 kW reactor using Ni–Ce/$Al_2O_3$ and Ru–Ce/$Al_2O_3$: Kinetics, catalyst degradation and process design

Manuel Bailera [a, b, *], Pilar Lisbona [b], Begoña Peña [b], Andreina Alarcón [c, d], Jordi Guilera [c, e], Jorge Perpiñán [b], Luis M. Romeo [b]

[a] Graduate School of Creative Science and Engineering, Waseda University, Okubo, Shinjuku-ku, Tokyo, 169-8555, Japan
[b] Escuela de Ingeniería y Arquitectura. Universidad de Zaragoza, Campus Río Ebro, María de Luna 3, 50018, Zaragoza, Spain
[c] Catalonia Institute for Energy Research (IREC), Jardins de Les Dones de Negre 1, 08930, Sant Adrià de Besòs, Spain
[d] Escuela Superior Politécnica del Litoral (ESPOL), Facultad de Ingeniería en Ciencias de La Tierra, Campus Gustavo Galindo Km.30.5 Vía Perimetral, P.O. Box 09-01-5863, Guayaquil, Ecuador
[e] Department of Chemical Engineering and Analytical Chemistry, University of Barcelona, Barcelona, 08028, Spain

ARTICLE INFO

*Article history:*
Received 10 January 2022
Received in revised form
15 June 2022
Accepted 30 June 2022
Available online 5 July 2022

*Keywords:*
Power-to-Gas
Hydrogen
Methanation
Synthetic natural gas
Catalyst

ABSTRACT

Nickel and ruthenium promoted by ceria were compared as catalyst active phase for the production of synthetic natural gas in a 1 kW fixed-bed reactor (49 cm in length and 3 cm in diameter). Both catalysts were tested in a broad range of conditions: 250–450 °C, 8000–16000 $h^{-1}$ GHSV, 3.5–5.5$H_2/CO_2$ ratio, and atmospheric pressure. The Ni-based catalyst presented higher $CO_2$ conversion and lower reduction of BET area and metal dispersion after utilization. Two kinetic models were elaborated according to the performance of the catalysts in this reactor. The minimum mean squared error between the kinetic model and experiments was 3.0% for the Ru-based catalyst and 1.4% for the Ni-based catalyst. The kinetic model of the Ni-based catalyst was implemented in Aspen Plus to evaluate potential methanation plant designs. The simulation minimized the amount of catalyst required to reach 95 vol% of $CH_4$, within proper technical limits (GHSV $\leq$ 5000 $h^{-1}$ and temperature $\geq$ 300 °C). The 3-reactor plant was the most adequate configuration. The total catalyst mass was 3.26 kg per kg/h of SNG, the heat removed from the reactors was 10.8 $MJ/kg_{SNG}$, and the preheating necessity was 4.90 $MJ/kg_{SNG}$. The electrolysis energy consumption was 86.4 $MJ/kg_{SNG}$.
© 2022 The Authors. Published by Elsevier Ltd. This is an open access article under the CC BY-NC license (http://creativecommons.org/licenses/by-nc/4.0/).

## 1. Introduction

The massive penetration of renewable energy resources in the energy system, as well as the development of large scale energy storage systems, is essential to achieve global emissions targets [1]. Different technologies are currently in operation and others have been proposed to overcome the current drawbacks of energy storage technologies. Among them, Power to Gas has received attention in the recent years [2,3]. Power to Gas includes all those technological concepts that convert renewable electricity into gaseous fuel by including an electrolysis stage [4]. Considering the benefits and drawbacks of the different synthetic fuels that can be obtained, Power to Methane is one of the most versatile options thanks to the possibility of storing and distributing the product (methane) through the natural gas network [5–7]. The core of the Power to Methane process is the methanation reactor where a metallic catalyst that exhibits high stability over a long time and high resistance to sintering and carbon deposition is required to promote the Sabatier reaction (Eq. (1)) [8].

$$CO_2 + 4H_2 \leftrightarrow CH_4 + 2H_2O \qquad \Delta H^0_{298} = -165.0 \text{ kJ}/\text{mol} \tag{1}$$

Heterogeneous catalysts based on metals primordially from VIII-XI group, nickel (Ni) and ruthenium (Ru), supported over mesoporous alumina ($\gamma$-$Al_2O_3$) have been found to be competitive for the methane production by $CO_2$ methanation process. Ru-based catalysts are typically synthetized using a low metal loading ($\leq$5 wt%), whereas Ni-based catalysts are fabricated using a high metal loading ($\leq$20 wt%) [9]. Between both, Ni-based catalysts are

* Corresponding author. Graduate School of Creative Science and Engineering, Waseda University, Okubo, Shinjuku-ku, Tokyo, 169-8555, Japan.
*E-mail address:* mbailera@unizar.es (M. Bailera).

https://doi.org/10.1016/j.energy.2022.124720
0360-5442/© 2022 The Authors. Published by Elsevier Ltd. This is an open access article under the CC BY-NC license (http://creativecommons.org/licenses/by-nc/4.0/).

preferred to be developed at industrial levels because of their excellent catalytic performance, easy availability, and low price. However, they are easily deactivated by sintering [10], coke deposition [11] or poisoning [12–15], in a higher extension than Ru-based catalysts [16,17], which in turn are much more expensive.

The influence of the support material ($SiO_2$ [15], $TiO_2$ [20], $Y_2O_3$ [18], $Sm_2O_3$ [11], $ZrO_2$ [23], $CeO_2$ [24], $La_2O_3$ [25], MgO [26], MCM-41 [27], carbon [28], zeolites [29–32] and KIT-6 [33]), the addition of 1 s metallic active phase (Fe [34], Pt, Pd, Rh [35], Co [36], V [37] and Ru [35]), and the addition of a metal oxide promoter ($ZrO_2$ [40], $CeO_2$ [41], $La_2O_3$ [42,43], $Mn_2O$ [44], CaO [45], $Gd_2O_3$ [46], MIL-101 [47]) to modify conventional $\gamma$-$Al_2O_3$ support are the main catalyst design strategies applied in order to improve the catalytic performance of the Ni-based catalysts. In our most recently works, it was reported that the addition of lanthanides promoters ($CeO_2$ and $La_2O_3$) on Ni/$\gamma$-$Al_2O_3$ microspheres was beneficial to enhanced both activity and stability [48]. Moreover, we also reported that lanthanides promoters play an important role to withstand sulphur poisoning, such in the case of $CeO_2$ [49,50]. Regarding to Ru-based catalysts, the strategy of addition $CeO_2$ as promoter has been also investigated, however its promoting effect over the physicochemical properties of the Ru/$\gamma$-$Al_2O_3$ catalysts has not been clearly reported. In literature, Rynkowski et al. [51] claimed that the stabilization of Ce (III) in $CeAl_2O_3$, which is a driving force enhancing $CO_2$ activation, is promoted by a high temperature catalyst reduction (T < 900 °C). However, taking into consideration that most of the reactor designs that are nowadays available in the market cannot operate at this high temperature reduction condition and that a stable catalyst is mandatory to carry out an industrial $CO_2$ methanation process, further research about scalable $CeO_2$ promoted Ni- and Ru- based catalysts should be conducted to clarify the $CeO_2$ promoter effects and to compare the catalytic performance between both catalytic systems at industrial levels.

In literature, the comparison and characterization of catalysts is usually performed at small lab-scale reactors whose operating conditions are easy to manage and fully controlled. Moreover, most of the reported catalyst are fabricated in powder shape with a particle size lower than 200 μm [52]. At industrial levels, powder catalysts are not technical feasible to be used in the conventional fixed-bed reactors because their small particle sizes promote the pressure drop across the catalyst bed. The use of relatively large particles (1–3 mm) can be required to avoid high pressure drop. Commercial methanation catalysts are currently manufactured in spherical (3–6 mm) [53], cylindrical (5.4 × 3.6 mm) [54] and ring (5 × 2.5 mm) [55] shapes, which are not compatible for the new generation of micro- and mm-fixed bed reactors. Therefore, the design of active catalysts at industrially relevant shape is required for a proper catalyst selection in these methanation fixed-bed reactors.

The main original contribution of the present study is the comparison of nickel and ruthenium as catalyst active phase at larger scale, and the characterization of its performance in a 1 kW mm-fixed bed reactor, including the elaboration of kinetic models for this scale. The paper is divided in three main sections: Methods, Results and Process design. The Methods section provides information on the catalyst preparation, the experimental setup, the experiment design, and the elaboration of the kinetic models. The Results section shows the reduction protocol, the analysis on the temperature profile of the reactor, the comparison between mm-sized Ni and Ru active phases performance, and the study on the degradation of the catalysts after their utilization. Finally, the Process design section presents an Aspen Plus model of potential methanation plant configurations, based on the elaborated kinetics at 1 kW scale, which optimizes the operating parameters to minimize the required amount of catalyst to reach 95 vol% of $CH_4$ in the final gas.

## 2. Methods

### 2.1. Catalyst preparation

Two mm-sized catalyst with spherical shape were considered in this work based on different active phase, nickel (Ni) and ruthenium (Ru). Both catalysts, Ni and Ru, were promoted by cerium oxide ($CeO_2$) and supported on $\gamma$-alumina spheres (dp = 2–2.2 mm). Catalyst composition was selected according to preliminary works on Ni- [56] and Ru-based catalyst promoted by $CeO_2$ [57].

The catalyst preparation is described as follows. A typical synthesis consisted on 50 g-catalyst batch. The salt precursors; nickel (II) nitrate hexahydrate [$Ni(NO_3)_2 \cdot 6H_2O$] (98% purity, Alfa Aesar), or ruthenium (III) chloride hydrate [$RuCl3 \cdot xH_2O$] (Sigma-Aldrich), and cerium (III) nitrate hexahydrate [$Ce(NO_3)_2 \cdot 6H_2O$] (99% purity, Alfa Aesar) were dissolved in a rotary evaporator at constant stirring (140 rpm) for 1 h at 120 °C. Then, pre-dried $\gamma$-$Al_2O_3$ spheres (SA 62240, Norpro Saint-Gobain) were added to the solution and kept for 3 h for impregnation. Catalyst were calcined at 450 °C for 30 min (1 °C·min$^{-1}$).

### 2.2. Catalyst characterization

Physiochemical characterization of the fresh and used catalysts included Scanning Electron microscopy (SEM), Energy dispersive X-ray (EDX), Helium pycnometry, Hydrogen temperature programed reduction ($H_2$-TPR), Nitrogen physisorption, X-ray diffraction (XRD) and CO-chemisorption. Prior to measurements, fresh catalysts were activated on a tubular furnace at 300 °C for 3 h (1 °C·min$^{-1}$) and under 5 vol% $H_2$/Ar flow (100 NmL·min$^{-1}$).

SEM (Zeiss Auriga 60) was used to study the morphology of the samples, while the experimental composition was studied by EDX (Oxford Inca Energy). SEM images and EDX analysis were performed by using the procedure measurement described in Ref. [48]. The true densities of catalysts were estimated by using helium pycnometer (Ultrapyc pycnometer 1200e, Quantachrome Instruments) Experiments were performed using a large sample cell that was filled by catalyst at 75% vol. to ensure accuracy (±0.02). True density was estimated by the average of collected data points from three runs measured at 1.38 bar.

Textural analyses were carried out from the corresponding $N_2$ adsorption-desorption isotherms at −196 °C using a static automatic volumetric apparatus (TriStar II 3020-meritics analyser). Before the measurements, the samples were degassed at 90 °C for 1 h, and then at 250 °C for 4 h. Brunauer-Emmett-Teller (BET) method was applied for calculation of the BET surface area for a relative pressure ($P \cdot P_0^{-1}$) range of 0.05–0.30. The total pore volume and the average pore size were determined by applying Barrett-Joyner-Halenda (BJH) method to the desorption branch of the isotherms at value $P \cdot P_0^{-1} = 0.999$.

$H_2$-TPR and CO-Chemisorption were carried out using an automated chemisorption analyser (Autochem HP-meritics). In the case of $H_2$-TPR measurements 70 mg of synthetized material was kept under a 12 vol% $H_2$/Ar flow (50 NmL·min$^{-1}$), while the temperature was increased from 25 to 800 °C with a heating ramp of 10 °C·min$^{-1}$. The signal of $H_2$ consumption was detected by a thermal conductivity detector (TCD). CO-Chemisorption measurements were held at 35 °C under a 10 vol% CO/He flow over samples (50 mg), which were pre-reduced at 300 °C under a 12 vol% $H_2$/Ar flow (50 NmL·min$^{-1}$) for 3 h (heating ramp of 1 °C·min$^{-1}$). CO pulses were periodically introduced until full saturation of the system. Metal dispersion of the catalysts was calculated assuming a stoichiometric ratio CO/Ni and CO/Ru equal to 1, an atomic weight for Ni to 58.71 and Ru to 101.07, an atomic cross-sectional area for

Ni to 0.0649 $nm^2$ and for Ru to 0.0613 $nm^2$, and a density for Ni to 8.90 g $cm^{-3}$ and Ru to 12.2 g $cm^{-3}$.

XRD spectra were collected on a Bruker type XRD D8 Advance A25 diffractometer (Cu Kα radiation, λ = 1.5406 Å, 40 kV, 40 mA) with a scanning range of 2Θ form 20° to 80° and step size of 0.05°/3s. The average crystal sizes of the metallic nickel, ruthenium and cerium oxide nanoparticles were derived from Scherrer's equation at the most intense peaks: 2Θ = 44.55° for Ni (111), 2Θ = 44.07° for Ru (101) and, 2Θ = 28.71° for $CeO_2$ (220): D=(Kλ/βCosΘ), where λ is the X-ray wavelength, β is the full width of the diffraction peak at half maximum (FWHM), and Θ is the Bragg angle.

### 2.3. Experimental setup

The methanation facility (Fig. 1) consisted on a $CO_2$ cylinder (≥99.5% purity, Air products ×50S) connected to a mass flow controller (EL-Flow Bronkhorst® model F–201CV-RAD-22-K, measuring range 0.16–0.80 kg/h), a $H_2$ cylinder (≥99.5 purity, Air products ×50S) connected to a mass flow controller (EL-Flow Bronkhorst® model F-201AV-RAD-22-V, measuring range 0.003–0.15 kg/h), a ceramic heater to pre-heat the reagent mixture (≤400 °C, custom-made by Tellsa SL), a fixed bed reactor (tube in stainless steel 310 and flanges in stainless steel 304, in-house design), three electrical resistances wrapped around the reactor (3 × 500 W, annealed copper, model Electricfor FFC4 T-175-E), a water condenser (custom-made Tellsa SL) and a burner to co-fire the synthetic methane with butane (custom-made Tellsa SL) [58]. For cleaning and safety purposes, the facility also included a $N_2$ entry ($N_2$ bottle ≥99.998% purity, Air products ×50S).

The gas composition was analyzed before and after the methanation step using a gas analyser, which consisted on a thermal conductivity detector (Calomat 6, Siemens) for $H_2$ quantification and an infrared detector (Ultramat 23, Siemens) for $CO_2$, $CH_4$ and CO quantification. Pressure and temperature were measured with standard instrumentation at different points of the installation, and were monitored using a Labview system.

The reactive channel consisted on a tubular fixed bed (30 mm diameter and 490 mm in length). The prepared catalyst spheres were mixed and loaded with alumina spheres (3.56 mm in diameter with a true density of 3.81 g/$cm^3$, Goodfellow AL60-SP-000122) to have a homogenous axial distribution of temperature. Additionally, two inert layers of 35 mm of alumina spheres were used to place the catalytic bed in the desired location and a 60 mm layer of quartz wool was placed at the bottom. Table 1 describes the characteristics of the ruthenium and nickel fixed beds.

The reactor thermal design was based on a co-current "double pipe" (Fig. 2). Air flowed through the annular space to cool the inner tube (shell of 100 mm outer diameter), while the reactants flowed through the inner tube (620 mm length and 30 mm inner diameter). A total of 9 thermocouples were distributed along the reactor length (50 mm of separation), which were placed in contact with the inner tube wall. Thus, the temperature of the wall measured by the thermocouples is expected to be representative to the actual temperature of the catalytic bed.

### 2.4. Catalyst performance

The activation of the catalyst was carried out by passing a pure hydrogen flowrate of 0.015 kg/h during 3 h at 200–400 °C. After activation, the mass flows of $H_2$ and $CO_2$ corresponding to the operating point under study were set in the mass flow controllers. When the conversion and temperature of the reactor was stable, the measurement in the gas analyzer was recorded. The tests were performed in ascending order of operating temperature, in order to not cool the reactor between tests. When requiring increasing the temperature to reach the new operating temperature set point, the electrical resistances were set on.

The experimental plan (Fig. 3) was designed to evaluate the performance of both catalysts at different steady conditions of operating temperature (T = 250-450 °C), gas hourly space velocity (GHSV = 8000-16000 $h^{-1}$), molar ratio (3.5–5.5) and activation temperature (T = 200-400 °C). The operating pressure was 1 bar. The base case consisted on T = 350 °C, GHSV of 10000 $h^{-1}$ and $H_2$/

**Table 1**
Physical characteristics of the fixed beds.

| | Ru-based | Ni-based |
|---|---|---|
| Catalyst (g) | 41 | 39 |
| Inert spheres (g) | 750 | 750 |
| Total mass (g) | 791 | 789 |
| Bulk density (g/$cm^3$) | 2.285 | 2.283 |
| Void fraction (–) | 0.346 | 0.346 |

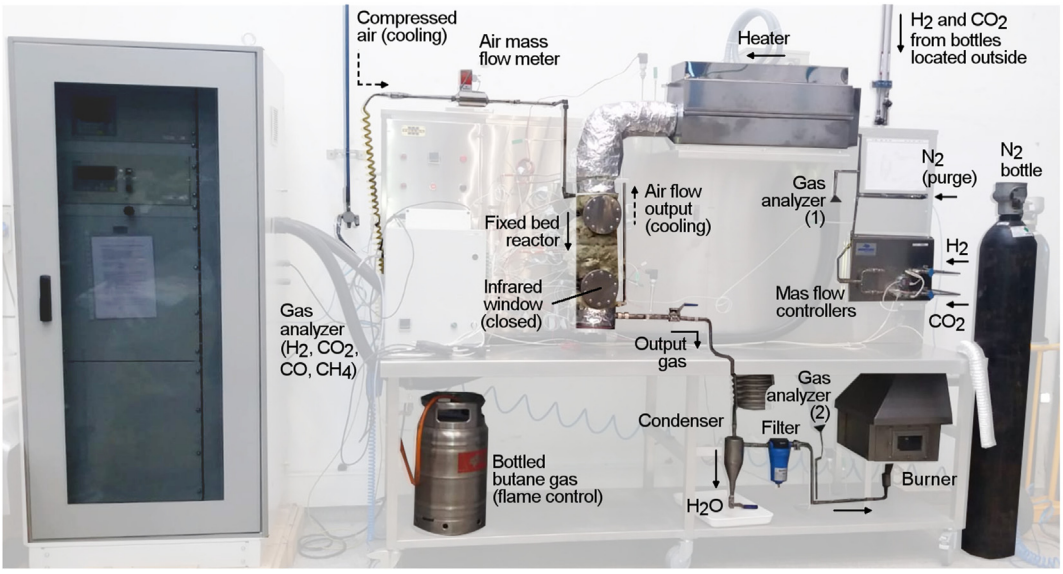


**Fig. 1.** Methanation test facility.

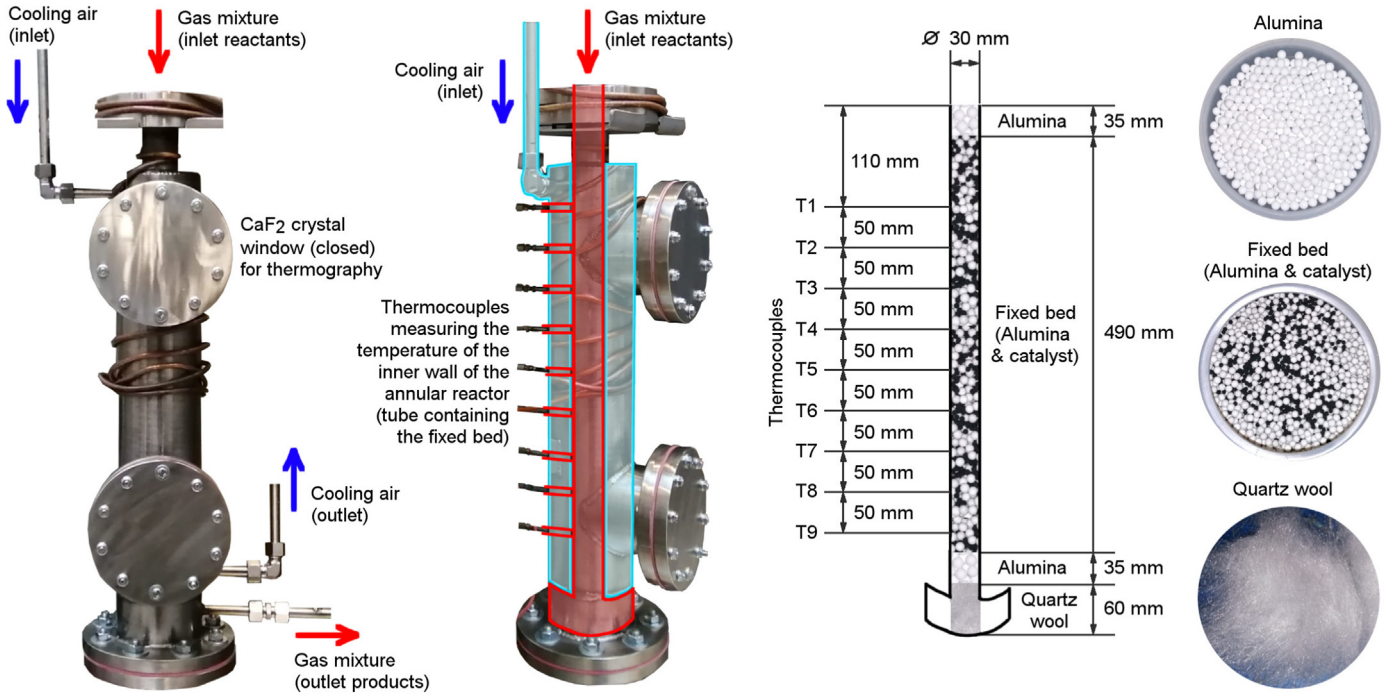


**Fig. 2.** Methanation reactor (without external insulation).

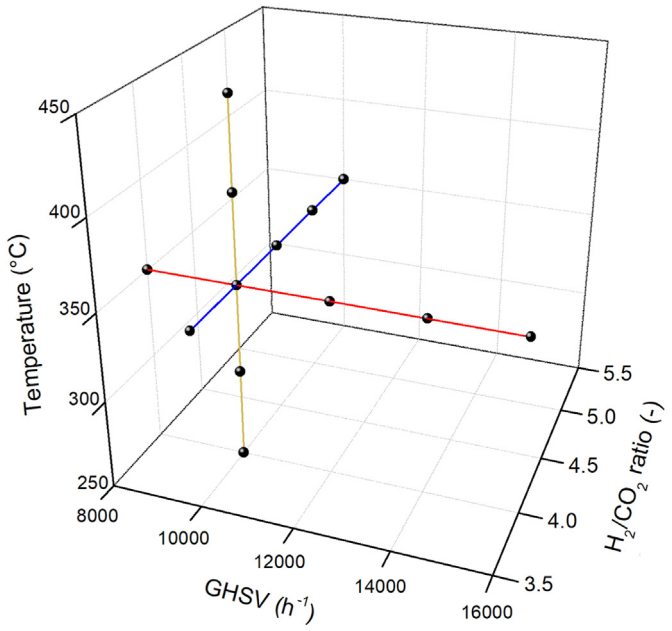


**Fig. 3.** Experimental design to evaluate catalyst performance. Sensitive analysis on Temperature (yellow), GHSV (red) and $H_2/CO_2$ ratio (blue).

$CO_2$ ratio of 4. The experimental design consisted of 13 independent points for each catalyst. Experiments were repeated twice for each catalyst (at different activation temperatures), therefore 52 experimental data points were measured in total. The experimental conditions of each experiments can be found at the appendixes (Table 5to Table 8).

The GHSV was calculated by Eq. (2), while the $CO_2$ conversion to $CH_4$ was experimentally calculated by Eq. (3) from the measurements of the gas analyzer:

$$GHSV = \frac{F}{m_{cat}/\rho_{cat}} \tag{2}$$

$$\eta_{CO2} = \frac{x_{CH4}}{x_{CO2} + x_{CO} + x_{CH4}} \cdot 100 \tag{3}$$

where $F$ is the volume flow of reactants (STP conditions), $m_{cat}$ the catalyst mass, $\rho_{cat}$ the bulk density of the catalyst and $x_j$ the molar fraction of component $j$ in the final gas.

### 2.5. Kinetic model

A kinetic model was elaborated for each catalyst by using the experimental results of the present study. The model was based in the equation proposed by Falbo et al. (Eq. (4)) [59], which is a modification of the model reported by Lunde et al. [16].

$$r_{CO2} = \frac{k}{1 + \alpha[P_{H2O}]} \cdot \left( [P_{CO2}]^n [P_{H2}]^{4n} - \frac{[P_{CH4}]^n [P_{H2O}]^{2n}}{{K_{eq}}^n} \right) \tag{4}$$

The term $[P_i]$ is the partial pressure of component $i$, the parameter $n$ adjusts the reaction order, the coefficient $\alpha$ gives the dependence on the water partial pressure, $K_{eq}$ is the equilibrium constant (Eq. (5)), and $k$ is the rate constant (Eq. (6), Arrhenius equation).

$$K_{eq}(T) = \exp\left[ \frac{1}{1.987} \cdot \left( \frac{56000}{T^2} + \frac{34633}{T} - 16.4 \cdot \ln T + 0.00557 \cdot T \right) + 33.165 \right] \tag{5}$$

$$k = k_0 \cdot \exp\left( -\frac{E_A}{R \cdot T} \right) \tag{6}$$

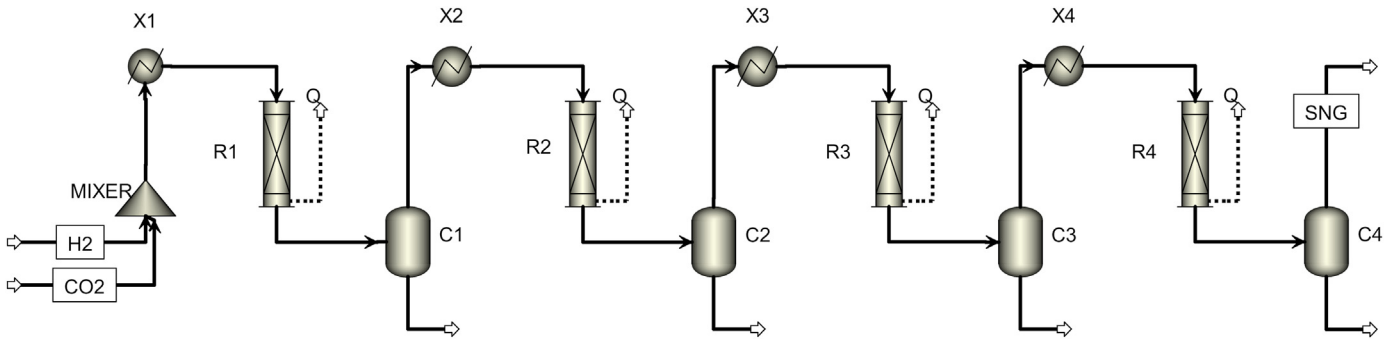


**Fig. 4.** Process flow diagram for the methanation plant in Aspen Plus (4-reactor configuration).

The parameters $k_0$ (pre-exponential factor), $E_A$ (activation energy), $n$ (reaction order) and $\alpha$ (dependence on water partial pressure) were obtained by minimizing the mean squared error (MSE) of the $CO_2$ conversion (Eq. (7)) over the total number $N$ of experimental tests. The MSE was minimized by using the Powell Method [60], with the following limits: 5–10000 mol/(s g $atm^{5n}$) for $k_0$, 50–90 kJ/mol for $E_A$, 0.001–1 for $n$, and 0–70 1/atm for $\alpha$.

$$\mathrm{MSE} = \sqrt{\frac{\sum_j^N \left(\eta_{\mathrm{CO2\,(model)},j} - \eta_{\mathrm{CO2(experimental)},j}\right)^2}{N}} \quad (7)$$

### 2.6. Process design

The kinetic model elaborated in this study was implemented in Aspen Plus to evaluate a methanation plant able to reach a 95 vol% of methane in the final synthetic natural gas. As case study, it was assumed an electrolysis capacity of 1 MW with 68% efficiency [61]. A conventional configuration of reactors in series with intermediate condensers was chosen (Fig. 4).

The simulation use the RKSMHV2 property method provided by Aspen Plus. This package is based on the Redlich-Kwong-Soave equation-of-state and modified Huron-Vidal mixing rules, which are valid for the tested temperatures and pressures. An optimization process based on the Sequential Quadratic Programming (SQP) method was followed in order to minimize the amount of catalyst required, constrained by the requirement of 95 vol% $CH_4$ in the final gas. In this optimization, the temperature of the reactors and the mass of catalyst was varied, as well as the number of reactors (2, 3 or 4 reactors in series). A second optimization was performed including additional technical constrains of typical methanation plants (GHSV $\leq$ 5000 $h^{-1}$ and T $\geq$ 300 °C [62]).

## 3. Results and discussion

### 3.1. Temperature profile along the fixed bed

During the elaboration of the kinetic model, as well as for the catalyst performance comparison, it was assumed that the reactor was isothermal. To check this condition, the temperature of the reactor was cautiously measured by 9 thermocouples spaced by 5 cm along the fixed bed (Fig. 2). The difference of temperature with respect to the isothermal set point, in °C, was presented in a boxplot in Fig. 5, covering all the tests (Table 9). This type of graph is a standardized way of displaying data based on the minimum, the maximum, the sample median, and quartiles.

In the case of Ru-based fixed bed, the median of the temperature differences for the third to eight thermocouples was in the range +3.3% to −8.2%. Moreover, the ninth thermocouple had a median of −14.3%, which is still reasonable since its influence will be minor taking into account its proximity to the end of the fixed bed. Deviations were found for the two first thermocouples only,

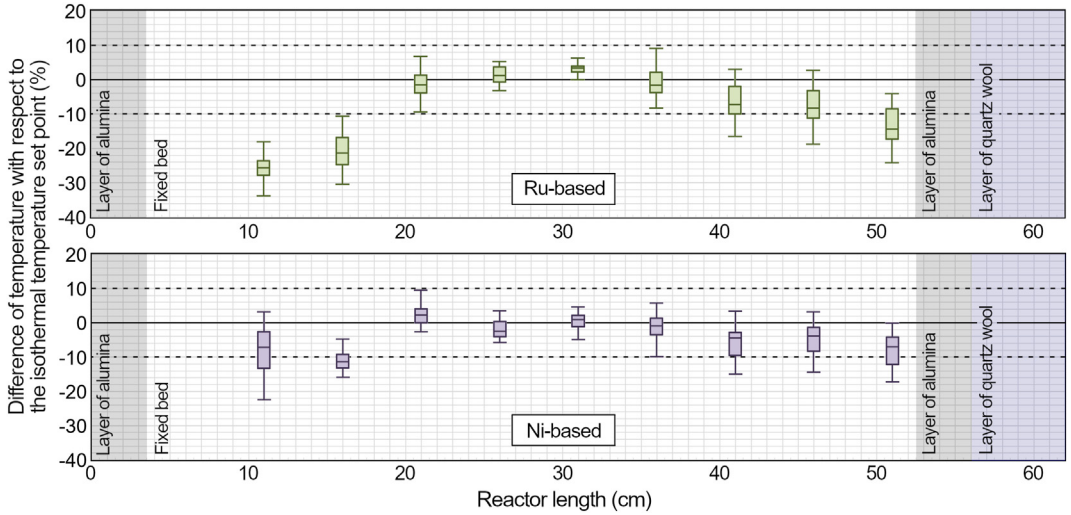


**Fig. 5.** Boxplot of the relative difference between the temperature (in °C) measured along the fixed bed and the isothermal set point.

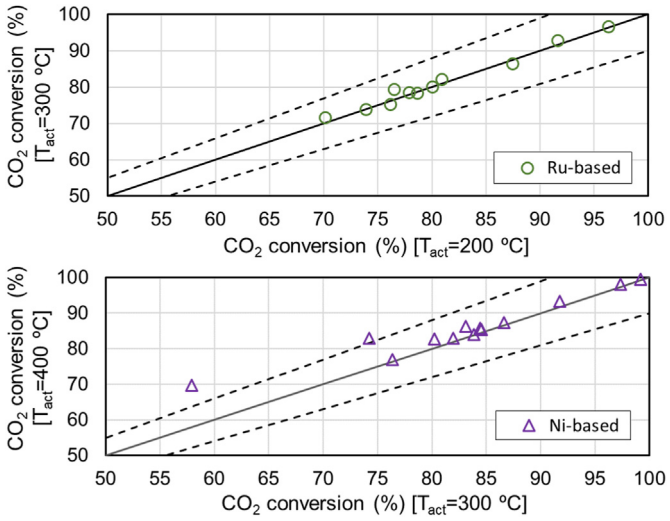


**Fig. 6.** Parity plot of $CO_2$ conversion at the outlet of the reactor, using different activation temperatures. The graph shows the results of Table 5, Tables 6 and 7 versus the results of Table 8. Dashed lines show ±10% error interval.

whose median were −25.7% and −21.3%, probably because of a loosely insulation or a bad positioning of the upper electrical resistance. Therefore, we concluded that about 70% of the length of the reactor was quasi-isothermal in practice, and the rest 30% presented small deviations with respect to the desirable set point temperature due to the scale of the reactor and the complexity of heat management. With regards to Ni-based fixed bed, the median of the temperature differences was in the range +2.2% to −11.3% accounting for all the thermocouples. Therefore, a lower temperature difference in the two first thermocouples of the tests compared to the Ru-based case. This behaviour was considered quasi-isothermal in practice.

### 3.2. Reduction protocol

The influence of the reduction temperature was evaluated for both catalysts. The obtained $CO_2$ conversion is compared through a parity plot in Fig. 6. As it can be seen, all these points laid over the line with a slope of 1 using Ru-based. Therefore, it was concluded that there is no influence of the reduction temperature at the range of 200−300 °C for the Ru-based catalyst. In the case of the Ni-based catalyst (activation temperatures of 300 °C and 400 °C), it was observed an improve in the activity for two operating points corresponding to conditions far from the equilibrium. For the rest of the operating points, at high $CO_2$ conversions, the activation temperature had no effect (points laying on the diagonal line of slope 1 in the parity plot). Since the variation in the $CO_2$ conversion with the activation procedure was negligible in most cases, an intermediate value of 300 °C was chosen for the reduction protocol during the comparison of the catalyst performance.

**Table 2**
Calculated kinetic parameters and minimum mean squared error.

| | Ru-based | Ni-based |
|---|---|---|
| $k_0$ (mol/(s·g·atm$^{5n}$)) | 300.4 | 3421 |
| $E_A$ (kJ/mol) | 77.37 | 69.38 |
| $n$ (−) | 0.2397 | 0.4309 |
| $\alpha$ (1/atm) | 0.6856 | 36.22 |
| MSE (%) | 7.4 (3.0) | 1.4 |

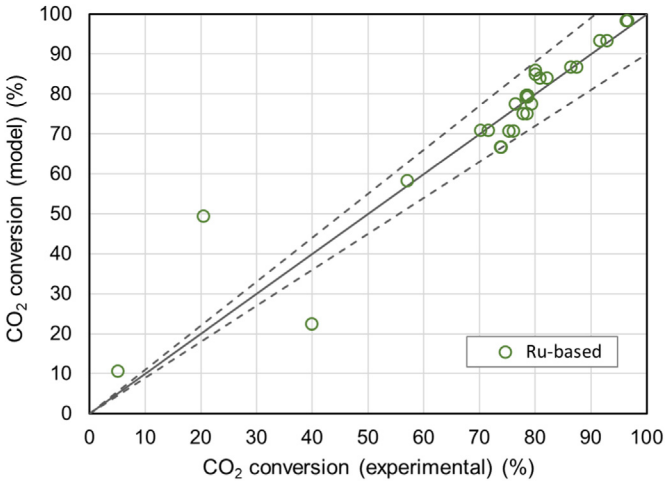


**Fig. 7.** Parity plot for model and experimental $CO_2$ conversion (Ru-based catalyst). Dashed lines show ±10% error interval.

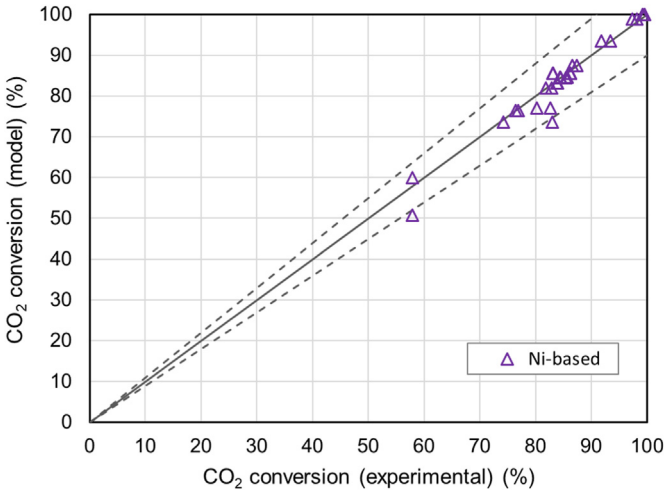


**Fig. 8.** Parity plot for model and experimental $CO_2$ conversion (Ni-based catalyst). Dashed lines show ±10% error interval.

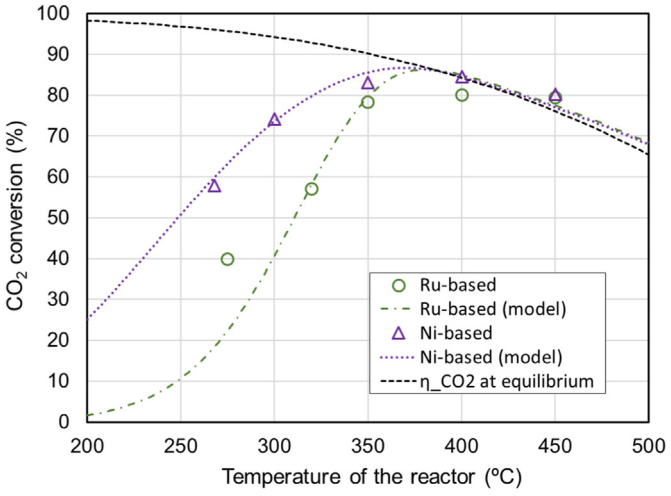


**Fig. 9.** $CO_2$ conversion at the outlet vs. isothermal temperature of reactor. Each point corresponds to one steady state operation. GHSV = 10000 $h^{-1}$; $H_2/CO_2$ ratio = 4; P = 1 atm (Table 5).

### 3.3. Kinetic model

The calculated parameters of the kinetic model, after the minimization of the mean squared error, are presented in Table 2. The mean squared error was 7.4% for the Ru-based catalyst, and 1.4% for the Ni-based catalyst. The activation energy was 77.4 kJ/mol for the Ru-based and 69.4 kJ/mol for the Ni-based, which are in the range of the typical values found in literature (60–80 kJ/mol [59]).

The model results were compared to the experimental data through parity plots to validate the model (Fig. 7 and Fig. 8). Only major deviations were found in two operating points for the Ru-based catalyst, which corresponded to the transient in which the fixed bed starts the auto-thermal behaviour (between 275 and 310 °C, Tests #Ru-T1 and #Ru-T2b, see the Appendix). If these two points are not considered when computing the MSE, we found a mean squared error of 3.0%.

### 3.4. Catalyst performance

The influence of methanation temperature on the $CO_2$ conversion was assessed through experimental tests which make use of both catalysts activated at 300 °C (Table 5). The experiments were carried out under atmospheric pressure, with a gas hourly space velocity of 10000 $h^{-1}$ and a $H_2/CO_2$ ratio equal to 4. Results illustrated in Fig. 9 follow the typical curve of a $CO_2$ methanation conversion versus temperature which may be predicted through a kinetic model. The conversion achieved with Ni-based material was higher for every tested temperature although similar conversions were reached for temperatures from 350 °C. According to results of the kinetic model, the activity of Ni-based catalyst is about 3 times higher than the activity of Ru-based catalyst at 275 °C, while the activity at temperatures greater than 375 °C is nearly the same because equilibrium is reached.

The influence of gas flow was also evaluated through experimental tests carried out with both catalysts activated at 300 °C. The experiments were performed under atmospheric pressure, with a constant temperature of 350 °C and a $H_2/CO_2$ ratio equal to 4 (Table 6). The performance of Ni-based catalyst was better for every tested GHSV between 8000 and 16000 $h^{-1}$ and the trend of the experimental results for both catalysts was coherent and analogous, decreasing with the increase of the gas flowrate through the reactor (Fig. 10). It must be highlighted that the carbon conversion obtained for a doubled flowrate (16000 $h^{-1}$) using Ni-based catalyst was similar than the conversion achieved with Ru-based catalyst (8000 $h^{-1}$). Thus, the Ni-based catalyst would allow for the treatment of a doubled gas flowrate without impact on carbon conversion. The higher GHSV, the wider difference between the conversions obtained for both catalysts.

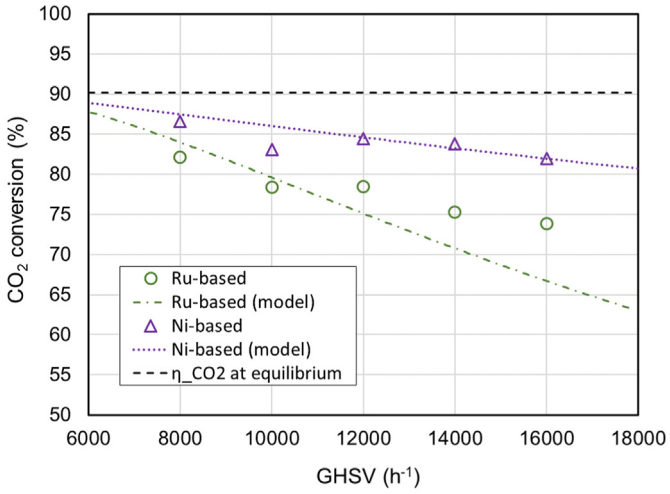


**Fig. 10.** $CO_2$ conversion at the outlet vs. GHSV. Each point corresponds to one steady state operation. T = 350 °C; $H_2/CO_2$ ratio = 4; P = 1 atm (Table 6).

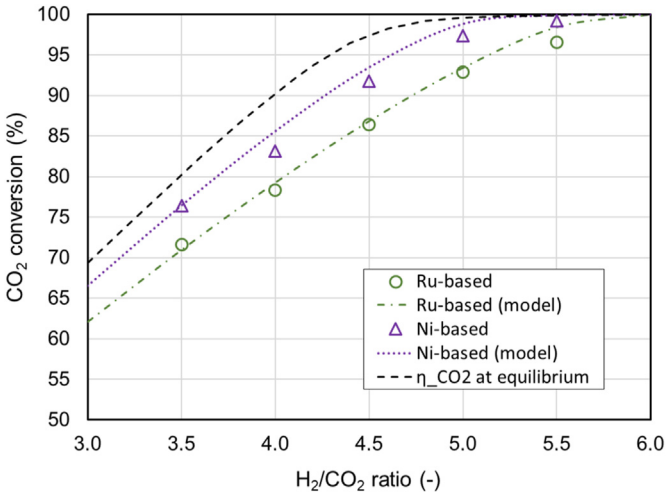


**Fig. 11.** $CO_2$ conversion at the outlet vs. $H_2/CO_2$ ratio at the inlet. Each point corresponds to one steady state operation. GHSV = 10000 $h^{-1}$; T = 350 °C; P = 1 atm (Table 7).

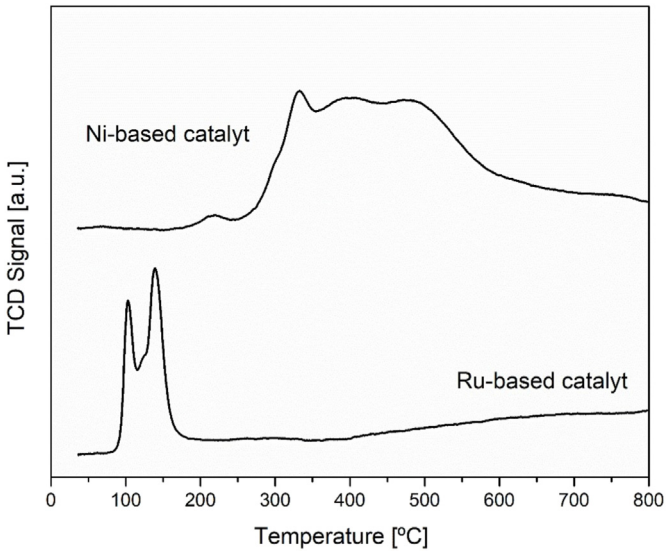


**Fig. 12.** $H_2$-TPR profiles of the Ni- and Ru-based catalysts.

The influence of increasing the $H_2/CO_2$ ratio was analyzed through experimental tests carried out with both catalysts activated at 300 °C. The experiments were performed under atmospheric pressure, with a constant temperature of 350 °C and a GHSV equal to 10000 $h^{-1}$ (Table 7). Again, the $CO_2$ conversion achieved with Ni-based catalyst were higher than those obtained with Ru-based catalyst. The trend shown by the experimental data is a linear increase of carbon conversion with $H_2/CO_2$ ratio until the equilibrium conditions are reached. The activity of the Ni-based catalyst was about 6%–8% greater than the activity of Ru-based catalyst between the $H_2/CO_2$ ratios of 3.5 and 5 (Fig. 11).

### 3.5. Catalyst characterization

Fig. 12 shows $H_2$-TPR profiles of both fresh Ni- and Ru-based catalysts. In the case of the Ni-based catalyst, it was identified a small reduction peak around 225 °C with a shoulder at 300 °C, suggesting an interaction between $CeO_2$ and Ni. In addition, the main reduction peaks detected at around 325, 400, and 475 °C were attributed to the reduction of NiO particles interacted weakly and strongly with the support, respectively. For the Ru-based catalyst, its main reduction peaks were identified at very low temperatures ($\leq$150 °C). This behaviour can be attributed to the fact that the high amount of promoter phase weakens the strong RuO-support interactions, causing over the Ru-based catalyst a better dispersion of their metal components. For comparison purposes, the temperature of 300 °C was selected to estimate the percentage of reducibility of the catalysts. At this conditions, Ru-based catalyst (100%) showed a higher metallic phase activation than Ni-based catalyst (13%), implying that a higher reduction temperature ($\geq$300 °C) can be positive to achieve the activation of Ni sites in a high percentage, as it was also identified in the experiments carried out in section 3.2. Despite the Ni-based catalyst showed a low percentage of reduction at 300 °C, its high catalytic performance estimated in section 3.3 can be justified by the its favourable catalyst activation during the evaluation of the reaction condition parameters, as for example temperature. In this series of experiments, temperatures of 450 °C were used, and therefore the catalyst can be activated during reaction.

The morphology (surface shape) and elemental composition of the Ni- and Ru-based catalyst in their two estates fresh and used were evaluated by SEM images and EDX analysis, respectively. SEM images revealed that after impregnation, both fresh Ni- (Fig. 13 (a)) and Ru-based (Fig. 14 (a)) catalyst kept the shape and mm-size of the alumina support. It was designed spherical catalysts with a verge diameter of 2.2 mm. Compared to fresh Ru-based catalyst (Fig. 14 (b)), microcracks were identified into the surface of some particles of the fresh Ni-based catalyst (see Fig. 13 (a)). The formation of small cracks into the surface can be negative since it structural phenomena can promote to the catalyst attrition by fragmentation, as it can be identified for the used Ni-based catalyst (Fig. 13 (b)). In this catalytic system, it was confirmed the breakages of the particles and particle attrition. The most probably is that during the $CO_2$ metahantion process, Ni-based particles may undergo different forces in different directions when colliding with other particles or the wall of the attrition tube, which causes fragmentation. Therefore, it can be claimed that surface features have effect on attrition resistance, and they can influence attrition mechanisms. However, it is important to note that this new microparticles had not a negative impact in the catalytic performance of the Ni-based catalyst since it showed a superior catalytic activity than that Ru-based catalyst. On the other hand, EDX analysis suggested that the experimental compositions of active and promoter phase of both catalysts, Ni-based (19.04 w.% of Ni and 13.95 wt% of $CeO_2$) and Ru-based (2.23 w.% of Ru and 40.24 wt% of $CeO_2$), were very close to the selected theoretical ones. In the case of the used samples, it was determined a slight reduction of the active phase. The reduction for Ni-based catalyst was 3%, while for the Ru-based catalyst was 8%. Concerning the promoter phase, an opposite behaviour was observed in the used samples. For the used Ni-based catalyst, the $CeO_2$ promoter phase was reduced a 4%. In contrast, an increase in the promoter phase of 2% was determined for the Ru-based catalyst. This reduction of active and promoter phase can be attributed to the attrition particles, A summary of the elemental composition of the two samples in their different estates is summarized in Table 3.

Fig. 15 shows XRD patterns of both Ni-based catalyst (left) and Ru-based catalyst (right) in their fresh and used estates. At the selected temperature reduction of 300 °C, the diffraction peaks found in the Ni-based catalysts around at $2\Theta = 37.24$, 43.28 and 62.91° were indexed to the NiO (101), (012) and (104) lattice planes. Although the NiO phase was detected on both catalysts, these peaks were weaker in the used sample, suggesting that the reduction of the Ni-based catalyst was carried out even during the reaction. This

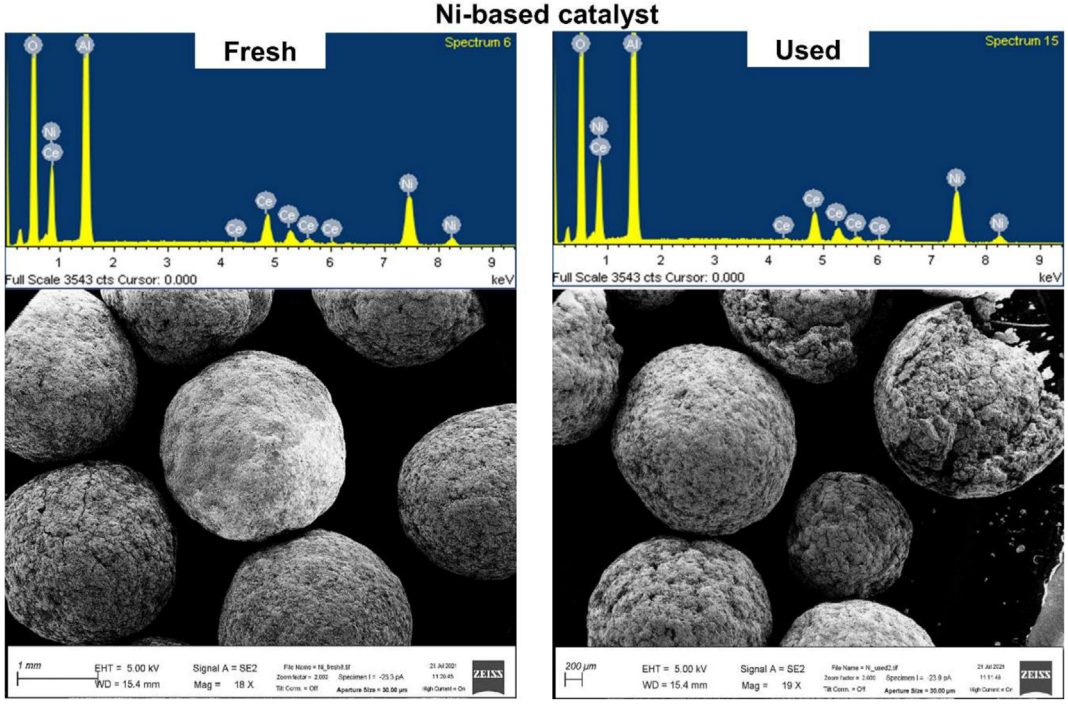


**Fig. 13.** SEM images of the a) fresh and b) used Ni-based catalyst.

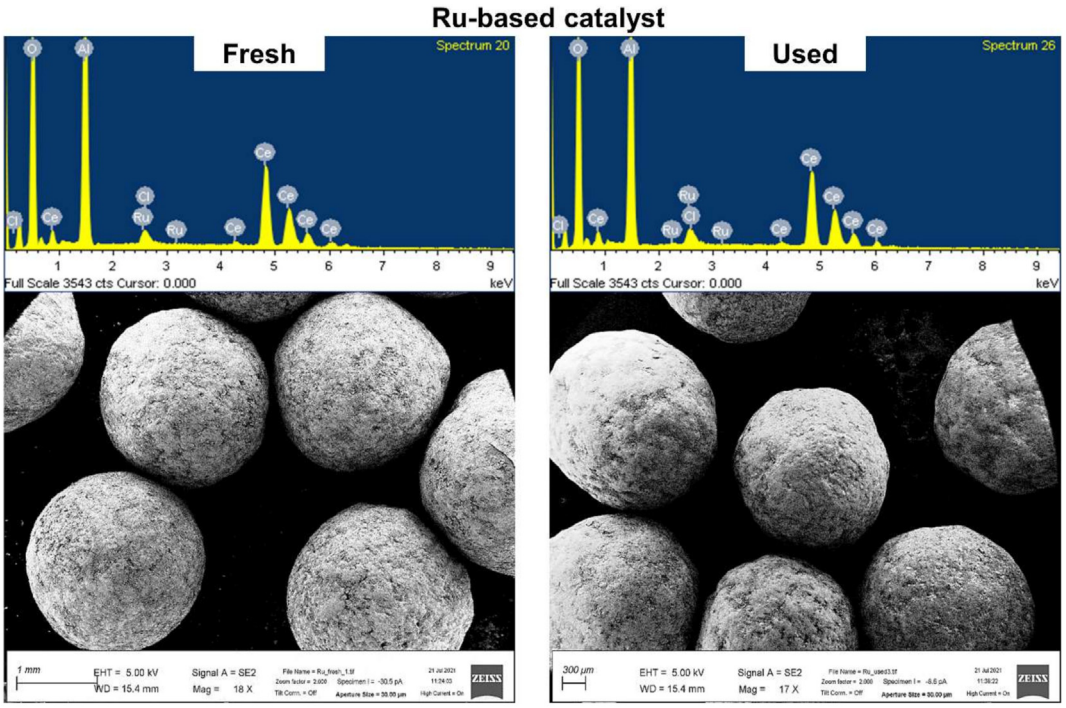


**Fig. 14.** SEM images of a) fresh and b) used Ru-based catalyst.

**Table 3**
Physico-chemical properties of Ni- and Ru-based catalysts.

| Property | Ni-based | | Ru-based | |
|---|---|---|---|---|
| State | Fresh | Used | Fresh | Used |
| Elemental composition (wt%) | | | | |
| Ni | 19.04 | 18.56 | – | – |
| Ru | – | – | 2.23 | 2.06 |
| $CeO_2$ | 3.75 | 13.41 | 40.24 | 41.07 |
| Shape | Spherical | Spherical | Spherical | Spherical |
| Average Diameter (mm) | 2.2 | 2.2 | 2.2 | 2.2 |
| Density (g/cm$^3$) | 1.33 | – | 1.39 | – |
| True density (g/cm$^3$) | 3.75 | – | 3.94 | – |
| Metallic phase reduced (%) | 13 | – | 100 | – |
| BET (m$^2$/g) | 132 | 126 | 122 | 103 |
| Pore volume (cm$^3$/g) | 0.34 | 0.35 | 0.29 | 0.28 |
| Pore diameter (nm) | 9.25 | 9.17 | 9.12 | 9.47 |
| Metal dispersion (%) | 0.21 | 0.14 | 2.89 | 1.63 |
| XRD | | | | |
| dNi (nm) | 24.55 | 14.89 | – | – |
| dRu (nm) | – | – | 27.42 | 27.86 |
| d$CeO_2$ (nm) | 6.72 | 7.39 | 6.29 | 6.85 |

fact can be also confirmed with the behaviour of the peaks diffraction associated with the Ni (111), (200), and (220) lattice planes identified at $2\Theta = 44.50$, 51.84, and 76.37°, respectively. As it can be observed, the peaks of the Ni phase detected in the used catalyst were stronger than those identified in the fresh catalyst. With regard to $CeO_2$ phase, diffraction peaks at $2\Theta = 28.55$, 33.07, and 47.49° were related to the (111), (200), (220), and (222) lattice planes. Between fresh and used catalysts, slight alterations in the intensity of the diffraction peaks were distinguished, implying mainly sintering of the $CeO_2$ particles. Regarding to Ru-based catalysts, for the fresh catalyst, the diffraction peaks identified at $2\Theta = 44.00$ were linked to Ru (101) lattice plane. Similar to Ni-based catalyst, a diffraction peak associated with the $Al_2O_3$ (214) lattice plane was detected at $2\Theta = 66.52°$. Besides Ru and $Al_2O_3$, $CeO_2$ (111), (200), (311), (222), (400) and (331) lattice planes were recorded at $2\Theta = 28.55$, 33.08, 47.47, 56.33, 69.40 and 76.7°, respectively. Between fresh and used Ru-based catalysts, slight alterations in the intensity of the diffraction peaks were distinguished, implying sintering of the Ru and $CeO_2$ particles. According to XRD analysis, Ni-based catalyst shown competitive structural properties in comparison with Ru-based catalyst. After reaction, the average crystal size of the metallic nickel was 14.84 nm, whereas the metallic ruthenium was 27.86 nm. However, an opposite behaviour was observed in the average particle size of $CeO_2$. The average particle size was of approximately 7.39 nm for Ni-based catalyst and 6.85 nm for Ru-based catalyst.

Other structural properties, such as metal dispersion and metallic surface area of Ni- and Ru-based catalysts in their two states were also evaluated and estimated by means of CO-Chemisorption data. According to the results summarized in Table 3, between both fresh catalysts, the better structural properties were measured in the fresh Ru-based catalyst. These enhanced structural effects were in concordance with Ru reducibility (100%), as estimated by $H_2$-TPR measurements. Compared to fresh Ru-based catalyst (2.89% and 10.54 m$^2$/g), a metal dispersion of 0.21% and metal surface area of 1.43 m$^2$/g were achieved for the fresh Ni-based catalyst. After the reaction, a reduction in the structural properties of both catalysts was detected. For the case of the used Ni-based catalyst, its metal dispersion is reduced to 0.14% and its metallic surface area decreased to 0.95 m$^2$/g. Concerning the used Ru-based catalysts, their structural properties were reduced by 43%. It was determined a metal dispersion of 1.63% and metallic surface area of 5.96 m$^2$/g. These results can be linked to the increase of $CeO_2$ particles, as estimated by XRD measurements.

The nitrogen isotherms obtained for Ni-based and Ru-based catalysts were type IV of IUPAC classification, exhibiting H1 hysteresis loops with correspond to mesoporous solids. The main textural properties, such as BET surface area, pore volume and average pore diameter for both catalysts are displayed in Table 3. In overall, Ni-based catalyst shown the best textural properties compared to Ru-based catalyst. As can be observed, BET surface area of fresh Ni-based sample was 132 m$^2$/g, while decreased to

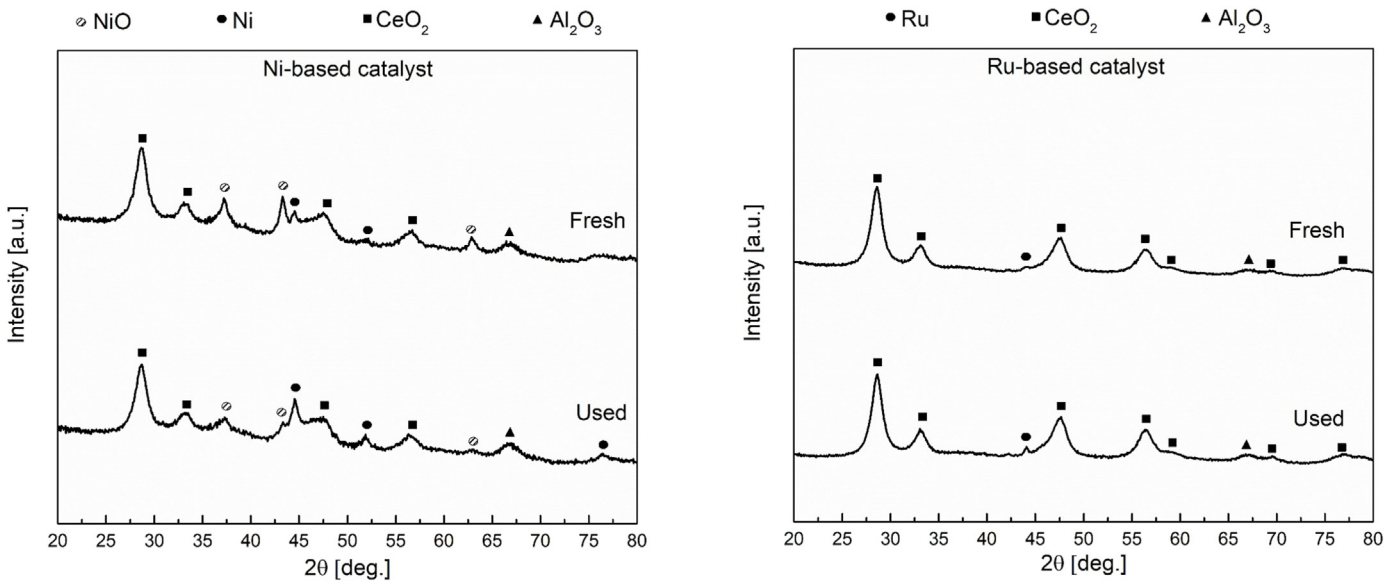


**Fig. 15.** Left: XRD profile of the Ni-based catalyst. [○] NiO: (101), (012) and (104); [•] Ni: (111), (200) and (220); [■] $CeO_2$: (111), (200), (220) and (222); [▲] γ-$Al_2O_3$: (214). Right: XRD profile of the Ru-based catalyst. [•] Ru: (101); [■] CeO2: ((111), (200), (311), (222), (400) and (331); [▲] γ-$Al_2O_3$: (214).

126 $m^2/g$ for used Ni-based sample. With regard to its other textural properties, compared to the fresh sample, an increase of 3% in the pore volume and a reduction of 1% in the pore diameter were measured for the used sample. In the case of the fresh Ru-based catalysts, its BET surface area was 122 $m^2/g$, and even lower than the fresh Ni-based catalyst. This behaviour can be mainly attributed to the high amount of $CeO_2$ promoter. After the reaction, this property decreased to 103 $m^2/g$. Compared to the used Ni-based catalyst, an opposite behaviour was detected in the pore volume and pore diameter of the used Ru-catalyst. The pore volume was reduced by 1%, while the pore diameter increased by 4%. In concordance with SEM, XRD and CO-chemisorption analysis, the modification of the textural properties in the used samples can be mainly attributed to the attrition problems detected for Ni-based catalysts and the thermal degradation of $CeO_2$ particles identified for Ru-based catalysts.

Catalytic performance test showed that the Ni-based catalyst was more active. Characterization techniques revealed that Ru-based catalyst was beneficial as active catalyst at low temperatures. However, this catalytic system showed a low catalytic activity, especially with reaction temperatures below 350 °C. From this temperatures, both catalysts shown similar catalytic activities; however, it was revealed that after reaction, the physicochemical properties of Ni-based catalyst were more stable than the ones Ru-based catalysts. Therefore, considering the favourable catalytic performance and the competitive physicochemical properties achieved over the $CeO_2$ promoted Ni-based catalyst makes it catalytic system promising for industrial applications.

### 3.6. Process design

After comparing the performance of both catalyst, the Ni-based catalyst was selected as the best option for evaluating a process design. It presented higher $CO_2$ conversion under all tested conditions, as well as lower decrease of BET and metal dispersion during operation. Thus, its kinetic model was implemented in Aspen Plus to analyse a methanation plant (Fig. 4). An optimization process was followed to minimize the amount of catalyst required, constrained by the requirement of 95 vol% $CH_4$ in the final gas (independent variables: temperature and mass of catalyst in each reactor, and number of reactors). Cases #2, #3 and #4 of Table 4 correspond to configuration of 2, 3 or 4 reactors in series. The optimization was also performed with additional technical constrains typical for large scale plants (GHSV $\leq$ 5000 $h^{-1}$ and T $\geq$ 300 °C [62]), corresponding to cases #2C, #3C and #4C.

When no technical restrictions were included, the total mass of catalyst required in a 3-reactor plant was almost a quarter of the catalyst required when only 2 reactors were used (Fig. 16). However, including a fourth reactor allowed diminishing the catalyst mass only by an additional 10% (with respect to the 2-reactor configuration). Moreover, the 4-reactor plant required a 26% more energy for the preheating of the gases than the 3-reactor configuration (Fig. 17), and would lead to greater economic costs due to the additional equipment. Thus, 3 was the number of reactors that provided the best results at first approach (using low temperatures of reaction and high GHSV).

When technical restrictions were considered, 95 vol% of $CH_4$ in the final gas could not be achieved in a 2-reactor configuration (temperatures below 300 °C would be required). The difference between the 3-reactor plant and the 4-reactor plant was similar to the previous case. The mass of catalyst was diminished by 27%, but the preheating consumption increased by 20%. This save in the mass of catalyst cannot justify increasing the cost with additional equipment and extra energy consumption. The problem in this case came from the limitation of the GHSV at 5000 $h^{-1}$, which prevented from further diminishing the amount of catalyst mass. In the 4-reactor plant, the two first reactors were at the upper limit of GHSV, and the third one close to it, so the minimization of the mass of catalyst gets remarkably constrained when 4 or more reactors are installed.

Thus, the 3-reactor plant was found to be the most adequate configuration when considering isothermal fixed-bed reactors operating with the Ni-based catalyst studied in this paper. In this configuration, the total amount of catalyst was 3.26 kg per kg/h of SNG produced, the preheating requirement was 4.90 $MJ/kg_{SNG}$, and the heat evacuated in the reactors was 10.8 $MJ/kg_{SNG}$. The preheating needs could be partially satisfied with the heat removed from the reactors and condensers. The average temperature of the three isothermal reactors was 320 °C (300–348 °C), and the GHSV varied from 1150 to 5000 $h^{-1}$, which is in total agreement with

**Table 4**
Operating parameters of the studied configurations for the methanation plant. Each configuration corresponds to an optimization that minimizes the required amount of catalyst mass.

| Configuration | #2 | #2C | #3 | #3C | #4 | #4C |
|---|---|---|---|---|---|---|
| Electrolysis capacity (MW) | 1.0 | 1.0 | 1.0 | 1.0 | 1.0 | 1.0 |
| $m_{H2}$ (kg/h) | 20.42 | 20.42 | 20.42 | 20.42 | 20.42 | 20.42 |
| $m_{CO2}$ (kg/h) | 111.45 | 111.45 | 111.45 | 111.45 | 111.45 | 111.45 |
| Pressure (atm) | 1 | 1 | 1 | 1 | 1 | 1 |
| Number of reactors | 2 | 2 | 3 | 3 | 4 | 4 |
| Type of catalyst | Ni-based | Ni-based | Ni-based | Ni-based | Ni-based | Ni-based |
| Technical constrains | | | | | | |
| - GHSV ($h^{-1}$) | – | $\leq$ 5000 | – | $\leq$ 5000 | – | $\leq$ 5000 |
| - T (°C) | – | $\geq$ 300 | – | $\geq$ 300 | – | $\geq$ 300 |
| - $CH_4$ in SNG (vol% dry) | 95.0 | 95.0 | 95.0 | 95.0 | 95.0 | 95.0 |
| - Condensers (°C) | 35.0 | 35.0 | 35.0 | 35.0 | 35.0 | 35.0 |
| Reactor 1 | | | | | | |
| - T (°C) | 320.0 | – | 380.5 | 348.0 | 411.9 | 351.8 |
| - $m_{cat}$ (kg) | 152.7 | – | 17.5 | 48.8 | 7.3 | 48.8 |
| - GHSV ($h^{-1}$) | 1598.6 | – | 13938 | 5000.0 | 33461 | 5000.0 |
| - $CO_2$ conversion (%) | 92.5 | – | 85.7 | 89.4 | 81.6 | 89.4 |
| - $CH_4$ in outlet gas (vol% dry) | 71.1 | – | 54.4 | 62.8 | 46.9 | 62.8 |
| - Cooling (kW) | 116.1 | – | 108.9 | 113.0 | 104.4 | 113.0 |
| Reactor 2 | | | | | | |
| - T (°C) | 266.3 | – | 325.9 | 310.7 | 351.8 | 334.6 |
| - $m_{cat}$ (kg) | 258.5 | – | 25.1 | 37.7 | 10.8 | 14.7 |
| - GHSV ($h^{-1}$) | 260.1 | – | 3240.8 | 1955.6 | 8326.8 | 5000 |
| - $CO_2$ conversion (%) | 86.3 | – | 79.4 | 79.5 | 75.9 | 73.3 |
| - $CH_4$ in outlet gas (vol% dry) | 95.0 | $\leq$ 94.0 | 86.7 | 89.9 | 81.1 | 87.2 |
| - Cooling (kW) | 8.0 | – | 14.3 | 10.6 | 17.6 | 9.7 |
| Reactor 3 | | | | | | |
| - T (°C) | – | – | 285.2 | 300.0 | 311.8 | 318.1 |
| - $m_{cat}$ (kg) | – | – | 61.7 | 49.0 | 21.5 | 11.8 |
| - GHSV ($h^{-1}$) | – | – | 938.1 | 1149.0 | 2827.9 | 4881.9 |
| - $CO_2$ conversion (%) | – | – | 65.5 | 53.2 | 63.9 | 45.9 |
| - $CH_4$ in outlet gas (vol% dry) | – | – | 95.0 | 95.0 | 92.3 | 92.7 |
| - Cooling (kW) | – | – | 2.4 | 1.4 | 3.5 | 1.6 |
| Reactor 4 | | | | | | |
| - T (°C) | – | – | – | – | 293.6 | 300.0 |
| - $m_{cat}$ (kg) | – | – | – | – | 24.4 | 23.5 |
| - GHSV ($h^{-1}$) | – | – | – | – | 2258.0 | 2338.9 |
| - $CO_2$ conversion (%) | – | – | – | – | 36.6 | 33.2 |
| - $CH_4$ in outlet gas (vol% dry) | – | – | – | – | 95.0 | 95.0 |
| - Cooling (kW) | – | – | – | – | 0.7 | 0.6 |
| Total cooling at reactor (kW) | 124.1 | – | 125.6 | 125.0 | 126.3 | 125.0 |
| Total cooling at condensers (kW) | 90.5 | – | 109.0 | 104.6 | 124.4 | 115.7 |
| Total preheating (kW) | 41.9 | – | 61.8 | 56.7 | 77.9 | 68.0 |
| Total $m_{cat}$ – optimization variable (kg) | 411.2 | No solution | 104.3 | 135.5 | 64.0 | 98.8 |

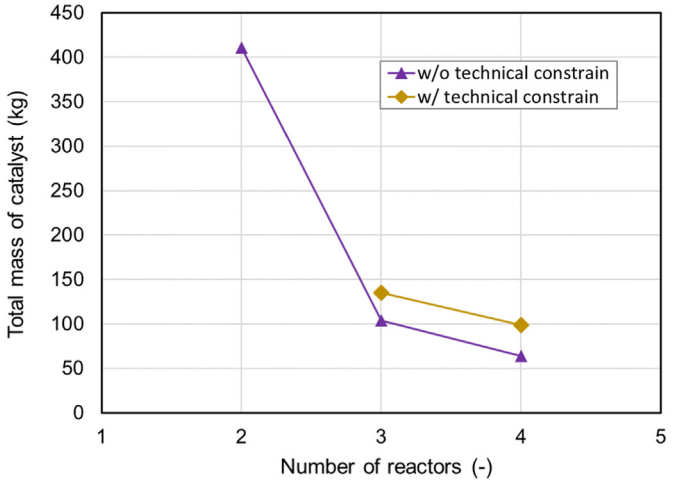


**Fig. 16.** Minimum total mass of Ni-based catalyst necessary to reach 95 vol% of $CH_4$ in the SNG vs. number of reactors in the methanation plant (1 MW electrolysis capacity) with and without technical constrains.

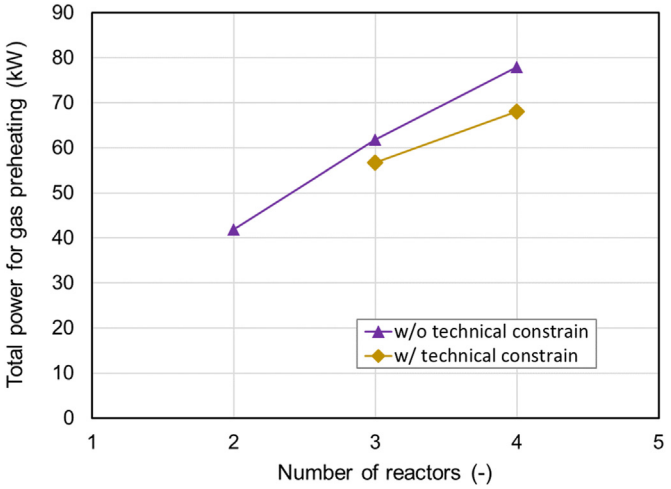


**Fig. 17.** Total power required for gas preheating vs. number of reactors in the methanation plant (1 MW electrolysis capacity) with and without technical constrains. The results correspond to the operation with the minimum total mass of Ni-based catalyst necessary to reach 95 vol% of $CH_4$ in the SNG.

literature [62]. The $CO_2$ conversion in the first reactor was 90%, in the second 80% and in the third one 53%, leading to a SNG with $CH_4$ content of 95 vol%. The required electrolysis power capacity was 86.4 MJ/$kg_{SNG}$.

## 4. Conclusions

In this paper, we compared nickel and ruthenium as catalyst active phase for synthetic natural gas production at a 1 kW reactor, using in-house catalysts with ceria as promoter. The catalysts were tested in a fixed-bed reactor with bottled $CO_2$ and $H_2$. The fixed bed was 49 cm in length and 3 cm in diameter. The catalyst spheres were mixed with alumina spheres to have a homogenous distribution of temperature, which was monitored with 9 thermocouples distributed along the reactor length. The tested conditions were 250−450 °C at intervals of 50 °C, gas hourly space velocities from 8000 to 16000 $h^{-1}$ spaced by 2000 $h^{-1}$, and $H_2/CO_2$ ratios in the range 3.5−5.5 by steps of 0.5. All the experiments were performed at atmospheric pressure. The following conclusions were found:

- The behaviour of the reactor was considered isothermal in practice (considering the size of the reactor): The median of the difference between the measured temperature and the isothermal set point temperature was in the range +2.2% to −11.3% for the Ni-based catalyst (accounting for all the thermocouples and tests). In the case of the Ru-based catalyst, the median was between +3.3% and −14.3% for 7 out of 9 thermocouples, with variations smaller than −26% for the other two thermocouples.
- The Ni-based catalyst presented higher $CO_2$ conversion under all tested conditions: The activity of Ni-based catalyst is 3 times higher than the activity of Ru-based catalyst at 275 °C, while the activity at temperatures greater than 375 °C is nearly the same because equilibrium is reached.
- The Ni-based catalyst is the preferred option in terms of physicochemical properties for this reactor: The decrease of the BET and metal dispersion in Ni-based catalyst was lower than for the Ru-based catalyst.
- Two kinetic models were successfully elaborated: The models are valid for the catalysts studied in this paper and for the type of reactor used. The minimum mean squared error between the kinetic model and the experimental measurements was 3.0% for the Ru-based catalyst and 1.4% for the Ni-based catalyst.
- In terms of plant design, the 3-reactor plant was found to be the most adequate configuration: Different potential designs of a methanation plant were evaluated in Aspen Plus for the Ni-based catalyst. The designs considered 2 to 4 reactors in series with intermediate condensers. The simulation was optimized using the SQP method in order to minimize the amount of catalyst required to reach 95 vol% of $CH_4$ in the final gas within proper technical limits (GHSV $\leq$ 5000 $h^{-1}$ and temperature $\geq$ 300 °C). In the case of the 3-reactor plant, the total amount of catalyst was 3.26 kg per kg/h of SNG produced. The total useful heat removed from the reactors was 10.8 MJ/$kg_{SNG}$, while the preheating necessity was 4.90 MJ/$kg_{SNG}$. The temperature of the reactors was in the range 300−348 °C, and the GHSV varied between 1150 and 5000 $h^{-1}$. The required electrolysis energy consumption was 86.4 MJ/$kg_{SNG}$. In the case of a 2-reactor plant, the 95 vol% of $CH_4$ could not be achieved in the final gas, while in the 4-reactor plant, the decrease in the required catalyst mass (−27%) does not justify the increment in preheating necessities (+20%) and the additional costs of a 4th reactor.

## Credit author statement

Conceptualization, M.B., P.L., B.P., A.A., J.G., LM.R.; Methodology, M.B., B.P., A.A., J.G.; Software, M.B.; Validation, M.B., B.P., A.A., J.G.; Formal analysis, M.B., B.P., A.A., J.G.; Investigation, M.B., P.L., B.P., A.A., J.G., LM.R., J.P.; Writing − original draft, M.B., P.L., A.A., J.G.; Visualization, M.B., A.A., J.G.; Funding acquisition, M.B., P.L., B.P., LM.R. All authors have read and agreed to the published version of the manuscript.

## Declaration of competing interest

The authors declare that they have no known competing financial interests or personal relationships that could have appeared to influence the work reported in this paper.

## Data availability

The data is available in the appendix.

## Acknowledgments

The work described in this paper is supported by the R+D Spanish National Program from Ministerio de Economía y Competitividad, MINECO (Spanish Ministry of Economy and Competitiveness) and the European Regional Development Funds (European Commission), under project ENE2016-76850-R. This work has also been supported by the Government of Aragon (Research Group DGA T46_17R) and co-financed by FEDER 2014−2020 "Construyendo Europa desde Aragón" (ALEN OXY-PtG). This project has received funding from the European Union's Framework Programme for Research and Innovation Horizon 2020 (2014−2020) under the Marie Skłodowska-Curie Grant Agreement No. 887077. IREC is grateful to Producte19 project (AGAUR, 2019 PROD 00091) for catalyst development activities. Authors would like to acknowledge the use of "Servicio General de Apoyo a la Investigación-SAI", Universidad de Zaragoza.

## Nomenclature

*Symbols*

| | |
|---|---|
| $E_A$ | activation energy, kJ/mol |
| $F$ | volumetric flow (STP), $cm^3/h$ |
| $GHSV$ | gas hourly space velocity, 1/h |
| $k_0$ | pre-exponential factor, kmol/(s·$g_{cat}$·$atm^{5n}$) |
| $K_{eq}$ | equilibrium constant, $1/atm^2$ |
| $m$ | mass, g |
| MSE | mean squared error, % |
| $n$ | calculation parameter indicating the reaction order, |
| $N$ | number of experimental tests, |
| $R$ | ideal gas constant, kJ/K·mol |
| $T$ | temperature, K |
| $x$ | molar fraction in the final gas, |

*Greek symbols*

| | |
|---|---|
| $\alpha$ | calculation parameter, 1/atm |
| $\eta_{CO2}$ | $CO_2$ conversion to $CH_4$, % |
| $\rho$ | bulk density, $g/cm^3$ |

*Subscripts and superscripts*

| | |
|---|---|
| *cat* | catalyst |

## Appendix. Experimental data

**Table 5**
Experimental data for the comparison of catalyst performance under different operating temperatures.

| Test | Fixed bed | Reduction | | $m_{H2}$ (kg/h) | $m_{CO2}$ (kg/h) | T (°C) | GHSV ($h^{-1}$) | $H_2/CO_2$ (−) | $\eta_{CO2}$ (%) | $\eta_{CO2}$ (%) at equil | $CH_4$ | $CO_2$ | CO | $H_2$ |
|---|---|---|---|---|---|---|---|---|---|---|---|---|---|---|
| | | T(°C) | $m_{H2}$ (kg/h) | | | | | | | | (%vol. dry) | | | |
| #Ru-T1 | Ru | 300 | 0.015 | 0.03241 | 0.17827 | 275 | 10,000 | 4.0 | 39.9 | 95.7 | 13.0 | 19.6 | 0.0 | 69.6 |
| #Ru-T2 | Ru | 300 | 0.015 | 0.03241 | 0.17827 | 320 | 10,000 | 4.0 | 57.0 | 92.9 | 23.0 | 17.3 | 0.0 | 60.0 |
| #Ru-T3 | Ru | 300 | 0.015 | 0.03241 | 0.17827 | 350 | 10,000 | 4.0 | 78.4 | 90.2 | 44.7 | 12.3 | 0.1 | 42.3 |
| #Ru-T4 | Ru | 300 | 0.015 | 0.03241 | 0.17827 | 400 | 10,000 | 4.0 | 80.0 | 84.3 | 47.0 | 11.7 | 0.1 | 40.5 |
| #Ru-T5 | Ru | 300 | 0.015 | 0.03241 | 0.17827 | 450 | 10,000 | 4.0 | 79.4 | 76.1 | 46.2 | 11.8 | 0.2 | 41.4 |
| #Ni-T1 | Ni | 300 | 0.015 | 0.03204 | 0.17623 | 268 | 10,000 | 4.0 | 57.9 | 95.7 | 23.5 | 17.0 | 0.1 | 60.3 |
| #Ni-T2 | Ni | 300 | 0.015 | 0.03204 | 0.17623 | 300 | 10,000 | 4.0 | 74.2 | 92.9 | 38.7 | 13.4 | 0.1 | 46.9 |
| #Ni-T3 | Ni | 300 | 0.015 | 0.03204 | 0.17623 | 350 | 10,000 | 4.0 | 83.1 | 90.2 | 52.2 | 10.5 | 0.1 | 36.2 |
| #Ni-T4 | Ni | 300 | 0.015 | 0.03204 | 0.17623 | 400 | 10,000 | 4.0 | 84.5 | 84.3 | 54.2 | 9.8 | 0.1 | 34.8 |
| #Ni-T5 | Ni | 300 | 0.015 | 0.03204 | 0.17623 | 450 | 10,000 | 4.0 | 80.2 | 76.1 | 47.9 | 11.5 | 0.3 | 40.5 |

**Table 6**
Experimental data for the comparison of catalyst performance under different GHSV.

| Test | *Fixed bed* | Reduction | | *$m_{H2}$ (kg/h)* | *$m_{CO2}$ (kg/h)* | *T (°C)* | *GHSV ($h^{-1}$)* | *$H_2/CO_2$ (−)* | *$\eta_{CO2}$ (%)* | *$\eta_{CO2}$ (%) at equil.* | $CH_4$ | $CO_2$ | CO | $H_2$ |
|---|---|---|---|---|---|---|---|---|---|---|---|---|---|---|
| | | *T (°C)* | *$m_{H2}$ (kg/h)* | | | | | | | | (%vol. dry) | | | |
| #Ru-G1 | Ru | 300 | 0.015 | 0.02593 | 0.14262 | 350 | 8000 | 4.0 | 82.1 | 90.3 | 49.7 | 10.8 | 0.1 | 36.6 |
| #Ru-G2 | Ru | 300 | 0.015 | 0.03241 | 0.17827 | 350 | 10,000 | 4.0 | 78.4 | 90.3 | 44.7 | 12.3 | 0.1 | 42.3 |
| #Ru-G3 | Ru | 300 | 0.015 | 0.03890 | 0.21393 | 350 | 12,000 | 4.0 | 78.5 | 90.3 | 44.8 | 12.2 | 0.1 | 42.3 |
| #Ru-G4 | Ru | 300 | 0.015 | 0.04538 | 0.24958 | 350 | 14,000 | 4.0 | 75.3 | 90.3 | 40.1 | 13.0 | 0.1 | 46.5 |
| #Ru-G5 | Ru | 300 | 0.015 | 0.05186 | 0.28524 | 350 | 16,000 | 4.0 | 73.8 | 90.3 | 38.2 | 13.4 | 0.2 | 48.4 |
| #Ni-G1 | Ni | 300 | 0.015 | 0.02563 | 0.14098 | 350 | 8000 | 4.0 | 86.6 | 90.3 | 60.0 | 9.2 | 0.1 | 30.0 |
| #Ni-G2 | Ni | 300 | 0.015 | 0.03204 | 0.17623 | 350 | 10,000 | 4.0 | 83.1 | 90.3 | 52.2 | 10.5 | 0.1 | 36.2 |
| #Ni-G3 | Ni | 300 | 0.015 | 0.03845 | 0.21147 | 350 | 12,000 | 4.0 | 84.4 | 90.3 | 55.2 | 10.1 | 0.1 | 34.4 |
| #Ni-G4 | Ni | 300 | 0.015 | 0.04486 | 0.24672 | 350 | 14,000 | 4.0 | 83.8 | 90.3 | 53.3 | 10.2 | 0.1 | 36.2 |
| #Ni-G5 | Ni | 300 | 0.015 | 0.05127 | 0.28197 | 350 | 16,000 | 4.0 | 81.9 | 90.3 | 50.5 | 11.0 | 0.1 | 39.1 |

**Table 7**
Experimental data for the comparison of catalyst performance under different $H_2/CO_2$ ratios.

| Test | *Fixed bed* | Reduction | | *$m_{H2}$ (kg/h)* | *$m_{CO2}$ (kg/h)* | *T (°C)* | *GHSV ($h^{-1}$)* | *$H_2/CO_2$ (−)* | *$\eta_{CO2}$ (%)* | *$\eta_{CO2}$ (%) at equil.* | $CH_4$ | $CO_2$ | CO | $H_2$ |
|---|---|---|---|---|---|---|---|---|---|---|---|---|---|---|
| | | *T (°C)* | *$m_{H2}$ (kg/h)* | | | | | | | | (%vol. dry) | | | |
| #Ru-R1 | Ru | 300 | 0.015 | 0.03151 | 0.19808 | 350 | 10,000 | 3.5 | 71.6 | 80.3 | 46.7 | 18.4 | 0.1 | 34.0 |
| #Ru-R2 | Ru | 300 | 0.015 | 0.03241 | 0.17827 | 350 | 10,000 | 4.0 | 78.4 | 90.3 | 44.7 | 12.3 | 0.1 | 42.3 |
| #Ru-R3 | Ru | 300 | 0.015 | 0.03315 | 0.16207 | 350 | 10,000 | 4.5 | 86.4 | 97.4 | 44.1 | 6.9 | 0.0 | 47.9 |
| #Ru-R4 | Ru | 300 | 0.015 | 0.03376 | 0.14856 | 350 | 10,000 | 5.0 | 92.9 | 99.6 | 42.5 | 3.2 | 0.0 | 53.4 |
| #Ru-R5 | Ru | 300 | 0.015 | 0.03428 | 0.13713 | 350 | 10,000 | 5.5 | 96.6 | 99.9 | 38.0 | 1.4 | 0.0 | 60.0 |
| #Ni-R1 | Ni | 300 | 0.015 | 0.03115 | 0.19581 | 350 | 10,000 | 3.5 | 76.4 | 80.3 | 56.7 | 17.4 | 0.1 | 25.9 |
| #Ni-R2 | Ni | 300 | 0.015 | 0.03204 | 0.17623 | 350 | 10,000 | 4.0 | 83.1 | 90.3 | 52.2 | 10.5 | 0.1 | 36.2 |
| #Ni-R3 | Ni | 300 | 0.015 | 0.03277 | 0.16021 | 350 | 10,000 | 4.5 | 91.8 | 97.4 | 54.6 | 4.9 | 0.0 | 40.4 |
| #Ni-R4 | Ni | 300 | 0.015 | 0.03338 | 0.14686 | 350 | 10,000 | 5.0 | 97.3 | 99.6 | 47.3 | 1.3 | 0.0 | 56.6 |
| #Ni-R5 | Ni | 300 | 0.015 | 0.03389 | 0.13556 | 350 | 10,000 | 5.5 | 99.2 | 99.9 | 40.1 | 0.3 | 0.0 | 59.2 |

**Table 8**
Repetition of experimental data of Table 5, Tables 6 and 7 at different reduction temperature.

| Test | *Fixed bed* | Reduction | | *$m_{H2}$ (kg/h)* | *$m_{CO2}$ (kg/h)* | *T (°C)* | *GHSV ($h^{-1}$)* | *$H_2/CO_2$ (−)* | *$\eta_{CO2}$ (%)* | *$\eta_{CO2}$ (%) at equil.* | $CH_4$ | $CO_2$ | CO | $H_2$ |
|---|---|---|---|---|---|---|---|---|---|---|---|---|---|---|
| | | *T (°C)* | *$m_{H2}$ (kg/h)* | | | | | | | | (%vol. dry) | | | |
| #Ru-T1b | Ru | 200 | 0.015 | 0.03241 | 0.17827 | 250 | 10,000 | 4.0 | 5.1 | 95.7 | 1.2 | 22.2 | 0.0 | 79.7 |
| #Ru-T2b | Ru | 200 | 0.015 | 0.03241 | 0.17827 | 310 | 10,000 | 4.0 | 20.5 | 92.9 | 5.5 | 21.3 | 0.0 | 76.0 |
| #Ru-T3b | Ru | 200 | 0.015 | 0.03241 | 0.17827 | 350 | 10,000 | 4.0 | 78.6 | 90.2 | 45.0 | 12.1 | 0.1 | 42.0 |
| #Ru-T4b | Ru | 200 | 0.015 | 0.03241 | 0.17827 | 390 | 10,000 | 4.0 | 80.1 | 84.3 | 48.6 | 11.9 | 0.2 | 39.3 |
| #Ru-T5b | Ru | 200 | 0.015 | 0.03241 | 0.17827 | 450 | 10,000 | 4.0 | 76.5 | 76.1 | 40.4 | 12.2 | 0.2 | 42.3 |
| #Ru-G1b | Ru | 200 | 0.015 | 0.02593 | 0.14262 | 350 | 8000 | 4.0 | 80.9 | 90.3 | 48.6 | 11.4 | 0.1 | 38.8 |
| #Ru-G2b | Ru | 200 | 0.015 | 0.03241 | 0.17827 | 350 | 10,000 | 4.0 | 78.6 | 90.3 | 45.0 | 12.1 | 0.1 | 42.0 |
| #Ru-G3b | Ru | 200 | 0.015 | 0.03890 | 0.21393 | 350 | 12,000 | 4.0 | 77.9 | 90.3 | 44.0 | 12.4 | 0.1 | 43.0 |

(*continued on next page*)

**Table 8** (*continued*)

| Test | *Fixed bed* | Reduction | | $m_{H2}$ (kg/h) | $m_{CO2}$ (kg/h) | *T* (°C) | *GHSV* ($h^{-1}$) | $H_2/CO_2$ (−) | $\eta_{CO2}$ (%) | $\eta_{CO2}$ (%) at equil. | $CH_4$ | $CO_2$ | CO | $H_2$ |
|---|---|---|---|---|---|---|---|---|---|---|---|---|---|---|
| | | *T* (°C) | $m_{H2}$ (kg/h) | | | | | | | | (%vol. dry) | | | |
| #Ru-G4b | Ru | 200 | 0.015 | 0.04538 | 0.24958 | 350 | 14,000 | 4.0 | 76.1 | 90.3 | 41.8 | 12.9 | 0.1 | 45.4 |
| #Ru-G5b | Ru | 200 | 0.015 | 0.05186 | 0.28524 | 350 | 16,000 | 4.0 | 73.9 | 90.3 | 39.5 | 13.8 | 0.1 | 47.7 |
| #Ru-R1b | Ru | 200 | 0.015 | 0.03151 | 0.19808 | 350 | 10,000 | 3.5 | 70.2 | 80.3 | 43.6 | 18.4 | 0.2 | 36.5 |
| #Ru-R2b | Ru | 200 | 0.015 | 0.03241 | 0.17827 | 350 | 10,000 | 4.0 | 78.6 | 90.3 | 45.0 | 12.1 | 0.1 | 42.0 |
| #Ru-R3b | Ru | 200 | 0.015 | 0.03315 | 0.16207 | 350 | 10,000 | 4.5 | 87.5 | 97.4 | 46.3 | 6.6 | 0.1 | 46.4 |
| #Ru-R4b | Ru | 200 | 0.015 | 0.03376 | 0.14856 | 350 | 10,000 | 5.0 | 91.6 | 99.6 | 40.9 | 3.7 | 0.0 | 54.6 |
| #Ru-R5b | Ru | 200 | 0.015 | 0.03428 | 0.13713 | 350 | 10,000 | 5.5 | 96.3 | 99.9 | 38.2 | 1.5 | 0.0 | 60.0 |
| #Ni-T1b | Ni | 400 | 0.015 | 0.03204 | 0.17623 | 250 | 10,000 | 4.0 | 57.9 | 95.7 | 21.9 | 15.9 | 0.1 | 57.9 |
| #Ni-T2b | Ni | 400 | 0.015 | 0.03204 | 0.17623 | 300 | 10,000 | 4.0 | 83.0 | 92.9 | 49.4 | 10.1 | 0.0 | 34.6 |
| #Ni-T3b | Ni | 400 | 0.015 | 0.03204 | 0.17623 | 350 | 10,000 | 4.0 | 86.2 | 90.2 | 55.5 | 8.9 | 0.0 | 30.1 |
| #Ni-T4b | Ni | 400 | 0.015 | 0.03204 | 0.17623 | 400 | 10,000 | 4.0 | 85.4 | 84.3 | 54.7 | 9.3 | 0.1 | 31.0 |
| #Ni-T5b | Ni | 400 | 0.015 | 0.03204 | 0.17623 | 450 | 10,000 | 4.0 | 82.7 | 76.1 | 50.0 | 10.3 | 0.1 | 35.2 |
| #Ni-G1b | Ni | 400 | 0.015 | 0.02563 | 0.14098 | 350 | 8000 | 4.0 | 87.4 | 90.3 | 59.0 | 8.5 | 0.0 | 27.2 |
| #Ni-G2b | Ni | 400 | 0.015 | 0.03204 | 0.17623 | 350 | 10,000 | 4.0 | 86.2 | 90.3 | 55.5 | 8.9 | 0.0 | 30.1 |
| #Ni-G3b | Ni | 400 | 0.015 | 0.03845 | 0.21147 | 350 | 12,000 | 4.0 | 85.7 | 90.3 | 54.2 | 9.0 | 0.1 | 31.7 |
| #Ni-G4b | Ni | 400 | 0.015 | 0.04486 | 0.24672 | 350 | 14,000 | 4.0 | 83.9 | 90.3 | 51.5 | 9.8 | 0.1 | 34.4 |
| #Ni-G5b | Ni | 400 | 0.015 | 0.05127 | 0.28197 | 350 | 16,000 | 4.0 | 82.9 | 90.3 | 49.1 | 10.0 | 0.1 | 36.4 |
| #Ni-R1b | Ni | 400 | 0.015 | 0.03115 | 0.19581 | 350 | 10,000 | 3.5 | 76.9 | 80.3 | 55.7 | 16.7 | 0.1 | 22.6 |
| #Ni-R2b | Ni | 400 | 0.015 | 0.03204 | 0.17623 | 350 | 10,000 | 4.0 | 86.2 | 90.3 | 55.5 | 8.9 | 0.0 | 30.1 |
| #Ni-R3b | Ni | 400 | 0.015 | 0.03277 | 0.16021 | 350 | 10,000 | 4.5 | 93.4 | 97.4 | 51.9 | 3.7 | 0.0 | 39.3 |
| #Ni-R4b | Ni | 400 | 0.015 | 0.03338 | 0.14686 | 350 | 10,000 | 5.0 | 98.1 | 99.6 | 43.8 | 0.9 | 0.0 | 50.4 |
| #Ni-R5b | Ni | 400 | 0.015 | 0.03389 | 0.13556 | 350 | 10,000 | 5.5 | 99.6 | 99.9 | 36.0 | 0.2 | 0.0 | 59.6 |

**Table 9**
Temperatures (°C) measured at the wall of the tube containing the fixed bed.

| Test | Set point (°C) | Thermocouple | | | | | | | | |
|---|---|---|---|---|---|---|---|---|---|---|
| | | 1 | 2 | 3 | 4 | 5 | 6 | 7 | 8 | 9 |
| #Ru-T1 | 275 | 225.2 | 231.0 | 258.2 | 272.2 | 285.5 | 270.2 | 254.9 | 249.9 | 231.9 |
| #Ru-T2 | 320 | 246.7 | 271.4 | 292.0 | 309.7 | 328.0 | 320.9 | 304.9 | 295.5 | 274.9 |
| #Ru-T3 | 350 | 260.7 | 276.5 | 324.2 | 347.0 | 353.6 | 336.5 | 315.4 | 307.0 | 283.7 |
| #Ru-T4 | 400 | 264.9 | 313.0 | 396.2 | 407.9 | 406.4 | 378.6 | 345.6 | 335.8 | 3136 |
| #Ru-T5 | 450 | 326.8 | 374.5 | 443.2 | 451.6 | 449.7 | 421.1 | 390.9 | 372.3 | 341.0 |
| #Ru-T1b | 250 | 223.9 | 242.4 | 248.9 | 259.8 | 258.4 | 264.7 | 245.1 | 242.7 | 230.6 |
| #Ru-T2b | 310 | 261.4 | 299.4 | 310.5 | 317.9 | 301.6 | 306.7 | 274.6 | 274.2 | 261.0 |
| #Ru-T3b | 350 | 266.7 | 278.3 | 339.0 | 342.7 | 367.3 | 368.5 | 352.6 | 352.7 | 335.7 |
| #Ru-T4b | 390 | 289.9 | 313.9 | 378.6 | 396.9 | 403.0 | 383.7 | 361.7 | 346.7 | 312.9 |
| #Ru-T5b | 450 | 317.6 | 374.1 | 439.8 | 447.0 | 441.5 | 412.7 | 375.9 | 365.7 | 344.1 |
| #Ru-G1 | 350 | 253.1 | 259.5 | 344.5 | 340.8 | 361.5 | 356.1 | 343.8 | 341.9 | 324.6 |
| #Ru-G2 | 350 | 260.7 | 276.5 | 324.2 | 347.0 | 353.6 | 336.5 | 315.4 | 307.0 | 283.7 |
| #Ru-G3 | 350 | 251.0 | 259.9 | 356.0 | 355.0 | 365.2 | 351.6 | 338.0 | 336.8 | 317.4 |
| #Ru-G4 | 350 | 238.7 | 249.8 | 326.5 | 347.5 | 357.2 | 337.8 | 323.8 | 320.0 | 299.2 |
| #Ru-G5 | 350 | 229.7 | 243.5 | 317.0 | 353.2 | 358.5 | 328.0 | 309.9 | 303.2 | 278.9 |
| #Ru-G1b | 350 | 286.2 | 312.9 | 355.5 | 363.1 | 371.9 | 364.8 | 344.2 | 338.4 | 319.2 |
| #Ru-G2b | 350 | 266.7 | 278.3 | 339.0 | 342.7 | 367.3 | 368.5 | 352.6 | 352.7 | 335.7 |
| #Ru-G3b | 350 | 265.4 | 274.2 | 352.6 | 347.8 | 371.2 | 363.8 | 347.3 | 347.5 | 332.3 |
| #Ru-G4b | 350 | 250.1 | 263.7 | 348.8 | 365.6 | 365.5 | 340.5 | 325.9 | 321.6 | 300.2 |
| #Ru-G5b | 350 | 260.0 | 273.6 | 373.7 | 392.2 | 404.4 | 382.1 | 360.8 | 359.3 | 334.1 |
| #Ru-R1 | 350 | 259.8 | 273.5 | 343.2 | 357.9 | 362.6 | 347.9 | 324.1 | 318.2 | 296.8 |
| #Ru-R2 | 350 | 260.7 | 276.5 | 324.2 | 347.0 | 353.6 | 336.5 | 315.4 | 307.0 | 283.7 |
| #Ru-R3 | 350 | 255.1 | 261.4 | 338.0 | 348.5 | 358.0 | 347.7 | 324.7 | 325.6 | 306.0 |
| #Ru-R4 | 350 | 254.6 | 262.5 | 354.4 | 359.4 | 361.6 | 342.7 | 320.5 | 320.8 | 299.3 |
| #Ru-R5 | 350 | 255.6 | 264.2 | 363.9 | 365.2 | 363.0 | 337.2 | 315.1 | 313.8 | 291.6 |
| #Ru-R1b | 350 | 261.1 | 270.3 | 331.7 | 339.0 | 362.5 | 362.1 | 348.4 | 349.4 | 333.9 |
| #Ru-R2b | 350 | 266.7 | 278.3 | 339.0 | 342.7 | 367.3 | 368.5 | 352.6 | 352.7 | 335.7 |
| #Ru-R3b | 350 | 265.9 | 279.2 | 356.2 | 362.8 | 361.4 | 339.9 | 327.2 | 322.7 | 302.1 |
| #Ru-R4b | 350 | 268.3 | 282.7 | 338.7 | 353.1 | 359.3 | 344.4 | 333.6 | 329.2 | 309.2 |
| #Ru-R5b | 350 | 266.8 | 279.4 | 367.8 | 368.5 | 363.3 | 336.6 | 322.1 | 317.4 | 296.7 |
| #Ni-T1 | 268 | 237.0 | 233.4 | 274.2 | 268.9 | 266.2 | 258.8 | 250.1 | 247.3 | 234.9 |
| #Ni-T2 | 300 | 236.4 | 241.1 | 299.4 | 292.8 | 313.1 | 317.4 | 310.4 | 309.5 | 299.8 |
| #Ni-T3 | 350 | 271.6 | 294.6 | 343.7 | 346.5 | 361.2 | 363.1 | 352.5 | 347.6 | 334.5 |
| #Ni-T4 | 400 | 335.9 | 360.3 | 389.8 | 401.5 | 413.5 | 421.2 | 401.3 | 399.8 | 391.0 |
| #Ni-T5 | 450 | 414.7 | 426.7 | 459.7 | 463.7 | 462.0 | 456.0 | 431.4 | 428.2 | 416.8 |

**Table 9** (*continued*)

| Test | Set point (°C) | Thermocouple | | | | | | | | |
|---|---|---|---|---|---|---|---|---|---|---|
| | | 1 | 2 | 3 | 4 | 5 | 6 | 7 | 8 | 9 |
| #Ni-T1b | 250 | 238.1 | 229.4 | 260.8 | 254.6 | 253.6 | 247.0 | 242.8 | 245.6 | 241.5 |
| #Ni-T2b | 300 | 265.4 | 269.7 | 313.2 | 299.4 | 301.3 | 292.0 | 279.9 | 280.8 | 273.6 |
| #Ni-T3b | 350 | 361.1 | 330.7 | 383.3 | 356.8 | 366.3 | 358.0 | 335.9 | 341.4 | 333.6 |
| #Ni-T4b | 400 | 389.2 | 380.8 | 419.4 | 409.4 | 406.5 | 391.8 | 362.8 | 361.3 | 351.7 |
| #Ni-T5b | 450 | 428.2 | 437.1 | 464.7 | 465.8 | 454.7 | 433.7 | 398.2 | 389.4 | 375.3 |
| #Ni-G1 | 350 | 325.6 | 306.9 | 357.7 | 337.9 | 348.6 | 344.6 | 329.9 | 337.9 | 328.4 |
| #Ni-G2 | 350 | 271.6 | 294.6 | 343.7 | 346.5 | 361.2 | 363.1 | 352.5 | 347.6 | 334.5 |
| #Ni-G3 | 350 | 335.6 | 311.9 | 364.0 | 341.2 | 355.7 | 354.9 | 338.7 | 348.0 | 339.8 |
| #Ni-G4 | 350 | 303.4 | 301.1 | 350.5 | 335.4 | 352.9 | 352.3 | 341.4 | 347.4 | 339.1 |
| #Ni-G5 | 350 | 315.0 | 312.4 | 374.6 | 344.7 | 355.9 | 349.7 | 337.7 | 344.6 | 333.8 |
| #Ni-G1b | 350 | 357.9 | 314.0 | 359.4 | 338.3 | 349.1 | 345.8 | 334.8 | 334.0 | 325.6 |
| #Ni-G2b | 350 | 361.1 | 330.7 | 383.3 | 356.8 | 366.3 | 358.0 | 335.9 | 341.4 | 333.6 |
| #Ni-G3b | 350 | 342.1 | 304.6 | 348.7 | 330.0 | 332.9 | 319.5 | 303.5 | 309.9 | 300.3 |
| #Ni-G4b | 350 | 354.1 | 309.1 | 359.2 | 335.5 | 332.9 | 318.0 | 300.3 | 307.1 | 296.7 |
| #Ni-G5b | 350 | 337.0 | 304.3 | 357.4 | 331.4 | 340.8 | 334.3 | 314.0 | 322.6 | 316.0 |
| #Ni-R1 | 350 | 280.3 | 299.9 | 358.0 | 348.3 | 357.6 | 353.1 | 341.6 | 340.1 | 325.0 |
| #Ni-R2 | 350 | 271.6 | 294.6 | 343.7 | 346.5 | 361.2 | 363.1 | 352.5 | 347.6 | 334.5 |
| #Ni-R3 | 350 | 303.9 | 308.6 | 368.7 | 348.9 | 357.6 | 351.6 | 334.1 | 337.5 | 324.0 |
| #Ni-R4 | 350 | 294.4 | 295.9 | 344.3 | 335.9 | 354.6 | 356.1 | 347.7 | 350.2 | 339.9 |
| #Ni-R5 | 350 | 307.4 | 302.4 | 353.9 | 337.2 | 350.6 | 347.7 | 338.6 | 342.9 | 331.8 |
| #Ni-R1b | 350 | 324.6 | 319.3 | 355.5 | 340.2 | 336.5 | 320.3 | 303.5 | 302.8 | 294.3 |
| #Ni-R2b | 350 | 361.1 | 330.7 | 383.3 | 356.8 | 366.3 | 358.0 | 335.9 | 341.4 | 333.6 |
| #Ni-R3b | 350 | 342.8 | 317.5 | 360.8 | 338.7 | 334.7 | 315.7 | 297.7 | 299.5 | 289.9 |
| #Ni-R4b | 350 | 340.5 | 307.9 | 349.4 | 331.0 | 342.0 | 343.5 | 322.8 | 326.1 | 319.9 |
| #Ni-R5b | 350 | 350.9 | 311.9 | 355.6 | 335.8 | 347.8 | 351.9 | 334.2 | 335.8 | 328.9 |

## References


[1] Capros P, De Vita A, Florou A, Kannavou M, Fotiou T, Siskos P, et al. EU reference scenario 2020. 2021. https://doi.org/10.2833/35750.

[2] Daiyan R, Macgill I, Amal R. Opportunities and challenges for renewable power-to-X. ACS Energy Lett 2020;5:3843–7. https://doi.org/10.1021/acsenergylett.0c02249.

[3] Bailera M, Lisbona P, Peña B, Romeo LM. A review on CO2 mitigation in the Iron and Steel industry through Power to X processes. J CO2 Util 2021;46:101456. https://doi.org/10.1016/j.jcou.2021.101456.

[4] Bailera M, Lisbona P, Romeo LM, Espatolero S. Power to Gas projects review: lab, pilot and demo plants for storing renewable energy and CO2. Renew Sustain Energy Rev 2017;69. https://doi.org/10.1016/j.rser.2016.11.130.

[5] Bailera M, Lisbona P. Energy storage in Spain: forecasting electricity excess and assessment of power-to-gas potential up to 2050. Energy 2018;143. https://doi.org/10.1016/j.energy.2017.11.069.

[6] Katla D, Jurczyk M, Skorek-Osikowska A, Uchman W. Analysis of the integrated system of electrolysis and methanation units for the production of synthetic natural gas (SNG). Energy 2021;237. https://doi.org/10.1016/j.energy.2021.121479.

[7] Uchman W, Skorek-Osikowska A, Jurczyk M, Węcel D. The analysis of dynamic operation of power-to-SNG system with hydrogen generator powered with renewable energy, hydrogen storage and methanation unit. Energy 2020;213. https://doi.org/10.1016/j.energy.2020.118802.

[8] Gao J, Liu Q, Gu F, Liu B, Zhong Z, Su F. Recent advances in methanation catalysts for the production of synthetic natural gas. RSC Adv 2015;5:22759–76. https://doi.org/10.1039/c4ra16114a.

[9] Garbarino G, Bellotti D, Riani P, Magistri L, Busca G. Methanation of carbon dioxide on Ru/Al2O3 and Ni/Al2O3 catalysts at atmospheric pressure: catalysts activation, behaviour and stability. Int J Hydrogen Energy 2015;40:9171–82. https://doi.org/10.1016/j.ijhydene.2015.05.059.

[10] Ewald S, Kolbeck M, Kratky T, Wolf M, Hinrichsen O. On the deactivation of Ni-Al catalysts in CO2 methanation. Appl Catal Gen 2019;570:376–86. https://doi.org/10.1016/j.apcata.2018.10.033.

[11] Muroyama H, Tsuda Y, Asakoshi T, Masitah H, Okanishi T, Matsui T, et al. Carbon dioxide methanation over Ni catalysts supported on various metal oxides. J Catal 2016;343:178–84. https://doi.org/10.1016/j.jcat.2016.07.018.

[12] Wolf M, Wong LH, Schüler C, Hinrichsen O. CO2 methanation on transition-metal-promoted Ni-Al catalysts: sulfur poisoning and the role of CO2 adsorption capacity for catalyst activity. J CO2 Util 2020;36:276–87. https://doi.org/10.1016/j.jcou.2019.10.014.

[13] Méndez-Mateos D, Barrio VL, Requies JM, Cambra JF. A study of deactivation by H2S and regeneration of a Ni catalyst supported on Al2O3, during methanation of CO2. Effect of the promoters Co, Cr, Fe and Mo. RSC Adv 2020;10:16551–64. https://doi.org/10.1039/d0ra00882f.

[14] Legras B, Ordomsky VV, Dujardin C, Virginie M, Khodakov AY. Impact and detailed action of sulfur in syngas on methane synthesis on Ni/γ-Al2O3 catalyst. ACS Catal 2014;4:2785–91. https://doi.org/10.1021/cs500436f.

[15] Müller K, Fleige M, Rachow F, Schmeiber D. Sabatier based CO2-methanation of flue gas emitted by conventional power plants. Energy Proc 2013;40:240–8.

[16] Lunde PJ, Kester FL. Rates of methane formation from carbon dioxide and hydrogen over a ruthenium catalyst. J Catal 1973;30:423–9. https://doi.org/10.1016/0021-9517(73)90159-0.

[17] Schoder M, Armbruster U, Martin A. Heterogen katalysierte Hydrierung von Kohlendioxid zu Methan unter erhohten Drucken. Chem-Ing-Tech 2013;85:344–52. https://doi.org/10.1002/cite.201200112.

[18] Wu HC, Chang YC, Wu JH, Lin JH, Lin IK, Chen CS. Methanation of CO2 and reverse water gas shift reactions on Ni/SiO2 catalysts: the influence of particle size on selectivity and reaction pathway. Catal Sci Technol 2015;5:4154–63. https://doi.org/10.1039/c5cy00667h.

[20] Zhou R, Rui N, Fan Z, Liu C. Effect of the structure of Ni/TiO2 catalyst on CO2 methanation. Int J Hydrogen Energy 2016;41:22017. https://doi.org/10.1016/J.IJHYDENE.2016.08.093. –25.

[23] Everett OE, Zonetti PC, Alves OC, de Avillez RR, Appel LG. The role of oxygen vacancies in the CO2 methanation employing Ni/ZrO2 doped with Ca. Int J Hydrogen Energy 2020;45:6352–9. https://doi.org/10.1016/j.ijhydene.2019.12.140.

[24] Winter LR, Gomez E, Yan B, Yao S, Chen JG. Tuning Ni-catalyzed CO2 hydrogenation selectivity via Ni-ceria support interactions and Ni-Fe bimetallic formation. Appl Catal B Environ 2018;224:442–50. https://doi.org/10.1016/j.apcatb.2017.10.036.

[25] Song H, Yang J, Zhao J, Chou L. Methanation of carbon dioxide over a highly dispersed Ni/La2O3 catalyst. Chin J Catal 2010;31:21–3. https://doi.org/10.1016/s1872-2067(09)60036-x.

[26] Yan Y, Dai Y, He H, Yu Y, Yang Y. Applied Catalysis B : environmental A novel W-doped Ni-Mg mixed oxide catalyst for CO 2 methanation. Appl Catal B Environ 2016;196:108–16. https://doi.org/10.1016/j.apcatb.2016.05.016.

[27] Bacariza MC, Graça I, Bebiano SS, Lopes JM, Henriques C. Micro- and mesoporous supports for CO2 methanation catalysts: a comparison between SBA-15, MCM-41 and USY zeolite. Chem Eng Sci 2018;175:72–83. https://doi.org/10.1016/j.ces.2017.09.027.

[28] Romero-Sáez M, Dongil AB, Benito N, Espinoza-González R, Escalona N, Gracia F. CO2 methanation over nickel-ZrO2 catalyst supported on carbon nanotubes: a comparison between two impregnation strategies. Appl Catal B Environ 2018;237:817–25. https://doi.org/10.1016/j.apcatb.2018.06.045.

[29] Graça I, González LV, Bacariza MC, Fernandes A, Henriques C, Lopes JM, et al. CO2 hydrogenation into CH4 on NiHNaUSY zeolites. Appl Catal B Environ 2014;147:101–10. https://doi.org/10.1016/j.apcatb.2013.08.010.

[30] Zhang W, Machida H, Takano H, Izumiya K, Norinaga K. Computational fluid dynamics simulation of CO2 methanation in a shell-and-tube reactor with multi-region conjugate heat transfer. Chem Eng Sci 2020;211:115276. https://doi.org/10.1016/j.ces.2019.115276.

[31] Czuma N, Zarębska K, Motak M, Gálvez ME, Da Costa P. Ni/zeolite X derived

from fly ash as catalysts for CO2 methanation. Fuel 2020;267. https://doi.org/10.1016/j.fuel.2020.117139.
[32] Bacariza MC, Bértolo R, Graça I, Lopes JM, Henriques C. The effect of the compensating cation on the catalytic performances of Ni/USY zeolites towards CO2 methanation. J CO2 Util 2017;21:280–91. https://doi.org/10.1016/j.jcou.2017.07.020.
[33] Cao H, Wang W, Cui T, Wang H, Zhu G, Ren X. Enhancing CO2 hydrogenation to methane by Ni-based catalyst with V species using 3D-mesoporous KIT-6 as support. Energies 2020;13. https://doi.org/10.3390/en13092235.
[34] Pandey D, Deo G. Effect of support on the catalytic activity of supported Ni–Fe catalysts for the CO2 methanation reaction. J Ind Eng Chem 2016;33:99–107. https://doi.org/10.1016/j.jiec.2015.09.019.
[35] Mihet M, Lazar MD. Methanation of CO2 on Ni/γ-Al2O3: influence of Pt, Pd or Rh promotion. Catal Today 2018;306:294–9. https://doi.org/10.1016/j.cattod.2016.12.001.
[36] Xu L, Lian X, Chen M, Cui Y, Wang F, Li W, et al. CO2 methanation over Co-Ni bimetal-doped ordered mesoporous Al2O3 catalysts with enhanced low-temperature activities. Int J Hydrogen Energy 2018;43:17172–84. https://doi.org/10.1016/j.ijhydene.2018.07.106.
[37] Le TA, Kim J, Kang JK, Park ED. CO and CO2 methanation over M (M[dbnd]Mn, Ce, Zr, Mg, K, Zn, or V)-promoted Ni/Al@Al2O3 catalysts. Catal Today 2019. https://doi.org/10.1016/j.cattod.2019.08.058.
[40] Zhan Y, Wang Y, Gu D, Chen C, Jiang L, Takehira K. Ni/Al2O3-ZrO2 catalyst for CO2 methanation: the role of γ-(Al, Zr)2O3 formation. Appl Surf Sci 2018;459:74–9. https://doi.org/10.1016/j.apsusc.2018.07.206.
[41] Rahmani S, Rezaei M, Meshkani F. Preparation of promoted nickel catalysts supported on mesoporous nanocrystalline gamma alumina for carbon dioxide methanation reaction. J Ind Eng Chem 2014;20:4176–82. https://doi.org/10.1016/j.jiec.2014.01.017.
[42] Rivero-Mendoza DE, Stanley JNG, Scott J, Aguey-Zinsou KF. An alumina-supported ni-la-based catalyst for producing synthetic natural gas. Catalysts 2016;6:1–15. https://doi.org/10.3390/catal6110170.
[43] Garbarino G, Wang C, Cavattoni T, Finocchio E, Riani P, Flytzani-Stephanopoulos M, et al. A study of Ni/La-Al2O3 catalysts: a competitive system for CO2 methanation. Appl Catal B Environ 2018. https://doi.org/10.1016/j.apcatb.2018.12.063.
[44] Zhao K, Li Z, Bian L. CO2 methanation and co-methanation of CO and CO2 over Mn-promoted Ni/Al2O3 catalysts. Front Chem Sci Eng 2016;10:273–80. https://doi.org/10.1007/s11705-016-1563-5.
[45] Liu Q, Wang S, Zhao G, Yang H, Yuan M, An X, et al. CO2 methanation over ordered mesoporous NiRu-doped CaO-Al2O3 nanocomposites with enhanced catalytic performance. Int J Hydrogen Energy 2018;43:239–50. https://doi.org/10.1016/j.ijhydene.2017.11.052.
[46] Frontera P, Malara A, Modafferi V, Antonucci V, Antonucci P, Macario A. Catalytic activity of Ni-Co supported metals in carbon dioxides methanation. Can J Chem Eng 2020. https://doi.org/10.1002/cjce.23780.
[47] Grad O, Mihet M, Blanita G, Dan M, Barbu-Tudoran L, Lazar MD. MIL-101-Al2O3 as catalytic support in the methanation of CO2 – comparative study between Ni/MIL-101 and Ni/MIL-101-Al2O3 catalysts. Catal Today 2020. https://doi.org/10.1016/j.cattod.2020.05.003.
[48] Guilera J, del Valle J, Alarcón A, Díaz JA, Andreu T. Metal-oxide promoted Ni/Al2O3 as CO2 methanation micro-size catalysts. J CO2 Util 2019;30:11–7. https://doi.org/10.1016/j.jcou.2019.01.003.
[49] Alarcon A, Guilera J, Soto R, Andreu T. Higher tolerance to sulfur poisoning in CO2 methanation by the presence of CeO2. 2019. https://doi.org/10.1016/j.apcatb.2019.118346.
[50] Guilera J, Soto R, Alarcón A, Andreu T. Satisfactory catalyst stability in SNG production using real biogas despite sulfur poisoning evidences at different reactor zones. Fuel 2021;306. https://doi.org/10.1016/j.fuel.2021.121682.
[51] Rynkowski JM, Paryjczak T, Lewicki A, Szynkowska MI, Maniecki TP, Jóźwiak WK. Characterization of Ru/CeO2-Al2O3 catalysts and their performance in CO2 methanation. React Kinet Catal Lett 2000;71:55–64. https://doi.org/10.1023/A:1010326031095.
[52] Nam H, Kim JH, Kim H, Kim MJ, Jeon SG, Jin GT, et al. CO2 methanation in a bench-scale bubbling fluidized bed reactor using Ni-based catalyst and its exothermic heat transfer analysis. Energy 2021;214:118895. https://doi.org/10.1016/j.energy.2020.118895.
[53] Clariant.. METH® 134 Catalyst for methanation in ammonia or syngas production. 2019.
[54] Matthey J. Methanation catalysts. 2020.
[55] Topsøe H. PK-7R Pre-reduced methanation catalyst. 2020.
[56] Alarcón A, Guilera J, Díaz JA, Andreu T. Optimization of nickel and ceria catalyst content for synthetic natural gas production through CO2 methanation. Fuel Process Technol 2019;193:114–22. https://doi.org/10.1016/j.fuproc.2019.05.008.
[57] Martin San José C. Catalizadores de alta actividad a baja temperatura para la producción de gas natural sintéctico. Universitat de Barcelona; 2020.
[58] Bailera M, Peña B, Lisbona P, Marín J, Romeo LM. Lab-scale experimental tests of power to gas-oxycombustion hybridization: system design and preliminary results. Energy 2021;226:120375. https://doi.org/10.1016/j.energy.2021.120375.
[59] Falbo L, Martinelli M, Visconti CG, Lietti L, Bassano C, Deiana P. Kinetics of CO2methanation on a Ru-based catalyst at process conditions relevant for Power-to-Gas applications. Appl Catal B Environ 2018;225:354–63. https://doi.org/10.1016/j.apcatb.2017.11.066.
[60] Vassiliadis VS, Conejeros R. Powell method. Encycl. Optim.. Boston, MA: Springer US; 2008. p. 3012–3. https://doi.org/10.1007/978-0-387-74759-0_516.
[61] Bailera M, Lisbona P, Peña B, Romeo LM. Energy storage. Cham: Springer International Publishing; 2020. https://doi.org/10.1007/978-3-030-46527-8.
[62] Götz M, Lefebvre J, Mörs F, McDaniel Koch A, Graf F, Bajohr S, et al. Renewable Power-to-Gas: a technological and economic review. Renew Energy 2016;85:1371–90. https://doi.org/10.1016/j.renene.2015.07.066.